

# Northumbria Research Link

Citation: Kyriakou, Sotiris (2019) Synthesis and biological evaluation of metal chelators of the hydroxypyridinone family as potential treatment of Parkinson's disease and cancer. Doctoral thesis, Northumbria University.

This version was downloaded from Northumbria Research Link:  
<http://nrl.northumbria.ac.uk/id/eprint/42400/>

Northumbria University has developed Northumbria Research Link (NRL) to enable users to access the University's research output. Copyright © and moral rights for items on NRL are retained by the individual author(s) and/or other copyright owners. Single copies of full items can be reproduced, displayed or performed, and given to third parties in any format or medium for personal research or study, educational, or not-for-profit purposes without prior permission or charge, provided the authors, title and full bibliographic details are given, as well as a hyperlink and/or URL to the original metadata page. The content must not be changed in any way. Full items must not be sold commercially in any format or medium without formal permission of the copyright holder. The full policy is available online: <http://nrl.northumbria.ac.uk/policies.html>

**Synthesis and Biological Evaluation  
of Metal Chelators of the  
Hydroxypyridinone Family  
as Potential Treatment of Parkinson's  
Disease and Cancer**

Sotiris Kyriakou

PhD

**Synthesis and Biological Evaluation  
of Metal Chelators of the  
Hydroxypyridinone Family  
as Potential Treatment of Parkinson's  
Disease and Cancer**

Sotiris Kyriakou

BSc (Hons), MSc

A thesis in partial-fulfilment of the requirements of the University of Northumbria at  
Newcastle for the degree of Doctor of Philosophy. Research undertaken in the  
Faculty of Health and Life Sciences.

September 2019

## ABSTRACT

A series of 9 hydroxypyridinones (HOPO) metal-based iron chelators (from which 6 of them are novel) have been prepared, characterised and derivatized in a manner to exploit an active transport mechanism; Large neutral Amino Acid Transporter-1 (LAT-1), which is found to be overexpressed in various types of cancer as well as to be presented in the blood-brain barrier (BBB) (**Figure i**).

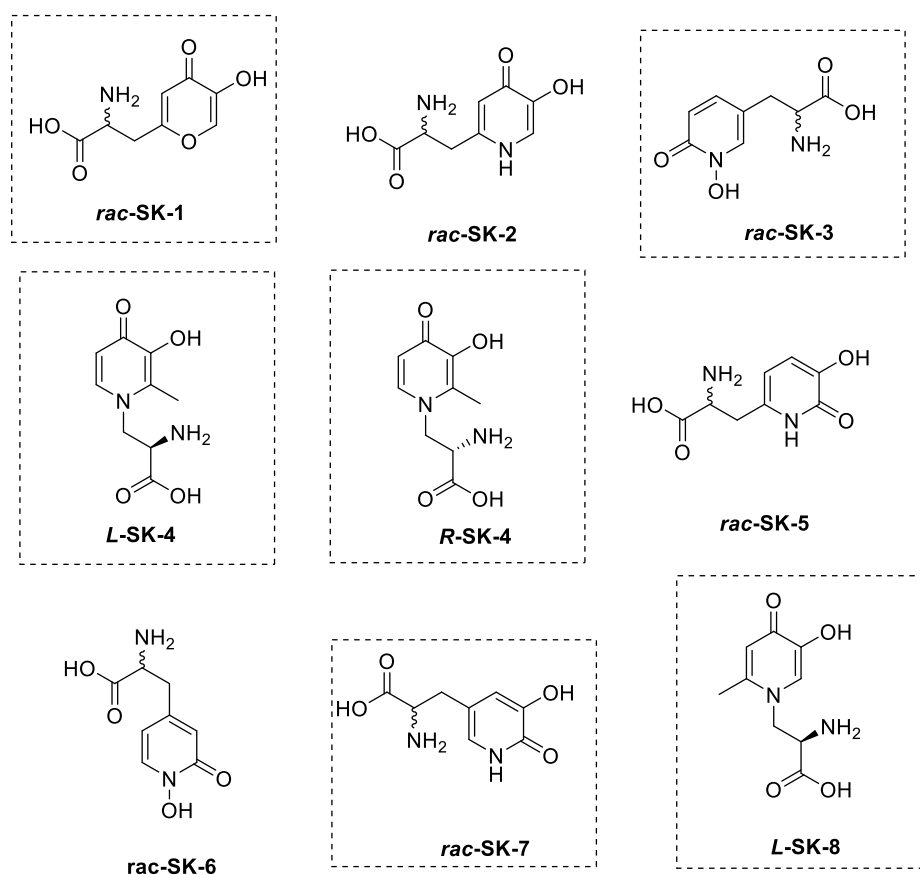


**Figure (i):** Structure of HOPO based compounds synthesised. Novel compounds are in the dotted frames.

Additionally, it appears that the involvement of iron into metabolic pathways and/or the formation of low levels of reactive oxygen species (ROS) enhances the survival and proliferation of various types of cancer including malignant melanoma. The anticancer capacity of the series of HOPO based metal chelators, have been evaluated in an *in vitro* model

consisting of human (eg. A375, VVM1, HS-294T) and rodent (eg. B16F-10) melanoma cells as well as non-melanoma epidermoid carcinoma (eg. A431) and immortalized, non-malignant keratinocyte (eg. HaCaT) cells. The results of this study demonstrated that a single compound a methylated analogue of *L*-mimosine, can exert anticancer capacity as at the administered concentration it acts as a pro-oxidant triggering the production of high (toxic) levels of ROS, selectively in melanoma cell lines. The accumulation of ROS, drives the cells to apoptosis via activation of a well characterised downstream cascade that includes that activation of the terminal caspase 3/7 via the action of intrinsic (activation of caspase-9 pathway) and extrinsic (activation of caspase-8 pathway)

Additionally, the excessive production of oxidative cellular stress and iron misregulation may be substantially involved in the dopaminergic neuron degeneration seen in the brains of Parkinson's disease (PD) patients. Here we evaluated the effectiveness of the synthesised iron chelators, based on the hydroxypyridinone core with the ability to cross the BBB and penetrate the brain. Immortalised human dopaminergic neuronal precursor cells (LUHMES) were treated with the PD-related toxins 6-hydroxydopamine (6-OHDA), which generates superoxide radicals, 1-methyl-4-phenylpyridinium (MPP<sup>+</sup>), a mitochondrial complex I inhibitor, and the ferroptosis activator, erastin. Extensive cytotoxicological profiling revealed that three (*rac*-SK-2, *rac*-SK-3 and *L*-SK-4) out of the five tested compounds (*rac*-SK-1, *rac*-SK-2, *rac*-SK-3, *L*-SK-4 and *rac*-SK-5) rescue dopaminergic neuronal cells without inducing any toxic effects to cells, revealed through multiple cytotoxicological assays.

In order to validate which structural features were essential for the transportation and the action of the compound, a series of control compounds (which they were lacking either the amino acid moiety or the coordination unit) have also been designed and screened against both melanoma cancer as well as PD cell lines. These control compounds of the associated molecules supported the rational design behind them according to which, the HOPO core is essential for the metal binding and the amino acid side vector for the transportation across the biological membranes via LAT-1.

## **DECLARATION**

I declare that the work contained in my thesis has not been submitted for any other award and that is all my own work. Where metadata are being used for further data analysis, the source are appropriately acknowledged. I declare that the word count for the thesis is 50822.

Name: Sotiris Kyriakou

Signature:

Date: 24/09/2019

## **ACKNOWLEDGEMENTS**

Firstly, I would like to thank my supervisor Dr David Tetard for his help, support and guidance over the duration of this research. His consistent motivation and enthusiasm were of great help during the more challenging parts of the project.

I would also like to thank Prof Mihalis Panayiotides for his support, guidance and financial support of the biological screening part of the compounds against melanoma cancer. Many thanks also belong to our collaborators; Dr Jeremy Brandel from the university of Strasbourg in France who helped us with the physicochemical characterisation of the compound, Dr Marcel Leist and Dr Simon Gutbier from the university of Konstanz in Germany for assisting us in the biological evaluation of our compounds against in PD.

My sincerest thanks go to the technical staff at Northumbria University; Dr Karen Haggerty, Gordon Forrest, Anthea Wilde, Gary Askwith and Paul Broom for their continued help throughout the project.

I am extremely grateful to my colleagues in EBA510, the support and enthusiasm that they provided me through the last three years. Special thanks go to Dr Andrey Zaytzev, Dr Hannah Sykes, Dr Rachel Bulmer, Dr Matt Knight, Dr Ross Martinscroft, Dr Jeffrey McGeorge, Dr William Cheung, Dr Theodora Mantso, Melina Mitsiogianni, Charlotte Marsh, Thong Truong, Joe Watson, Joe O'Sullivan, Elliot Sharp, Craig Hodgson and Kristian Poll for encouraging and motivating me through my studies.

Finally, my greatest thanks to my parents and brother for their uncanny support and encouragement especially through the last three years. Thank you to my fiancée who has been a constant source of reassurance, support and for talking through the difficult parts of the study and, in many cases, helping me to find the best way to proceed, no matter the obstacles.

## Table of Contents

<b>1</b>	<b>Introduction.....</b>	<b>1</b>
1.1	Skin Cancer – Classes of the disease .....	1
1.1.1	Malignant melanoma .....	2
1.1.2	Origin of the disease .....	2
1.1.3	Cancer stem cells in skin cancer progression.....	3
1.2	Clinical diagnosis and therapy .....	4
1.2.1	Current therapeutic approaches .....	5
1.2.1.1	Immunotherapeutic approach .....	6
1.2.1.2	Chemotherapeutic agents and radiotherapy .....	7
1.3	The involvement of metals in cancer development and metastasis .....	8
1.3.1	The role of copper in cancer .....	8
1.3.2	The role of zinc in cancer .....	9
1.3.2.1	The role of iron in cancer.....	10
1.4	Metal chelation based treatment .....	13
1.4.1	Toxicity of metal chelators and prodrugs .....	20
1.5	Neurodegenerative diseases.....	23
1.6	Parkinson’s disease .....	23
1.6.1	Epidemiology .....	23
1.6.2	Pathology and symptoms.....	24
1.6.3	Genetic origin of PD.....	26
1.6.4	The contribution of metal-induced oxidative stress into PD development.....	28
1.7	Toxin-induced PD for <i>in vitro</i> and <i>in vivo</i> studies .....	28
1.7.1	6-hydroxydopamine (6-OHDA) .....	29
1.7.2	MPTP/ MPP <sup>+</sup> .....	30
1.7.3	Erastin .....	31
1.8	Current Treatments.....	33
1.8.1	Non-pharmacological therapies .....	33
1.8.2	Pharmacological therapies – Existing treatments.....	34
1.8.2.1	<i>L</i> -DOPA supplements.....	36
1.8.2.2	Catechol-O-Methyl Transferase Inhibitors (COMT) .....	37
1.8.2.3	Monoamine Oxidase (MAO) Inhibitors.....	38
1.8.2.4	Dopamine agonists .....	38
1.8.3	New strategies - Metal chelators.....	40
1.8.3.1	Toxicity of metal chelators .....	43
1.9	Transportation across the BBB.....	44
1.10	The Blood-Brain Barrier .....	45

1.11	Overcoming the BBB .....	46
1.11.1	Passive diffusion.....	47
1.11.2	Prodrugs to improve passive diffusion .....	48
1.12	Transportation process .....	50
1.12.1	The transport system.....	51
1.12.1.1	Active Efflux Transporter (AET).....	51
1.12.1.2	Receptor Mediated Transport .....	51
1.12.1.3	Carrier mediated transport (CMT) .....	52
1.12.1.3.1	The Glucose-Transporter-1 (GLUT-1) .....	54
1.12.1.3.1.1	Transportation of metal chelators through GLUT-1.....	55
1.12.1.3.2	Large Amino acid Transporter-1 (LAT-1).....	57
1.12.1.3.2.1	Structure of LAT-1-4F2hc .....	57
<b>2</b>	<b>Design and Synthesis of Metal Chelators .....</b>	<b>60</b>
2.1	Factors affecting the Fe(III)-chelator stability .....	60
2.1.1	Redox activity – Fenton Chemistry .....	60
2.2	Thermodynamic considerations of complex formation .....	61
2.3	Stability of Fe <sup>3+</sup> - chelator complexes .....	63
2.4	pFe <sup>3+</sup> as measure of ligand binding efficiency .....	65
2.5	Metal sensitivity .....	65
2.6	Dioxygenated coordination units.....	68
2.6.1	Catechols .....	69
2.6.2	Hydroxamic acids.....	69
2.6.3	α-hydroxycarboxylic acid .....	70
2.6.4	Hydroxypyridinones .....	70
2.6.4.1	HOPOs can induced redox silencing .....	72
2.7	Denticity.....	73
2.8	Pharmaco–physicochemical parameters .....	80
2.8.1	Lipophilicity and molecular weight .....	81
2.8.2	Protonation constants.....	82
2.8.3	Stability constants.....	83
2.8.4	Partition coefficient .....	83
2.8.5	Lipinski's rule .....	83
<b>3</b>	<b>Rational LAT-1 substrate design .....</b>	<b>84</b>
3.1	LAT-1 active site.....	84
3.2	Interactions of the amino acid group. ....	85
3.3	Pharmacophore design .....	86
3.3.1	Side Chain design.....	91

3.4	Lipophilicity of LAT-1 substrates .....	92
3.5	Stereochemistry of LAT-1 substrates .....	93
<b>4</b>	<b>Scope of the study .....</b>	<b>95</b>
<b>5</b>	<b>Organic synthesis of the target molecules and control compounds .....</b>	<b>99</b>
5.1	1, 2- HOPOs .....	99
5.2	Synthesis of the amino acid moiety .....	100
5.2.1	Synthesis of <i>rac</i> -SK-3 .....	103
5.2.2	Synthesis of <i>rac</i> -SK-6 .....	108
5.3	3, 2- HOPOs .....	121
5.3.1	Synthesis of <i>rac</i> -SK-5 .....	121
5.3.2	Results – Synthesis of <i>rac</i> -SK-7 .....	123
5.4	3, 4- HOPOs .....	129
5.4.1	Synthesis of <i>rac</i> -SK-1 and <i>rac</i> -SK-2 .....	129
5.4.2	Synthesis of <i>N</i> -substituted 3, 4-HOPOs .....	130
5.4.2.1	Synthesis of <i>L</i> - and <i>D</i> - SK-4 .....	130
5.4.2.2	Synthesis of <i>L</i> -SK-8 .....	132
5.5	Synthesis of the control compounds .....	133
5.5.1	Controls of <i>L</i> -SK-4 .....	133
5.5.2	Control of <i>rac</i> -SK-2 .....	134
5.6	Synthesis of LAT-1 non-selective substrate .....	135
<b>6</b>	<b>Physicochemical characterisation .....</b>	<b>137</b>
6.1	Protonation constants .....	137
6.2	Stability constants .....	146
6.2.1	Complexation with Fe(III) .....	146
6.2.2	Complexation with Cu(II) and Zn(II) .....	154
<b>7</b>	<b>Results and Discussion – Evaluation of the anticancer capacity of the chelators in an <i>in vitro</i> model of Malignant Melanoma. ....</b>	<b>157</b>
7.1	Biological Characterization .....	157
7.1.1	Assessing the cytotoxicity of the SK- <i>n</i> compounds .....	157
7.2	<i>In vitro</i> validation of Structure Activity Relationship (SAR) .....	163
7.2.1	Transportation through LAT-1 .....	163
7.2.2	Control compounds of <i>L</i> -SK-4 .....	168
7.3	Characterization of molecular mechanism of action .....	169
7.3.1	Ability of <i>L</i> -SK-4 to induce ROS .....	169
7.3.2	Determination of mode of cell death .....	174
7.3.3	Ability of <i>L</i> -SK-4 to arrest cell cycle growth .....	178
7.4	Biological mode of action .....	183
7.4.1	Time-dependence determination of ROS fold of induction .....	183

7.5	<i>L</i> -SK-4 generates oxidative stress on malignant melanoma cells .....	185
7.5.1	Effect of oxidative stress been induced by <i>L</i> -SK-4.....	185
7.5.2	ROS scavenging effect by GSH .....	187
7.5.3	Cell death driven by ROS .....	197
7.5.4	ROS elevation activate apoptotic cascades .....	208
7.6	Lipidomic analysis .....	210
7.6.1	Effect of myriocin in cell survival - The role of ceramide. ....	216
7.6.2	Ceramide triggers the direct activation of the extrinsic apoptosis.....	222
7.6.3	Ceramide elevation triggers the indirect activation of intrinsic apoptosis....	223
<b>8</b>	<b>Results and Discussion – Evaluation of the neuroprotective capacity of the SK-n compounds in an in vitro model of Parkinson’s disease (PD) .....</b>	<b>229</b>
8.1	Neuroprotection against 6-OHDA.....	229
8.1.1	Cytotoxicity of the SK-n compounds .....	229
8.2	Neuronal protection.....	232
8.3	Neuroprotection against MPP <sup>+</sup> .....	234
8.3.1	Cytotoxicity of the SK-n compounds .....	234
8.4	In vitro model of ferroptosis.....	238
8.5	<i>In vitro</i> validation of Structure Activity Relationship (SAR) .....	245
8.6	Antioxidant properties of SK-n. ....	248
8.6.1	Interaction of the SK-n compounds with superoxide.....	248
8.6.2	Interactions of SK-n compounds with peroxynitrite .....	249
<b>9</b>	<b>Final discussion .....</b>	<b>254</b>
9.1	Summary and Conclusions.....	254
9.2	Further studies.....	259
9.2.1	Novel Molecules.....	259
9.2.2	Mode of action .....	260
<b>10</b>	<b>Experimental procedures – organic synthesis .....</b>	<b>262</b>
10.1	Equipment and chemical reagents. ....	262
10.2	Synthesis of 1.2 HOPOs.....	263
10.2.1	Synthesis of <i>rac</i> -SK-3 .....	263
10.2.1.1	Synthesis of 5-bromo-2-methoxypyridine (1).....	263
10.2.1.2	Synthesis of 6-methoxypyridine-3-carbaldehyde (2) .....	263
10.2.1.3	Synthesis of 4-[(6-methoxypyridin-3-yl)methylidene]-2-methyl-4,5-dihydro-1,3-oxazol-5-one (3) .....	264
10.2.1.4	Synthesis of 2-acetamido-3-(6-methoxypyridin-3-yl)prop-2-enoic acid (4)	265
10.2.1.5	Synthesis of <i>rac</i> -2-acetamido-3-(6-methoxypyridin-3-yl)propanoic acid (5)	266

10.2.1.6	Synthesis of <i>rac</i> -5-(2-carboxy-2-acetamidoethyl)-2-methoxypyridin-1-ium-1-olate (6) .....	266
10.2.1.7	<i>rac</i> - 2-amino-3-(1-hydroxy-6-oxo-1,6-dihydropyridin-3-yl)propanoic acid ( <i>rac</i> -SK-3).....	267
10.2.2	Synthesis of <i>rac</i> -SK-6 .....	268
10.2.2.1	Synthesis of 4-carboxy-2-chloropyridin-1-ium-1-olate (30) .....	268
10.2.2.2	Synthesis of 1-hydroxy-2-oxo-1,2-dihydropyridine-4-carboxylic acid (31) .....	268
10.2.2.3	Synthesis of methyl 1-hydroxy-2-oxo-1,2-dihydropyridine-4-carboxylate (32) .....	269
10.2.2.4	Synthesis of methyl 1-(benzyloxy)-2-oxo-1,2-dihydropyridine-4-carboxylate (33) .....	270
10.2.2.5	Synthesis of 1-(benzyloxy)-4-(hydroxymethyl)-1,2-dihydropyridin-2-one (34) .....	271
10.2.2.6	Synthesis of [1-(benzyloxy)-2-oxo-1,2-dihydropyridin-4-yl]methyl 4-methylbenzene-1-sulfonate (38) .....	272
10.2.2.7	Synthesis of 1,3-diethyl 2-[[1-(benzyloxy)-2-oxo-1,2-dihydropyridin-4-yl]methyl]-2-acetamidopropanedioate (40).....	273
10.2.2.8	Synthesis of 2-amino-3-(1-hydroxy-2-oxo-1,2-dihydropyridin-4-yl)propanoic acid ( <i>rac</i> -SK-6) .....	274
10.3	Synthesis of 3,2-HOPOs.....	275
10.3.1	Synthesis of <i>rac</i> -SK-5 .....	275
10.3.1.1	Synthesis of 5-(benzyloxy)-2-(hydroxymethyl)-4H-pyran-4-one (41). .....	275
10.3.1.2	Synthesis of 5-(benzyloxy)-2-(hydroxymethyl)-1,4-dihydropyridin-4-one (42) .....	275
10.3.1.3	Synthesis of 5-(benzyloxy)-4-chloro-2-(chloromethyl)pyridine (43)... ..	276
10.3.1.4	Synthesis of 1,3-diethyl-2-[[5-(benzyloxy)-4-chloropyridin-2-yl]methyl]-2-acetamidopropane dioate (44).....	277
10.3.1.5	Synthesis of 1,3-diethyl 2-acetamido-2-[(5-hydroxypyridin-2-yl) methyl] propanedioate (45) .....	278
10.3.1.6	Synthesis of 1,3-diethyl-2-acetamido-2-[(5-hydroxy-6-iodopyridin-2-yl)methyl] propanedioate (46).....	278
10.3.1.7	Synthesis of <i>rac</i> -2-amino-3-(5-hydroxy-6-oxo-1,6-dihydropyridin-2-yl)propanoic acid ( <i>rac</i> -SK-5) .....	279
10.3.2	Synthesis of <i>rac</i> -SK-7 .....	280
10.3.2.1	Synthesis of 2-chloro-3-methoxy pyridine (50) .....	280
10.3.2.2	Synthesis of 2, 3-dimethoxypyridine (51).....	281
10.3.2.3	Synthesis of 5-bromo-2,3-dimethoxypyridine (52).....	281
10.3.2.4	Synthesis of 5,6-dimethoxypyridine-3-carbaldehyde (53) .....	282
10.3.2.5	Synthesis of 4-[(5,6-dimethoxypyridin-3-yl)methylidene]-2-methyl-4,5-dihydro-1,3-oxazol-5-one (54) .....	283

10.3.2.6	Synthesis of <i>rac</i> -3-(5,6-dimethoxypyridin-3-yl)-2-acetamidoprop-2-enoic acid (55).....	284
10.3.2.7	Synthesis of <i>rac</i> -3-(5,6-dimethoxypyridin-3-yl)-2-acetamidopropanoic acid (56)	284
10.3.2.8	Synthesis of <i>rac</i> -2-amino-3-(5-hydroxy-6-oxo-1,6-dihydropyridin-3-yl)propanoic acid ( <i>rac</i> -SK-7) .....	285
10.4	Synthesis of 3, 4-HOPOS .....	287
10.4.1	Synthesis of <i>rac</i> -SK-1 and <i>rac</i> -SK-2.....	287
10.4.1.1	Synthesis of [5-(benzyloxy)-4-oxo-4H-pyran-2-yl]methyl 4-methylbenzene-1-sulfonate (57) .....	287
10.4.1.2	Synthesis of 1,3-diethyl 2-[[5-(benzyloxy)-4-oxo-4H-pyran-2-yl]methyl]-2-acetamidopropanedioate (58).....	288
10.4.1.3	Synthesis of 2-amino-3-(5-hydroxy-4-oxo-4H-pyran-2-yl)propanoic acid ( <i>rac</i> -SK-1) 289	
10.4.1.3.1	Synthesis of 2-amino-3-(5-hydroxy-4-oxo-1,4-dihydropyridin-2-yl)propanoic acid ( <i>rac</i> -SK-2) .....	289
10.4.2	Synthesis of <i>D</i> -SK-4.....	290
10.4.2.1	Synthesis of 3-(benzyloxy)-2-methyl-1,4-dihydropyridin-4-one (60)..	290
10.4.2.2	Synthesis of (2 <i>R</i> )-3-amino-2-[[ <i>(tert</i> -butoxy)carbonyl]amino]propanoic acid ( <i>D</i> -59) 291	
10.4.2.3	Synthesis of 2-amino-3-(3-hydroxy-2-methyl-4-oxo-1,4-dihydropyridin-1-yl)propanoic acid ( <i>D</i> -SK-4) .....	292
10.4.3	Synthesis of <i>L</i> -SK-4 .....	293
10.4.3.1	Synthesis of (2 <i>S</i> )-3-amino-2-[[ <i>(tert</i> -butoxy)carbonyl]amino]propanoic acid ( <i>L</i> -59) 293	
10.4.3.2	Synthesis of 2-amino-3-(3-hydroxy-2-methyl-4-oxo-1,4-dihydropyridin-1-yl)propanoic acid ( <i>L</i> -SK-4).....	293
10.4.4	Synthesis of <i>L</i> -SK-8 .....	294
10.4.4.1	Synthesis of 2-(chloromethyl)-5-hydroxy-4H-pyran-4-one (61).....	294
10.4.4.2	Synthesis of 5-hydroxy-2-methyl-4H-pyran-4-one (62) .....	295
10.4.4.3	Synthesis of 5-(benzyloxy)-2-methyl-4H-pyran-4-one (63) .....	296
10.4.4.4	Synthesis of (2 <i>S</i> )-2-amino-3-(5-hydroxy-2-methyl-4-oxo-1,4-dihydropyridin-1-yl)propanoic acid ( <i>L</i> -SK-8) .....	296
10.5	Synthesis of the control compounds .....	298
10.5.1	Synthesis of <i>L</i> -SK-4 control compounds .....	298
10.5.1.1	Synthesis of 3-methoxy-2-methyl-4H-pyran-4-one (64).....	298
10.5.1.2	Synthesis of (2 <i>S</i> )-amino-3-(3-methoxy-2-methyl-4-oxo-1,4-dihydropyridin-1-yl)propanoic acid (SK-4C1) .....	299
10.5.1.3	Synthesis of 1-(2-aminoethyl)-3-(benzyloxy)-2-methyl-1,4-dihydropyridin-4-one (65).....	300

10.5.1.4	Synthesis of 1-(2-aminoethyl)-3-(benzyloxy)-2-methyl-1,4-dihydropyridin-4-one (SK-4C2).....	301
10.5.1.5	Synthesis of 3-[3-(benzyloxy)-2-methyl-4-oxo-1,4-dihydropyridin-1-yl]propanoic acid (66) .....	301
10.5.1.6	Synthesis of 3-(3-hydroxy-2-methyl-4-oxo-1,4-dihydropyridin-1-yl)propanoic acid (SK-4C3) .....	302
10.5.2	Synthesis of <i>rac</i> -SK-2 control .....	303
10.5.2.1	Synthesis of <i>rac</i> -3-amino-3-(4-chloro-5-hydroxypyridin-2-yl)propanoic acid (SK-2C1) .....	303
10.6	Synthesis of LAT-1 competitive substrate.....	304
10.6.1	Synthesis of 1,3-diethyl 2-acetamido-2-[(naphthalen-2-yl)methyl]propanedioate (67).....	304
10.6.2	Synthesis of <i>rac</i> -2-acetamido-3-ethoxy-2-[(naphthalen-2-yl)methyl]-3-oxopropanoic acid (68).....	305
10.6.3	Synthesis of <i>rac</i> - ethyl 2-acetamido-3-(naphthalen-2-yl)propanoate (69) ...	305
10.6.4	Synthesis of ethyl (2 <i>S</i> )-2-acetamido-3-(naphthalen-2-yl)propanoate (70) and (2 <i>R</i> )-2-acetamido-3-(naphthalen-2-yl)propanoic acid (71) .....	306
10.6.5	Synthesis of (2 <i>R</i> )-2-amino-3-(naphthalen-2-yl)propanoic acid (R-72) .....	307
10.6.6	Synthesis of (2 <i>S</i> )-2-amino-3-(naphthalen-2-yl)propanoic acid (S-72).....	308
<b>11</b>	<b>Experimental procedures – Biological screening and evaluation of the SK-n compounds.....</b>	<b>309</b>
11.1	Cell Culture and Methodologies .....	309
11.1.1	Cell lines.....	309
11.1.2	Materials for cell culture.....	311
11.1.3	Cells recovery .....	312
11.1.4	Cells propagation.....	312
11.1.5	Cells plating .....	312
11.2	Morphological observation of cells .....	313
11.3	Determination of cell viability – Alamar Blue Assay .....	313
11.3.1	Principle of the assay:.....	313
11.3.1.1	Experimental procedure:.....	314
11.4	Flow Cytometry Methodologies .....	315
11.4.1	Determination of ROS kinetics.....	315
11.4.1.1	Principle of the assay:.....	315
11.4.1.1.1	Experimental procedure:.....	316
11.4.2	Determination of apoptosis.....	317
11.4.2.1	Principle of the assay:.....	317
11.4.2.1.1	Experimental procedure:.....	317
11.4.3	Determination of mitochondria membrane depolarization.....	318
11.4.3.1	Principle of the assay:.....	318

11.4.3.1.1	Experimental Procedure:.....	319
11.4.4	Determination of cell cycle kinetics .....	319
11.4.4.1	Principle of the assay:.....	319
11.4.4.1.1	Experimental procedure:.....	320
11.4.5	Protein Methodologies.....	320
11.4.5.1	Preparation of cell lysates and protein determination .....	320
11.4.5.2	Western immunoblotting .....	321
11.4.6	Biochemical Assays .....	323
11.4.6.1	TBARS assay .....	323
11.4.6.1.1	Principle of the assay:.....	323
11.4.6.1.1.1	Experimental procedure:.....	324
11.4.6.2	Protein Carbonyl Colorimetric Assay .....	324
11.4.6.2.1	Principle of the assay:.....	324
11.4.6.2.1.1	Experimental procedure:.....	325
11.4.6.3	DNA oxidative Damage Elisa Assay .....	326
11.4.6.3.1	Principle of the assay:.....	326
11.4.6.3.1.1	Experimental procedure:.....	327
11.5	Lipidomics .....	328
11.5.1	Lipidomic extraction protocol:.....	328
11.5.2	Sample analysis .....	329
11.5.3	LC profile.....	329
11.5.4	Mass spectrometer.....	329
11.5.5	Mass spectral acquisition parameter .....	329
11.5.6	Peak table generations .....	329
11.5.7	Statistical analysis .....	330
<b>12</b>	<b>Appendices.....</b>	<b>331</b>
12.1	Appendix I: derivatization of <i>L</i> -SK-4.....	331
12.2	Appendix II: List of publications.....	334
<b>13</b>	<b>List of References .....</b>	<b>335</b>

## List of abbreviations

±ESI	Electrospray ionisation in positive or negative mode
<sup>13</sup> C-NMR	isotopic carbon 13 nuclear magnetic resonance
<sup>1</sup> H-NMR	proton nuclear magnetic resonance
2,4-DNPH	2,4-dinitrophenyl hydrazine
3D-QSAR	3 dimensional quantitative structure activity relationship
6-OHDA	6-hydroxydopamine
8-OHdG	8-oxo-2-deoxy guanosine
Å	Angstrom
Ac	Acetyl
AChE	Acetyl Choline esterase
AdiC	Arginine bound <i>Escherichia Coli</i>
AET	Active Efflux Transporters
AMT	absorptive-mediated transcytosis
Apaf-1	Apoptotic protease activating factor-1
ApcT	broad-specific Amino acid Transporter
aq	aqueous
Ar	aromatic
ATP	Adenosine triphosphate
BAK	Bcl-2- antagonist Killer protein
BCC	Basal skin Carcinoma
BAX	Bcl-2-associated X protein
BBB	Blood Brain Barrier
BCA	Bicinchoninic acid
BCH	2-aminobicyclo-(2,2,1)-heptane-2-carboxylic acid
BCRP	Breast Cancer Resistance Protein
BID	BH3 Interacting Domain
Bn	benzyl
Boc	<i>Tert</i> -butyloxycarbonyl
br	broad
BRAF	B-Rapidly Accelerated Fibrosarcoma oncogene
BSA	Bovine Serum Albumin

CAM	catecholamide
Cer	Ceramide
CMT	Carrier-mediated Transporter
CNS	Central Nervous System
CoMFA	Comparative Molecular Field Analysis
COMT	Catechol O-Methyl Transferase
d	doublet
Da	Dalton
DAPI	4'-6-diaminidino-2-phenylindole
DAT	Dopamine Antagonist Transporter
DCM	dichloromethane
DEAD	Diethyl azodicarboxylate
DHE	Dihydroethidium
dd	double doublet
DDC	Dopamine Decarboxylase
DDCI	Dopamine Decarboxylase Inhibitor
DF	Dilution Factor
DFO	Desferrioxamine
DFP	Deferiprone
DHR 123	Dihydrorhodamine 123
DMEM	Dulbecco's Modified Eagle Medium
DMF	<i>N, N</i> -dimethylformamide
DMHB	<i>N, N</i> -dimethyl-2,3-dihydrobenzamine
DMS	Dimethyl sulphide
DMSO	Dimethyl sulfoxide
DMSO- <i>d</i> <sub>6</sub>	Deuterated dimethyl sulfoxide
DNA	Deoxyribonucleic acid
DTT	Dithiothreitol
DTPA	Diethylenetriamine Pentaacetic Acid
EC <sub>50</sub>	Half maximal effective Concentration
ED	Extracellular Domain
EDTA	<i>N,N,N',N'</i> -ethylenediamine tetraacetic acid

EGFR	Epidermal Growth Factor
$E^\circ$	Standard Electrode Potential
eq	equivalent
EtOH	Ethanol
FADD	FAS associated domain with death domain
FITC	Fluorescein Isothiocyanate
FTL	Ferritin Light chain
$g$	gravity
GadC	Glutamate/GABA antiporter
GLUT-1	Glucose Transporter-1
GABA	$\gamma$ -aminobutyric acid
GPX-4	Glutathione peroxidase-4
GSH	glutathione (reduced)
HEPES	2-[4-(2-hydroxyethyl)piperazin-1-yl]ethanesulfonic acid
HESI	Heated Electron Spray Ionisation
HPLC	High Performance Liquid Chromatography
hr	hour
$IC_{50}$	Half maximal inhibitory concentration
IRP-2	Iron Regulatory Protein-2
$J$	coupling constant
JC-1	5,5,6,6-tetraethyl benzimidazolyl carbocyanine iodide
K	Equilibrium constant
$k_{rot}$	Rate of bond rotation
LAT-1	Large (neutral) Amino acid Transporter-1
LC	Liquid Chromatography
L-DOPA	Levodopa
LeuT	Leucine Transporter
LDH	Lactate dehydrogenase
LG	Leaving Group
LIP	Liable Iron Pool
LMTC	Ligand-to-Metal Charge Transfer
$\log P$	-log of partition coefficient

LOX	Lysyl oxidase
LOXL	Lysyl oxidase like
M	Molarity
mA	Milli Ampere
MAO-A and B	MonoAmine Oxidase A and B
MAPK	Mitogen-Activated Protein Kinase
MHz	Mega Hertz
MMP	Matrix metalloproteases
<i>m</i> -CPBA	<i>meta</i> chloroperoxybenzoic acid
MCT	Monocarboxylate transporter
MDA	Malondialdehyde
MeOH	methanol
MFS	Major Facilitators Superfamily
MITF	microphthalmia transcription factor
min	minute
mL	mililiter
mM	Mili molar concentration
mmol	milimol
MPP <sup>+</sup>	1-methyl-4-phenylpyridin-1-ium
MPTP	1-methyl-4-phenyl-1,2,6-tetrahydropyridine
MRP	Multidrug Resistance associated Proteins
MS(1)	Mass Spectroscopy
MS(2)	Molecular sieves
Ms-	Mesyl
NADH	Nicotinamide Adenine Dinucleotide
NBS	<i>N</i> -bromo succinimide
NHE	Normal Hydrogen Electrode
nM	nano Molar concentration
nm	Nano metres
NMSC	non-malignant skin cancers
NP40	Ethoxylated nonylphenol
NRAS	N-RAS sarcoma protein

°C	degrees Celsius
OCT	Organic cation transporter
PBS	Phosphate Buffer Saline
PC	Phosphatidyl Choline
PCA	Principal Components Analysis
PD	Parkinson's Disease
Pd/C	palladium over charcoal
PE (1)	Phosphatidyl ethanolamine
PE (2)	Phycoerythrin
PEG	Polyethylene glycol
PG	Protetective group
pFe	'free' metal constant (-log [Fe] <sub>free</sub> )
P-gp	p-glycoprotein
pH	potential of hydrogen
phSM	Sphingomyelin (phytosphingosine)
PI	Propidium iodide
pKa	-log of acid dissociation constant
PLS-DA	Partial Least Squares –Discriminated Analysis
PNS	Peripheral Nervous System
ppm	parts per million
PS	Phosphatidyl serine
PVDF	Polyvinylidene difluoride
q	quarter
R	generic group
<i>rac</i>	racemic
RMT	receptor-mediated transcytosis
RNA	Ribonucleic acid
ROS	Reactive Oxygen Species
Rpm	Revolutions per minute
RT	Room Temperature
RT	room temperature
s	singlet

SAR	Structure Activity Relationship
SD	Standard deviation
SDS	Sodium Dodecyl Sulphate
SIN-1	5-amino-3-(4-morpholinyl)-1,2,3-oxadiazolium chloride
SM	Sphingomyelin
S <sub>N</sub> 2	Bimolecular nucleophilic substitution
S <sub>N</sub> Ar	Nucleophilic aromatic substitution
SCC	squamous cell carcinoma
t	triplet
TBARS	Thiobarbitouric acid
TBST	Tris-Buffer Saline with Tween-20 (polysorbate -20)
TCA	Trichloroacetic acid
Tf-	triflic
TFAA	Trifluoroacetic anhydride
TFA	trifluoroacetic acid
TfR1	Transferrin Receptor 1
THF	tetrahydrofuran
TIC	Total Ion Chromatogram
TLC	Thin Layer chromatography
TM	Transmembrane
Ts-	Tosyl
TPP	Triphenylphosphine
TPSA	Topological surface area
UPH	Urea hydrogen peroxide
UHPLC	Ultra-high performance liquid chromatography
UV	UltraViolet
V	volts
v/v	Volume/volume
w/v	Weight/volume
x,y-HOPO	x-hydroxypyridin-y-one
β	Cumulative equilibrium constant
δ	chemical shift

$\Delta\Psi$	Membrane potential difference
$\varepsilon$	Molar extinction coefficient
$\lambda$	Wavelength

# 1 Introduction

## 1.1 Skin Cancer – Classes of the disease

Skin cancer is one of the most common types of cancer worldwide with an increasing incidence rate over the past decade, and it can be categorised into several classes according to the kind of skin cells that it involves (**Figure 1**).<sup>1</sup>

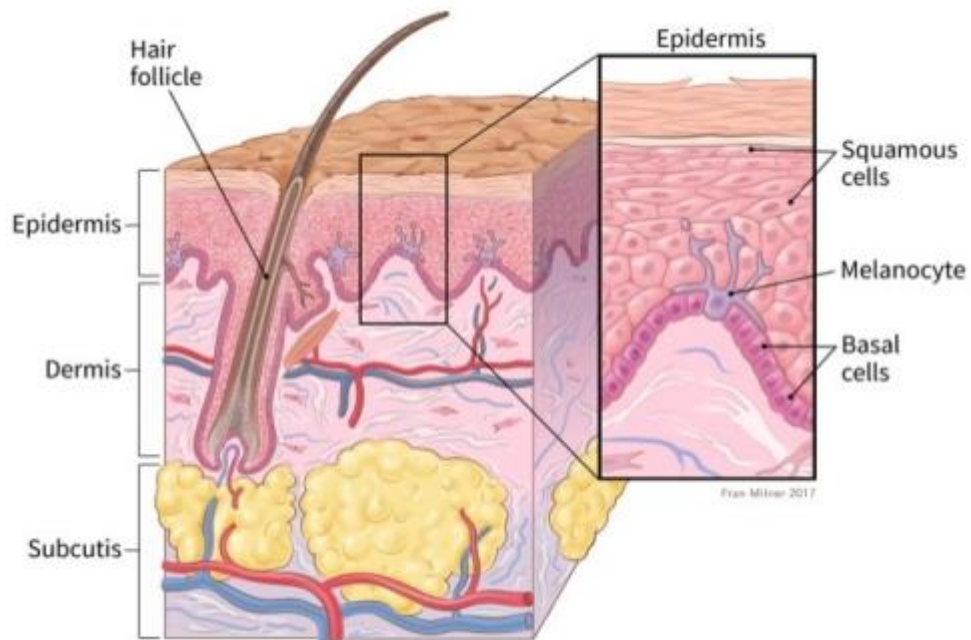


**Figure 1:** Layers from which skin is composed.<sup>2</sup>

There are three main classes of skin cancer. Basal skin carcinoma (BCC) originates from basal cells that are located in the basal layer epidermis or the follicular epithelium and it has the highest prevalence amongst skin cancer rates.<sup>3</sup> Another class of skin cancer is the squamous cell carcinoma (SCC) that derives from the cells that compose the top surface of epidermis.<sup>3</sup> Malignant melanoma is the third class of skin cancer that originates from the melanocytes; cells that are responsible for the melanin production and the most aggressive known type of skin cancer.<sup>3</sup> Both BCC and SCC are subcategorised as non-malignant skin cancers (NMSC) and the most common histologic subtypes (~20%) of all malignancies diagnosed across the UK per annum, whilst worth wide about 5.5 million patients are diagnosed with NMSC.<sup>4,5</sup>

Most of the BCC cases tend to be curable through surgical excision by erosion of the local anatomical structure (mainly on head or neck) and are rarely metastatic.<sup>6</sup> On the contrary, the prognosis for SCCs is less favourable because it can metastasize with significantly higher rate of mortality. SCCs are characterised by the present of atypical keratinocytes, however they can also exhibit a broad spectrum of clinical manifestations.<sup>3</sup> Barton V. *et al.* suggested that the development of NMSC can also lead to an increased risk of other malignancies.<sup>7</sup>

### **1.1.1 Malignant melanoma**

Malignant melanoma is the most aggressive form of skin cancer and one of the most lethal amongst all solid tumour types.<sup>8,9</sup> According to international demographic reports, ~250000 people are diagnosed with malignant melanoma annually, with the overall trend being increasing over the last decade.<sup>10</sup> In the UK, 1 in 54 people will be diagnosed with melanoma during their life, rendering the disease the fifth most common of type of cancer.<sup>10</sup> Over that last two decades the disease incidence rates have been increased dramatically (134%), while it seems that is one of the most common cancers among young (between ages 15-35) and fair-skinned people.<sup>10</sup> The incident rate projections report for 2035 suggest an additional increase of 7%.<sup>10</sup> The late diagnosis is mainly observed in 1 in 10 cases and 59000 patients diagnosed with the disease, were reported for 10 years survival post-diagnosis.<sup>10</sup>

### **1.1.2 Origin of the disease**

The development of the disease is a result of a combination of genetic and metabolic abnormalities at the pigment producing cells (melanocytes) that are located in the neural crest and can migrate to the skin (mainly) during embryonic development<sup>11</sup>. Additionally, melanoma can originate from the cutaneous melanocytes or it can be developed in the mucosal surfaces (uveal tract of the eye, leptomeninges, gastrointestinal sites, oral cavity, and genital mucosa).<sup>11</sup> Unfortunately, the exact pathogenesis of melanoma cancer still remains unclear. However, skin phototype, hair colour, numerous atypical naevi (pigmented moles), and genetic predisposition appear to be the most dominant factors that affect the development of

the disease.<sup>12</sup> Changes in socio-economic status and in lifestyle habits, such as intense and sporadic exposure to sun - mainly during childhood, has been linked to the steadily rising numbers of new diagnosed cases.<sup>13</sup> However, the main reason for the observed trends still remains the prolonged exposure to solar ultraviolet (UV) radiation.<sup>14-16</sup>

Interestingly, melanoma genome analysis demonstrated the strong association between the frequency of mutational events and UV radiation exposure, suggesting the latter as the leading risk factor.<sup>17,18</sup>

### **1.1.3 Cancer stem cells in skin cancer progression**

During the last few decades, there has been research that aims to investigate the stem cell theory of cancer. According to this theory, a small population of cancer cells within a specific tumour seems to exhibit stem cell properties.<sup>19,20</sup> Thus, this can explain the ability of cancer cells to reproduce themselves generating the range of cancer cells that compose the tumour and also that promote the development of malignancy.<sup>19,20</sup> An important implication of this theory is that cancer stem cells can promote metastasis of a tumour type to different sites (ability to migrate), whereas in the event of resistance to a treatment, they can potentially cause a future relapse.<sup>21</sup>

One of the most extensively studied tissue with a well-defined structural hierarchical organization is mouse skin, hence it has been widely used for studying skin carcinogenesis. Skin carcinogenesis is characterised by multiple steps including hyperplasia, dysplasia and benign papilloma to squamous invasive carcinoma and spindle carcinoma.<sup>22</sup> In addition to this, the elevated levels of DNA alterations of the target cells have been linked with the progression of this process.<sup>23</sup> Although, it still remains unclear whether the target cancer stem cell pre-possess the capacity to reproduce indefinitely or the genetic modifications results in the immortalisation of more committed cells with limited life span.<sup>23</sup> It has been documented from different studies that tumours of different malignancies can arise from different target cells.<sup>24,25</sup> More specifically, it was suggested that malignant tumours are developed from cells residing in the bulge of the hair follicle and have a high self-renewal potency, while papilloma may

arise from stem cells of the interfollicular epidermis.<sup>24,25</sup> These findings suggest that cells with mutation on their RAS gene remained on the epidermis for an extended period of time without the formation of lesions, hence, those cells belong to a stem cell population.<sup>26</sup> Several reports have demonstrated the implication of cancer stem cells in the development and progression of malignant melanoma as well as their ability to exhibit resistance to current therapies.<sup>27</sup> Melanoma cells can form spheres of non-adherent cells that maintain their renewal properties over long periods, thus supporting the presence of cell with stem cells features within the melanoma population.<sup>28</sup> Furthermore, the development of melanoma tumours is mainly characterised by substantial changes in their genome including chromosomal translocations, deletions, amplifications or mutations which suggest the extensive heterogeneity in melanoma population.<sup>29</sup> Moreover, it has been shown by Kaplan R *et al.* that melanoma cells can secrete factors capable of directing the migration of hematopoietic progenitor cells to metastatic sites.<sup>29</sup> For example, nodal (which is secreted by melanoma cells) acts as a morphogen for progenitor cells and it can also contribute to the determination of sites for tumour metastasis.<sup>30</sup> Additionally, important stem cell markers such as CD133, CD166, nestin, NoTCh etc. seem to be upregulated in melanoma cancer.<sup>22,31,32</sup> On the contrary, others suggest that melanoma heterogeneity is mainly based on a clonal variation while the formation of tumours arise from different clones induced by other molecular mechanism.<sup>32</sup> As a result of this, the unsuccessful results of current treatments can be attributed to the potential participation and activation of different molecular mechanisms during the progression of the disease.<sup>32,33</sup>

## **1.2 Clinical diagnosis and therapy**

The clinical diagnosis of malignant melanoma is mostly unambiguous and in most cases accurate. However, in some instances, the non-pigment malignant melanocytic lesions are misinterpreted as NMSC.<sup>34</sup> On the other hand, prognosis of the diagnosed metastatic deposits remains extremely poor highlighting the need for a more effective eradication of the primary tumour deposits.<sup>35,36</sup>

The clinical examination of the neoplasm mainly relies on dermoscopy, computerised imaging, whole body digital scanning and confocal laser microscopy.<sup>37</sup> In addition to this, excisional biopsy is required for the histological evaluation, classification and staging according to the protocols of the American Joint Commission of Cancer (AJCC) TNM system.<sup>38,39</sup> Technological advances in molecular biology allowed the identification of genes and key pathogenic events responsible for melanoma tumorigenesis including UV-induced DNA damage, reactive oxygen species (ROS) (over)production, the secretion of growth factors derived from keratinocytes, as well as the suppression of T-cell mediated immune responses.<sup>40,41</sup> Early disease can be treated by surgical tumour removal, whereas, upon disease progression to metastatic stages, the available treatment options are poor.<sup>42</sup> Moreover, current therapeutic strategies are not promising.<sup>42</sup> Despite the fact that several therapeutic regimens based on the combination therapy entered clinical trials, none of them have been proven to improve survival rates. Therefore, the establishment of new therapeutic strategies or the improvement of the already existing ones, is pivotal.

### 1.2.1 Current therapeutic approaches

The development of malignant melanoma is strongly associated with the dysregulation of several proteins including, the mitogen-activated protein kinase (MAPK), the microphthalmia transcription factor (MITF), the epidermal growth factor (EGFR), the N-Ras sarcoma protein (NRAS) protooncogene as well as the B-rapidly accelerated fibrosarcoma (BRAF) oncogene.<sup>43-47</sup> Therefore, the recent molecular drugs aim to target the MAPK pathway which contributes by 90% in the development of the disease.<sup>45</sup> In fact, 50% of cases present activating mutations in BRAF. Vemurafenib (**Figure 2A**) and dabrafenib (**Figure 2B**) shown some exceptional inhibitory ability against BRAF activation whereas trametinib (**Figure 2C**), which is a MAPK kinase (MEK) inhibitor was found to be effective in blocking the downstream signalling activation of BRAF.<sup>48-50</sup> Others suggested that combination treatment with BRAF and MEK inhibitors has elicited considerable tumour regression.<sup>51,52</sup>

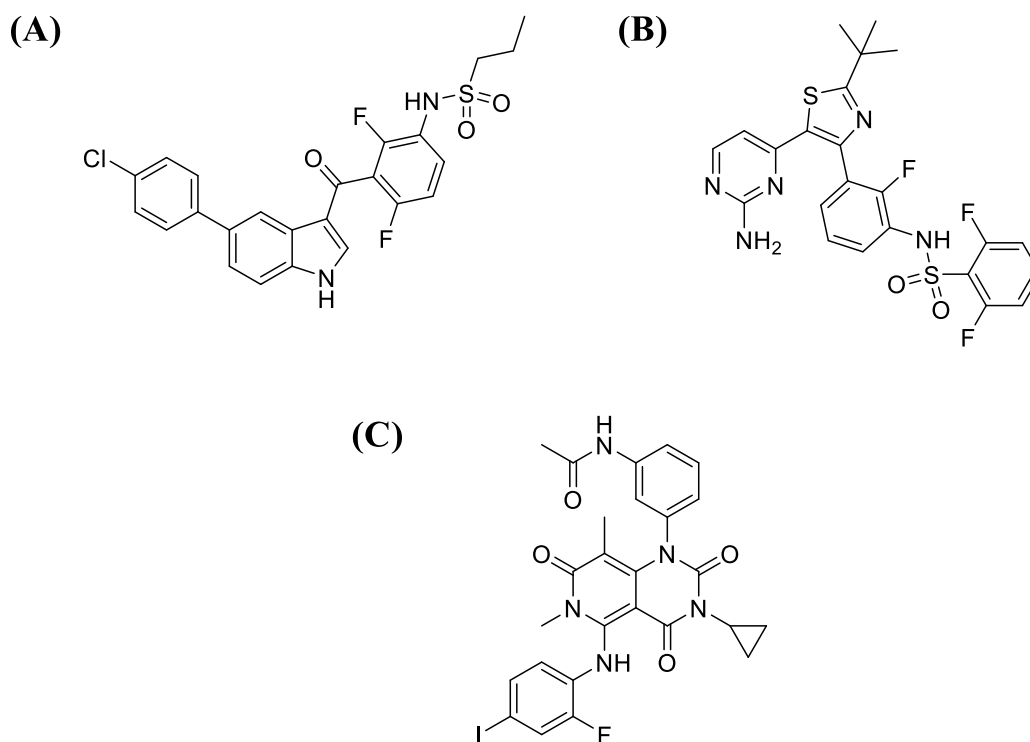


**Figure 2:** Structure of (A) vemurafenib, (B) dabrafenib and (C) trametinib

### 1.2.1.1 Immunotherapeutic approach

Nowadays, molecular immunotherapy is an attractive therapeutic approach that has shown promising results towards malignant melanoma treatment.<sup>53</sup> Initially, adaptive immunotherapy exploiting tumour infiltrating lymphocytes (TIL) or genetically engineered T-cells expressing chimeric antigen receptors (CAT-T 5 cells) has been correlated with 50-70% response rates.<sup>54,55</sup> Afterwards, administration of interleukin-2 (IL-2) or interferon-alpha (IFN- $\alpha$ ) as a single agent or adjuvant therapy was found to be an effective approach in sustaining disease's control.<sup>51,56,57</sup> It has been also demonstrated that patients diagnosed with advanced or even intermediate stage of the disease can undergo adjuvant systemic therapy including the administration of intermediate doses of IFN- $\alpha$  or adjuvant radiotherapy post-surgical clearance.<sup>58,59</sup> Most recently, it has been reported that treatment with immune check-point regulators has been adopted as a way to oppose the induction of immunological tolerance

during melanoma development and formation.<sup>60,61</sup> T-Lymphocyte associated protein 4 (CTLA4) inhibitors including ipilimumab or tremelimumab were found to be effective as monotherapy or in combination with the cytotoxic drug dacarbazine (**Figure 3**).<sup>60,61</sup>

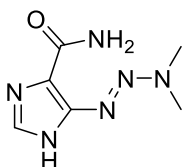


**Figure 3:** Structure of dacarbazine

Moreover, nivolumab and lambrolizumab (monoclonal antibodies) can target the pro-death receptor-1 ligand 1 (PD-L1) which is frequently expressed in melanoma cells suggesting an alternative therapeutic approach, towards the treatment of melanoma.<sup>62</sup>

#### 1.2.1.2 Chemotherapeutic agents and radiotherapy

Single agent chemotherapy involving treatment with dacarbazine (**Figure 3**), temozolamide (**Figure 4A**) and fotemustine (**Figure 4B**) is frequently used for the treatment of melanoma mainly due to their low toxicity and simplicity of administration.<sup>63</sup>

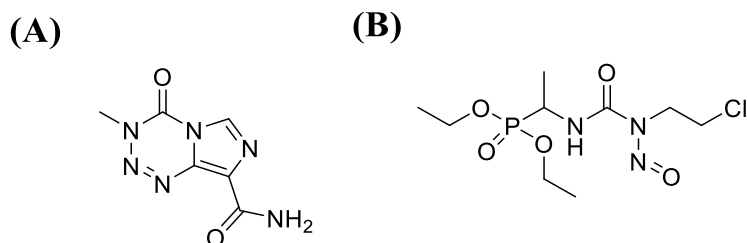


**Figure 4:** Structure of (A) temozolamide and (B) fotemustine

However, such a treatment approach is mainly associated with low responses rates (~10%).<sup>63</sup> Bio-chemotherapy, a combination of all the above mentioned regimens with administration of cytokines, is considered as a promising strategy with potentially better response rates.<sup>64</sup> Last but not least, radiation therapy in combination with the chemotherapeutic agents is widely

employed for the treatment of distant metastases including those in the lungs, lymph nodes, spleen liver, biliary, bones and gastrointestinal tract.<sup>65</sup>

### **1.3 The involvement of metals in cancer development and metastasis**

Several reports noted the importance of metals in human biology. It is well known that the human body uses essential metals; iron, zinc, copper manganese, molybdenum, selenium magnesium, calcium, potassium and sodium for the maintenance and the proper function of the organism.<sup>66</sup> Tracer amounts of those metals (apart from iron, copper and zinc) play a pivotal role in cellular organisations with most of them being integral for the function of enzymes required for the catalysis of biochemical reactions.<sup>66,67</sup> For example, ribonucleotide reductase, an enzyme that participates in the rate limiting step of the synthesis of DNA, contains iron atom as a cofactor, whereas zinc is contained in enzymes that are responsible for gene expression e.g. zinc transcription factor. In addition to this, copper is a cofactor in at least 13 enzymes, which most these have application in the rigidity, mechanical strength and competence of the bones, ATP synthesis, as well as the synthesis of myelin in brain.<sup>68-70</sup> On the contrary, depletion of those metals can be fatal or can associated with the development of several diseases, such as anaemia due to iron deficiency or ischaemic heart disease induced by copper deficiency.<sup>66</sup> Conversely, an excess of these metals can also lead to toxic effects that are linked with inflammation.<sup>66</sup> It has been also demonstrated in the past, that many metals contribute to development, progression and metastasis of several types of cancer by interfering on key biological process that mediate the cell motility, invasion and dissemination.<sup>66</sup>

#### **1.3.1 The role of copper in cancer**

It has been shown, that elevated levels of copper have the ability to induce malignancies by promoting the tumour growth, the angiogenesis and metastasis of cancer.<sup>71,72</sup> The role of copper in facilitating angiogenesis has been demonstrated to be crucial for the activity of lysyl oxidase (LOX) and lysyl oxidase-like (LOXL); enzymes that are necessary for the cross

linking of collagen and elastin fibres.<sup>73,74</sup> In addition to this, these two enzymes are participating in cell angiogenesis, proliferation and differentiation and upon dysregulation of their expression levels they can contribute to the development of metastasis.<sup>67</sup> The secretion of LOX allows the tumorigenic cell to induce alteration of the extracellular matrix to proffer a pre-metastatic phase.<sup>67</sup> Furthermore, LOXL2 can interact with E-cadherin gene suppressor; SNAIL causing in that way the downregulation of E-cadherin thus facilitating in that way the promotion of epithelial to mesenchymal transition.<sup>75</sup> Another cell motility protein that plays an important role in the development of breast cancer cell is the MEMO protein which required a Cu(II) for its oxidase activity.<sup>76</sup> It has been shown previously, that MEMO facilitates the migrator capacity of breast cancer cells.<sup>76</sup> Additionally, it is essential element for the invasion and metastasis of these cells. Furthermore, it has also been reported that MEMO protein can also induce elevation of ROS as the Cu(II) ion is redox active and it can therefore participate in Fenton Chemistry (2.1).<sup>66,68,72,76</sup>

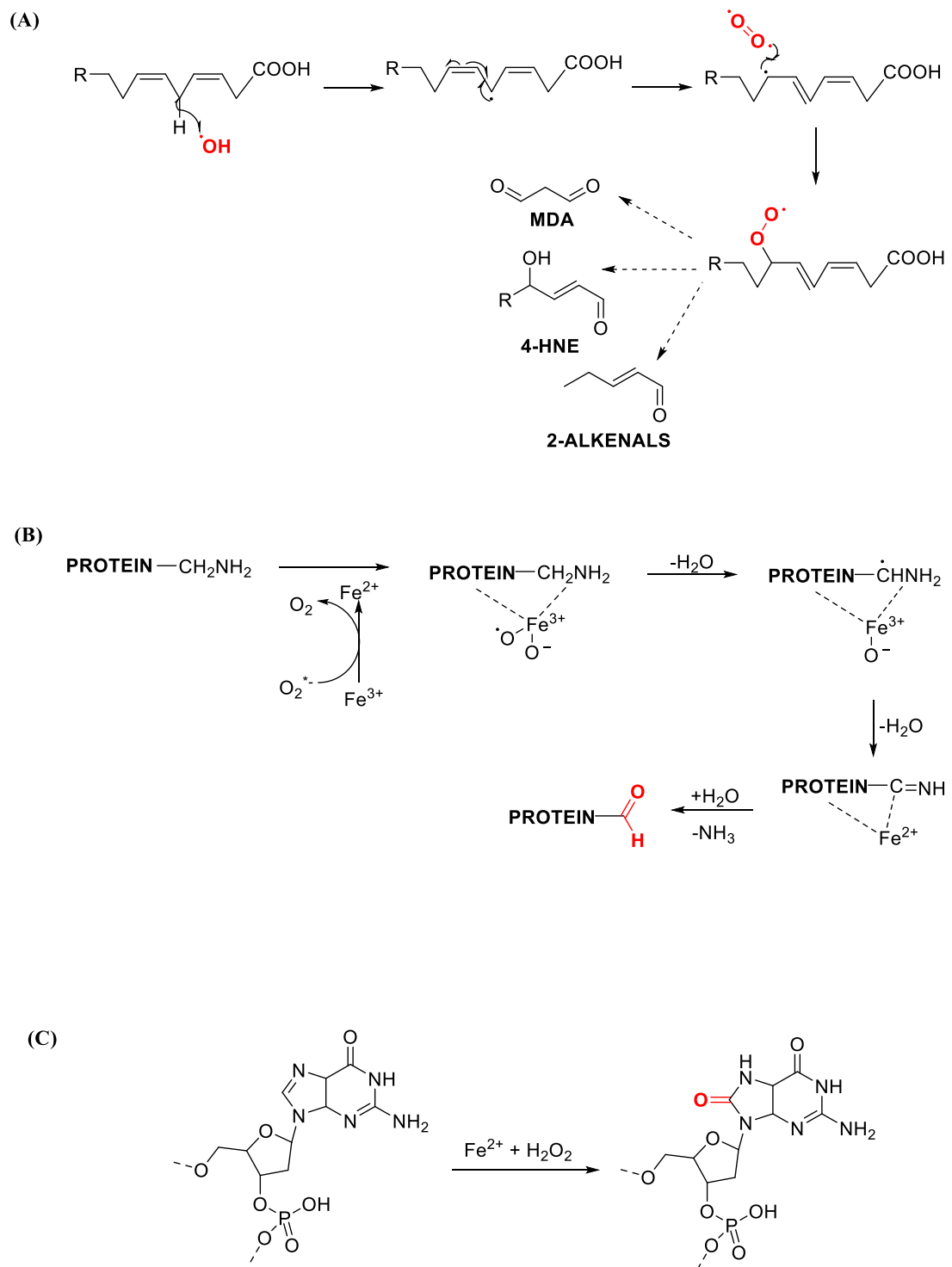
### **1.3.2 The role of zinc in cancer**

Matrix Metaloproteases (MMPs) play a crucial role in the invasion and metastasis of cancer as they can degrade the surrounding cellular tissue enabling the access of cancerous cells.<sup>77</sup> The catalytic action of most these particular superfamily of enzymes is mediated by zinc, which is located in their active centre.<sup>77</sup> Not surprisingly, evidence shown that elevation of zinc labile pool in cancer led to significant activation of MMP whereas their action was abolished upon chelation of zinc.<sup>78</sup> Interestingly, the expression levels of MPPs; MMP-1 and MMP-3 is mediated by the transcription factor zinc-binding protein-89 (ZBP-89).<sup>67,79</sup> Furthermore, the expression levels of ZBP-89 were significantly higher in cell renal carcinoma and it was demonstrated that its overall expression is significantly higher in metastasized cells compared to the non-metastasized ones.<sup>80-82</sup> Hence, through the involvement of zinc in key enzymes and molecules that regulate the cell motility and invasion it can be concluded that regulation of zinc can be a major contributor in cancer development and metastasis.<sup>66</sup>

### 1.3.2.1 The role of iron in cancer

Due to the poor bioavailability of iron, the contribution of different proteins involved in iron import storage and export has to be perfectly mediated as there is currently unknown way of excreting iron in humans.<sup>83</sup> Malignant cancer is mainly associated with dysregulated iron haemostasis.<sup>84</sup> It has been also demonstrated that cancer cells are not using the surplus of iron just for the transformation and proliferation but also during the late stages to promote metastasis and angiogenesis.<sup>85,86</sup> Moreover, the ability of iron to remodel the extracellular matrix was also correlated with cancer invasion.<sup>87</sup> The essential role of iron in cancer development has been assessed in animal models in the past.<sup>83</sup> The outcome of these studies was that mice fed with low iron diet prior to tumour implantation showed significantly delayed tumour growth.<sup>88</sup> The necessity of tumour cells to acquire iron leads to a depletion of the iron levels in liver and spleen (post implantation).<sup>88</sup> As a result, it was suggested that red blood cell recycling and iron storage in the liver and spleen are compromised, hence the erythropoiesis was significantly reduced, inducing anaemia.<sup>88,89</sup> Not surprisingly patients diagnosed with cancer tend to develop anaemia due to the dysregulation of iron metabolism.<sup>83</sup> The expression of a variety of iron regulated genes including the transferrin receptor1 (TfR1), ferritin light chain (FTL) and the iron regulatory protein (IRP-2) in cancerous cells was strongly associated with a series of events such as poor prognosis, higher tumour grade and increased chemoresistance.<sup>90-93</sup> However, the most important aspect of iron that makes it an essential component for the development of cancer is its ability to participate in the catalysis of ROS production via its redox potency – Fenton Chemistry (2.1.1).<sup>90-93</sup> In addition to this, it has been previously suggested that the contribution of ROS in cancer depends on its levels.<sup>84,94</sup> High ROS levels can be cytotoxic and that results in apoptosis, whereas low levels of ROS can activate oncogenes and consequently carcinogenesis.<sup>94-98</sup> Moreover, low levels of ROS have been shown to increase the expression levels of proteins that are associated with the angiogenesis and metastasis including; SNAIL, AP-1, VEGF as well as the activation of the NF- $\kappa$ B pathway.<sup>95,98-101</sup> Overall it has been demonstrated that some malignancies including malignant melanoma express significantly elevated amount of ROS in order to proliferate and

metastasize.<sup>102-104</sup> Excessive ROS accumulation has been associated with cancer development, as oxidative stress can induce lipid peroxidation (**Figure 5A**), protein carbonylation (**Figure 5B**) as well as DNA oxidative damage (**Figure 5C**).<sup>83</sup> This effect can lead to genetic instability and tumorigenesis.<sup>105</sup>

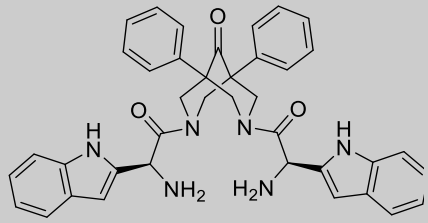
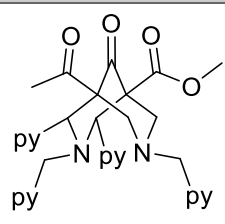
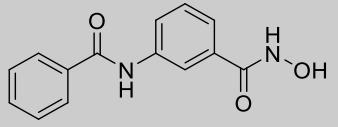


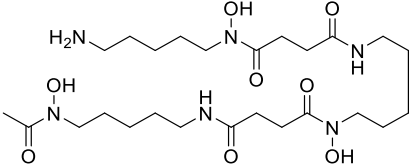
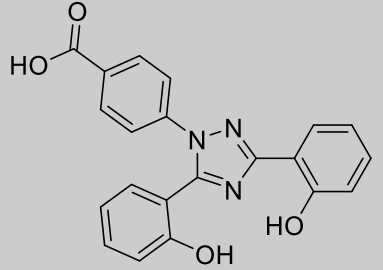
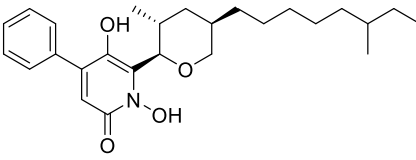
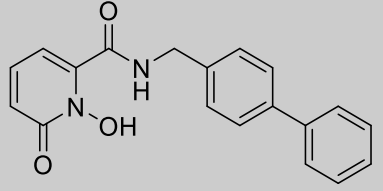
**Figure 5:** ROS driven (A) lipid peroxidation (B) protein carbonylation and (C) oxidation of DNA-bases (herein the formation of 8-oxo2-deoxyguanine is shown).

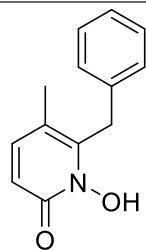
#### 1.4 Metal chelation based treatment

Due to the involvement of metals in cancer development and progression it is not surprising that metal chelators are being considered as potential therapeutic targets agents that would aim the restore of metal homeostasis by preventing the metal induced cell growth and proliferation.<sup>106</sup> As it was mentioned above, low levels of ROS are essential for cell proliferation whereas the high levels of ROS can be cytotoxic. Therefore, metal chelators should act either as anti-oxidants and promote the redox silencing of Fe(III) or Cu(II) or act as pro-oxidants (depending at the concentration).<sup>107</sup> Pro-oxidant metal chelators can induce toxic levels of ROS activating downstream apoptotic cascades.<sup>108,109</sup> To this end, according to the literature, a variety of metal chelators have been designed as potential anticancer therapeutic agents (**Table 1**).

**Table 1:** Selected classes of metal chelators that were used against various type of cancer.

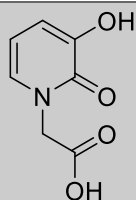
Class of chelator	Structure	Metal target	Activity against cancer
Bispidones		-	Human Pancreatic cancer; MiaPaCa-2 CFPAC1, BxPC3 <sup>110</sup>
		Cu(II)	Prostate cancer; PC3 <sup>111</sup>
Hydroxamic acids	 and derivatives	Zn(II)	Human Kidney epithelial; HEK293 <sup>112</sup> Neuroblastoma; BE(2)C <sup>113</sup>

	 <p>Desferoxamine (DFO)</p>	<p>Fe(III)</p> <p>Various cancer types<sup>114-117</sup></p>
<p><b>Deferasirox</b></p>		<p>Fe(III)</p> <p>Oesophageal adenocarcinoma; OE16, OE33 oesophageal; squamous carcinoma; OE21, TE4<sup>118</sup></p>
<p><b>Hydroxypyridinones (HOPOs)</b></p>		<p>Fe(III),</p> <p>Human colon carcinoma; HCT-116<sup>119</sup> B16 malignant melanoma<sup>119</sup> Lymphoid neoplasm; P388D1<sup>119</sup></p>
<p><b>1-hydroxypyridin- 2(H)-ones (1, 2-HOPOs)</b></p>		<p>Zn(II)</p> <p>MPPs inhibitor<sup>120,121</sup></p>



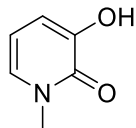
and derivatives

Glioma stem cells; BT-142<sup>122,123</sup>



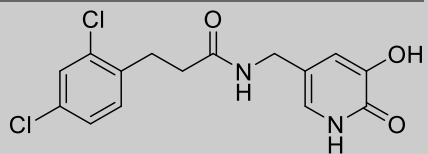
CDK-2 inhibitor<sup>124</sup>

**3-hydroxypyridin-  
2(*H*)-ones  
(3, 2-HOPOs)**



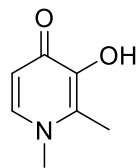
Zn(II),  
Fe(III),  
Cu(II)

MMPs inhibitor<sup>125</sup>  
Fibrosarcoma; HT-1080<sup>124</sup>



and derivatives

Human malignant melanoma; A375<sup>126</sup>

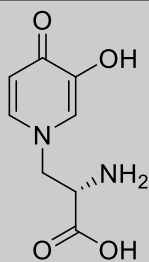


Various types of cancer<sup>127-135</sup>

**3-hydroxypyridin-  
4(*H*)-ones  
(3, 4- HOPOs)**

Deferiprone (DFP) and  
derivatives

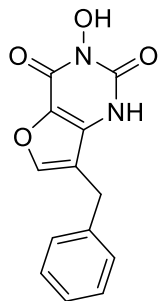
Zn(II),  
Fe(III),  
Cu(II),  
Al(III)



L-Mimosine

Various types of cancer<sup>136-140</sup>

**Hydroxypyrimidinones (HOPYs)**

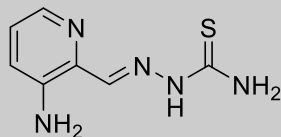


and derivatives

Fe(III),  
Zn(II)

Xeroderma pigmentosum G.<sup>141,142</sup>  
Bladder carcinoma; T4<sup>141,142</sup>  
DNA-repair complex; ERCG1-XPF<sup>141,142</sup>

**Thiosemicarbazole**

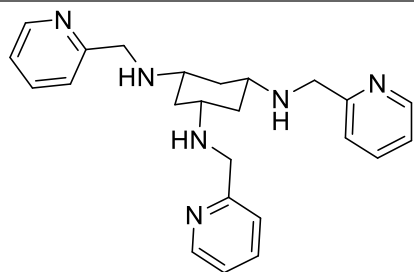


Fe(III)

Lung carcinoma; M109<sup>143</sup>  
Ovarian carcinoma; A278<sup>143</sup>  
Human Nasopharyngeal carcinoma; KB<sup>143</sup>  
Leukemia; L1210<sup>143</sup>  
Ribonucleotide reductase inhibitor<sup>144</sup>

---

**Tachpyridines**

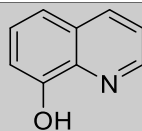


and derivatives

Fe(III),  
Zn(II) ,  
Cu(II)

Various cancer types<sup>145-153</sup>

**Quinolines**



8-hydroxy quinolones  
and derivatives

Fe(III),  
Zn(II) ,  
Cu(II)

Various cancer types<sup>154-161</sup>

### 1.4.1 Toxicity of metal chelators and prodrugs

The development of metal chelators can be associated with the appearance of side effects mainly due to the lack of either cellular or metal selectivity. For example, regardless the exceptional ability of deferiprone (DFP) to bind Fe(III) over Cu(II) and Zn(II) it was found that it inhibits non selectively lipoxygenases and tyrosine hydroxylase.<sup>162,163</sup> Additionally, administration of DFP also induces agranulocytosis.<sup>164</sup> A naturally occurring metal chelator; *L*-mimosine obtained from the plant *Mimosa* and *Leucaena genara* endowed with the range of biological functions including anti-cancer, anti-inflammatory, anti-viral and anti-fibrotic capacity.<sup>106</sup> It was also demonstrated that *L*-mimosine exerted anticancer activity against various melanoma cell lines (with EC<sub>50</sub>= 100 μM) by inducing cell cycle growth arrest and activating apoptotic cascades, however the side effects associated with its strong cytotoxicity, discouraged its further development.<sup>136–139</sup> In another example, thiocarbazon triapine and DFO also show some anticancer activity in clinical trials.<sup>83,117,165</sup> However, due to the serious side effects such as hearing abnormalities, optic neuropathy and growth failure in children, their further administration has been hampered.<sup>83</sup> In an attempt to limit the side effects associated with the administration of metal chelators the research was focused in the design of prodrugs that can undergo *in situ* action/activation.<sup>166</sup> For example, exploiting the disulphide bonds for the activation of the iron pro-chelators, show encouraging results *in vitro* mainly because iron coordination achieved via the intracellular reduction of disulphide forming high affinity tridentate thiolate chelators (**Figure 6**).<sup>167</sup>

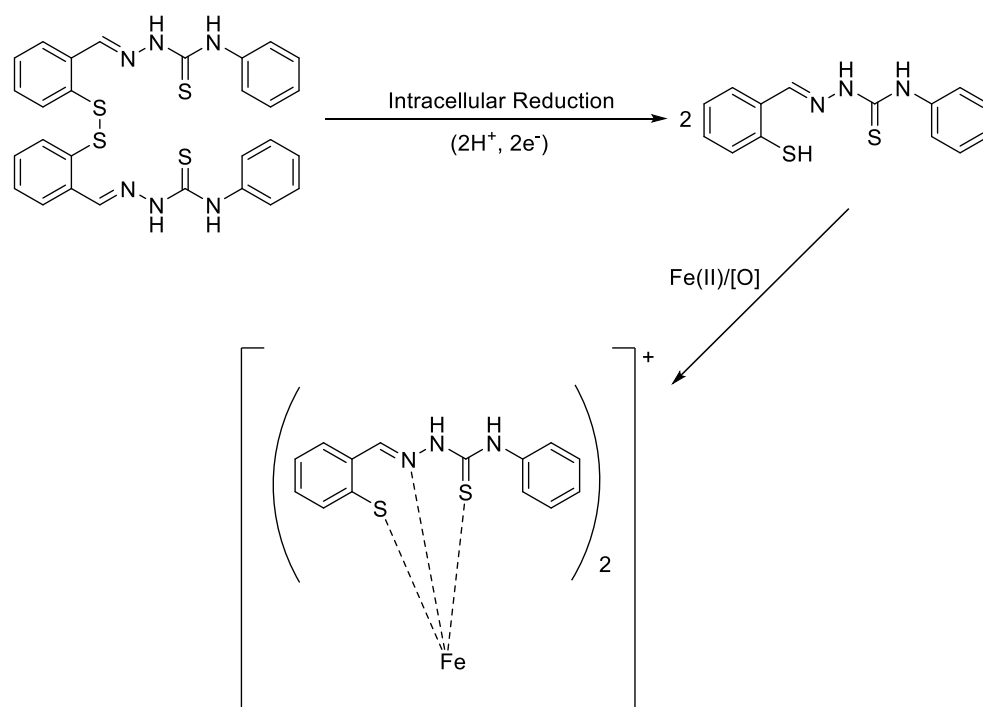


**Figure 6:** Intracellular reduction of disulphide bond leads to activation of anti-proliferative thiosemicarbazone chelator.<sup>167</sup>

Furthermore, cancer cells exhibit a higher reducing environment compared to the surrounding tissues, making the reductive activation an alternative strategy to enhance cancer cell specificity, owing to significantly higher amounts of reduced glutathione compared to the healthy cells.<sup>167,168</sup>

Additionally, Akam A. *et al.* used a glucose-conjugated thiosemicarbazole pro-chelator against colon carcinoma, proving that enhanced pro-chelator was accumulated and acted preferentially in cancer cells (**Figure 7**).<sup>169</sup>

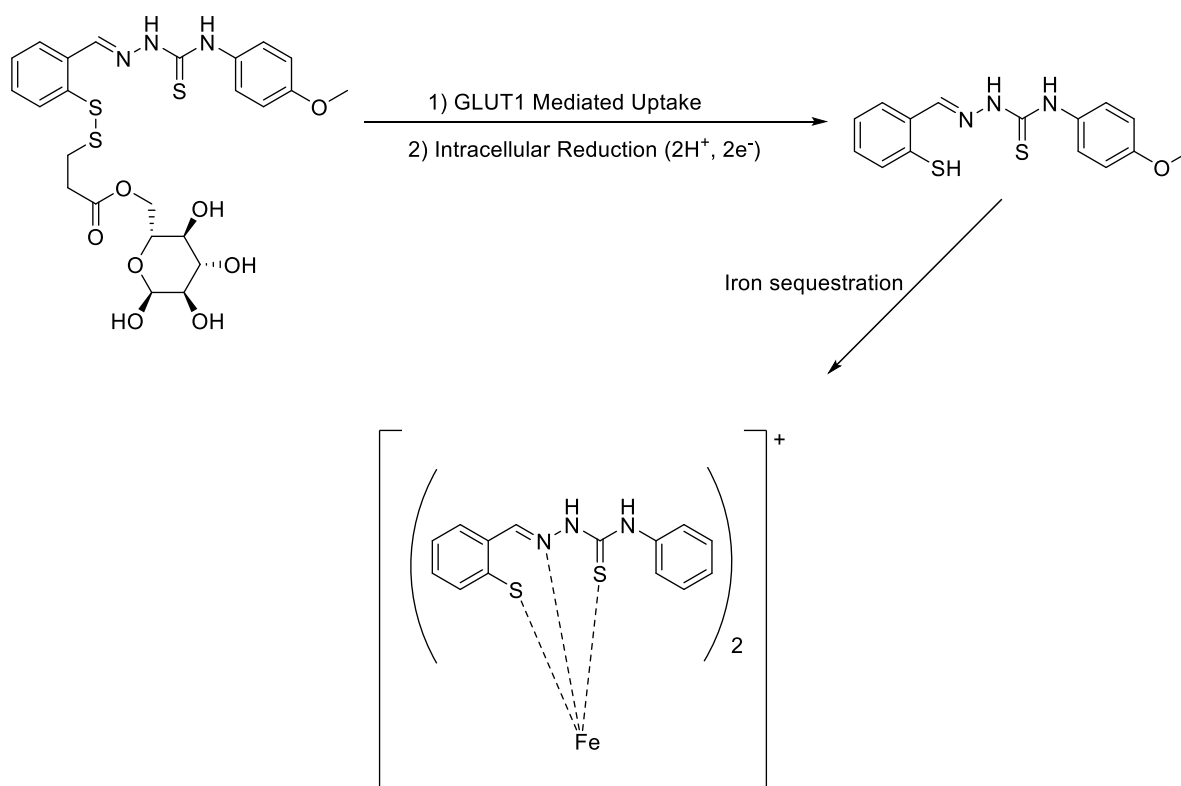


**Figure 7:** Redox directed glucoconjugate pro-chelator based strategy for iron coordination.<sup>169</sup>

This approach was based on the fact that malignant cancer cells tend to overexpress the GLUT1 transporter (more details can be found in **1.12.1.3.1** and **1.12.1.3.1.1**).<sup>170</sup> Glucose conjugates of several chemotherapeutic drugs including paclitaxel and doxorubicin experience significantly improved therapeutic efficacy *in vivo*.<sup>171–173</sup> Therefore, these strategies aim in the selective iron pool targeting of carcinogenic cells.

## **1.5 Neurodegenerative diseases**

Neurological disorders are a class of disorders - pathological conditions – that affect the nervous system. It has been previously documented that neurodegenerative disorders, constitute a major burden on modern society as they affect one in four people worldwide.<sup>174</sup> Particularly, in Europe, neurological disorders cause around 35% of years lost due to ill-health, disability or early death.<sup>175</sup> The primary risk factor for such disorder is mainly the age.<sup>176</sup> This will exacerbate the healthcare burden of the pathology of this disease as the average age of the global population is expected to rise rapidly, especially in countries with a rising life expectancy (i.e. industrialised developed or newly industrialised countries).<sup>176–178</sup> The common characteristic aspect of all the neurodegenerative diseases in the loss of neuronal structural composition and hence the loss of their function, with Alzheimer’s disease (AD), Parkinson’s disease (PD) and Huntington’s disease being the lead examples of such diseases.<sup>179</sup> The underlying cause is poorly understood in the majority of neurodegenerative diseases and the progression of the diseases in often unclear. The diagnosis relies on empirical clinical criteria but a definitive diagnosis requires post-mortem autopsy.<sup>180</sup> Interestingly, certain hallmarks and patterns have been identified in the most important neurodegenerative diseases including AD, PD, amyotrophic lateral sclerosis, prion diseases and Huntington’s disease.<sup>176</sup> All the mentioned disorders are characterised by the progressive loss of specific localised cell populations and the abnormal accumulation and aggregation of certain proteins.<sup>176,181–183</sup>

## **1.6 Parkinson’s disease**

### **1.6.1 Epidemiology**

Parkinson’s disease was first characterised by James Parkinson at the beginning of the 19<sup>th</sup> century and overall is the second most common neurodegenerative disease worldwide after AD.<sup>184,185</sup> The incidence rate of PD is estimated to be 8-18 cases per 100,000 persons per annum, but it varies across different geographical locations, and it is higher in populations with a higher average age.<sup>186</sup>

The prevalence of PD in the UK was estimated to exceed 150,000 cases or 5.1% of the overall population according to the last statistical analysis that was performed in 2018.<sup>187</sup> The prevalence was estimated based on medical records and it therefore likely that a significant undiagnosed cases exist in addition to these recorded cases.<sup>187</sup> According to the statistical analysis, the biggest risk for PD development is age, which is illustrated by the fact that over 90% of PD sufferers are aged 60 or older.<sup>187</sup> In addition to this, studies suggested that the disease more often appeared in men whereas others found no differences between sexes.<sup>177–179,186</sup> Most Western societies have a rapid ageing population, which lead to an increasing development of the diseases in future, whereas in the UK, studied pointed out that we should expect an approximately 50% increase of PD diagnosed cases by 2020.<sup>187</sup> Similarly, the number of diagnosed cases for 15 of the world's most populous nations is expected to double by 2030, driven by a pronounced increase of cases in the rapidly industrialised and developing countries including China, India, Indonesia, Brazil, Pakistan, Bangladesh, Russia, Nigeria, etc.).<sup>186,188</sup>

### **1.6.2 Pathology and symptoms**

PD as neurodegenerative disease is mainly characterised by the loss of the neuron in nigrostriatal pathway and the presence of intracellular proteins inclusions, known as Lewy bodies (**Figure 8**).<sup>182,189,190</sup>

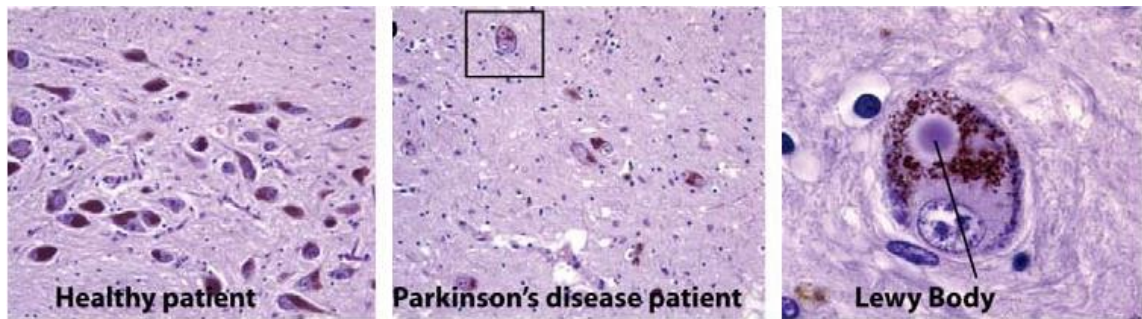


**Figure 8:** Formation of Lewy bodies is one of the common parameters that contributes to the development of PD.<sup>189</sup>

The loss of neuronal cells affects the dopaminergic neurons projecting into the *substantia nigra* of the midbrain striatum (**Figure 9**).<sup>182,189–192</sup>

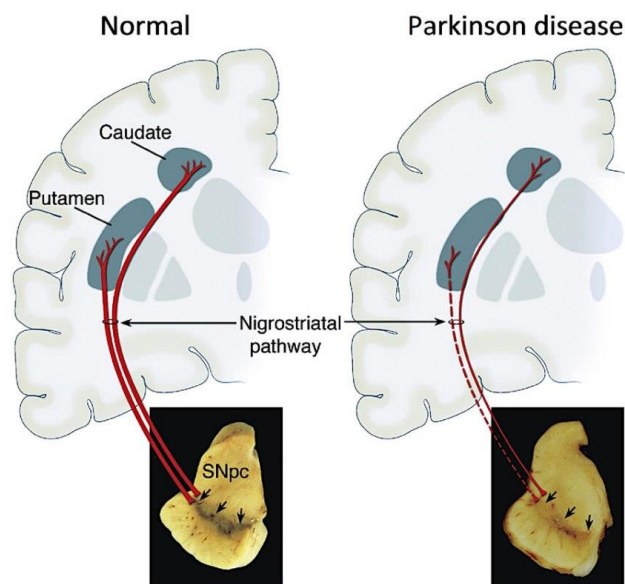


**Figure 9:** PD arises from the degradation of dopaminergic neuronal cells; *Substantia nigra* (SNpc) locates in the Putamen and Caudate of the midbrain.<sup>192</sup>

Additionally, the neurons projecting into the putamen are lost preferentially over the caudate.<sup>192</sup> At the time of death, it has been demonstrated that up to 70-80% of neurons in that area are lost.<sup>182,191,192</sup> The neuronal loss leads to a significant depletion of the levels of dopamine in the striatum, causing perturbation of the signal transduction to the areas responsible for motor

control.<sup>192–195</sup> In addition to this, depletion of dopamine is also correlated with the most common PD symptoms including; resting tremors, stiffness and bradykinesia.<sup>191,194,196,197</sup> Non-motor symptoms can also exist, however their cause is not clear yet. Interestingly it has been previously reported that a large population of dopaminergic neurons is lost prior to the appearance of the symptoms. The exact cause of neuronal degradation is still unknown, however the protein aggregation (Lewy bodies) and oxidative stress (both developed in PD brains) are known to be cytotoxic, hence they might contribute significantly to the development of the disease.<sup>198–200</sup> Moreover,  $\alpha$ -synuclein, is the most dominant species of aggregated proteins found in PD brains and unfortunately the exact role in both health and disease remains unclear.<sup>201</sup> It is thought that under healthy conditions it is neuroprotective for non-dopaminergic neurons, however, aggregates of the insoluble  $\alpha$ -synuclein exhibit toxicity in the presence of dopamine.<sup>201</sup> It has been shown previously in the literature that multiple mutations on the synuclein genes have been shown to be associated with the development of PD or to constitute a risk factor for sporadic PD.<sup>191,202</sup>

### **1.6.3 Genetic origin of PD**

Other pathological risk factors that are related to the development of the disease include gene polymorphism, however just a small amount of cases can be attributed to genetic factors.<sup>202</sup> So far, ten different *loci* are known; PARK1 to PARK10, however the exact mutations remained unknown.<sup>203</sup> The most well studied mutations concern the genes PARK1, -2 and -8.<sup>204,205</sup> For example, genetic mutation on PARK1 leads to a formation of an autosomal dominant PD family which is mainly characterised by an early onset with aggressive progress.<sup>206</sup> Furthermore, the PARK1 gene (as well as SNCA) encodes  $\alpha$ -synuclein.<sup>207,208</sup>  $\alpha$ -Synuclein plays a fundamental role into the supplement of synaptic vesicles in presynaptic terminals.<sup>209</sup> Additionally, it was found that  $\alpha$ -synuclein is responsible for the controlled release of dopamine.<sup>210</sup> Therefore, mutation on the respective genes leads (mainly) to a significant reduction of the dopamine's storage.<sup>207</sup> Another

mutation concerns PARK2, which is responsible for the expression of parkin protein – a component of the ubiquitin-proteasome system.<sup>211–213</sup> PARK2, participates into the regulation of monoamine oxidase (MAO) which is responsible for the regulation of dopamine's oxidation.<sup>212</sup> Mutation in this gene is known to cause a familiar form of PD known as autosomal recessive juvenile PD.<sup>204</sup> Finally, another mutation which is widely studied concerns PARK8 which encodes leucine-rich repeat kinase- 2 (LRRK2).<sup>214</sup> LRRK2 is associated with a variety of cellular functions including signal transductions, and apoptotic processes.<sup>214</sup> The relationship between the LRRK2 and neurodegeneration of dopamine endings in striatum has been previously studied and it was concluded that mutation in LRRK2 has been identified as risk factor for the development of PD.<sup>215–217</sup> On the contrary, selective inhibition of the mutated form of LRRK2 shown some neuroprotective effect and thus it could be used as an alternative therapeutic strategy against the disease.<sup>214,218,219</sup>

Another important class of genes those mutations can cause PD is the Pantothenic-Induced putative kinase-1 (PINK-1).<sup>220</sup> The expression of these genes lead to the formation of a mitochondrial serine/threonine kinase-1 which is involved in the mitochondrial response against cellular and oxidative stress, protecting in that way neurons from mitochondrial dysfunction and proteosomal induction of apoptosis.<sup>221–223</sup> In the unfortunate event of PARK-1 mutation, the defective protein is not able to act properly against the oxidative damage facilitating in that way the neuronal degradation and eventually PD development.<sup>224,225</sup> Nevertheless, more than 90% of the PD diagnosed cases are idiopathic.<sup>226,227</sup> Not surprisingly, environmental factors, such as smoking, diet, exposure to toxins, heavy metals or herbicides, have been marked as risk factors for PD, however their effect remains contested.<sup>177,182</sup>

#### **1.6.4 The contribution of metal-induced oxidative stress into PD development**

The elevated levels of redox active metals including Fe(III) and Cu(II) in the *substantia nigra* of the PD diagnosed patients is often correlated with the protein aggregation, while iron and copper levels in other part of the brain were not elevated.<sup>228–232</sup> As it has been mentioned in the previous chapter (1.3 and 1.4) above, Fe(III) and Cu(II) are participating in Fenton reaction to produce free radicals from hydrogen peroxide which is mainly produced in mitochondria as a by-product of natural metabolism mainly during the metabolic production of DOPAL by the action of monoamine oxidase-B (MAO-B).<sup>233,234</sup> The toxicity mediated by those metals in cells appears at least partly linked to the development of oxidative stress in mitochondrial DNA which leads to progressive mitochondrial dysfunction.<sup>235</sup>  $\alpha$ -Synuclein misfolding and aggregation has also been shown to be enhanced by the metal-induced oxidative damage.<sup>236,237</sup> It has been suggested that the dysregulated iron localization in PD exacerbates the stress on dopaminergic neurons caused by protein aggregates and oxidative stress on multiple levels.<sup>191,198,233,235–237</sup> Therefore, this effect can lead into the selective and preferential death of dopaminergic cells, hence, the contribution of iron in these process links to PD development and progression. The removal of iron and/or copper from PD brains is therefore a novel approach for the treatment of disease.

#### **1.7 Toxin-induced PD for *in vitro* and *in vivo* studies**

Prior to the screening of drugs against PD in either an *in vitro* or *in vivo* model it is essential to introduce a parkinsonian phenotype. This is because there is not currently an isolated cell line that is genetically modified to correspond to PD. PD pathogenesis can be studied using some experimental model been produced after exposure with some neurotoxins that tend to produce similar phenotypes to those of the disease.<sup>238,239</sup> Although a variety of natural and synthetic molecules can exert neurodegradation effect on dopaminergic neurons, only a handful are used in animal models to reproduce some of the hallmarks of PD.<sup>239</sup>

### 1.7.1 6-hydroxydopamine (6-OHDA)

One of the catecholaminergic neurotoxins that is widely used for both *in vitro* and *in vivo* study of PD is a noradrenergic analogue called 6-hydroxydopamine (6-OHDA) (**Figure 10A**).<sup>240</sup>

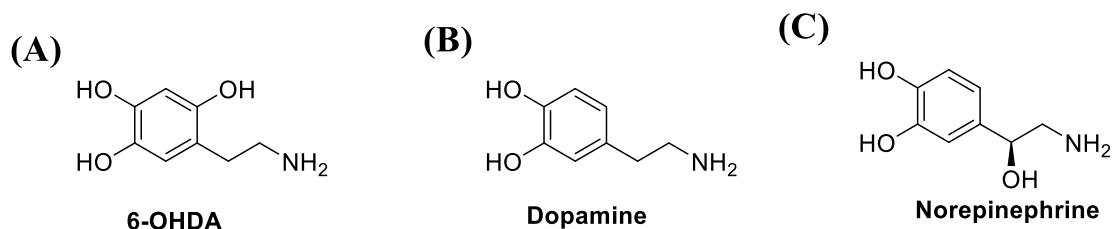


**Figure 10:** Structural similarities between the neurotoxin; (A) 6-OHDA and the neurotransmitters; (B) dopamine and (C) Norepinephrine.

As it can be observed from (**Figure 10**), 6-OHDA possess structural similarities with both dopamine (**Figure 10B**) and norepinephrine (**Figure 10C**) exhibiting in that way high affinity for a variety of catecholaminergic plasma membrane transported including dopamine (DAT) and norepinephrine transporters (NET).<sup>241,242</sup> Therefore, 6-OHDA can enter both dopaminergic and noradrenergic neurons inducing damage to the catecholaminergic pathways. The mode of action of this neurotoxin it is mainly associated with the induction of ROS.<sup>239</sup> Additionally, its auto-oxidation can lead to the formation of hydrogen peroxide and para-quinone which is known as a powerful electrophile which can react further with either side chains of proteins or DNA bases (**Figure 11**).<sup>239</sup>

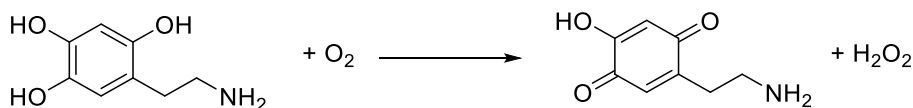


**Figure 11:** Oxidation of 6-OHDA into hydrogen peroxide and quinone.

Injection of 6-OHDA in mice and dogs directly in the SNpc or the striatum (as it can poorly cross the BBB) shown a maximal reduction of striatal dopamine as well as gradual degradation of the dopaminergic neuronal cells.<sup>239</sup> Another function of 6-OHDA is its ability to inhibit both complex I and IV of the mitochondrial respiratory chain preventing in that way the redox cycle of the coenzyme NADH and the binding of cytochrome C.<sup>243,244</sup> Additionally, the inhibition of these complexes can also lead to perturbation in the gradient across the membranes since the proton transportation is prevented.<sup>243,244</sup>

### 1.7.2 MPTP/ MPP<sup>+</sup>

Despite the variety of neurotoxins that can be used for the understanding of neuronal related pathologies that occur in basal ganglia and/or in the SNpc, a single toxin seems to target specifically and selectively those neurons that are involved in the development of PD.<sup>245</sup> This toxin is 1-methyl-4-phenyl-1,2,3,6-tetrahydropyridine (MPTP) (**Figure 12A**).

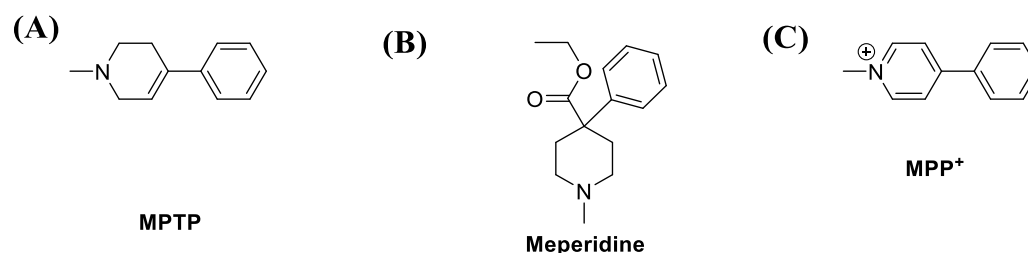


**Figure 12:** Structures of (A) MPTP, (B) Meperidine and (C) MPP<sup>+</sup>

MPTP is a narcotic synthetic compound that is related to meperidine (**Figure 12B**).<sup>245</sup> This toxin, is relatively water insoluble and therefore it can cross the BBB and easily reach easily the brain cells.<sup>246</sup> Furthermore, MPTP can be captured by organelles with an acidic environment including lysosomes and astrocytes.<sup>247</sup> Interestingly, MPTP is not toxic itself, however its oxidized form; 1-methyl-4-phenylpyridinium (MPP<sup>+</sup>) is toxic (**Figure 12C**).<sup>245,246</sup> The oxidation of MPTP into MPP<sup>+</sup> is regulated by MAO-B, which is located in astrocytes and serotonergic neurons.<sup>246</sup> Once

the toxic oxidized product reaches the extracellular fluid, via the DAT, it is taken to the dopaminergic neuronal terminals.<sup>246</sup> The mode of action of the MPP<sup>+</sup> is mainly to inhibit complex I of the mitochondrial respiration chain causing cyto(neuro) toxic effects. Initially, inhibition of complex I can cause perturbations in the production of ATP as the blockage prevents ion transportation.<sup>247–250</sup> Additionally, such inhibition leads to disruption of calcium hemostasis, as the concentration of the extracellular calcium is elevated, promoting in that way the activation of the calcium-dependent enzymes; protein kinase-1, calpain I and II.<sup>251–253</sup> The activation of these proteins is associated with the disruption of cell function and cell death.<sup>251,252</sup> Eventually, and most importantly, MPP<sup>+</sup> stimulates the generation of ROS via the faulty maintenance of NADH dehydrogenases. On the other hand, experiments on monkeys treated with MPP<sup>+</sup> show the elevation of the Fe(II) which is incorporated into Fenton chemistry. ROS and Fe(II) have been strongly implicated to the development of PD.<sup>254–256</sup>

### 1.7.3 Erastin

There are multiple cell death mechanisms that are associated with the development of PD, with ferroptosis being one those.<sup>257</sup> Ferroptosis, is an iron-dependent cell death pathway (that differs from apoptosis) which involves several molecular events that were previously found to be correlated with the pathogenesis of PD.<sup>258</sup> More specifically, ferroptosis, is triggered by small molecules or conditions that inhibit the biosynthesis of glutathione and/or the glutathione dependent antioxidant enzyme; glutathione peroxidase 4 (GPX4).<sup>258</sup> As a result of this, the intracellular levels of reduced glutathione are depleted and the levels of liable iron pool are elevated (as reduced glutathione acts as a natural ligand of iron in the liable iron pool).<sup>259</sup> These features of ferroptosis are strongly associated with the pathogenesis of PD as the increased availability of iron contributes significantly to the induction of the oxidative damage via ROS elevation and lipid peroxidation.<sup>258,260</sup> Erastin is one of the lead neurotoxins that can induce ferroptosis (**Figure 13**).

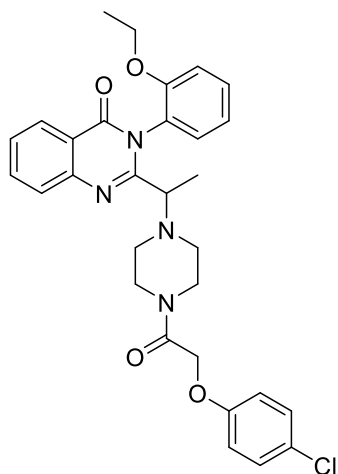


**Figure 13:** Structure of erastin.

The mode of action of this toxin is to inhibit the xCT cysteine/glutamate antiporter preventing the cysteine uptake into the cells (**Figure 14**).<sup>261</sup>

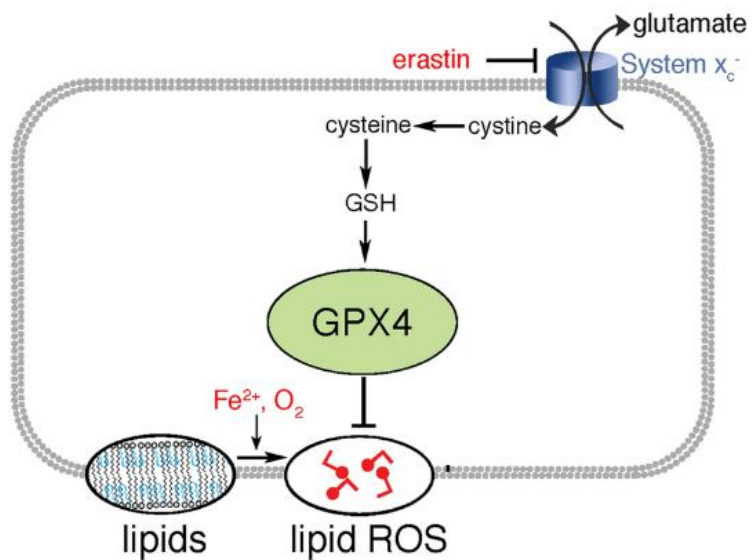


**Figure 14:** Erastin prevents the entrance of cysteine preventing the biosynthesis of glutathione.<sup>261</sup>

Starvation of cystine and hence cysteine can have detrimental effect into the antioxidant defense of the cell as both compounds act as precursor of glutathione.<sup>261</sup> In addition to this, the lack of glutathione prevents the detoxification of the cell and also allows the liable iron being unbound, promoting in that way the Fenton reaction with all the cytotoxic events that are associated.

## **1.8 Current Treatments**

At the present time, there is no cure for PD and the existing treatment options are only used to manage the motor symptoms of the disease and not reverse the cellular loss or prevent further neuronal degradation.<sup>191,199</sup>

### **1.8.1 Non-pharmacological therapies**

Non-pharmacological methods are used as potential therapeutic approaches against the disease and they include deep brain stimulation of the subthalamic nucleus.<sup>236,262</sup> This well-established technique was found to improve significantly the motor functions of the patients.<sup>263</sup> Despite the promising results of this therapeutic approach, it is only used for just 5-10% of diagnosed with PD patients due to strict patient criteria.<sup>264</sup> Another option that offers potential restoration of motor symptoms, involves the foetal mesencephalic graft transplantation.<sup>265,266</sup> According to this treatment option, the nigrostriatal dopaminergic pathway can be restored facilitating the reverse of motor function dysregulations.<sup>265,266</sup> However, the success of this graft is limited and post-mortem analysis indicates the presence of Lewy bodies in the dopaminergic neurons of the grafts.<sup>267</sup> Further development of this technique was hampered due to bioethical and legal limitations.<sup>268</sup>

Eventually, gene therapy is an alternative approach which has been employed in clinical trials in PD patients and due to the promising results, further research projects are in process.<sup>269</sup>

### **1.8.2 Pharmacological therapies – Existing treatments**

Because the main symptoms of PD are associated with the depletion of dopamine, the dopamine's metabolism is the main target of the current treatments (**Figure 15**).

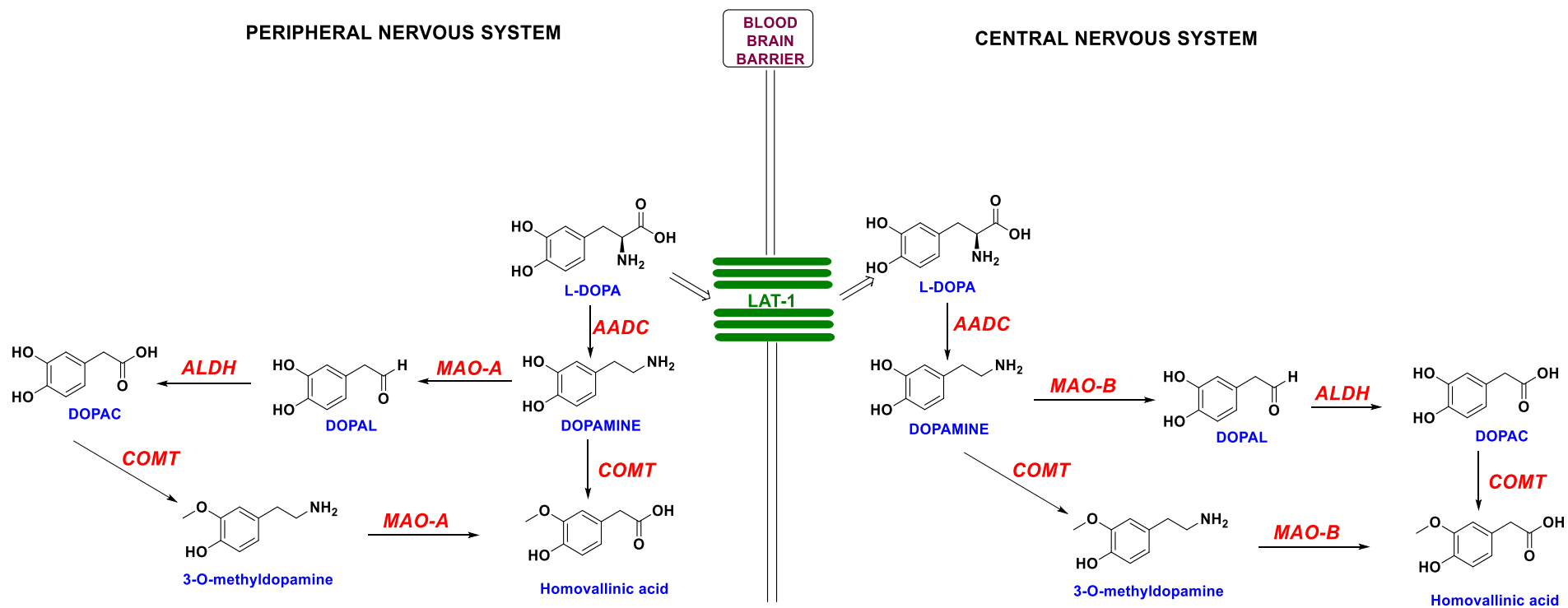


**Figure 15:** Metabolism of L-DOPA and dopamine in peripheral and central nervous system

### 1.8.2.1 L-DOPA supplements

Nowadays there is a variety of drugs on the market that are able to target proteins in order to increase the available dopamine in the striatum. The initial drug therapy against PD involved the administration of (*L*)-3,4-dihydroxyphenylalanine or levodopa (*L*-DOPA).<sup>191</sup> *L*-DOPA is the hydrophilic precursor of dopamine, which can be transported from the peripheral nervous system to the central nervous system by exploiting an active transport mechanism; Large neutral Amino Acid Transporter-1 (LAT-1) on the blood brain barrier (BBB).<sup>270–272</sup> Upon transportation of *L*-DOPA to the CNS, it is picked by the presynaptic dopaminergic endings and it converted to dopamine by the action of Amino Acid Decarboxylase (AADC) enzymes.<sup>273</sup> Apart from the CNS, *L*-DOPA has the ability to be decarboxylated into dopamine in the PNS.<sup>273</sup> The accumulation of dopamine into the PNS is often associated with adverse side effects including nausea and dyskinesia.<sup>274</sup> To bypass the development of the side effects, *L*-DOPA is co-administered with a peripheral *L*-DOPA decarboxylase inhibitor (DDCI) (not capable to cross the BBB) such as , benzerazide (**Figure 16A**) and carbidopa (**Figure 16B**).<sup>275–277</sup>

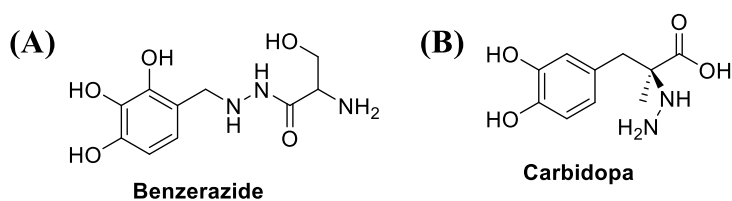


**Figure 16:** Structure of DDC inhibitors that used against PD.

The inhibition of peripheral *L*-DOPA decarboxylation reduces the development of the site effects by decreasing the concentration and accumulation of the systemic dopamine but also it can increase the bioavailability of the drug on the CNS.<sup>278</sup> However, prolong administration of *L*-DOPA seems to loss its activity due to the wearing-off effect according to which *L*-DOPA's activity is decreased because of a progressive destruction of dopaminergic neurons.<sup>279</sup>

### 1.8.2.2 Catechol-O-Methyl Transferase Inhibitors (COMT)

COMT inhibitors belong to a relatively new class of drugs against PD.<sup>280</sup> The role of COMT enzymes is to introduce a methyl group to the 3-hydroxy group of catecholamine core of both dopamine (in the CNS) and *L*-DOPA (in the PNS) which is denoted by the *S*-adenosyl methionine (SAM) as part of the metabolic decomposition of these molecules (**Figure 15**).<sup>281</sup> The methylation leads to the formation of the inactive compounds; 3-O-methoxytyramine and 3-O-methyldopa respectively (**Figure 15**).<sup>280</sup> The co-administration of inhibitor of DOPA-decarboxylase and *L*-DOPA reduces the production of dopamine but increases the concentration of *L*-DOPA that can be methylated by COMT.<sup>282</sup> The main therapeutic action of COMT inhibitor is to prevent the methylation of *L*-DOPA to 3-O-methyldopa in the PNS and increase the bioavailability of the drug.<sup>282</sup> Additionally, COMT inhibition can also prevent the methylation of dopamine in the CNS.<sup>282</sup> The two well-known COMT inhibitors are Tolcapone (**Figure 17A**) and entacapone (**Figure 17B**), opicapone (**Figure 17C**) and nitecapone (**Figure 17D**).<sup>282,283</sup>

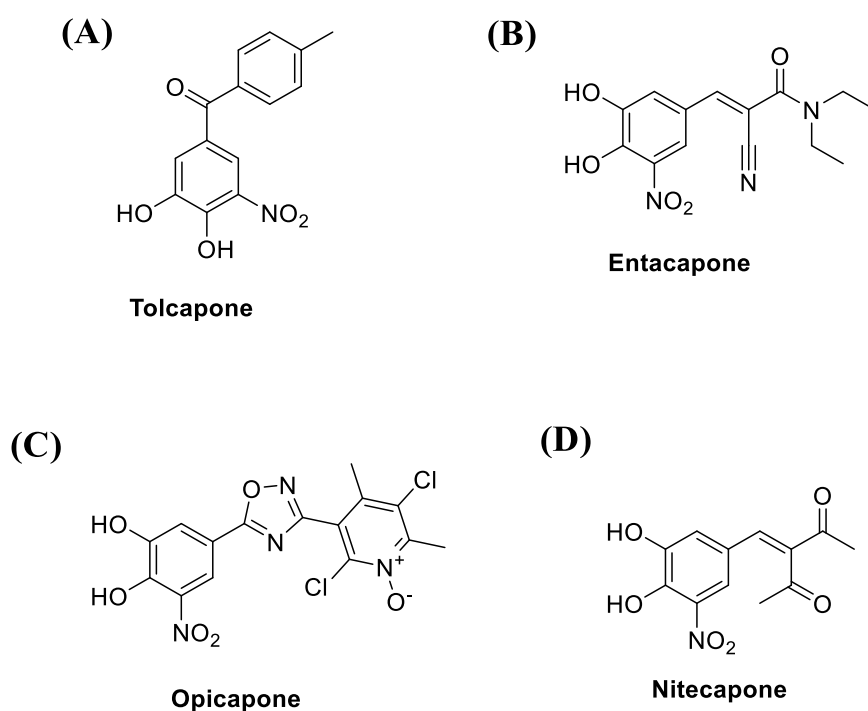
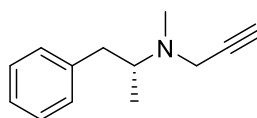


**Figure 17:** Structure of COMT inhibitors used against PD.

The advantages of tolcapone over entacapone are the longer duration and inhibition of COMT in both the PNS and CNS, whereas entacapone can only inhibit the peripheral COMT.<sup>284</sup> However, all of them show toxicity that is mainly associated with the nitro group and the catechol core. To this end a variety of COMT inhibitors based on HOPO core are known, however they are not used for the treatment of PD but against psychiatric disorders.<sup>285</sup>

### 1.8.2.3 Monoamine Oxidase (MAO) Inhibitors

Monoamine oxidases (MAOs) are enzymes that catalyze the oxidation reaction of the monoamine (dopamine) to the respective aldehyde; DOPAL (**Figure 15**).<sup>286</sup> In humans there are two types of MAO; MAO-A and B with MAO-B being the most dominant form in the striatum responsible for the oxidation of dopamine during metabolism (**Figure 15**).<sup>286,287</sup> Therefore, the development and usage of MAO-B inhibitors is of a particular interest against the treatment of PD.<sup>288</sup> A characteristic example of a MAO-B inhibitor is Selegiline, which can selectively inhibit the MAO-B on the striatum and not the peripheral MAO-A, hence it can be co-administered with *L*-DOPA (**Figure 18**).<sup>289</sup>



**Selegiline**

**Figure 18:** Structure of MAO-B inhibitor used against PD

However, the major disadvantage of this drug is its toxic metabolites; amphetamine and methamphetamine, which can cause anxiety and insomnia.<sup>290</sup>

### 1.8.2.4 Dopamine agonists

Another important class of drugs that are widely used against PD are dopamine agonists.<sup>291</sup> Dopamine agonists have the capability to cross the BBB, and they can act directly on dopamine

receptors by mimicking the endogenous neurotransmitter.<sup>292</sup> Overall, they have similar effects to *L*-DOPA, however an important difference is that the dopamine agonist can act to the site of action without any enzymatic conversion.<sup>292</sup> On the other hand, since they are selective for dopamine receptor binding, they usually have less side effects compared to *L*-DOPA.<sup>292</sup> Among the dopamine agonists, the most common ones are bromocriptin (**Figure 19A**) (an ergot alkaloid), ropinirole (**Figure 19B**) and pramipexole (**Figure 19C**).<sup>293–295</sup>

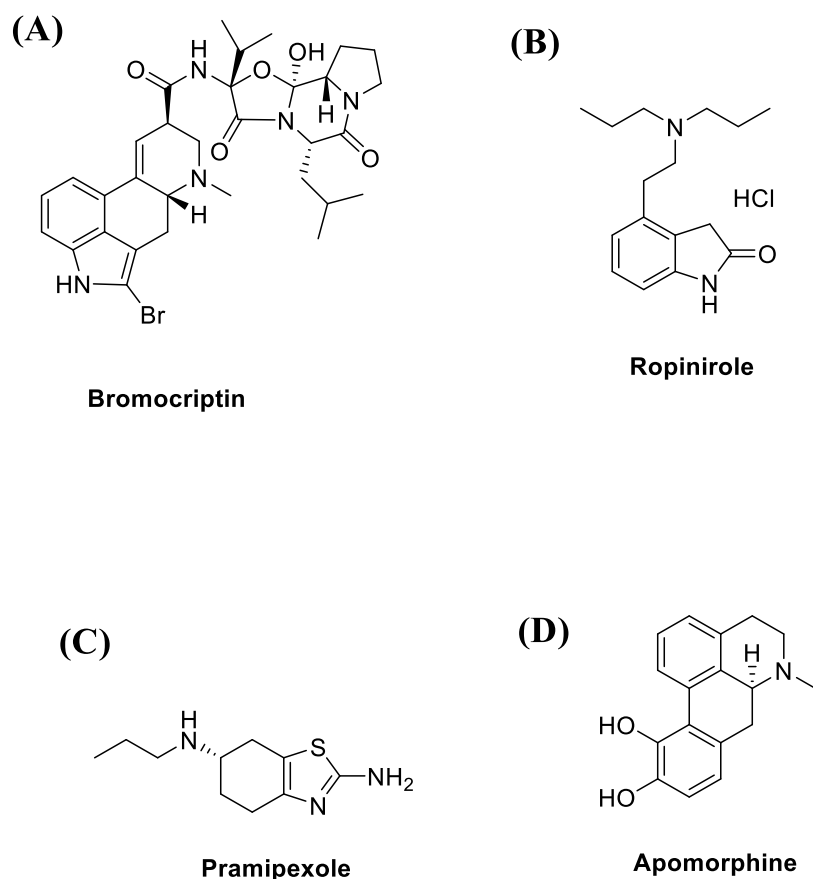


**Figure 19:** Structure of dopamine agonist that used against PD.

These dopamine agonist, can be orally absorbed and they have longer duration of action compared to *L*-DOPA.<sup>296</sup> The therapeutic effect of these class of drugs relies on their interaction with postsynaptic receptors of dopamine but they can also activate the presynaptic autoreceptors.<sup>297–299</sup> The receptor stimulation leads to a decrease in production and release of endogenous dopamine

reducing the intracellular oxidative stress.<sup>297-299</sup> The side effects that are associated with the administration of these drugs include hallucination, confusion and hypotension.<sup>300</sup> A drug that is also used with fewer side effects is apomorphine (**Figure 19D**), which is available as a subcutaneous injection with immediate release.<sup>301,302</sup> Apomorphine is a potent agonist with high affinity for D4 receptors, moderate activity for D2, 3 and 5 and low activity for D1 receptors.<sup>303,304</sup>

### 1.8.3 New strategies - Metal chelators

Despite the fact that a variety of drugs against PD have been designed and used in clinical trials none of them manage to prevent the development or affect the progression of the disease since they are only capable of treating the symptoms of PD.<sup>305</sup> As it was mentioned above, the involvement of iron in the pathogenesis of PD is an important factor that should be taken into consideration for the treatment of the disease as iron and/or copper, via oxidative stress, increase the rate of protein aggregation and consequently the neuronal degradation.<sup>181,183,198,228,231,232,236</sup> A variety of studies in the literature demonstrate the neurotoxic effect of iron on both *in vitro* and *in vivo* as well as the therapeutic effect of iron chelators (themselves or part of a multidrug regiment) that are capable of removing the iron liable pool.<sup>181,183,198,233,255</sup> Additionally, it was suggested by Zheng et al. that iron chelators; VK28 (**Figure 20A**), M30A (**Figure 20B**) and M30 (**Figure 20C**) can pose anti-oxidant effect on iron mediated lipid peroxidation in brain homogenate been treated with 6-OHDA (as a PD-induced toxin).<sup>306</sup> On the other hand, the presence of the propargyl side chain on both M30A and M30 leads to a dual mode of action as it was previously demonstrated that apart from the metal chelation, they can also inhibit the MAO-B enzymes.<sup>307</sup>

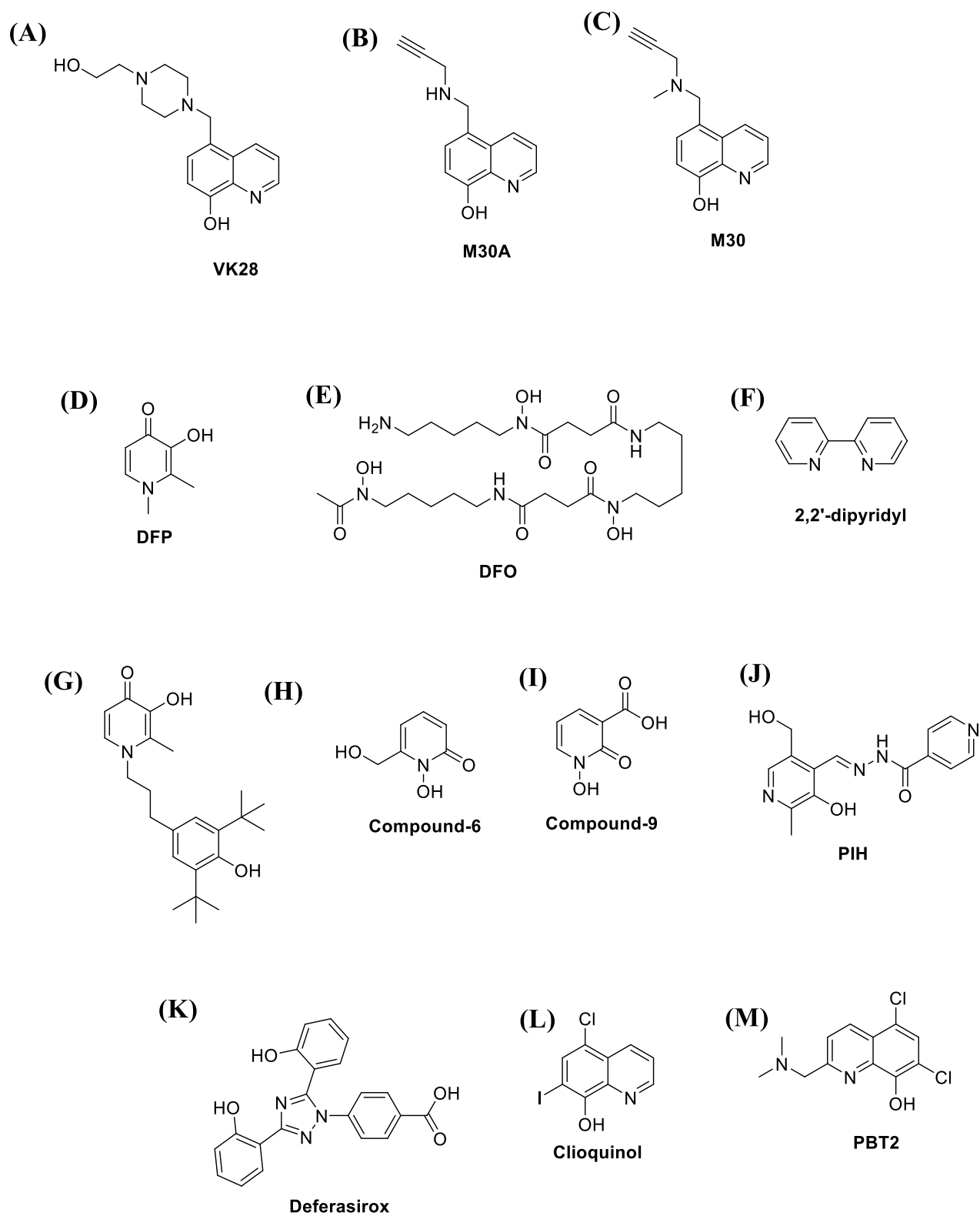


**Figure 20:** Selected structures of iron chelators used in several studies against PD.

Dexter D. *et al.* have shown using *in vitro* experiments the neuroprotection properties of iron chelators DFP (**Figure 20D**), DFO (**Figure 20E**) and desferal (DFO-mesylate) against 6-OHDA.<sup>308</sup> In the same study, treatment with DFP, rescued the loss of 6-OHDA tyrosine hydroxylase (an enzyme that is involved in biosynthesis of dopamine by hydroxylate tyrosine using molecular oxygen) from 15% to 45% whereas other clinically available chelators including desferal and DFO rescue to a lesser extent (25% and 35% respectively).<sup>308</sup> The therapeutic effect of DFP against the iron-induced damage cortical neurons as well as human neuroblastoma SHSY-5Y has also been observed by Molina H. *et al.*<sup>309</sup> The same group, also documented that DFP manage to rescue almost 50% of cell death by preventing the neuronal morphology alteration to a higher extent than the neuroprotective 2,2'-dipyridyl (**Figure 20F**). Chemical modification to DFP has also been conducted by Benbington D. *et al.*<sup>310</sup> According to this derivative of DFP (**Figure 20G**) a dual mode of action has also been enclosed. Namely, the coordination group of this molecule has the capacity to chelate Fe(II) and Cu(II), but also its side chain can act as radical trap in a similar way to Trolox. Therefore, it can prevent the Fenton cycle from taking place and also trap the ROS that are produced by the cycle. Apart from DFP, Workman D. *et al.* have shown the neuroprotective property of 1,2-HOPOs (**Figure 20H and I**) in an *in vitro* model composed of human neuroblastoma SHSY-5Y cells been exposed to 6-OHDA.<sup>311</sup> Moreover, synthetic metal chelator that has been previously used against PD is pyridoxal isonicotinoyl hydrazine (PIH) (**Figure 20J**).<sup>312</sup> PIH as tridentate ligand has shown exceptional results against neurodegradation by chelating preferentially Cu(II) over Fe(III), preventing the ROS formation.<sup>312</sup> To this end, numerous other reports have demonstrated the neuroprotective capacity of DFP (and analogues) against the related PD-induced toxins. In addition to this, the neuroprotective capacity of deferasirox (**Figure 20K**) has also been evaluated against neuroblastoma; BE2-M17 cells been

exposed to MPTP.<sup>313</sup> The results suggested that the tridentate chelator has the ability to act as a neuroprotective agent with therapeutic potency against the disease.<sup>313</sup>

Another class of chelators that show excellent neuroprotective capacity is 8-hydroxyquinoline and derivatives. It was reported in various citations in the literature that 8-hydroxyquinoline and derivatives of it have the ability to improve the motor function by preventing the formation of toxic aggregates of  $\alpha$ -synuclein by inhibiting the liable iron pool.<sup>314</sup> In addition to this, it was shown that this class of chelators has the ability to prevent the oxidative neuronal damage induced by the PD-related toxins including 6-OHDA and MPP<sup>+</sup> by posing antioxidant activity.<sup>315,316</sup> Additionally, it has been demonstrated that 8-hydroxyquinoline derivatives have also the capacity to act as MAO inhibitors.<sup>317</sup>

#### **1.8.3.1 Toxicity of metal chelators**

Despite the exceptional results obtained by DFP, some major disadvantages have been noticed during clinical trials. For example, DFP possessed relative low brain penetration (as it has been proven that DFP can pass the BBB via passive diffusion) and fast metabolism.<sup>318–320</sup> Additionally, the occurrence of some dangerous – albeit rare and transient – side effect including agranulocytosis requires constant monitoring especially for chronic treatment.<sup>321</sup> Therefore, it is of high importance the improvement of brain penetration as this might lower the rate of metabolism and consequently prevent the development of side effects due to lower drug concentration needed in systemic blood circulation.

Clioquinol (**Figure 20L**) a derivative of 8-hydroxyquinoline managed to enter clinical trials in the beginning of the 20<sup>th</sup> century and had many applications including; anti-parasite, anti-diarrhea.<sup>322</sup> Additionally, this specific compound show exceptional results against neurodegenerative disease including PD and Alzheimer's disease as it shown ability to prevent the neuronal degradation, by inhibiting the formation of  $\alpha$ -synuclein aggregates.<sup>322</sup> Additionally, it has been shown that is can

prevent the formation of Tau proteins as well as the formation of A $\beta$ -amyloids.<sup>322</sup> However, it was withdrawn from the market as its administration was associated with the development of sub-acute meylo-optic neuropathy in Japanese patients.<sup>322</sup> This syndrome, mainly involves disturbance in the sensor and motion of the lower limbs as well as visual changes due to symmetrical demyelination of lateral and posterior funiculi of the spinal cord, optic nerve and peripheral nerves.<sup>322</sup> It has also been reported that the majority of the symptoms were versatile however in 1/10 of the cases cause permanent disability. Nowadays, a big effort is being made in order to redesign clioquinol in a manner that would abolish the associated-side effects.<sup>322</sup> A derivative of clioquinol; PBT2 (**Figure 20M**) has shown a great potency against neurodegenerative diseases mainly AD and Huntington's disease due to its capacity to chelate the redox active Cu(II) and the redox inactive Zn(II) and it has successfully managed to enter clinical trials.<sup>323</sup>

In addition to this, as in the case of cancer, metal chelators were found to act as inhibitors of many metallo-enzymes including tyrosine hydroxylase (TH) mainly because TH contains Fe(III) as a cofactor.<sup>324</sup> Inhibition of TH can cause perturbations in *L*-DOPA biosynthesis by preventing its biosynthesis.<sup>325</sup> Therefore, the design of metal chelators with limited side effects should be considered against the treatment of PD.<sup>325</sup>

## 1.9 Transportation across the BBB

One of the key properties that a drug should have in order to treat neurodegenerative diseases is its ability to reach the brain. Therefore, the study of delivery systems that would allow the transportation of drugs to the brain is been of high interest for many years.<sup>326</sup> The main issue that has to be taken into consideration during the design of the active compounds is the BBB which its existence was confirmed in the beginning of the 20<sup>th</sup> century by Goldmann.<sup>327</sup> Not surprisingly, only a few classes of drugs are capable to be transported across the BBB. In 1999 Ghose *et al.* examined the capability of the 7000 drugs from the Comprehensive Medicinal Chemistry database to penetrate the BBB and interestingly it was found that only a 5% of these were CNS active

regardless of their mode of penetration (See below).<sup>328</sup> Of these drugs all are used for the treatment of depression, schizophrenia and other mental disorders but none for the treatment of neurodegenerative diseases.<sup>328</sup> CNS active drugs tend to be small with a recommended molecular weight of <400 Da however that doesn't mean that and compound with a molecular weight of <400 Da can enter the CNS and reach the brain.<sup>329</sup> This is mainly because the drug molecules need to have some properties to penetrate the BBB which are dictated by the properties of the BBB.<sup>330,331</sup> Therefore, the design of compounds that would be capable to reach the brain (by means of BBB penetration) requires profound understanding of the BBB structure and function.

### 1.10 The Blood-Brain Barrier

The BBB is composed by a well-defined multicellular layers that exists in all species with a developed CNS (**Figure 21**).<sup>332,333</sup>

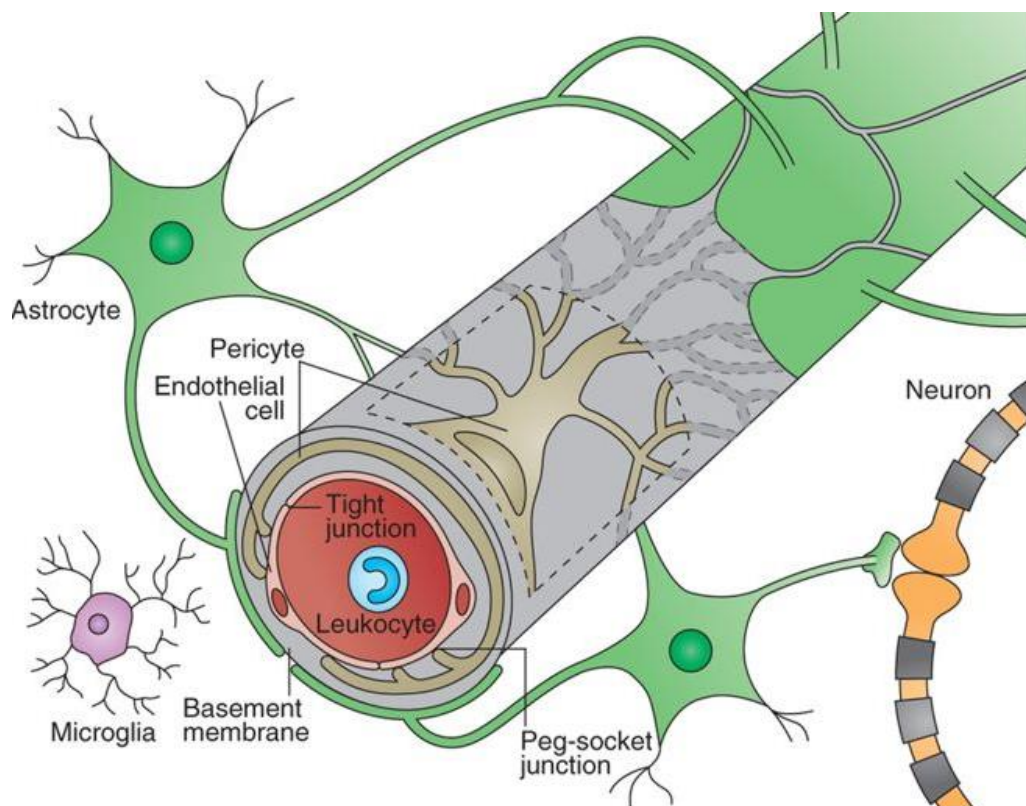


**Figure 21:** Cellular composition of Blood-Brain Barrier.<sup>332</sup>

The main role of BBB is to separate the brain from the systemic blood circulation maintain in that way the homeostasis of CNS for the proper synaptic signalling, hence the optimal neuronal function.<sup>332-334</sup> In mammalian species the BBB is built-up by endothelial cells of cerebral capillaries.<sup>334</sup> On the contrary, to the peripheral blood vessels the endothelium of the brain vasculature is not leaky due to the absence of fenestrations and consequently the tight junctions between the cells.<sup>335</sup> The role of tight junctions is mainly to prevent plasma proteins and other solutes found in the blood to enter the brain via paracellular diffusion.<sup>335</sup> Therefore the transportation of any compound from and to the brain has to be done through transcellular passage through the endothelium.<sup>335</sup> Another important aspect of the BBB is its ability to express metabolic enzymes; cytochrome P450, MAO, transaminases and glucoronosyl transferases that are capable to detoxified or degrade potentially harmful compounds during the transportation.<sup>336-338</sup> Moreover, the BBB is comprised of transporter systems that can efflux solutes entering endothelial back to the blood.<sup>334</sup> Despite the fact that other CNS barriers exist including the blood cerebrospinal fluid at the choroid plexuses and the arachnoid membrane under the dura mater have significantly smaller area play a localised role during the transportation.<sup>334</sup>

### **1.11 Overcoming the BBB**

So far, multiple strategies have been employed in order to overcome the issue that BBB causes in the drug delivery to the brain. For examples, drugs can be deliver to the brain by direct injection to the CNS (intrathecal administration).<sup>339</sup> For the synthetic point of view, it has been previously shown that the transportation across the BBB could be improved or achieved by utilising nanoparticle carrier systems for large drug delivery.<sup>340-342</sup> For smaller molecules, chemical modifications to their structure can be beneficial as they can either be transported via passive diffusion or they can take the advantage of the active or energy-independent transport systems of the BBB.<sup>343</sup>

### 1.11.1 Passive diffusion

As mentioned previously, some drugs can enter to the brain by passively diffusing the lipid bilayer of the BBB. The transportation is mainly driven by the gradient between the intra- and extracellular concentrations.<sup>344</sup> Moreover, the permeability of molecules is influenced by several factors including their lipophilicity, polarity and size.<sup>344</sup> Large molecules are mostly unlikely to cross the biological membranes via passive diffusion as large amount of lipid has to be displaced and the overall process is energetically disfavoured. The diffusion rate of the molecules is therefore inversely related to their size.<sup>345,346</sup> Additionally, the passive transportation of hydrophilic molecules is also disallowed as it cannot be partitioned into the lipophilic core of the membrane.<sup>346</sup> On the contrary, high lipophilicity increases the chances of molecule's permeability via diffusion, however it can reduce the aqueous solubility.<sup>347,348</sup> This can lead to low absorption and high plasma protein binding, hence the free drug concentration will be lower resulting in a flat concentration gradient and significantly slower diffusion rate.<sup>347,348</sup> For this reason, Lipinski suggested a set of rules for the drug discovery and development in terms of both oral, intestinal and hence CNS permeability.<sup>344</sup> To this end, a variety of free web-tools have been generated allowing the prediction of the ability of a compound to penetrate the BBB via passive diffusion taking into consideration of the physicochemical parameters associated with the passive diffusion.<sup>349–351</sup> These will be discussed in more details in **2.8** and **2.8.1**.

In 1999, Habgood *et al.* documented that the transportation of 3, 4-HOPOs via passive diffusion can be affected by varying the *N*-substituent as this affects the  $\log P$  value.<sup>352</sup> Namely, lengthening the *N*-alkyl chain leads to an elevation of the  $\log P$  value and consequently the brain penetration.<sup>352</sup> In contrast the addition of hydroxyl groups abolished the brain penetration, whereas the non-hydroxylated derivatives with similar  $\log P$  can enter the brain more easily. The more lipophilic HOPO was not advanced further as the increased lipophilicity can lead to higher partitioning into liver, where HOPOs can be metabolised and excreted.<sup>319,352</sup>

### 1.11.2 Prodrugs to improve passive diffusion

Prodrugs are derivative of drugs in which the active group is conjugated with a pro-moiety in order to avoid peripheral metabolism and/or improve uptake in the target area. Once the molecule enters the target tissue, the pro-moiety is cleaved, releasing the active drug.<sup>353,354</sup> A common strategy to improve the permeability of the drug is to mask the polar group (which they act as hydrogen bond donors) with non-polar groups and cross the BBB via passive diffusion or even using an active transporter.<sup>354–356</sup> In addition to this, once the prodrug reaches the brain, it is converted into the active drug via bioconversion.<sup>353,354</sup> Usually, the hydroxyl or carboxylic group of the molecule are been converted into the corresponding esters and once the compound reaches the target area (brain), the esters are cleaved by the action of esterases.<sup>353,354</sup> Example of a naturally occurring prodrugs is *L*-DOPA. As it is mentioned previously, dopamine cannot enter the CNS due to its hydrophilicity. Therefore its precursor, *L*-DOPA exploits LAT-1 to reach the CNS and afterwards is metabolised by ADDC into dopamine. Therefore, a pro-moiety can also be used in order to direct the drug to the brain via one of the endogenous systems. An example of synthetic metal pro-chelators can be found in **(Figure 22)**.<sup>357</sup>

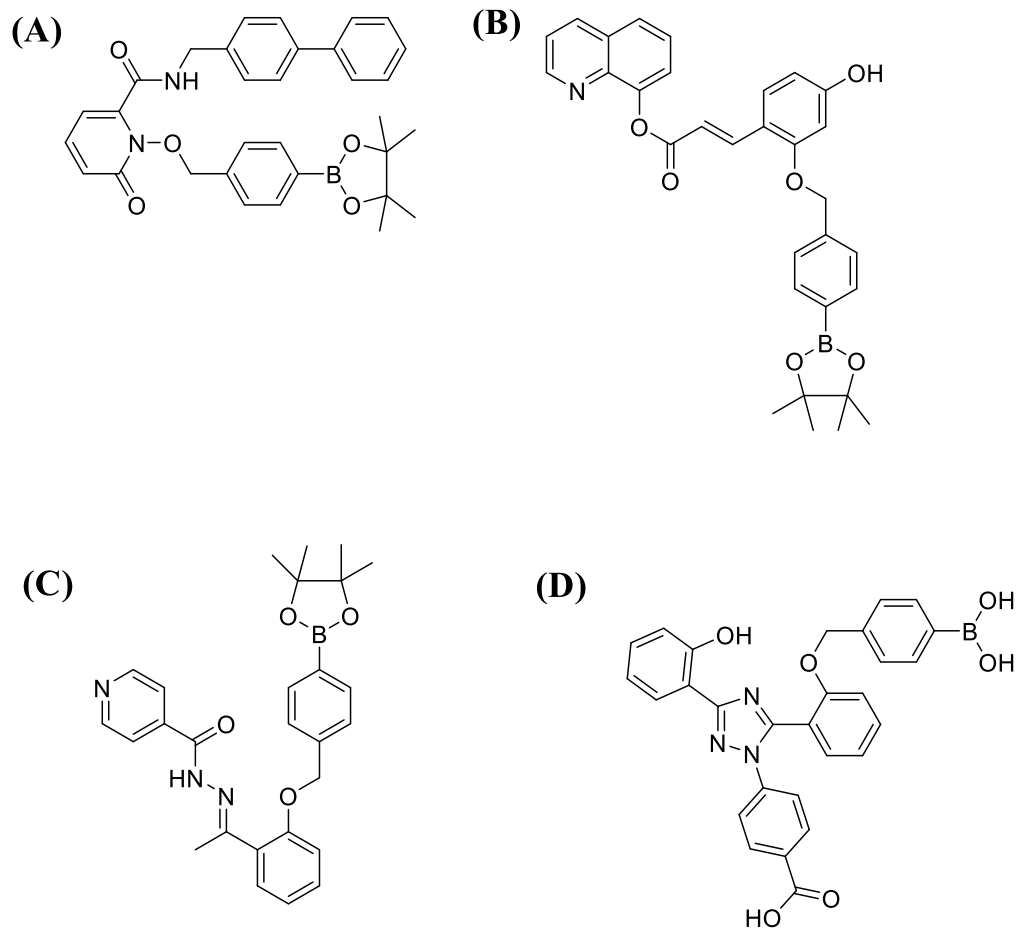


**Figure 22:** Selected boronic ester masked pro-chelators.

The addition of a boronic ester can mask the *N*-OH group of the hydroxypyridinone core and also can increase the lipophilicity of the molecule allowing its diffusion through the BBB (**Figure 22A**).<sup>357</sup> Due to the high concentration of hydrogen peroxide that is produced (mainly) by the action of MAO-B, the boronic ester can be cleaved eliminating the active chelator (**Figure 23**).<sup>357</sup>

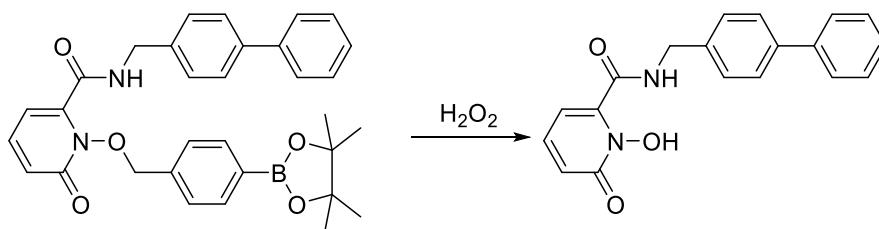


**Figure 23:** Conversion of the boronic ester masked pro-chelator into active chelator by the action of  $H_2O_2$ .

This approach has also been applied to 8-hydroxyquinoline (**Figure 22B**) derivatives as well as PIH (**Figure 22C**) and deferasirox (**Figure 22D**) based analogues and with promising results.<sup>357</sup>

### 1.12 Transportation process

The BBB has the capacity of utilising a variety of different classes of transporter mechanisms in order to supply all the brain regions with nutrients and also in order to remove the metabolites of those out of the brain (**Figure 24**).<sup>333,358</sup>

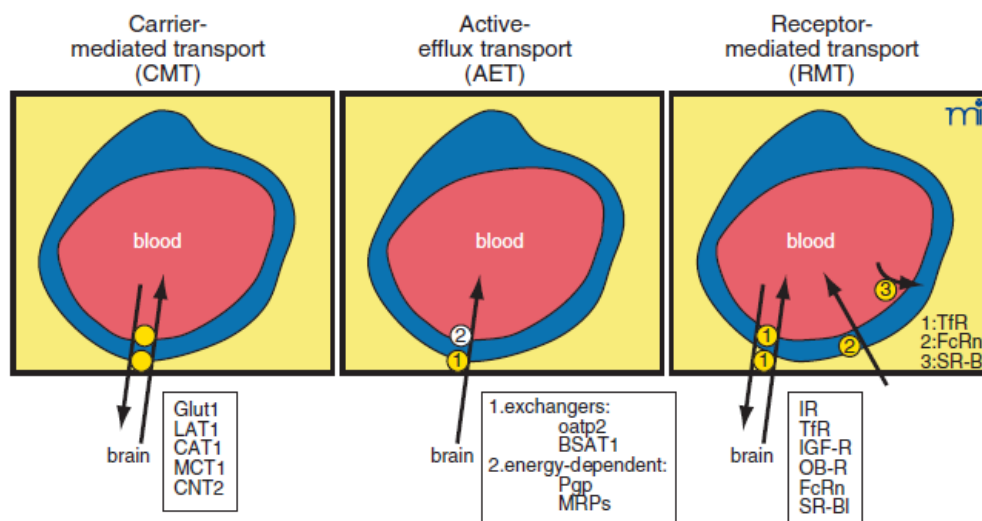


**Figure 24:** Transporter systems located in the endothelium of BBB.<sup>326</sup>

Additionally, the transporters that are located in the BBB can also be used to maintain the entry of xenobiotic and toxins into the CNS. Therefore, these transport systems can be used as for the

improvement of delivery systems and/or to be used as targets by means of selective inhibition.<sup>343,359,360</sup>

### **1.12.1 The transport system**

#### **1.12.1.1 Active Efflux Transporter (AET)**

AET is one of the three transport systems of the BBB and it is mainly responsible for the exportation of molecules from the brain endothelium.<sup>334</sup> The exportation process is usually achieved by the utilisation of ATP molecules or by the sodium-dependent co-transport. Some of the members of proteins that belong to this system are; P-glycoprotein (P-gp), breast cancer resistance protein (BCRP) and the multidrug resistance associated proteins (MRP 1-5).<sup>361,362</sup> Interestingly, this transport system can preferentially transport lipophilic molecules and increasing lipophilicity makes molecules a more likely substrate of the active efflux transporters.<sup>362-364</sup> Significant examples of drugs which exploit AETs include anti-retroviral such as; amperanivir, indinavir and saquinavir, anticancer agents such as; vincristine, vinblastine, etoposide, and doxorubicin, antibiotics such as; erythromycin, tetracycline and fluoroquinolones.<sup>362</sup>

#### **1.12.1.2 Receptor Mediated Transport**

This transport system is mainly responsible for the transportation of large molecules and macromolecules including signalling peptides and proteins across the BBB and the transportation relies in two sub-transportation process; the non-specific transcytosis and the specific transcytosis.<sup>365</sup> In both cases the (macro)molecule is transported to the brain enclosed in a vesicle. Initially, non-specific transcytosis occurred by absorptive-mediated transcytosis (AMT).<sup>366,367</sup> Positively charged macromolecules are the main substrates of such transportation process. The interaction between the charged macromolecules and the cell surface binding sites, triggers the internalisation via a conformational change, leads into the formation of a vesicle which is then transported across the cell (**Figure 25**).<sup>366,367</sup>

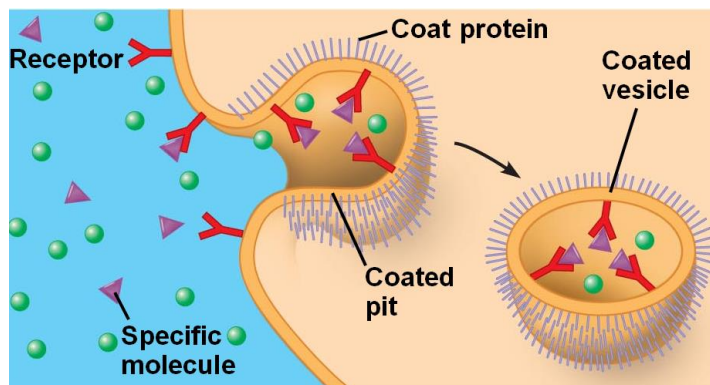


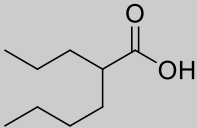
**Figure 25:** Formation of vesicles carrying macromolecules for their transportation across the BBB via RMT.<sup>368</sup>

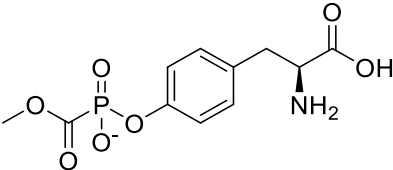
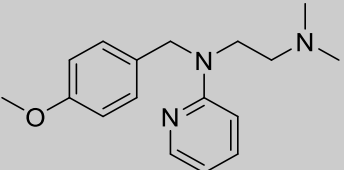
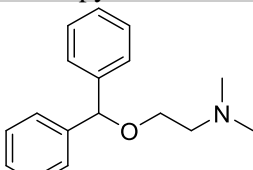
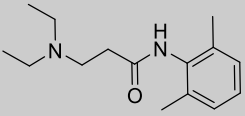
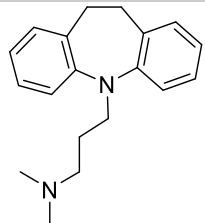
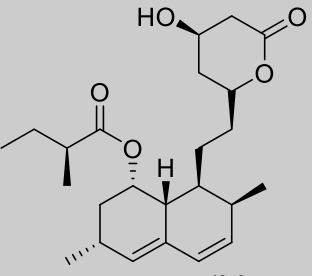
On the other hand, the receptor mediated transcytosis (RMT) requires specific ligand binding into specific receptor of the endothelial cell membrane.<sup>368,369</sup> The binding of the ligand to the receptor triggers the internalisation via the formation of a vesicle.<sup>368,369</sup> The vesicle is transported across as receptor-ligand pairs undergoing RMT include transferrin, insulin-like growth factor and LDL as well as particular large molecules such as ‘Trojan horse’.<sup>370–374</sup>

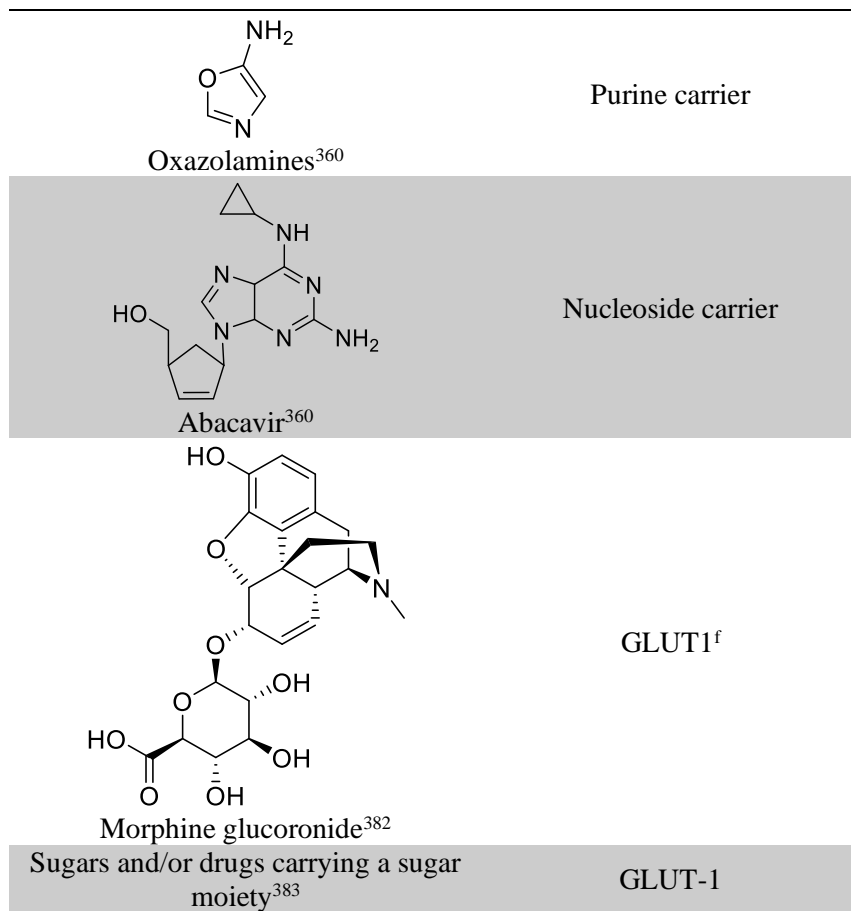
### 1.12.1.3 Carrier mediated transport (CMT)

The role of CMT which is located to the brain endothelium as well is primarily to supply the brain with the essential nutrients needed for metabolism purposes.<sup>375,376</sup> The transportation is often facilitated by sodium-dependend channels or it is driven by an exchange with other ions. Numerous drugs are known to enter the brain via CMT and the most important once are depicted in **Table 2**.<sup>377</sup>

**Table 2:** Selective drugs that uses CMT for their transportation across the BBB.

COMPOUND	TRANSPORTER
 Valproic acid	MC <sup>a</sup> fatty acid carrier <sup>378</sup>  MC fatty acid carrier

DHA <sup>b</sup> -dideoxycytidine <sup>379</sup>	
DHA-taxol <sup>360</sup>	MC fatty acid carrier
<i>L</i> -DOPA <sup>360</sup>	LAT-1
$\alpha$ -methyl-dopa <sup>360</sup>	LAT-1
	LAT-1
Tyrosine phosphoformate <sup>353</sup>	
	OCT family <sup>c</sup>
Mepyramine <sup>360</sup>	
	OCT family
Diphenylhydramine <sup>380</sup>	
	OCT family
Lidocaine <sup>381</sup>	
	OCT family
Imipramine <sup>360</sup>	
	MCT1 <sup>e</sup>
Lovostanine <sup>d360</sup>	



a=Medium Chain fatty acid carrier  
 b=DocosaHexanoic Acid  
 c= Organic Cation Transporter  
 d= open lactone form  
 e=MonoCarboxyl Acid transporter  
 f= Glucose Transporter-1

### 1.12.1.3.1 The Glucose-Transporter-1 (GLUT-1)

In order for the mammalian cells to acquire the essential for energy production glucose they acquire two transport mechanism one of which is the sodium-dependent glucose transporter (SGLT).<sup>384–386</sup> SGLT is responsible for the glucose uptake in the intestine and glucose re-uptake in nephron.<sup>386</sup> The GLUT-1 transporter belongs to a sodium independent glucose transporter family (GLUT) and its main endogenous substrate is *D*-glucose but not the *L*-glucose. More specifically, GLUT-1 belongs to a class of major facilitators superfamily (MFS) which is a very large

transporter superfamily.<sup>386–388</sup> The common structural characteristic of the MFS is that they composed of 12 transmembrane domain (**Figure 26**).<sup>389</sup>

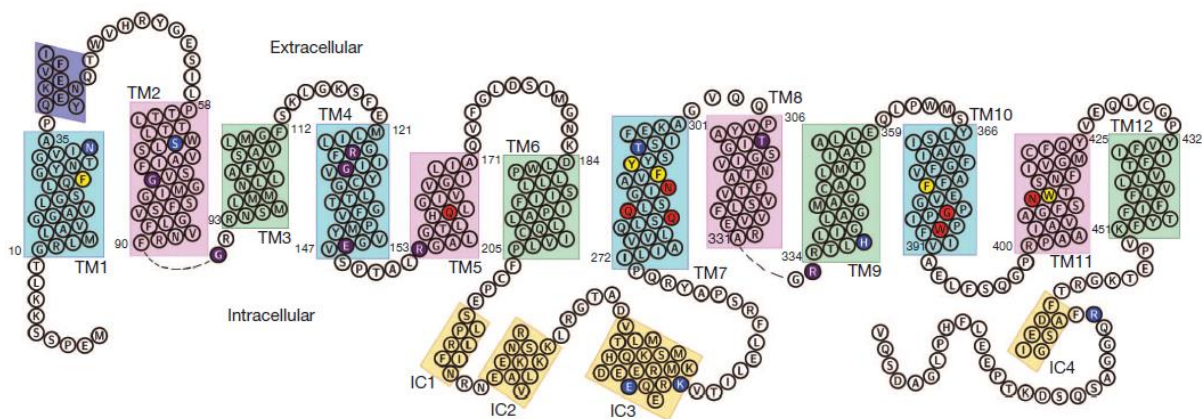


**Figure 26:** Predicted secondary structural components of GLUT-1. The polar and aromatic residues involved into the D-glucose binding (red and yellow shaded respectively). The residue whose mutation were found in GLUT1 deficiency syndrome are shaded in purple and blue for invariant and variant residues respectively.<sup>389</sup>

The presence of the GLUT-1 transporter in the brain can almost exclusively found to be in the BBB whereas other members of the GLUT family can also be found in astrocytes and neurons.<sup>390,391</sup> Interestingly, GLUT-1 is also expressed in erythrocyte membranes, retina, testes and the placenta.<sup>386,387,390–393</sup>

#### 1.12.1.3.1.1 Transportation of metal chelators through GLUT-1

In order to facilitate the delivery of DFP and/or its derivatives, for the treatment of neurodegenerative diseases, researchers modified the active molecule in order to exploit the GLUT1 transporter (active transport mechanism) making it as a prodrug.<sup>320,357,394–396</sup> This was achieved by conjugating the hydroxyl group of the pyridine core to a glucose, whereas other, have built an *N*-amide coupled to the glucose.<sup>320,357,394–396</sup> Orvig *et al.* have synthesised a variety of

glycosylated metal chelators based on the hydroxypyridinone (**Figure 27A**) and tetrahydrosalen (**Figure 27B**) classes as they assumed that the introduction of a glucose moiety on the chelators can lead into direct brain uptake.<sup>394–397</sup>

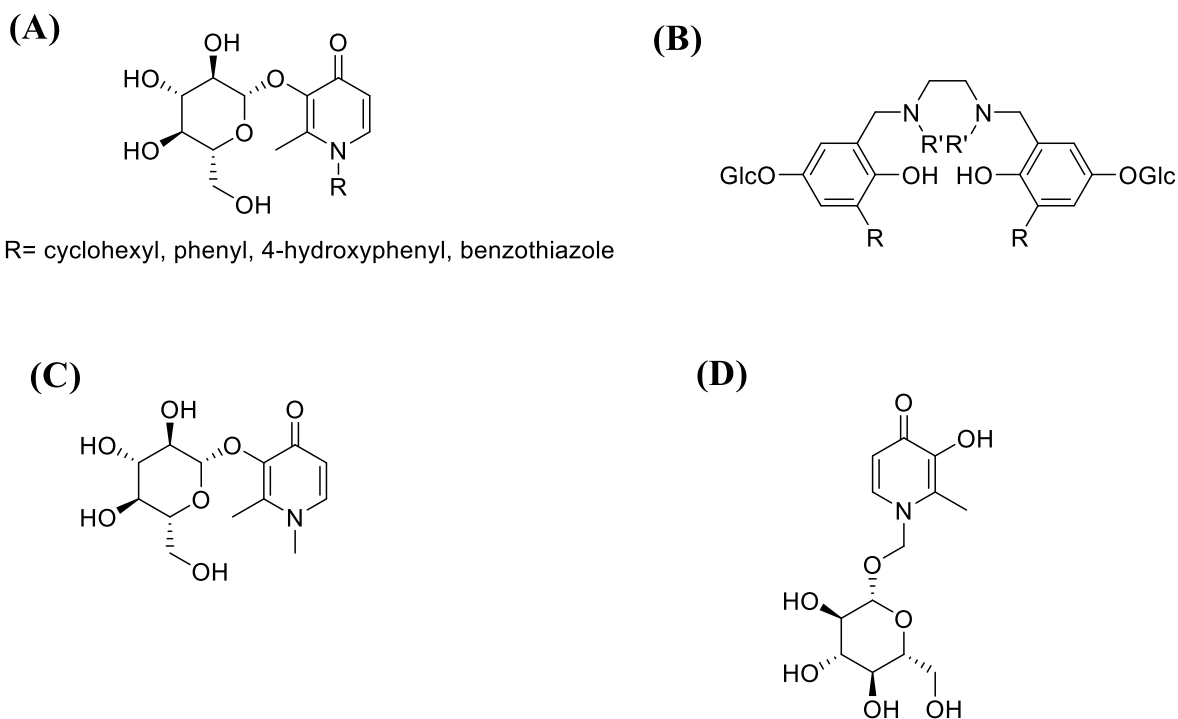


**Figure 27:** Structures of glycosylated metal chelators.

As it is mentioned above, glycosylated hydroxypyridinones were screened as prodrugs for the treatment of neurodegenerative diseases by copper chelation.<sup>394,395</sup> In another study, Roy *et al.* glycosylate DFP (**Figure 27C and D**) in an attempt to facilitate its transportation in the brain.<sup>320</sup> The brain uptake was measured by *in situ* brain perfusion of guinea pigs, however HPLC analysis could not detect the presence of the compound in the brain, showing that this methodology is probably not universal.<sup>320</sup>

### 1.12.1.3.2 Large Amino acid Transporter-1 (LAT-1)

LAT-1 (SLC7A5) is a sodium and pH-independent transmembrane protein (protein) that forms a heterodimeric complex with the glycoprotein 4F2hc (CD98 and SLC3A2) to bring large neutral amino acid in the CNS in exchange for intracellular amino acid.<sup>398,399</sup> Studies shown that the LAT-1 is the sole transport compete unit whereas the 4F2hc does not participate in the intrinsic transportation as it only functions as chaperone that allows LAT-1 to reach its definitive localisation in the cellular membrane.<sup>400</sup> This transported is overexpress into the BBB due to the continuous necessity of the neuron and glial cells for amino acids.<sup>401,402</sup> It has been suggested that LAT-1 in the BBB is stereospecific with preferential selectivity to the *L* enantiomers rather than the *D* ones, whereas the LAT-1 of the peripheral tissues is not.<sup>402,403</sup> It has also been demonstrated that the LAT-1 possess higher affinity for intracellular amino acid compared to the extracellular ones, denoting in that way that the transportation ratio is controlled by the concentration of intracellular amino acid.<sup>402,404</sup> Moreover, LAT has a preferential order of amino acid transportation as follow; Phe > Trp > Ile > Met > His > Tyr > Val.<sup>402</sup>

#### 1.12.1.3.2.1 Structure of LAT-1-4F2hc

LAT-1 transporter belongs to the family of Heterodimeric Amino acid Transporters (HATs) that are composed of a light chain (SLC7), which is responsible for the mediation of the amino acid transportation, and a heavy chain (SLC3) which is responsible for the catalysis of the plasma membrane localisation and stabilisation of the light chains (**Figure 28**).<sup>405</sup>

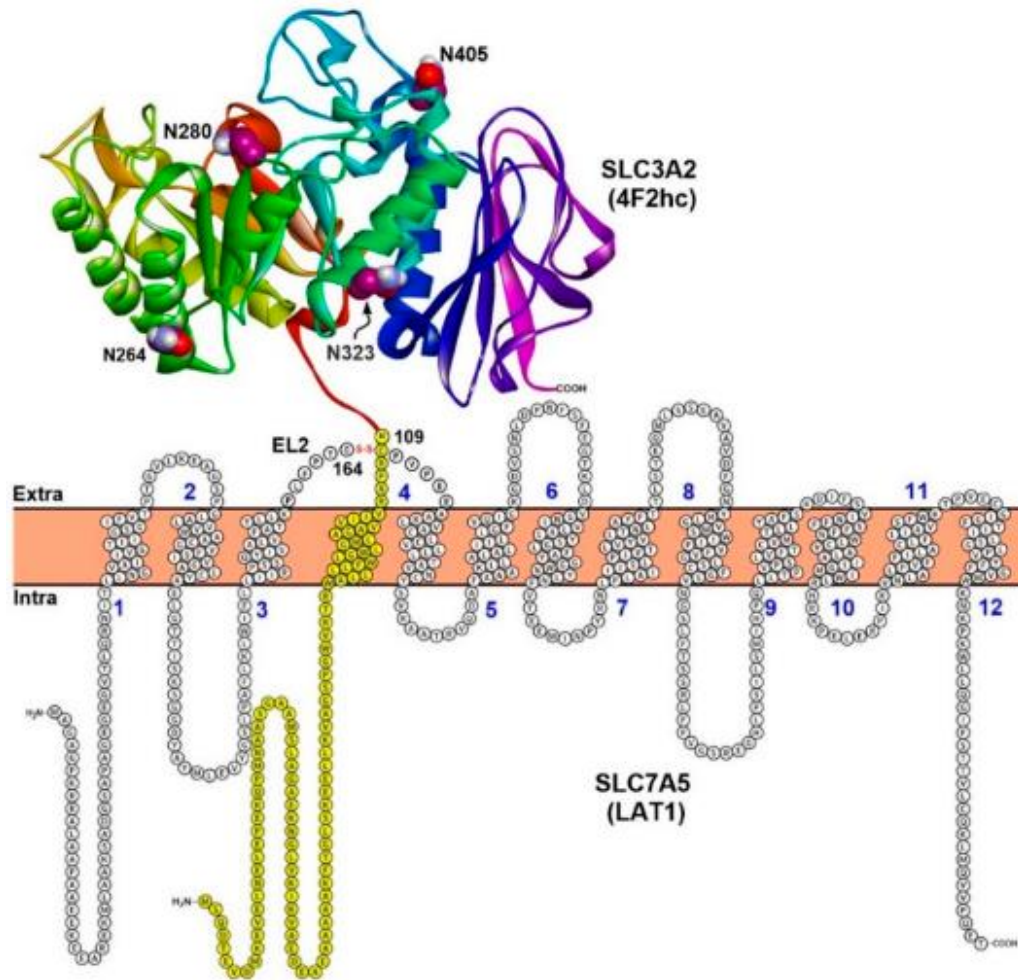


**Figure 28:** Topological representation of LAT-1 – 4F2hc. LAT-1 is consisted of 12 putative TM and is associated with 4F2hc though a disulphide bond. The crystal structure of the extracellular domain of human 4F2hc is shown as ribbon.<sup>399,406</sup>

Moreover, LAT1 is built up by 12 putative transmembrane segments (TMs) arranged in two layers. The inner layer is composed of TM1, 3, 6, 8 and 10 and is surrounded by the outer layer which is consisting of TM2, 4, 5, 7, 9, 11 and 12.<sup>405</sup> Moreover, *N*- and *C*- terminal of ends of LAT-1 are located intracellularly whereas the respective terminal ends of 4F2hc are located extracellularly.<sup>398,405,407</sup> As it is mentioned above, 4F2hc is a glycoprotein with the for putative *N*-glycosylation sites; N264, 286, 323 and 405.<sup>405</sup> Additionally, it has one TM domain and a large extracellular domain (ED).<sup>405</sup> LAT-1 and 4F2hc are covalently linked together by a disulphide

bond between the cysteine residues which are located in closed proximity with TM of the heavy subunit and in the putative extracellular loop-2 of the light subunit (between TM3 and TM4).<sup>405</sup> In a protein-protein docking study performed by Rosel *et al.* it was found that the desolvation energy of hydrophobic residues contributes to the binding of LAT-2 and 4F2hc-ED suggesting that LAT-1 and 4F2hc might be involved in a similar interactions.<sup>408</sup>

Since the beginning of 2019 the crystal structure of human LAT-1 – 4F2hc heterodimer was unknown.<sup>409</sup> Therefore, the arginine-bound AdiC crystal structure was previously used as a reliable template for molecular modelling studies.<sup>405,410</sup> Moreover, the broad-specific amino acid transporter (ApcT), the glutamate/  $\gamma$ -aminobutyric acid (GABA), the antiporter (GadC) and the Leucine transporter (LeuT) pose some structural and sequence similarities with the AdiC and therefore they were used as alternative templates (however of less preference) for LAT-1 transporter.<sup>405,411,412</sup>

## 2 Design and Synthesis of Metal Chelators

### 2.1 Factors affecting the Fe(III)-chelator stability

#### 2.1.1 Redox activity – Fenton Chemistry

The catalysis by Fe(III) and Cu(II) in the production of ROS in biological systems has been extensively documented in the past in attempt to characterise the pathological conditions (inducing cancer and PD) that are arisen due to elevation of toxic ROS levels.<sup>413–416</sup> It is also documented that Fe(II) can be oxidised into Fe(III) by the reduction of hydrogen peroxide, during the Fenton reaction, something that leads to the formation of hydroxyl radicals. This can also be confirmed from the fact that the redox potential of hydrogen peroxide/hydroxyl radical ( $E^{\circ}=+ 0.32$  V, pH 7, 25°C, NHE) is significantly higher compared to the potential of  $\text{Fe}^{3+}/\text{Fe}^{2+}$  (been coordinated by either EDTA or citrate).<sup>417</sup> Therefore, it is expected that hydrogen peroxide is more likely to oxidised  $\text{Fe}^{3+}$  into  $\text{Fe}^{2+}$  and the redox process is favourable with the respect to the ROS formation. On the other hand, according to the Haber-Weiss net reaction oxidation of hydrogen peroxide into superoxyl radicals can cause the reduction of Fe(III) can reduced back to Fe(II) (**Figure 29**).

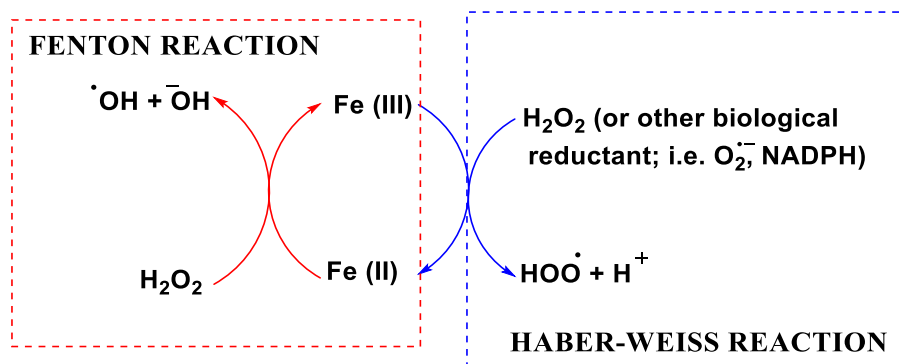


**Figure 29:** Formation of hydroxyl and superoxyl radicals through Fenton and Haber-Weiss reaction respectively.

Therefore, the inhibition of ROS formation can be achieved by preventing the redox cycling of metals. Liu et al reported that the high affinity Fe(III) ligands can indeed prevent redox cycling in biological systems.<sup>418</sup>

## 2.2 Thermodynamic considerations of complex formation

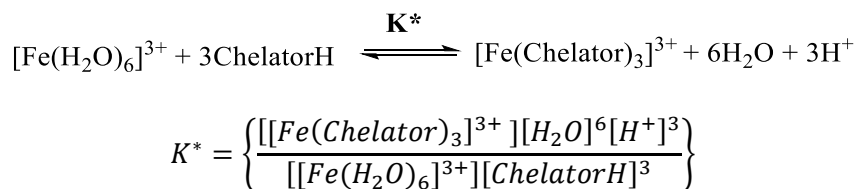
The complexation of a metal centre with a ligand is a process that is mainly controlled by thermodynamic factors. The thermodynamics of complex stability can therefore be described by the Gibbs free energy of reaction  $\Delta G^{\circ}$  (**Equation 1**).

$$\Delta G^{\circ} = \Delta H^{\circ} - T\Delta S^{\circ}$$

**Equation 1:** Gibbs free energy of reaction ( $\text{J mol}^{-1}$ ),  $\Delta H^{\circ}$  is the standard enthalpy of the reaction ( $\text{Jmol}^{-1}$ ), T is the temperature (K) and  $\Delta S^{\circ}$  is the standard entropy of the reaction ( $\text{JK}^{-1} \text{mol}^{-1}$ )

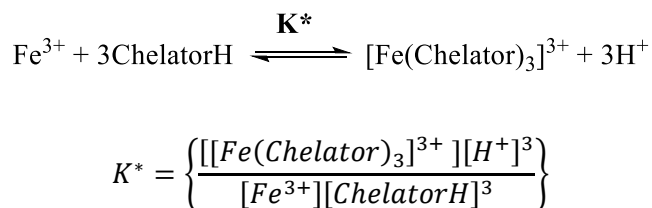
The existence of charged ion species in a solution that are mainly surrounded by solvent molecules that formed dipole interactions can be consider as a thermodynamically unfavourable process in terms of entropic contribution. As a result, the complexation process, which involves the participation of charged species leads to partial or complete cancelation of the charges of those species providing in that way favourable contribution to the entropic considerations within the free energy. In addition to this, the total or partial cancellation of the charges in solution has also a favourable enthalpic contribution due the combination of the oppositely charged species. Therefore, the partial or complete cancelation holds a significantly negative  $\Delta H^{\circ}$  favoured in terms of Gibbs free energy. Furthermore, for ligands of high denticity, an important impact in the thermodynamically favoured complexation process. Therefore, it appears that the chelate effect will have enthalpic and entropic contributions towards the stability of the complex. The stabilisation of the enthalpic contribution of the chelate effect would be the inductive contribution of the electron density gained from the atom adjacent to the coordinating sites. As a result of this the donor strength of the binding sites will be increased and hence the stability of the complex.

The overall entropic contribution is driven by two factors. Firstly, the entropy surrounding the metal-ligand complex formation is often favoured for reaction in which polydentate. This is because polydentate ligands can cause the dissolution of the metal centre leaving more species (eg. water molecules) on the product side of the reaction. Furthermore, this interaction increases the entropy of the system and thus increases the thermodynamic favourability.



**Scheme 1A:** Bidentate chelators displaces water molecules from ferric iron centre.

Based on the **Scheme 1A**, we can ignore the contribution of water as  $[\text{H}_2\text{O}]$  is constant and we can focus on  $K^*$  for (**Scheme 1B**);

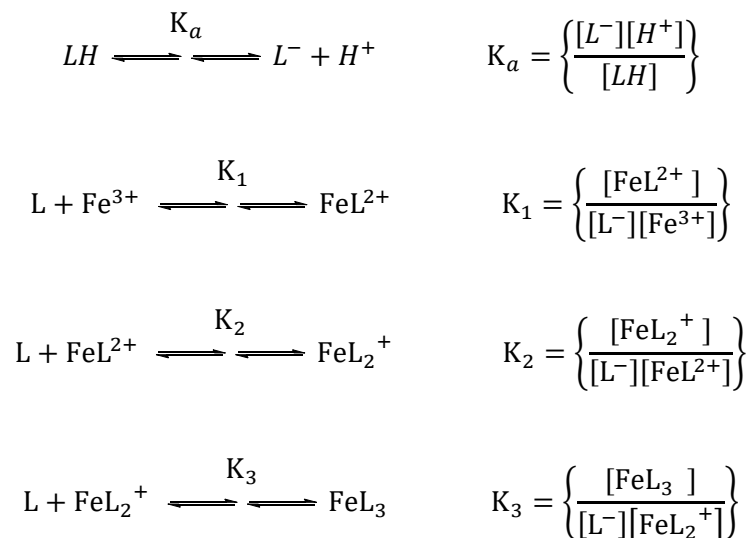


**Scheme 1B:** Revised equilibrium constant for bidentate chelators and Fe(III), ignoring the contribution of water

Therefore, in order to have a thermodynamically favoured reaction it is essential to shift the equilibrium towards the product formation, having in that way as high as possible  $K^*$  value. However, the  $[\text{Fe}^{3+}]$  (non-complexed  $\text{Fe}^{3+}$ ) should be as low as possible in order to have fully metal coordination.

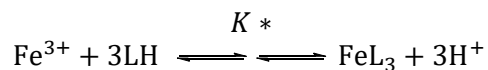
### 2.3 Stability of Fe<sup>3+</sup>-chelator complexes

Since most of the ligands are in their protonated state at neutral pH, the dissociation of protons is pivotal for the binding to Fe(III). The competition between the Lewis acids (Fe(III) and H<sup>+</sup>), is taken into consideration when calculating equilibrium constants K for Fe(III)-ligand complex formation as depicted in **Scheme 1** that encompasses that various equation in **Scheme 2**.<sup>419,420</sup>



**Scheme 2:** Stepwise addition of monoprotic bidentate ligand (L) to Fe(III) upon proton dissociation.

To simplify the expression of the stepwise stability constants it is often the case that these are expressed as the product of the overall stability constant ( $\beta$ ).<sup>420</sup> The overall stability constant when multiple ligands are incorporated (same denticity and structure) is displayed along with subscript notation in the form of  $\beta_{MLH}$  where, L= number of the same ligands involved, M= number of metal ligands involved and H= number of proton involved in the stoichiometry of the equilibrium process (**Scheme 3**).

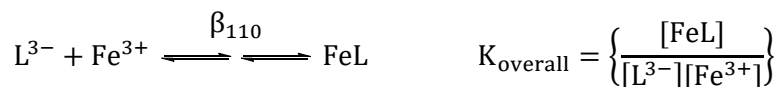
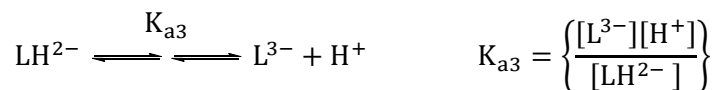
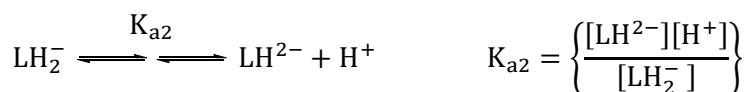
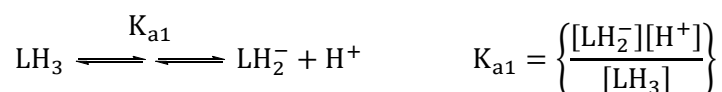


$$K^* = \left\{ \frac{[\text{FeL}_3]^{3+}[\text{H}^+]^3}{[\text{Fe}^{3+}][\text{LH}]^3} \right\} = K_a \times \beta_{130}$$

where  $K_a$  is the dissociation constant and  $\beta_{130} = K_1 \times K_2 \times K_3$

**Scheme 3:** Overall stability constant defined for the complexation of 3 bidentate monoprotic ligands and 1 Fe(III) centre.

The most powerful chelators are mainly hexadentate and for these the overall stability constant will be expressed as  $\beta_{110}$  for the fully deprotonated hexadentate ligand (**Scheme 4**).



**Scheme 4:** Stepwise deprotonation of a triprotic hexadentate ligand and the overall stability constant of such a ligand binding Fe.

Due to the fact the equilibrium is only favourable upon deprotonation of the ligand it can be concluded the overall stability constant is pH dependant. However, when we look at the equilibrium constant of the chelator, is often simpler to measure the condition for the proton free reaction, which is the  $\beta$  measured for the Fe(III)-ligand complex at equilibrium.<sup>421</sup>

## 2.4 pFe<sup>3+</sup> as measure of ligand binding efficiency

An accepted way to measure the efficacy of the complex is to measure the equilibrium concentration of the free Fe(III) in solution. This is the pFe<sup>3+</sup> value and is defined by analogously with pH;

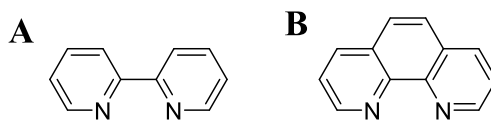
$$\text{pFe}^{3+} = -\log_{10} [\text{Fe}^{3+}]_{\text{free}}$$

The pFe<sup>3+</sup> value is a conditional value that takes into account all thermodynamic ( $K_a$  and  $\beta$ ) and conditional (pH= 7.4,  $[\text{Fe}^{3+}]_{\text{total}} = 1 \mu\text{M}$  and  $[\text{Chelator}]_{\text{total}} = 10 \mu\text{M}$ ) values. The Lewis acid competition of dissociated protons, ligand denticity and basicity as well as difference in metal – ligand stoichiometry is accounted for by the pFe<sup>3+</sup> and hence it is a more acceptable measure of the ability of a ligand to bind Fe<sup>3+</sup>. The  $[\text{Fe}^{3+}]_{\text{free}}$  refers to the unbound (non-complexed) Fe<sup>3+</sup> that remains in solution. Therefore, this value allows for the direct comparison of metal chelator strength as long as the conditions in which are taken are conserved in both cases. The one with the highest pFe<sup>3+</sup> value, will be the stronger chelator.<sup>422</sup>

## 2.5 Metal sensitivity

For the design of iron chelators as potential therapeutic agents, the properties of metal sensitivity should be examined. The design of a chelator for a particular metal complexation can be rationalised by the segregation of metals and ligands to the concept of soft and hard acids.<sup>423</sup> Despite the fact that Pearson's classification is overall outdated, in our case is still useful. Theoretically, iron chelators should be able to exhibit affinity for Fe(II) and Fe(III) species however according to the soft/ hard Lewis acids theory, this is not applicable. Mainly because high-spin Fe(III) is a spherically, symmetrical tri positive cation with radius 0.65 Å and due to its high charge density it can be classified as hard Lewis acid.<sup>418</sup> In contrast Fe(II) has a lower charged density and it can be said that less hard Lewis acid. Due to this effect, it is expected that Fe(III) would have higher affinity to hard Lewis bases (such as oxygen contained ligands) whereas, Fe(II)

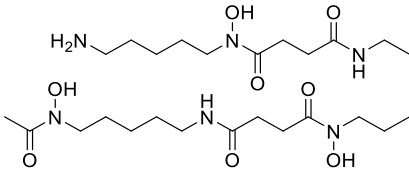
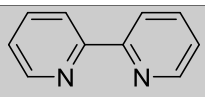
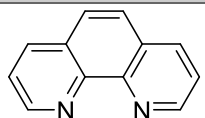
should have less affinity to hard Lewis base and greater affinity to the soft ones (nitrogenous ligands) eg; 2,2'-bipyridyl and 1, 10-phenanthroline (**Figure 30**).<sup>418</sup>



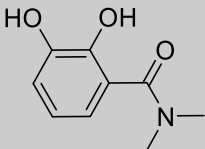
**Figure 30:** Structure of (A) 2,2'-bipyridyl and (B) 1, 10-phenanthroline

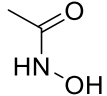
Furthermore, ligands with affinity to Fe(II) are expected to present some affinity for other bivalent metals including Cu(II) and Zn(II).<sup>418</sup> Therefore, this prevents the design of Fe(II) selective ligands difficult. On the contrary, Fe(III) ligands, (mainly oxyanions) have high selectivity over tri basic cations over dibasic. Due to the fact that tri basic cations such as Al(III) and Ga(III) are not essential for living cells, Fe(III) provides the best target for iron chelator under biological conditions (**Table 3**).<sup>424</sup>

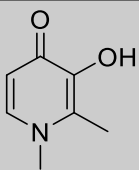
**Table 3:** Metal affinity constants for selected ligands.<sup>424</sup>

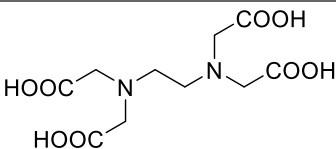
Ligand	Log cumulative stability					
	Fe(III)	Al(III)	Ga(III)	Cu(II)	Zn(II)	Fe(II)
<b>DFO</b>						
	30.6	25.0	27.6	14.1	11.1	7.2
	16.3	-	7.7	16.9	13.2	17.2
<b>2, 2'-Biphenyl</b>						
	14.1	-	9.2	21.4	17.5	21.0

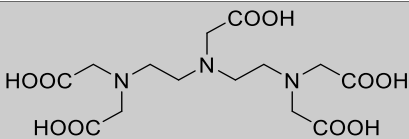
## 1, 10- Phenanthroline

	40.2	-	-	24.9	13.5	17.5
<b>DMHB</b>						

	28.3	21.5	-	7.9	9.6	8.5
<b>Acetohydroxamic acid</b>						

	37.2	35.8	32.6	21.7	13.5	12.1
<b>Deferiprone</b>						

	25.1	16.5	21.0	18.8	16.5	14.3
<b>EDTA</b>						

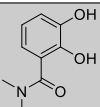
	28.0	18.6	25.5	21.6	18.4	16.5
<b>DTPA</b>						

Previously, Harris and co-worker demonstrate that high affinity Fe(III) chelators can bind to Fe(II) and these are rapidly oxidised them into the corresponding Fe(III) species under aerobic conditions.<sup>425</sup> Therefore, it is suggested that high affinity Fe(III) chelators can coordinate both Fe(II) and Fe(III) under physiological conditions, eventually leading to the ferric complex.

## 2.6 Dioxygenated coordination units

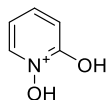
Some of the more commonly observed coordination units in siderophores are catechols, hydroxamic acids and  $\alpha$ -hydroxycarboxylic acid binding units. The common feature in all of these, is that their structure includes oxygen donor atoms as shown in (Table 4).<sup>418</sup>

**Table 4:** Common binding units of chelators and selected non-biologically occurring coordinating groups.<sup>418</sup>

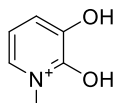
	Name	Structure	$pK_{a1}$	$pK_{a2}$	$\log\beta_{130}$	$pFe^{3+a}$
BIOLOGICALLY OCCURRING	N,N-Dimethyl-2,3-dihydroxybenzamine (DMHB)		8.4	12.1	40.2	15
	Acetoxyhydroxamic Acid		-	9.4	28.3	13
	$\alpha$ -hydroxyethanoic acid		3.8	14.8	-	-
	3-methyl-3-hydroxyl-pyran-4-one		-	8.7	28.5	15
	1-hydroxypyridin-2-one		-0.8*	5.8	27	16
NON-BIOLOGICALLY OCCURRING	1-methyl-3-hydroxypyridin-2-one		0.2**	8.6	32	16
	1,2-dimethyl-3-hydroxypyridin-4-one		3.6***	9.9	37.2	19

(a) [ligand] = 10  $\mu$ M,  $[Fe^{3+}]_{total}$  = 1  $\mu$ M, pH = 7.4

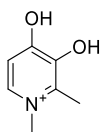
\* for



\*\* for



\*\*\* for



### 2.6.1 Catechols

As it can be observed by **Table 4**, catechols (represented by DMHB) exhibit the highest  $pK_{as}$  (8.4 and 12.1) and  $\log\beta_{130}$  (40.2). Those values are common for the biologically occurring Fe(III) coordinating units for siderophores demonstrating in that way the strongest binding interaction with Fe(III). This effect can be attributed to the fact that the high electron density located across the vicinal oxygen atoms as well as from the electron density across the aromatic ring. Interestingly despite their exceptional properties, catechols, at physiological pH the Fe(III)-catechol binding is inhibited due to competition by proton (hard Lewis). Therefore, the  $pFe^{3+}$  value (=15) drops significantly. In addition to this, the production of high negatively Fe(III) species ( $Fe(DMHB)_3^{3-}$ ) also affect the complexation through increased charged repulsion of the diprotic molecules. This is shown by statistically greater than expected decreases in the stepwise equilibrium, constants of the order  $K_1=20.4 > K_2=15.5 > K_3=9.4$ .<sup>426</sup>

### 2.6.2 Hydroxamic acids

Hydroxamic acids are monoprotic acids with relatively lower  $pK_a$  (~9.4) compared to catechols. It is expected that the Fe(III) affinity will be lower something which is validated by the  $\log\beta_{130}$  value (=28.3) for acetoxyhydroxamic acid. However, at physiological pH, hydroxamic acids, are less dependent to pH compared to catechols, hence the  $pFe^{3+}$  value of the complexation with metal is low (in comparison with catechols). In addition to this, as the acid is monoprotic, the coordination is occurring through the carbonyl and charged *N*-hydroxyl functionalities to the metal centre by 3 hydroxamate groups. Therefore, there is not any net charge something which is energetically more favourable compared to the formation of charged complexes. Moreover, it has

been proven before, that the dissociation rates of Fe(III) complexed hydroxamates has also been shown to be more kinetically inert compared to catecholates.<sup>427,428</sup> A major limitation of hydroxamic acids is the free rotation around the C-N bond which caused unfavourable chelation mode though the E isomer, as the Z/E ratio seems to have an impact in the rate of complex formation. In example, desferrioxamine B (DFO-B) has a Z/E ratio of 0.25 and rotational rate constants ( $k_{rot}$ ) of 9, 15 and 12 s<sup>-1</sup> whereas N-acetoxyhydroxamic acid, has values of 4 and 3 s<sup>-1</sup> respectively. Ring closure to form the Fe(III) chelate is rapid relative to the rate of C-N bond rotation in the latter however it becomes slow for DFO-B.<sup>429</sup>

### 2.6.3 $\alpha$ -hydroxycarboxylic acid

$\alpha$  - hydroxycarboxylic acid are the weakest of the common naturally occurring oxygenated chelators for Fe(III) in siderophores. Nevertheless, they are important molecules for iron acquisition by microbes in highly acidic environment such as fungi, where other coordinating groups would be fully protonated and hence less effective Fe(III) chelators. Additionally,  $\alpha$  - hydroxycarboxylic acid, demonstrate useful reductive properties under UV-light for Fe(II) release mechanism in marine bacteria.<sup>430</sup>

### 2.6.4 Hydroxypyridinones

Hydroxypyridinones combine the characteristics of both hydroxamates and catechol groups 'forming' 5-membered chelate rings in which the metal is chelated by two vicinal metal atoms. HOPOs are characterised by having a hydroxyl group *ortho*- to a carbonyl functionality within a pyridine ring of which there are three isomers; 1-hydroxypyridin-2(*H*)-one (1, 2-HOPO), 3-hydroxypyridin-2(*H*)-one (3, 2-HOPO) and 3-hydroxypyridin-4(*H*)-one (3, 4-HOPO).<sup>418,431</sup>

The HOPO coordinating groups are extremely close analogues to catechols in terms of electronic distribution and size. However, the fact that HOPOs have significantly lower pKa values compared to catechols is making them preferable for applications in biological systems. In addition to this, the HOPOs forms neutral ion complexes they do not show the dramatic decrease

in stepwise equilibrium constants been observed for catechols due to charged repulsion (**Figure 31**).<sup>432,433</sup>

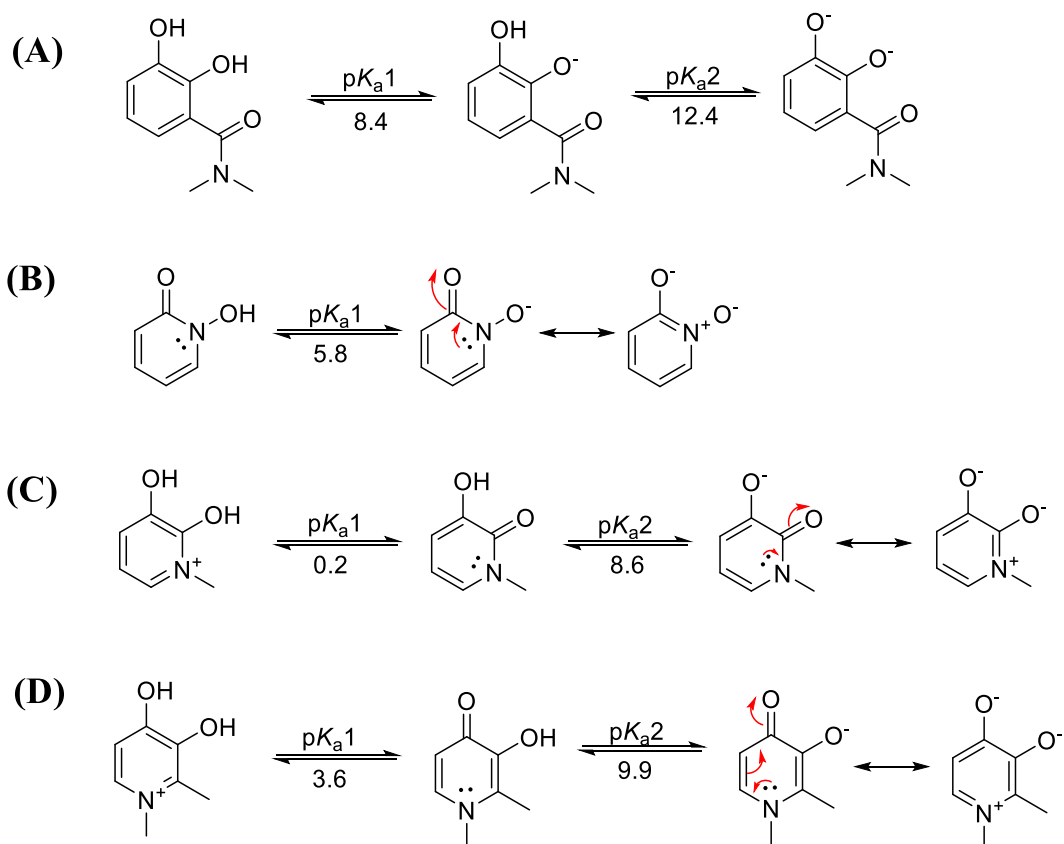


**Figure 31:** Acid dissociation constants and deprotonation reaction of (A) DMHB (catechol), (B) 1, 2-HOPO, (C) 1-Me-3, 2-HOPO and (D) DFP (3, 4-HOPO). Resonance forms for the fully deprotonated HOPOs are represented to show their bioisosteric equivalence to catechol binding unit.<sup>432</sup>

Despite the fact that HOPO's lower  $\text{p}K_a$  values, decrease the  $\log\beta$  value compared to DBMH, acetohydroxamic acid and maltol, however they can have a comparable or higher  $\text{pFe}^{3+}$  value. In example, DFP has  $\sim 5$  orders of magnitude greater  $\text{pFe}^{3+}$  value compared to the catecholate DMHB (mainly due to relative high affinity of catechols for protons) and  $\sim 7$  order of magnitude greater than acetohydroxamic acid. This suggests that the  $\text{p}K_a$ s of HOPOS are optimally balanced for the

formation of strong  $\text{Fe}^{3+}$  coordination spheres (trivalent complexes) and significant deprotonation at pH 7.4, similarly to hydroxamates.<sup>418</sup>

#### 2.6.4.1 HOPOs can induced redox silencing

HOPOs as high affinity Fe(III) chelators can be employed in order to inhibit the redox cycle. It has also been proven that upon fully complexation of iron by 3, 4- HOPO (DFP), the redox potential of the couple  $[\text{Fe(III)(DFP)}_3]/ [\text{Fe(III)(DFP)}_n]^{+x}$  was found to be extremely low ( $E^0 = \sim -0.45$  V, pH 7, 25°C, NHE) than the redox potential of hydrogen peroxide.<sup>417</sup> As a result of this, hydrogen peroxide is not capable of reducing Fe(III) back to Fe (II), hence Fenton reaction was quenched. This statement was validated later on by Devanur and co-workers who demonstrated that the fully coordinated  $[(\text{DFP})_3\text{Fe(III)}]$  complex wasn't able to produced hydroxyl radicals. In contrast, the hydroxyl production was maximised in the partially coordinated  $[(\text{DFP})_2\text{Fe(III)}]^+$  complex.<sup>434</sup> This suggested that the redox silence of Fe(III) is strongly depended in the concentration of chelators, as a 3:1 molar ratio allows full coordination of Fe(III), preventing in that way the access of the reductant to the iron cation.<sup>418,434</sup> In contrast, 2:1 or 1:1 stoichiometry, allows the generation of ROS since there is free site on iron centre, which allows the reduction of hydrogen peroxide and the oxidation of Fe(III).<sup>434,435</sup> This evidence was later confirmed by Timoshnikov VA et al which they prove that the formation of a  $[\text{Fe(III)(DFP)}_3]$  complex was redox inactive in an experimental model of photo-Fenton chemistry.<sup>436</sup> Furthermore, the formation of the unstable Fe (II) complex will dissociated to hexaquo Fe (II) that is a major endogenous source of labile iron pool.<sup>434</sup> Eventually they concluded that fully occupation of the binding sites by chelators can prevent the binding of hydrogen peroxide on Fe(II) hence the silence of Fenton reaction. Finally, it has been demonstrated that 3, 4-HOPOs are also capable to inhibit Cu(II) catalysed hydroxyl radical formation.<sup>437,438</sup> Therefore, it can be concluded that HOPOs are capable to act as antioxidants by inhibiting the Fenton reaction.<sup>438-444</sup> This is achieved by the formation of fully coordination Fe(III) spheres that prevent the reduction of Fe(III) to Fe(II). Nevertheless, the saturation of Fe(III) doesn't abolish the formation of ROS from already existing as Fe(II) will

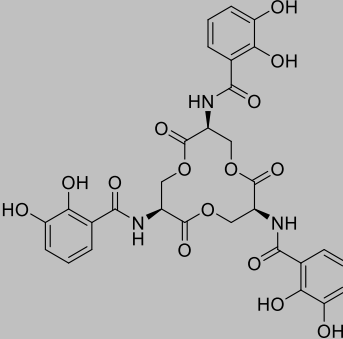
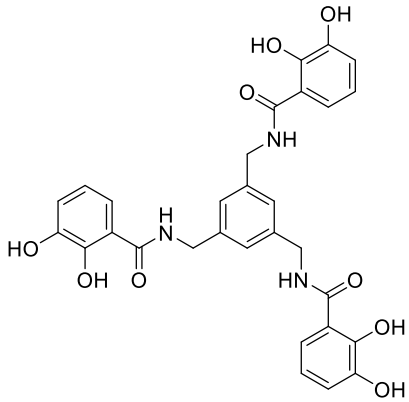
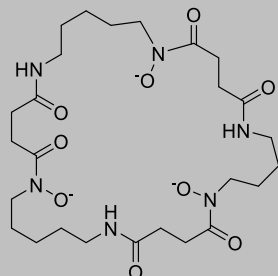
oxidised once and a hydroxyl radical will be formed however this process is expected that is going to be irreversible since the Fe(III) will be blocked.

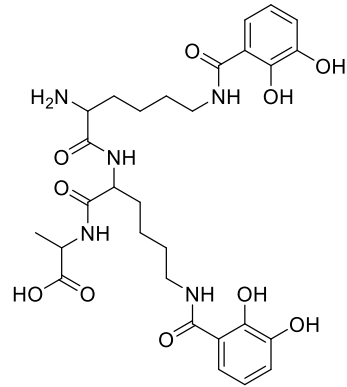
## 2.7 Denticity

In the case of PD, we have already suggested that full saturation of Fe(III) is important. This is strongly influenced by denticity. Iron chelators can possess a variety of denticities with the bidentate, tridentate, tetradentate and hexadentate being the most common. However, the various contributions to the stability of Fe(III)-chelator complex are not entirely enthalpic driven in nature, but also have significant entropic contributions upon complexation. As noted above, the hydroxypyridinone unit is a bidentate ligand that provides more thermodynamically stable complex with iron than the monodentate ligand. This is something that is validated (with some exceptions) by the 'chelate effect' which states that the increase of the denticity will cause an increase in the stability of the complex as denoted by both  $pFe^{3+}$  and  $\log\beta$ .<sup>421</sup>

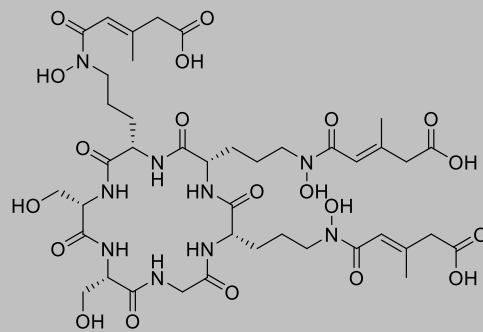
Therefore, it is expected that hexadentate ligands will form more Fe(III) stable complexes in an octahedral arrangement. A general trend of ligand denticity and Fe(III) ligand formation constant is displayed in (Table 5).<sup>421</sup>

**Table 5:** Binding affinity for a range of ligands for Fe<sup>3+</sup>, displayed in descending order of pFe<sup>3+</sup>.<sup>421</sup>

Ligand	Denticity	logβ (Fe <sup>3+</sup> )	pFe <sup>3+</sup>
<p><b>Enterobactin</b></p> 	6	49.0	35.5
<p><b>MECAM</b></p> 	6	45.9	29.1
<p><b>Ferrioxamine E</b></p> 	6	32.5	26.6
<p><b>Amonabactin</b></p>	4	34.5	26.0

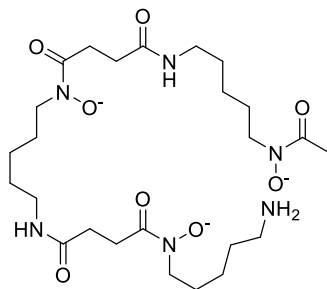


**Ferrichrome A**



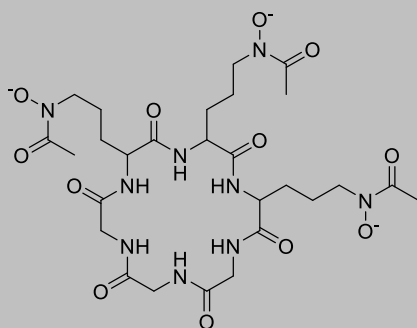
6 32.0 25.2

**Ferrioxamine B**



6 30.5 25.0

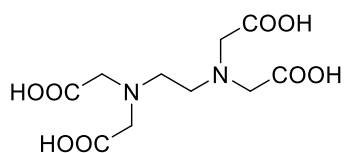
---

**Ferrichrome**

6

29.1

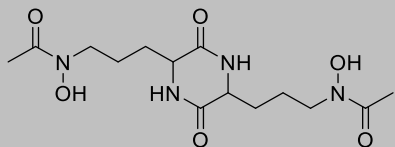
25.0

**EDTA**

6

25.1

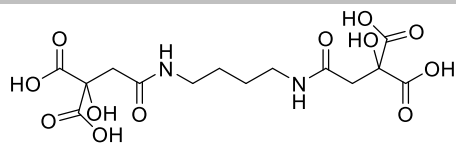
23.4

**Rhodotorulic acid**

4

31.2

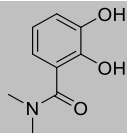
22.0



6

25.3

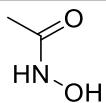
20.0

**Rhizoferrin**

2

40.2

15.0

**N,N-Dimethyl-2,3-dihydroxybenzene**

2

28.3

14.8

**Acetohydroxamic acid**

 <b>DFP</b>	2	37.2	19
<b>OH<sup>-</sup></b> <b>Hydroxide anion</b>	1	11.7	14.6

Interestingly, this denticity is not always found. Hider and co-workers have denoted an exception of this trend, which correlated the complex stability and the increased denticity.<sup>445</sup> Namely, it has been demonstrated that a hexadentate chelator containing a tripodal 3, 2-HOPO coordination unit; CP130 exhibited lower  $\log\beta$  value ( $\log\beta= 28.1$ ) when compared to the  $\log\beta$  value of its bidentate analogue 2-(3-hydroxy-2-oxo-1,2-dihydropyridin-1-yl) acetic acid ( $\log\beta= 32.5$ ) (**Figure 32**).<sup>445</sup>

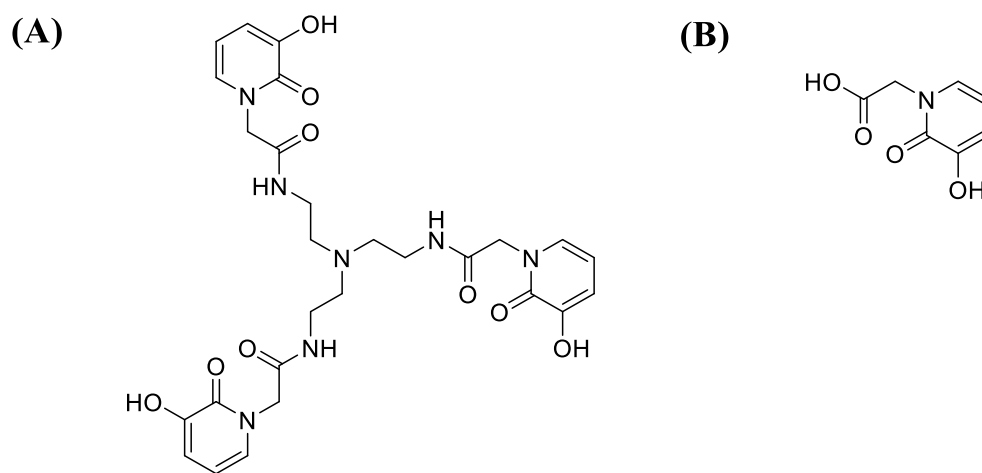
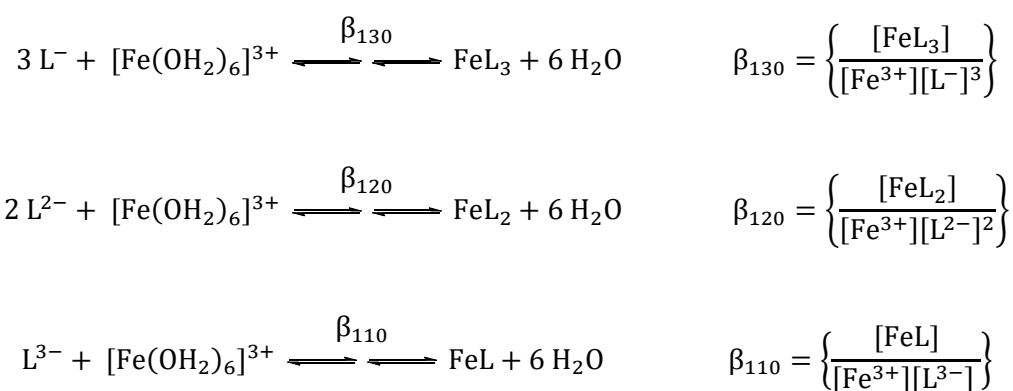


**Figure 32:** Structure of **(A)** CP130 and **(B)** 2-(3-hydroxy-2-oxo-1,2-dihydropyridin-1-yl) acetic acid.

This might be due to steric entropic effects.<sup>446</sup> Namely, the limited rotation of the amide bond might inhibit the Fe(III) coordination. In contrast, 2-(3-hydroxy-2-oxo-1,2-dihydropyridin-1-yl) acetic acid which lacks the amide bond can access to Fe(III) centre much more easily. Hence, apart from the coordination group, the skeletal backbone and the linker are important factors for biological functions.<sup>446</sup>

A concentration effect is also apparent when we consider different denticities of ligands and those of higher denticity are favoured (**Scheme 5**).<sup>447</sup>



**Scheme 5:** Equations displaying the equilibrium constants for bi-, tri- and hexadentate Fe<sup>3+</sup>- ligand complexation.

Namely, it is expected that the increased denticity of hexadentate ligand reduced the concentration of ligand required for complete Fe(III) coordination, whereas higher ligand concentration is required in the case of bidentate ligands to achieve Fe(III) saturation. As a consequence of this, the iron-hexadentate ligand complex pFe<sup>3+</sup> it is expected to be higher than the respective complexation constant of a bidentate ligand-iron complex.

In the case of PD we aimed to inhibit the redox cycling by increasing the concentration of Fe(III)L<sub>3</sub> in the brain i.e. the full coordination of Fe(III). It has been previously shown that labile ligands on Fe(III) are required for the production of hydroxyl radicals via the hydrogen peroxide redox

cycling.<sup>435</sup> The authors, provided evidences that at least one free coordination site in the iron centre is required for the generation of hydroxyl radicals from hydrogen peroxide. Moreover, the availability of a free coordination site (upon EDTA or DTPA binding) (or a site that is occupied by easily displaceable ligands – water) facilitates the reduction of Fe(III) by superoxyl radicals. Even if the ligand is hexadentate, full saturation is not guaranteed as shown in **Figure 33**.<sup>435</sup>

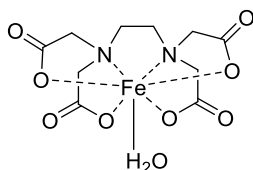


**Figure 33:** EDTA-Fe(III) complexation allows a free binding site.

Despite the various advantage of hexadentate ligands, the dioxygenated bidentate ligands have been utilised in this study. This is mainly because, hexadentate ligands exhibit high molecular weights >500 Da making them not appropriate lead candidates for orally bioavailable drugs.<sup>418</sup>

On the other hand the synthesis of tridentate ligand with only oxygen anion coordination sites is not feasible for HOPOs. Even if an extra hydroxyl group employed in the pyridinone core, will cause distortion of the geometry of the coordinated complex by forming macrocyclic rings, which are thermodynamically unstable (**Figure 34**).

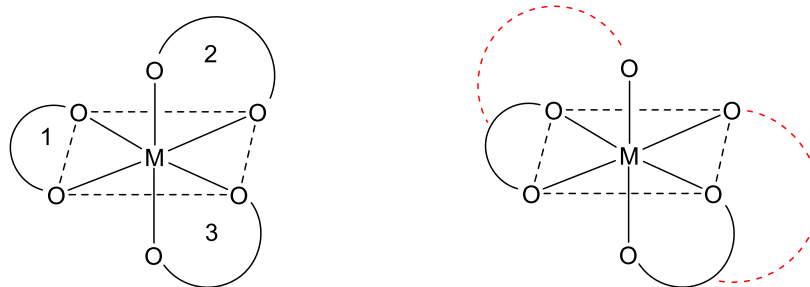


**Figure 34:** (A)Schematic representation of chelate ring formation in metal-bidentate ligand complex (B) formation of thermodynamically unstable macrocycle by a tri-oxygen tridentate ligand.

Therefore, tridentate ligands typically contained nitrogen atoms at the coordination sites (**Figure 35**).<sup>448</sup>

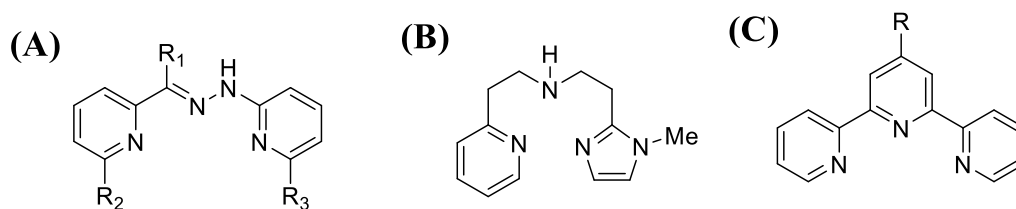
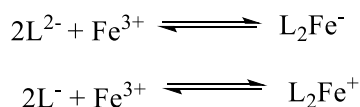


**Figure 35:** Selected nitrogenous tridentate ligands. (A) 2-substituted-6-[(Z)-substituted [2-(6-substituted pyridin-2-yl)hydrazin-1-ylidene]methyl]pyridine<sup>449</sup> (B) [2-(1-methyl-1H-imidazol-2-yl)ethyl][2-(pyridin-2-yl)ethyl]amine<sup>450</sup> and (C) 6-(pyridin-2-yl)-4-substituted 2,2'-bipyridine<sup>451</sup>.

Furthermore, the presence of nitrogen atoms in the coordination spheres is associated with cytotoxicity since; it reduced the selectivity of Fe(III) over Zn(II).<sup>452</sup> In addition issue that is arisen from the use of tridentate ligands is that they can formed charged complexes with Fe(III) which is an undesirable feature for the efficient Fe extraction from intracellular sites (**Scheme 6**).<sup>418</sup>



**Scheme 6:** Formation of charged Fe(III) complexes with tridentate ligands.

Finally, it has been demonstrated that tridentate ligands can generate complexes which are more susceptible towards redox cycling and ROS formation.<sup>453</sup>

## 2.8 Pharmaco–physicochemical parameters

The exact link between chemical structure and various biological and pharmacological activity is usually extremely difficult to establish. This is due to the complex influence of primary mode of action (e.g. metal chelation in this case) with need for low toxicity, stability towards metabolic transformations, systemic distribution. The ability of the molecule to cross the BBB, penetrate

inside neuron, distribute in the neuron and general pharmacokinetics will be influenced by  $pK_a$ ,  $\log P$ , number of H-bond donor and acceptors. The biological activity will be largely influenced by the following physicochemical parameters that can be somewhat controlled/studied in our case

### 2.8.1 Lipophilicity and molecular weight

An important property for an orally active iron chelator is its ability to be efficiently absorbed by the gastrointestinal tract and cross through the biological membranes in order to reach the desired sites (eg brain in the case of PD or lymph nodes in the case of a metastatic cancer). The major factors that can affect the ability of the compounds to freely permeate a bilipid membrane are the molecular weight, the ionisation state and eventually the lipophilicity. It has suggested that the partition coefficient ( $C_{logP}$ ) of a molecule should be  $>-1$  in order to penetrate the gastrointestinal tract, whereas highly lipid soluble chelators can diffuse through the BBB and placental barriers potentially causing toxic side effects.<sup>454</sup> The anticipated optimal  $\log P$  for an ideal iron chelator, clearly indicates that there is no single compound that fulfil these criteria since the ideal  $\log P$  for the gastrointestinal tract differ for the optimal value for access to brain and placenta (Table 6).<sup>418</sup>

**Table 6:** Anticipated optimal  $\log P$  of an ideal chelator.<sup>418</sup>

	$\log P$
Good absorption from the gastrointestinal tract	$> -1$
Efficient liver extraction	$> 0$
Poor entry into peripheral cells (thymus, muscles, heart, bone marrow)	$< -3$
Poor ability to penetrate the BBB and maternal/placental barriers	$< -3$

Hider and co-workers shown before that some lipophilic HOPOs manage to enter the BBB whereas via passive diffusion.<sup>455</sup>

The permeability across the biological membranes is also affected by the ionic states of the compounds as uncharged molecules can penetrate faster compared to the charged ones.<sup>418</sup>

Finally, the molecular weight is a crucial factor for the effective transportation and absorption of the chelator.<sup>418,456</sup> Generally, it has been stated that passive diffusion is mainly followed by drugs with molecular weight > 200, whereas the ‘cut-off’ molecular weight value for the paracellular in the human small intestine is ~ 400 and thus is not quantitatively important for drugs with molecular weight > 200. In contrast, the penetration of compounds with molecular weight > 500 falls rapidly as indicated by PEG permeability.<sup>457,458</sup> Furthermore, it was recommended that the molecular weight of a chelator should be >300 for a ~70% absorption.<sup>457</sup> The limited range of molecular weights excludes therefore, the use of hexadentate chelators as orally available drugs. Interestingly, it was found the EDTA (as a hexadentate ligand) with molecular weight 292 (too small to fully encompass the chelated iron) promoted the toxicity of the metal possibly by promoting Fenton chemistry.<sup>459</sup> On the contrary, bidentate chelators have significantly lower molecular weights and it has been proven before that 3, 4-HOPOs were absorbed between 50 and 70% in rabbit.<sup>460</sup>

### **2.8.2 Protonation constants**

If the  $pK_a$  of the acidic groups (-OH, -CO<sub>2</sub>H) is too low, or the  $pK_a$  of conjugate acid of the amine group too high, the molecule will be present in its ionic form at physiological pH. It is known that molecules in their ionic form are less likely to be drug-like and have poor cell penetration. Also, the overall charge of the compounds (associated with their lipophilicity as measured by  $\log P$ ) will likely influence their distribution in the cell’s organelle. The amino-acid moiety is expected to be in the zwitterion form. However, that should not be an issue as it has been previously demonstrated that gut contains amino acid sensing receptors and transporters in order to supply the organism with nutrients.<sup>461</sup> Moreover The form taken by the coordinating hydroxyl group is unknown until  $pK_a$  values are determined. The  $pK_a$  will also influence the efficacy of metal chelation via the

$pFe^{3+}$ . Therefore, the  $pK_a$  will have a complex influence on cell penetration, cell distribution and metal chelation.

### 2.8.3 Stability constants

$\beta_{130}(Fe^{3+})$  and  $\beta_{130}(Fe^{2+})$ : The stability constant for coordination of Fe(III) will influence the affinity of the compound to efficiently coordinate iron at low concentration (together with  $pK_a$ ) as it critically influences the  $pFe^{3+}$ . The aim is to reach a  $pFe^{3+}$  value that is high enough to make the dose-response pharmacologically relevant but not too high as there are then risks of demetallation/inhibition of essential metallo-enzymes as it was previously proven.<sup>462-464</sup> Furthermore,  $\beta$  values for other biologically relevant metals will have an impact on dose response, safety, distribution and overall metal redox-silencing.

### 2.8.4 Partition coefficient

A Lipinski rule of 5, the molecule must not be too hydrophilic to be able to penetrate cells (this is linked to the  $pK_a$  and existence of atoms with high electronegativity like N and O). The  $\log P$  is also likely as mentioned to influence the distribution of the compounds in the cell's organelles.

### 2.8.5 Lipinski's rule

The synthesised compounds should pose some essential characteristics in order to make them orally bioavailable drug candidate. Namely, the structure of the synthesised compounds should contain  $\leq 10$  hydrogen bonds acceptor and  $\leq 5$  hydrogen bond donor elements. In addition to this, the molecular weight should be maintained below 500.

### 3 Rational LAT-1 substrate design

#### 3.1 LAT-1 active site

For the design and synthesis of molecules that would be capable of being transported across the BBB, exploiting the LAT-1 active mechanism the substrate-binding site was studied. Initially, Uchino and co-workers, suggested that both amino- and carboxylate group of the substrate should be in the zwitterion form.<sup>465</sup> This is because, it has been proposed that LAT-1 transporter contains specific recognition sites in the peptide backbone that mediates the binding of charged head groups of amino acids through electronic interactions. Therefore, a LAT-1 substrate should contain a free  $\alpha$ -carboxylated group, an unsubstituted  $\alpha$ -amino group. Interestingly, either a hydrogen or a methyl group can be present on the  $C_{\alpha}$ . Furthermore, the binding of the substrate in the active site is mediated by hydrophobic residues (F252, C335, S342, C407) denoting the need of lipophilic side chain in order to be able to fit in this zone (**Figure 36**).<sup>466</sup>

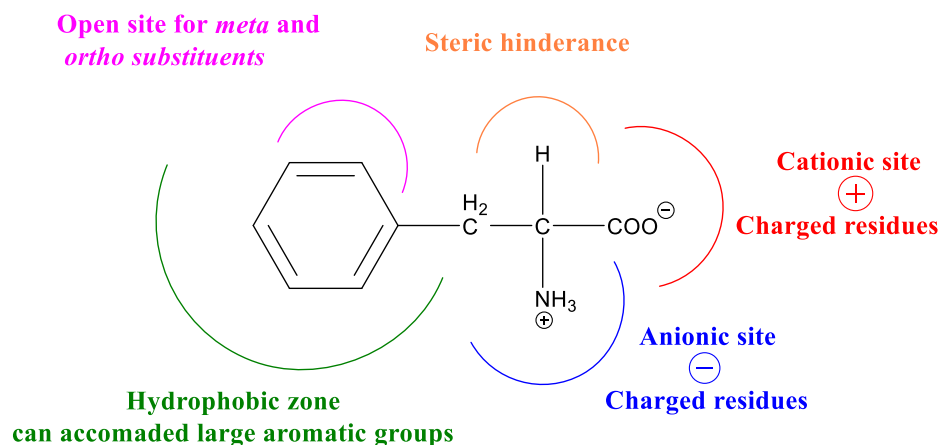


**Figure 36:** The essential features of the binding site of LAT-1 in relation to the amino acid phenylalanine.

### 3.2 Interactions of the amino acid group.

In an *in silico* study, where a model of arginine bound to AdiC active site has been employed, the  $\alpha$ -amino group of arginine (as hydrogen bond donor) interactions with the TM1 and TM6 by forming hydrogen bonds with the backbone oxygen atom of I23, W202 and I205.<sup>272</sup> In addition to this, the  $\alpha$ -amino group seems to contribute in a cation- $\pi$  interaction with the indole ring of W202.<sup>467</sup> On the other hand, the  $\alpha$ -carboxyl group (as hydrogen bond acceptor) accepted two hydrogen bonds from S26 and G27 at the TM1 site (Figure 37).<sup>467</sup>

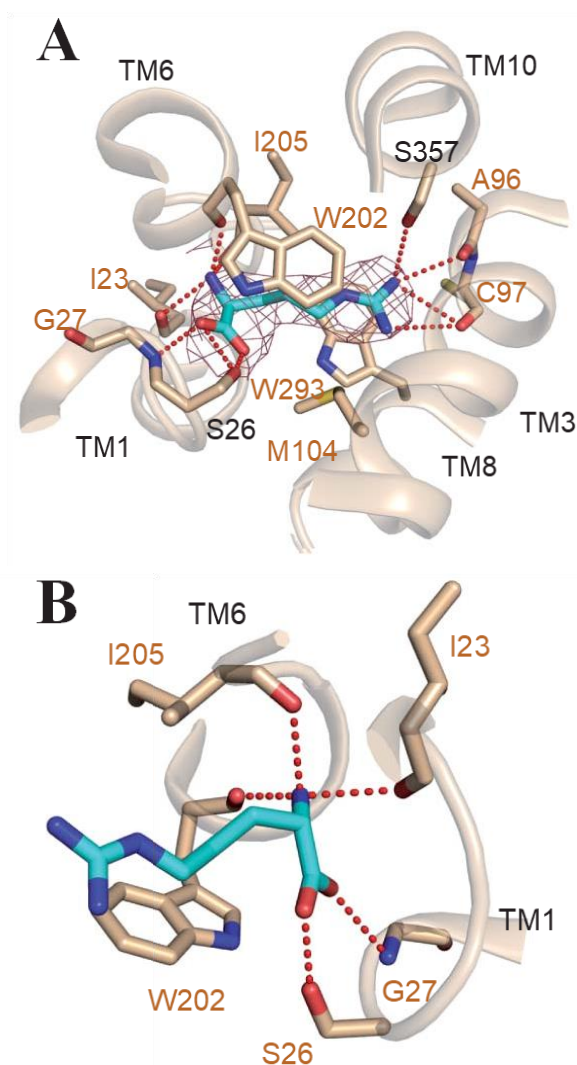


**Figure 37:** (A) Arginine is bound at the active site of ‘putative LAT-1’ forming interactions with TM1, TM3, TM6, TM8 and TM10. (B) The amino group donates three hydrogen bonds whereas the carboxylic group accepts two hydrogen bonds.<sup>467</sup>

In contrast, the respective residues that interacted with phenylalanine in LAT-1 include I63 (TM1), F252 (TM6) and G255 (TM6) (by accepting hydrogen bonds from the  $\alpha$ -amino group) and S66, G67 (TM1) (by donating hydrogen bonds to  $\alpha$ -carboxyl group) (**Figure 38**).<sup>272</sup>

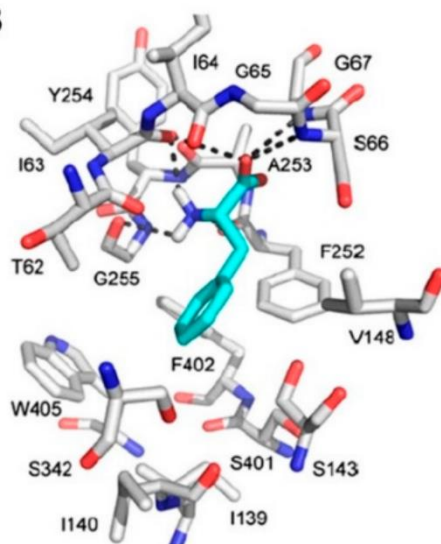


**Figure 38:** Predicted binding of Phenylalanine in ‘putative LAT-1’ active site.<sup>272</sup>

In another study, it has been shown that the residues F252, C335, S342 and C407 are mediating the binding of histidine in the active site of the transporter.<sup>468</sup> However, it was suggested that since the  $\alpha$ -amino and  $\alpha$ -carboxyl group are conserved among the LAT-1 substrates it has been assumed that most of the compounds will display a similar binding mode.<sup>468</sup>

### 3.3 Pharmacophore design

For the determination of the ‘ideal’ pharmacophore, Ylikangas and co-worker generated a small library of LAT-1 substrates with various side chains.<sup>469</sup> The pharmacophore was designed based

on four features including hydrogen bond donor, hydrogen bond acceptor negative charge and aromatic ring (**Figure 39**).<sup>469</sup>

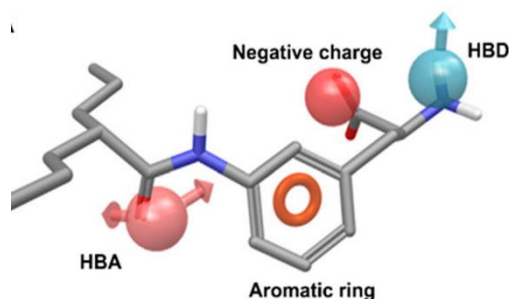


**Figure 39:** 3D pharmacophore model for LAT-1 with four features; hydrogen bond donor/acceptor, aromatic ring and negative charge.<sup>469</sup>

The structure activity relationship (SAR) of the substrates suggested that the present of negatively charged features, as well as moieties capable to donate hydrogen bonds were essential for good activity since their removal or modification resulted in a weaker affinity (or completely lost of affinity) for LAT-1 binding.<sup>469</sup> In addition to this, it has been proven that the present of aromatic (planar) rings in the compounds were preferred towards the ligand affinity compared to the equally lipophilic non-planar cores. Moreover, the introduction of hydrogen bond acceptor groups follow the aromatic region demonstrated an improve substrate binding in LAT-1 active site.<sup>469</sup> In another study 3D-Quantitative SAR (3D-QSAR) was performed in 39 substrates using classical and topomer comparative molecular field analysis (CoMFA).<sup>470,471</sup> The outcome of this analysis was that the contribution of steric interactions was stronger than the electrostatic once in two tomomers; R1: amino acid group, R2: side chain, prodrug and parent drug) (**Figure 40**).<sup>470,471</sup>



**Figure 40:** CoMFA model for LAT-1. Green and red represent areas where adding steric features and negative charge or hydrogen bond acceptors are favoured, respectively. Blue represents areas where a more positive charge or hydrogen bond donors are preferred, whereas yellow contours designate sterically disfavoured regions. R1 and R2 indicate the common core, amino acid function and variable topomer, side chain and parent drug.<sup>470,471</sup>

Through this model it was revealed that the addition of steric features above the aromatic core and below the amino acid terminal (yellow contour in R1) decrease the affinity. In contrast, by increasing the positive charge near the amino group (blue contour in R1) and by adding negatively charged moieties closed to carboxylic acid (red contour in R1) can lead to an increase LAT-1 affinity.<sup>470,471</sup> In addition to this, the model suggested that the moiety for the design of prodrugs should be relatively planar as large branched substituent can reach areas that can lower the affinity (yellow contour in R2).<sup>470,471</sup> Therefore, the addition of steric groups near the 5- and 6- position of *L*-tryptophan is favourable for ligand binding as depicted by the green contour in R2. These position are equivalent to the 3- and 4- position of phenylalanine.<sup>470,471</sup> Considering this substituent pattern, the cytotoxicity of the three structural analogues of the alkylating phenylalanine mustards with a *bis*(2-chloroethyl) amine chain in *ortho*- (**Figure 41D**), *meta*- (**Figure 41A**) and *para*- (**Figure 41B**) positions has been assessed in a human neoplasm model.<sup>472-475</sup>

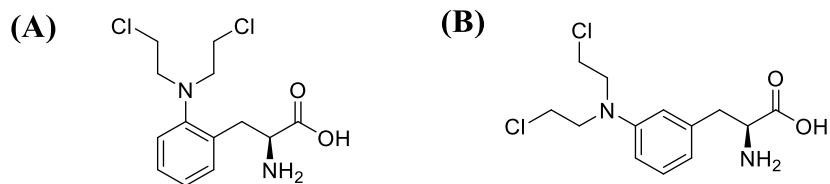


**Figure 41:** Structure of (A) *meta*- phenylalanine alkylating mustard and (B) *para*- phenylalanine alkylating mustard.

The results denoted that the *ortho*- substituted substrate was the most effective once (as it exhibits the highest  $IC_{50}$ ), whereas the *para* substituent shown the least activity.<sup>474</sup> These observations demonstrated a clear selectivity of the position that each pharmacophore should have in order to exploit LAT-1. Previously, Augustyn et al demonstrate that by adding lipophilic substituents in the planar pharmacophore can induced inhibition of LAT-1.<sup>476</sup> For example, compound 41 (**Figure 42A**) KYT-0353 (**Figure 42B**), KYT-0285 (**Figure 42C**), 3-([1,1'-biphenyl]-3-yl)-2-aminopropionic acid (**Figure 42D**), 2-amino-3-(3-benzylphenyl)propanoic acid (**Figure 42E**) were able to inhibit the [<sup>3</sup>H]-gabapentin uptake in HEK human LAT-1 cells.<sup>476-478</sup>

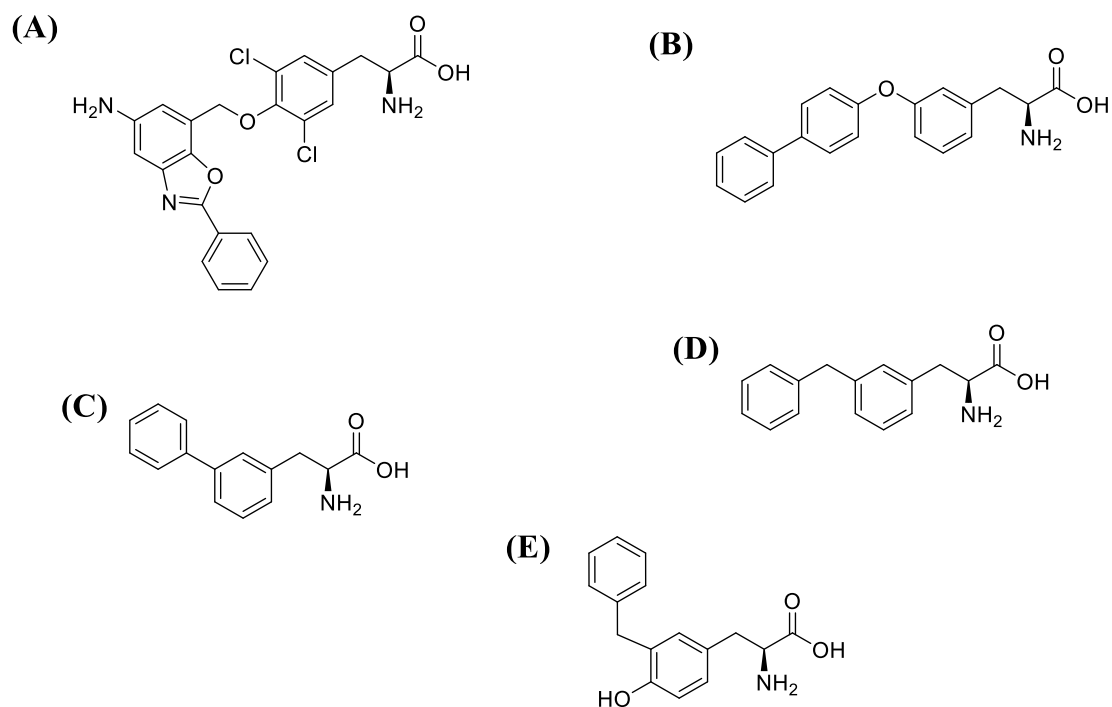


**Figure 42:** Structure of (A) compound 41, (B) KYT-0353, (C) KYT-0285, (D) 3-([1,1'-biphenyl]-3-yl)-2-aminopropionic acid and (E) 2-amino-3-(3-benzylphenyl)propanoic acid.<sup>476</sup>

Interestingly 3-([1,1'-biphenyl]-3-yl)-2-aminopropionic acid (**Figure 42D**) with a phenyl group at the *meta* position, prevented strongly the [<sup>14</sup>C]Phenylalanine uptake by LAT-1. The ortho and meta analogs of phenylalanine were found to be lesser active substrates relative to meta isomer.<sup>476</sup> SAR- guide computational modeling suggested that large lipophilic groups (such as phenyl group in 3-([1,1'-biphenyl]-3-yl)-2-aminopropionic acid) can increase the affinity towards the LAT-1 active site due to hydrophobic interactions that are developed with the subpocket PA.<sup>476</sup> However, the strong interactions resulted in decreased transport capacity (low  $V_{max}$ ). As a consequent of this, the compound behaves more like an inhibitor rather than a substrate. Similar observations have been seen with compounds; KYT-0353 (**Figure 42B**) 2-amino-3-(3-benzylphenyl)propanoic acid (**Figure 42E**).<sup>476</sup> Namely, the increase lipophilicity on both meta position developed strong interactions with the subpocket generating in that way strong inhibitors of LAT-1.<sup>476</sup> On the other hand, compound 41 has a large lipophilic group in the para position which can rotate around the

two flexible rotatable atoms (oxygen and -CH<sub>2</sub> group). As a result of the rotation, it can mimic the meta conformation and therefore it can acquire the same position in the subpocket and develop similar interactions.<sup>476</sup>

### 3.3.1 Side Chain design

Docking studies where thyroxine (T<sub>4</sub>) (**Figure 43A**), 3,3',5-triiodothyroxine (T<sub>3</sub>) (**Figure 43B**), Gabapentin (**Figure 43C**) and Melphanal (**Figure 43D**) have been used as substrates, demonstrate that the residues that are located near the helix break of TM1 (I63, S66 and G67) and TM6 (F252 and G255) are mainly responsible for the substrate binding through hydrogen bond interactions. On the other hand, it is assumed that residues I139, V148, F252, F252, F402 and W405 facilitate the binding of the site chain via hydrophobic interactions.<sup>468</sup>

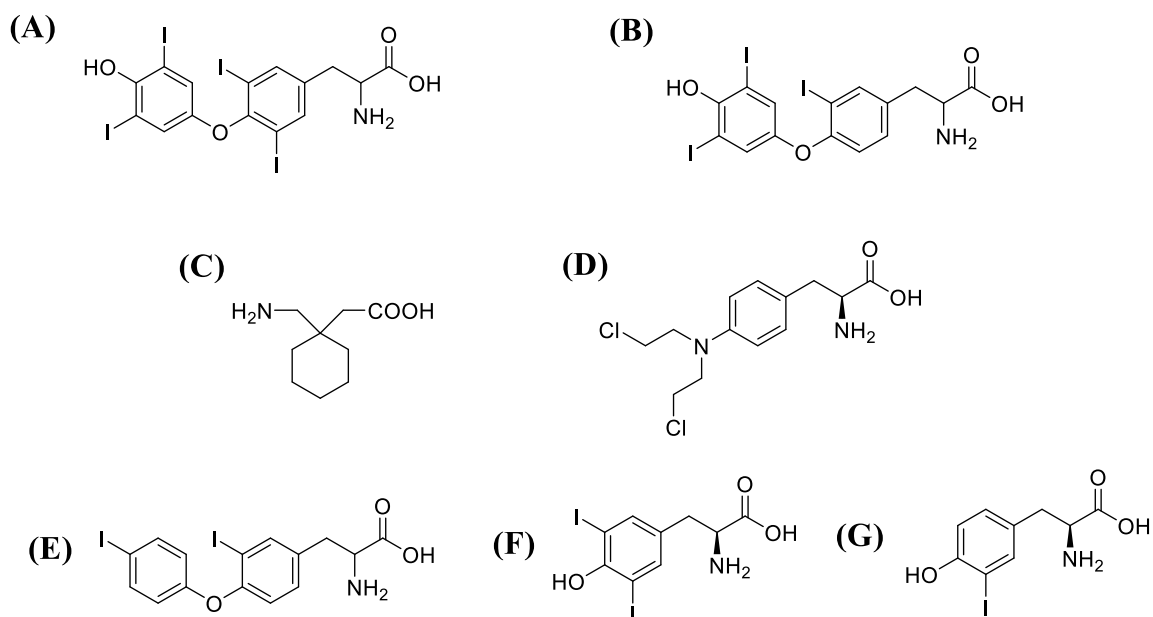


**Figure 43:** Structure of (A) Thyroxine (T<sub>4</sub>), (B) 3,3',5-triiodothyroxine (T<sub>3</sub>), (C) Gabapentin, (D) Melphanal, (E) 3,3'-diiodothyronine, (F) 3,5-diiodo-*L*-tyrosine and (G) 3-iodo-*L*-tyrosine.

Ligands, such as T<sub>4</sub> (**Figure 43A**), T<sub>3</sub> (**Figure 43B**), 3,3'-diiodothyronine (**Figure 43E**), 3,5-diiodo-*L*-tyrosine (**Figure 43F**) and 3-iodo-*L*-tyrosine (**Figure 43G**) might be involved in the halogen bond interaction of polarized halogens contributing substantially to the to the binding

affinity for LAT-1.<sup>477</sup> Moreover, the halogen bond is an electrostatic interaction where halogens can exhibit electropositive crown in the  $\sigma$ -hole, that acts as a Lewis acid with high affinity towards electron-rich Lewis bases (oxygen, nitrogen sulfur) in a similar manner as hydrogen bonds.<sup>479</sup> In addition to this, the ability of halogens to act as both halogen bond donors to carboxyl/carbonyl oxygen and aromatic  $\pi$ -systems in the direction of the  $\sigma$ -hole and hydrogen bond acceptor in the perpendicular direction.<sup>479,480</sup> These factors can explain why the active site of LAT-1 is not consisting only with aromatic residues which provide  $\pi$ -electrons, but it is also consist of polar residues (S143, N258, T345) contributing hydrogens for the hydrogen bond interaction.<sup>476</sup> Furthermore, the carboxyl group of E236 and the backbone oxygen of residues in LAT-1 may serve as halogen bond acceptor.<sup>476</sup>

It has been previously demonstrated that halogen substituents in the *meta* position of phenylalanine can also lead to either the formation of an excellent LAT-1 substrate or inhibitor depending on the size of the halogen.<sup>481</sup> In example, the addition of iodine in the *meta* position can lead to a powerful inhibitor whereas the addition of fluorine can generate a very potent LAT-1 substrate. This suggests that halogen substituted analogues might be developed higher affinity for halogen bonding increase in lipophilicity with halogen size of both.<sup>479,480</sup>

### 3.4 Lipophilicity of LAT-1 substrates

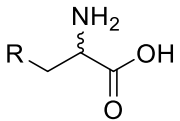
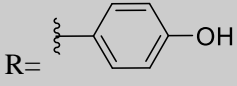
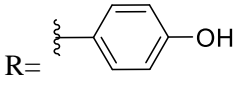
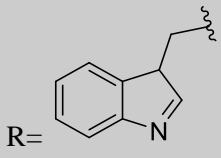
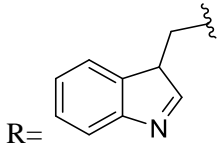
Another factor that should be taken into consideration during LAT-1 substrates design is the lipophilicity. In example, the LAT-1 affinity of phenylalanine, tyrosine, and *L*-DOPA varies with the number of phenolic hydroxyl groups in the aromatic ring and therefore the trend of affinity can be drawn as follow; *L*-DOPA (2 -OH) < *L*-Tyrosine (1 -OH) < Phenylalanine, with *L*-DOPA to behave more like an inhibitor rather than substrate.<sup>482,483</sup> The inhibitor constant (*K<sub>i</sub>*) trend (*L*-DOPA > *L*-tyrosine > phenylalanine) in in agreement with the *ClogP* values (determined by octanol/water method); 0.0984 > -0.0524 > -0.0498 demonstrating in that way that the lipophilicity is an important parameter for the binding of the side chain of LAT-1 substrates.<sup>482,483</sup> According

to the Connolly accessible surface area and Clog $P$  calculations for the studied compounds, authors concluded that a LAT-1 substrate becomes an inhibitor when its Connolly accessible surface becomes  $> 500 \text{ \AA}^2$  and/or has a calculated Clog $P > 2.0$  such as for melphanal (**Figure 43D**), T<sub>3</sub> (**Figure 43B**) and T<sub>4</sub> (**Figure 43A**).<sup>484</sup>

### 3.5 Stereochemistry of LAT-1 substrates

Since the amino acid moiety of the LAT-1 substrate contains a chiral centre, the effect of stereochemistry should also be taken into consideration during the design of LAT-1 substrates. To begin with, it has been reported that the LAT-1 transporter that is expressed in the BBB is a stereospecific transporter with the preference on *L*- enantiomeric amino acid.<sup>405</sup> This statement was confirmed by which they observed that the *L*- enantiomer of phenylalanine mustards exhibits a significantly higher cytotoxicity in an experimental model of human neoplasm compared to the respective *D*- enantiomer.<sup>472</sup> In addition to this, Schlessinger et al, demonstrated the inability of *D*- enantiomers to inhibit (i) the *L*- phenylalanine efflux and (ii) the LAT-1 transporter in general (**Table 7**).<sup>485</sup>

**Table 7:** The ability of selected amino acids with the side chain being in different stereochemistry to inhibit *L*-Phe uptake and LAT-1. <sup>485</sup>

		(%) <i>L</i> -Phe efflux	(%) Inhibition
<b><i>L</i>-Phe</b>		100	85
<b><i>D</i>-Phe</b>		96	74
<b><i>L</i>-Ala</b>	R = (CH <sub>3</sub> ) <sub>2</sub> CHCH <sub>2</sub> -	120	73
<b><i>D</i>-Ala</b>	R = (CH <sub>3</sub> ) <sub>2</sub> CHCH <sub>2</sub> -	100	56
<b><i>L</i>-Trp</b>		81	79
<b><i>D</i>-Trp</b>		59	29

On the other hand, others claimed that the stereochemistry is not necessarily a factor that should be taken into account since it has been proven that some *D*- amino acids can inhibit the [<sup>14</sup>C]-Leucine uptake. <sup>485-489</sup>

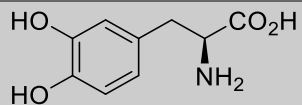
## 4 Scope of the study

The first aim of this study is associated with the design and synthesis of neuroprotective HOPOs iron derived chelators with the capability of transportation across the BBB in a similar manner to *L*-DOPA in order to prevent the Fe(III) redox cycling in the brain that is responsible for the development of PD by the excessive ROS formation. As it was stated previously, HOPOs are analogues of catechols; therefore, the compounds would be analogues of *L*-DOPA that will contain several of HOPO coordination group instead of catechol. In addition to this, our HOPOs will carry an amino acid vector that would be essential for the transportation across the BBB in the same manner as *L*-DOPA (**Table 8**).

**Table 8:** Structure of HOPO based chelators – analogues of *L*-DOPA- with the potential capability of transportation across the BBB.

---

**L-DOPA**



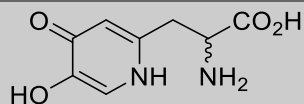
**1,2- HOPOs**



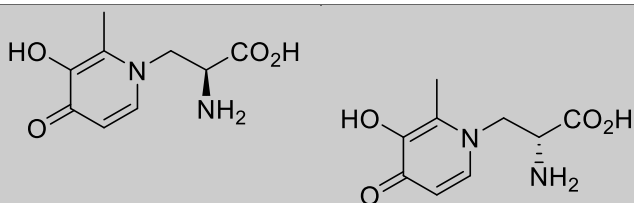
**3, 2- HOPOs**



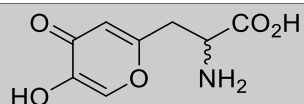
**3, 4- HOPO**



**N-substituted 3, 4-HOPOs**



**Hydroxypyranone**

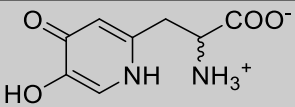
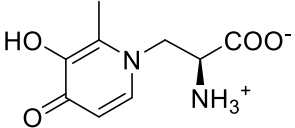
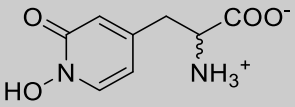
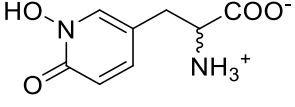
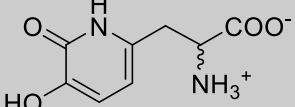
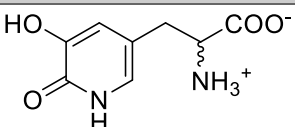


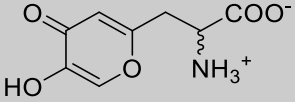
Of all the coordinating groups that appear suitable, there is not one of them that provides the optimum combination of structural features. We therefore had to investigate a library of compounds to select the lead candidate. The second aim was to evaluate whether, the synthesised compounds would have the potency to target the cancer cells and induced cytotoxicity once again

by minimising the essential for cancerous cell survival, ROS levels. Our proposed compounds can be regarded as the first HOPO derivatives specifically designed for LAT-1

The pharmacological properties of all the proposed compounds were also calculated in an attempt to rationalise the overall design (**Table 9**)

**Table 9:** Pharmacological properties calculated by SwissADME – Swiss Institute of Bioinformatics.

Compound	Molecular Weight	log <i>P</i>	TPSA (Å)	H-Bond donor	H-Bond acceptor
	198.18	-2.22	120.86	3	4
	212.20	-2.39	110.0	2	4
	198.18	-2.19	110.0	2	4
	198.18	-2.29	111.0	2	4
	198.18	-2.13	120.86	3	4
	198.18	-2.22	120.86	3	4

	199.16	-2.22	118.21	2	5
---	--------	-------	--------	---	---

According to (**Table 9**), all of the proposed compounds will exist as zwitterions and based on the predicted pharmaco-physicochemical properties, all of them fulfil Lipinski's rule of 5 apart from the  $\log P$  as the respective values were significantly below 5. Therefore, it is expected that these compounds will not be able to cross the BBB via diffusion. Additionally, as demonstrated in (**Table 6**), these chelators cannot be absorbed from the gastrointestinal tract (by diffusion – but possibly can be absorbed due to the presence of amino acid receptors/channels in the GI) as the  $\log P < -1$ . However, the proposed chelators can potentially penetrate the BBB as the corresponding  $\log P > -3$ .

## 5 Organic synthesis of the target molecules and control compounds

During the last years, much work has been conducted towards the development of the chemistry associated with the synthesis, functionalisation and characterisation of the physicochemical parameters of the HOPO coordinating group.

### 5.1 1, 2- HOPOs

The chemistry of 1, 2-HOPO is overall undeveloped in terms of variety and accessibility of the functionalities currently been available as previously published in tetra-, hexa- and octadentate chelate literature. The synthesis of the 1, 2- HOPOs mainly relies into two synthetic approaches (**Figure 44**).

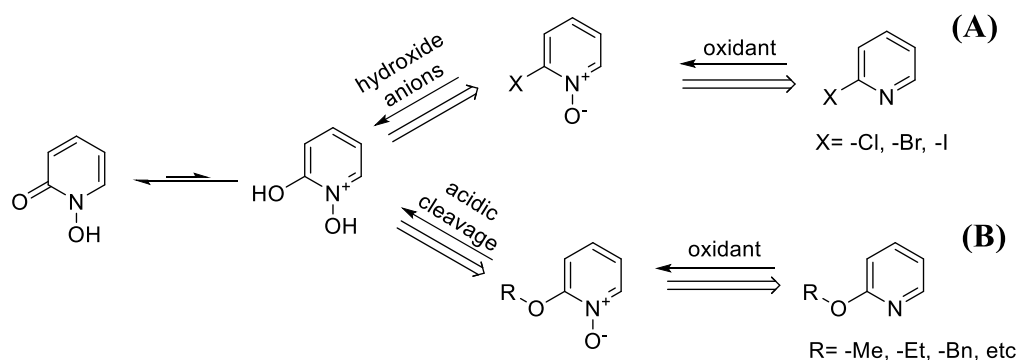


**Figure 44:** The two synthetic approaches for the synthesis of 1, 2- HOPOs

The first strategy involves the *N*-oxidation of the 2-halogenated pyridine and afterwards the substitution of the halogen atom with hydroxides (**Figure 44A**). The second approach involves the participation of a 2-alkoxy substituted pyridine. The *N*-oxidation of this starting material leads to the formation of a 2-*O*-protected *N*-oxide pyridine intermediate which its deprotection (mainly) under acidic conditions gives the pyridone (**Figure 44B**) The expected product in both cases predominates as 1, 2-hydroxypyridone rather than 1,2-dihydroxypyridine.

## 5.2 Synthesis of the amino acid moiety

The synthesis of unnatural amino acid is widely report into the literature. Herein, the most common ways of synthesising amino acids were described. One of the most abundant method for synthesising an amino acid is using the Strecker reaction (**Figure 45**).<sup>490</sup>

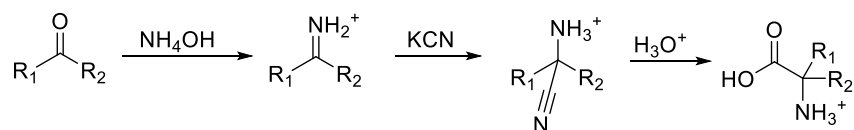


**Figure 45:** Strecker amino acid synthesis.<sup>490</sup>

According to this procedure, the first step involves the condensation of an aldehyde or a ketone with ammonia or (substituted amine) towards the formation of an imine.<sup>491</sup> Afterwards, nucleophilic substitution of the cyanide salt with the imine can lead to the formation of versatile  $\alpha$ -aminonitrile intermediates. Eventually, treatment of the  $\alpha$ -aminonitrile with acidic aqueous solution could afford the  $\alpha$ -amino acid as a racemic mixture.<sup>491</sup>

The synthesis of amino acids can be also be achieved by applying a modified version of Strecker synthesis which involves the synthesis of hydantoins as amino acid precursors (**Figure 46**).<sup>492,493</sup>

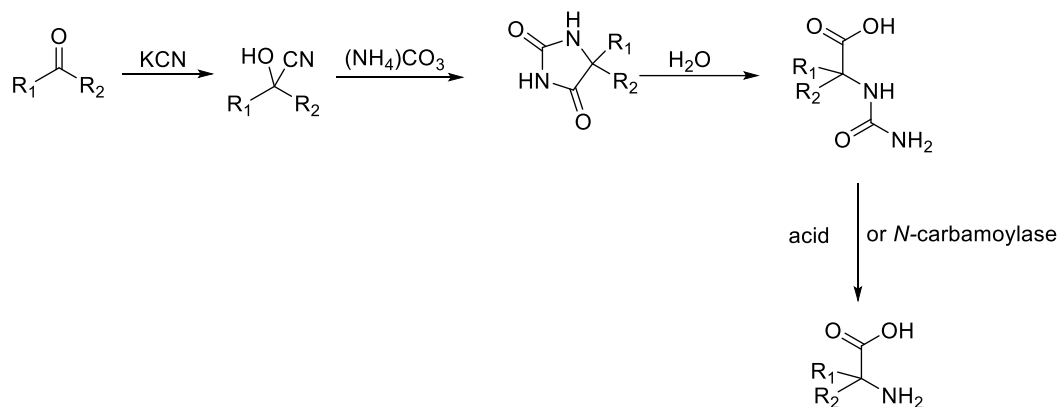


**Figure 46:** Bucherer-Bergs amino acids synthesis.<sup>494</sup>

According to this reaction an aldehyde or a ketone can react with potassium cyanide in order to form a cyanohydrin which in the presence of ammonium carbonate it is cyclised into the corresponding hydantoin.<sup>492-494</sup> Hydrolytic ring opening of the hydantoin core can lead to the formation of *N*-carbamoyl amino acid which in the presence of acid or an appropriate enzyme (*N*-carbamoylase) can yield to racemic amino acid mixture.<sup>492-494</sup> The overall pathway is known as Bucherer-Bergs reaction.

It has been previously reported that an alternative method for synthesising  $\alpha$ - amino acids can be achieved by using a Gabriel synthesis.<sup>495</sup> According to this methodology, alkyl halides react with phthalimide core and the formed intermediate can then be deprotonated and substituted with the alkyl or aryl halide. Alkaline hydrolysis of this intermediate can cause the elimination of the amino acid precursor as a dicarboxylate intermediate which after heat in the presence of acid it can be mono-decarboxylated eliminating the amino acid as a racemic mixture (**Figure 47**).<sup>495</sup>

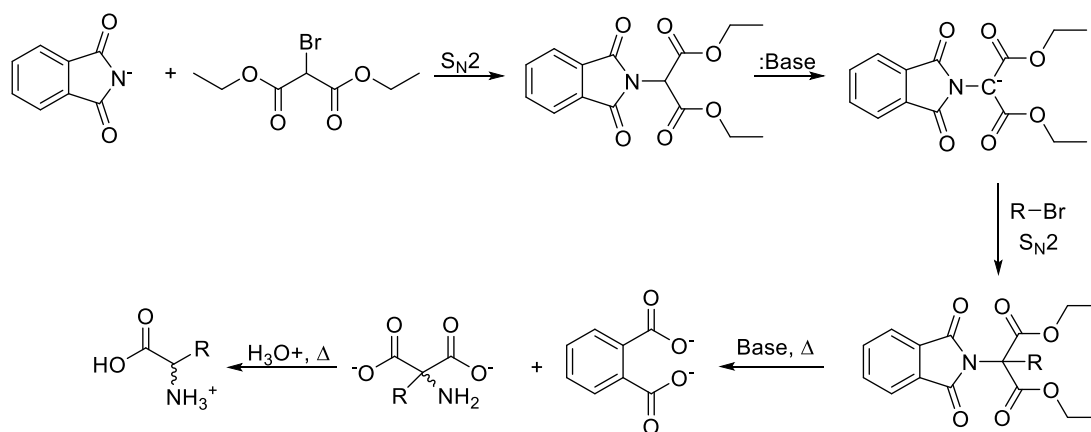


**Figure 47:** Gabriel Synthesis of amino acids.<sup>495</sup>

Another way of introducing an amino acid synthesis involved the condensation of a substituted (aromatic) aldehyde with glycine anhydride (diketopiperazine) and sodium acetate in acetic anhydride (**Figure 48**).<sup>496</sup>

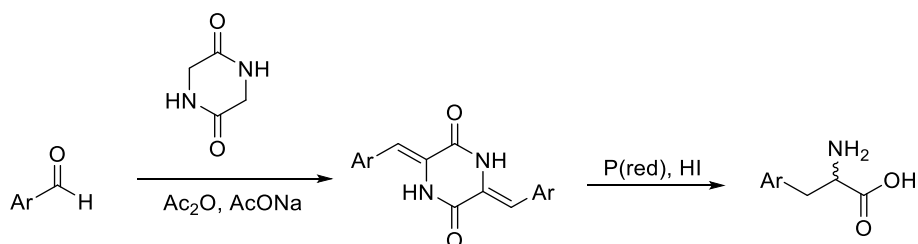


**Figure 48:** Synthesis of amino acids via the formation of aldehyde-glycine anhydride intermediate.

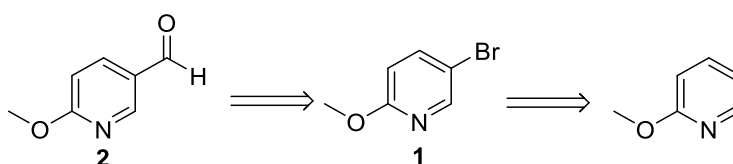
The formed intermediate was then reduced to the corresponding amino acid in the presence of phosphorus red, hydriodic acid.<sup>496</sup>

The synthesis of amino acids in the following chapter afforded the final products as racemic mixtures (unless the starting material was available as pure enantiomer). Racemic mixture resolution was performed if the compound presents any biological activity towards melanoma cancer and/or PD.

### 5.2.1 Synthesis of *rac*-SK-3

Reports regarding the synthesis of HOPO carrying an amino acid functionality have been previously established by Harris in attempt to synthesised analogues of *L*-mimosine in order to minimise its toxicity which has shown to act as a de-fleecing agent.<sup>497,498</sup>

The synthesis of novel 5-substituted 1, 2-HOPO, was initiated primarily by constructing the amino acid functionality prior to the coordinating group. Moreover, the synthetic procedures that have been followed for the introduction of amino acid moiety involved the participation of aldehyde as a precursor hence, the first part of the synthesis aimed to the formation of such intermediate (**Scheme 7**).

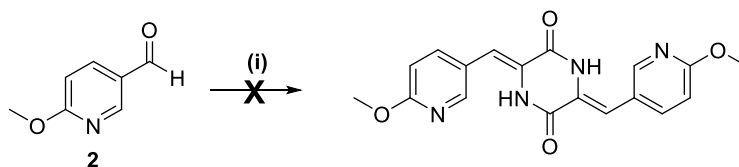


**Scheme 7:** Retrosynthetic approach for the synthesis of 2-methoxy-5-pyridine carbaldehyde (**2**).

The synthesis was initiated by the bromination of 2-methoxypyridine at the 5- position. It has been previously reported in the literature, that the bromination reaction of the substituted pyridine can be achieved by the addition of bromine in acetic acid solution containing the substrate and sodium acetate.<sup>499</sup> However, this approach is known to lead to the formation of both 3- and 5- brominated intermediates and that their separation could not be performed.<sup>499</sup> Therefore, the bromination reaction was performed using *N*-bromosuccinimide as a source of electrophilic bromine and the reaction proceed affording exclusively the brominated intermediate (**1**) which was purified by column chromatography. However, in our hands the yield of the reaction was significantly lower (18%) compared to what others obtain.<sup>500</sup> Afterwards, intermediate (**1**) underwent formylation reaction as it was previously described in the literature with some modifications.<sup>500</sup> The addition

of *n*-BuLi in a solution of (**1**) in dry diethyl ether led to the formation of organolithium which was then reacted further with *N,N*-dimethylformamide in order to introduce the carbonyl functional group. Elimination of dimethylamine led to the formation of aldehyde (**2**) as yellow crystals which were purified by column chromatography.

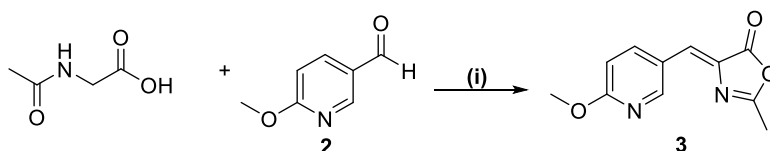
Initially, for the introduction of the amino acid functionality, the experimental method described by Kunishima M. *et al.* using glycine anhydride was followed.<sup>496</sup> However, the first part of the reaction where the aldehyde (**2**) reacted with glycine anhydride in the presence of sodium acetate and acetic anhydride failed to produce the expected intermediate (as mixture of *E/E*, *E/Z* and *Z/Z* isomers) even after several attempts to repeat the reaction varying the stoichiometry of the reactants, the temperature as well as the time of the reaction (**Scheme 8**).



**Scheme 8:** Attempted synthetic approach for the introduction of the amino acid functionality.

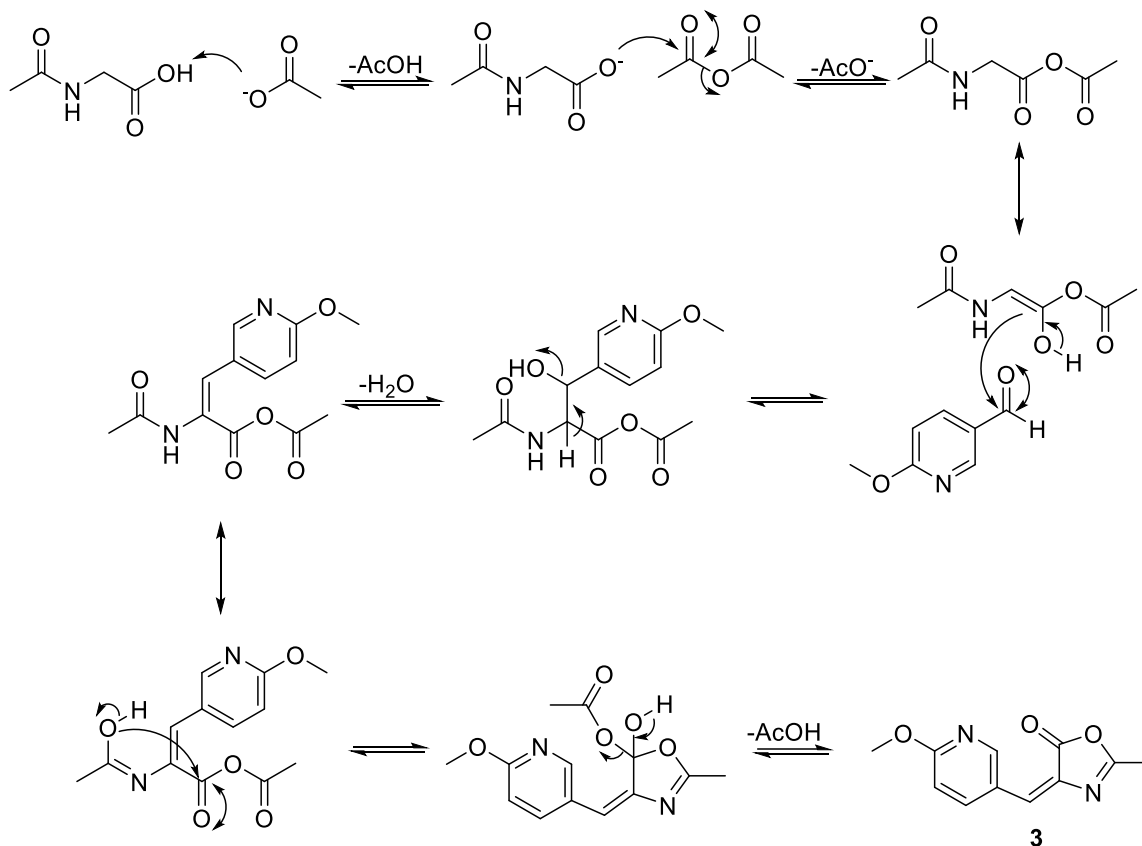
Reagents and conditions; (i) glycine anhydride, AcONa, Ac<sub>2</sub>O reflux, 6 hr.

Therefore, in order to overcome this issue, a slightly different approach was followed. For the introduction of the amino acid functionality we followed the Erlenmeyer's azalactone synthesis by reacting (**2**) with *N*-acetyl glycine, sodium acetate and refluxed in acetic anhydride as it was previously described (**Scheme 9**).<sup>501-503</sup>



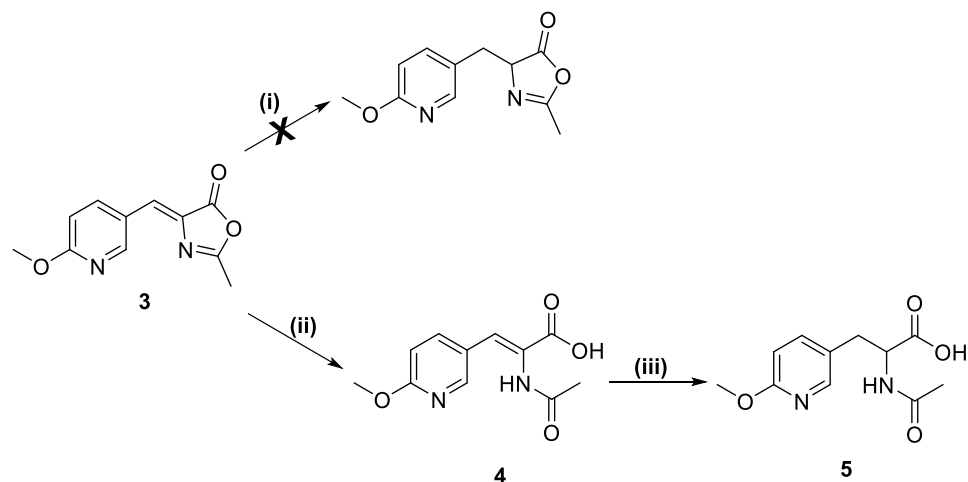
**Scheme 9:** Reagents and conditions for the synthesis of azalactone intermediate (**3**); (i) Ac<sub>2</sub>O, AcONa, reflux, 7 hr, 63%.

The cyclisation reaction that took place led to the formation of an azalactone intermediate **3** that was precipitated out by the hydrolysis of acetic anhydride in the presence of ice, as a yellow solid which was purified by recrystallization from methanol (**Scheme 10**).



**Scheme 10:** Proposed mechanism for the formation of the azalactone intermediate.

An attempt to reduce the synthesised alkene prior to hydrolytic ring opening of the azalactone was contacted by bubbling H<sub>2</sub> gas in a solution of (**3**) containing a catalytic amount of Pd/C (10%) (**Scheme 11**). The expected reduced product has not been formed and the starting material was almost fully recovered. Attempts to allow the reaction to proceed for longer with a slight increase of the reaction temperature were conducted, however, TLC shown almost exclusively the existence of the starting material.



**Scheme 11:** Unsuccessful reduction of the alkene (**3**) prior to hydrolysis of azalactone. Reagents and conditions: (i) H<sub>2</sub>(g), Pd/C (10%), MeOH, RT, 6 hr; (ii) See **Table 10**; same as (i), 53%

Therefore, hydrolysis of the azalactone ring before reduction (**Scheme 11**) was attempted using various conditions that were reported in the literature with some modifications (**Table 10**).

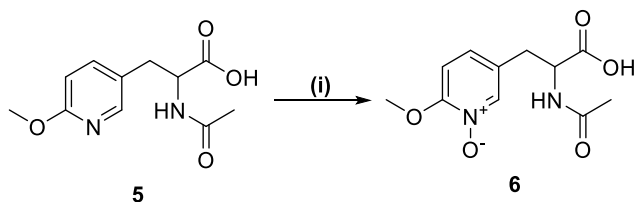
**Table 10:** Various experimental conditions towards the hydrolysis of azalactone (**3**)

Conditions <sup>[a]</sup>			Yield (%)
Water <sup>504</sup>	Reflux	4 hr	81
Acetone/ water <sup>505</sup>	Reflux	9 hr	60
HCl <sub>aq</sub> (5% v/v) <sup>506</sup>	RT	18 hr	No reaction
HCl <sub>aq</sub> (5% v/v) <sup>506</sup>	Reflux	18 hr	10
MeOH/ NaOH <sup>507</sup>	RT	2 hr	92

<sup>[a]</sup> Based upon literature procedure upon some modifications.

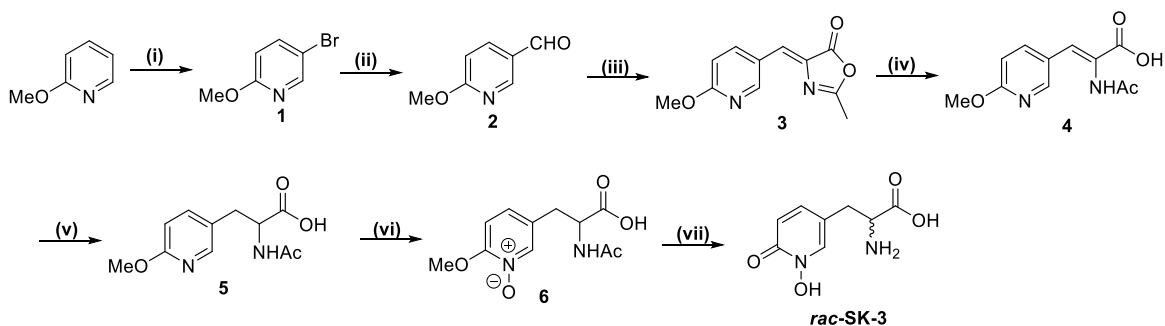
As it can be observed from **Table 10** the alkali hydrolysis of the azalactone afforded intermediate (**4**) as a pale brown crystals that was precipitated by acidification of the MeOH/NaOH mixture to pH ~1. Afterwards, the reduction of the alkene was conducted successfully in methanol solution containing a catalytic amount of Pd/C (10%), under hydrogen atmosphere (**Scheme 11**). The crude product was purified by column chromatography affording intermediate (**5**) as a pale yellow oil

which solidified on standing. Afterwards the HOPO core had to be formed and for this purpose, intermediate (**5**) underwent *N*-oxidation using *m*-CPBA (**Scheme 12**).



**Scheme 12:** Reagents and conditions for the synthesis of *N*-oxide intermediate (**6**); (i) *m*-CPBA, MeOH, DCM, RT, 48 hr, 77%.

Due to the poor solubility of the starting material in dichloromethane, a small volume of methanol was added and the overall reaction mixture as stirred at RT for 48 hrs. The unreacted *m*CPBA as well as the by-product; *m*-CBA were removed by trituration of the crude product in diethyl ether, causing in that way the precipitation of the *N*-oxidised intermediate (**6**). The formation of the *N*-oxide was verified by the change of the chemical shift in both <sup>1</sup>H and <sup>13</sup>C-NMR as well as the change of mass as denoted by HRMS. Eventually, reflux of the intermediate (**6**) in conc. HCl caused the demethylation of the methyl ether and also the deprotection of the amine group by cleavage of the acetyl group, affording the final product racemic product as a hydroscopic HCl salt. The overall pathway that followed can be found in **Scheme 13**.

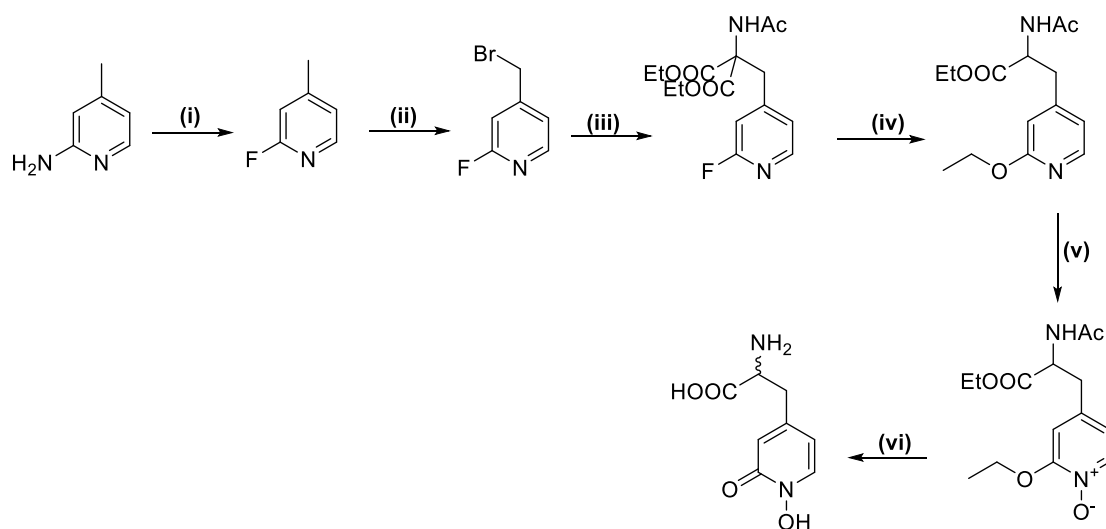


**Scheme 13:** Reagents and conditions for the synthesis of *rac*-SK-3. (i) NBS, CH<sub>3</sub>CN, 90°C, 2 hr, 18%; (ii) *n*-BuLi, Et<sub>2</sub>O, DMF<sub>dry</sub>, -35°C, 7 hr, 67%; (iii) *N*-acetyl glycine, AcONa, Ac<sub>2</sub>O, 130°C, 4

hr, 63%; (iv) *see Table 10*; (v) H<sub>2</sub>, Pd/ C (10%), MeOH, RT, 9 hr, 53%; (vi) *m*-CPBA, DCM, MeOH, RT, 48 hr, 77%; (vii) conc. HCl, reflux, 1 hr, 54%.

### 5.2.2 Synthesis of *rac*-SK-6

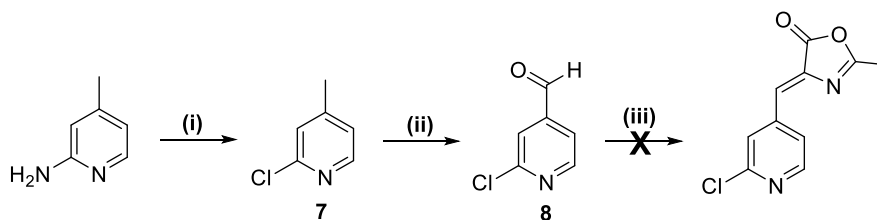
The synthesis of 4- substituted 1, 2-HOPO was the most challenging part of the overall synthesis since numerous synthetic approaches have been optimised and applied for the formation of the expected product. Despite the fact that the synthesis of *rac*-SK-6 was reported in the literature, the overall synthesis involved several steps with the overall yield been significantly low (**Scheme 14**).<sup>498</sup>



**Scheme 14:** Reagents and conditions for the synthesis of 4-substituted 1, 2-HOPO according to the literature; (i) HBF<sub>4</sub>, NaNO<sub>2</sub>; 60%, (ii) NBS, dibenzoyl peroxide, CCl<sub>4</sub>, reflux, 48%; (iii) diethyl acetamidomalonate, NaH (60% in mineral oil), DMF<sub>dry</sub>, RT, 16 hr; (iv) Na<sub>(s)</sub>, EtOH, reflux, 16 hr, 73%; (v) H<sub>2</sub>O<sub>2</sub> (30%), AcOH, 50%; HCl conc. reflux, 16 hr, 31%.<sup>498</sup>

Several attempts were conducted towards the reproducibility of the compounds without any results as the formation of the expected N-oxide intermediate couldn't be synthesised under the literature procedures. Therefore, herein we attempted to identify a procedure that would allow the synthesis of the compound within less synthetic steps (if possible) and higher overall yield.

Initially, as in the case of *rac*-SK-6, the synthesis of the 4- substituted 1, 2-HOPO was initiated by the synthesis of amino acid prior to the formation of the HOPO core using the same established methodologies with some modifications (**Scheme 15**).

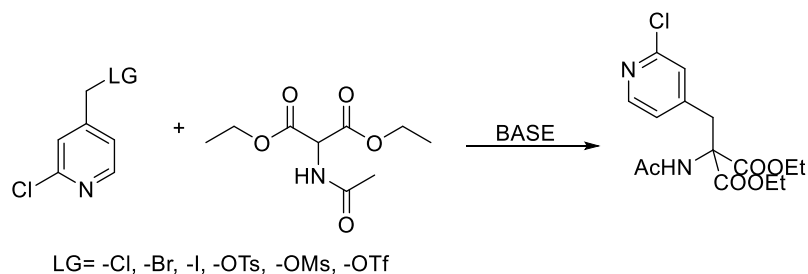


**Scheme 15:** Reagents and conditions towards the formation of azalactone intermediate: (i) NaNO<sub>2</sub>, HCl conc., H<sub>2</sub>SO<sub>4</sub> conc., 0°C, 3 hr, 96% ; (ii) SeO<sub>2</sub>, 1, 4- dioxane, reflux, 12 hr, 46%; (iii) *N*-acetyl glycine, AcONa, Ac<sub>2</sub>O, 130°C, 4 hr.

Therefore, the synthesis was initiated by the conversion of 2-aminopicoline into the 2-chloropicoline (**7**) via the formation of a diazonium salt using sodium nitrate and concentrated hydrochloric acid as it was described before with some modifications.<sup>508</sup> The expected intermediate was afforded in excellent yield (96%) and used directly without further purification to the next step which involved the oxidation of the methyl group of intermediate **7** into the corresponding aldehyde **8**. This was done by using an established procedure from the literature using selenium dioxide in 1, 4-dioxane.<sup>509</sup> The aldehyde **8** was obtained in a moderate to low yield (46%). However, the cytotoxicity of selenium containing species was reported several times in the literature.<sup>510-512</sup> Therefore, as it was used in the early steps of the synthesis we hoped that any traces of selenium would have been removed after purification of the followed intermediates. The Erlenmeyer reaction of azalactone formation was attempted however the reaction failed even after several changes of the reaction conditions.

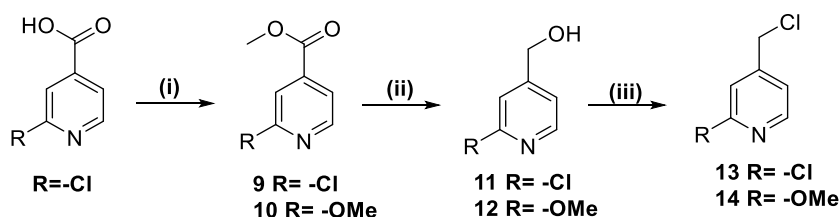
In order to overcome this issue a different synthetic approach was attempted. One of the most abundantly used method for the formation of amino acids is the alkylation of diethyl

acetamidomalonate followed by  $S_N2$  substitution of an intermediate with a good leaving group (eg halogen or tosylate, mesylate, triflate) (**Scheme 16**).



**Scheme 16:** Synthesis of amino acid using diethyl acetamidomalonate as an amino acid precursor.

Therefore, the synthesis was initiated with an  $S_N2$  substitution of the chlorine atom of 2-chloroisonicotinic acid using sodium methoxide (**Scheme 17**).<sup>513</sup>

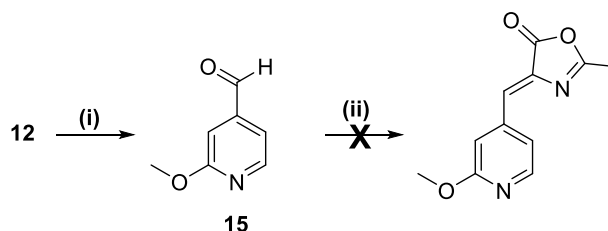


**Scheme 17:** Reagents and conditions for the formation of amino acid moiety or *rac*-**SK-6** : (i) for **9** MeI, NaH (60%), DMF, 60°C, 3 hrs, 73%; for **10** (a), MeONa, 1, 4- dioxane, reflux, 12 hr, 80%, (b) MeI, NaH, DMF, 60°C, 3 hr, 84% (ii), NaBH<sub>4</sub>, CaCl<sub>2</sub>, THF<sub>dry</sub>, 12 hr, RT, 48% (for **11**), 53% (for **12**); (iii) SOCl<sub>2</sub>, CHCl<sub>3</sub> 0°C, 2 hr, 89% (for **14**), (87% for **15**).

The etherification reaction was successful as the expected intermediated was formed in high yield (80%). Esterification of the carboxylic acid of the intermediates using iodomethane afforded the respective esters **9** and **10** intermediates in good yield (73% and 84% respectively).<sup>513</sup> Afterwards, the reduction of the ester was performed upon a literature procedure using calcium chloride and

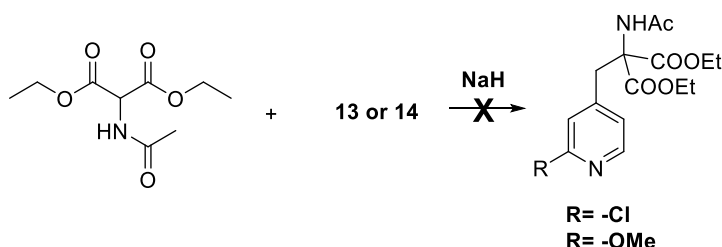
sodium borohydride forming the respective alcohols **11** and **12** in a moderate yield (48% and 53% respectively).<sup>514</sup> Then the formed alcohols (**11** and **12**) were converted into the respective aryl alkyl chlorides (**13** and **14**) after treating them with thionyl chloride.<sup>513</sup>

Additionally, a small portion of alcohol **12** was oxidised to the respective aldehyde (**15**) using the Swern oxidation method as a last attempt to follow the Erlenmeyer reaction (**Scheme 18**).<sup>515</sup>



**Scheme 18:** Reagents and conditions for the formation of azalactone intermediate using aldehyde **13** as a starting material; (i) oxalyl chloride, DMSO, DCM, 2 hr, -78 °C, 84%; (ii) *N*-acetyl glycine, AcONa, Ac<sub>2</sub>O, 130 °C, 4 hr

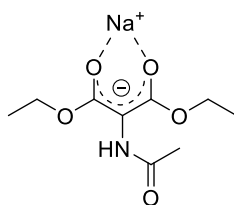
Therefore, the aryl alkyl chlorides (**13** and **14**) have been considered as the key intermediate towards the formation of the amino acid (**Scheme 19**).



**Scheme 19:** Attempted synthetic approach for the introduction of amino acid moiety. Reagents and conditions; NaH (60%), DMF<sub>dry</sub>, various temperatures, 48 hr.

Intermediates **13** and **14**, were then added (separately) in a solution *N,N*-dimethyl formamide containing the sodium salt of acetamidomalonnate (been prepared by treatment of

acetamidomalonate with sodium hydride). The overall reaction was monitored by TLC and  $^1\text{H-NMR}$  at RT initially for 48 hrs without any sign of product formation. As a result of this the temperature of the reaction was gradually increased and once again the reaction didn't proceed as expected as there wasn't any indication of the product. A possible explanation of this behaviour can be attributed to the fact that possibly the negative charge that has been introduced to diethyl acetamidomalonate upon treatment with sodium hydride is stabilised by sodium ion (**Figure 49**), making the carbanion too weakly nucleophilic.

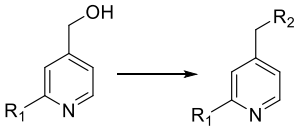


**Figure 49:** Stabilisation of the negative charge of diethyl acetamidomalonate by sodium cation.

The reaction was therefore repeated, this time by adding a 15-crown-5 in an attempt to coordinate sodium and prevent it from stabilising the charge. Surprisingly, the reaction failed to proceed neither after prolonged monitoring nor after increasing the reaction temperature.

In an attempt to identify the best precursor molecule, a small library of analogues have been prepared varying the aryl alkyl substituent (**Table 11**).

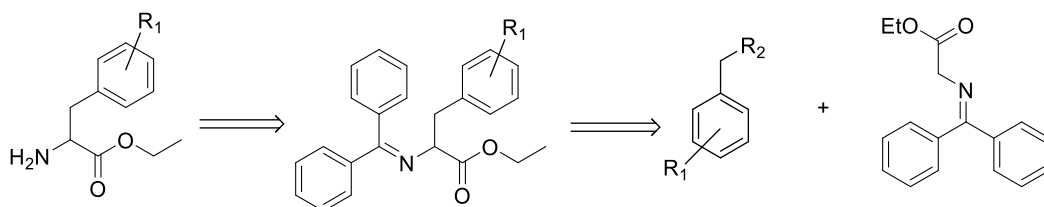
**Table 11:** Small library of intermediates that have been prepared in an attempt to optimise the reaction procedure.

		Reagents and Conditions <sup>[a]</sup>	Yield (%)	Intermediate
<b>R<sub>2</sub>=</b>				
<b>R<sub>1</sub>= -Cl</b>	-Br	PBr <sub>3</sub> , DCM, 0°C, 2 hr <sup>516</sup>	57	<b>16</b>
	-OTs	TsCl, KOH, THF, 0°C, 18 hr <sup>517</sup>	69	<b>17</b>
	-OMs	MsCl, Et <sub>3</sub> N, DCM, 0°C, 3 hr <sup>518</sup>	89	<b>18</b>
<b>R<sub>2</sub>=</b>				
<b>R<sub>1</sub>= -OMe</b>	-Br	CBr <sub>4</sub> , PPh <sub>3</sub> , DCM, 0°C, 2 hr <sup>519</sup>	63	<b>19</b>
	-OTs	TsCl, KOH, THF, 0°C, 12 hr <sup>517</sup>	75	<b>20</b>
	-OMs	MsCl, Et <sub>3</sub> N, DCM, 0°C, 3 hr <sup>518</sup>	82	<b>21</b>

<sup>[a]</sup> Based upon literature procedure upon some modifications.

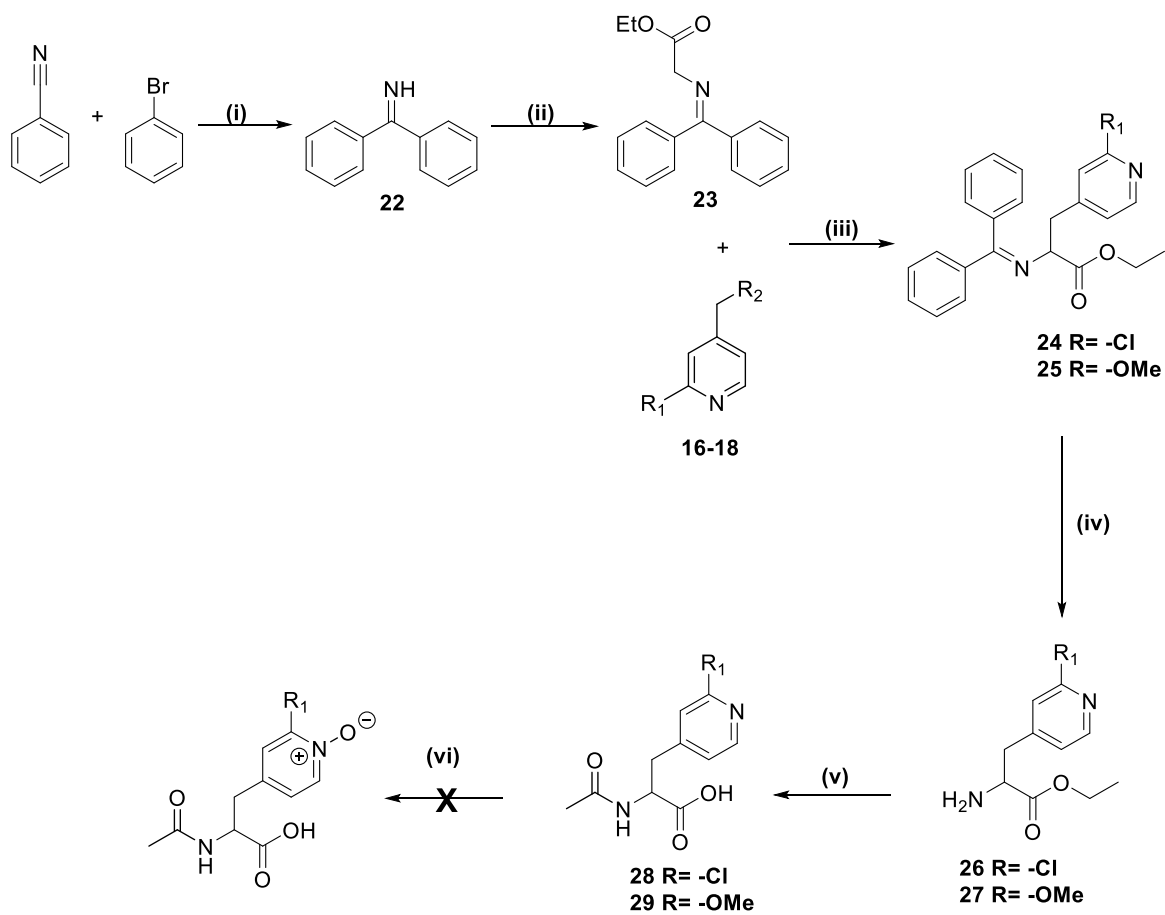
The same experimental procedures have been repeated varying the time of the reaction and the temperature however unfortunately none of them gave the expected intermediate.

According to the literature, the amino acid functionality can also be introduced by the nucleophilic substitution of benzophenone imine glycine ester as a starting material (O'Donnell Amino Acid synthesis) as shown in (Scheme 20).<sup>520</sup>



**Scheme 20:** Retrosynthesis of amino acids using benzophenone imine glycine ethyl ester as the carrier of amino acid functionality.

Therefore, benzophenone imine glycine ethyl ester was synthesised by reacting benzophenone imine with glycine ethyl ester hydrochloride as it was previously described in the literature (Scheme 21).<sup>521</sup>



**Scheme 21:** Reagents and conditions for the synthesis of the precursor of *rac*-SK-6. (i) Mg, I<sub>2</sub>, Et<sub>2</sub>O, 40 °C, 3 hr, 90%; (ii) glycine ethyl ester hydrochloride, RT, 20 hr, 95%; (iii) KO<sup>t</sup>Bu, THF, -78°C - -40°C; (vii) HCl (1M), Et<sub>2</sub>O, H<sub>2</sub>O, RT, 18 hr, 52% for **26**, 63% for **27**; (viii) Ac<sub>2</sub>O, NaOH, H<sub>2</sub>O, 0 °C – RT, 4 hr, 98% for **28** and **29**; (vi) see **Table 10**.

Afterwards, the product (23) has been deprotonated by the addition of potassium *tert* butoxide in order to generate the nucleophile and then it was exposed with the electrophilic compounds listed in **Table 11**. The process of the reaction was monitored by TLC and after a few hours

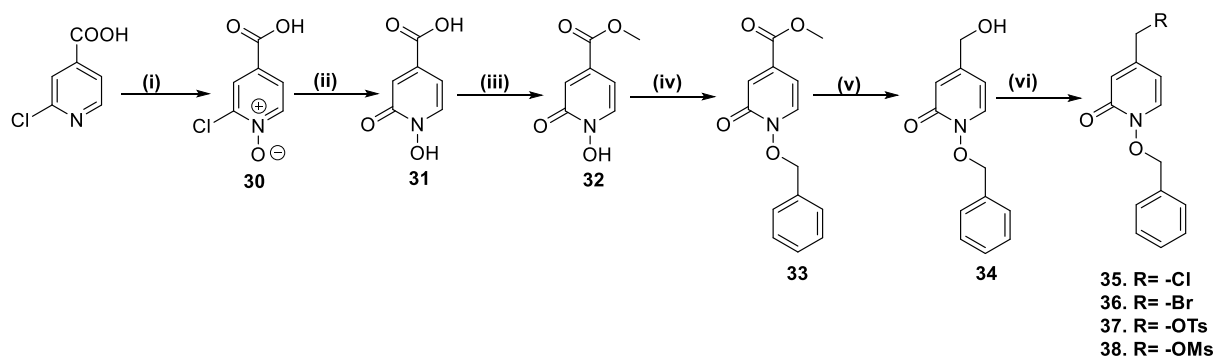
(~3 hr) the expected intermediates (**24-25**) were formed, isolated and used directly to the next step which involved the acid hydrolysis of the imine to towards the formation of (**26-27**). The amine of the formed amino acids was then protected by acetylation as it was previously described. The expected intermediates (**28-29**) were formed in an almost quantitative yield (~98%) and they were taken directly to the next step which involved the *N*-oxidation. For the *N*-oxidation several oxidising agents have were employed however none of them gave the expected *N*-oxide intermediate even after varying the time and the temperature of the reaction (**Table 12**).

**Table 12:** Reagents and conditions for the *N*-oxidation of intermediates **28** and **29**.

Conditions <sup>[a]</sup>		Yield
R= -Cl	<i>m</i> CPBA, DCM, reflux, 48-96 hr <sup>522</sup>	No reaction
R= -OMe		No reaction
R= -Cl	AcOOH, H <sub>2</sub> O <sub>2</sub> , 80°C, 12 -72 hr <sup>311</sup>	No reaction
R= -OMe		No reaction
R= -Cl	UHP, TFAA, DCM, RT, 24 hr <sup>523</sup>	No reaction
R= -OMe		No reaction
R= -Cl	TFA, H <sub>2</sub> O <sub>2</sub> , 80 °C, 48 hr <sup>311</sup>	No reaction
R= -OMe		No reaction
R= -Cl	HOREO <sub>3</sub> , H <sub>2</sub> O <sub>2</sub> , DCM, RT, 48 hr <sup>524</sup>	No reaction
R= -OMe		No reaction

<sup>[a]</sup> Based upon literature procedure upon some modifications.

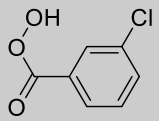
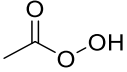
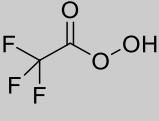
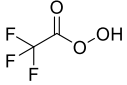
Due to the numerous unsuccessful attempts to *N*-oxidise the intermediates **28** and **29** moiety we decided that the HOPO group could be built prior to construction of the amino acid functionality as it was concluded that the presence of amino acid moiety at the 4- position prevented the *N*-oxidation. The synthesis was directed towards the formation of intermediate **35** as the key intermediate that would allowed to the introduction of the amino acid moiety (**Scheme 22**).



**Scheme 22:** Reagents and conditions for the synthesis of intermediates **35-38**. **(i)** See **Table 13**, **(ii)** KOH (10% w/v), 70°C, 16-18 hr, 92%; **(iii)** SOCl<sub>2</sub>, MeOH, reflux, 6 hr, 95%; **(iv)** BnBr, K<sub>2</sub>CO<sub>3</sub>, DMF, 80°C, 18 hr, 54 %; **(v)** NaBH<sub>4</sub>, MeOH, THF<sub>dry</sub>, reflux, 2 hr, 95 %; **(vi)** See **Table 14**.

The formation of 1, 2-HOPO was begun by the *N*-oxidation of 2-chloroisonicotinic acid using various oxidising methods in order to determine the optimum one that would afford the expected *N*-oxide (**30**) in the highest yield and purity (**Table 13**).

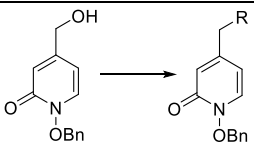
**Table 13:** Reagents and conditions for the *N*-oxidation of the 2-chloroisonicotinic acid

Oxidant	Conditions <sup>[a]</sup>	Yield (%)
	<i>m</i> CPBA, DCM, reflux, 48hr <sup>522</sup>	28
	AcOH, H <sub>2</sub> O <sub>2</sub> , 80°C, 12hr <sup>311</sup>	42
	TFA, H <sub>2</sub> O <sub>2</sub> , 80 °C, 18 hr <sup>311</sup>	74
	UHP, TFAA, DCM, RT, 6 hr <sup>523</sup>	82

<sup>[a]</sup> Based upon literature procedure upon some modifications.

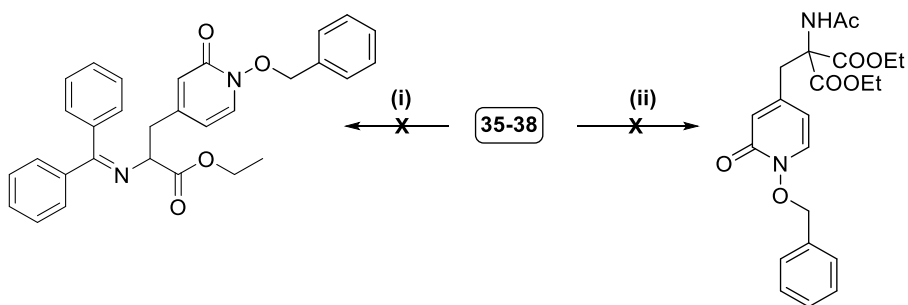
The *in situ* formation of trifluoro peracetic acid led to the formation of a strong oxidant which has the capacity to *N*-oxidise the starting material in an excellent yield without any by-products, whereas the other methods either gave the final product in poor yield (e.g. AcOH/H<sub>2</sub>O<sub>2</sub>) or the purification of the final product was difficult (e.g. *m*CPBA). Afterwards, the reaction of **30** with aqueous solution of potassium hydroxide (10% w/v) led to the formation of the *ortho* 1,2-HOPO. The next step evolved the functionalisation of the carboxylic acid group and thus it was converted to the respective methyl ester (**32**) by treatment with thionyl chloride in methanol. Then the *N*-oxide group was protected by the addition of benzyl group using benzyl bromide in the present of potassium carbonate. Afterwards, the intermediate **33** was reduced to the respective alcohol (**34**) according to the procedure obtained by Boechat N. *et al.* in an excellent yield.<sup>525</sup> The alcohol was functionalised further in a range of molecules with various leaving groups (**Table 14**).

**Table 14:** Reagents and conditions for the functionalisation of intermediate **34**.

	Reagents and Conditions <sup>[a]</sup>	Yield (%)	Intermediate
R=	Cl- CCl <sub>4</sub> , PPh <sub>3</sub> , RT, 1 hr <sup>526</sup>	36	<b>35</b>
	Br- CBr <sub>4</sub> , PPh <sub>3</sub> , DCM, 0°C, 3 hr <sup>519</sup>	89	<b>36</b>
	-OMs MsCl, Et <sub>3</sub> N, DCM, 0°C, 1 hr <sup>518</sup>	61	<b>37</b>
	-OTs TsCl, KOH, THF, 0°C, 5 hr <sup>517</sup>	70	<b>38</b>

<sup>[a]</sup> Based upon literature procedure upon some modifications.

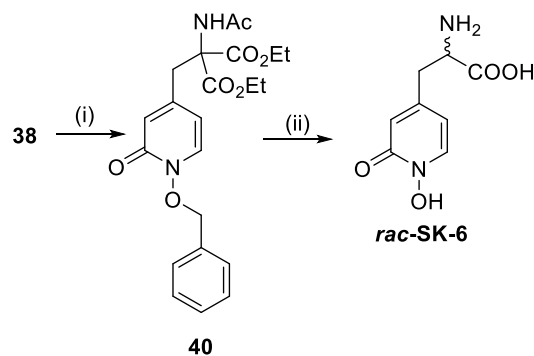
Subsequently, the two pathways that have been follow above, were repeated as it was previously described using various temperatures and time (**Scheme 23**) Unfortunately, none of the above listed intermediates gave the expected product.



**Scheme 23:** Attempted synthesis for the introduction of the amino acid group at the 4- position of the 1, 2-HOPO. Reagents and conditions; (i) intermediate **23**, KO<sup>t</sup>Bu, THF, -78°C - -40 °C; (ii) NaH (60%), diethyl acetamidomalonate, DMF<sub>dry</sub>, RT, 48 hr.

In another literature report, by Quanxuan Z. and co-workers, it was suggested that the amino acid synthesis would be achieved by reacting tosylate intermediates with diethyl acetamidomalonate in the presence of potassium *tert* butoxide rather than sodium hydride and also by using aprotic non

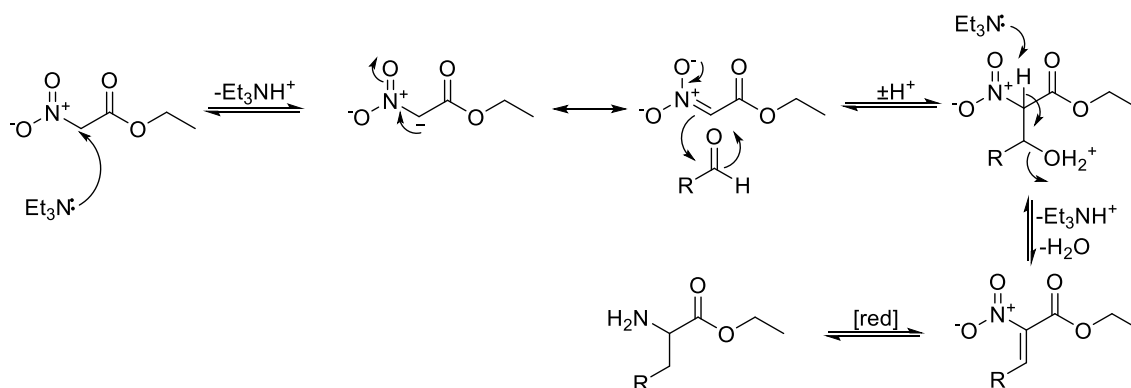
polar solvent such as 1, 4-dioxane rather than *N,N*-dimethyl formamide (polar solvent).<sup>527</sup> In addition to this, they recommend to maintain the reaction initially at 50-60°C and then reflux.<sup>527</sup> Taking into account the above recommendation the tosylate intermediate (**38**) was used as a proper starting material towards the formation of the amino acid group (**Error! Reference source not found.**).



**Scheme 24:** Reagents and conditions for the synthesis of *rac*-SK-6; (i) diethyl acetamidomalonate, KO<sup>t</sup>Bu, 1, 4-dioxane, reflux, 16 hr, 73%; (ii) HCl conc, reflux, 9 hr, 23%.

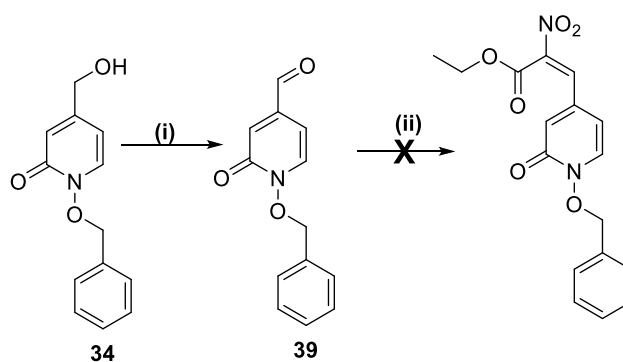
Therefore, **38** reacted with diethyl acetamidomalonate potassium salt (generated by heating at 60°C a solution of diethyl acetamidomalonate in 1, 4-dioxane in the presence of potassium *tert* butoxide) forming the expected intermediate **40** in a good yield (73%). Acidic hydrolysis by means of reflux in conc. HCl of the intermediate (**40**) led to the cleavage of the ethyl esters, the acetyl deprotection, affording the expected amino acid (*rac*-SK-6) as a racemic mixture in a low yield (23%). This can be attributed to the fact the potassium *tert*-butoxide has a *pK*<sub>a</sub> of ~17 whereas the *pK*<sub>a</sub> of sodium hydride that has been previously used is ~35. The use of a stronger base might cause the deprotonation of the amide bond (and the α-proton) forming an intermediate which it could react further with the series of pyridines, whereas the use of a milder non-nucleophilic base led to the selective deprotonation of the acidic protons allowing the S<sub>N</sub>2 reaction to proceed.

In order to solve those issues, a different approach has been followed. It has been previously reported that an alternative method for synthesis of  $\alpha$ - amino acid precursors is the conversion of aldehydes into the respective  $\alpha$ - amino esters (Henry's reaction) (**Scheme 25**).



**Scheme 25:** Proposed mechanism for the synthesis of  $\alpha$ -nitro esters using ethyl nitroacetate.

For this purpose, the alcohol **34** was oxidised into the corresponding aldehyde via the Swern oxidation in a low yield (32%) (**Scheme 26**).<sup>515</sup>



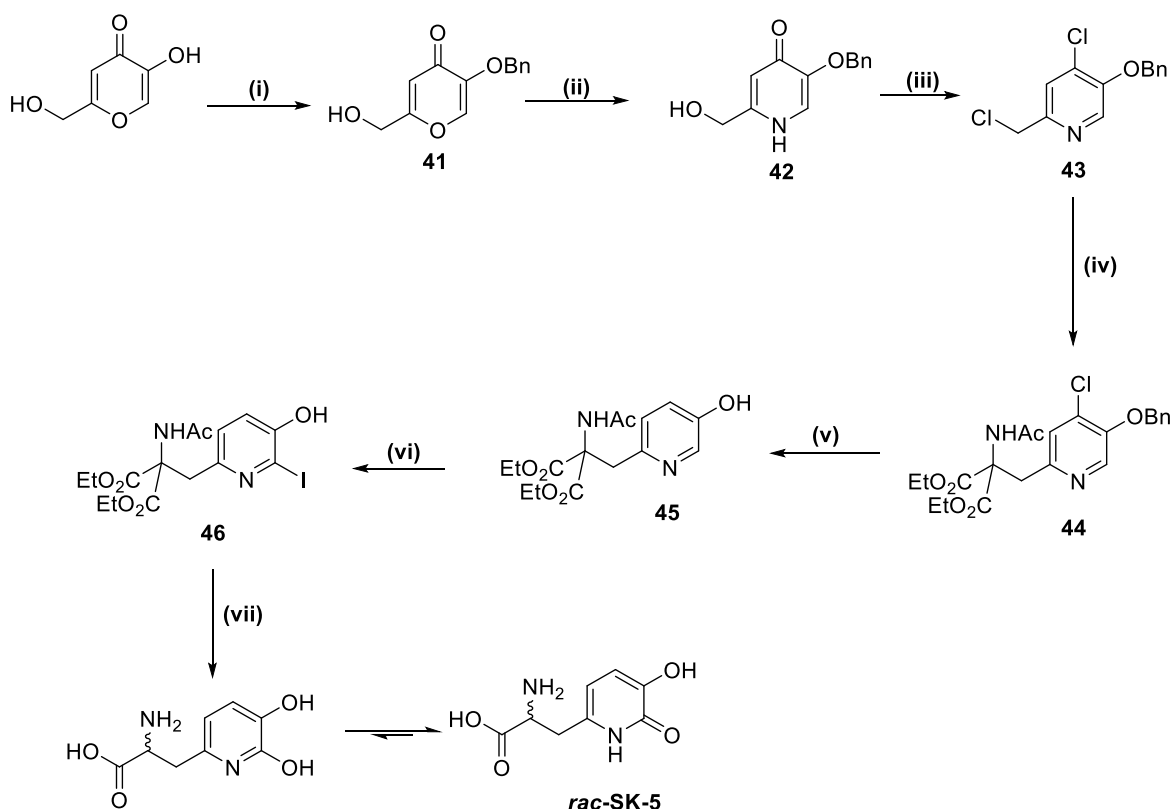
**Scheme 26:** Attempted synthesis of  $\alpha$ -nitro ester via Henry's reaction. Reagents and conditions: (i) oxalyl chloride, DMSO, DCM, 2 hr,  $-78\text{ }^{\circ}\text{C}$ , 32%; (ii) Ethyl nitroacetate,  $\text{Et}_3\text{N}$ ,  $\text{THF}_{\text{dry}}$ , MS (4 Å MS),  $\text{ZrCl}_4$ , reflux, 3 hr.

Afterwards, the aldehyde **39** was reacted with ethylnitroacetate in the presence of trimethylamine and molecular sieves.<sup>528,529</sup> It has been also recommended the use of a catalytic amount of zirconium tetrachloride as a Lewis acid catalyst.<sup>529</sup> However, the reaction failed to proceed. The <sup>1</sup>H-NMR revealed the decomposition of the HOPO core and therefore further attempts were avoided.

### 5.3 3, 2- HOPOs

#### 5.3.1 Synthesis of *rac*-SK-5

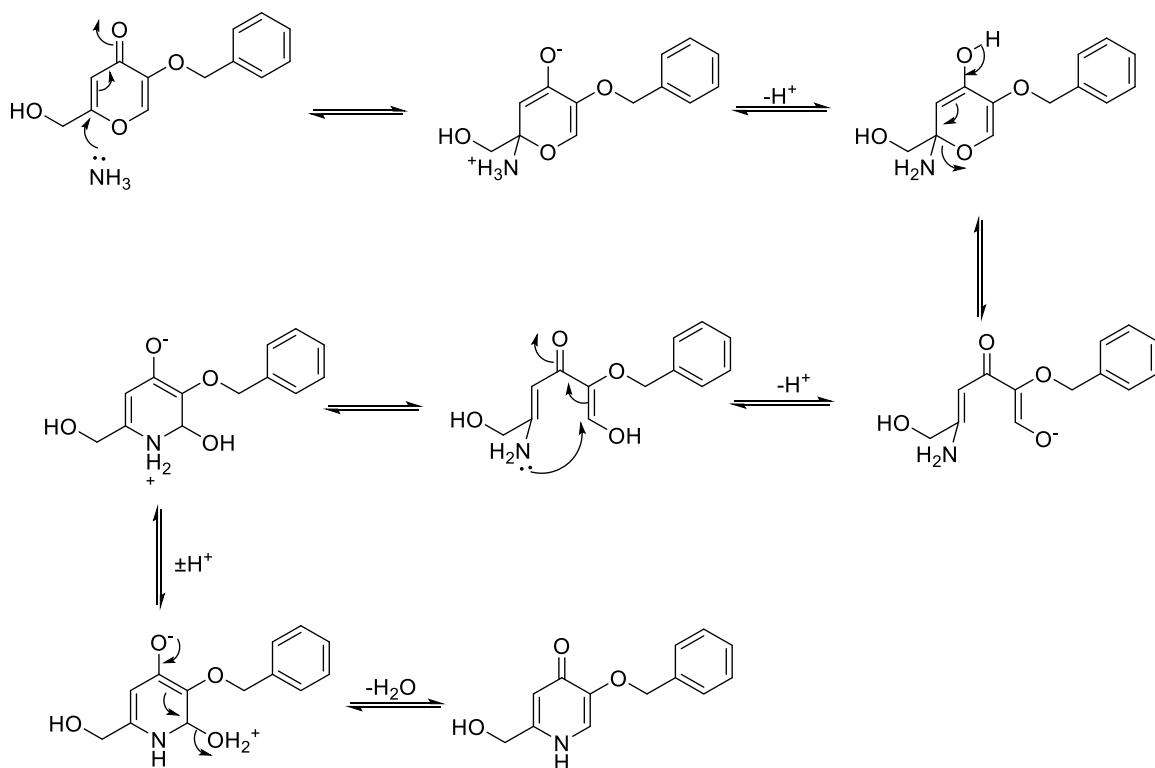
The synthesis of *rac*-SK-5 (*ortho*- substituted) 3, 2-HOPO was first reported by Harris and co-workers and the same methodology was followed (**Scheme 27**).<sup>498</sup>



**Scheme 27:** Reagents and conditions for the synthesis of *rac*-SK-5: (i) BnBr, NaOH, MeOH, 18 hr, reflux, 82%; (ii) conc. NH<sub>4</sub>OH, 5 hr, 120°C, 80%; (iii) POCl<sub>3</sub>, 40 min, 120°C, 87%; (iv) Diethyl

acetamidomalonate, NaH (60% in mineral oil), DMF<sub>dry</sub>, 18 hr, RT, 98%; (v) H<sub>2</sub> (g), Pd/C (10%), MeOH, RT, 68%; (vi) Na<sub>2</sub>CO<sub>3</sub> aq, I<sub>2</sub>, KI, 18 hr, RT, 98%; (vii) a) Ba(OH)<sub>2</sub> aq, 24 hrs, 120°C, 24 hrs b) conc. HCl, 180°C, 1 hr, c) conc. NH<sub>4</sub>OH, pH 5, 5°C, 95%.

The overall synthesis was initiated by the formation of the amino acid moiety, prior to the development of HOPO core. Initially, for the *O*-protection of the reactive hydroxyl group of kojic acid its deprotonation in the present of sodium hydroxide towards the formation of nucleophile was necessary.<sup>498</sup> Afterwards the formed nucleophile reacted with benzyl bromide forming the *O*-benzyl protected intermediate in a high yield (**41**). The *O*-benzyl protected pyranone was then converted to the respective pyridinone (**42**) by heating it in a solution of concentrated ammonium hydroxide in a stainless steel bomb (**Scheme 28**).<sup>498</sup>

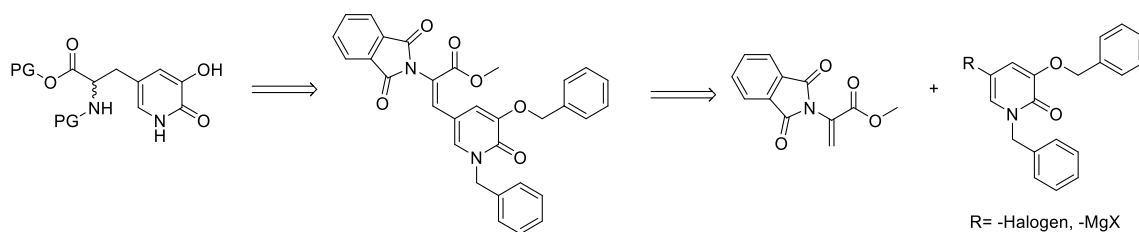


**Scheme 28:** Proposed mechanism for the conversion of *O*-benzyl protected pyranone into the respective *O*-benzyl pyridinone by condensation with ammonium hydroxide.

The *O*- benzyl pyridinone was then converted into to the corresponding chloropyridine (**43**) after reflux with phosphorous oxychloride. That reaction also led to the conversion of the primary alcohol into the respective alkyl chloride.<sup>498</sup> This substrate was then reacted further with diethyl acetamidomalonate in the present of sodium hydride.<sup>498</sup> As a result of this substitution reaction the amino acid precursor (**44**) was generated in almost quantitatively yield (98%). The next part of the synthesis begun by the formation of the HOPO core. Namely, intermediate **44** was reductively de-chlorinated via catalytic (Pd/C – 10%) hydrogenation in the presence of sodium acetate.<sup>498</sup> Apart from the reduction of chloropyridine, the hydrogenation deprotected the *O*-benzyl group, leading to the formation of the hydroxypyridine intermediate **45** in good yield (68%). Afterwards, iodination of **45** using I<sub>2</sub>, KI<sub>aq</sub> led to the formation of the **46** in excellent yield (98%).<sup>498</sup> The next step involved the nucleophilic aromatic substitution (S<sub>N</sub>Ar) reaction using barium hydroxide forming the HOPO core. The formed intermediate barium salt was taken directly to the next step which evolved the acid cleavage of the diethyl ester group and the acetyl de-protection of the amino group.<sup>498</sup> The final product (*rac*-SK-5) was formed as salt free racemic mixture after its dissolution in water and its re-precipitation by the addition of conc. ammonium hydroxide until pH~5 in an excellent yield (95%).

### 5.3.2 Results – Synthesis of *rac*-SK-7

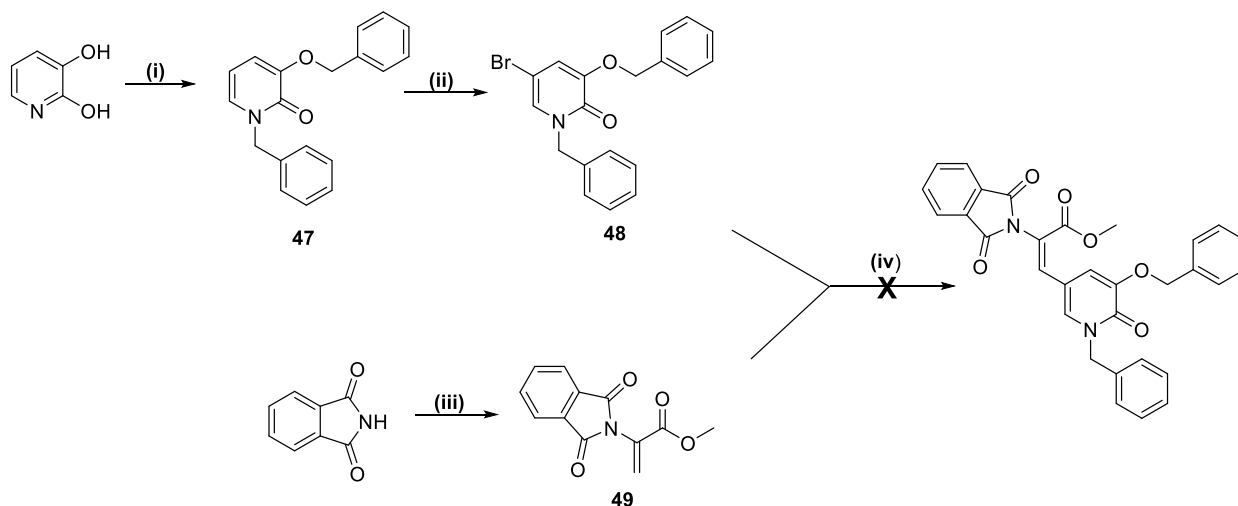
Being inspired from the Gabriel synthesis of amino acids we utilised the phthalimide core as a carrier of the amine component of the amino acid functionality (**Scheme 29**).



**Scheme 29:** Retrosynthetic analysis towards the synthesis of the amino acid group using *N*-alkyl phthalimide.

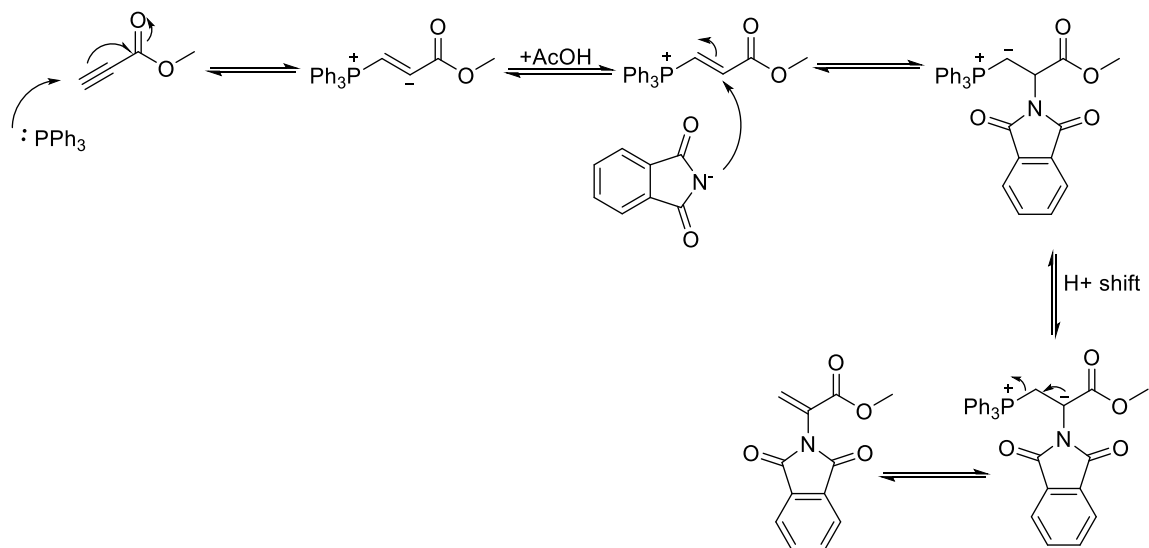
Additionally, one of the two building blocks would also carry an electrophilic centre that would allow the nucleophilic addition towards the formation of the amino acid group.

Therefore, the synthesis of the novel compound; *rac*-SK-7 was initiated with the synthesis of both building blocks; the HOPO core and amino acid precursor (**Scheme 30**).



**Scheme 30:** Reagents and conditions: (i) CsCO<sub>3</sub>, BnBr, DMF, RT, 7 days, 80%; (ii) Br<sub>2</sub>, DCM, RT, 40 hr, 69%; (iii) a) TPP, AcONa, toluene, reflux, 10 min, b) AcOH, ethyl propiolate, reflux, 18 hr, 46% (iv) see **Table 15**.

The synthesis of the HOPO core involved the protection of both nitrogen atom and the 3-hydroxyl group of the 2,3-dihydropyridine using caesium carbonate in the presence of DMF, as it was previously described with some modifications. The di-benzyl protected product (**47**) was afforded in a good yield (80%) upon purification by recrystallization from ethanol.<sup>530</sup> Afterwards, intermediate **47** underwent bromination at the 4 position by treating it with bromine. The synthesis of the amino acid precursor **49** was carried out by refluxing the phthalimide in toluene in the presence of methyl propiolate, triphenylphosphine, sodium acetate and acidic acid (**Scheme 31**).<sup>531,532</sup>



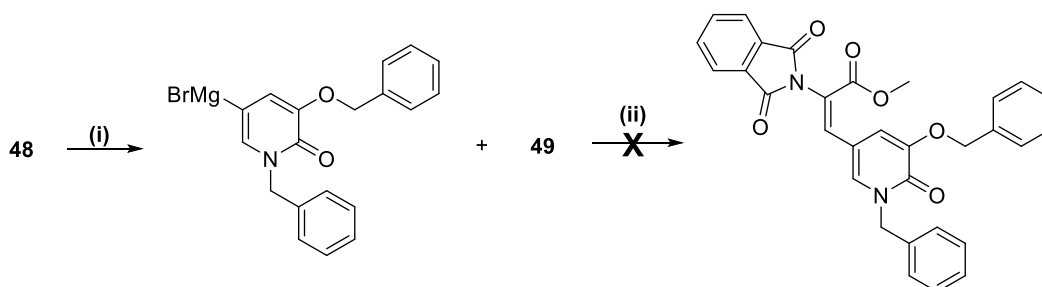
**Scheme 31:** Proposed mechanism of the triphenylphosphine catalyzed nucleophilic addition to methyl propiolate towards the synthesis of  $\alpha$ -substituted alkyl acrylate.

Afterwards, the Heck coupling was used in order to form a new C-C bond between the two building blocks. The overall procedure failed to afford the expected intermediate even after optimizing the reagents and the conditions of the reaction (**Table 15**).

**Table 15:** Optimization of the reagents and the conditions for the synthesis of the amino acid group via Heck coupling.

Attempt 1 <sup>533,534</sup>	Attempt 2 <sup>535,536</sup>
PdCl <sub>2</sub>	Pd(OAc) <sub>2</sub>
P( <i>O</i> -tol) <sub>3</sub>	P( <i>O</i> -tol) <sub>3</sub>
DMF	ACN
NaHCO <sub>3</sub>	Et <sub>3</sub> N
100°C	90°C
4 hr	18 hr
Tetrabutylammonium bromide	-

Afterwards, an alternative method was followed for the formation of the C-C group between the alkene **49** and the brominated intermediate **48** towards the synthesis of the target molecule (**Scheme 32**).<sup>537</sup>

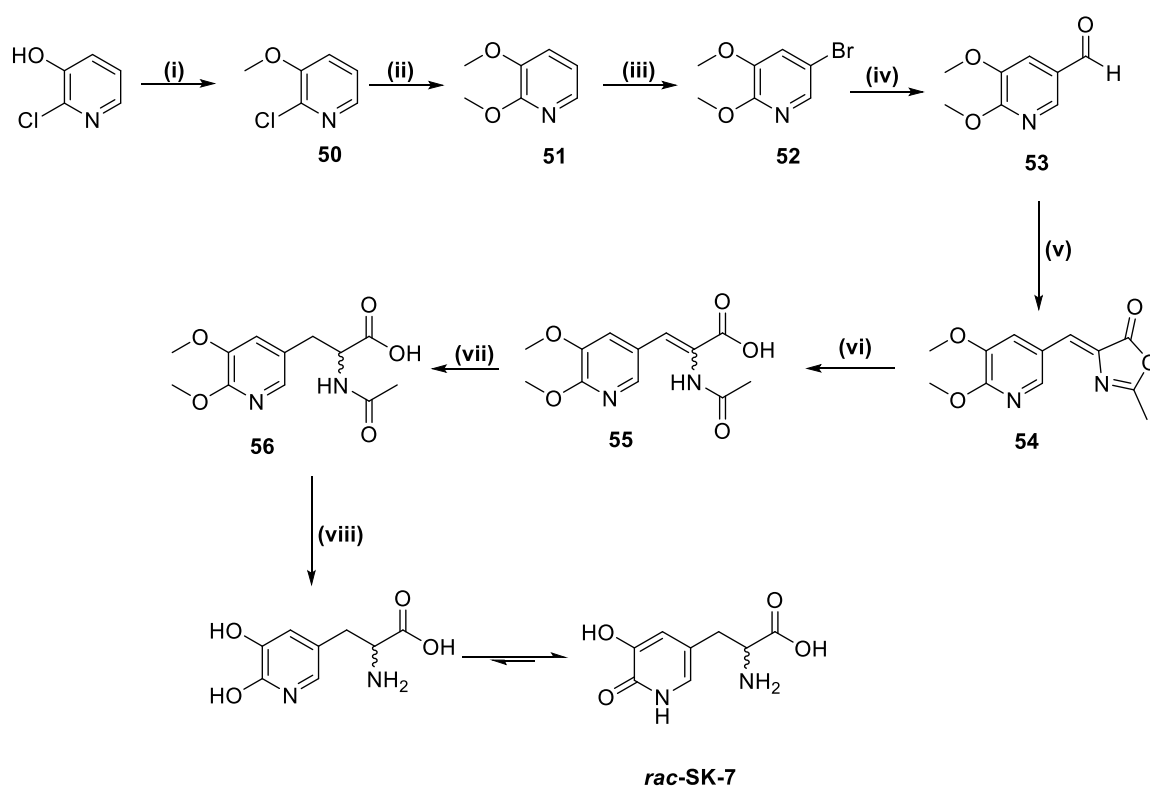


**Scheme 32:** Attempted Grignard conjugated addition to the electrophilic centre of **49**. Reagents and conditions: (i) Mg grinds, I<sub>2</sub> cat, THF<sub>dry</sub>, RT, 2 hr; (ii) THF<sub>dry</sub>, 0°C to reflux, 3-6 hr.

Namely, **48** has been converted to the respective Grignard reagent by treating it with magnesium in the presence of a catalytic amount of iodide crystals in THF. Moreover, the conjugated Grignard addition proceed by mixing the organomagnesium product with the electrophile **49** in the presence

of a catalytic amount of copper iodide as it was previously suggested by Gardhelicchio C. and co-workers.<sup>537</sup> The overall reaction occurred at 0°C and after several hours there was no sight of product formation and hence, the reaction was heated gradually until reflux. The <sup>1</sup>H-NMR of the reaction suggested the decomposition of the HOPO group and as a result of this, further optimisations were not conducted.

Therefore, the synthesis was oriented towards the Erlenmeyer synthesis as it was described before (Scheme 33).



**Scheme 33:** Reagents and conditions for the synthesis of **rac-SK-7**: (i) MeI, K<sub>2</sub>CO<sub>3</sub>, Acetone, RT, 48 hr, 98%; (ii) MeONa, DMF<sub>dry</sub>, 60°C, 18 hr, 76%; (iii) Br<sub>2</sub>, NaHCO<sub>3sat</sub>, DCM, RT, 4 hr, (iv) *n*-BuLi, Et<sub>2</sub>O, DMF<sub>dry</sub>, -35°C, 2 hr, 53%; (iv) *N*-acetyl glycine, AcONa, Ac<sub>2</sub>O, 130°C, 3 hr, 80%; (vi) MeOH, NaOH<sub>aq</sub>, RT, 2 hr, 95%; (vii) H<sub>2</sub> (g), Pd/ C (10%), MeOH, RT, 4 hr, 63%; (viii) HBr (48%), AcOH, reflux, 4 hr, 40%.

Initially, the HOPO core was built first by using 2-chloro-3-hydroxy pyridine. Therefore, the synthesis was initiated by alkylation with iodomethane.<sup>538</sup> The formed intermediate (**50**) was then treated with sodium methoxide in dry *N,N*-dimethyl formamide in order to substitute the chlorine atom.<sup>539</sup> It can be noticed that this sequence is necessary as direct demethylation of the 2,3-dihydroxypyridine leads instead to the *N*-methyl-3-methoxypyridinone. Afterwards bromination of **51** by using bromine in solution mixture of sodium bicarbonate/ dichloromethane afforded the 5-bromo intermediate as the major isomer.<sup>540</sup> In addition to this, the <sup>1</sup>H-NMR revealed the present of the 6-bromo intermediate as the minor isomer. According to the literature, the separation of the two regioisomers is not feasible, whereas the separation of their respective aldehydes is.<sup>541</sup> Therefore, the reaction mixture was taken directly to the next step without further purification. The formylation reaction was performed as it was described above by treating the cool solution of the mixture (**52**) in diethyl ether with *n*-BuLi, followed by the addition of dry DMF.<sup>540</sup> The two aldehydes were separated by recrystallization and the aldehyde (**53**) was afforded in a moderated yield (53%). Afterwards, the azalactone **54** intermediate was formed as described before by refluxing the aldehyde (**53**) in acetic anhydride with sodium acetate and *N*-acetyl glycine. The azalactone then underwent alkali hydrolysis as described previously, affording the alkene (**55**) in a good yield (95%). The reduction of the **55** into the respective alkane (**56**) was achieved via catalytic (Pd/C-10%) hydrogenation. Reflux of the **56** in a solution mixture of hydrobromic acid (48%) and acetic acid lead to the demethylation of the two ethers and also the acetyl de-protection of the amino group of the amino acid affording the *rac*-**SK-7** as salt which was dissolved in water and re-precipitated by the addition of ammonium hydroxide until pH 5.

## 5.4 3, 4- HOPOs

The synthesis of 3, 4- HOPOs began almost 30 years ago where Kontoghiorghes and Sheppard reported a cost effective conversion of the *O*-benzyl protected maltol to the corresponding 3, 4- HOPO following reaction with primary amine and subsequent deprotection (**Figure 50**).<sup>542</sup>

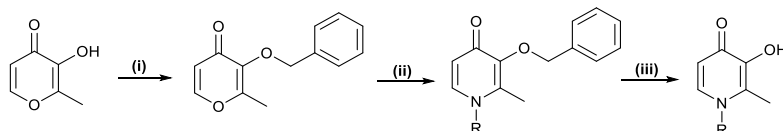
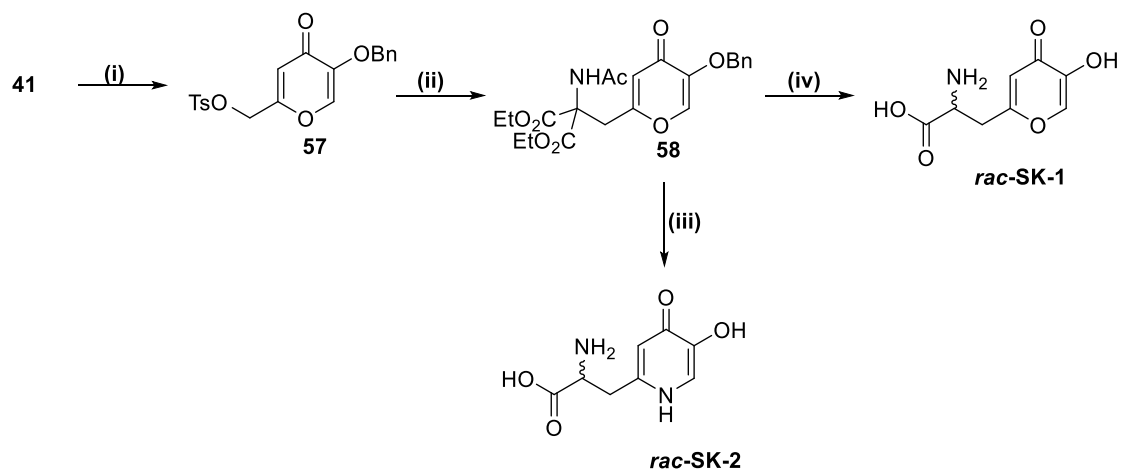


**Figure 50:** The various methodologies for the preparation of 3, 4-HOPOs. Reagents: (i) BnBr, K<sub>2</sub>CO<sub>3</sub>, (ii) RNH<sub>2</sub>, NaOH, (iii) Pd/C, MeOH.

### 5.4.1 Synthesis of *rac*-SK-1 and *rac*-SK-2

The synthesis *rac*-SK-1 and *rac*-SK-2 was based upon a modified literature procedure (**Scheme 34**).<sup>497</sup>



**Scheme 34:** Reagents and conditions for the synthesis of *rac*-SK-1 and *rac*-SK-2; (i) TsCl, NaOH<sub>(aq)</sub>, acetone, 20 min, RT, 94%; (ii) Diethyl acetamidomalonate, NaH (60% in mineral oil)

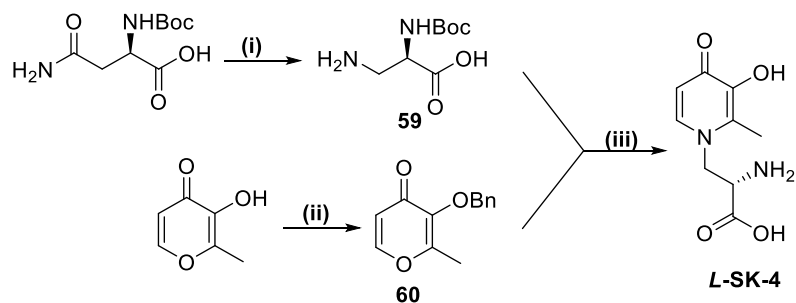
DMF<sub>(dry)</sub>, overnight, RT, 95%; (iii) **a**) conc. HCl, 180°C, 3 hr, **b**) conc. NH<sub>4</sub>OH, pH 5, 5°C, 89%; (iv) **a**) conc. NH<sub>4</sub>OH, 130°C, 3 hr, **b**) conc. HCl, 180°C, 3 hr, **c**) conc. NH<sub>4</sub>OH, pH 5, 5°C, 91%.

The free primary alcohol was converted to the corresponding tosylate upon exposure of **41** with tosyl chloride as was previously described by Thomas F.A.<sup>543</sup> Then, intermediate **57** was reacted with diethyl acetamidomalonate (sodium salt been prepared upon its reaction with sodium hydride in DMF<sub>(dry)</sub>) via an S<sub>N</sub>2 reaction affording intermediate **58** in a good yield. Acidic cleavage (by means of refluxing in conc. HCl) of the ethyl esters and decarboxylation as well as de-protection of the *O*-benzyl protected hydroxide group and the acetyl protected amine afforded the novel hydroxypyranone (*rac*-**SK-1**) as a hydrochloric acid salt which was dissolved in water and re-precipitated by the addition of ammonium hydroxide until pH 5, in an excellent yield (89%). In addition to this, intermediate **58** was converted to the respective pyridinone by heating with ammonia in a stainless still bomb. The formed intermediate then underwent the acidic cleavage as described before for *rac*-**SK-1**. *Rac*-**SK-2** was also afforded as the hydrochloric acid salt which was dissolved in water and re-precipitated by the addition of ammonium hydroxide until pH 5, in an excellent yield (91%).

## 5.4.2 Synthesis of *N*-substituted 3, 4-HOPOs

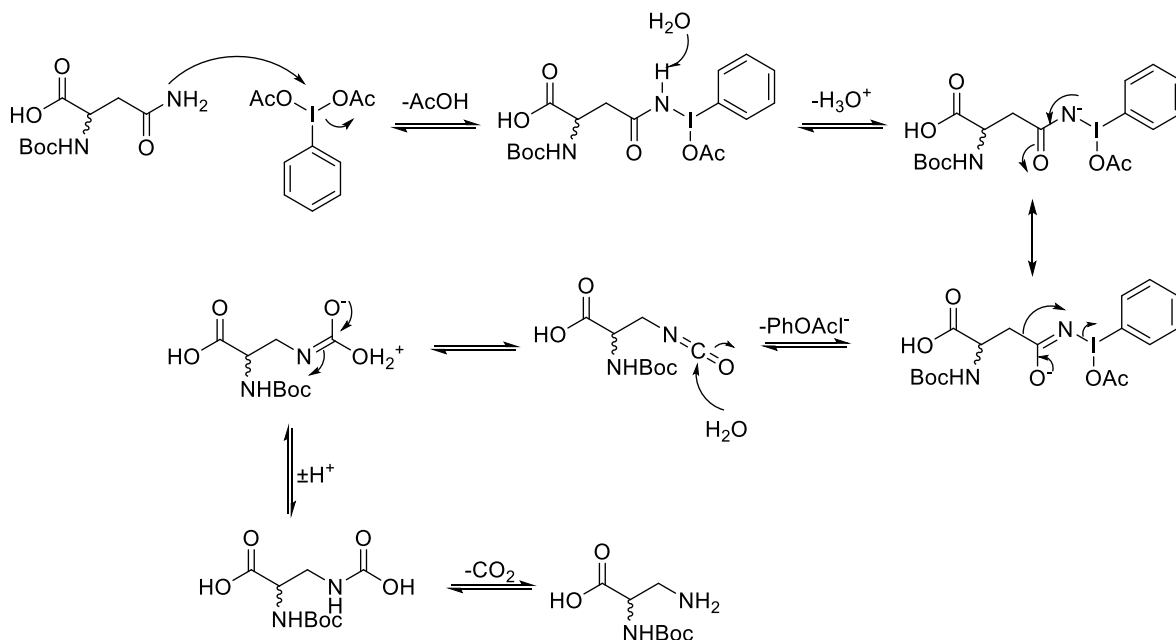
### 5.4.2.1 Synthesis of *L*- and *D*- SK-4

The synthesis of the enantiomerically pure *N*-substituted 3, 4-HOPOs (*L* and *D*- **SK-4**) (methylated analogues of *L*-mimosine) was achieved by condensing the *O*-benzyl protected maltol (**60**) with intermediate **59** (Scheme 35).<sup>544</sup>



**Scheme 35:** Reagents and conditions for the synthesis of *L*-SK-4; (i) **a**) *N*-Boc-*L*-Asn, Iodosobenzene diacetate, EtOAc: MeCN: H<sub>2</sub>O, RT, 4hr, 76%; (ii) BnBr, K<sub>2</sub>CO<sub>3</sub>, DMF, 80°C, 1 hr, 76%; (iii) **a**) EtOH: H<sub>2</sub>O, NaOH (aq) 8 days, **b**) conc. HBr, reflux, 20 mins, **c**) conc. NH<sub>4</sub>OH, pH 5, 5°C, 72 hr, 90%. For *D*-SK-4 (47%) the same procedure followed for *D*-SK-4

Intermediate **59** was performed by applying Hoffmann rearrangement of carboxamides (*L* and *D*-*N*-Boc-protected asparagine) as it was previously described by Mitra R. *et al.* using hypervalent iodine species (iodosobenzene diacetate) (**Scheme 36**)<sup>545</sup>.

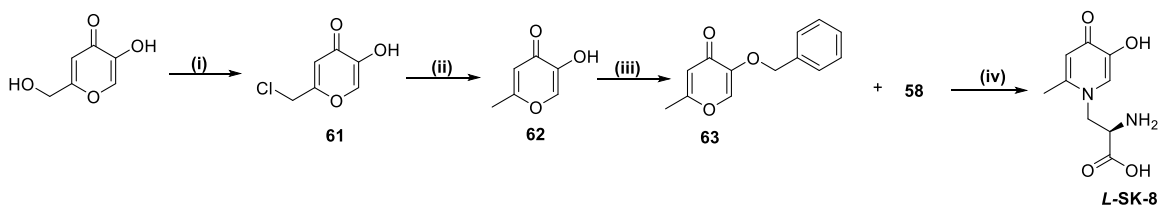


**Scheme 36:** Proposed mechanism for the conversion of *L*- and *D*- *N*-Boc protected asparagine into intermediate **59**.<sup>546,547</sup>

The condensation reaction occurred in the presence of sodium hydroxide and after a week, the crude product was refluxed with hydrobromic acid (48%). That, caused the *O*-benzyl as well as the *N*-Boc deprotection affording the enantiomerically pure compound (*L*- and *D*- respectively **SK-4**) as a hydrobromic acid salt which was dissolved in water and re-precipitated by the addition of ammonium hydroxide until pH 5, in moderated yields (90% for the *L*- and 47% for the *D*- enantiomer).

#### 5.4.2.2 Synthesis of *L*-SK-8

The next part involved the synthesis of a novel isomer of *L*-SK-4 where the methyl group would be in the position 5- rather than 2- (**Scheme 37**)



**Scheme 37:** Reagents and conditions for the synthesis of *L*-SK-8: (i) SOCl<sub>2</sub>, RT, 1 hr, 97%; (ii) Zn (dust), conc. HCl, 70-80°C, 5 hr, 82%; (iii) BnBr, K<sub>2</sub>CO<sub>3</sub>, DMF, 18 hr, 80°C, 68%; (iv) **a**) NaOH, RT, 8 days, **b**) HBr (48%), reflux, 20 min, **c**) NH<sub>4</sub>OH, pH 5, 5°C, 2 weeks, 18%.

Therefore, the synthesis was initiated with the conversion of the primary alcohol of kojic acid into the respective alkyl chloride intermediate (**61**) by using thionyl chloride.<sup>548</sup> Then the alkyl chloride group of intermediate **61** reduced to the respective methyl group using zinc dust and hydrochloric acid forming the allo maltol (**62**) in 81%.<sup>549</sup>

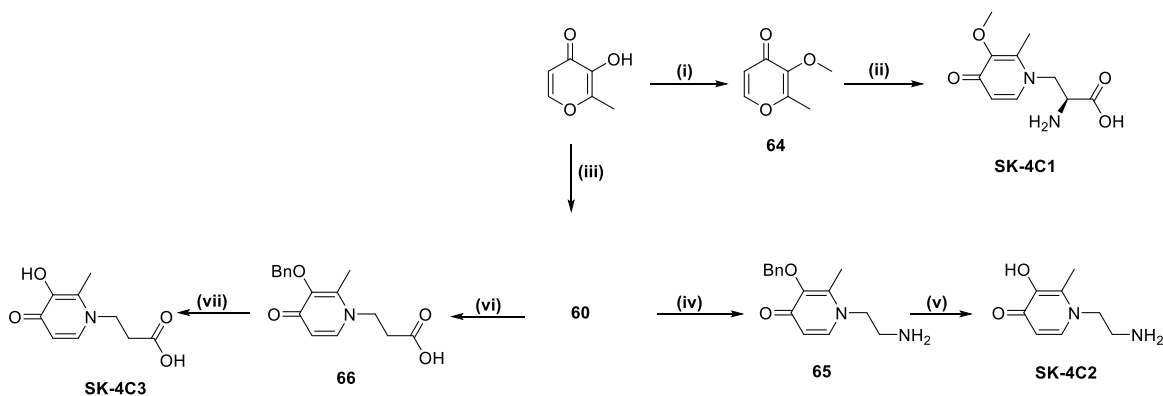
Then, the hydroxyl group of **62** underwent *O*-benzylation via benzyl chloride in the presence of potassium carbonate.<sup>550</sup> The protected intermediate **63** formed in a good yield (68%). Afterwards, **63** was condensed with *L*-59 as it was described previously forming the protected *L*-SK-8 which it was de-protected using the same methodology as described for *L*-SK-4. The hydrobromic acid

salt of **L-SK-8** was dissolved in water and re-precipitated by the addition of ammonium hydroxide until pH 5 affording the salt free *L*- enantiomer in a poor yield (18%).

## 5.5 Synthesis of the control compounds

### 5.5.1 Controls of *L*-SK-4

Due to the high biological potency of *L*-SK-4 in both cancer and PD biological evaluation control compounds have been synthesised (full justification of control compounds can be found in 7.2 and 7.2.2) (Scheme 38)



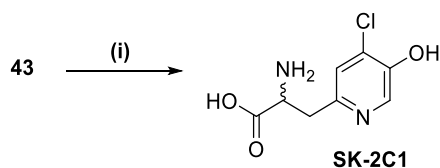
**Scheme 38:** Reagents and conditions for the synthesis of the control compounds; **SK-4C1-3:** (i) MeI, K<sub>2</sub>CO<sub>3</sub>, acetone, reflux, 3 hr, 94%; (ii) (a) **60**, NaOH, RT, 8 days, (b) HBr (48%), reflux 20 min, (c) NH<sub>4</sub>OH, pH 5, 5 °C, 72 hrs, (iv) Ethylenediamine, NaOH, MeOH, H<sub>2</sub>O, reflux, 4 hr, 95%, (v) H<sub>2(g)</sub>, Pd/C (10%), MeOH, 3 hr, 95%; (vi) β-alanine, NaOH, MeOH, H<sub>2</sub>O, reflux, 18 hr, 73%; (vii) H<sub>2</sub>, Pd/C (10%), MeOH, 6 hr, 83%;

Initially, for the synthesis of **SK-4C1**, the hydroxyl group of maltol underwent methylation using iodomethane in the present of potassium carbonate according to the literature.<sup>551</sup> The formed intermediate (**64**) was condensed with **59** as it was described above forming the control compound in a moderate to low yield (42%). Afterwards, **60** underwent condensation reaction with ethylenediamine and β-alanine towards the formation of **SK-4C2** and **SK-4C3** *O*-benzyl protected

intermediates (**65** and **66** respectively) as it was previously suggested.<sup>552,553</sup> In addition, the de-protection of intermediates **65** and **66** was achieved via catalytic hydrogenation (Pd/C – 10%) affording both **SK-4C2** and **SK-4C3** as solids with yields 95 and 83% respectively.

### 5.5.2 Control of *rac*-SK-2

The ability of *rac*-**SK-2** to exert neuroprotective properties against various Parkinsonian induced toxins suggested the synthesis of a control compound (**Scheme 39**).

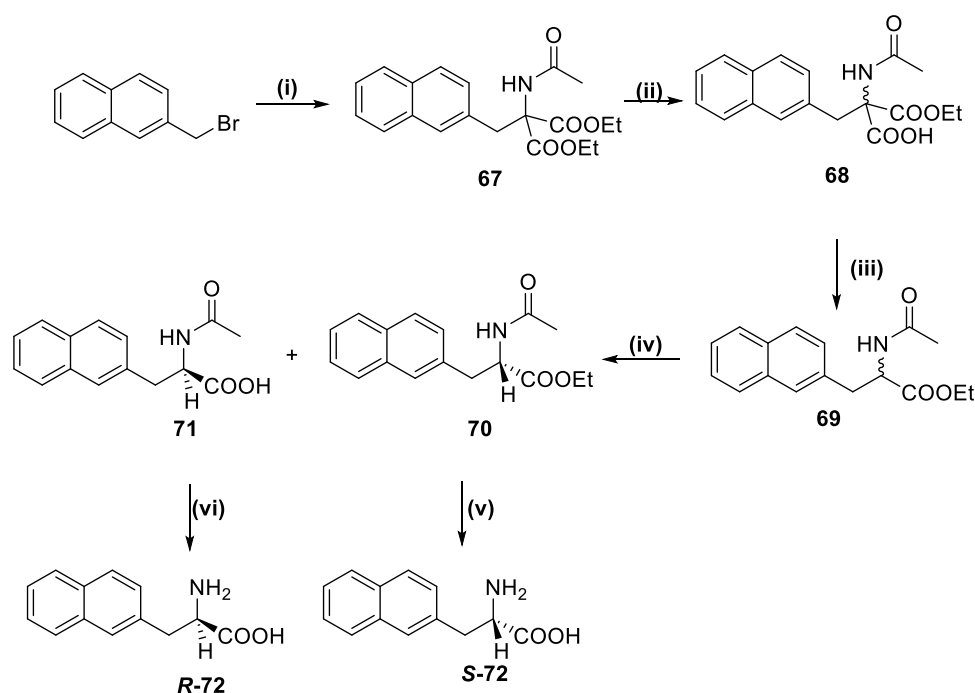


**Scheme 39:** Reagents and conditions for the synthesis of **SK-2C1**: (i) conc. HCl, reflux, 5 hr, 95%

The amino acid vector of this control; **SK-2C1** was retained and the coordination group has been modified in manner that either would prevent the metal binding or would have minimal binding affinity. The synthesis was straight forward as intermediate **44** underwent directly acidic cleavage (by means of refluxing in conc. HCl), and the expected control compound afforded in an excellent yield (95%).

## 5.6 Synthesis of LAT-1 non-selective substrate

It has been previously suggested by the literature that compound **72** has the ability to act as competitive substrate LAT-1 preventing the uptake of <sup>14</sup>C-Leucine.<sup>554</sup> This would allow us to investigate whether the synthesised SK-n compounds have the capability to exploit LAT-1 transporter and therefore been delivered to the targeted area. Since **72** is not commercially available it has to be synthesised. The synthesis of the competitive LAT-1 substrate was achieved upon a modified literature procedure (Scheme 40).<sup>555</sup>



**Scheme 40:** Reagents and conditions for the synthesis of the LAT-1 non selective substrate: (i) Na, EtOH, diethyl acetamidomalonate, reflux, 18 hr, 77%; (ii), NaOH<sub>(aq)</sub> 4M, RT, 45 min, 57%; (iii) 1, 4-dioxane, reflux, 2 hr, 87%; (iv) Subtilisin (Type VIII), KCl<sub>(aq)</sub> (0.01 M), NaHCO<sub>3</sub>, H<sub>2</sub>O, MeCN, RT, 18 hr, pH 7.8, 57% for **69** and 42% for **70**; (v) HCl<sub>(aq)</sub> 6M, reflux, 4 hr, 92%; (vi) HCl<sub>(aq)</sub> 6M, reflux, 4 hr 90%.

Several reports suggested that the stereoselectivity of the LAT-1 substrates is not an important factor that can affect the transportation, whereas others suggest that this transporter has a

preference for the *L*-enantiomers.<sup>405,485</sup> As a result of this, compound **72** has been synthesised and isolated as pure enantiomers and the biological activity of both enantiomers has been evaluated.

The overall reaction was initiated by the  $S_N2$  substitution of bromide with diethyl acetamidomalonate using sodium ethoxide as base (77%). Intermediate **67** underwent initially mono- (alkaline) hydrolysis of the diethyl ester (**68**) and following by mono- decarboxylation by refluxing in 1, 4-dioxane, affording intermediate racemic **69** as solid in good yield (87%). The next step involved the utilisation of the enzyme; Subtilisin (type VIII) in order to resolve the racemic **69**. Namely upon addition of the enzyme, the *S* ester (**70**) was precipitated out of the solution upon removal of the volatiles (51%) and the *R* acid (**71**) was isolated upon acidification of the filtrates (from which the *S* ester was precipitated) (42%). Acidic cleavage of the ethyl ester and also acetyl de-protection afforded the *S*-**72** as white solid (92%) whilst acidic acetyl de-protection afforded *R*-**72** as white solid (90%).

## 6 Physicochemical characterisation

The potentiometric data were refined with the Hyperquad 2008 program, which uses non-linear least-squares methods, taking into account the formation of metal hydroxide species.<sup>556</sup> The distribution curves as a function of pH of the protonated forms of *rac*-SK-2, *rac*-SK-3 and *L*-SK4 and their complexes were calculated using the Hyss2009 program.<sup>557</sup> All the spectrophotometric data were fitted with Hypspec software (<http://www.hyperquad.co.uk>), which allowed the determination of the protonation constants ( $Ka_n$ ) of the chelators, the stability constants ( $\log \beta$ ) of the formed species and the coordination model of the studied systems.<sup>556</sup> The following results on pages 137-156 were kindly prepared by our collaborator: Dr Jérémy Brandel at the University of Strasbourg, France.

### 6.1 Protonation constants

The protonation properties of ligands *rac*-SK-2, *rac*-SK-3 and *L*-SK-4 were studied by both potentiometric titrations and UV–vis absorption spectrophotometric titrations versus pH between pH 2 and 12 (**Figure 51B, D and F**). The acido-basic properties of the three chelators were also studied in strongly acidic conditions between  $p[H] - 0.75$  and 2.25 by means of spectrophotometric batch titrations vs  $p[H]$  (brackets indicate that the pH value was calculated) (**Figure 51A, C and E**).

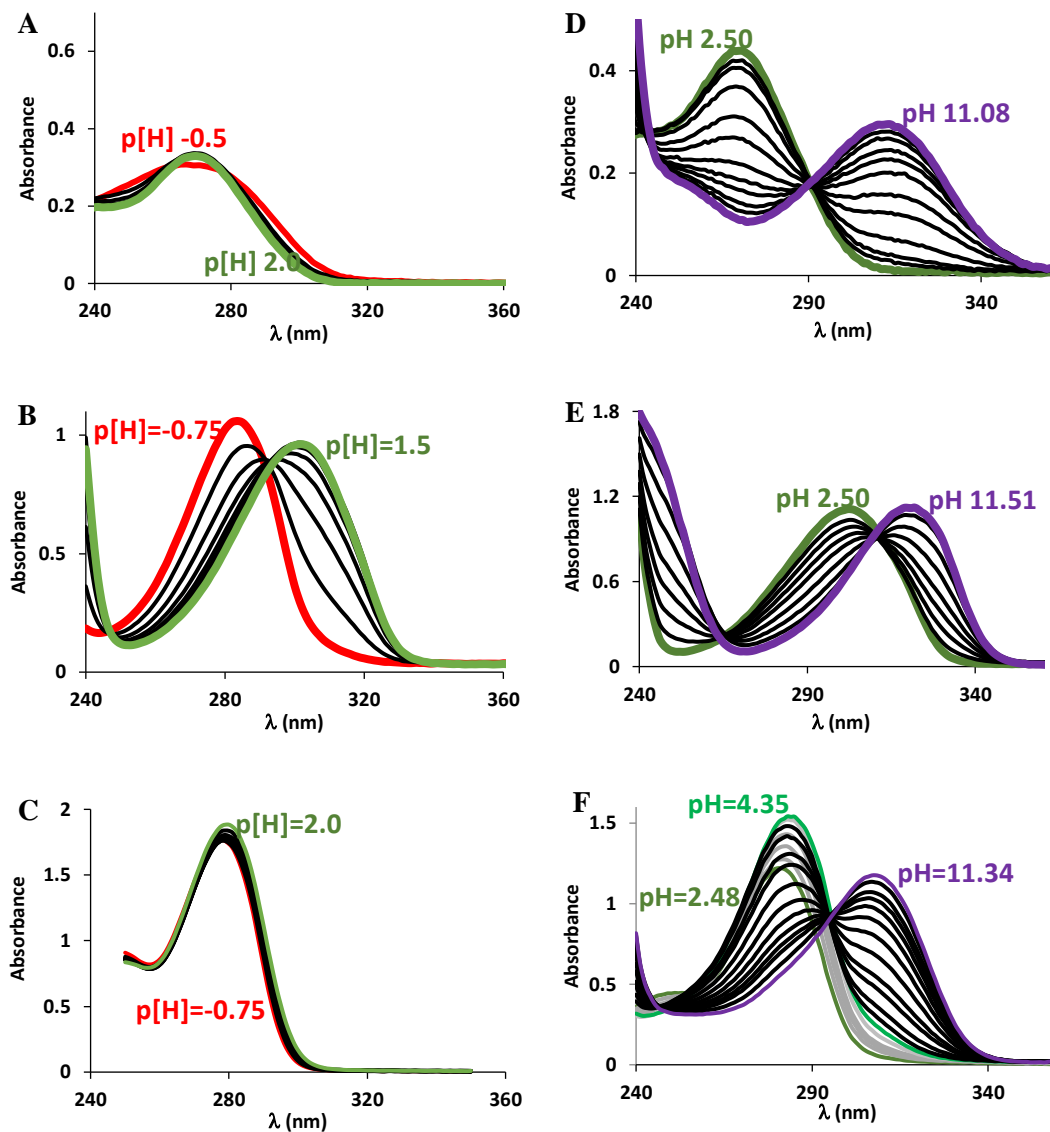


**Figure 51:** Spectrophotometric titrations vs pH of *rac*-SK-2 between (A)  $-0.75 \leq \text{p[H]} \leq 2$  ( $[\textit{rac}\text{-SK-2}] = 2.56 \times 10^{-4}$  M, batch titration) and (B)  $2.50 < \text{pH} < 11.08$  ( $[\textit{rac}\text{-SK-2}] = 3.00 \times 10^{-4}$  M, direct titration); of *rac*-SK-3 between (C)  $-0.75 \leq \text{p[H]} \leq 1.5$ . (batch titration,  $[\textit{rac}\text{-SK-3}] = 2.56 \times 10^{-4}$  M and (D)  $2.50 \leq \text{pH} \leq 11.51$  (direct titration,  $[\textit{rac}\text{-SK-3}] = 1.59 \times 10^{-4}$  M) and of *L*-SK-4 between (E)  $-0.75 \leq \text{p[H]} \leq 2.0$ . (batch titration,  $[\textit{L}\text{-SK-4}] = 2.59 \times 10^{-4}$  M and (F)  $2.48 \leq \text{pH} \leq 11.34$  (direct titration,  $[\textit{L}\text{-SK-4}] = 2.59 \times 10^{-4}$  M).

The exported results suggested that the protonation constants of the functional features of *rac*-SK-2; -OH, -NH<sub>2</sub> and -NH/-CO are in agreement with those reported in the literature for isomimosine (*rac*-SK-2), considering the differences in experimental conditions eg. 37°C in 0.15 M KNO<sub>3</sub> rather than 25°C in 0.1 M NaClO<sub>4</sub> (**Table 16**).<sup>558</sup>

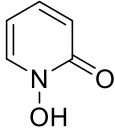
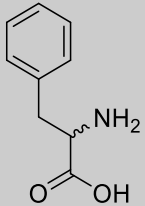
**Table 16:** Correlation between the obtained by the literature and experimental determined p*K*<sub>as</sub> of *rac*-SK-2 ± SD expressed to the last significant digit.

	p <i>K</i> <sub>a1</sub> LH <sub>4</sub>	p <i>K</i> <sub>a2</sub> LH <sub>3</sub>	p <i>K</i> <sub>a3</sub> LH <sub>2</sub>	p <i>K</i> <sub>a4</sub> LH
Literature <sup>558</sup>	1.4	3.13	7.84	9.29
Experimental determination	< -0.5	4.72±0.001	7.48±0.001	8.84±0.01

However, titration at very low pH showed small spectral variations that may be due to the protonation of the HOPO's carbonyl group but the *K*<sub>a1</sub> of this functional could not be calculated and can only be suggested inferior to -0.5.

In the case of *rac*-SK-3 the protonation of its hydroxyl function is in agreement with the respective values found in the literature for a 1, 2-HOPO based molecule (**Table 17**).<sup>418,559</sup>

**Table 17:** Correlation between the obtained by the literature and experimental determined p*K*<sub>as</sub> of *rac*-SK-3, 1, 2-HOPOs and phenylalanine, ± SD expressed to the last significant digit.

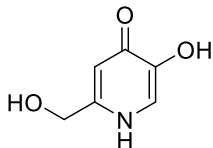
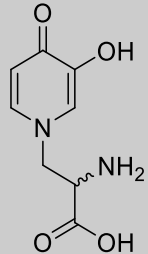
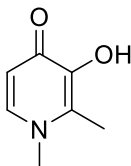
	p <i>K</i> <sub>a1</sub> LH <sub>4</sub>	p <i>K</i> <sub>a2</sub> LH <sub>3</sub>	p <i>K</i> <sub>a3</sub> LH <sub>2</sub>	p <i>K</i> <sub>a4</sub> LH	Conditions
1, 2- HOPO <sup>418,560</sup> 	-	-	5.8	-	25°C, 0.1M KNO <sub>3</sub>
Phenylalanine 	-	1.83	-	9.13	

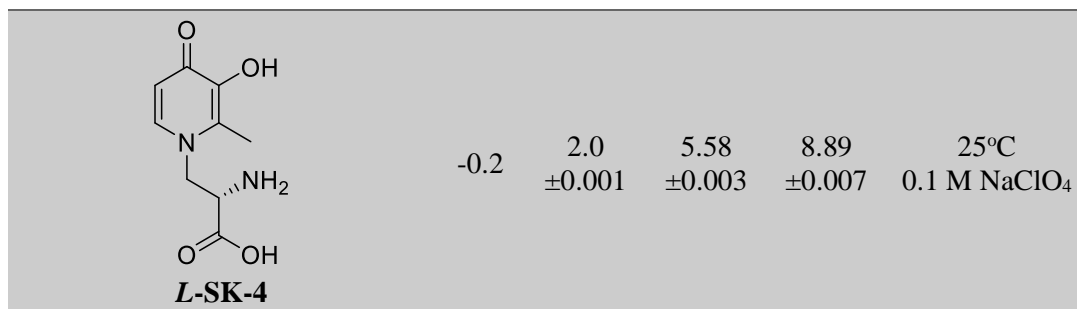
<i>rac</i> -SK-3	-1	2.86 ±0.001	7.0 ±0.001	9.82 ±0.002	25°C, 0.1M NaClO <sub>4</sub>
------------------	----	----------------	---------------	----------------	-------------------------------

The second ( $K_{a2}$ ) and fourth ( $K_{a4}$ ) protonation constants were attributed to the amino and carboxylic acid functions, respectively, by comparison to phenylalanine (**Table 17**). Strong spectral variations were observed between p[H] -0.5 and 1.5, suggesting an additional protonation on the chromophoric group that was attributed to 2-oxo group of the pyridine core as it was suggested before by Scarrow RC.<sup>560</sup>

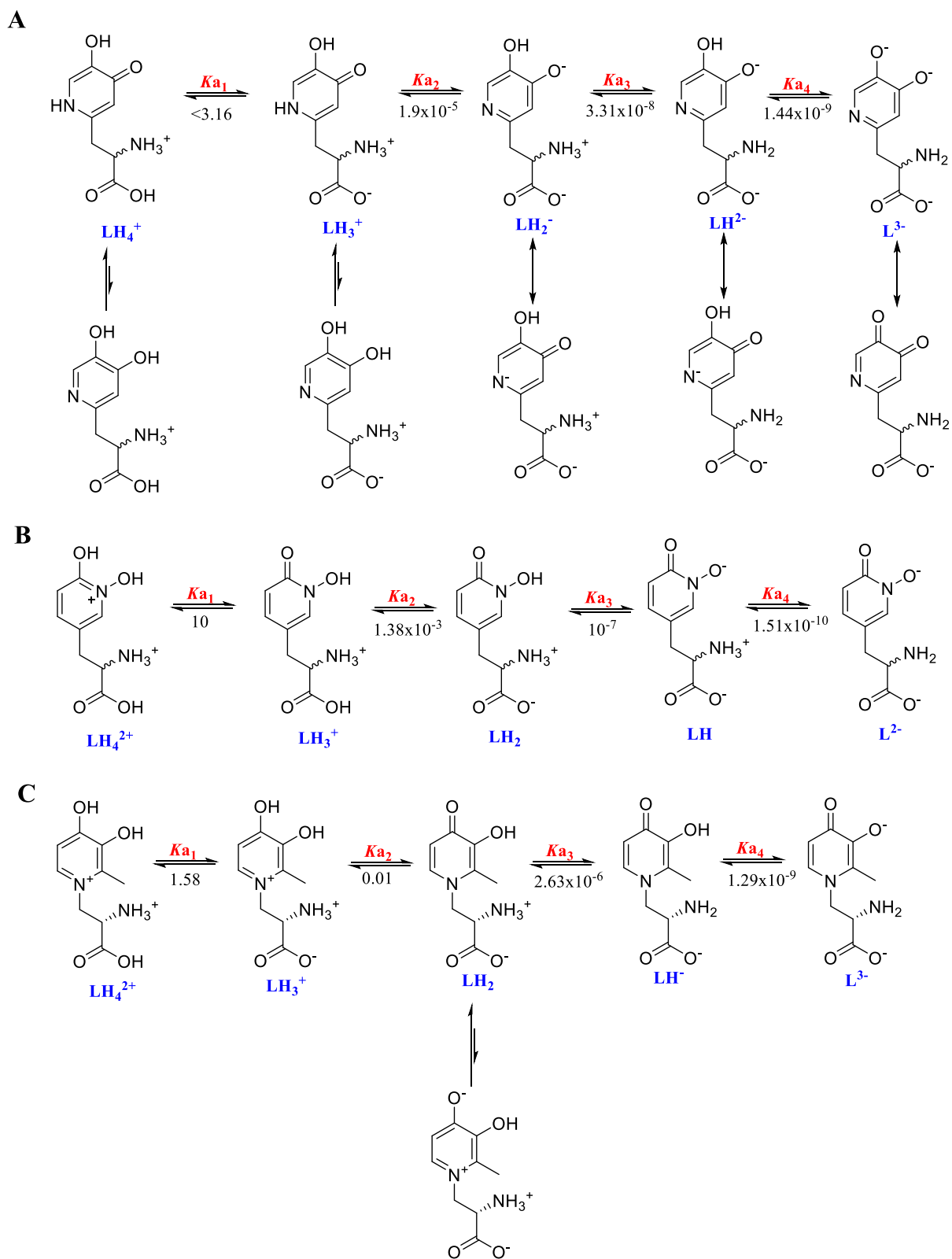
Finally, the protonation constants of *L*-SK-4 in agreement with those reported for Mimosine, with one significant difference on  $pK_{a3}$  ( $7.18 \pm 0.001$  vs  $5.58 \pm 0.003$ ) due to the presence of an additional methyl substituent in position 2 of the pyridine ring of *L*-SK-4 (**Table 18**).<sup>558,561</sup>

**Table 18:** Correlation between the obtained by literature and experimental determined  $pK_{as}$  of *L*-SK-4, *L*-mimosine and P1 ± SD expressed to the last significant digit..

COMPOUND	$pK_{a1}$ LH <sub>4</sub>	$pK_{a2}$ LH <sub>3</sub>	$pK_{a3}$ LH <sub>2</sub>	$pK_{a4}$ LH	CONDITIONS
<b>5-hydroxy-2-(hydroxymethyl)pyridine4(1H)-one (P1)</b> <sup>562</sup> 	3.37	9.00	12.16	12.6	25°C in 0.1 M KCl
<b><i>L</i>-Mimosine</b> <sup>558,561</sup> 	<1	2.56 ±0.001	7.18 ±0.001	9.02 ±0.001	25°C in 0.1 M KNO <sub>3</sub>
<b>DFP</b> <sup>418,563</sup> 	-	-	3.6	9.9	25°C in 0.1 M KNO <sub>3</sub>



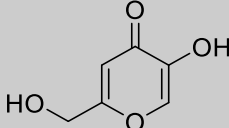
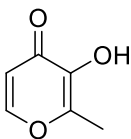
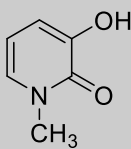
In addition to these, the exported data seems to be consistent with Hider's work on methyl substituted 3, 4-HOPOs (however lack the amino acid group) as they pose similar pK<sub>a</sub>s with the calculated ones for **L-SK-4** (Table 18).<sup>418,563,564</sup> In addition to this, similar protonation constants seems to be noticed between **L-SK-4** and P1 ligand (3, 4-HOPO).<sup>562</sup> Some, significant spectral variations could be observed under very acidic conditions in the batch titration suggesting that the carboxylate moiety pK<sub>a</sub> would be inferior to -1. Based on literature and the values of the protonation constants, the following protonation schemes were proposed for ligands **rac-SK-2** (Figure 52A), **rac-SK-3** (Figure 52B) and **L-SK-4** (Figure 52C).



**Figure 52:** Protonation scheme of (A) *rac*-SK-2, (B) *rac*-SK-3, (C) *L*-SK-4.

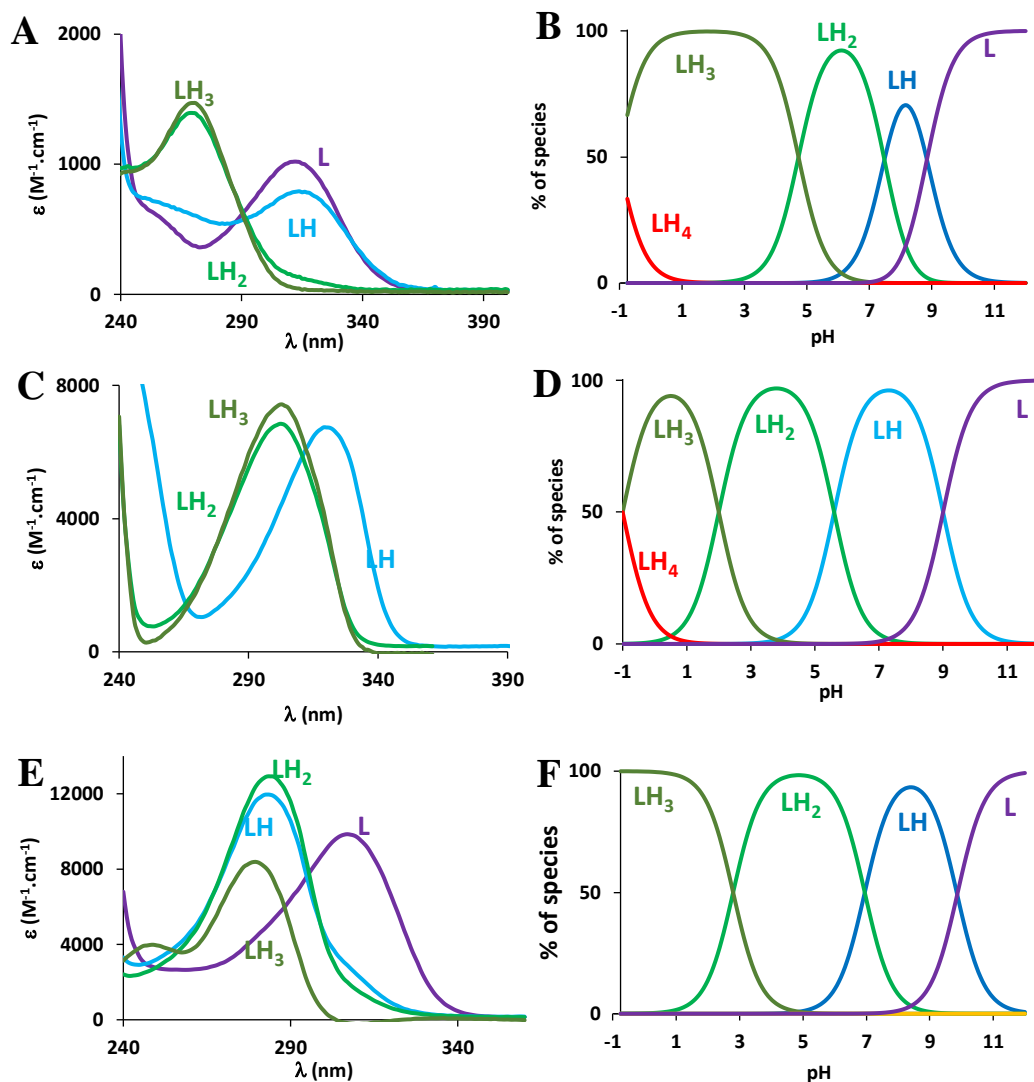
Since the  $pK_{as}$  of *rac*-SK-1 and *rac*-SK-5 have not been measured experimentally, the  $pK_{as}$  of the compounds that contained either the hydroxypyranone or the 3, 2-hydroxypyridinone core, were estimated from the literature of parent compounds (Table 19).

**Table 19:**  $pK_{as}$  of kojic acid, maltol and 1-methy-3-hydroxypyridin-2-one.

COMPOUND	$pK_{a1}$	$pK_{a2}$
<b>Kojic acid</b> <sup>565,566</sup> 	-1.86	7.70
<b>Maltol</b> <sup>418</sup> 	-	8.7
<b>1-methyl-3-hydroxypyridin-2-one</b> <sup>567</sup> 	0.2	8.6

Overall, based on the product of protonation constants ( $K_{a1} \times K_{a2}, \times K_{a3} \times K_{a4}$ ) (calculated and ones obtained from the literature), the order of acidity between the SK-n compounds can be drawn as follow; *rac*-SK1 > *rac*-SK5 > *rac*-SK3 > *rac*-SK2 > > *L*-SK4, demonstrating that *L*-SK-4 is the weakest acid of all.

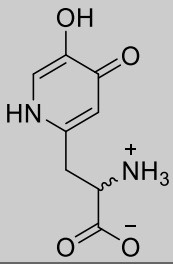
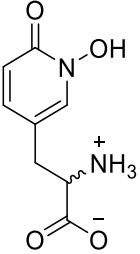
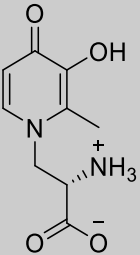
From these protonation constants of the *rac*-SK2, 3 and *L*-SK-4, the electronic spectra of the protonated species of each ligand and their distribution curves as function of pH were calculated (Figure 53).



**Figure 53:** Electronic spectra of the protonated species of (A) *rac*-SK-2, (C) *rac*-SK-3 and (E) *L*-SK-4 and distribution curves as function of pH of the protonated species of (B) *rac*-SK-2 ( $[rac-SK-2] = 2.56 \times 10^{-4} M$ ), (D) *rac*-SK-3 ( $[rac-SK-3] = 2.56 \times 10^{-4} M$ ) and (F) *L*-SK-4 ( $[L-SK-4] = 2.59 \times 10^{-4} M$ ). Solvent: H<sub>2</sub>O, I = 0.1 M (NaClO<sub>4</sub>), T = 25.0°C.

Afterwards, based on the distribution curves of the protonated species, the percentage of each protonated species at pH 7.4 was calculated (Table 20).

**Table 20:** Percentage (%) of the protonated species or *rac*-SK-2, 3 and *L*-SK-4 at pH 7.4 and structure of the protonated state for each compound most likely to be a LAT-1 substrate.

	LH <sub>3</sub>	LH <sub>2</sub>	LH	L
<i>rac</i> -SK-2	0.1 	53.5	44.7	1.2
<i>rac</i> -SK-3	0.0	1.5 	96.0	2.5
<i>L</i> -SK-4	0.0	28.3 	71.4	0.3

The calculation suggested that at physiological (pH 7.4), the majority of *rac*-SK-2 (53.5%) exists as LH<sub>2</sub>, followed by 44.7% of LH form and 1.2% at the fully deprotonated (L) state. In addition to this, just 0.1% exists in its neutral form (LH<sub>3</sub>) with the zwitterion form of amino acid. Moreover, 96% of *rac*-SK-3 exists at LH form whereas 2.5% and 1.5% exists in the L and LH state respectively. Interestingly at this pH there is not any neutral species as expected for amino acids. In the case of *L*-SK-4, 71.4% exists as LH whereas 23% exists as neutral molecule with amino acid group as zwitterion. A 0.3% of the total species is also appeared in the fully de-protonated state. Those data could give insights into the quantity of each of these compound that enters the cells. Namely, based on the fact that LAT-1 transporter can only accommodate neutral amino acids

(amino acid group as zwitterion) it is suggested that only a 0.1% of *rac*-SK-2 can enter the cell (if it exploits the LAT-1), whereas a 1.5% of the total *rac*-SK-3 will be transported through the LAT-1.<sup>568</sup> In contrast, ~ 30% of the total concentration of *L*-SK-4 will be able to be transported in the cells. Therefore, it can be assumed from these findings that biological order of activity if only influenced by penetration will be *L*-SK-4 >> *rac*-SK-3 > *rac*-SK-2. As a validation of the biological activity of the SK-n compounds, the % of the neutral species should also be taken into consideration.

## 6.2 Stability constants

### 6.2.1 Complexation with Fe(III)

Similar to the protonation study, spectrophotometric batch ( $-0.5 < \text{p[H]} < 2$ ) and classic titrations ( $2 < \text{pH} < 12$ ) were then carried out on the Fe(III) complexes of ligands *rac*-SK-2 (**Figure 54A, B**), *rac*-SK-3 (**Figure 54C, D**) and *L*-SK-4 (**Figure 54E, F**).

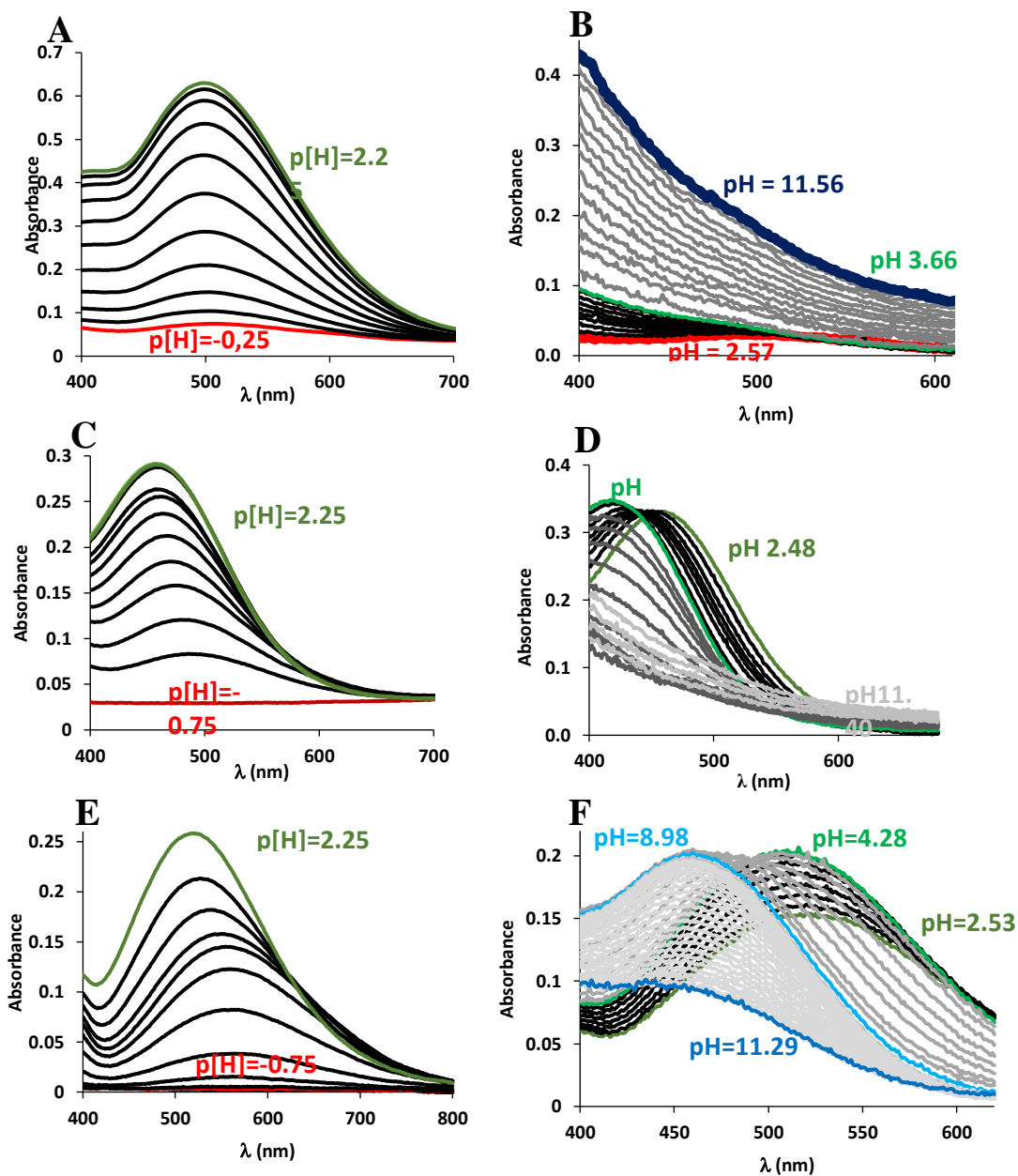


**Figure 54:** Spectrophotometric titrations vs pH of the Fe(III) complexes of ligands *rac*-SK-2 between (A)  $-0.75 \leq \text{p[H]} \leq 2$  (batch titration,  $[\textit{rac}\text{-SK-2}] = 2.77 \times 10^{-3} \text{ M}$ ,  $[\text{Fe}]/[\textit{rac}\text{-SK-2}] = 0.33$ ) and (B)  $2.50 < \text{pH} < 11.08$  (classic titration,  $[\textit{rac}\text{-SK-2}] = 2.97 \times 10^{-4} \text{ M}$ ,  $[\text{Fe}]/[\textit{rac}\text{-SK-2}] = 0.31$ ); of *rac*-SK-3 between (C)  $-0.75 \leq \text{p[H]} \leq 1.5$ . (batch titration,  $[\textit{rac}\text{-SK-3}] = 2.56 \times 10^{-4} \text{ M}$ ,  $[\text{Fe}]/[\textit{rac}\text{-SK-3}] = 0.33$ ) and (D)  $2.50 \leq \text{pH} \leq 11.51$  (classic titration,  $[\textit{rac}\text{-SK-3}] = 3.03 \times 10^{-4} \text{ M}$ ,  $[\text{Fe}]/[\textit{rac}\text{-SK-3}] = 0.30$ ) and of *L*-SK-4 between (E)  $-0.75 \leq \text{p[H]} \leq 2.25$ . (batch titration,  $[\textit{L}\text{-SK-4}] = 2.59 \times 10^{-4} \text{ M}$ ,

[Fe]/[L-SK-4]= 0.33) and (F)  $2.53 \leq \text{pH} \leq 11.25$  (classic titration,  $[L\text{-SK-4}] = 1.47 \times 10^{-4} \text{ M}$ , [Fe]/[L-SK-4]= 0.31)

The averaged overall stability constants of the Fe(III) complexes were calculated in the pH range where the species were soluble (**Table 21**).

**Table 21:** Overall stability constants ( $\log \beta$ ) of the Fe(III) complexes of ligands *rac*-SK-2, *rac*-SK-3 and *L*-SK-4  $\pm$  SD (expressed to the last significant place). H<sub>2</sub>O,  $I = 0.1 \text{ M}$  (NaClO<sub>4</sub>),  $T = 25.0 \text{ }^\circ\text{C}$ .  $\beta_{\text{ML}_x\text{H}_y} = [\text{ML}_x\text{H}_y]/([\text{M}][\text{L}]^x[\text{H}]^y)$ ; charges were omitted for the sake of clarity

	<i>rac</i> -SK-2	<i>rac</i> -SK-3	<i>L</i> -SK-4	PI <sup>562</sup>	1, 2- HOPO <sup>55</sup> <sub>9</sub>	DFP <sup>569</sup>
<b>ML<sub>2</sub>H<sub>2</sub></b> ( $\beta_{122}$ )	22.9	39.06 $\pm 0.001$	40.65 $\pm 0.0011$	49.12 $\pm 0.001$	-	-
<b>MLH</b> ( $\beta_{111}$ )	-	21.83 $\pm 0.001$	21.58 $\pm 0.001$	25.92 $\pm 0.009$	-	-
<b>ML</b> ( $\beta_{110}$ )	-	-	-	-	10.6	15.0
<b>ML<sub>2</sub></b> ( $\beta_{120}$ )	-	-	-	-	19.3	27.3
<b>ML<sub>3</sub>H<sub>3</sub></b> ( $\beta_{133}$ )	-	53.89 $\pm 0.001$	58.87 $\pm 0.006$	71.43 $\pm 0.006$	-	-
<b>ML<sub>3</sub>H<sub>2</sub></b> ( $\beta_{132}$ )	-	-	-	65.33 $\pm 0.003$	-	-
<b>ML<sub>3</sub></b> ( $\beta_{130}$ )	-	-	40.62 $\pm 0.007$	46.03 $\pm 0.005$	27.2	37.43
<b>ML<sub>2</sub>(OH)<sub>2</sub></b>	-	-	13.54 $\pm 0.002$	-	-	-

According to the results obtained, the appearance of a typical ligand-to-metal charge transfer band (LMCT) in the 400-700 nm region of the spectra in the titrations of the three chelators with Fe(III) versus pH showed that complexation started at very low pH.

The batch titration of Fe(III) and *rac*-SK-2 between p[H] -0.25 and 2.25 showed the appearance of a LMCT band at 500 nm suggesting the formation of a single species in this range of p[H] that was tentatively attributed to the formation of the FeLH<sub>2</sub> species in accordance with *rac*-SK-2 protonation scheme (**Figure 52A**). Titration between pH 2.50 and 11.56 showed a hypsochromic shift of this band, suggesting the formation of a new species but precipitation, indicated by simultaneous increase of the baseline and the spectral noise on the whole spectrum, occurred around pH 3.7 and precluded further analysis of the data.

In the case of *rac*-SK-3, the Fe(III) complex LMCT band appeared at 487nm at p[H] -0.5 and shifted gradually hypsochromically to 458 nm (pH 2.48) and 411 nm (pH 6.93), suggesting the successive formation of FeLH, FeL<sub>2</sub>H<sub>2</sub> and FeL<sub>3</sub>H<sub>3</sub> (possibly Fe(LH)<sub>2</sub> and Fe(LH)<sub>3</sub>) with the amino group protonated, in accordance with *rac*-SK-3 protonation scheme (**Figure 52B**). The LMCT band then started to decrease gradually with simultaneous precipitation, sign of release of Fe(III) from the ligand and its precipitation as Fe(OH)<sub>3</sub>.

The spectral variations of the Fe(III)-*L*-SK-4 titrations also showed the successive formation of the FeLH, FeL<sub>2</sub>H<sub>2</sub> and FeL<sub>3</sub>H<sub>3</sub> complexes. We suggest that Fe(III) is coordinated by the (CO, O-) donor set as it was observed previously for mimosine.<sup>7</sup> Further increase of the pH till around 9 lead to the formation of the deprotonated FeL<sub>3</sub> complex, possibly due to the deprotonation of the ammonium functions. Above pH 9, the LMCT band started to gradually decrease but it was still present at the end of the titration (pH 11.29) with no sign of precipitation, which suggested the presence of a hydroxylated FeL<sub>2</sub>(OH)<sub>2</sub> species.

No evidence of dinuclear species could be observed in our experimental conditions for any of the three ligands.

Since the stability constants for both *rac*-SK-1 and 5 has not been determined experimentally, the

respective values obtained from the literature suggested that maltol and kojic acid (as hydroxypyranones) have  $\log\beta_{130} = 28.5$  and  $24.15$  respectively, whereas 3, 2-hydroxypyridinone and 1-methyl-3-hydroxypyridin-2-one have  $\log\beta_{130} = 29.3$  and  $32$  respectively.<sup>418,562,566,570</sup>

From these stability constants, the electronic spectra of the complexed species and their distribution curves were calculated for *rac*-SK-3 (**Figure 55A, B**) and *L*-SK-4 (**Figure 55C, D**)

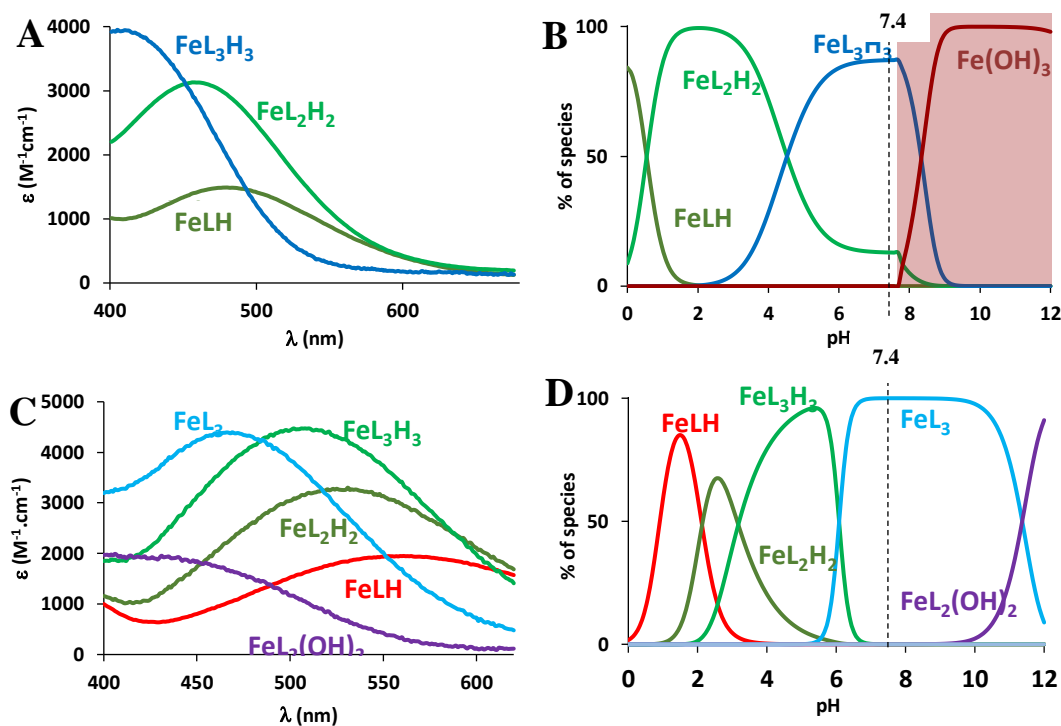


**Figure 55:** Electronic spectra of the protonated species of (A), Fe-*rac*-SK-3 and (C) Fe-*L*-SK-4 and distribution curves of the protonated species of (B) Fe-*rac*-SK-3 ( $[rac\text{-SK-3}] = 3.03 \times 10^{-4} M$ ,  $[Fe]/[rac\text{-SK-3}] = 0.3$ ) and (D) Fe-*L*-SK-4 ( $[L\text{-SK-4}] = 1.54 \times 10^{-4} M$ ,  $[Fe]/[L\text{-SK-4}] = 0.30$ ). Solvent:  $H_2O$ ,  $I = 0.1 M$  ( $NaClO_4$ ),  $T = 25.0^\circ C$  for all measurements.

The distribution curves show that, at physiological pH (pH 7.4), ligand *rac*-SK-3 exists primarily as its  $Fe(rac\text{-SK-3})_3H_3$  (**Figure 56A**) species and *L*-SK-4 as almost exclusively its  $Fe(L\text{-SK-4})_3$  complex (**Figure 56B**).

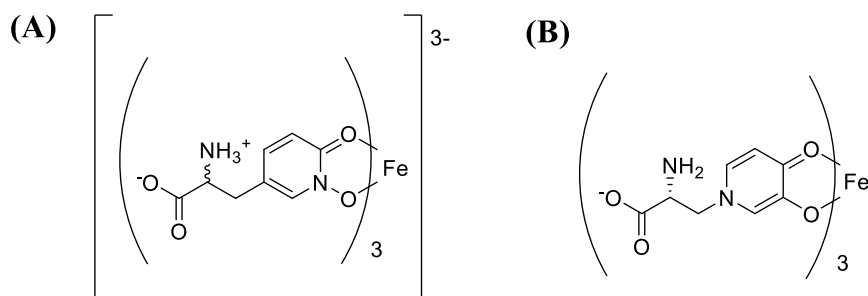


**Figure 56:** Main (A) Fe(III) – *rac*-SK-3 and (B) Fe(III) – *L*-SK-4 complexes being formed at pH 7.4.

To compare the chelation power of the three chelator, and other chelators from literature, for Fe(III), the amount of metal not complexed by the chelators ( $[M^{n+}]_{\text{free}}$ ) was calculated at every pH from the distribution curves (with  $[\text{Chelator}]_{\text{tot}} = 10^{-5}\text{M}$  and  $[M^{n+}]_{\text{total}} = 10^{-6}\text{M}$ ) and  $-\log([M^{n+}]_{\text{free}})$  was plotted against pH for clarity (**Figure 57**). A higher value thus indicates a higher chelation power.

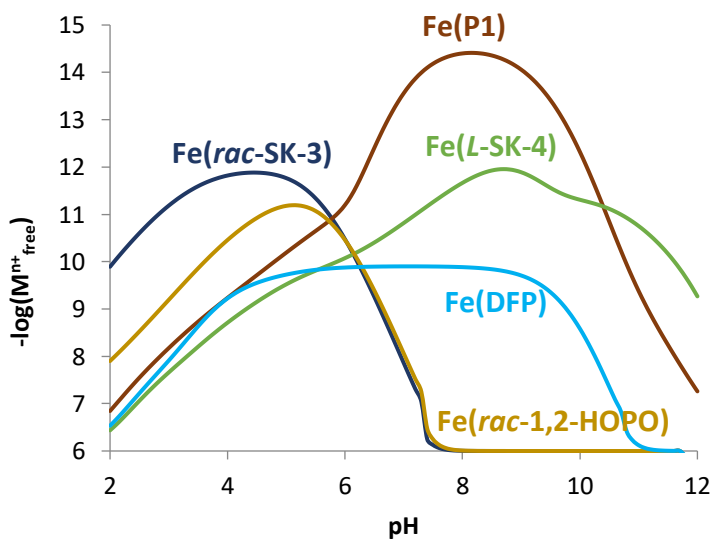


**Figure 57:** Chelating power of selected chelators versus pH, represented by the inverse log of the non-complexed (free)  $\text{Fe}^{3+}$  concentration, ( $-\log([M^{n+}]_{\text{free}})$ ) ( $[\text{Chelator}] = 10^{-5}\text{M}$ ,  $[\text{Fe}^{3+}] = 10^{-6}\text{M}$ ), taking into confederation the precipitation of  $\text{Fe}_2\text{O}_3$  species.

If we consider the affinity for Fe(III), we can observe that *rac*-SK-3, possessing a 1,2-HOPO chelating group, is the best chelator (when compared with the 1, 2-HOPO) between pH 2 and 5.8. From this pH, ligands based on the 3, 4-HOPO chelating unit like *L*-SK-4, DPF and ligand P1 become the best chelators. Interestingly, those data suggested that *L*-SK-4 exhibits a higher affinity than DFP however lower than ligand P1. As for *rac*-SK-2, its precipitation above pH 4 precluded any calculation. Therefore, the order of stability constants towards Fe(III) binding can be drawn as follow; *L*-SK-4 >> *rac*-SK-5 > *rac*-SK-3 > *rac*-SK-1.

Our bidentate ligands are giving a series of different complexes of stoichiometry LFe, L<sub>2</sub>Fe, L<sub>3</sub>Fe. Based on literature, only the L<sub>3</sub>Fe complex is considered suitable to prevent redox cycling and thus formation of ROS.<sup>434,571,572</sup> Therefore, the concept of pFe<sup>3+</sup> (-log[Fe<sup>3+</sup>]<sub>free</sub>) is not entirely satisfactory as it only considers [Fe<sup>3+</sup>]<sub>free</sub> to quantify the efficacy of a ligand but does not give any information about the 1:1 and 2:1 stoichiometries. Therefore, by defining pL<sub>3</sub>Fe<sup>3+</sup> as -log[L<sub>3</sub>Fe<sup>3+</sup>] complex, in the same conditions: [Fe<sup>3+</sup>]<sub>total</sub> = 10<sup>-6</sup> M with [L]<sub>total</sub> = 10<sup>-5</sup> M, pH 7.4, the closest pL<sub>3</sub>Fe<sup>3+</sup> is to 6 (full Fe(III) chelation) the more effective the ligand to prevent redox cycling and formation of ROS (**Figure 58**).

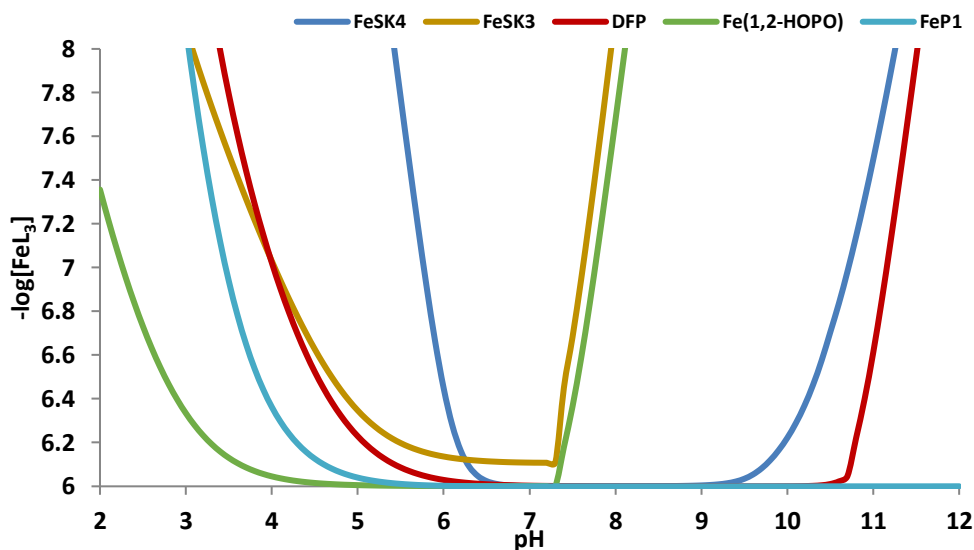


**Figure 58:** Saturated  $\text{Fe}^{3+}$  binding of selected chelators versus pH, represented by the inverse log of the  $\text{FeL}_3$  species ( $-\log([\text{FeL}_3])$ ) ( $[\text{Chelator}] = 10^{-5}\text{M}$ ,  $[\text{Fe}^{3+}] = 10^{-6}\text{M}$ ).

**Table 22:** Percentage (%) of  $\text{Fe}^{3+}$  redox silenced based on the  $\text{p}[\text{L}_3\text{Fe}^{3+}]$  at pH 7.4

	$\text{p}[\text{L}_3\text{Fe}^{3+}]$ at pH 7.4	% of $\text{Fe}^{3+}$ redox silenced
<b>Fe-L-SK-4</b>	6.00	100
<b>Fe-rac-SK-3</b>	6.45	35.5
<b>Fe-1, 2-HOPO</b>	6.18	66
<b>Fe-P1</b>	6.00	100
<b>DFP</b>	6.00	100

According to the exported data (**Table 22**), it can be concluded that at the **given** conditions;  $[\text{Fe}^{3+}]_{\text{total}} = 10^{-6}\text{M}$  with  $[\text{L}]_{\text{total}} = 10^{-5}\text{M}$ , pH 7.4, 3, 4-HOPOs were capable of forming fully saturated coordination spheres. As a result of this, 100% of the  $\text{Fe}^{3+}$  is redox inactive (silenced). In contrast, the  $\text{Fe}^{3+}$  centre of the 1, 2-HOPO- $\text{Fe}^{3+}$  complexes, is more susceptible to promote ROS formation since only the % of chelatable  $\text{Fe}^{3+}$  is below 100%. This approach could give as insights into whether the treatment with these compounds can prevent the redox cycling and ROS formation in biological system. However, the challenging part of this would be the calculation the liable iron pool (LIP) in the different cellular systems as LIP can found in various organelles

including cytosol, mitochondria and liposomes and the concentration of chelators there too. In addition to these, the pH at these organelles is not strictly 7.4.

### 6.2.2 Complexation with Cu(II) and Zn(II)

The next part of this study involved the potentiometric determination of the stability constants and the binding efficacy of the SK-n compounds against Cu(II) and Zn(II). It has been previously demonstrated that Cu(II) is also a redox active metal that can catalyzed the ROS formation, whereas Zn(II) is not.<sup>438,573,574</sup> Therefore, the determination of the stability constant could give insights on whether the SK-n compounds can prevent the Cu(I)/Cu(II) redox cycle and inhibit the ROS formation. In addition to this, the binding efficacy against Zn(II) could illustrate whether it can bind to HOPOs and remove some of them, preventing in that way the complete inhibition of Fenton chemistry (**Table 23**).

**Table 23:** Overall stability constants ( $\log \beta$ ) of the Cu(II) and Zn(II) complexes of ligands *rac*-SK-2, *rac*-SK-3 and *L*-SK-4  $\pm$  SD expressed to the last significant place. Solvent: H<sub>2</sub>O, *I* = 0.1 M (NaClO<sub>4</sub>), T = 25.0 °C.

	MLH	ML <sub>2</sub> H <sub>2</sub>	ML <sub>2</sub> H	ML <sub>2</sub>
<i>rac</i> -SK-2	nd	nd	nd	nd
Zn- <i>rac</i> -SK-3	13.9 $\pm 0.002$	27.86 $\pm 0.007$	21.56 $\pm 0.007$	12.5 $\pm 0.002$
Cu- <i>rac</i> -SK-3	nd	nd	nd	nd
Zn- <i>L</i> -SK-4	14.56 $\pm 0.006$	28.35 $\pm 0.006$	22.00 $\pm 0.005$	13.55 $\pm 0.007$
Cu- <i>L</i> -SK-4	16.7 $\pm 0.002$	33.44 $\pm 0.006$	25.79 $\pm 0.007$	15.8 $\pm 0.002$
Zn-P1 <sup>562</sup>	18.79 $\pm 0.006$	36.70 $\pm 0.004$	26.02 $\pm 0.009$	-
Cu-P1 <sup>562</sup>	21.78 $\pm 0.007$	41.42 $\pm 0.007$	34.21 $\pm 0.005$	24.68 $\pm 0.005$

In the case of *L*-SK-4, a successive formation of MLH, ML<sub>2</sub>H<sub>2</sub>, followed by successive deprotonation to ML<sub>2</sub>H and ML<sub>2</sub> for both Cu(II) and Zn(II) with stronger stability constants for Cu(II) than for Zn(II) was observed (**Table 23**).

*Rac*-SK-3 exhibited the same complexation pattern as *L*-SK-4 with Zn(II) but the stability of the Cu(II) complexes could not be determined as the complex was already fully formed at pH 2 due to the lower pKa values of this 1,2-HOPO-based ligand. This suggested, as observed for *L*-SK-4, a stronger stability of the Cu(II) complex than the Zn(II) complex. No evidence of dinuclear species could be observed in our experimental conditions.

To compare the chelation power of the three chelator, and other chelators from literature, for different metals, the amount of metal not complexed by the ligands ( $[M^{n+}]_{\text{free}}$ ) was calculated at every pH from the distribution curves (with  $[\text{Chelator}]_{\text{tot}} = 10^{-5}\text{M}$  and  $[M^{n+}]_{\text{total}} = 10^{-6}\text{M}$ ) and  $-\log([M^{n+}]_{\text{free}})$  was plotted against pH for clarity (**Figure 59**). A higher value thus indicates a higher chelation power.

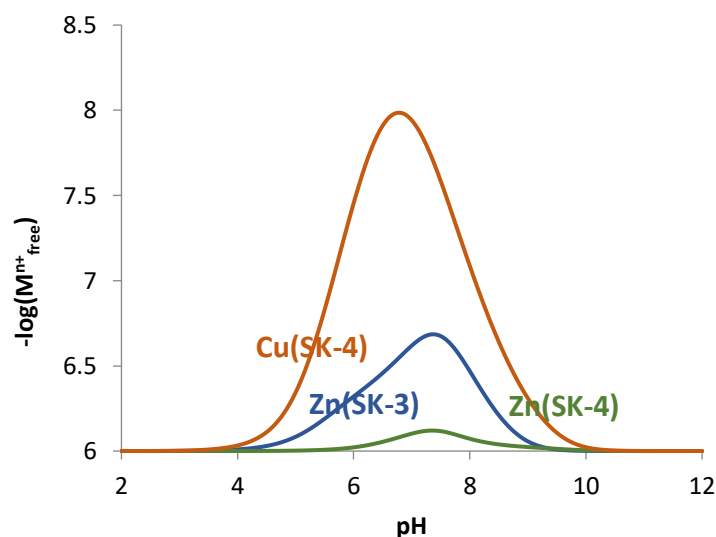


**Figure 59:** Chelating power of selected ligands versus pH, represented by the inverse log of the non-complexed (free)  $M^{n+}$  concentration, ( $-\log([M^{n+}]_{\text{free}})$ ) ( $[\text{Chelator}] = 10^{-5}\text{M}$ ,  $[M^{n+}] = 10^{-6}\text{M}$  [ $\text{Fe}^{3+}] = 10^{-6}\text{M}$ ), taking into confederation the precipitation of  $\text{Fe}_2\text{O}_3$  species.

As for divalent cations, both *rac*-SK-3 and *L*-SK-4 show a high selectivity for Fe(III) over Cu(II) and Zn(II), similarly to other ligands of the 3,4-HOPO family like DFP or ligand P1. That means

that even if cells contained elevated amount of Cu(II) or Zn(II), the redox silencing of Fe(III) is expected to dominate. As PD is linked with the abnormal elevation of Fe(III), treatment with the chelators can lead to the beneficial inhibition of ROS production by the prevention of redox cycling of Fe(III) and consequently Cu(II).

## 7 Results and Discussion – Evaluation of the anticancer capacity of the chelators in an *in vitro* model of Malignant Melanoma.

### 7.1 Biological Characterization

#### 7.1.1 Assessing the cytotoxicity of the SK-n compounds

The ability of a series of hydroxypyridinone (HOPO) including 1, 2-HOPO (*rac*-SK-3), 3, 2-HOPO (*rac*-SK-5), 3, 4-HOPO (*rac*-SK-2 and *L/D*-SK-4) as well as a hydroxypyranone (*rac*-SK-1) to induce cytotoxic effect has been evaluated in an *in vitro* model of malignant melanoma consisting of human malignant melanoma (A375) cells. (The cytotoxicity of 6 out of the 9 compounds has been evaluated due to the fact that the *rac*-SK-6, *rac*-SK-7 and *L*-SK-8 weren't synthesised by the time of biological characterisation). For the cytotoxicity assay, all the compounds have been assessed in a range of concentrations (10-1000  $\mu$ M) and time points (24-72 hr)(**Figure 60A-F**). The results revealed that A375 cells appeared to be more resistant to the treatment of *rac*-SK-1 and 5 since the viability levels after the exposure remained in the same levels as their respective untried controls, whereas some noteworthy activity has been noticed on *rac*-SK-2 and 3 as at high concentrations as 1000  $\mu$ M, 72 hr post-treatment (**Figure 60A-D**). In contrast, both enantiomeric forms of a methylated analogue of *L*-mimosine (*L/D*-SK-4) shown a potency to induce cytotoxic effect on A375 cells in a dose (concentration)-time dependent manner. In particular, a statistically significant reduction ( $p < 0.01$ ) in viability levels was initially observed when A375 cells were treated with 10  $\mu$ M of *L*-SK-4, an effect which was further potentiated as the concentration of the compound and/or time of exposure were increased (**Figure 60E**). Overall, cell viability levels reached an  $EC_{50}$  at a concentration of 100  $\mu$ M after 48 hr. In the case of the evaluation of the *D*-enantiomer (*D*-SK-4), a similar time- and concentration-dependent response was evident to that *L* enantiomer (**Figure 60F**). However, this was the case only at 48-72 hr of exposure while at 24 hr it remained almost at control levels (90-100%) except at very high

concentrations (e.g. 1000  $\mu\text{M}$ ). Furthermore, such treatment was not as potent as with *L*-SK-4, evident by a much higher  $\text{EC}_{50}$  value of approximately 250  $\mu\text{M}$  at 48-72 hr of exposure. Although it is appeared that both enantiomers have similar activity, the preference for the *L* enantiomer is more likely to occur due to the small preference of LAT-1 for the *L*-enantiomers of amino acids.<sup>476</sup> In addition to this, it seems that the structure of *L*-SK-4 (*N*-substituted 3,4 HOPO) can fit preferentially into the active site of the transporter compared to the structure of other screened molecules.

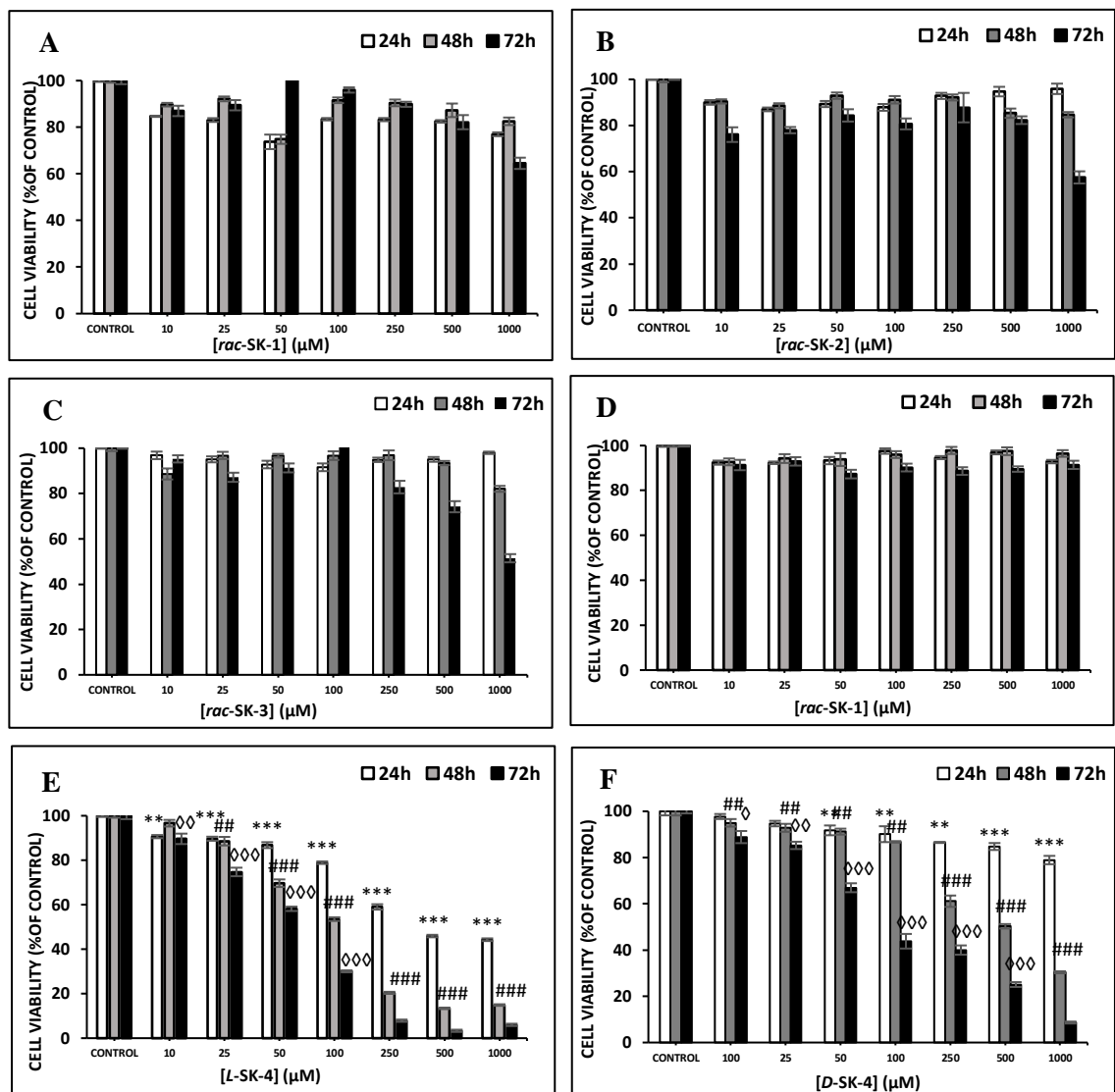


**Figure 60:** The ability of hydroxypyridones to induce cytotoxicity in A375 cells. Cells were exposed to a range of 10-1000  $\mu\text{M}$  concentrations of (A) *rac*-SK-1, (B) *rac*-SK-2, (C) *rac*-SK-3, (D) *rac*-SK-5, (E) *L*-SK-4 and (F) *D*-SK-4 for 24, 48 and 72 hr. Data shown are means  $\pm$  SD of 5 replicates from three independent experiments.

The cytotoxic phenotype that has been induced by the treatment of 100  $\mu\text{M}$  of *L*-SK-4 has also been observed under inverted phase contrast microscopy (**Figure 61**) as the number of cells in the treated groups decreases over the time compared to their respective untreated controls.

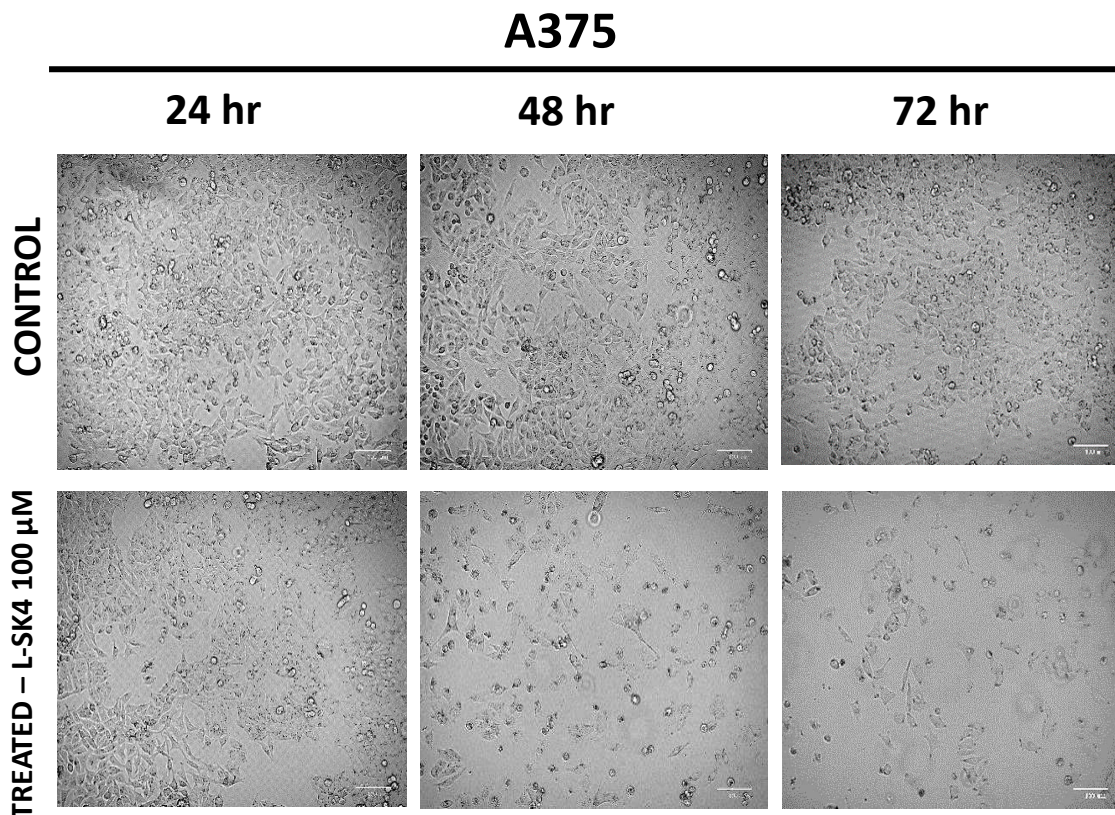


**Figure 61:** The ability of *L*-SK-4 to induce cytotoxicity in A375 cells. Control cells and those exposed to 100  $\mu\text{M}$  of *L*-SK-4 at 24 hr, 48, and 72 hr were visualized under inverted phase contrast microscope.

Finally, we evaluated the cytotoxic effect of 100  $\mu\text{M}$  of *L*-SK-4 in a non-melanoma epidermoid cancer (A431) and a non-malignant immortalized human keratinocyte (HaCaT) cell line in order to demonstrate any specificity towards the melanoma (A375) cell line. Our observations revealed that these cells were also affected at 100  $\mu\text{M}$  of *L*-SK-4 but nevertheless were shown to be more resistant than A375 (**Figure 62**). More specifically, in the case of A431 cells, the effect was comparable with that of A375 (at 24 hr of exposure) but it was a lot more intensified at 48 and 72 hr of exposure respectively as the number of viable cells was significantly higher compared to A375 cells (**Figure 62A**). In contrast, a comparable cytotoxicity pattern was also observed in the case of HaCaT cells as well (**Figure 62B**). Together, our cytotoxicity data indicate that *L*-SK-4 exerts a higher degree of cytotoxic potency against A375 cells while A431 and HaCaT cells were more resistant.

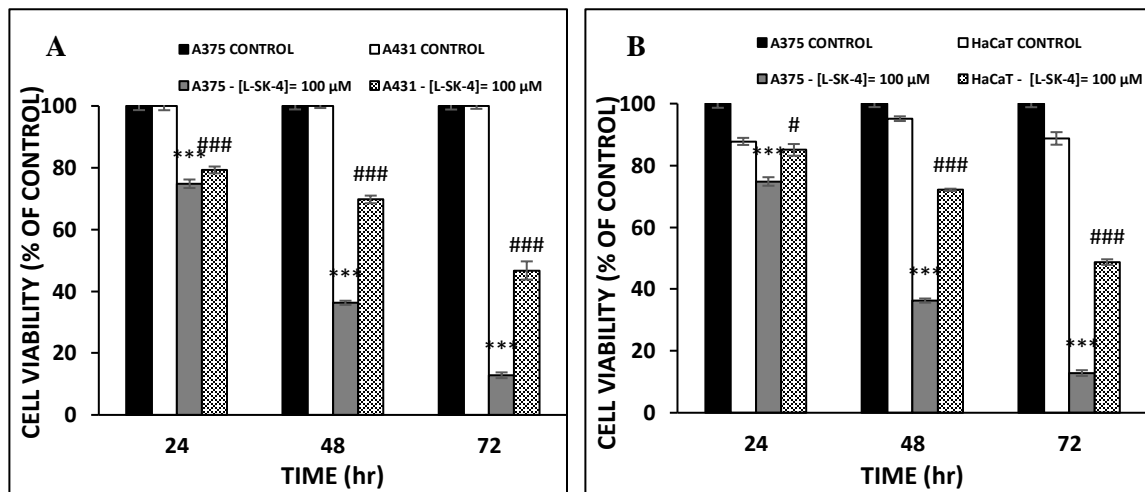


**Figure 62:** The ability of *L*-SK-4 to induce cytotoxicity in (A) non-melanoma (A431) cells and (B) non-malignant keratinocyte (HaCaT) cells. Cells were exposed to 100  $\mu\text{M}$  of *L*-SK-4 for 24, 48 and 72 hr. Data shown are means  $\pm$  SD of 5 replicates from three independent experiments.

The resistant phenotype of A431 and HaCaT cells post exposure to 100  $\mu\text{M}$  of *L*-SK-4 was also observed under inverted phase contrast microscopy (**Figure 63A and B**). Initially, the A431 cell

clusters that can be seen in the 24 hr control are retained upon the treatment whereas some shrinkage of the clusters is indicated on the 48 hr. In the case of 72 hr, cell clusters can still be seen, however the induced cytotoxicity, de-touched them from the bottom of the plate and they appeared as floaters. Similar observations are pointed for the HaCaT cells, since the cells remained in clumps as their respective untreated controls for 24 and 48 hr, whereas at 72 hr they appear as floaters.

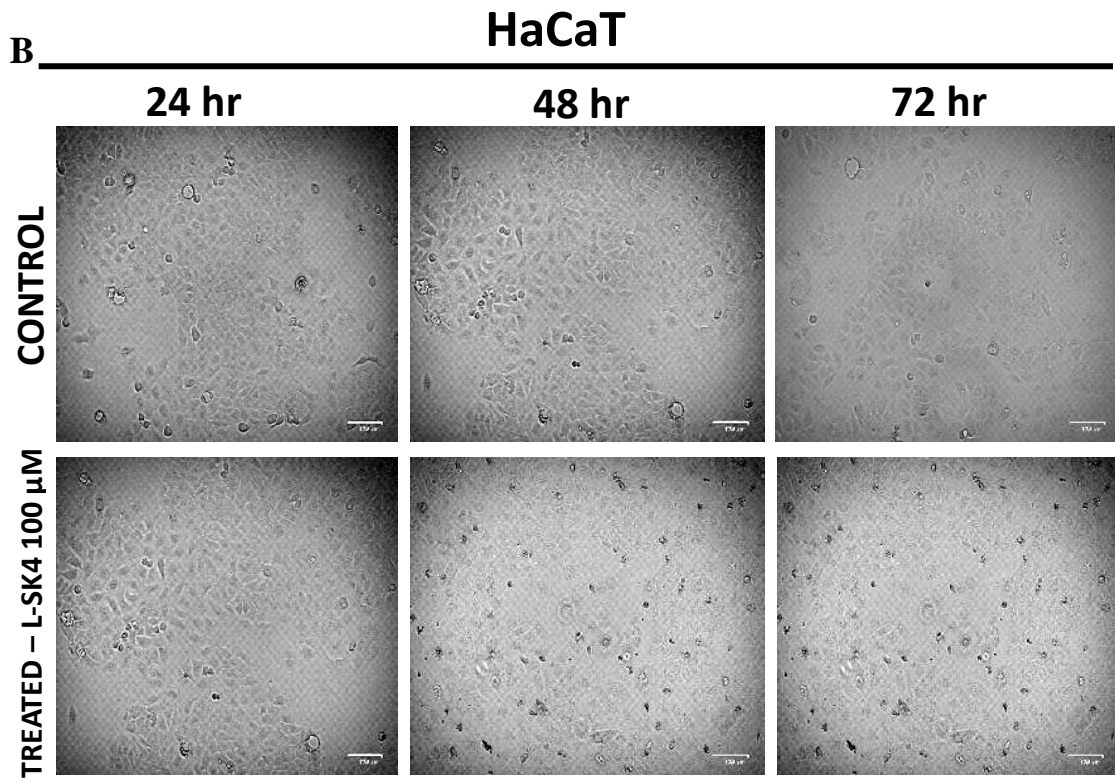
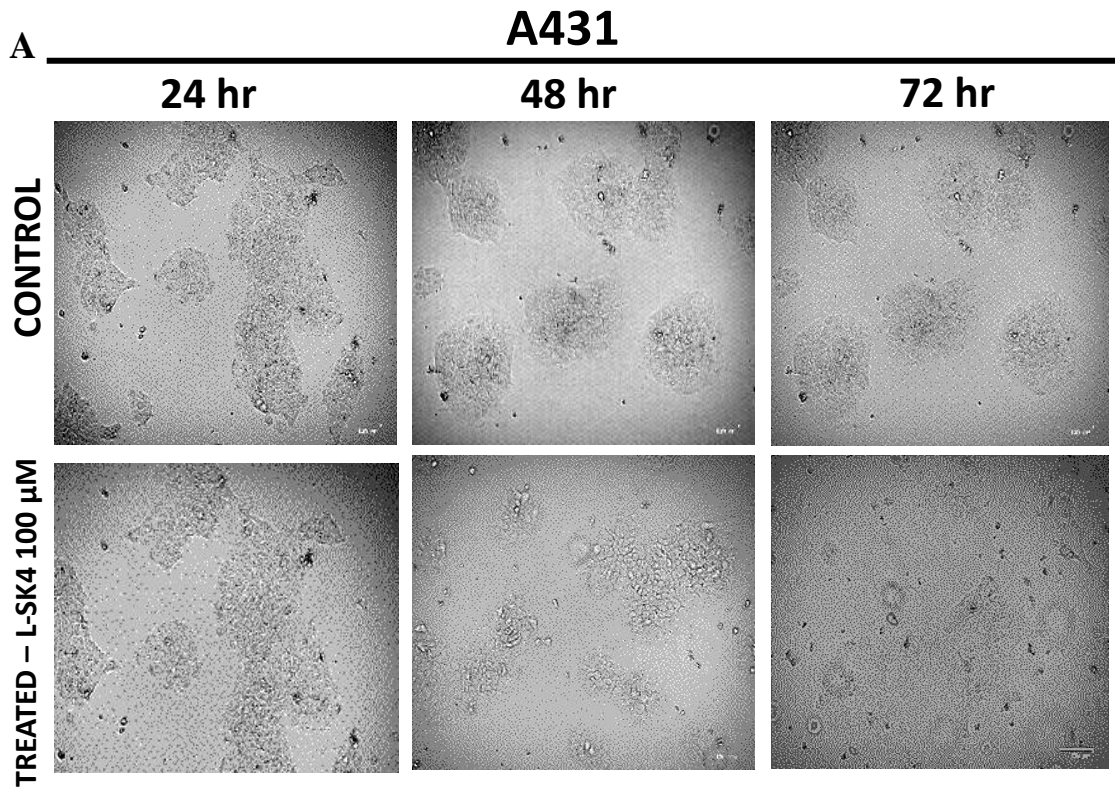


**Figure 63:** The ability of *L*-SK-4 to induce cytotoxicity in (A) A431 and (B) HaCaT cells. Control cells and those exposed to 100  $\mu$ M of *L*-SK-4 at 24 hr, 48 hr and 72 hr were visualized under inverted phase contrast microscope.

## 7.2 In vitro validation of Structure Activity Relationship (SAR)

### 7.2.1 Transportation through LAT-1

As mentioned before, the screened HOPOs contain an amino-acid vector in order to be transported through the LAT-1 transporters as proposed in the literature.<sup>465,469,484</sup> However, even if SK-n were designed to be LAT-1 substrates, it does not mean they use it. This hypothesis needed to be checked. In order to validate the assumption, the active site of the LAT-1 transporter has been blocked with either an inhibitor or a non-selective substrate which competes the efflux/uptake of amino-acids. For the purpose of this experiment, *L*-thyroxin (**Figure 64A**) was used as LAT-1 inhibitor, whereas 2-amino-norbornanecarboxylic acid (BCH) (**Figure 64B**) was used as a LAT-1 non selective substrate as it competes with leucine towards the same active site of the transporter.

554,575–577

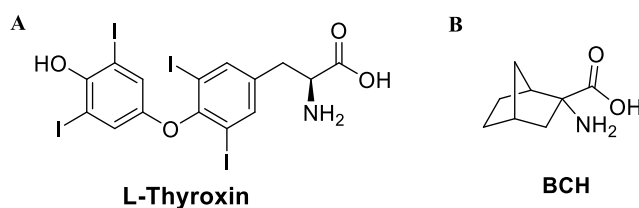


**Figure 64:** Structure of (A) L-Thyroxin and (B) BCH.

The addition of either the inhibitor or the non-selective substrate will induce cell death due to the cell starvation of amino acids, masking in that way the toxic effect of the lead compound. In order to overcome this effect both *L*-thyroxin and BCH have been applied to A375 cells, in a

range of concentrations (0.1-1 mM and 0.5-10 mM respectively) and time (24-72 hr) in the absence of *L*-SK-4 in order to determine the tolerated dose (**Figure 65A and B**).

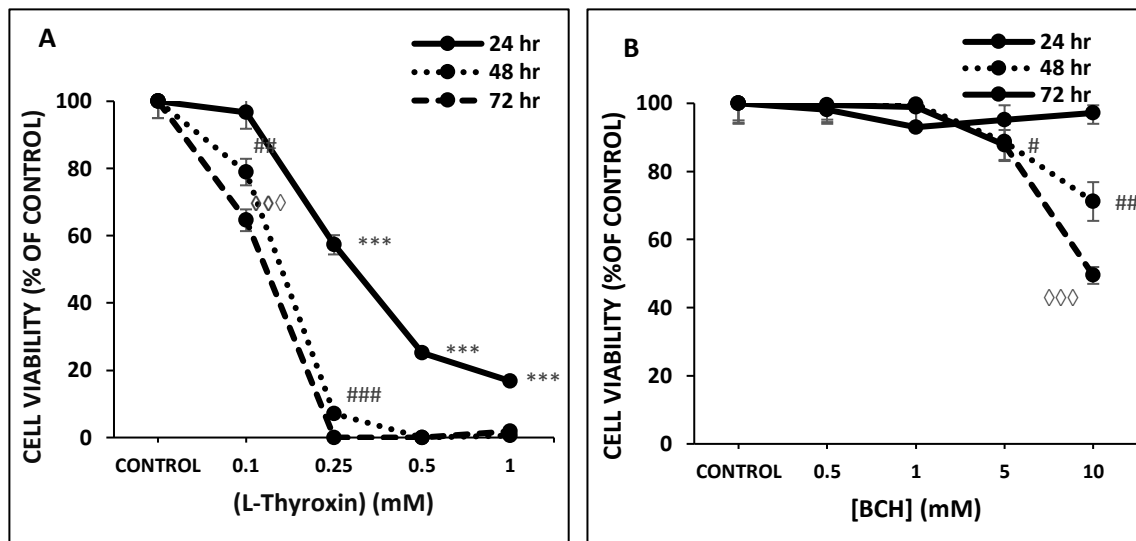


**Figure 65:** Determination of cytotoxicity of LAT-1 inhibitor; *L*-Thyroxin and non-selective substrate; BCH. A375 cells have been exposed in a range of concentrations (0.1-1 mM) of *L*-thyroxin (**A**) and (0.5-10 mM) of BCH (**B**) for 24, 48 and 72 hr. Data shown are means  $\pm$  SD of 5 replicates from three independent experiments.

The optimum concentration was found to be equal to 100  $\mu$ M for *L*-Thyroxin and 5 mM for BCH as at higher concentrations they induced toxicity. To investigate the use of LAT-1 by *L*-SK-4, A375 cells have been treated with *L*-Thyroxin (100  $\mu$ M) and BCH (5 mM) (separately) in the presence or the absence of 100  $\mu$ M of *L*-SK-4 for 24, 48 and 72 hr and the viability levels were monitored again utilizing Alamar Blue assay (**Figure 66**).

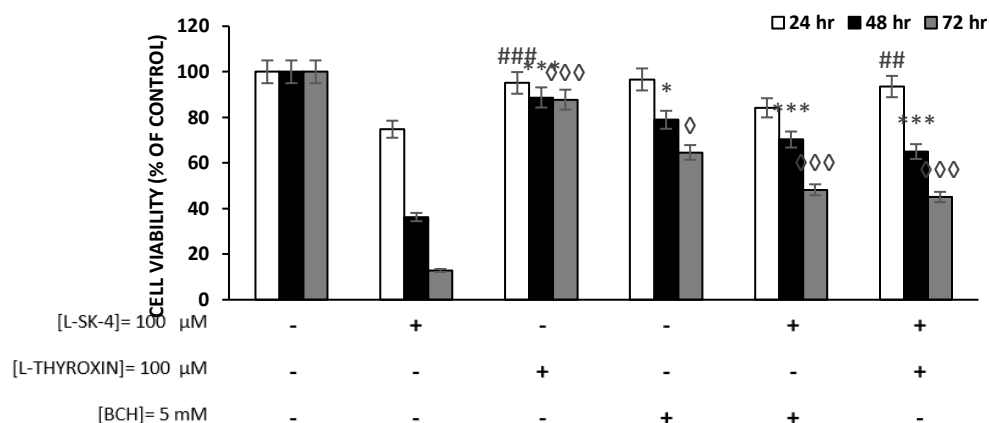


**Figure 66:** A375 cells have been exposed to 100 μM of *L*-SK-4 in the presence or the absence of 100 μM of *L*-Thyroxin or 5 mM of BCH respectively for 24, 48 and 72 hr. Data shown are means ± SD of 5 replicates from three independent experiments.

The results revealed that inhibition of the active site of LAT-1 transporter, and therefore preventing the entrance of *L*-SK-4 into the cells, leading to a significant cell rescue, since the viable levels of the co-treated groups were significantly higher compared to the respective ones been treated just with *L*-SK-4 (**Figure 66**). However, the limitations of this study didn't allow for final conclusions. This is because *L*-Thyroxin appears to be less selective towards LAT-1 inhibition compared to other synthetically accessible inhibitors which they can inhibit the Leucine uptake by 99±4%.<sup>272,465,484,578,579,580</sup> In addition to this, BCH is reported to cause inhibition of Leucine uptake by 75.3±6.7, 78±3.5 and 73±4.5% in KB, Saos2 and C6 cell lines respectively.<sup>577</sup> Therefore, the use of alternative inhibitor with higher inhibitory capacity was essential. Moreover, since BCH as a non-specific LAT substrate it might present some selectivity and/or specificity over LAT-2 or LAT-4 as it was demonstrated before.<sup>581,582</sup> Therefore, in an attempt to optimize and improve the above findings, two enantiomerically pure forms of a 2-amino-3-(2-naphthyl) propanoic acid were synthesized (**Figure 67**).<sup>580</sup>

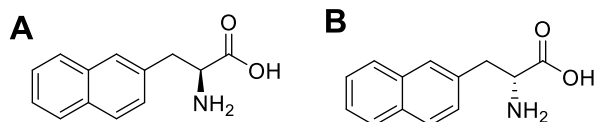


**Figure 67:** Structure of (A) *L*- and (B) *D*-2-amino-3-(2-naphthyl) propanoic acid.

According to the literature, the *L*- enantiomer form of this molecule exerts higher selectivity over LAT-1 with the capability of inhibiting Leucine uptake by  $94 \pm 2\%$ .<sup>580</sup> The addition of the LAT-1 inhibitors is expecting to induce cytotoxicity concealing in that way the cytotoxic effect of the *L*-SK-4. In order to overcome this effect both *L*- and *D*- 2-amino-3-(2-naphthyl) propanoic acid have been applied to A375 cells, in a range of concentrations (2-10 mM) and time (24-72 hr) in the absence of *L*-SK-4 in order to determine the tolerated dose (**Figure 68**).

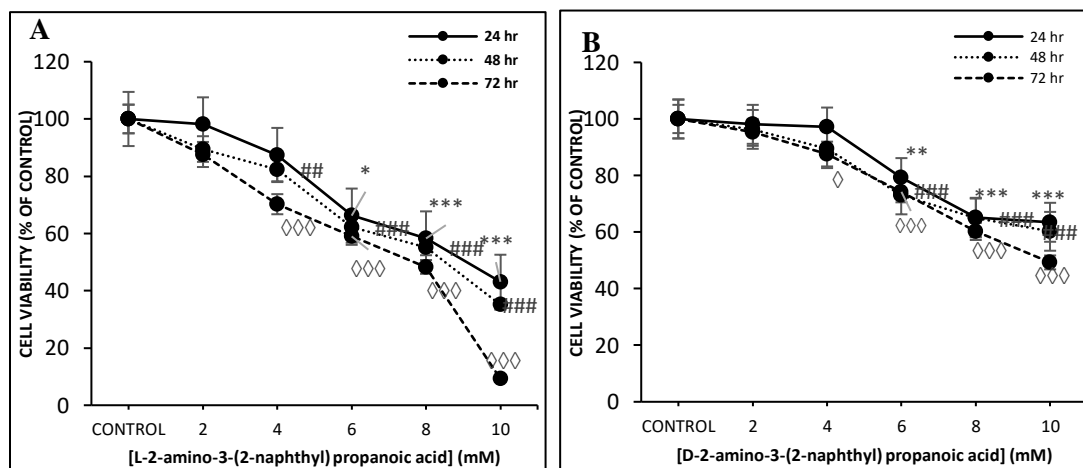


**Figure 68:** Determination of cytotoxicity of LAT-1 inhibitor; *L*- and *D*- 2-amino-3-(2-naphthyl) propanoic acid. A375 cells have been exposed in a range of concentrations (2-10 mM) of *L*- and *D*- 2-amino-3-(2-naphthyl) propanoic acid for 24, 48 and 72 hr respectively. Data shown are means  $\pm$  SD of 5 replicates from three independent experiments.

The optimum concentration was found to be equal to 2 mM for the *L*- enantiomer (**Figure 68A**) and 4 mM for the *D*- enantiomer (**Figure 68B**) as at higher concentrations it became cytotoxic.

However, for the rationalization of their inhibitory potency, both enantiomers have been screened under the same conditions and concentrations. For the validation of all the above, A375 cells have been treated with *L*- and *D*- 2-amino-3-(2-naphthyl) propanoic acid (2 mM) in the presence or the absence of 100  $\mu$ M of *L*-SK-4 for 24, 48 and 72 hr and the viability levels were monitored as described previously (**Figure 69**).

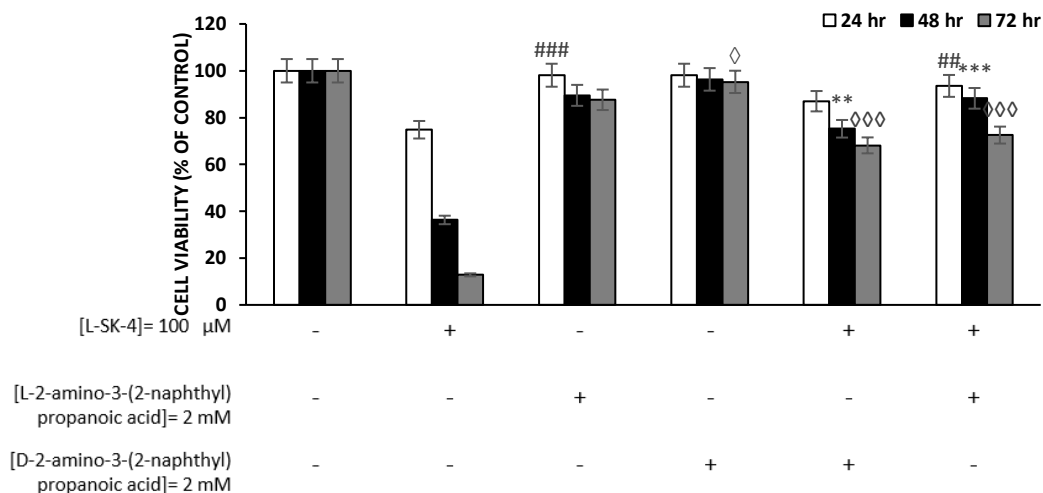


**Figure 69:** A375 cells have been exposed to 100  $\mu$ M of *L*-SK-4 in the presence or the absence of 100  $\mu$ M of *L*- and *D*- 2-amino-3-(2-naphthyl) propanoic acid for 24, 48 and 72 hr respectively. Data shown are means  $\pm$  SD of 5 replicates from three independent experiments.

The results obtained, suggested that indeed, the *L*-2-amino-3-(2-naphthyl) propanoic acid is preferred as LAT-1 inhibitor over the respective *D*- enantiomer validating once again the previously reported findings for the preference of LAT-1 on *L*- enantiomers.<sup>485</sup> Namely, the viability levels of the cell groups that have been exposed to *L*- enantiomer were lower compare to the once been treated with the *D*- enantiomer (**Figure 69**). Moreover, an almost 100% cell rescue was noticed in the cell groups that have been co-treated with both *L*-SK-4 and *L*-2-amino-3-(2-naphthyl) propanoic acid mainly after 24 hr, whereas a small drop in the viability levels has been noticed at 48 and 72 hr (**Figure 69**). This can be attributed to either to the cell starvation of amino-acid or because some percentage of the *L*-SK-4 managed to penetrate the cell. Some inhibition has

also been illustrated by the cell groups exposed to both *L*-SK-4 and the *D*-2-amino-3-(2-naphthyl) propanoic acid. However, the viability levels were lower compared to the respective once of the *L*- enantiomer (**Figure 69**).

### 7.2.2 Control compounds of *L*-SK-4

Eventually, in order to establish an *in vitro* Structure Activity Relationship (SAR), by means of investigating which structural features of the lead molecule (*L*-SK-4) are essential for its activity-potency and transportation as well as to demonstrate the importance of the chelating group, a range of control has been synthesized and screened on A375 cells (**Figure 70**). Control compounds 1-3 are derivatives of the parental molecule (*L*-SK-4) with a functional inactivation of one of their active features. Control-1 and -2 are primary amine and a carboxylic acid respectively, rather than amino acids and Control 3 has a methyl ether protected pyridone rather than hydroxypyridone (**Figure 70A**).

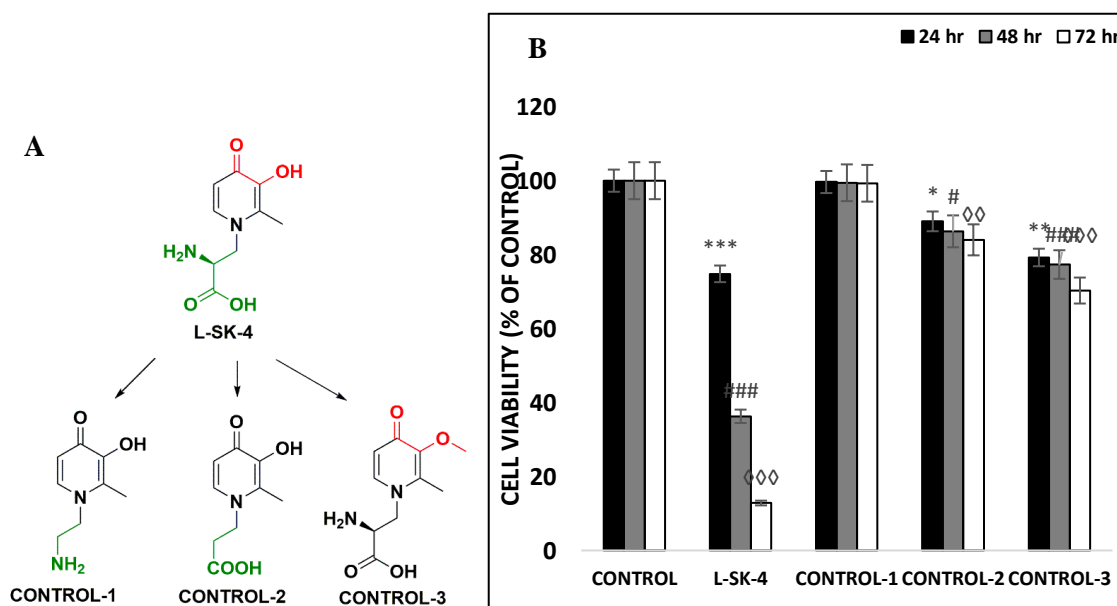


**Figure 70:** Metal chelators that have been used in this study were designed for both strong and selective  $\text{Fe}^{3+}$  binding and coordination and enhanced transportation to the cytosol. (**A**) Structures of the control compounds. (**B**) Cytotoxic evaluation of the control compounds on A375. A375

cells, were treated with a 100  $\mu\text{M}$  of Control compounds 1-3 in a range of time (24-72 hr). Data shown are means  $\pm$  SD of 5 replicates from three independent experiments.

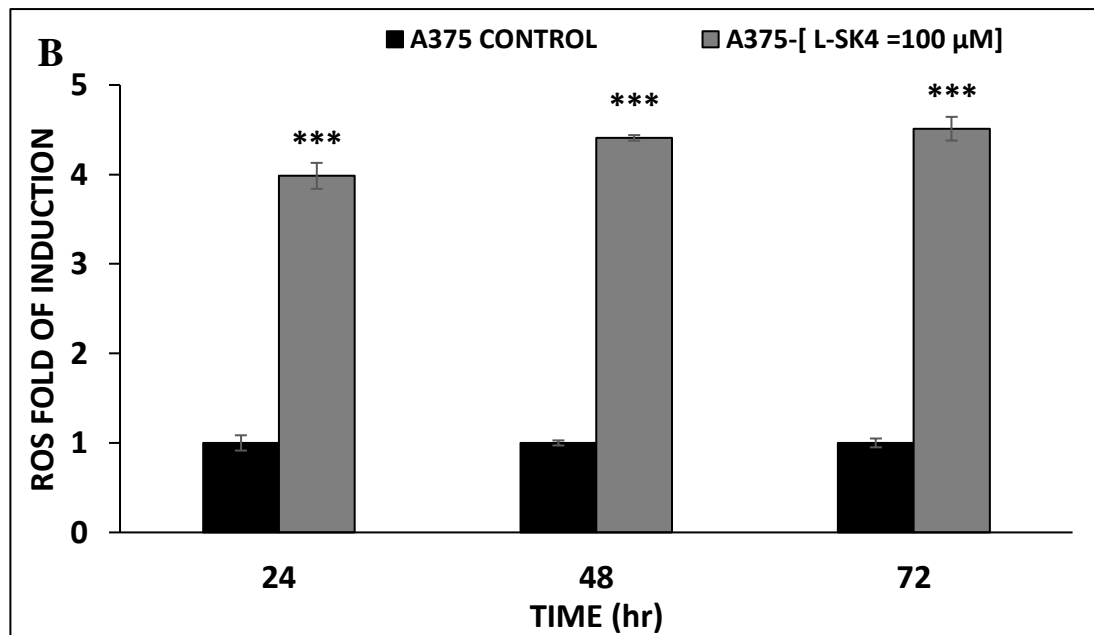
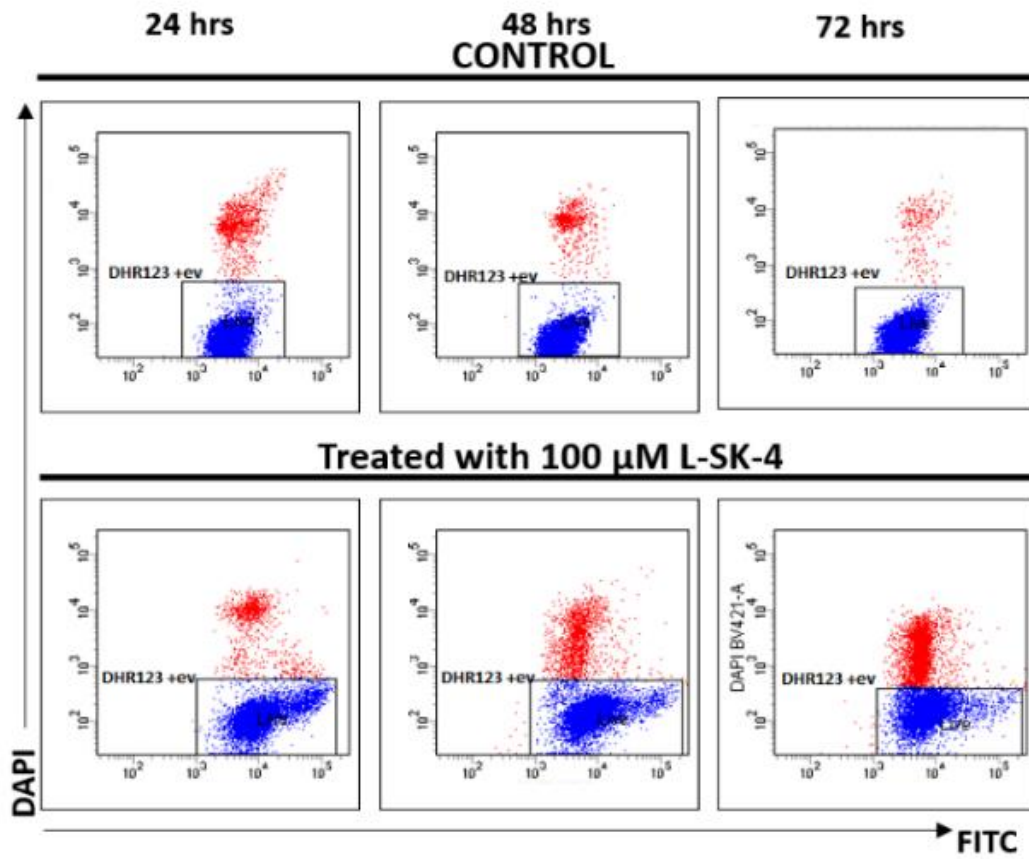
The results revealed that Control-1 was totally inactive since it couldn't induce any cytotoxic effect not even after 72 hr of exposure. Additionally, similar observation has been noticed when A375 have been treated with Control-2 especially after 24 and 48 hr as there wasn't any significant drop of the viability levels. A significant decrease on the number of viable cells has only been noticed 72 hr post-exposure to the compound. Eventually, Control-3 shown some cytotoxic effect which has been induced at 24 hr and slightly intensified over the course of 72 hr, however the magnitude of cytotoxic induction was not as intense as it was in the case of *L-SK-4* (**Figure 70B**). The small decrease of the viability levels can be attributed to the fact, that either the methyl ether protected pyridone can still bind to the  $\text{Fe}^{3+}$  but with less affinity or it can exhibit a weak alternative activity which is not related to  $\text{Fe}^{3+}$  chelation. On the other hand, it has been previously shown, that cytochrome P450s can de-methylate aryl ethers during the process of compounds metabolism.<sup>583</sup>

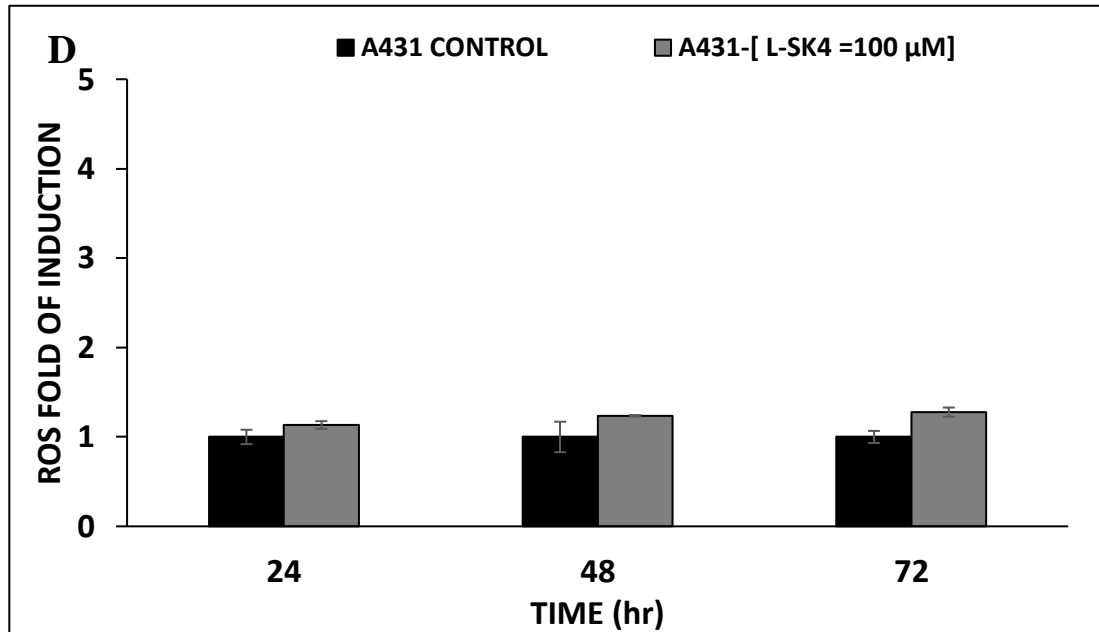
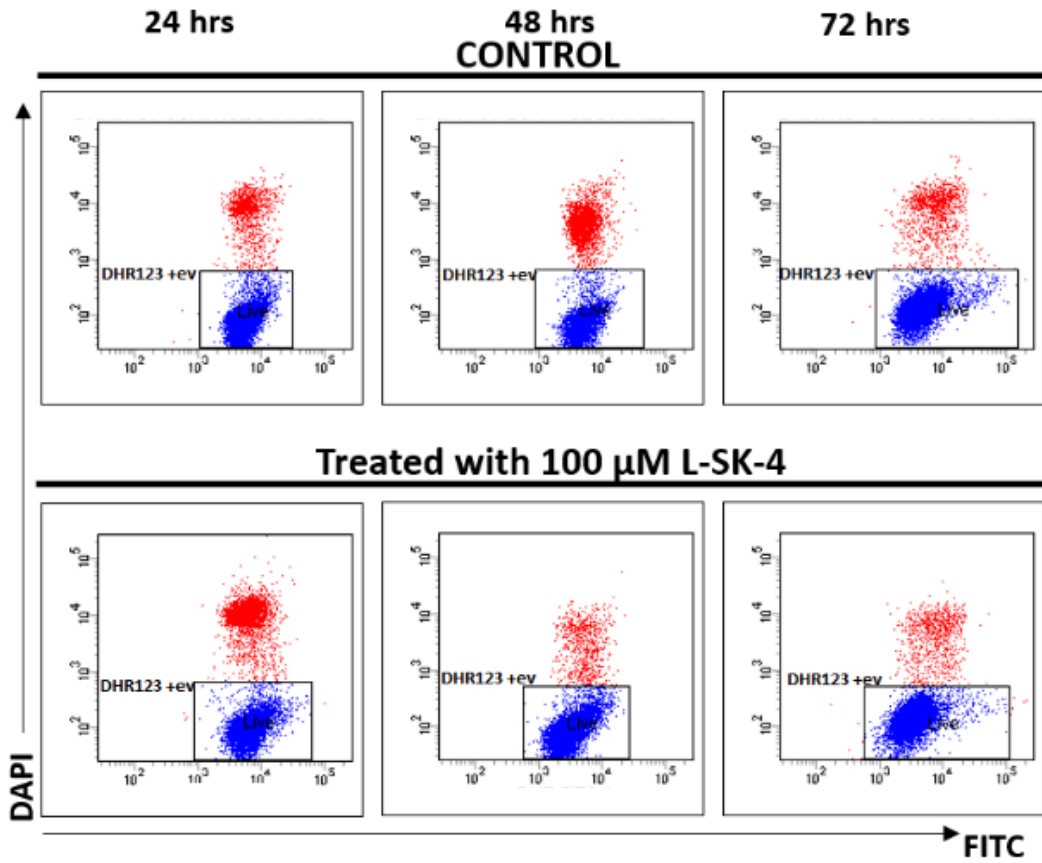
### **7.3 Characterization of molecular mechanism of action**

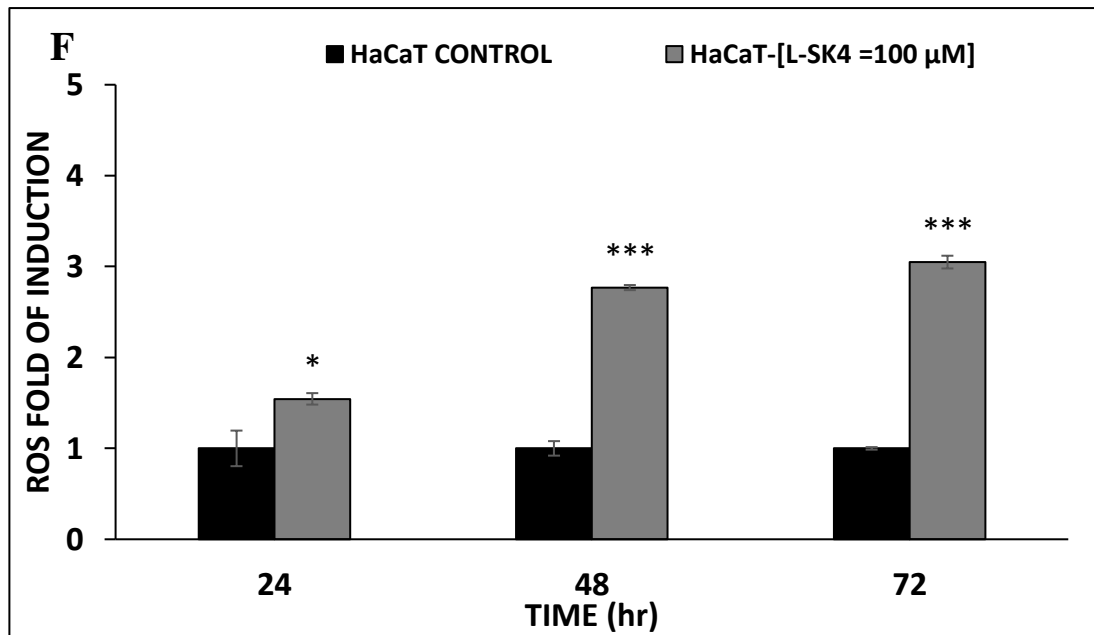
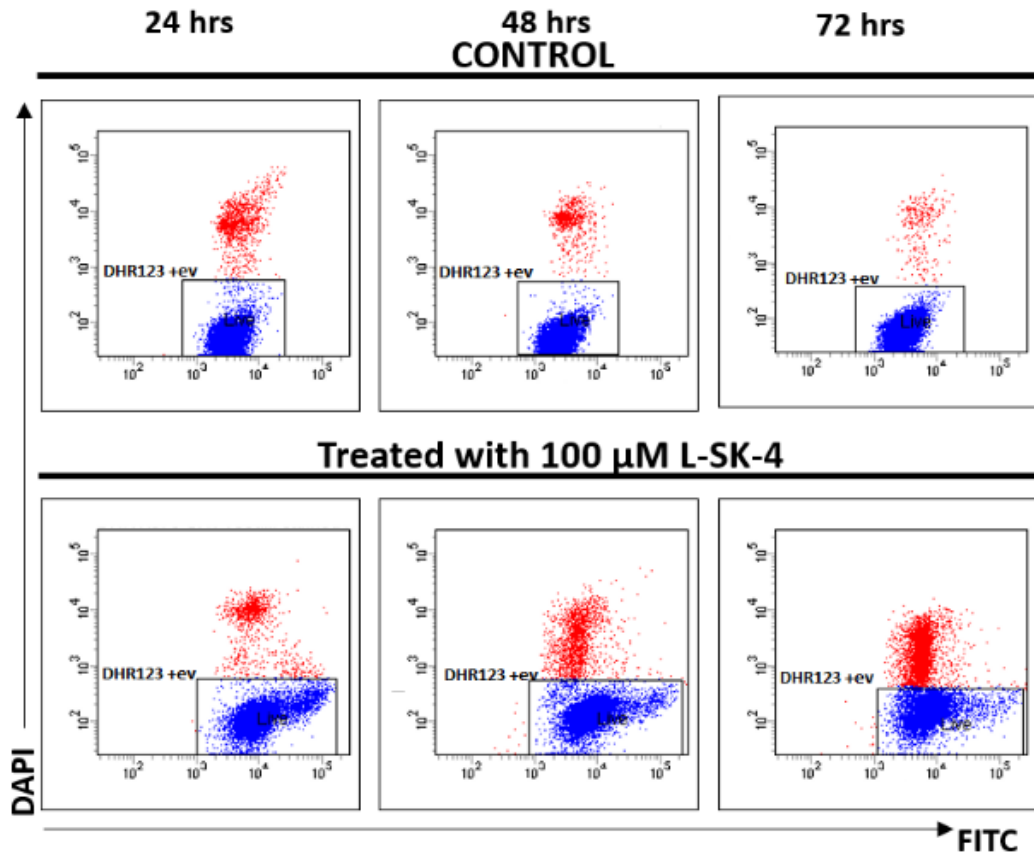
#### **7.3.1 Ability of *L-SK-4* to induce ROS**

The next part involved a synoptic characterization of the main mode of action of *L-SK-4* on the three working cell line by means of investigating the mode of cell death induction. The ability of 100  $\mu\text{M}$  of *L-SK-4* to induce intracellular reactive oxygen species (ROS) has been evaluated by means of flow cytometry, utilizing the DHR-123 fluorescent probe on A375, A431 and HaCaT cells as a ROS detector. The results obtained indicated that the treatment with 100  $\mu\text{M}$  of *L-SK-4* had the ability to increase dramatically the FITC spectrum in the exposed A375 group compared to the unexposed (control) group (**Figure 71A**). Interestingly, treatment of A375 cells with 100  $\mu\text{M}$  of *L-SK-4* induced a significant increase ( $p < 0.001$ ) in intracellular ROS levels, during the first

24 hr, which were sustained at each time point thereafter (**Figure 71B**). In the case of A431, the FITC spectrum retained at the same levels as the respective control (untreated cells) after the exposure to 100  $\mu$ M of *L*-SK-4 (**Figure 71C**). This observation was an indication that the treatment with the chelator couldn't promote any statistically significant alteration in the ROS levels (**Figure 71D**). Eventually, 100  $\mu$ M of *L*-SK-4 have the ability to induce ROS on HaCaT cells in a time dependent manner since the FITC spectrum increased with respect to the time (**Figure 71E**). Namely, an almost 1.5 fold of ROS induction has been observed during the first 24 hr with the effect been intensified over the time as at the 48 and 72 hours the ROS fold of induction was approximately and 3.1 respectively (**Figure 71F**). Overall it appears that A375 and HaCaT cells seems to be more vulnerable to the induction of ROS by the treatment with A375 been even more sensitive. In contrast, the ROS fold of induction on A431 was not of any statistically significant change.

**A****A375**

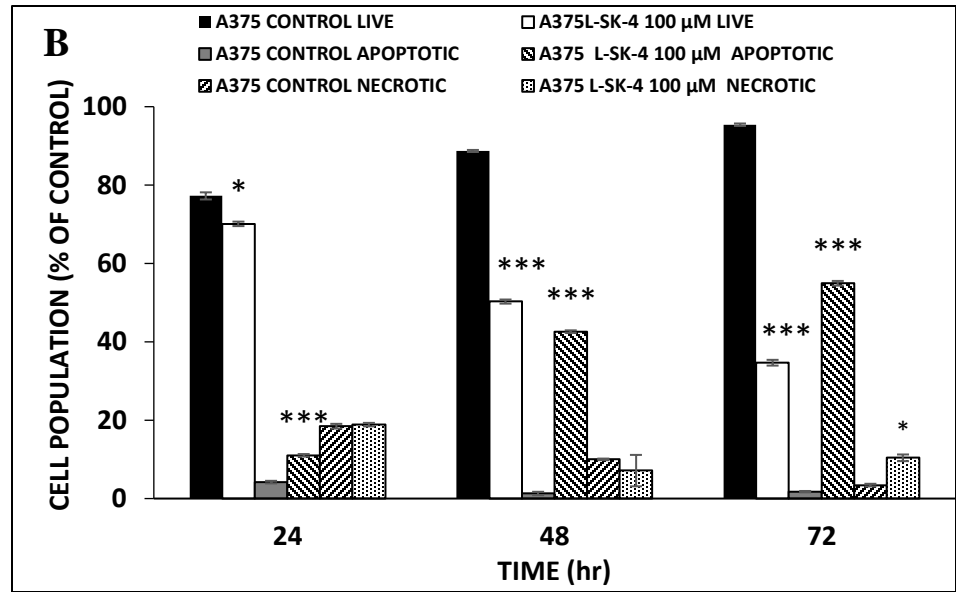
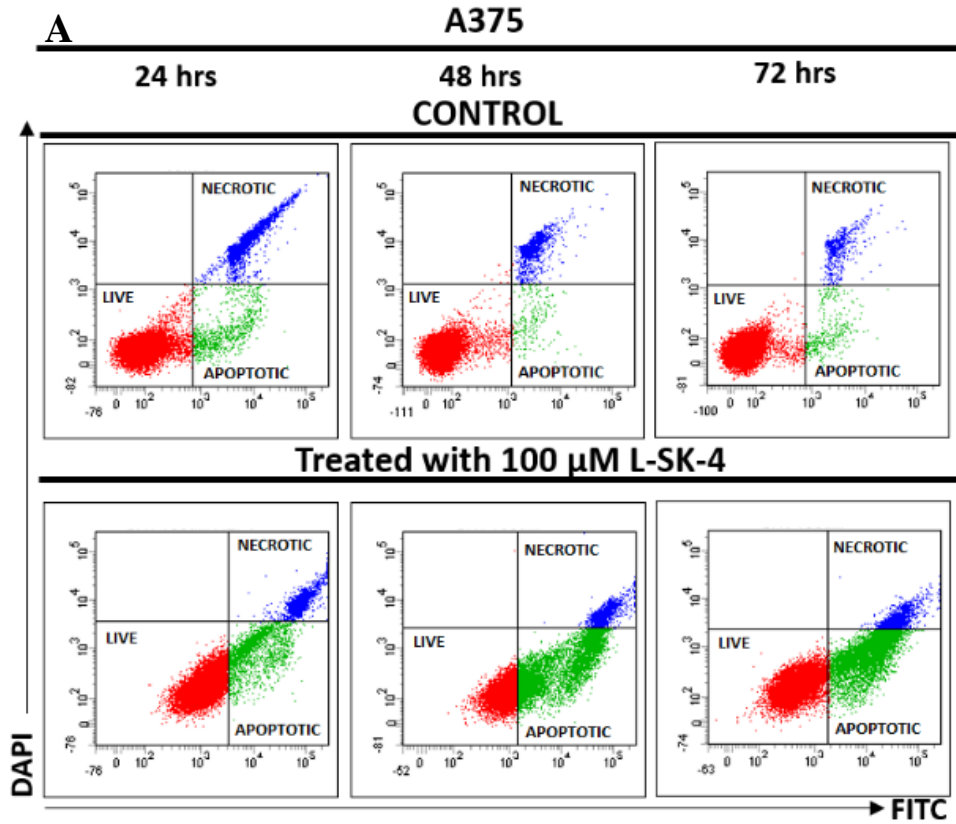
**C****A431**

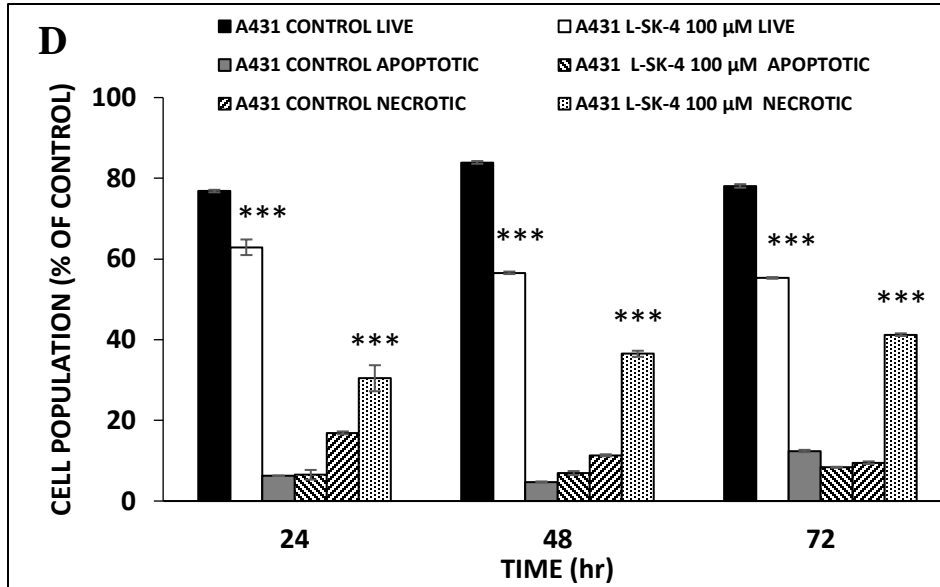
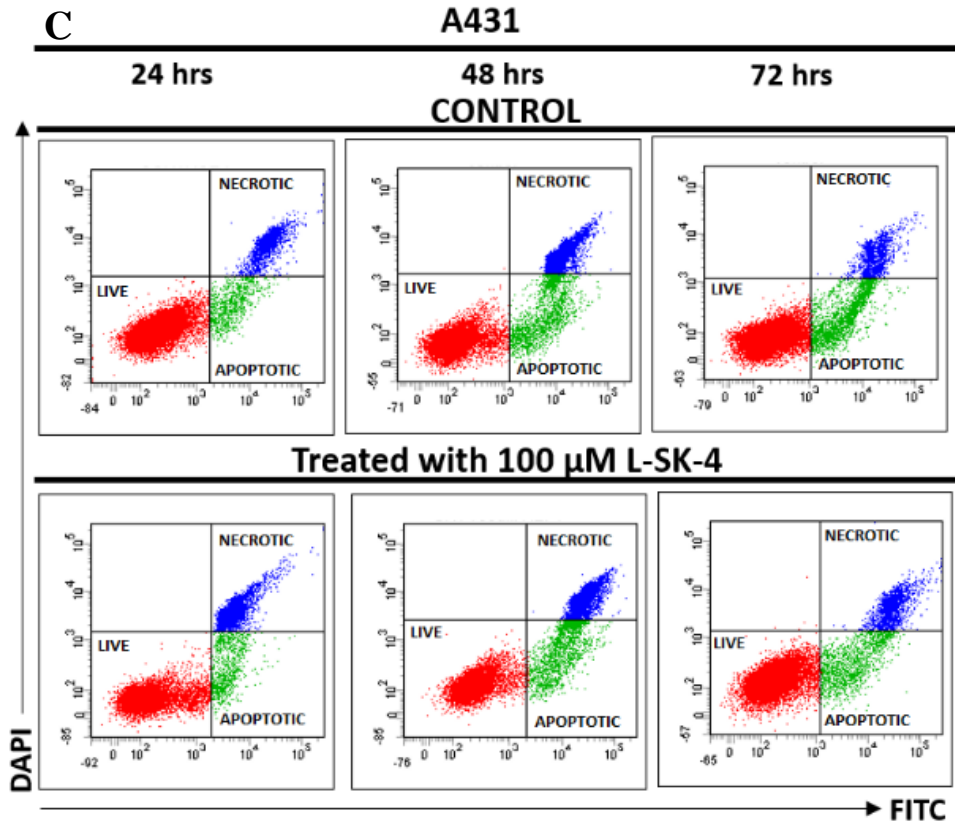
**E****HaCaT**

**Figure 71:** The ability of *L*-SK-4 to induce generation of oxidative stress in A375, A431 and HaCaT cells. A375, A431 and HaCaT were exposed to 100  $\mu$ M of *L*-SK-4 for 24, 48 and 72 hr and monitored by means of (A), (C), (E) flow cytometry in addition to being quantitated as (B), (D), (F) ROS fold induction respectively. Data shown are means  $\pm$  SD of 3 replicates from three independent experiments.

### 7.3.2 Determination of mode of cell death

In an attempt to evaluate the mode of cell death as a result of the induced cytotoxicity of the lead compound, the number of apoptotic and necrotic A375, A431 and HaCaT cells was evaluated after exposure to 100  $\mu$ M of *L*-SK-4. The importance of this study was to give insights into whether the treatment can induce either necrosis which is correlated to acute inflammation or apoptosis which is linked to the programmed cell death. To distinguish between the two modes of cell death, the CellEvent Caspase 3/7 Green detection reagent was utilized as an activated caspase 3/7 activity indicator whereas DAPI as an indicator for necrosis (Figure 72A, C, E) on A375, A431 and HaCaT respectively. Our data showed significant cell death on A375 that have been treated with 100  $\mu$ M of *L*-SK-4 during the first 24 hr ( $p < 0.01$ ), an effect which was intensified, over time, in a manner where live cells were significantly reduced ( $p < 0.001$ ) while necrotic cells remained at steady levels (Figure 72B). On the other hand, the number of apoptotic cells is increasing significantly over the time (Figure 72B). The same pattern seems to be followed by A431 as the treatment with 100  $\mu$ M of *L*-SK-4 induce a significant drop in the number of live cells during the first 24 hr ( $p < 0.001$ ), with the effect been intensified over 72 hr (Figure 72D). In this case, the number of necrotic cells is elevated significantly ( $p < 0.001$ ) over 72 hr while the number of the apoptotic cells remained steady at the control levels (Figure 72D). Finally, the number of live HaCaT cells drops significantly ( $p < 0.01$ ) at 48 hr and ( $p < 0.001$ ) at 72 hr (Figure 72F). Although the drop of live cells seems to be accompanied with a necroptotic effect as both apoptotic and necrotic cells are elevated at almost the same levels by the end of 72 hr (Figure 72F).





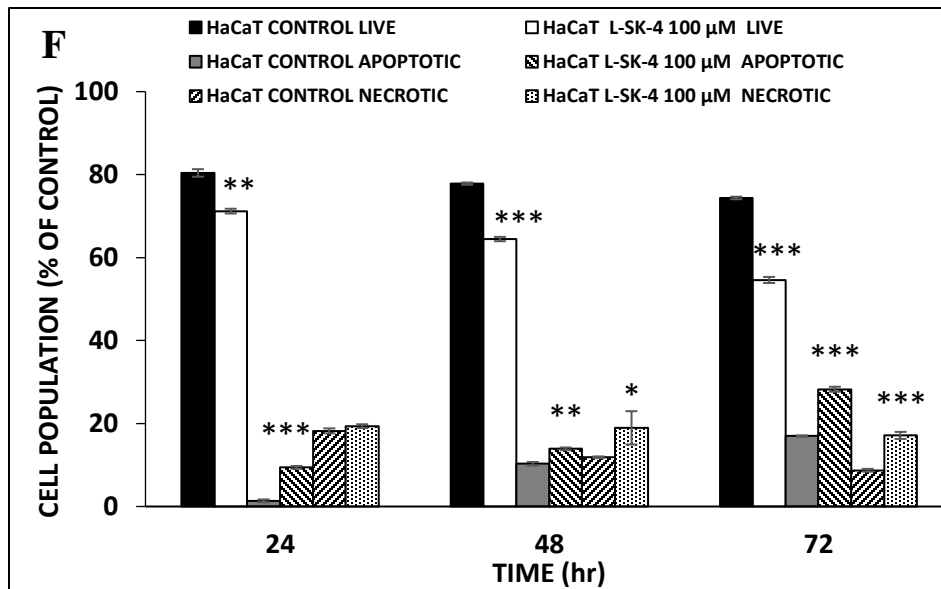
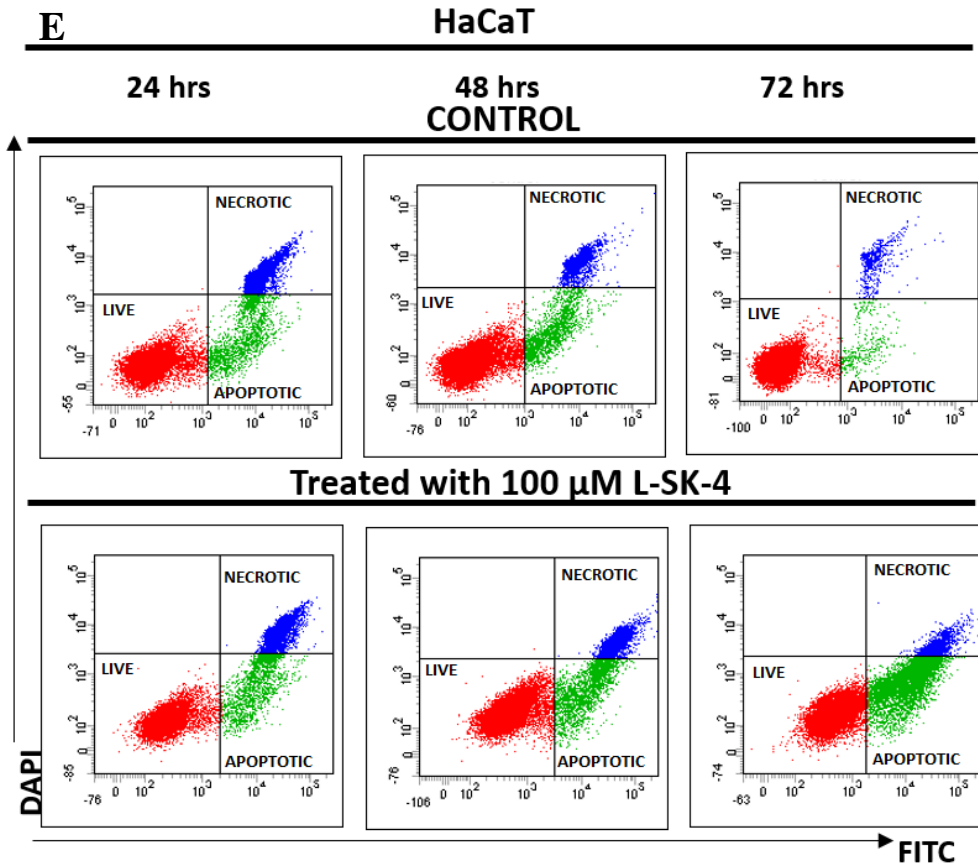


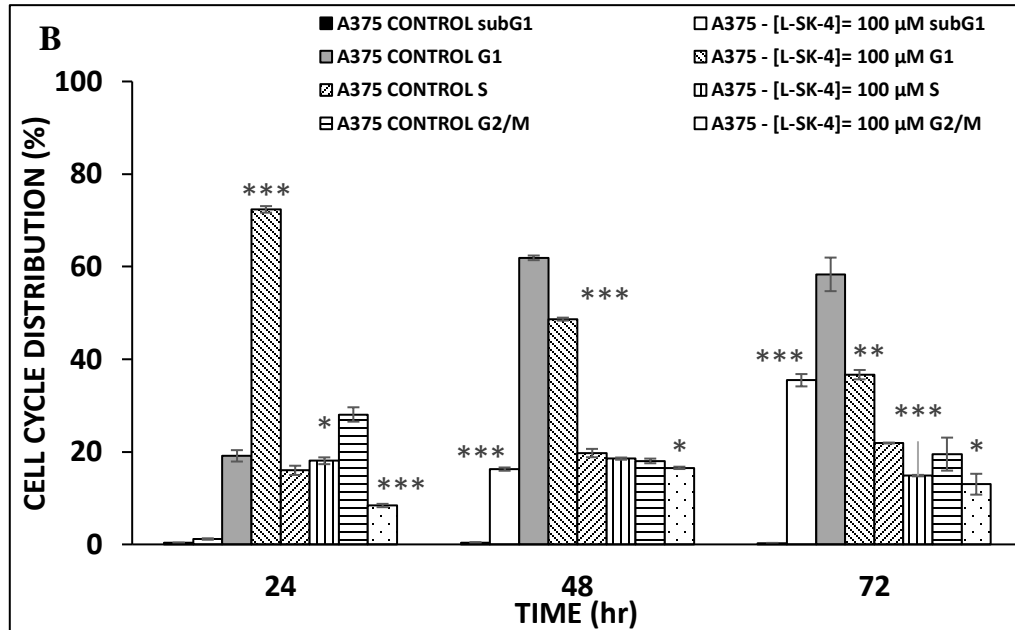
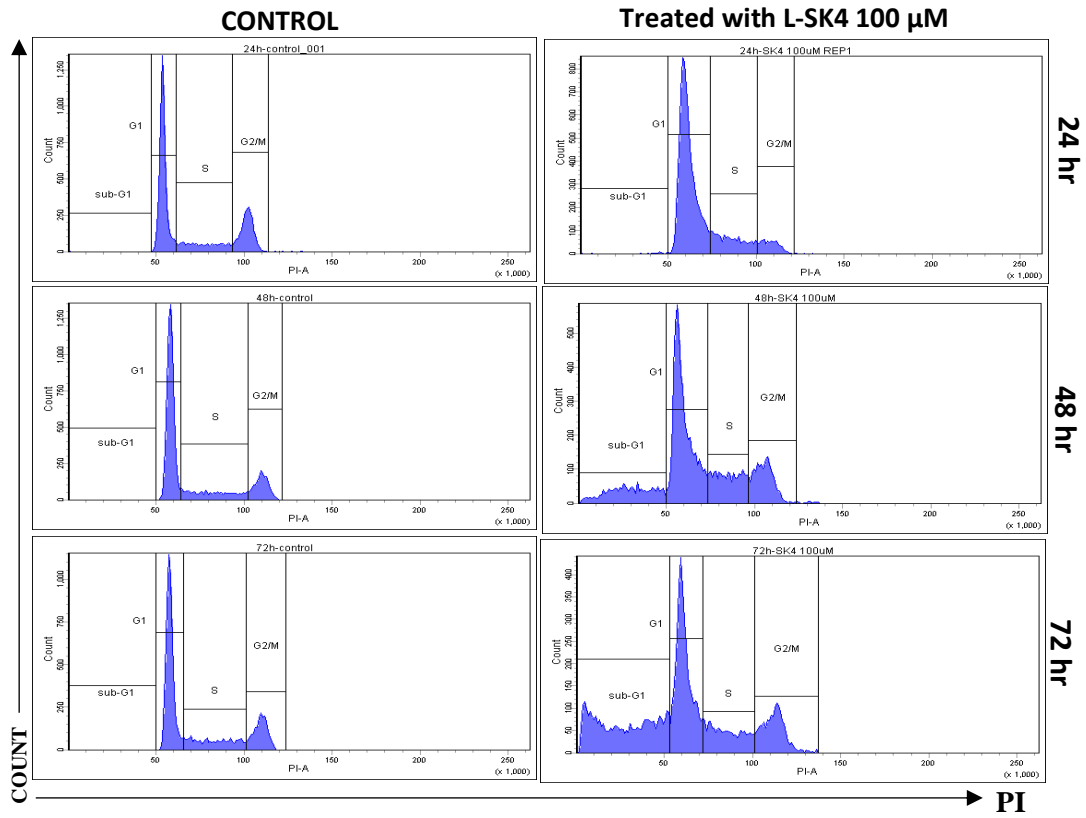
**Figure 72:** The ability of *L*-SK-4 to induce apoptosis in A375, A431 and HaCaT cells. Briefly, A375, A431 and HaCaT cells were exposed to 100  $\mu$ M of *L*-SK-4 at 24, 48 and 72 hr and then the number of live, apoptotic and necrotic cells were recorded by means of (A), (C), (E) flow cytometry and also quantified as (B), (D), (F) percent of total cell population. Data shown are means  $\pm$  SD of 3 replicates from three independent experiments.

### 7.3.3 Ability of *L*-SK-4 to arrest cell cycle growth

Finally, the ability of 100  $\mu$ M of *L*-SK-4 to induce cell cycle growth arrest was assessed by using the FxCycle PI/RNase staining solution for quantification of DNA content under each phase of the cell cycle and subsequent analysis by flow cytometry (Figure 73A, C, E) on A375, A431 and HaCaT cells respectively. Our results show that, 24 hr after exposure, there was a statistically significant elevation of the G1 phase on A375, followed by a reduction of the G2/M phase ( $p < 0.001$ ) while the S phase remained unaffected. Interestingly, at 48 hr, a significant increase of the sub-G1 phase was also observed followed by a marked reduction of the G1 phase ( $p < 0.001$ ) while the S- and G2/M phases remained relatively unaffected. Furthermore, this effect was intensified at 72 hr of exposure (Figure 73B). In the case of A431, there wasn't any significant alterations in the phases of cell growth during the first 24 hr (Figure 73D). However, a statistically significant increase of the G1 phase is observed at 48 hr with this effect been intensified over 72 hr. The increase of the G1 phase was also correlated with the statistically significant decrease of the S phase at 48 and 72 hr. Additionally, a statistically significant drop of the DNA levels been accumulated in the G2/M phase is also observed at 72 hr post treatment with 100  $\mu$ M *L*-SK-4 (Figure 73D). Finally, in the case of HaCaT cell a similar cell cycle growth arrest seems to be observed as it was in A431, with the exception that the significant increase of the G1 phase began at 24 hr and continues over 72 hr (Figure 73F). Once again, the increase of the G1 phase is accompanied with the statistically significant decrease;  $p > 0.01$  and  $p > 0.001$  of the S- and G2/M phase respectively (Figure 73F).

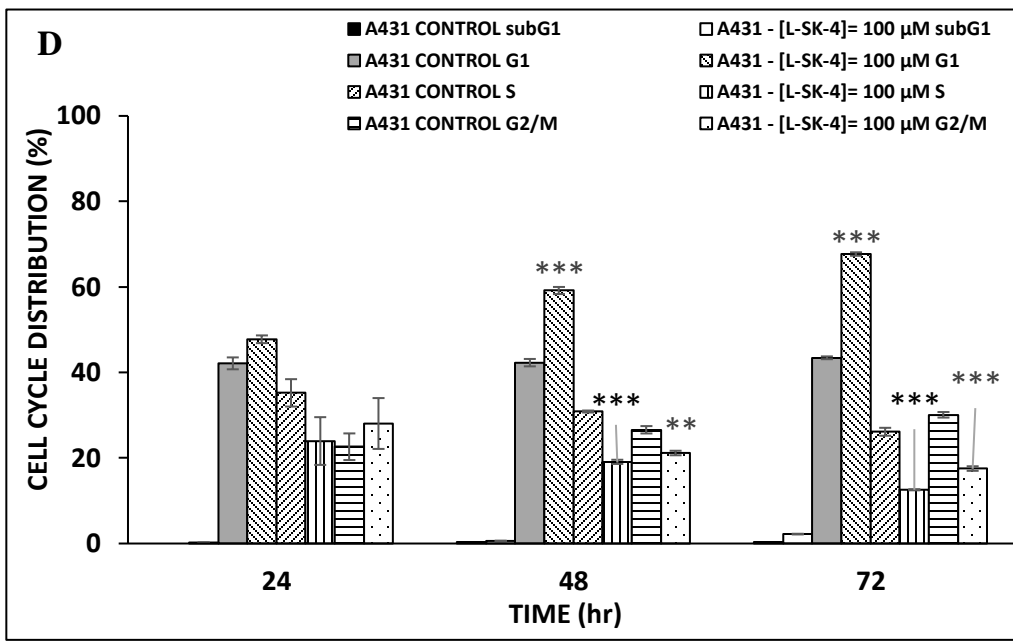
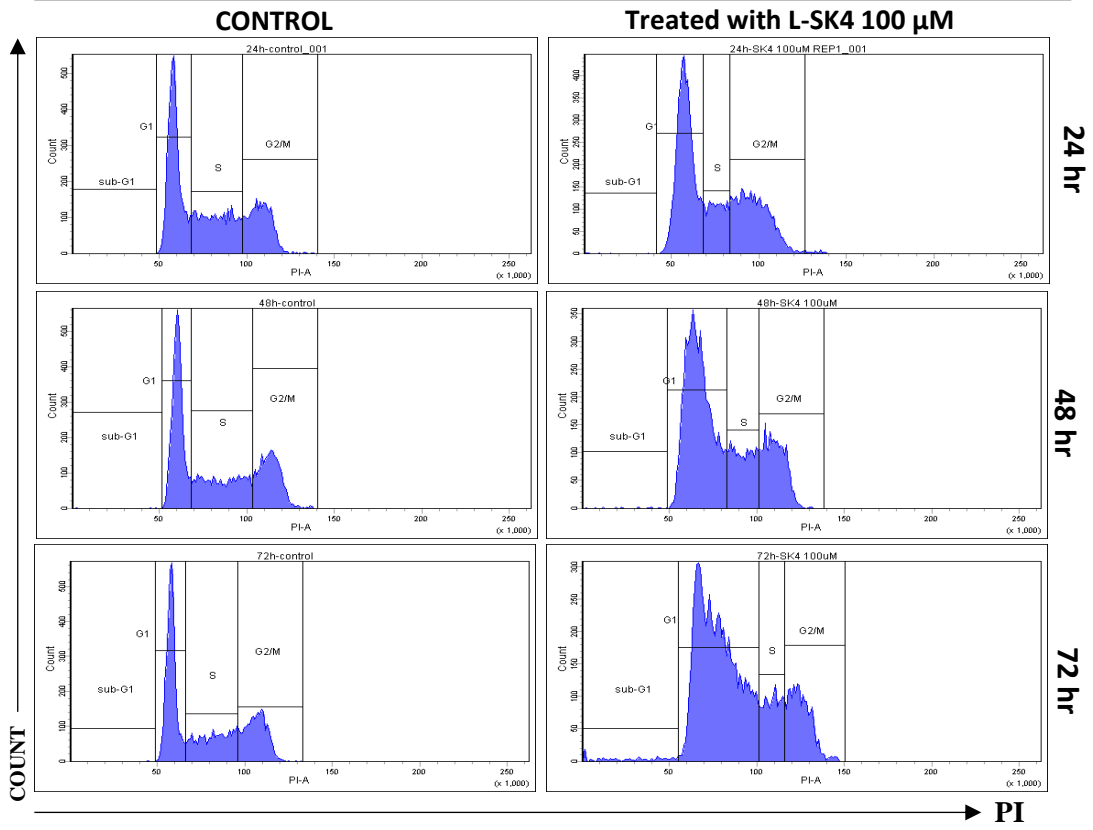
A

A375



C

A431



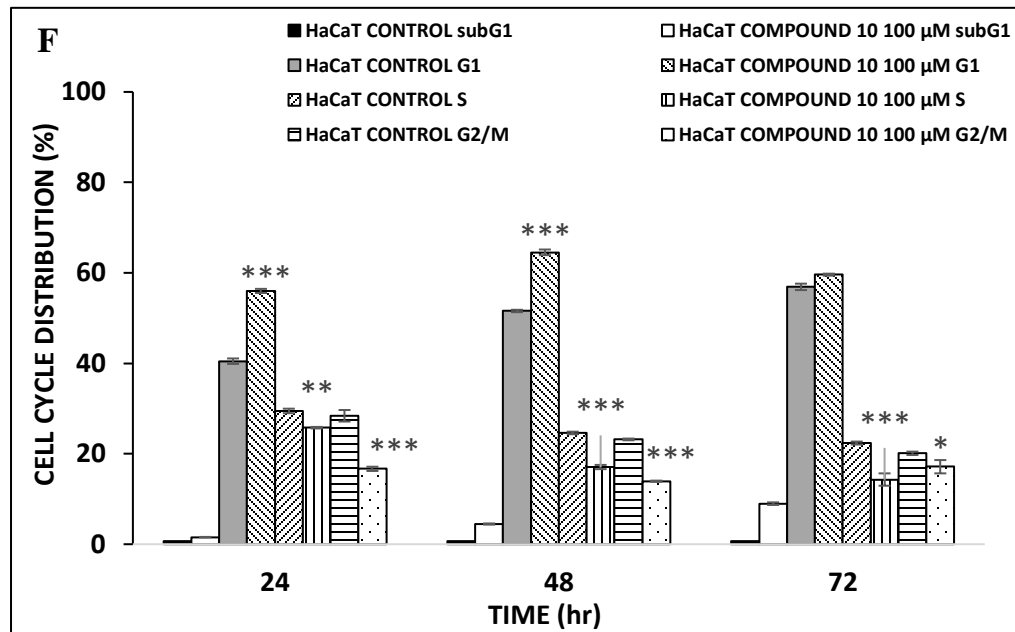
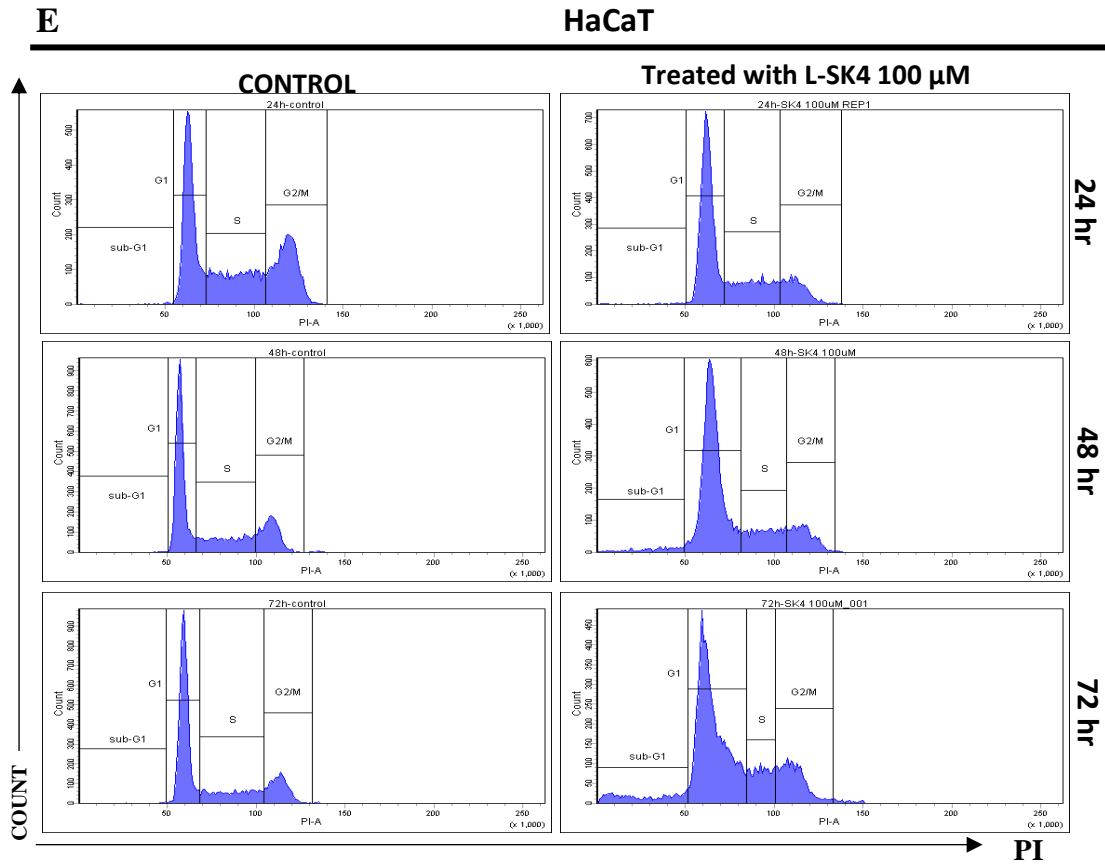


**Figure 73:** The ability of *L-SK-4* to induce cell cycle growth arrest in A375, A431 and HaCaT cells. Cells were exposed to 100 μM of *L-SK-4* at 24, 48 and 72 hr and then the number of cells

were recorded at each stage of the cell cycle by means of **(A)**, **(C)**, **(E)** flow cytometry and also quantified as **(B)**, **(D)**, **(F)** percent of total DNA cellular content accumulated at each phase of the cell cycle (e.g. sub-G1, G1, S or G2/M). Data shown are means  $\pm$  SD of 3 replicates from three independent experiments.

The main outcome of this study is that in the case of A375 cells, the compound induced growth arrest at the late of sub-G1 – early G1- phase of the cell cycle. This is strongly associated with the acute effect of the lead compound as it prevents the cell cycle to be completed due to the arrest at the very early stages. Therefore, the cell proliferation is inhibited. In contrast, the treatment of 100  $\mu$ M of *L*-SK-4 seems to arrest the cell cycle of A431 at the late G1 - early S-, whereas the growth arrest on HaCaT noticed at the G1- phase. That was an evidence of the resistance that two cell lines have to the treatment. Namely, in these cases, the treatment does not influence the cell cycle progression especially during the first 24 hr. In addition to this, it is demonstrated that cell cycle is allowed to progress unless its arrest to the mid stage of the procedure. Our findings are in agreement with the literature as it has been shown previously that *L*-mimosine and DFP (both 3, 4-HOPOs) have the ability to induced cell cycle growth arrest at the G1- phase before the entrance to the S- phase of the cell cycle.<sup>584–586</sup> It has been also suggested that the metals chelators interfere with the cell cycle by chelating the iron that exist in the active site of enzymes that are regulating the progression and maintenance of cell cycle grow.<sup>587</sup> In example, DFP, chelates the Fe<sup>2+</sup> ion that exist in the active site of essential for cell cycle enzymes; iron-depended histone lysine demethylases (KDMs).<sup>587</sup> In addition to this it has been shown before, that DFP, inhibits ribonucleotide reductase by chelating the intracellular liable zinc pool, whereas in other cases it prevents the demethylation of H3K4me3 and H3K27me3; enzymes that participate in the post translation modifications of chromatins.<sup>588–590</sup>

## 7.4 Biological mode of action

### 7.4.1 Time-dependence determination of ROS fold of induction

A kinetic characterization of the ability of HOPO metal chelators to induce toxic levels of ROS was evaluated in human malignant melanoma cells including those of 1,2-HOPO (*rac*-SK-3), 2,3-HOPO (*rac*-SK-5), 3,4-HOPO (*rac*-SK-2, *D/L*-SK-4) and a hydroxypyranone (*rac*-SK-1). Each compound was assessed on a range of concentrations (25-500  $\mu$ M) at three time points (24, 48 and 72 hr) (**Figure 74**). Our results shown that none of the compounds; *rac*-SK-1, 2, 3 and 5 was able to induce elevation of ROS, not even at concentrations as high as 500  $\mu$ M after 72 hr of treatment since the ROS levels were remained almost at the same as to their respective controls levels (**Figure 74A-C and F**). On the other hand, two enantiomerically pure forms of an *N*-substituted-3,4-HOPO (*L*- and *D*-SK-4) had the capacity to induce a statistically significant elevation of ROS at a concentration of 100  $\mu$ M after 24 hr of exposure (**Figure 74D and E**). However, the magnitude of ROS fold of induction was much more intense in the case *L*-SK-4 (~ 4x VS ~2.5x higher than the control). Additionally, when A375 cells have been treated with 100  $\mu$ M of *L*-SK-4 the ROS levels were maintained over the course of 72 hr at the same levels whereas in the case of *D*-SK-4 there was a slight elevation of the ROS level over the time of exposure. Interestingly, when cells were treated with 500  $\mu$ M of *L*-SK-4, the ROS levels were of less magnitude compare with the

once been induced by 100  $\mu\text{M}$  whereas in the case *D*-SK-4 the ROS fold of induction at the respective concentration retained almost at the same levels (**Figure 74D and E**).

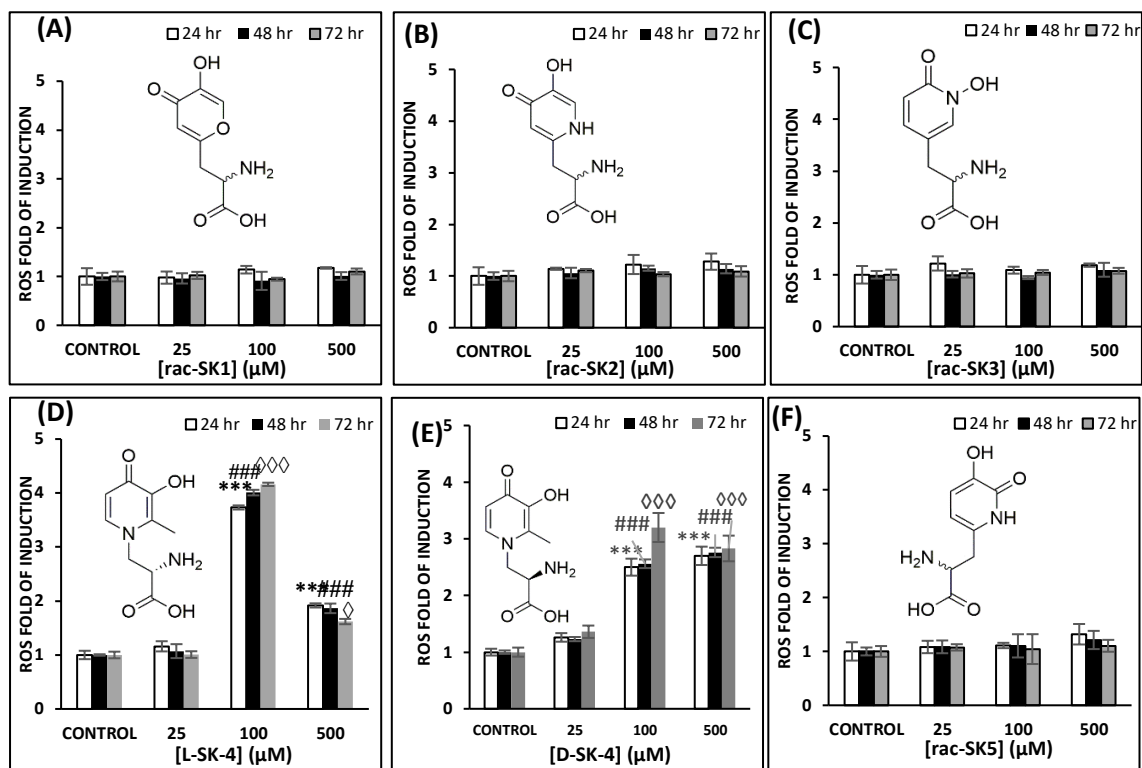


**Figure 74:** The ability of hydroxypyridinones to induce alterations on the ROS levels in A375 cell lines. A375 cells were exposed to a range of concentrations (0-500  $\mu\text{M}$ ) of (A) *rac*-SK-1, (B) *rac*-SK-2, (C) *rac*-SK-3, (D) *L*-SK-4, (E) *D*-SK-4 and (F) *rac*-SK-5 for 24, 48 and 72 hr. Data shown are means of  $\pm$  SD of 3 replicated from 3 independent experiments.

Finally, we evaluated the pro oxidant capacity of *L*-SK-4 in a range of concentrations (25-500  $\mu\text{M}$ ) and time (24-72 hr) against non-malignant melanoma (A431) as well as non-malignant keratinocytes (HaCaT) cells in an attempt to document any potential selectivity over A375 cells. Our observations revealed that the ROS levels, in A431 and HaCaT cells were also affected by the treatment with *L*-SK-4 (**Figure 75B and C**). In the case of HaCaT cells an elevation of ROS has been noticed at 100  $\mu\text{M}$  with the effect been intensified over 72 hr whereas at 500  $\mu\text{M}$  the

ROS levels were sustained almost the same over time. Despite the fact, that an increase on the ROS levels has been noticed, the magnitude of the induction was significantly lower than the respective one on A375 (**Figure 75B** and **Figure 74D**). On the other hand, a none-meaningful elevation of ROS has been noticed on A431 (**Figure 75B**). Taken together, our data, indicate that *L*-SK-4 exerts a higher degree of potency to induce ROS in A375 rather than A431 and HaCaT.

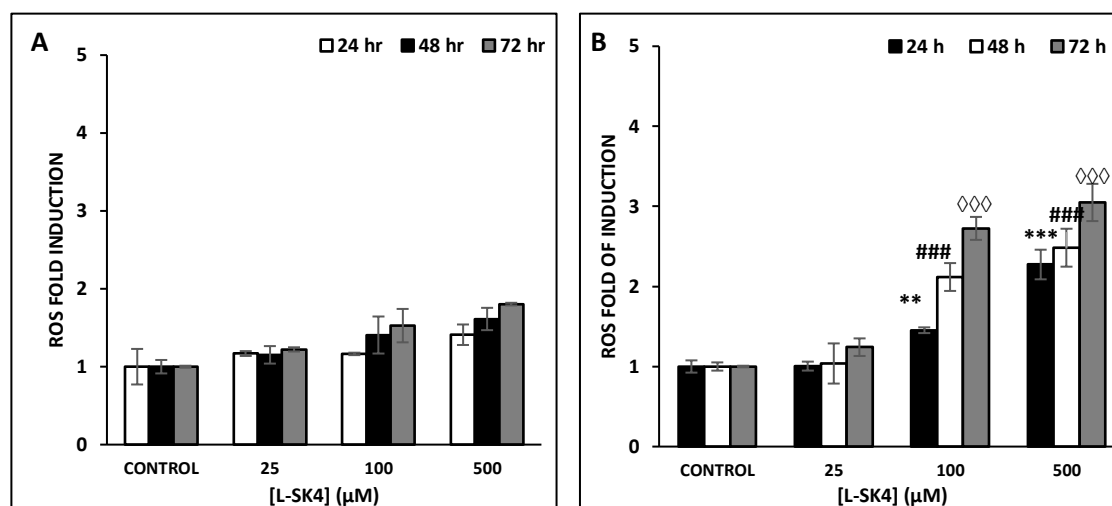


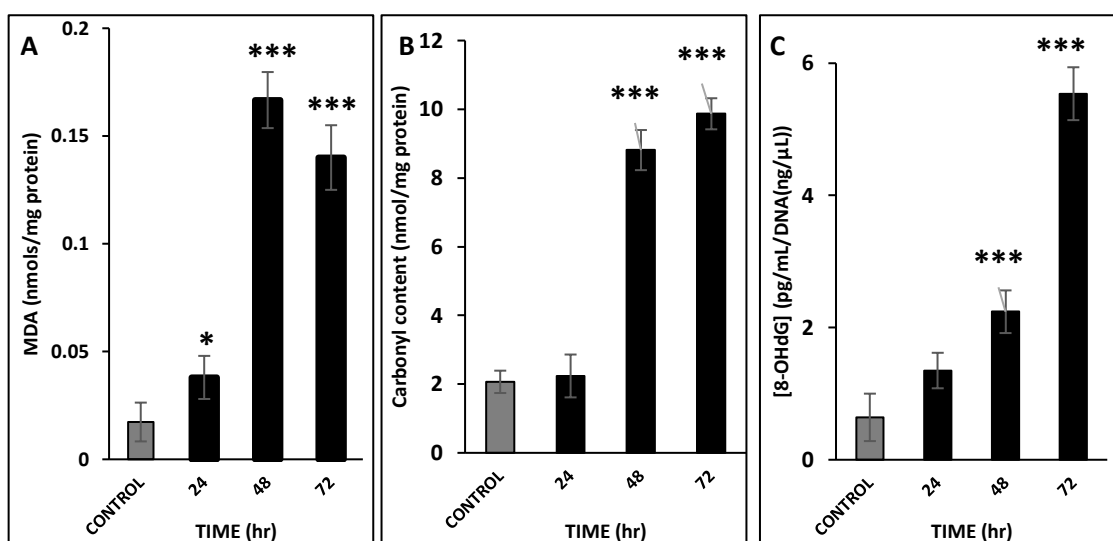
**Figure 75:** The ability of *L*-SK-4 to induce alterations on the ROS levels in (A) A431 and (B) HaCaT cells. Data shown are means of  $\pm$  SD of 3 replicated from 3 independent experiments.

## 7.5 *L*-SK-4 generates oxidative stress on malignant melanoma cells

### 7.5.1 Effect of oxidative stress been induced by *L*-SK-4

Afterwards, a descriptive characterization of the oxidative stress that 100  $\mu$ M of *L*-SK-4 can induce on A375 was performed by means of investigating its effect on lipid, protein and DNA level, at 24, 48 and 72 hr. Initially, the concentration of MDA, a marker of lipid peroxidation was measured (**Figure 76A**).<sup>591,592</sup> The results obtained indicated a statistically significant elevation of MDA at 24 hr whereas sharp elevation was noticed at 48 and 72 hr. Furthermore, we analyzed the levels of protein carbonyl as marker of proteins that underwent oxidative damage (**Figure**

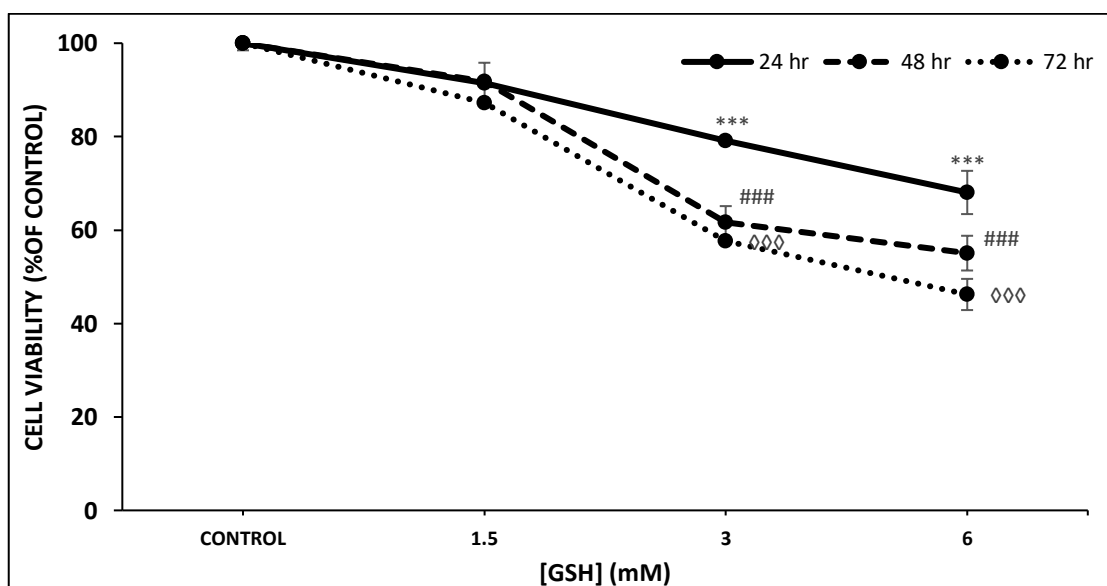
**76B).**<sup>593,594</sup> According to the exported results, there was not any significant change between the untreated cells and the ones that have been treated with *L*-SK-4 at the first 24 hr. On the other hand, a reverse effect seems to be illustrated, as a dramatic increase has been noticed at 48 hr and the effect was then intensified at 72 hr. Eventually, we examined whether the ROS induction could cause any DNA oxidative damage, by means of measuring the levels of its respective marker; 8-oxo-2-deoxy guanosine (8-OHdG) (**Figure 76C**).<sup>595,596</sup> Our observations suggested that there is an elevation of 8-OHdG at 24 hr which is not of statistical importance. However the concentration of the examined marker was significantly elevated at 48 hr and at the end-point (72 hr) of the experiment it reached the maximum levels.



**Figure 76:** The effect of ROS induction on lipids, proteins and DNA in A375 cell line. **(A)** The level of MDA on A375 cells post-treated with 100  $\mu$ M of *L*-SK-4 for 24, 48 and 72 hr. **(B)** The carbonyl protein content on A375 cells been treated with 100  $\mu$ M of *L*-SK-4 for 24, 48 and 72 hr. **(C)** The quantification of 8-OHdG species on DNA of A375 cells been treated with 100  $\mu$ M of *L*-SK-4 for 24, 48 and 72 hr. Data shown are means of  $\pm$  SD of 3 replicates from 3 independent experiments.

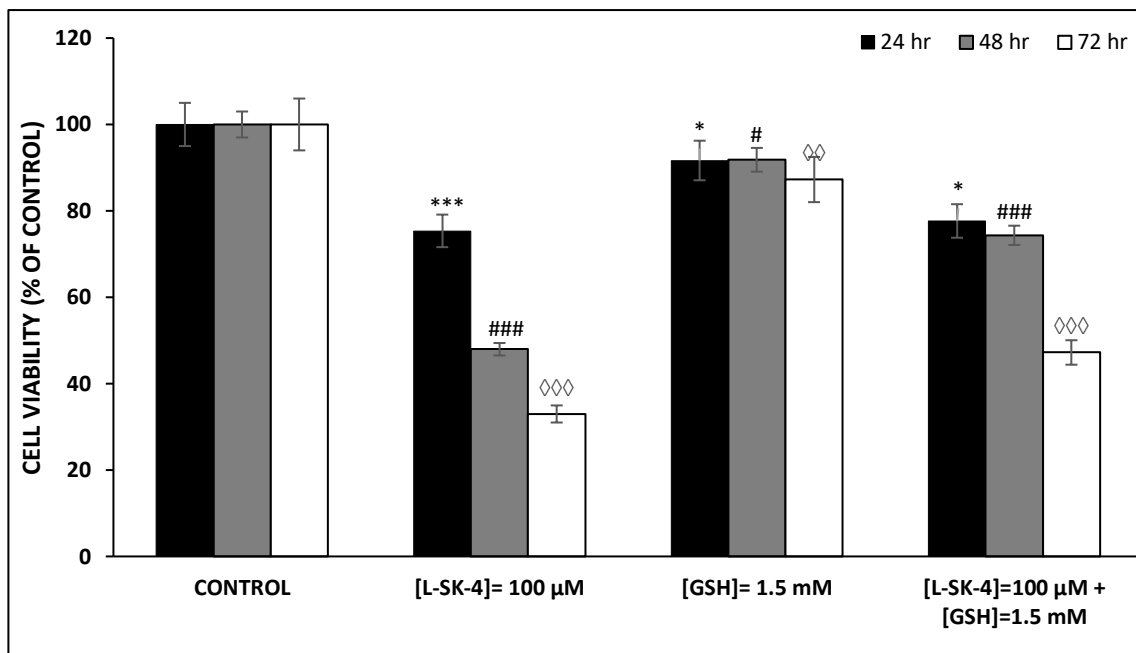
### 7.5.2 ROS scavenging effect by GSH

We subsequently, attempted to introduce a ROS scavenger; reduced glutathione (GSH), in order to examine whether we can reverse the phenotype from the cell survival rate point of view as the elevation of ROS in combination with oxidative stress induced by the treatment appeared to be the determinant factors for cell death induction.<sup>597,598</sup> Primarily, a dose-response curve was performed in A375 cells, with a range of concentrations of GSH (1.5-6 mM) and time (24-72 hr) in order to determine the optimum concentration that would not mask the cytotoxic effect of *L*-SK-4 (Figure 77).



**Figure 77:** The cytotoxicity of GSH on A375 cell line. A375 cells were exposed to a range of 1.5-6 mM concentrations of GSH for 24, 48 and 72 hr. Data shown are means  $\pm$  SD of 5 replicates from three independent experiments.

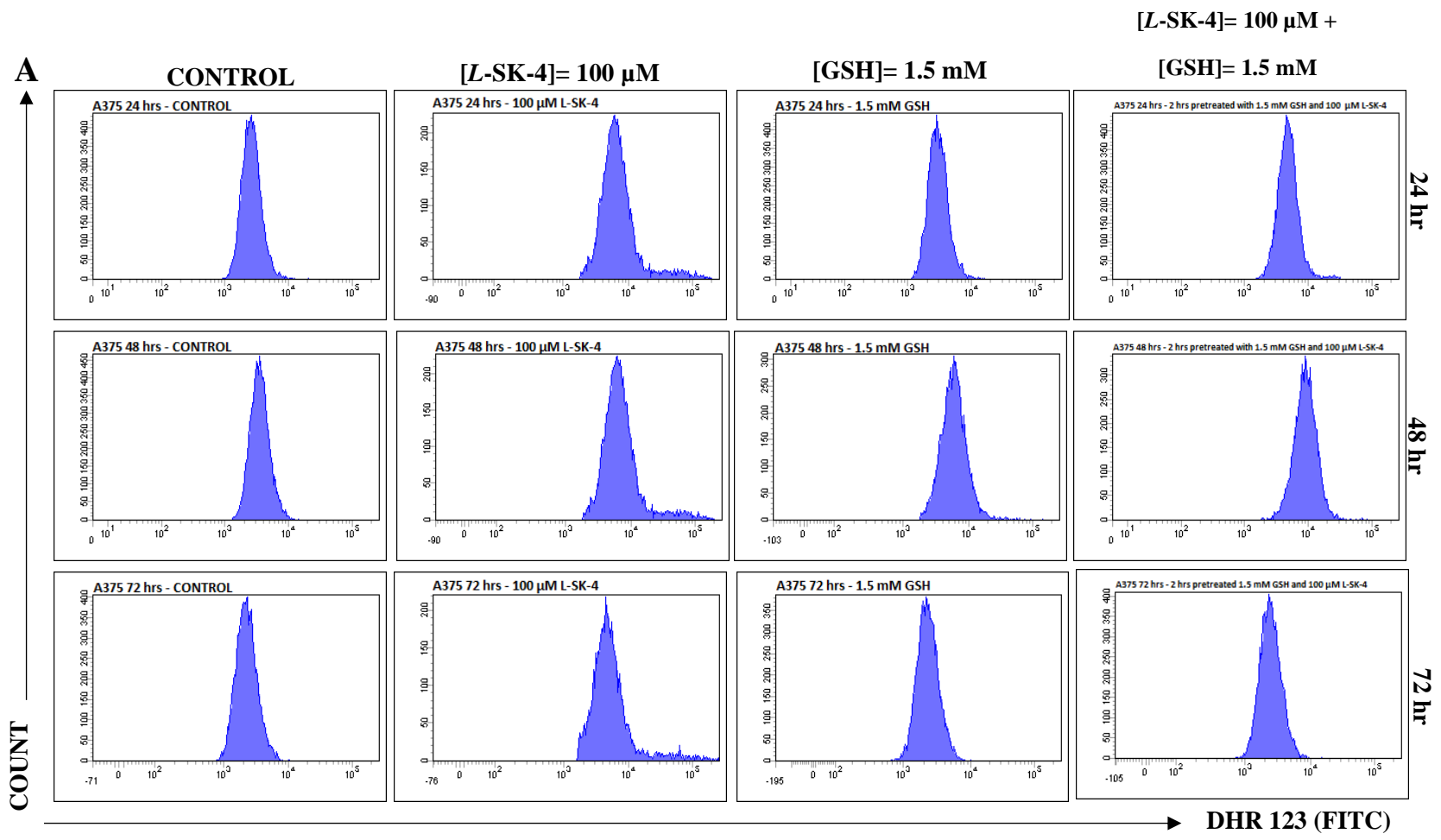
The results obtained shown that 1.5 mM of GSH was the tolerated concentration that could applied in cells, as at higher concentrations (3 and 6 mM) GSH exerts a toxic effect. Cell viability assay was then performed where cells were co-treated with 100  $\mu$ M of *L*-SK-4 and 1.5 mM GSH and interestingly our experimental data were in agreement with our initial assumption (Figure 78).

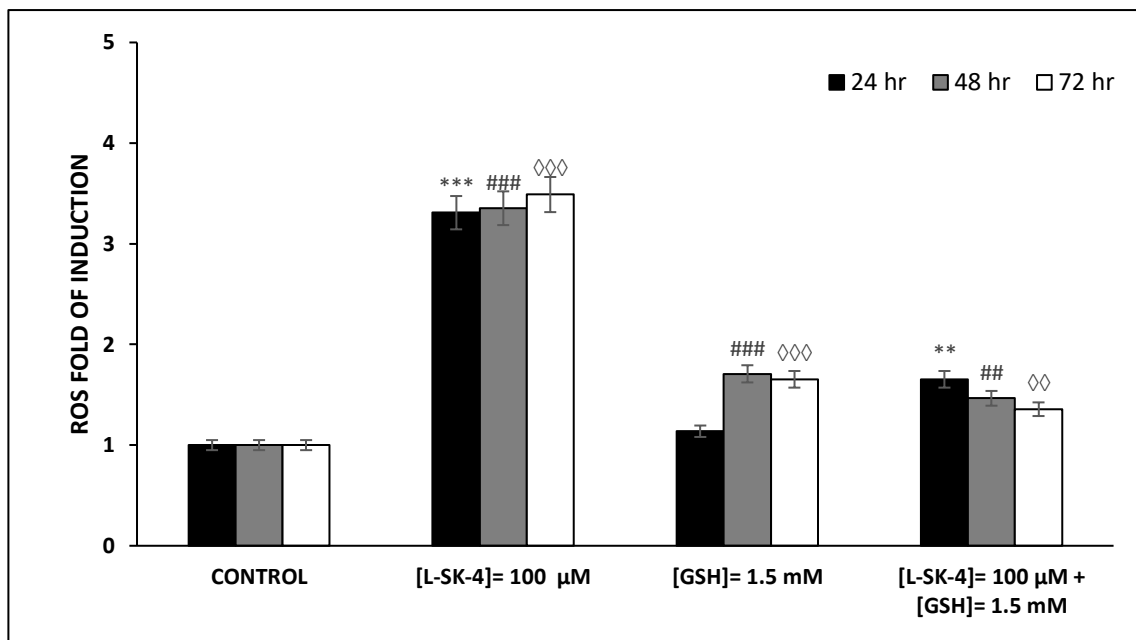


**Figure 78:** The ability of the GSH to rescue cell from cell death induced by *L*-SK-4. A375 cells were treated with 100 μM of *L*-SK-4 in the presence of the absence of 1.5 mM of GSH for 24, 48 and 72 hr. Data shown are the means ± SD of 5 replicates from 3 independent experiments.

Namely, the co-treatment with GSH and *L*-SK-4 led to cell rescue rather than cell death as the viability levels were at higher levels compared to respective cells which were treated only with GSH. As it can be observed from **Figure 78** there is a significant decrease of the viability levels in the co-treated group (*L*-SK-4 + GSH), however that magnitude was significantly elevated compared to the *L*-SK-4 treated group. That was a strong indication that the increasing accumulation of ROS can promote cell death in A375 and this is reduced by the antioxidant GSH. In order to validate this assumption, ROS levels were re-measured in the presence of GSH and *L*-SK-4. Our data showed that the FITC spectrum decreased dramatically in the co-treated groups compared to those been treated with only *L*-SK-4 (**Figure 79A**). Not surprisingly, co-treatment of A375 cells with 100 μM of *L*-SK-4 and 1.5 mM of GSH can cause a significant drop of the ROS levels compared to the respective values of ROS induction by just *L*-SK-4 (**Figure 79B**).

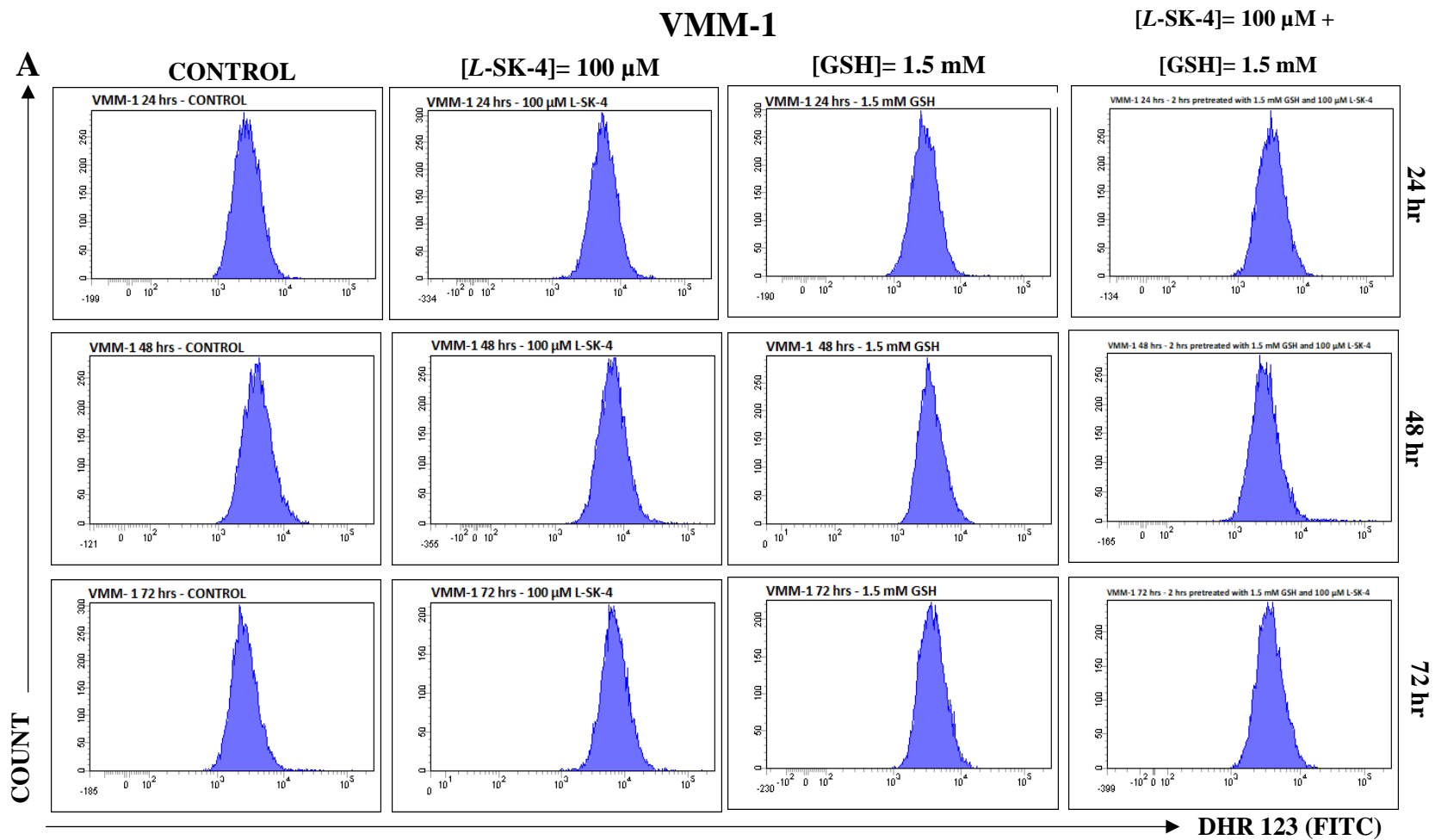
However, despite this difference, the ROS levels in the co-treated cells were significantly higher at 24, 48 and 72 hr compared to their respective control which has been treated simply with GSH.

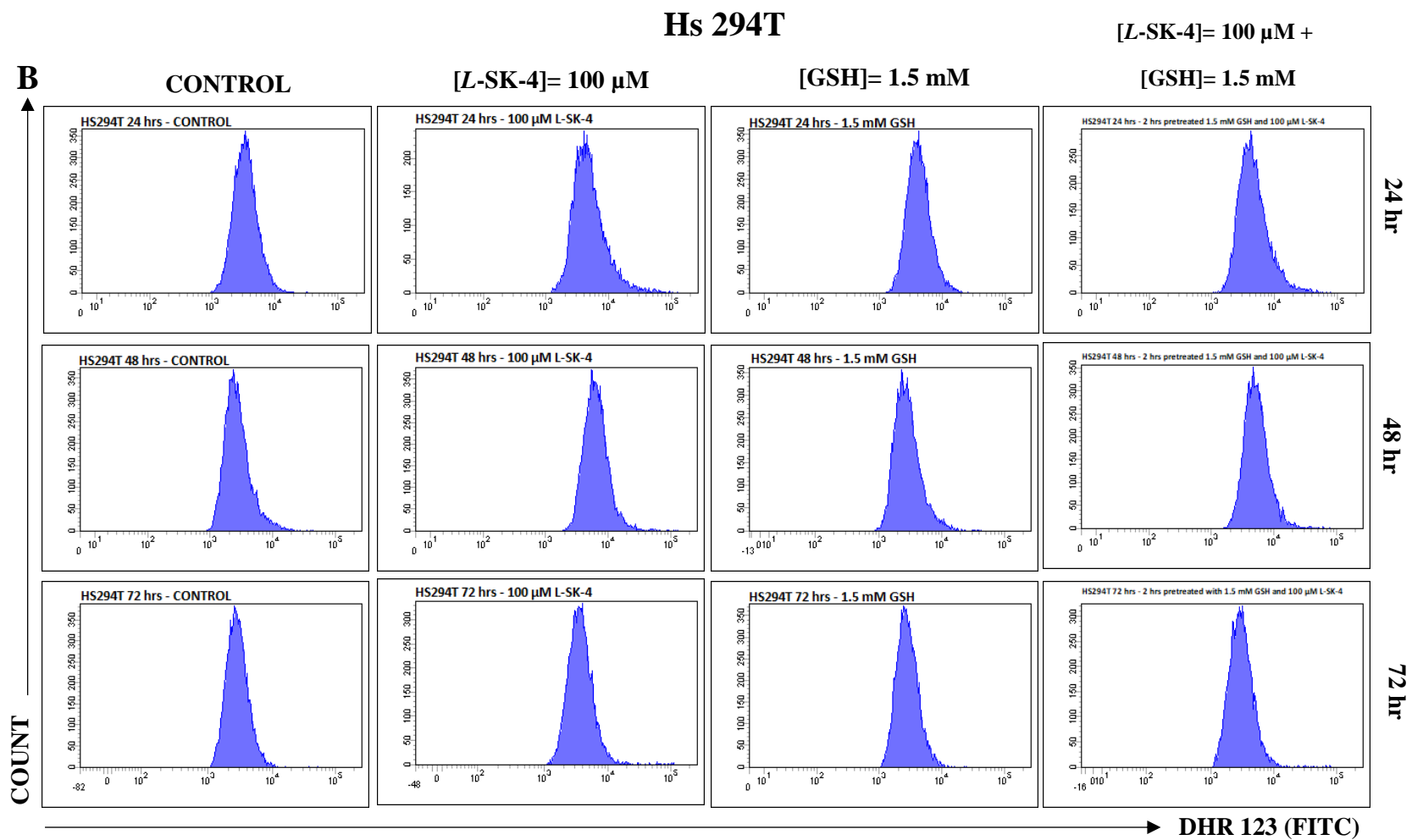




**Figure 79:** The ability of GSH to scavenge intracellular ROS that have been induced by *L-SK-4* in melanoma cell lines. A375 cells were treated with 100 µM of *L-SK-4* in the presence of the absence of 1.5 mM of GSH for 24, 48 and 72 hr and ROS levels were monitored by means of (A) flow cytometry in addition to being quantified as (B) ROS fold of induction.

Finally, we have examined the capacity of 100 µM of *L-SK-4* to induce ROS and also the potency of 1.5 mM of GSH to scavenge any accumulation of ROS in different classes of melanoma such brain metastatic melanoma (VMM-1) (**Figure 80A and D**), lymph node metastatic melanoma (Hs 294T) (**Figure 80B and E**) as well as murine malignant melanoma (B16 F10) (**Figure 80C and F**).





# B16 F10

[L-SK-4]= 100  $\mu$ M +

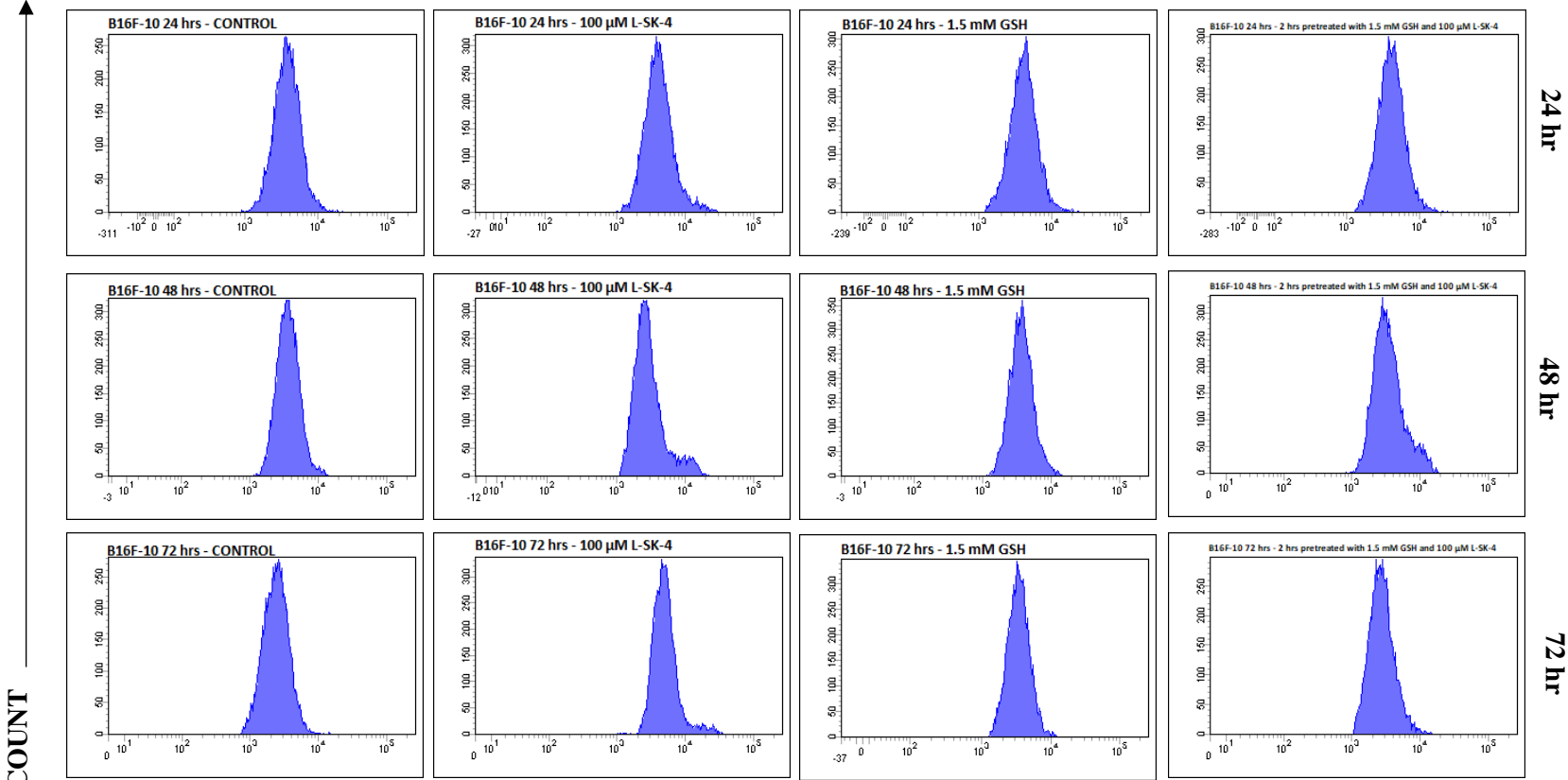
C

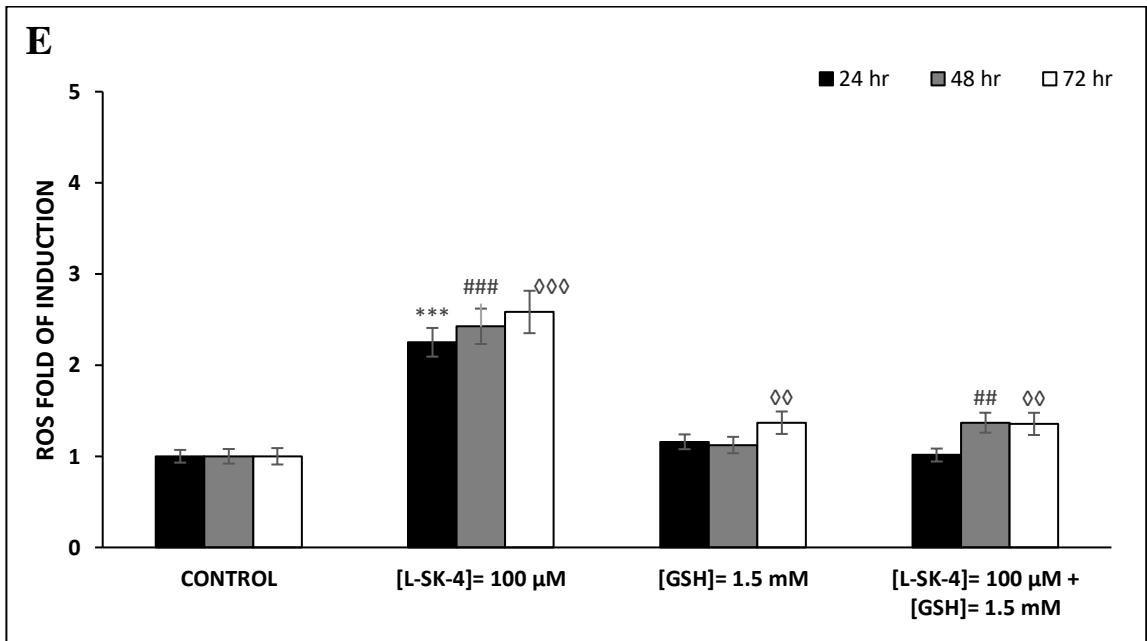
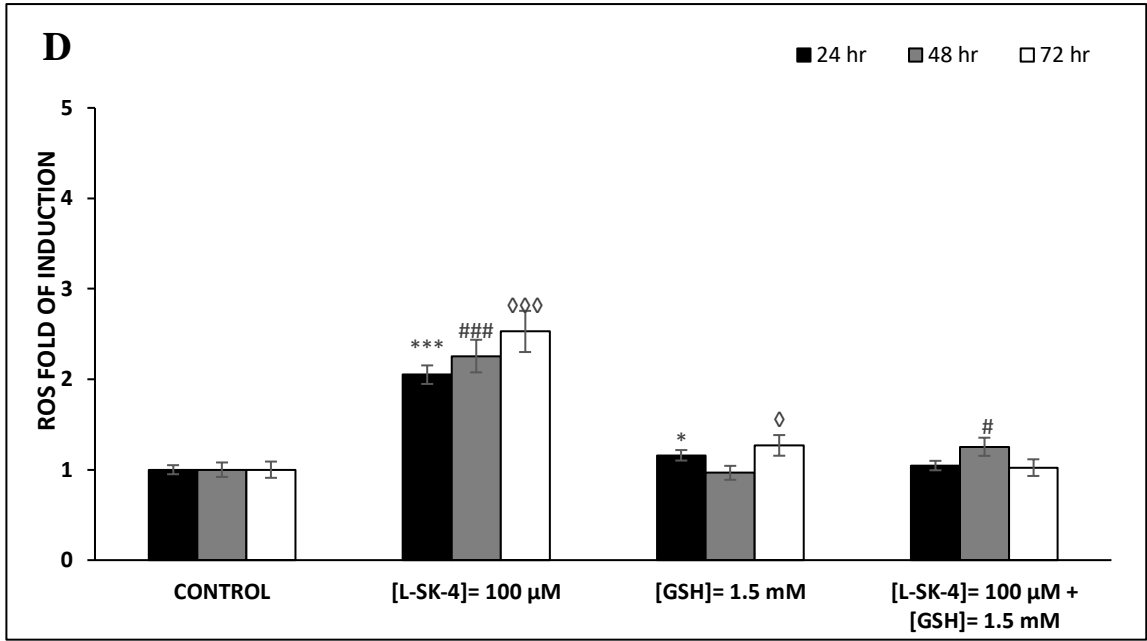
CONTROL

[L-SK-4]= 100  $\mu$ M

[GSH]= 1.5 mM

[GSH]= 1.5 mM





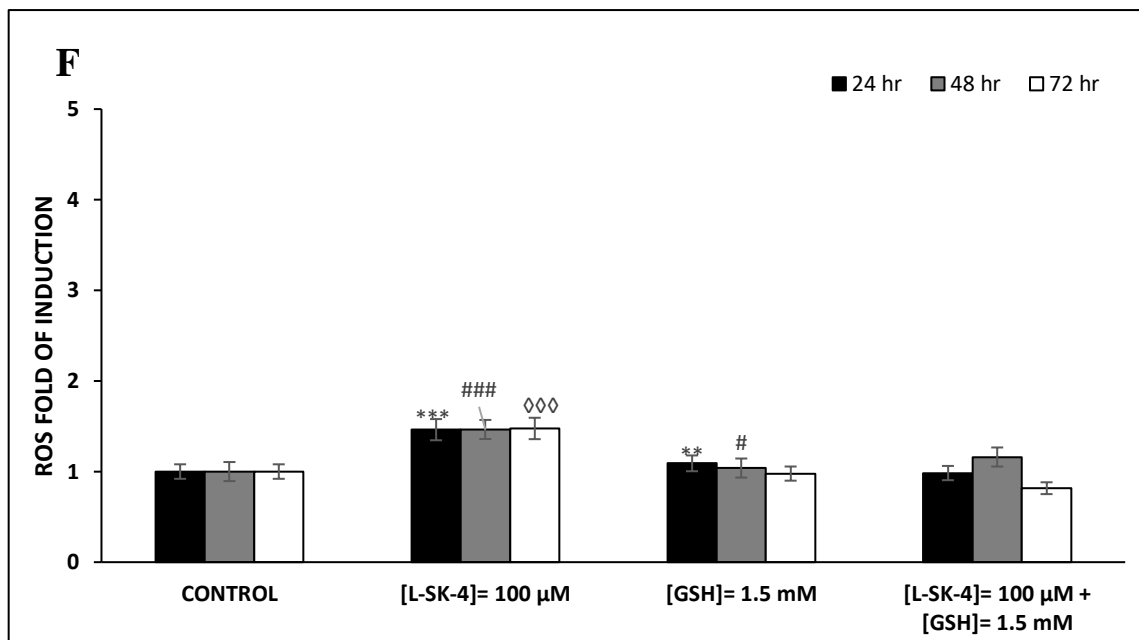


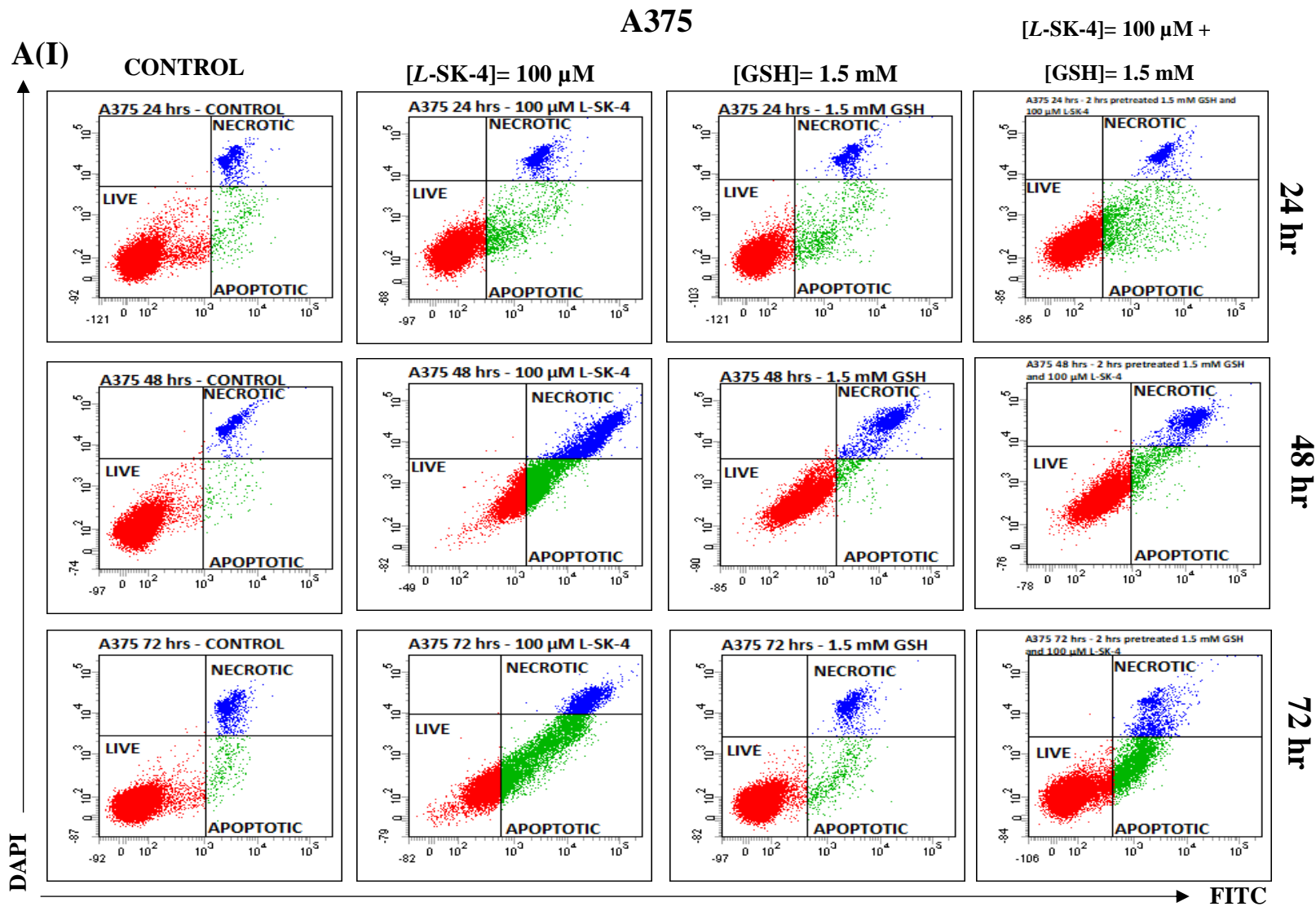
**Figure 80:** The ability of GSH to scavenge intracellular ROS that have been induced by *L-SK-4* in VMM-1, Hs 294T and B16 F10. All cell lines were treated with 100 μM of *L-SK-4* in the presence or the absence of 1.5 mM of GSH for 24, 48 and 72 hr and ROS levels were monitored by means of flow cytometry(A), (B) and (C) in addition to being quantified as ROS fold of induction for (D), (E) and (F) for VMM-1, Hs 294T and B16 F10 respectively. Data shown are means of ± SD of 3 replicates from 3 independent experiments.

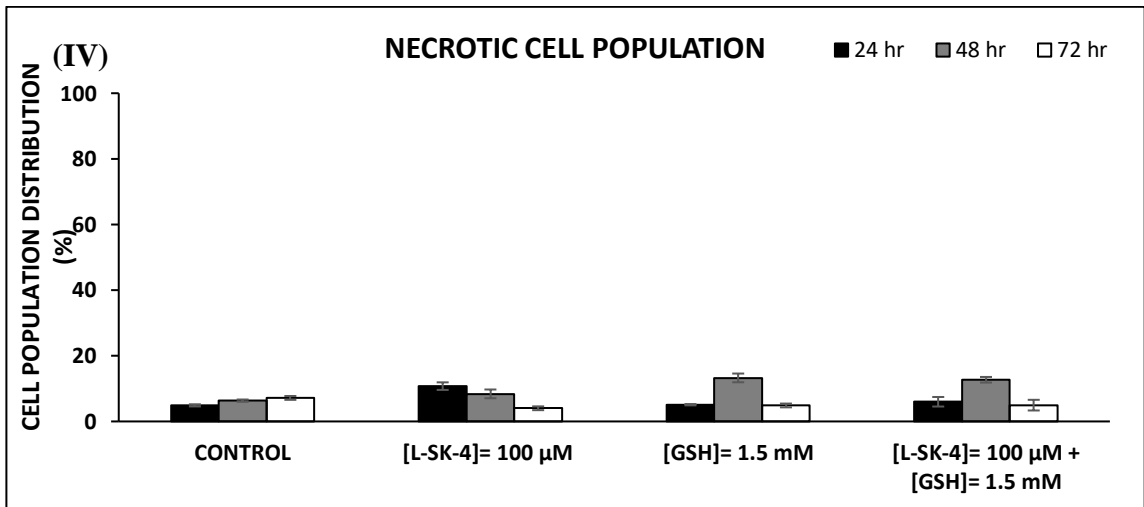
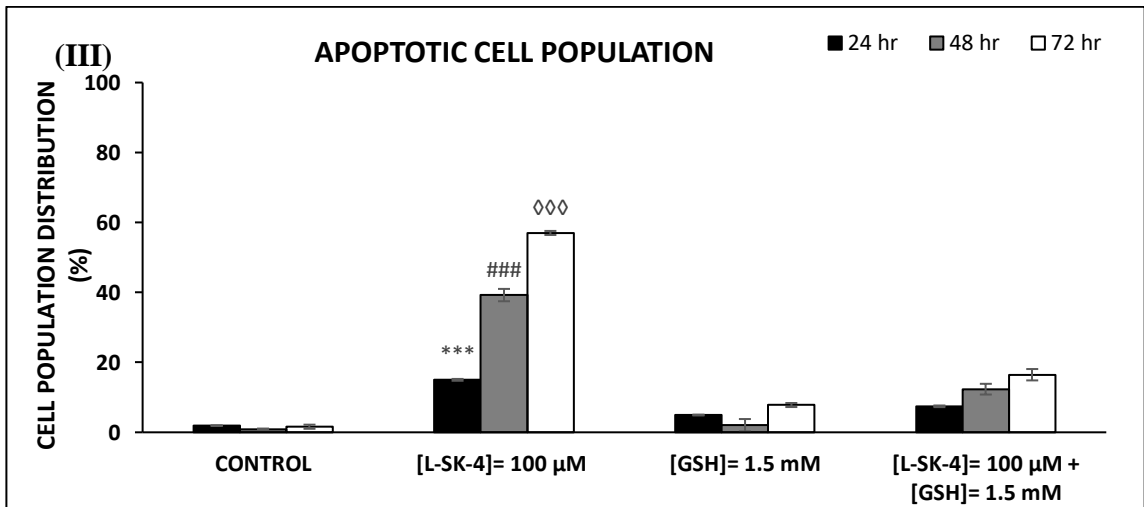
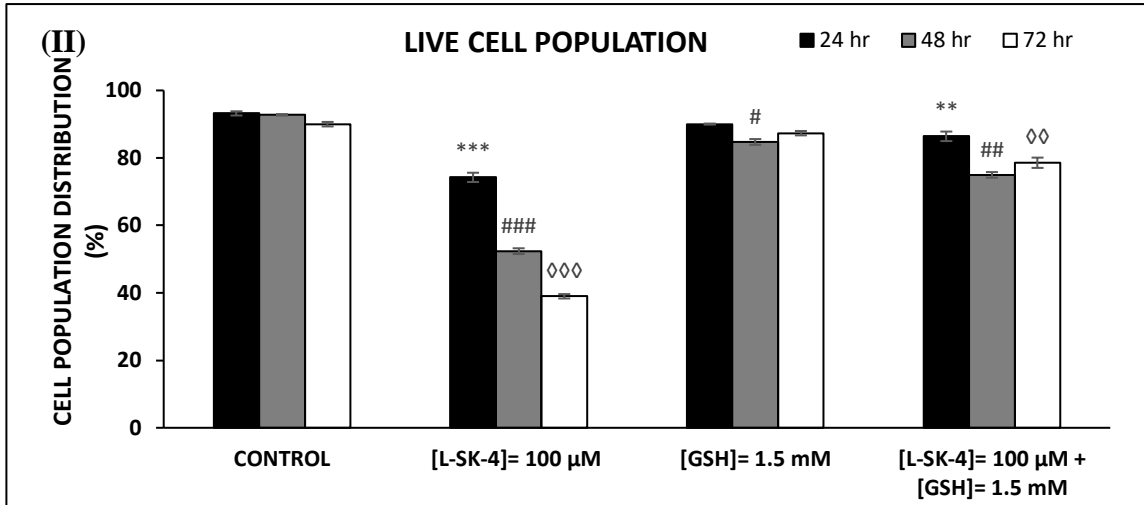
The exported phenotype was the same in all three cell lines. Namely, the treatment has the ability to induce a significant increase of ROS levels during the first 24 hr, which were sustained at each time point thereafter. More specifically in VMM-1 (Figure 80A and D) and Hs 294T (Figure 80B and E) the ROS induced levels were almost at the same magnitude. In contrast the ROS levels been induced in B16-F10 (Figure 80C and F) were not at the same high levels as they observed previously in VMM-1 and Hs 294T. Ultimately, the co-treatment with 1.5 mM of GSH and 100 μM of *L-SK-4* shown that the ROS levels were dropped, almost back to their respective control levels (Figure 80). However, it is also demonstrated that the ROS levels of induction were not as intense as it was in the case of A375, an indication that is pointing out a predominant selectivity

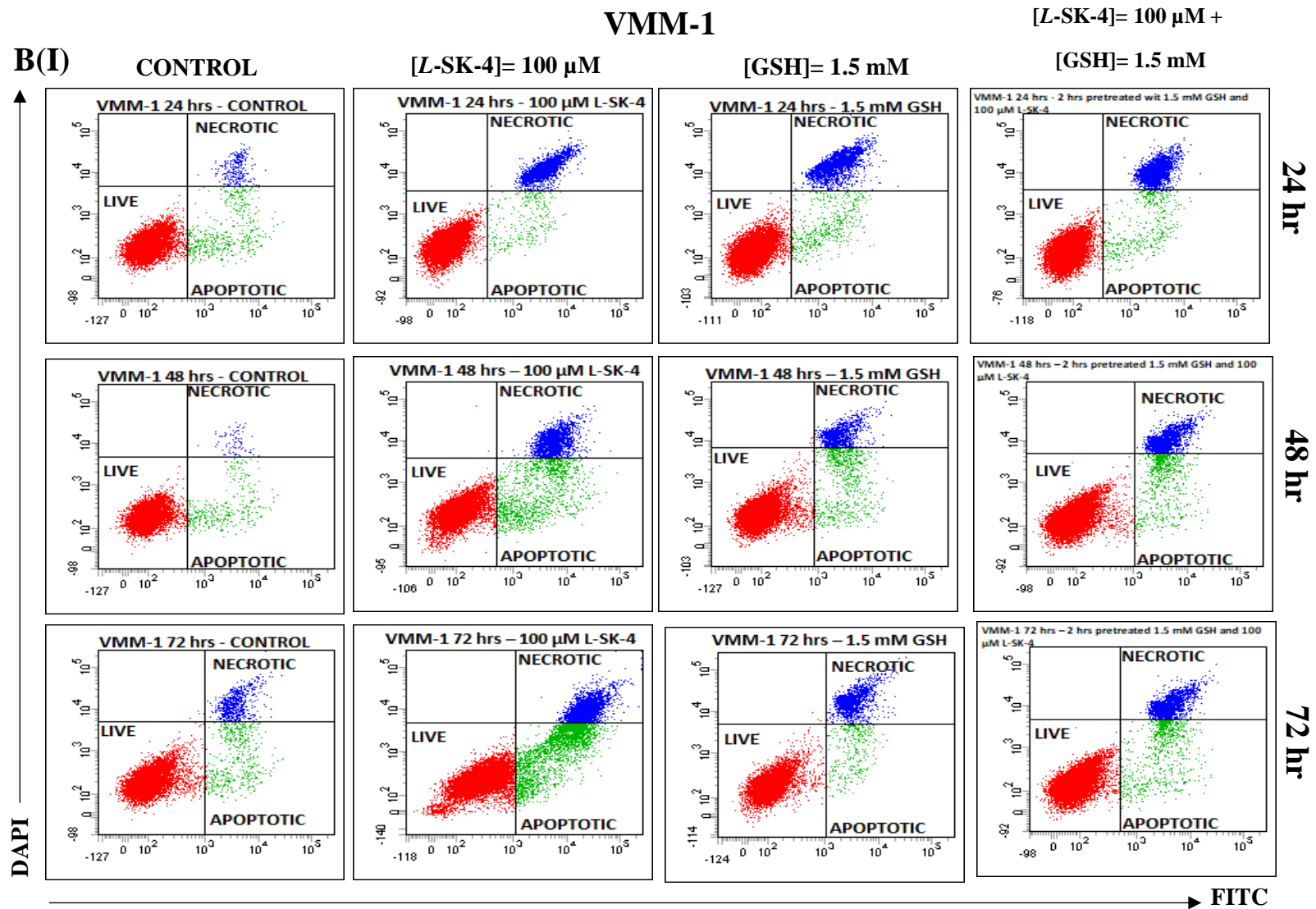
of the treatment on the primary class of malignant melanoma (A375) rather than the metastatic ones.

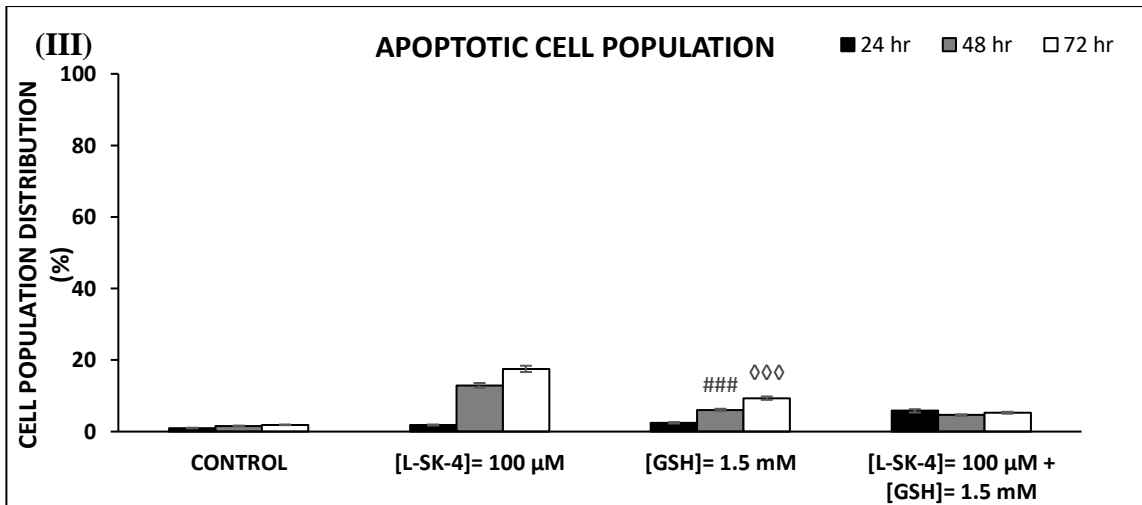
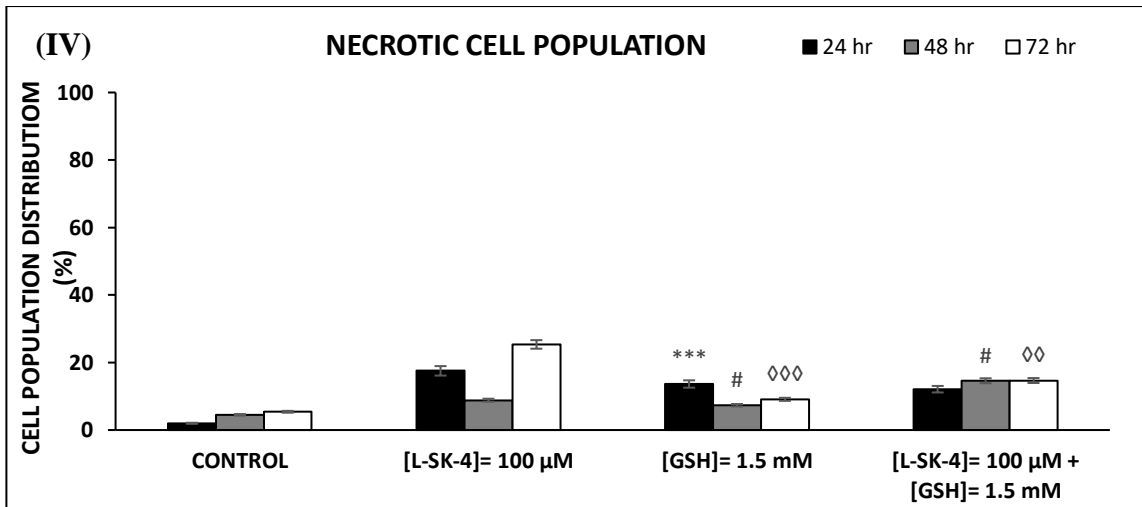
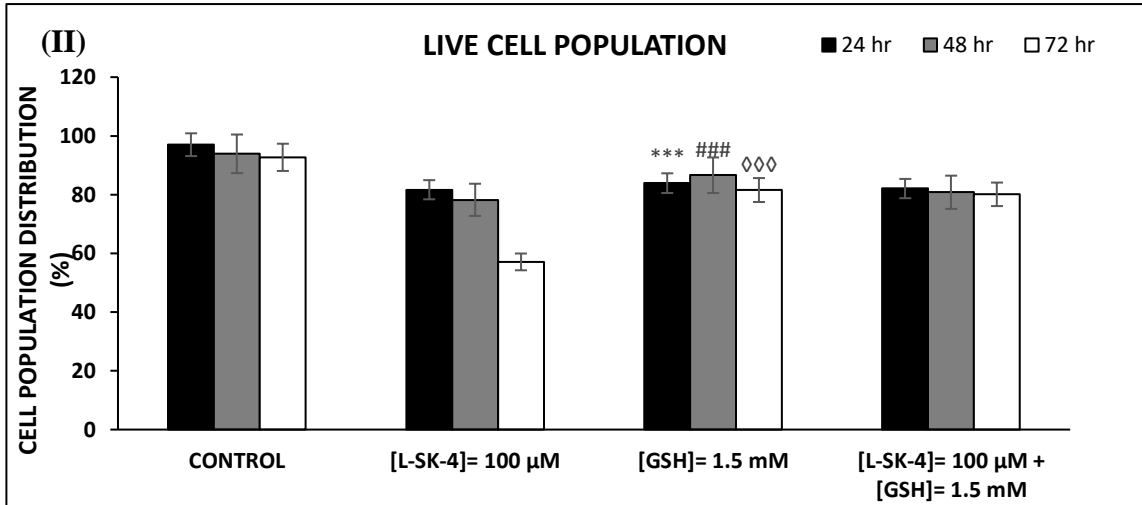
### **7.5.3 Cell death driven by ROS**

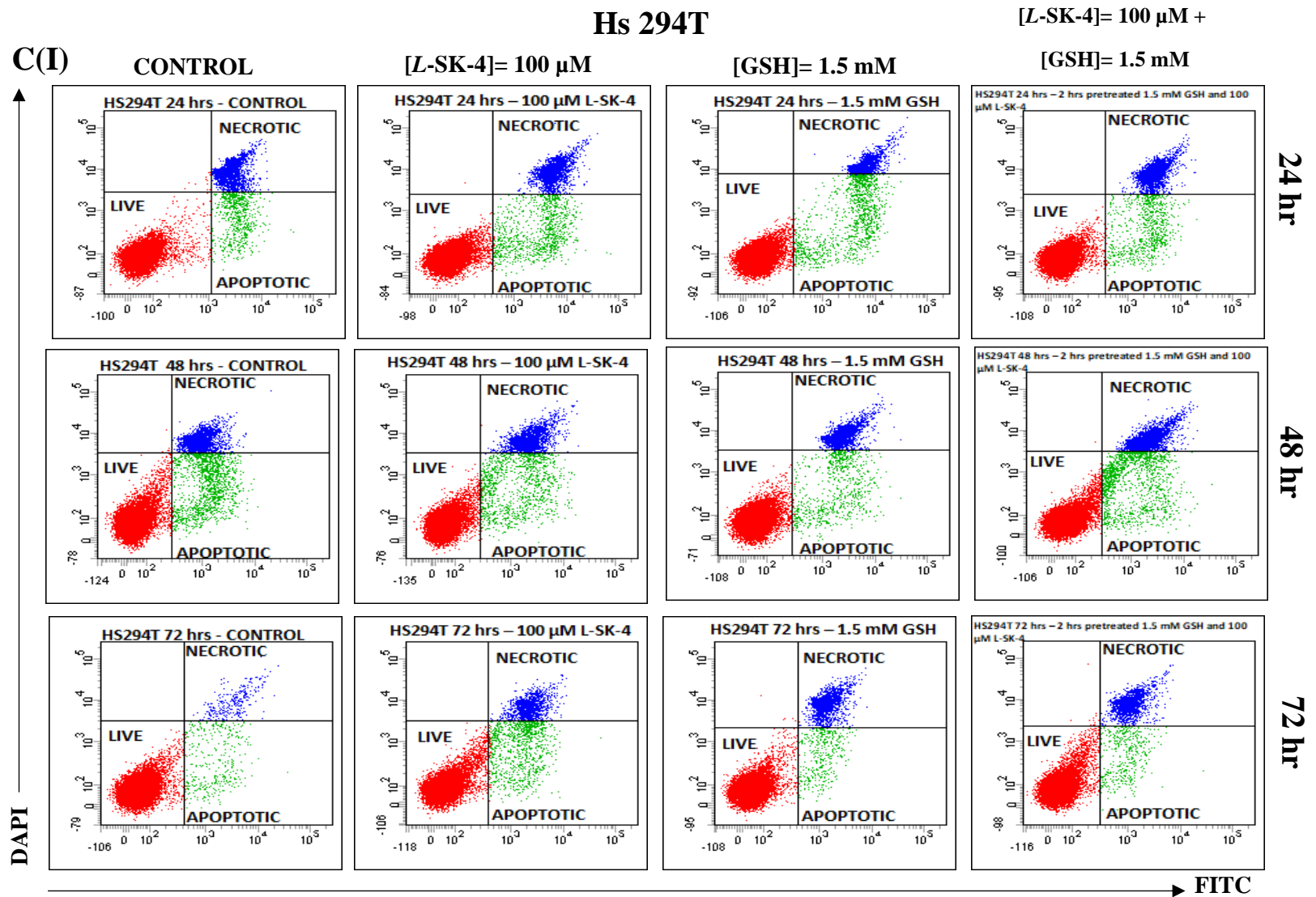
The number of apoptotic and necrotic A375, VMM-1, Hs 294T and B16-F10 cells, was evaluated after exposure to *L*-SK-4 in the presence and the absence of GSH in order to verify that cell death is ROS driven. To distinguish between the two mode of cell death in all cells, the CellEvent Caspase 3/7 Green reagent detection reagent was used as an indicator of activated Caspase 3/7 whereas DAPI as an indicator for necrosis (**Figure 81A-I, B-I, C-I and D-I**).

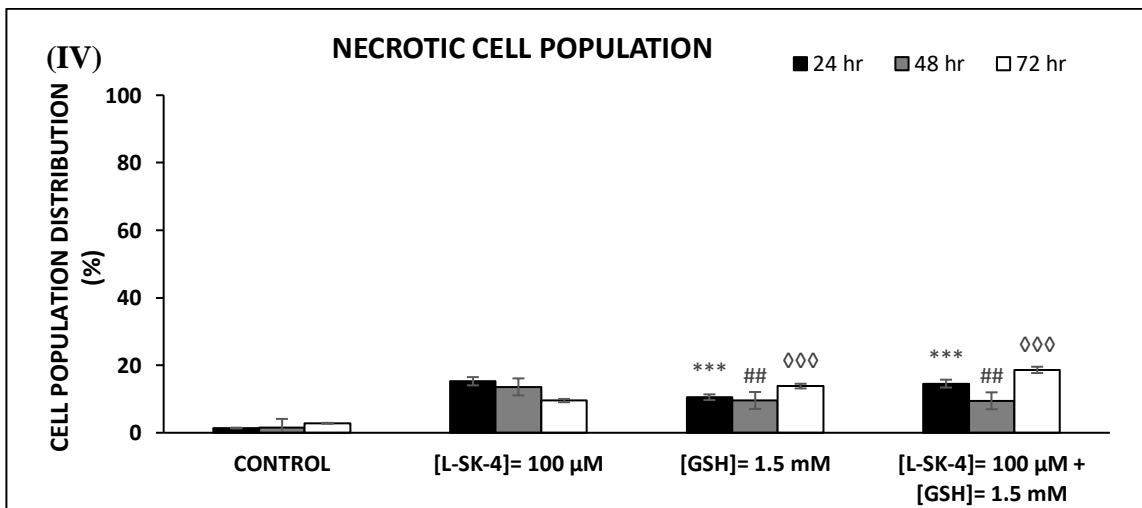
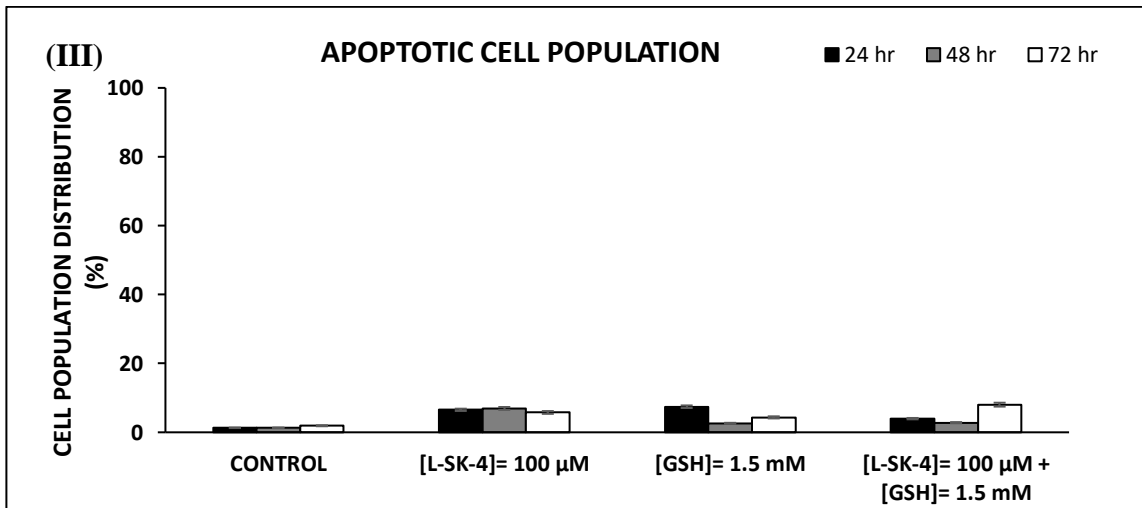
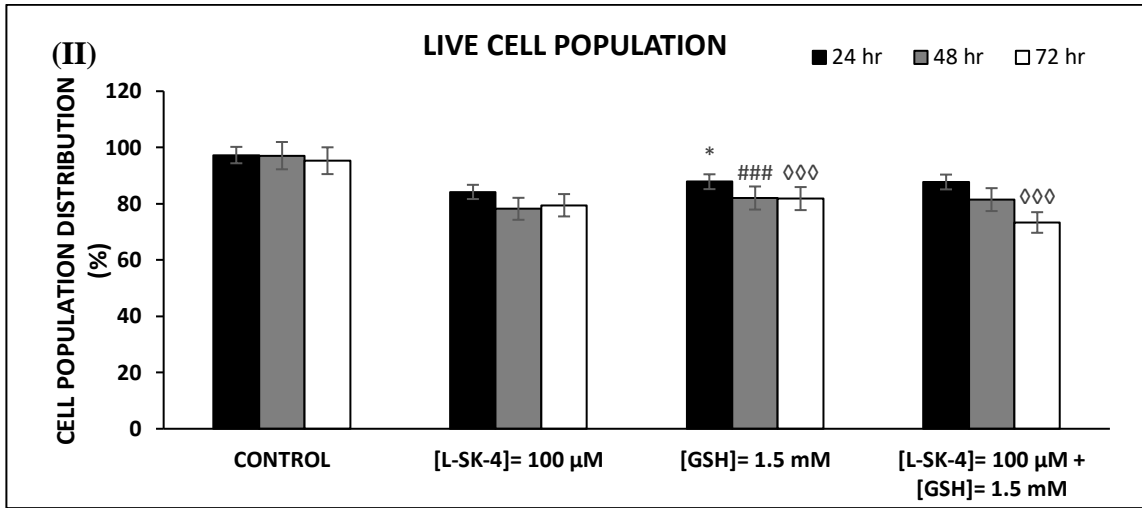


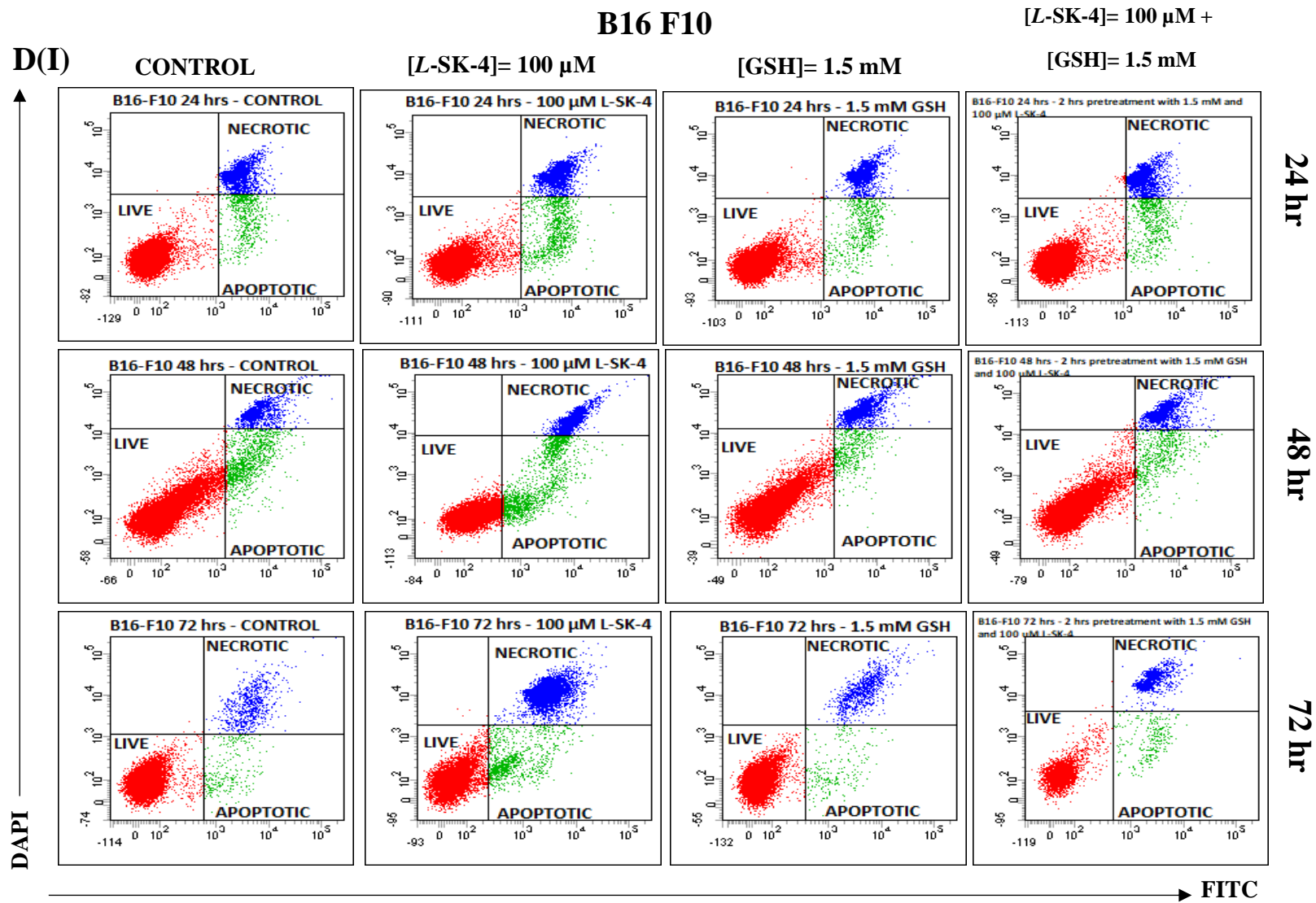












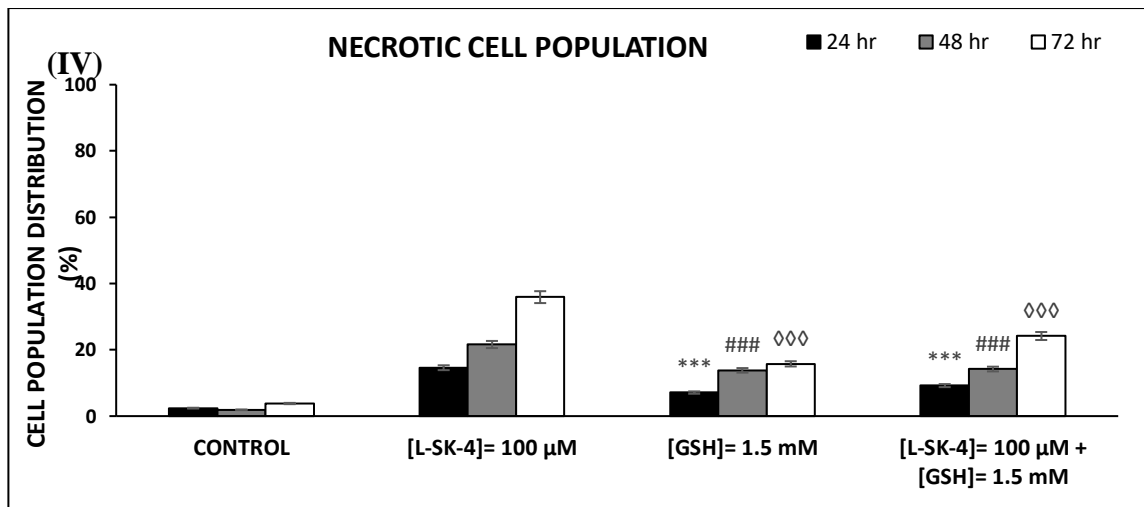
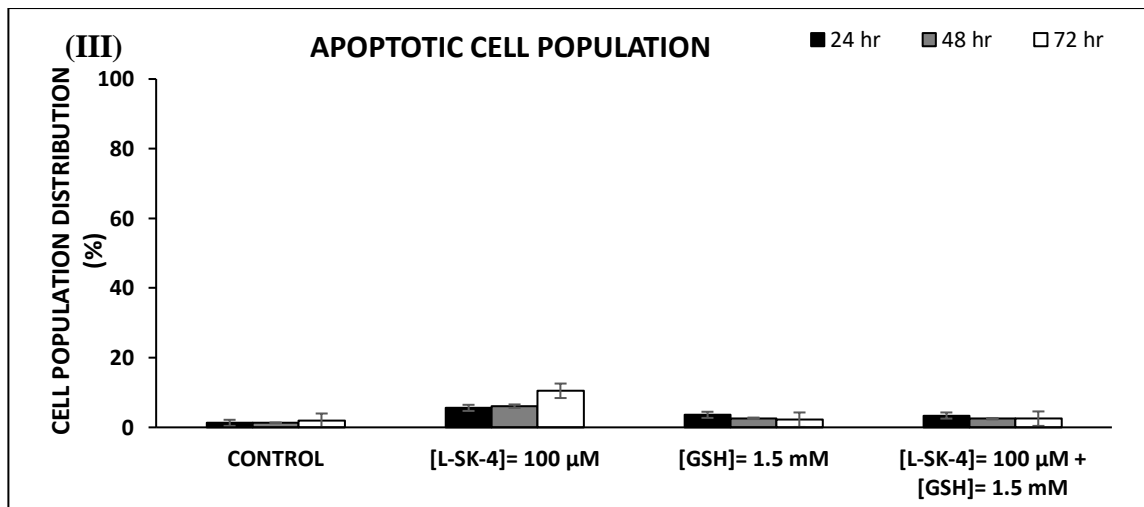
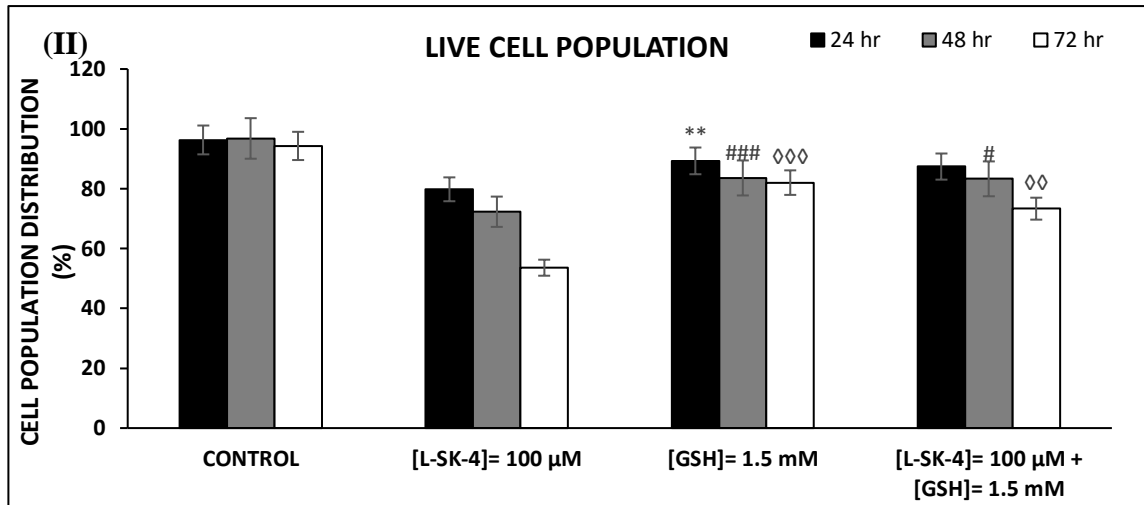


**Figure 81:** The ability of GSH to prevent (A) A375, (B) VMM-1, (C) Hs 294T and (D) B16 F10 cell from undergoing apoptosis after been treated with L-SK-4. Briefly cells were treated with 100

$\mu\text{M}$  of *L*-SK-4 in the presence or the absence of 1.5 mM of GSH or 24, 48 and 72 hr and the distinction between the live, apoptotic and necrotic cells has been done by means of flow cytometry (**A-I, B-I, C-I and D-I**) and then live (**A-II, B-II, C-II and D-II**), apoptotic (**A-III, B-III, C-III and D-III**) and necrotic (**A-IV, B-IV, C-IV and D-IV**) cells were quantified as percentages. Data shown are means of  $\pm$  SD of 3 replicates from 3 independent experiments.

Our data showed significant cell death (by means decreasing live cells) on A375 which was initiated during the first 24 hr, and intensified over time (**Figure 81A-II**). At the same time, the number of apoptotic cells was significantly increased at 24 hr and boosted at 48 and 72 hr (**Figure 81A-III**) while the necrotic population remained unaffected at low levels (**Figure 81A-IV**). However, the co-treatment with GSH reversed that phenotype. Namely, the addition of GSH caused significant elevation of the live cells levels by scavenging ROS, whereas the previously elevated apoptotic cell levels have been decreased dramatically (**Figure 81A-II and III**). Once again the levels of necrotic cells remained steady as to the control (**Figure 81A-IV**). Additionally, it appeared that 100  $\mu\text{M}$  of *L*-SK-4 can be cytotoxic in the other malignant melanoma cell lines that have been used in the *in vitro* model; VMM-1, Hs 294T and B16 F10 with the mode of cell death been differed in each cell line (**Figure 81B, C and D**). Primarily, in the case of VMM-1 cells, the treatment with 100  $\mu\text{M}$  of *L*-SK-4 has the ability to decrease significantly the levels of live cells at 24 hr with the effect to be retained over 48 hr and intensified at 72 hr (**Figure 81B-II**). Additionally, it can be observed that there is significant elevation of the number of apoptotic cells at 48 and 72 hr whereas the necrotic cell population was increasing over the time (**Figure 81B-III and B-IV**). The co-treatment of GSH seems that cause some cell rescue mainly after 72 hr of exposure as the number of live cells remained steady at 24 and 48 hr and increased at 72 hr (**Figure 81B-II**). Moreover, addition of GSH abolished the elevated levels of apoptosis and drops

the levels of necrosis after 24 hr (**Figure 81B-III and B-IV**). A small reduction of necrosis levels was also noticed at 48 and 72 hr (**Figure 81B-IV**).

Afterwards, treatment with 100  $\mu$ M of *L*-SK-4 induced cytotoxicity on Hs 294T cells 24 hr after the exposure with the effect be intensified at 48 hr and retained until 72 hr (**Figure 81C-II**). Interestingly, the treatment did not promote any apoptosis, however it induced necrosis at 24 hr and those levels were generally sustained over 72 hr (**Figure 81C-III and IV**). Co-treatment with GSH didn't cause any significant cell rescue at 24 and 48 hr, whereas a statistically significant ( $p>0.05$ ) has been noticed at 72 hr (**Figure 81C-II**). In this case, GSH didn't decrease the necrosis levels as those were remained unaffected over the entire course of screening (**Figure 81C-IV**).

Finally, exposure of B16 F10 to 100  $\mu$ M of *L*-SK-4 induced a statistically significant ( $p<0.01$ ) cytotoxic effect as the level live cells dropped at 24 hr and those levels decreased further after 48 and 72 hr of exposure (**Figure 81D-II**). The analysis of the mode of cell death didn't show any activation of apoptosis as the apoptotic levels were retained at almost the same levels as the controls (**Figure 81D-III**). In contrast a statistically significant elevation of the necrotic population seems to be illustrated 24 hr post treatment with the effect been intensified over 48 and 72 hr (**Figure 81D-IV**). Co-treatment with GSH didn't cause any beneficial cell rescue at 24 and 48 hr whereas a statistically significant cell rescue was noticed at 72 hr (**Figure 81D-II**). In this case it can be observed that GSH couldn't manage to cause any significant decrease of the necrotic cell population (**Figure 81D-IV**).

Overall it has been demonstrated that treatment with *L*-SK-4 can be cytotoxic in VMM-1, Hs 294T and B16 F10. However, those cell lines seem to be more resistance to the treatment compared to A375. This can be attributed to the fact, that melanoma cells have generally low levels of GSH and therefore they cannot overcome the high levels of ROS been induced by the pro-oxidant chelator.<sup>599</sup> Additionally, the elevated levels of ROS induced different mode of cell death in each

cell line. In some cases, the mode of cell death was not driven by ROS as scavenging them didn't cause any alterations to the either live or dead (including apoptotic and necrotic) cells.

#### 7.5.4 ROS elevation activate apoptotic cascades

Finally, a more descriptive characterization of a variety of proteins that are associated with intrinsic and extrinsic apoptotic cascades was performed (by means of western immunoblotting) in A375 cells that have been exposed to 100  $\mu$ M of *L*-SK-4 with or without pre-treatment with 1.5 mM of GSH (**Figure 82**).

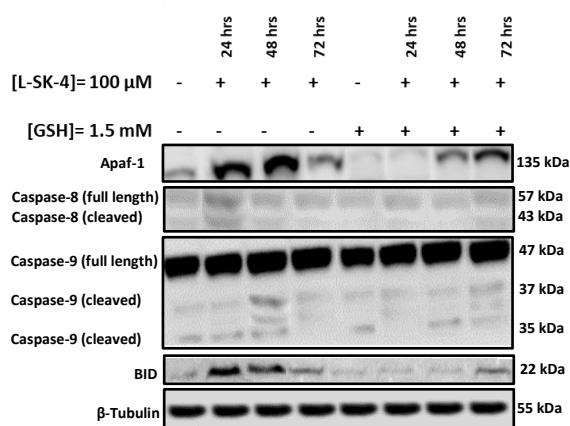


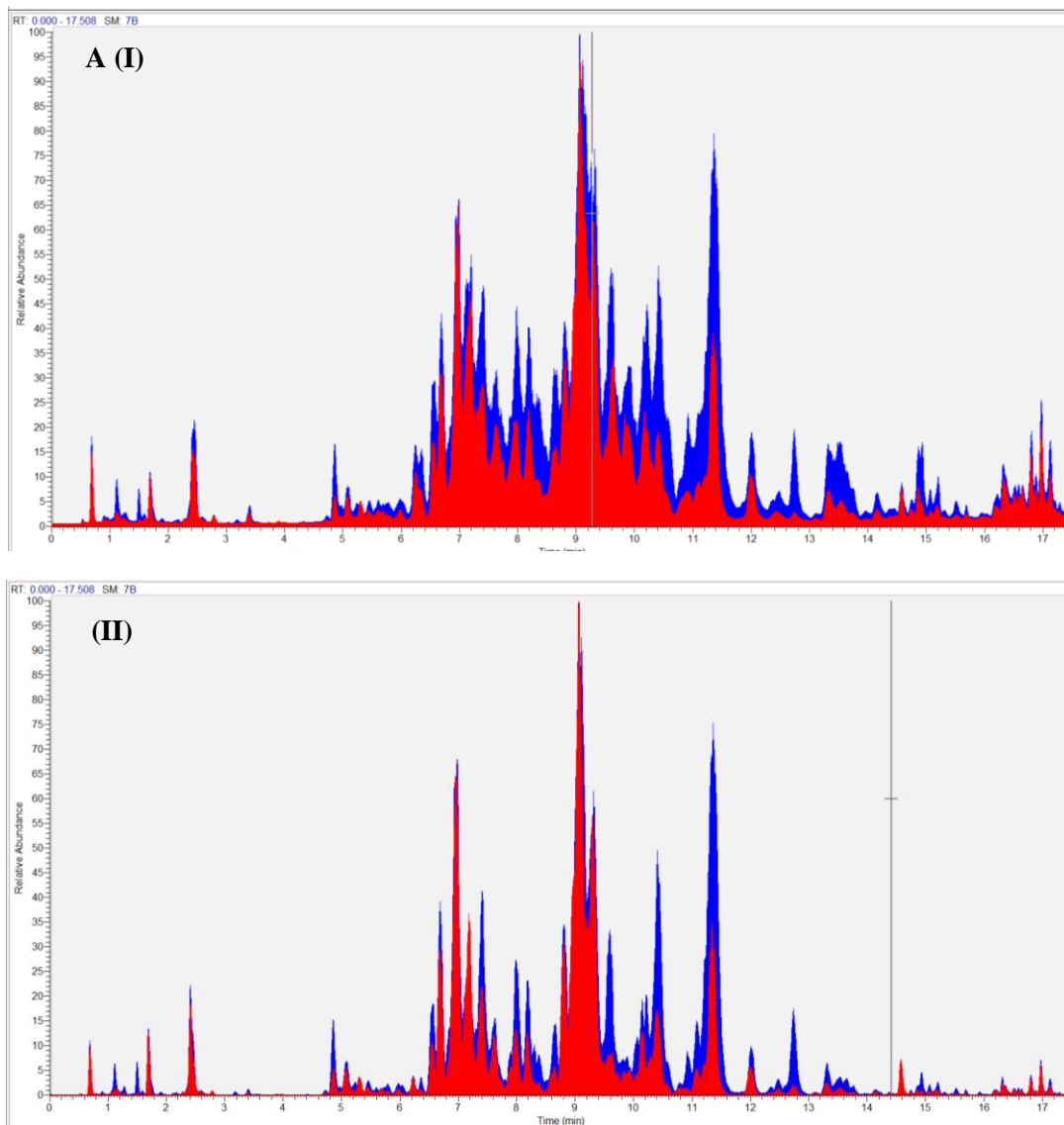
**Figure 82:** The ability of GSH to prevent A375 cell from undergoing apoptosis after been treated with *L*-SK-4. Cell were subjected to 100  $\mu$ M of *L*-SK-4 in the presence of the absence of 1.5 mM of GSH for 24, 48 and 72 hr and protein expression levels of full length and cleaved caspases-8 and -9 were recorded in addition to those of BID and Apaf-1.

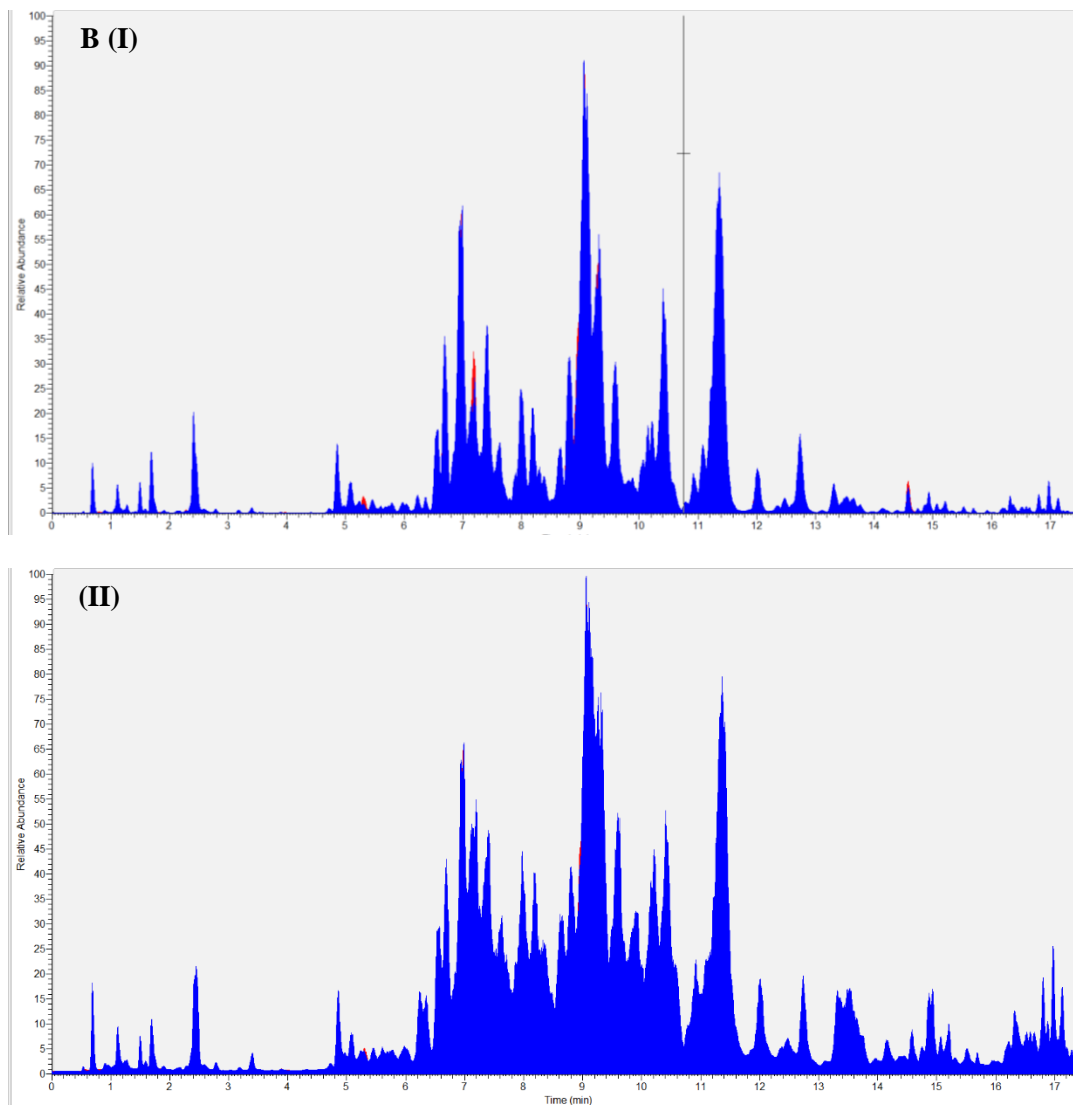
The expression levels of cleaved and full length Caspase-8 (indication of extrinsic apoptosis) and also the respective levels of cleaved and full length Caspase-9, as well as the Apoptotic protease-activating factor (Apaf-1) which are indicative markers for the intrinsic apoptosis were observed.<sup>600-606</sup> In addition to these, the expression levels of BID were determined due to its ability

to link the two apoptotic pathways.<sup>607-611</sup> Overall, the activation of Caspase-8 was proved by the present of increased cleaved length protein expression levels which was observed as early as 24 hr after the exposure to *L*-SK-4 and remained as such through the entire time course. In contrast, when cells co-treated with GSH and *L*-SK-4, the respective proteins expression levels were sustained at the same levels as the control (cell been treated with just GSH) for 24 and 48 hr. A small activation of Caspase-8 (by means of Cleaved length protein expression) was observed at 72 hr. Furthermore, the expression levels of BID were also elevated during 24-48 hr on the groups been exposed to *L*-SK-4 (indication of a concomitant activation of the intrinsic apoptosis) while reduced back to the control levels after 72 hr of exposure. The expression levels of BID in the cell population being co-treated with GSH were remained at the control levels over 24 and 48 hr whereas a small activation seems to be denoted after 72 hr. Further evidence for the concomitant activation of the intrinsic apoptotic activation was documented after examining the expression levels of caspase-9 and Apaf-1 through the time course in the groups been treated with *L*-SK-4 either with or without pre-treatment with GSH. To this end, several studies revealed the activation of Caspase-8 as well as that of Caspase-9 and Apaf-1 (via the formation of apoptosome) can eventually lead to the activation of Caspase-3 which is an establish mechanism for the execution of apoptosis.<sup>607-615</sup> On the other hand, we proved that accumulation of ROS is strongly associated with the activation of apoptotic pathways. These observations were documented by the expression levels of apoptotic markers that were remained at low levels (or slightly elevated after 72 hr of exposure) by scavenging the ROS that *L*-SK-4 has induced (by adding GSH). Therefore, this finding can lead us to the conclusion that (i) low levels of GSH cannot scavenge the excessive amount of ROS been induced by the chelator and also (ii) the cell death/rescue is well regulated by the ROS levels since scavenging them can rescue cell from apoptotic cell death. Our findings are in agreement with literature as it has been proven before that metal chelators can induce oxidative stress driven apoptosis.<sup>114,616-618</sup> Additionally, the ability of GSH to prevent the activation of apoptosis has been previously reported.<sup>619-622</sup>

## 7.6 Lipidomic analysis

In order to see how the elevated levels of ROS affect the lipidome profile of the A375 cells a lipidomic analysis was performed between the A375 cells treated for 24 hr with 100  $\mu$ M *L*-SK-4 and the respective untreated controls. The results suggested that 1800 lipidome MS1 features differentiated between the control and the treated group (**Figure 83**).

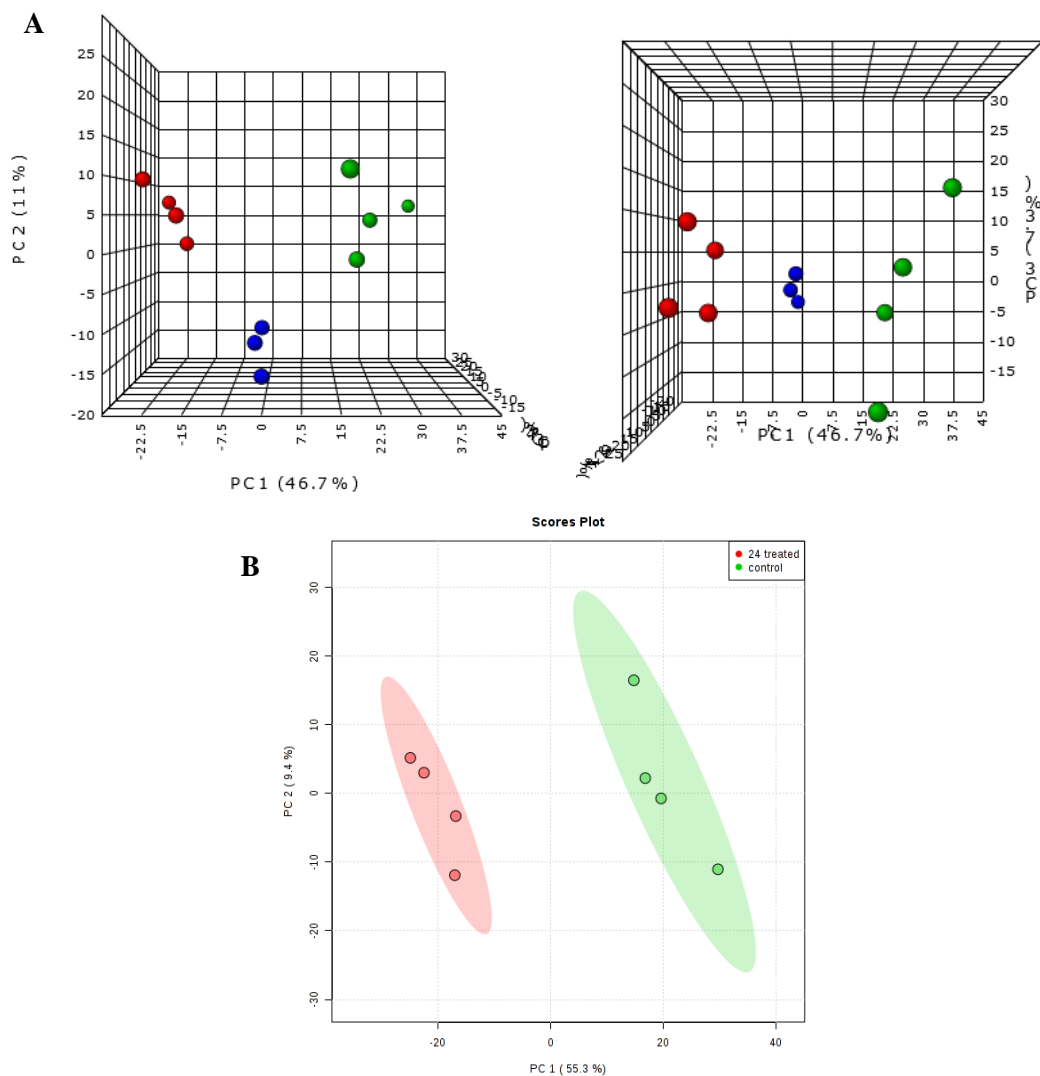




**Figure 83:** Overlapped (A) (I) Total Ion Chromatogram (TIC) and (II) Base Peak chromatograph of the A375 untreated cells (red chromatograph) and A375 24 hr treated with 100  $\mu$ M of *L*-SK-4 (blue chromatograph) (B) (I) Total Ion Chromatogram (TIC) and (II) Base Peak chromatograph of the A375 untreated cells (red chromatograph) of the A375 24 hr 100  $\mu$ M of *L*-SK-4 (blue chromatograph) and A375 untreated cells (red chromatograph) treated with respectively using positive Electron Ionization Mode (+ev EIM).

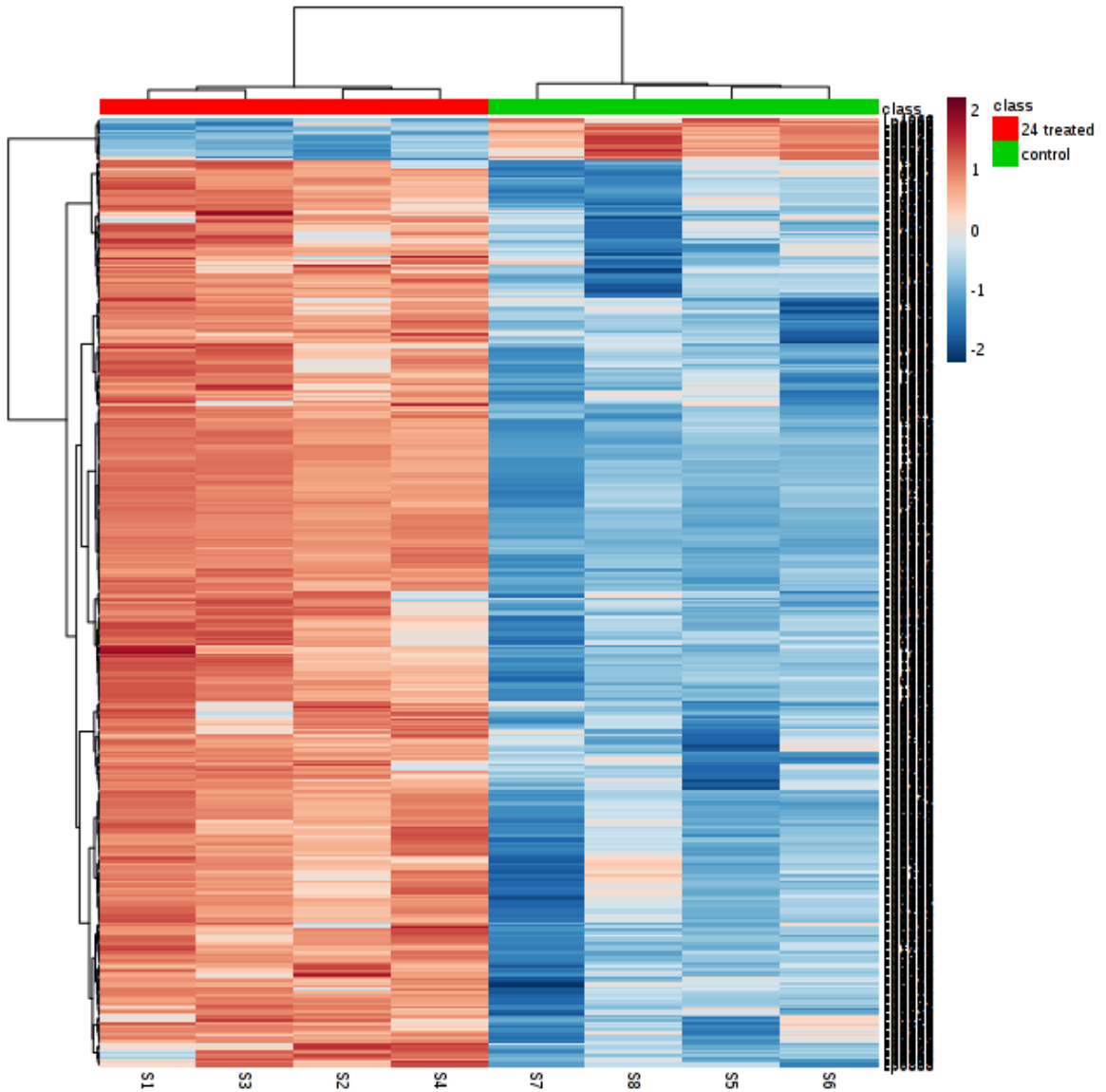
Principal Component Analysis (PCA) and visualization was used in order to examine the presence of any underlying trends within the data sets and the results revealed a planar separation between

the control, treated cells and quality control (**Figure 84A**). Afterwards, partial least square-discriminated analysis (PLS-DA, 1 latent variable) was then performed to identify and retain the most statistically significant features (VIP<1) (**Figure 84B**).



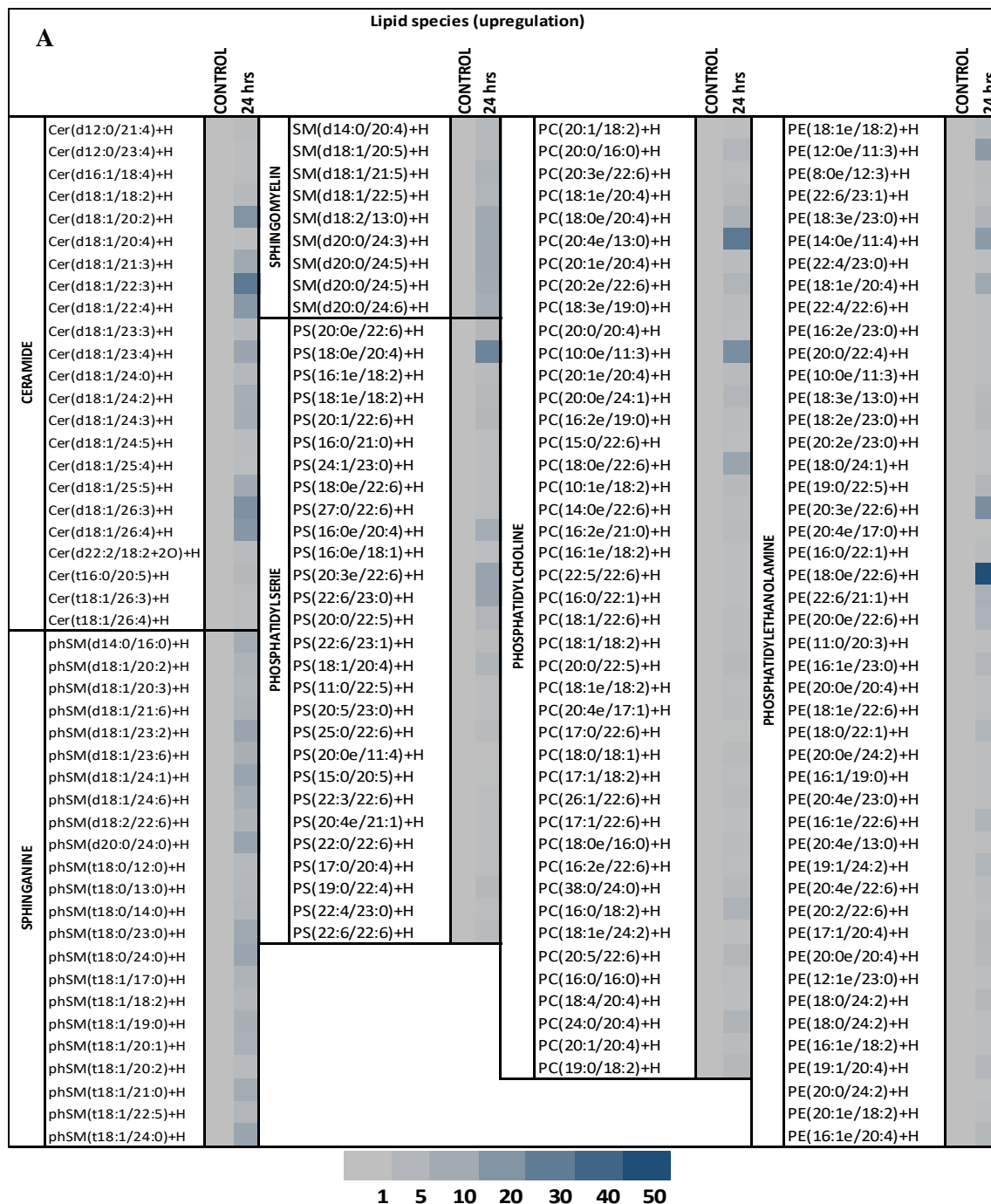
**Figure 84:** (A) 3D PCA of the the 1800 upregulated lipidated features present in A375 cells generated by MetaboAnalyst 4.0 using the ‘Statistical Analysis’ node. Blue spheres represent the quality control whereas red and green represent the lipidated features of 24 hr treated with 100  $\mu$ M *L*-SK-4 and untreated control respectively. (B) PLS-DA analysis of A375 untreated cells VS 24 hr A375 cells treated with 100  $\mu$ M *L*-SK-4.

The outcome of this analysis is that approximately 400 MS-1 validated features were upregulated in the treated cells compared to the respective control ones (**Figure 85**).



**Figure 85:** Heatmap representing the top 400 discriminated features that were significantly up or down regulated in the A375 cells treated with 100  $\mu\text{M}$  of *L*-SK-4 compared to the respective untreated control.

From those it can be confirmed (*via* MS-1) that the elevated lipid classes were associated with the *de novo* biosynthesis of sphingolipids with the most significant unregulated species of this class been known as ceramides (**Figure 86**).



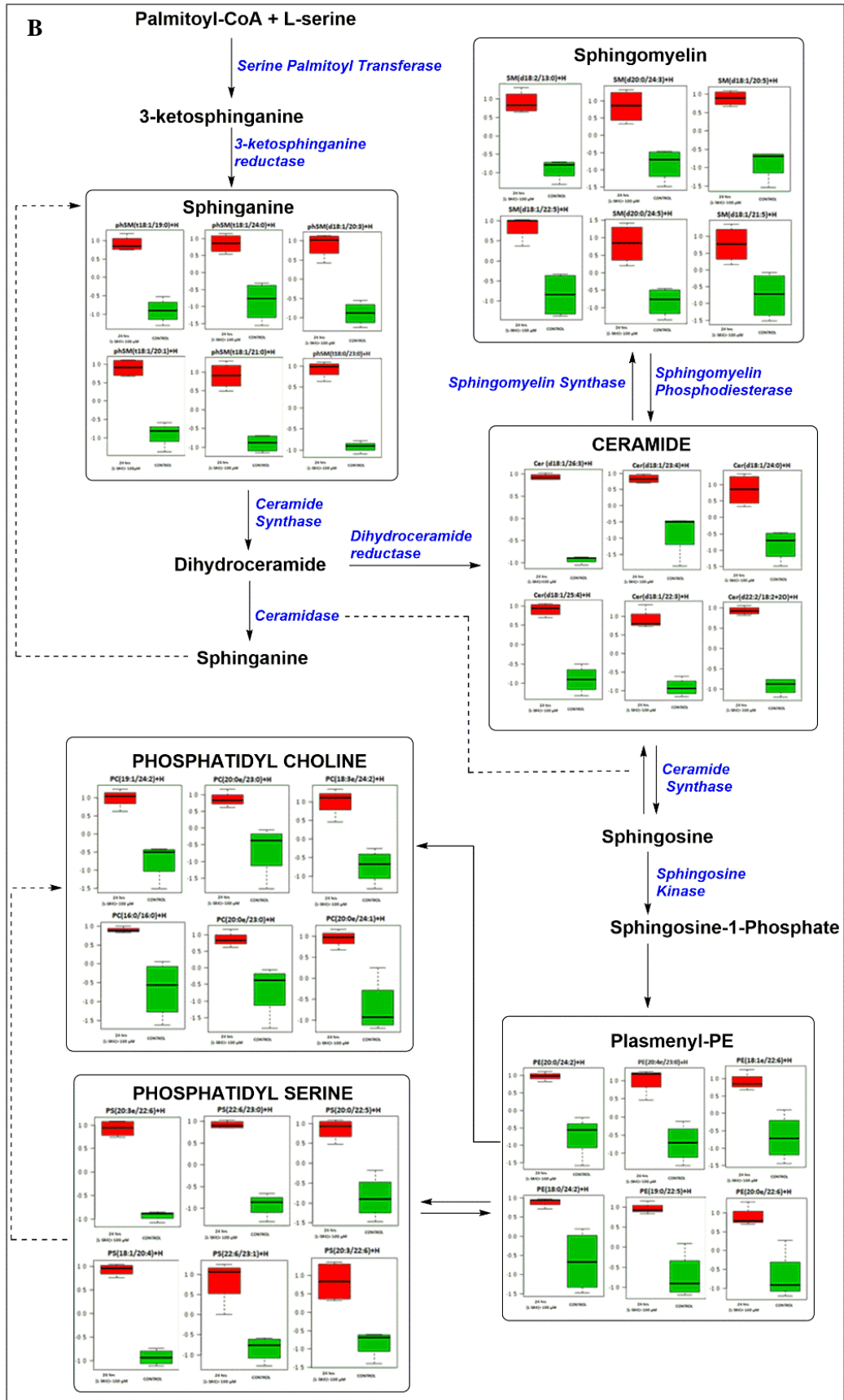


**Figure 86:** (A) Heatmap showing the relative fold of change in the biosynthesis of sphingolipids in A375 cell line, 24 hr post-treatment with 100  $\mu$ M of *L*-SK-4 for 24 hr. Lipidomic analysis revealed the significant elevation of sphingolipids. (B) Overall sphingolipids de novo biosynthetic map shows the upregulation of sphingolipids (Whisker's box) in the cell groups been treated with 100  $\mu$ M of *L*-SK-4 (red bar) compared with the respective control (green bar).

### 7.6.1 Effect of myriocin in cell survival - The role of ceramide.

According to the literature, it is suggested that elevation of ROS can stimulate the release of ceramide species which they can serve messengers for the activation of apoptotic cascades.<sup>623</sup> Our findings seems to agree with the literature since elevation of ROS stimulates the biosynthesis and release of ceramide lipids (as well as other sphingolipids) via ceramide releasing enzymes resulting in the generation of a ceramide-enriched membrane, suggesting that this is a response – adaptation – mechanism that cells tend to follow before the activation of the downstream apoptotic cascades.<sup>624-635</sup> Moreover, in order to validate whether the elevated (by ROS) levels of ceramide species can induce cell death, we treated the cells with myriocin, an inhibitor of serine palmitoyl transferase, an enzyme that catalyze the first step in *de novo* sphingolipids biosynthesis (**Figure 87A and B**).<sup>636-640</sup> Initially, cells were exposed to a range of concentrations of myriocin (0-50  $\mu$ M) and time (24-72 hr) for the determination of the tolerated dose which was found to be 50 nM (**Figure 87C**).

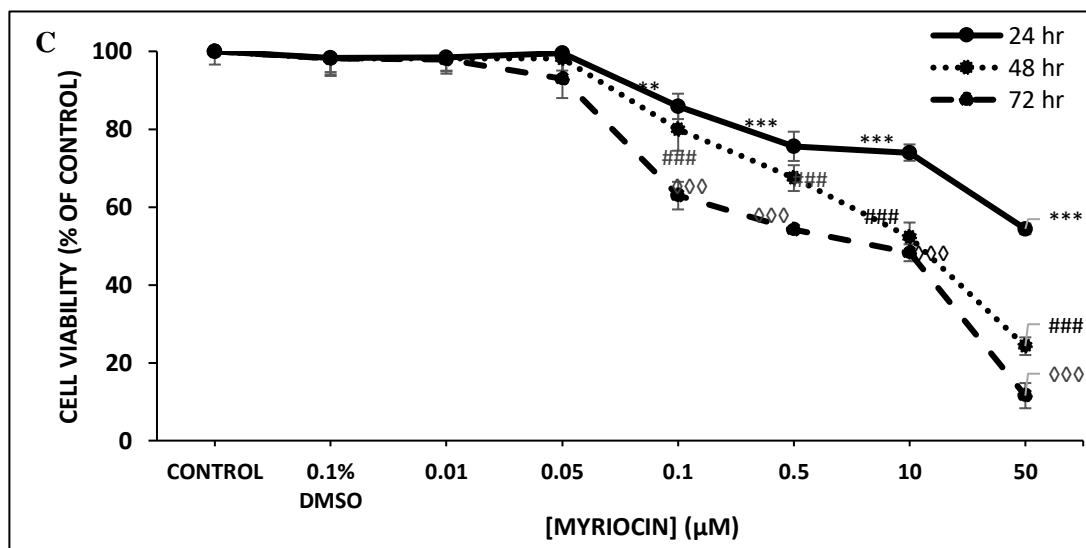
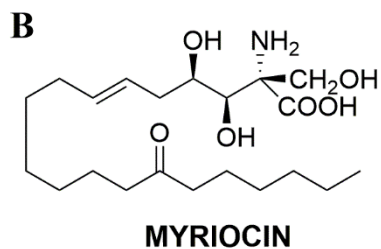
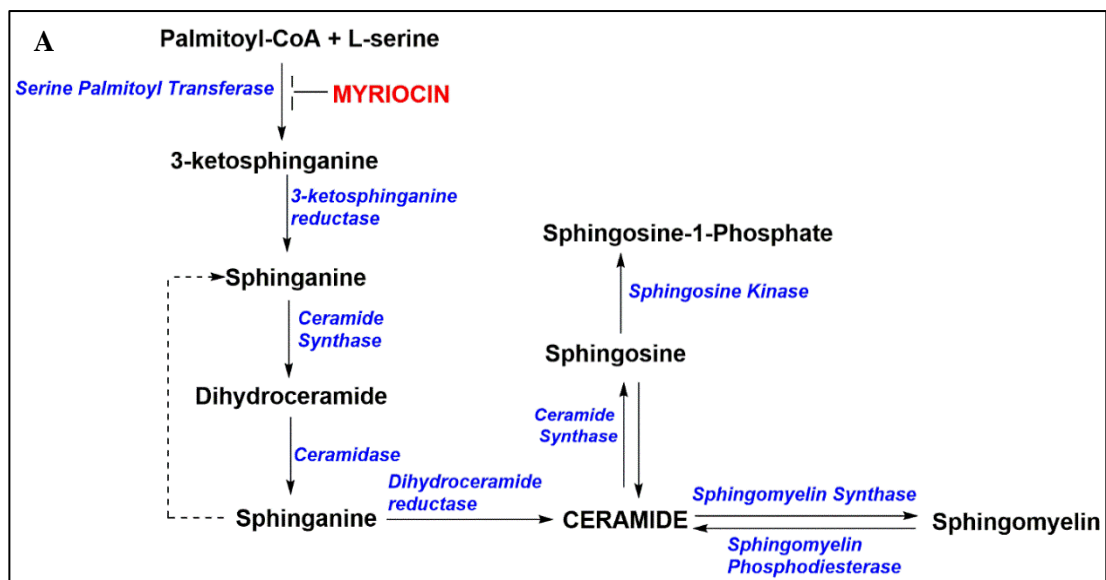


**Figure 87:** (A) Myriocin prevents ceramide biosynthesis by inhibiting the enzyme Serine Palmitoyl Transferase. (B) The structure of myriocin. (C) The ability of myriocin to induce cytotoxicity in A375 cells. Cells were exposed to a range of 0.01-50 μM concentrations of

myriocin for 24, 48 and 72 hr. Data shown are the means  $\pm$  SD of 5 replicates from 3 independent experiments.

Finally, cells were pretreated with 100  $\mu$ M of *L*-SK-4 either in the presence or the absence of 50 nM of myriocin in order to determine whether inhibition of sphingolipids biosynthesis and consequently ceramide elevation can prevent the induction of cell death (**Figure 88**).

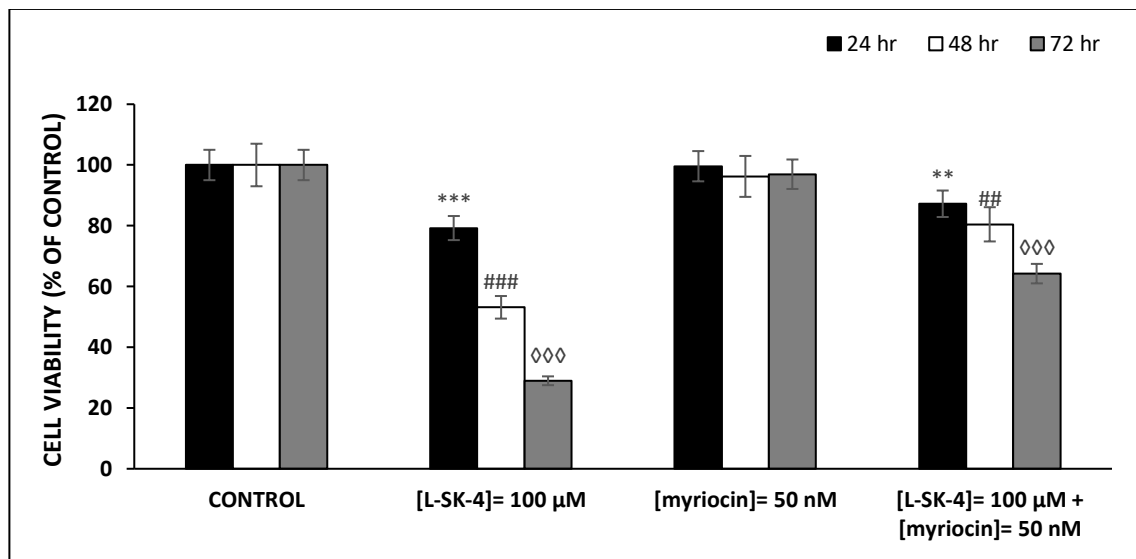
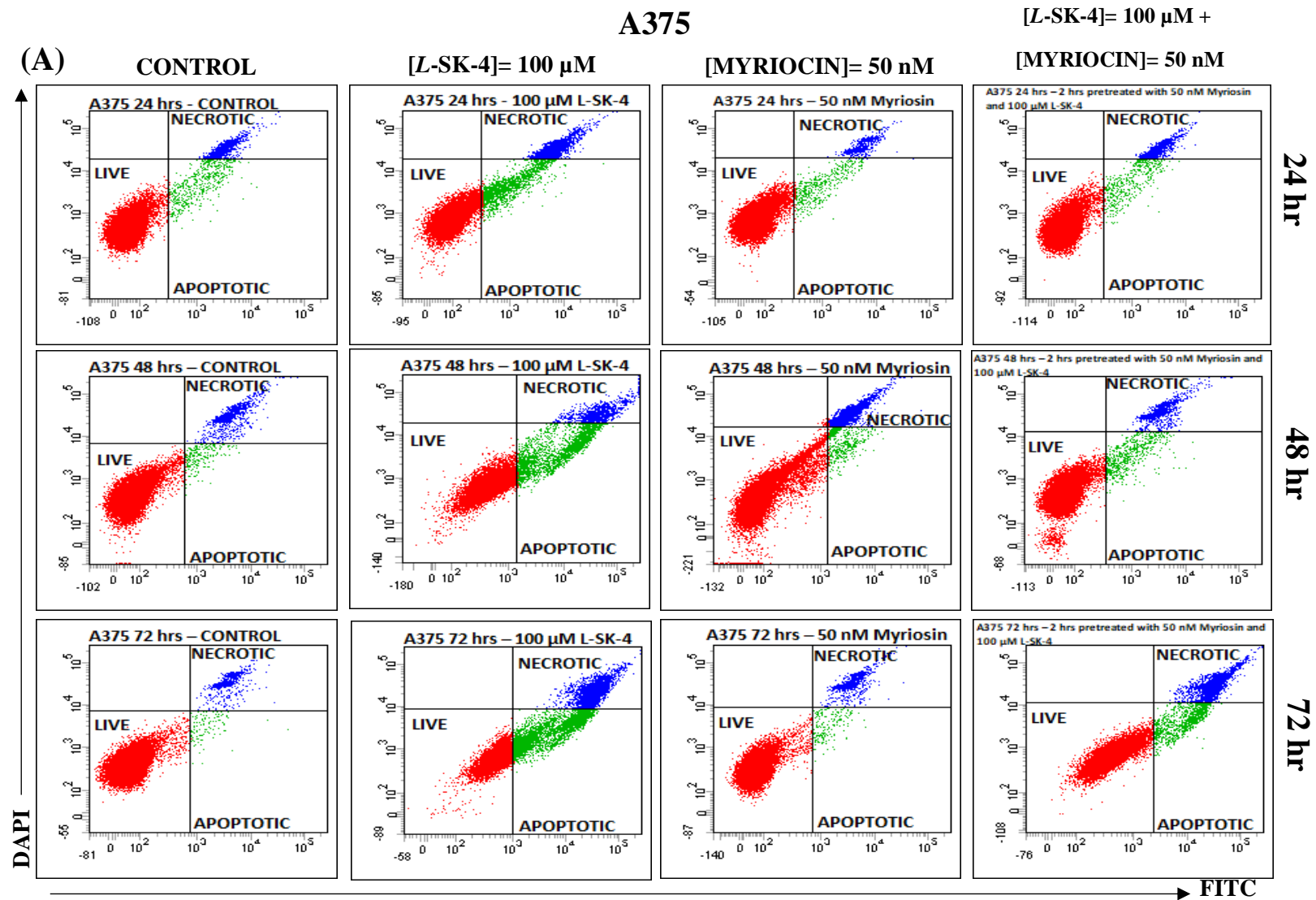


**Figure 88:** Myriocin can rescue cells from cell death by inhibiting the overproduction of ceramide been induced by *L*-SK-4. A375 cells were treated with 100  $\mu$ M of *L*-SK-4 in the presence of absence of 50 nM of myriocin for 4 24, 48 and 72 hr. Data shown are the means  $\pm$  SD of 5 replicates from 3 independent experiments.

Not surprisingly, a significant drop in the viability levels of the cells been exposed to *L*-SK-4 was noticed once again. However, the viability levels of the cell population that it was co-treated with *L*-SK-4 and myriocin was significantly elevated compared to those been treated with *L*-SK-4 implying in that way that myriocin has the ability to induce cell rescue rather than cell death (**Figure 88**).

Afterwards, we evaluated whether the treatment with myriocin can prevent the induction of apoptosis been induced by *L*-SK-4 by measuring the number of apoptotic and necrotic A375 cells

after exposure to *L*-SK-4 either with or without co-treatment with myriocin by means of flow cytometry (**Figure 89**). To distinguish between the two mode of cell death in all cells, the CellEvent Caspase 3/7 Green reagent detection reagent was used as an indicator of activated Caspase 3/7 whereas DAPI as an indicator for necrosis (**Figure 89A**).



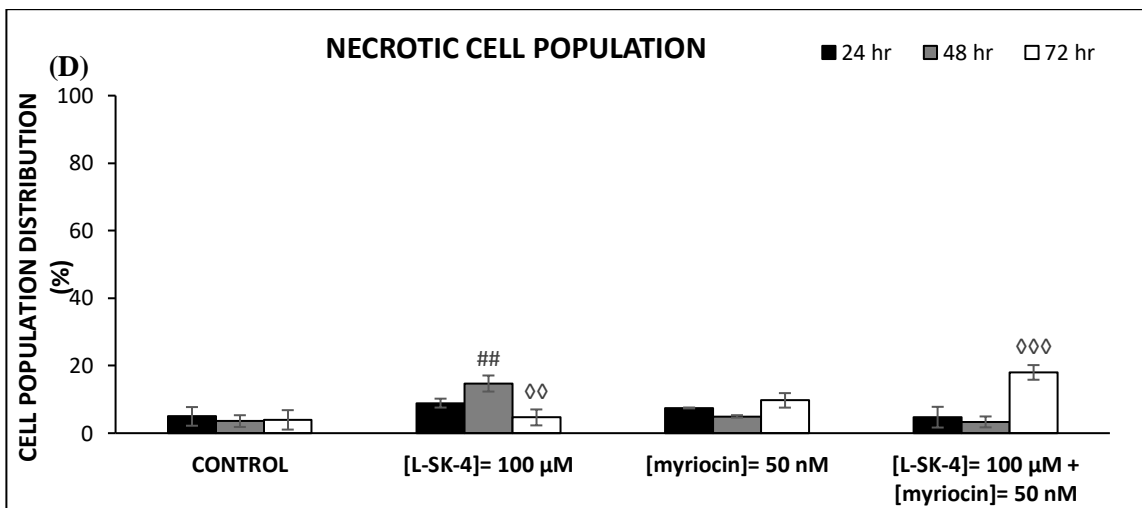
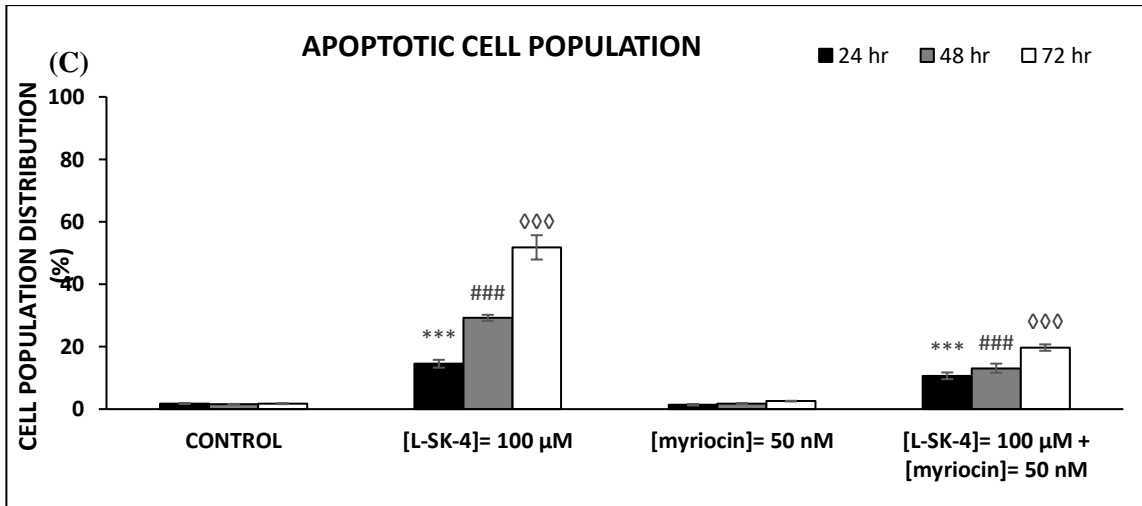
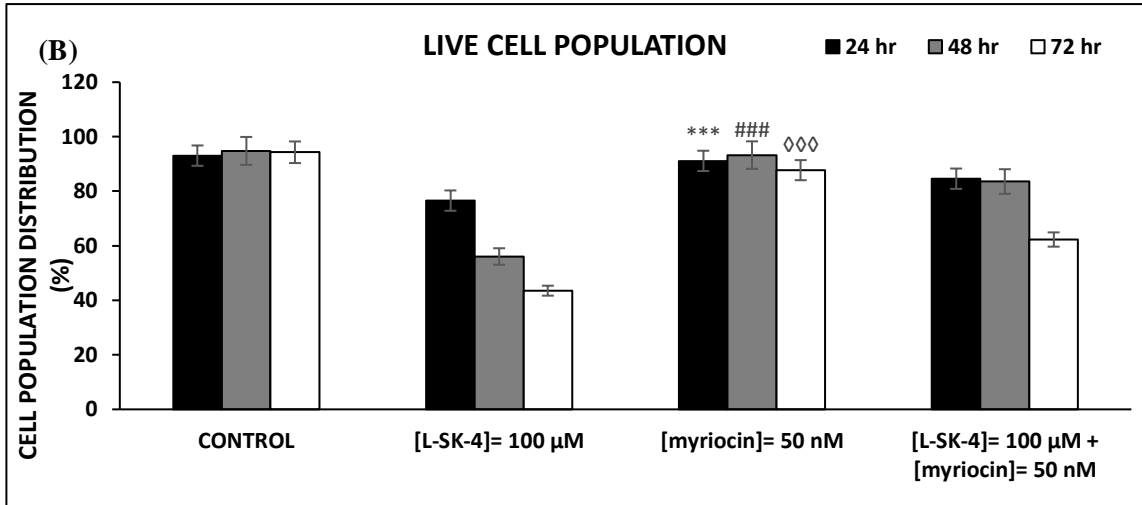


**Figure 89:** The ability of myriocin to prevent A375 cell from undergoing apoptosis after been treated with *L*-SK-4. Briefly, A375 cells were treated with 100  $\mu$ M of *L*-SK-4 in the presence or the absence of 50 nM of myriocin for 24, 48 and 72 hr and the distinguish between the live, apoptotic and necrotic cells has been done by means of (A) flow cytometry and then (B) live (C) apoptotic and (D) necrotic cells were quantified as percentages. Data shown are means of  $\pm$  SD of 3 replicates from 3 independent experiments.

The same pattern as described above was observed once again since the number of live cells in the cell population been treated with 100  $\mu$ M of *L*-SK-4 dropped significantly over the whole time course whereas the respective population of the cell being co-treated with *L*-SK-4 and myriocin sustained at almost the same levels as control for 24 and 48 hr (**Figure 89B**). After 72 hr of co-treatment a significantly drop of the viable levels has been noticed, which is not as intense as in the case of the treatment with *L*-SK-4 (**Figure 89B**). Similar pattern seems to be followed by apoptotic cells, since the significant elevation that has been noticed at 24 hr and intensified over 72 hr, abolished after the co-treatment with myriocin (**Figure 89C**), whereas not any significant alterations have been noticed on necrotic population (**Figure 89D**).

### 7.6.2 Ceramide triggers the direct activation of the extrinsic apoptosis

The capacity of ceramide to activate the extrinsic apoptosis by inducing FasL activation is well documented in the literature.<sup>641-645</sup> Therefore we examined how the elevated levels of ceramide can influence the expression level of Fas as well as this of Fas-Associated Death Domain (FADD) and how these levels can then correlated with the activation of extrinsic apoptosis by means of expression of full and/or cleaved length caspase-8 and BID in A375 cells been treated with *L*-SK-4 either in the presence or the absence of myriocin (**Figure 90**).

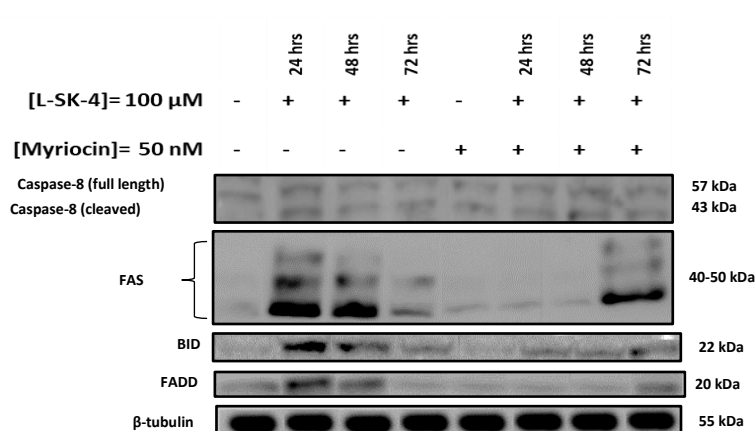


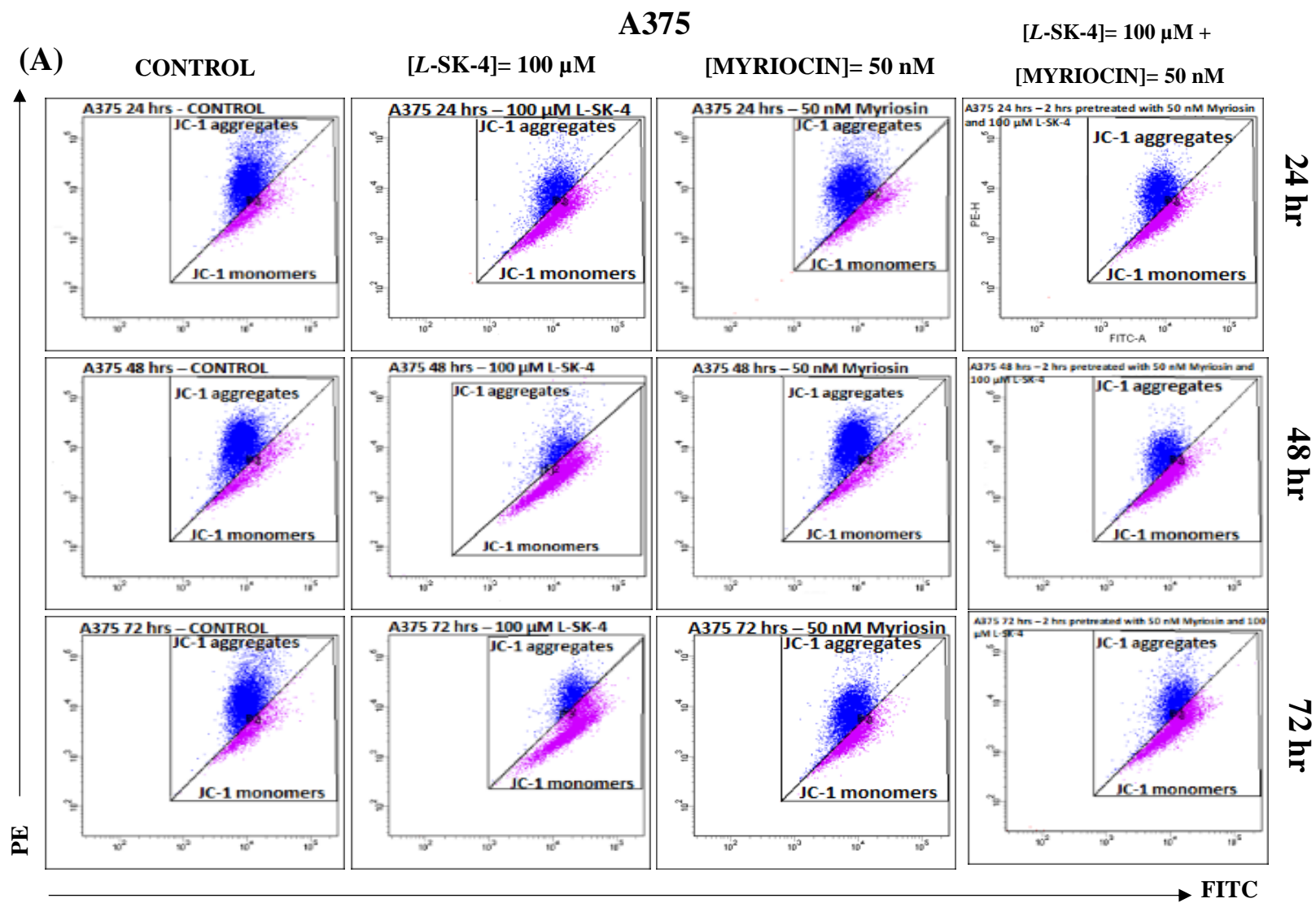
**Figure 90:** The ability of myriocin to prevent the activation of intrinsic apoptotic markers that have been elevated by the treatment of *L-SK-4* in A375 cells. Cell were subjected to 100  $\mu$ M of *L-SK-4* in the presence of absence 50 nM of myriocin for 24, 48 and 72 hr and protein expression levels of full length and cleaved caspases-8 were recorded in addition to those of BID, FADD and FAS.

According to the results exported it is indicated that the expression levels of Fas and FADD induced the activation of caspase-8 in the treated with *L-SK-4* population. In contrast, the expression levels of those proteins are dropped when the inhibitor of ceramide is added illustrating that the activation of the extrinsic apoptosis is driven and modulated by the levels of ceramide. Furthermore, the expression levels of BID were shown to be elevated during the 24 and 48 hr in the group that has been treated with *L-SK-4* whereas in the respective group where myriocin was added, the expression levels sustained to the same levels as control.

### 7.6.3 Ceramide elevation triggers the indirect activation of intrinsic apoptosis.

Finally, we analyzed whether the elevation of ceramide can trigger the activation of intrinsic apoptosis by examination of mitochondrial membrane depolarization ( $\Delta\Psi_m$ ) (as a marker of

mitochondrial dysfunction) in flow cytometry by utilizing the JC-1 stain (**Figure 91A**) and  $\Delta\Psi_m$  was calculated as the ratio of JC-1 aggregates over the JC-1 monomers. (**Figure 91B**).<sup>646-651</sup>



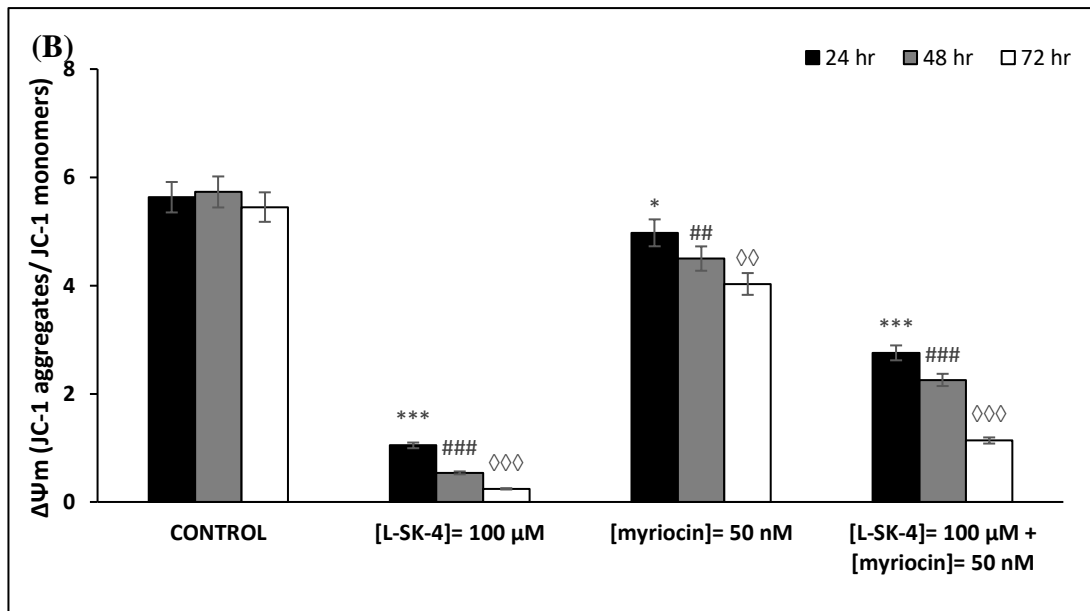


**Figure 91:** Myriocin prevents the mitochondria membrane depolarization by inhibiting the overproduction of ceramide been induced by *L*-SK-4. A375 cells were exposed to 100 μM *L*-SK-4 in the presence or the absence of 50 nM of myriocin for 24, 48 and 72 hr and the number of JC-1 monomers and aggregates by means of (A) flow cytometry and also quantified as (B) the ratio of JC-1 aggregates over JC-1 monomers. Data shown are means of ± SD of 3 replicates from 3 independent experiments.

According to the results, it is suggested that the treatment with 100 μM of *L*-SK-4 can induce a dramatic depolarization of mitochondria even after 24 hr of treatment with the effect been intensifies over 48 and 72 hr (**Figure 91B**). Interestingly, co-treatment with *L*-SK-4 and myriocin managed to show much lower membrane depolarization; however, the depolarized levels were significantly higher compared to the respective control (**Figure 91**). Those results demonstrate that the depolarization of mitochondrial membrane is regulated by the levels of ceramide been released by stimulation of ROS.

In order to validate our findings, we examined the levels of proteins that are associated with the formation of apoptosome by means of Apaf-1 as well as these of full and/ or cleaved length

Caspase-9 as markers of intrinsic apoptosis (**Figure 92**).

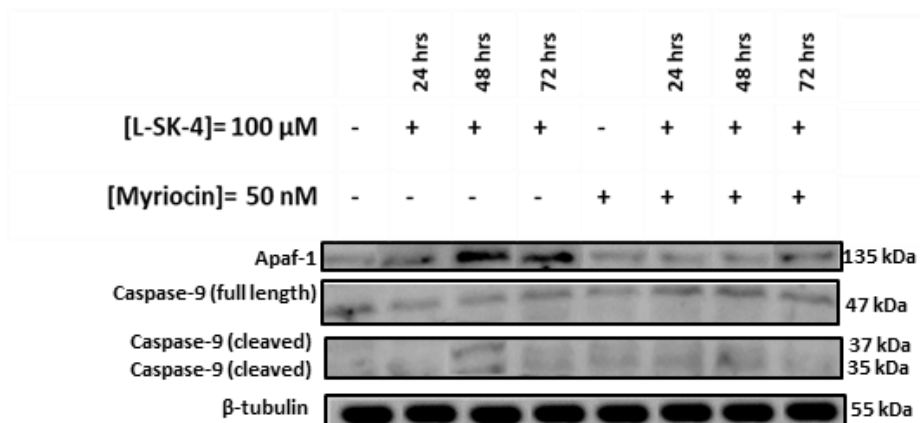


**Figure 92:** The ability of myriocin to prevent the activation of extrinsic apoptotic markers that have been elevated by the treatment of *L-SK-4* in A375 cells. Cell were subjected to 100  $\mu$ M of *L-SK-4* in the presence of absence 50 nM of myriocin for 24, 48 and 72 hr and protein expression levels of full length and cleaved caspases-9 were recorded in addition to this of Apaf-1.

The results suggest that elevation of the expression levels of Apaf-1 and the activation of caspase-9 in the treated with *L-SK-4* population were following the same pattern as before, whereas the addition of ceramide biosynthesis inhibitor caused a significantly dropped into the expression of the respective proteins. In addition to this, we examined the expression levels of the pro-apoptotic factors - regulators; BAX and BAK as markers of mitochondria degradation (**Figure 93**).<sup>652-658</sup>

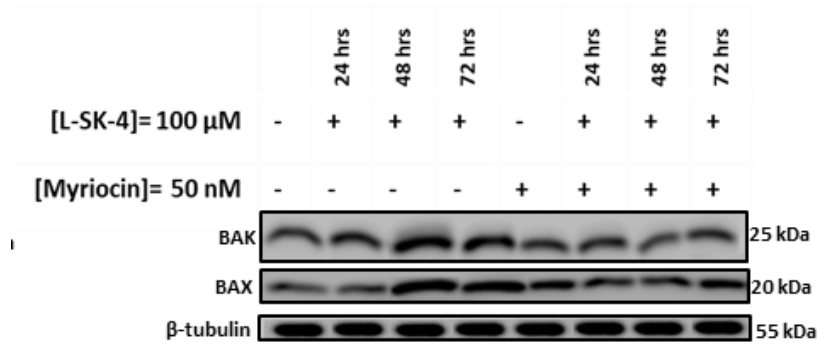


**Figure 93:** Effect of myriocin to the decrease of the pro-apoptotic markers that were elevated by the treatment of *L-SK-4* in A375 cells. Cells, were subjected to 100  $\mu$ M of *L-SK-4* in the presence of absence 50 nM of myriocin for 24, 48 and 72 hr and the protein expression levels of BAK and BAX were recorded.

The results revealed that there was an activation of those proteins at 48 and 72 hr in the cell population been treated with *L-SK-4*, with these findings been in agreement with the activation of intrinsic apoptosis. In contrast, the expression levels of BAK and BAX to the cells which were exposed to *L-SK-4* and myriocin remained steady to the same levels as the respective control, implying in that way that ceramide is needed for the activation of the pro-apoptotic proteins and consequently the activation of the downstream intrinsic apoptotic cascade.

This is mainly because ceramide as bioactive lipid plays the role of a secondary messenger that modulated (directly) the activation of extrinsic apoptotic pathway and also (indirectly) the activation of intrinsic apoptotic pathway.<sup>659-663</sup> Therefore, in this model we were able to see that *L-SK-4* has the ability to induce enough ROS just after 24 hr that allowed the stimulation of lipid biosynthesis (sphingolipids) and consequently, the elevation of ceramide. However, 48 and 72 post treatment the ROS level were still at the same levels as those of 24 hr. The excessive exposure of the cells to ROS led eventually to lipid peroxidation, protein carbonylation and DNA oxidative damage after 48 hr with the effect retained or intensified after 72 hr of the treatment, something that is confirmed by the findings above (**Figure 76**).

## **8 Results and Discussion – Evaluation of the neuroprotective capacity of the SK-n compounds in an in vitro model of Parkinson’s disease (PD)**

The neuroprotective capacity of a series of hydroxypyridinones including 1, 2-HOPO (*rac*-SK-3), 3, 2-HOPO (*rac*-SK-5), 3, 4-HOPO (*rac*-SK-2 and *L*-SK-4) as well as a hydroxypyranone (*rac*-SK-1), was evaluated in an *in vitro* model of PD consisting of Lund Human Mesecephalic (LUHMES) cells that have been differentiated to mature post-mitotic cells with biochemical morphological and functional features of dopaminergic neurons. For the induction of parkinsonian phenotype, LUHMES cells were exposed in a range of neurotoxins including; 6-hydroxydopamine (6-OHDA), 1-methyl-4-phenylpyridinium (MPP<sup>+</sup>) and erastin. Our collaborators; Dr Simon Gutbier, Dr Stefan Schildknecht and Prof Marcel Leist at the Konstanz University, Germany have kindly generated the results obtained.

### **8.1 Neuroprotection against 6-OHDA**

#### **8.1.1 Cytotoxicity of the SK-n compounds**

LUHMES cells, have been treated with a range of concentration (12.5-500  $\mu$ M) of the SK-n compounds 1 hr prior to exposure to 6-OHDA (50  $\mu$ M). Then, cells were incubated for further 24 hr before taking further measurements. The neuroprotective or neurotoxic ability of the SK-n compounds assessed using two metabolic assays: **(A)** reasazurin reduction and **(B)** Lactate Dehydrogenase (LDH) release (**Figure 94**).

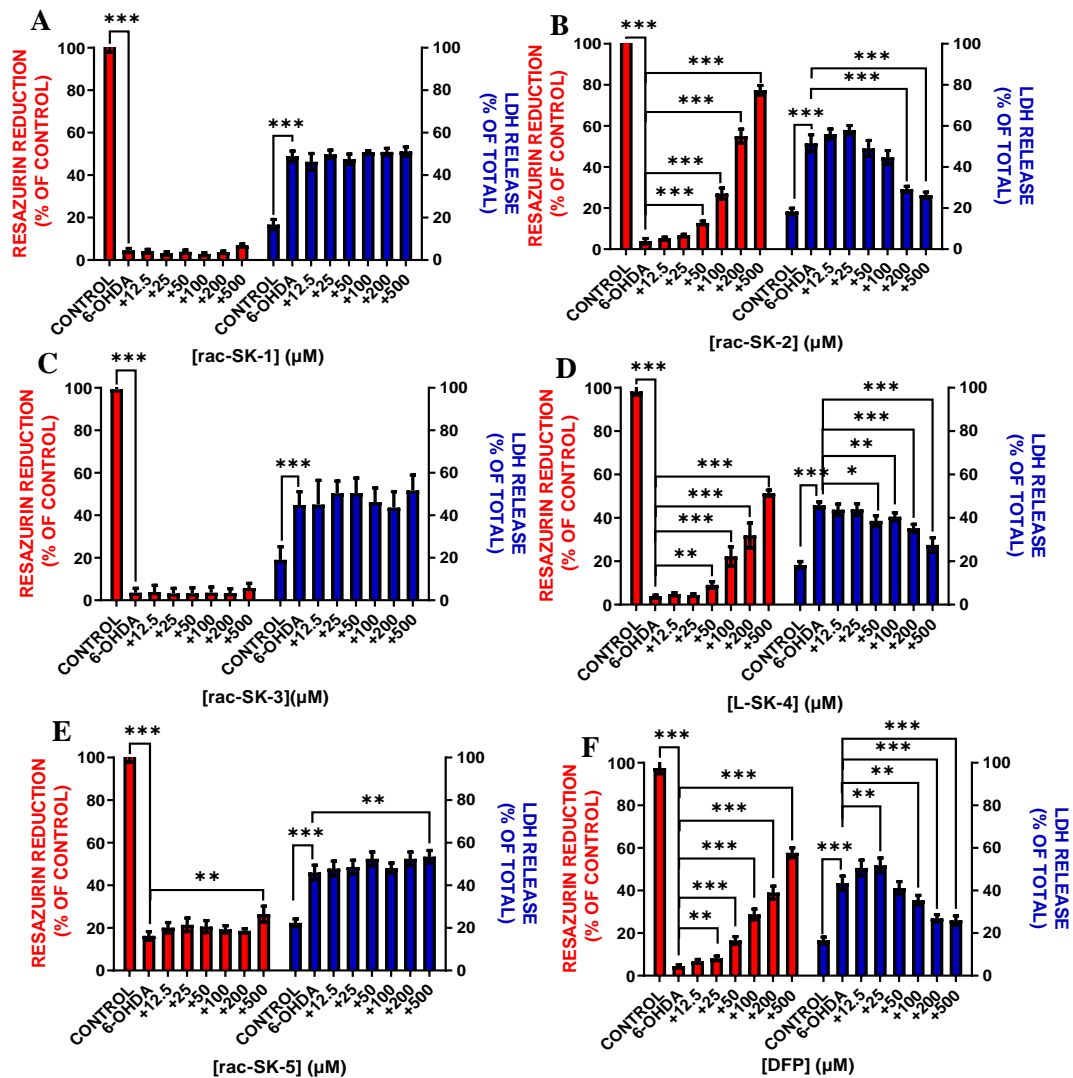


**Figure 94:** The ability neuroprotective capacity of hydroxypyridones against 6-OHDA induced parkinsonian phenotype. LUHMES cells have been exposed to a range of 12.5-500 μM concentrations of the SK-n compounds prior to the addition of 6-OHDA (50 μM). Red bars represent the viability assays performed by means of resazurin reduction whereas the blue bars show the outcome of LDH release assay. Data shown are means ± SD of at least 3 replicates from 3 independent experiments.

Primarily, the results revealed that treatment with 6-OHDA led to a significant cell death as the viability levels (by means of resazurin reduction) were at almost zero, whereas the LDH that has been released decreased by almost 50% (**Figure 94A**). In contrast, none of the SK-n

compounds induced further cytotoxicity as the levels of viabilities as well as those of LDH been released did not go below the respective levels of 6-OHDA treated groups (**Figure 94A-E**). In addition to this, *rac*-SK-1, 3 and 5 did not show any cell rescue event at high concentrations when compared with their respective control (cells treated with 6-OHDA) (**Figure 94A, C and E**). This can be attributed to the fact that either these compounds cannot penetrate the neuronal cell wall (by means of LAT-1) or they cannot prevent the extensive ROS production been Induced by the by the toxin. On the other hand, two 3, 4-HOPOs; *rac*-SK-2 and *L*-SK-4 seems to induce a statistically significant cellular protection against the neurotoxin. Namely, *rac*-SK-2 protects the cells at a concentration of 50  $\mu$ M with the effect been intensified at higher concentrations as the viability levels reached almost 80% implying an approximately 75% cellular rescue (from the viability perspective) (**Figure 94B**). In addition to this, the levels of the extracellular LDH decreased by approximately 50% compared to the respective control, showing in that way the neuroprotective potency of the compound (**Figure 94B**). Interestingly, these finding suggest that the treatment with *rac*-SK-2 is even more potent compared to the positive control (DFP) (**Figure 94F**). Furthermore, *L*-SK-4 demonstrated a neuroprotective capacity, which has not the same magnitude as this of *rac*-SK-2. Namely, *L*-SK-4, shown neuroprotective potency at 100  $\mu$ M with the effect to be intensified, showing almost 50% increase in the viability levels (**Figure 94D**). Moreover, these observations are in agreement with the level of LDH measured extracellularly as a significant decrease in its concentration has been notice (**Figure 94D**). In this case, the neuroprotective potency of DFP and *L*-SK-4 is towards the same line, due to the almost identical effect that they present in the evaluation.

## 8.2 Neuronal protection

For the verification of the above findings, LUHMES cells were visualised under automated fluorescent microscope in the presence or the absence of 6-OHDA with or without the SK-n compounds or DFP. The neuronal density (by means of neurite area determination) was then measured using Calcein [channel 2 ( $475\pm 40/525\pm 15$  nm)] for the detection of viable cells and H-33342 dye [channel 1 ( $365\pm 50/461\pm 15$  nm)] for the execution of non-viable cells. All calcein positive pixels outside of these masks (somatic area) were counted as neurite area. (**Figure 95**)

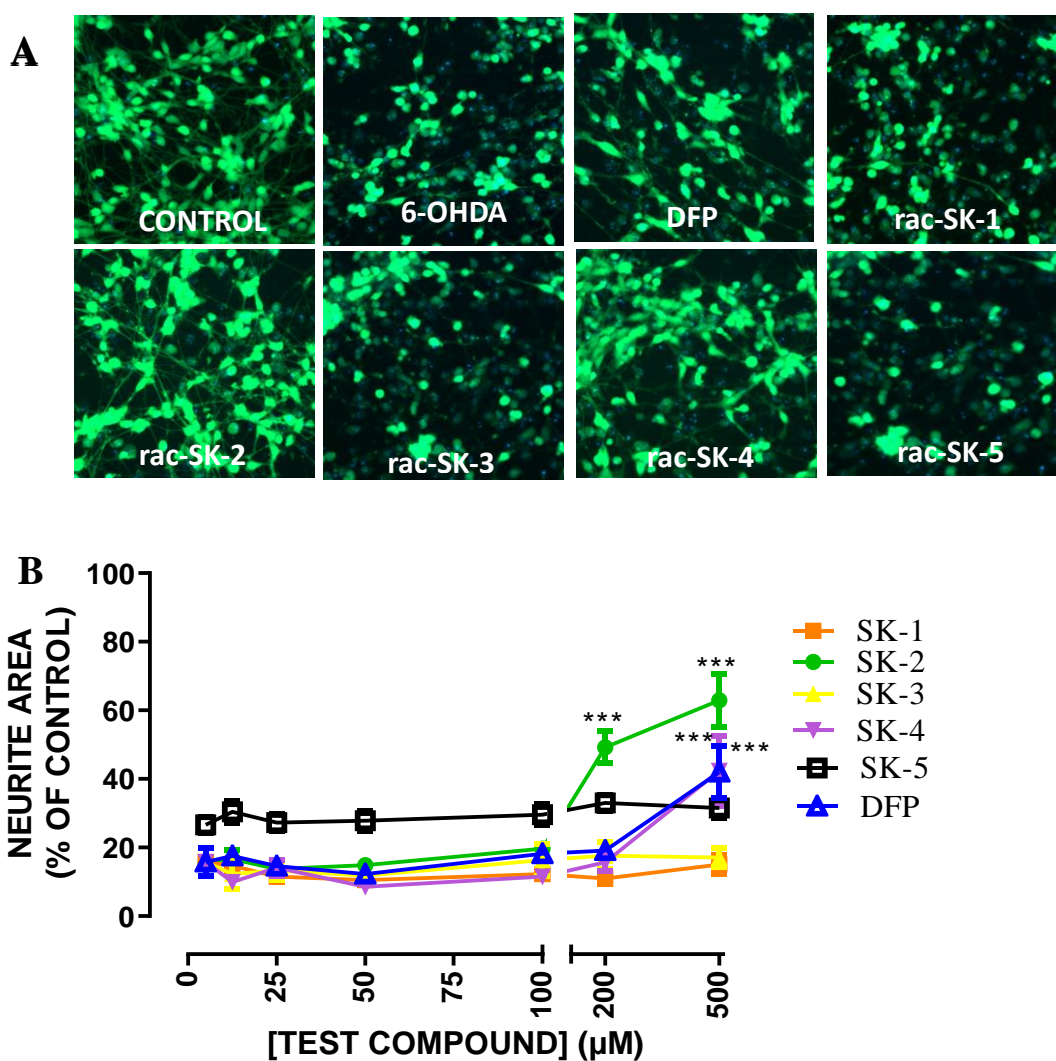


**Figure 95:** The ability of the SK-n compounds to protect from neuronal degradation phenotype been induced by 6-OHDA. LUHMES cells were exposed to a range of 12.5-500  $\mu\text{M}$  concentrations of each compound prior to the addition of 6-OHDA (50  $\mu\text{M}$ ). **(A)** LUHMES cells were labelled with Calcein-AM (1  $\mu\text{M}$ ) and H-33342 (1  $\mu\text{g}/\text{mL}$ ). Images were collected using automated microscope. **(B)** An algorithm quantified all calcein positive cells as viable and only H-33342 positive nuclei as “not viable” cells. All calcein positive pixels outside of these masks (somatic area) were counted as neurite area.

The exported data confirmed the loss of the neuronal cells upon exposure with 6-OHDA. That was indicated by the existence of the blue stained nucleus (indicative of non-viable LUHMES cells) predominate the viable cells been stained with Calcein (**Figure 95A**). In addition to this, the inability of *rac*-SK-1, 3 and 5 to protect neuronal cells from the toxin, can also be visualised since the H-33342 positively stained nucleus are the most prevalent cellular components (**Figure 95A**). Moreover, the neurite area of the exposed to *rac*-SK-1 and 3 groups retained at the same significantly low levels (compared to positive control) even after high concentration treatment (**Figure 95A and B**). On the other hand, a reverse phenotype seems to be illustrated in the cases where cells have been exposed to *rac*-SK2 and *L*-SK-4 confirming the above findings. More specifically, pre-incubation with *rac*-SK-2 protects from neuronal degradation been induced by 6-OHDA as the existence of the Calcein stained somatic components of the neurons seems to be retained (compared to the both positive and negative control) (**Figure 95A**). Furthermore, the neurite area of the *rac*-SK-2 treated cells group was increased significantly at a concentration as high as 500  $\mu\text{M}$  (**Figure 95B**). At this particular concentration, the neurite area was even larger compare to the positive control. Once again, the phenotype of cells been exposed to DFP was almost the same with the respective one of the cells been treated with *L*-SK-4, something which can be attributed to the structural similarity of the two compounds (**Figure 95A**). This is also be confirmed by the densitometric analysis as both *L*-SK-4 and positive control follow the same trend (**Figure 95B**).

Our findings suggested that the observed order of activity (*L*-SK-4 ~ *rac*-SK-2 >> *rac*-SK-5 > *rac*-SK-3 > *rac*-SK-1) match the order expected from their metal binding activity.<sup>442,452,570,664,665</sup> Namely, the higher the  $\log\beta_3[\text{Fe}^{3+}]$  the least free iron and consequently better neuroprotective capacity. Additionally, our data are in agreement with the current literature findings as it has been demonstrated before that 3, 4-HOPOs shown as exceptional ability of neuroprotection against the cytotoxic effect of 6-OHDA, mainly by chelating the elevated by the toxin levels of iron.<sup>439,666</sup> On the other hand, Workman DG and co-workers suggested that 1, 2-HOPOs can also exert neuroprotective potency against 6-OHDA.<sup>311</sup> Interestingly, the order of compounds activity differs from the one shown against cancer (7.1.1). Namely, it appears that the chelators presented different sensitivity and potency. This can be attributed to the fact, that either the compounds exploited other transport mechanism (apart of LAT-1) that is located in the neuronal cells, or because the concentration of redox active metals was in different proportions across the model of the two diseases.

### **8.3 Neuroprotection against MPP<sup>+</sup>**

#### **8.3.1 Cytotoxicity of the SK-n compounds**

The next part involved the induction of parkinsonian phenotype on LUHMES cells by utilizing a different toxin such as MPP<sup>+</sup>, the active metabolite of 1-methyl-4-phenyl-1,2,3,6-tetrahydropyridine (MPTP) that induces dopaminergic neuronal toxicity by inhibiting mitochondrial complex I activity.<sup>250,667</sup> Therefore, LUHMES cells have been treated with a range of concentration (12.5-500  $\mu\text{M}$ ) of the SK-n compounds 1 hr prior to exposure to MPP<sup>+</sup> (5  $\mu\text{M}$ ). Then, cells were incubated for further 72 hr before taking further measurements (Figure 96).

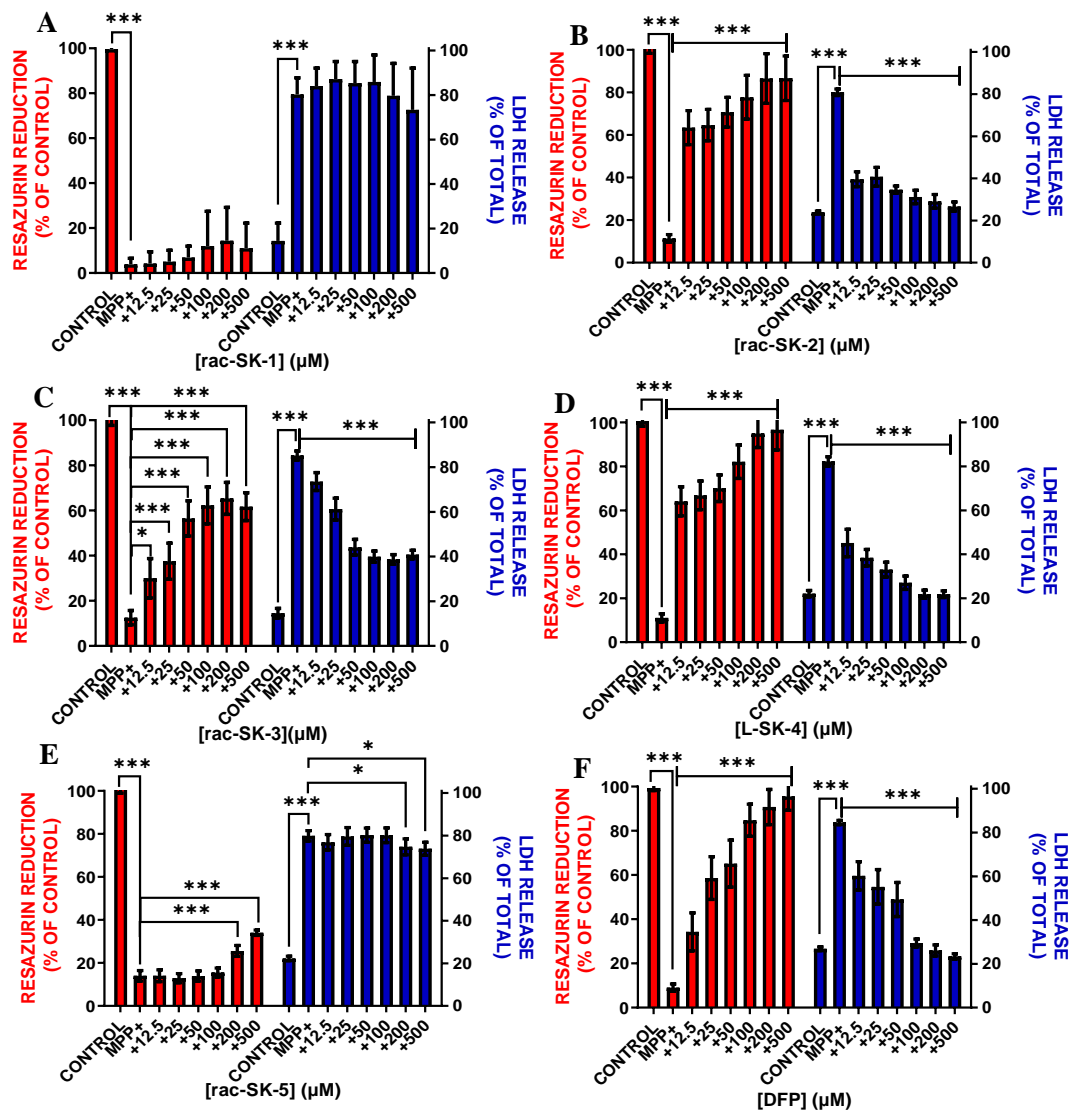


**Figure 96:** The ability neuroprotective capacity of hydroxypyridones against MPP<sup>+</sup> induced parkinsonian phenotype. LUHMES cells have been exposed to a range of 12.5-500 μM concentrations of the SK-n compounds prior to the addition of MPP<sup>+</sup> (5 μM) . Red bars represent the viability assays performed by means of resazurin reduction whereas the blue bars show the outcome of LDH release assay. Data shown are means ± SD of at least 3 replicates from 3 independent experiments.

The results suggested that the treatment with MPP<sup>+</sup> induced a statistically significant of toxicity since the viability levels of the exposed to the toxin cells, were decreases dramatically

(**Figure 96A-E**). In addition to this, the LDH that is been released due to the cytotoxicity of the compound reached almost the 80% of the total (**Figure 96A-E**). Moreover, as it can be observed from **Figure 96**, none of the screened molecules induced any further cytotoxicity since comparison of the viability and the LDH release levels of treated with MPP<sup>+</sup> and those that have been treated with MPP<sup>+</sup> did not revealed any statistically significant alterations. Furthermore, according to (**Figure 96A**), *rac*-SK-1, does not have any capacity of rescuing cells as the viability levels remained steady even after treatment with high concentrations. Similar behaviour can be illustrated by the LDH release profile, since there is not any reduction in the levels of the released LDH (**Figure 96A**). Interestingly, a significant cell rescue was noticed in the cell population that have been co-treated with *rac*-SK-2, 3 as well as *L*-SK-4. Namely, *rac*-SK-2 managed to increase the viability levels by approximately, 45% even at the lowest concentration (12.5  $\mu$ M) and prevented the release of LDH by approximately 40% (**Figure 96B**). This phenomenon was intensified in a dose-depended manner since at the maximal concentration the viability levels reached 80% and only a 20% of LDH has released (same as control – untreated cells) (**Figure 96B**). In the case of *rac*-SK-3, a similar dose-depended cell rescuing is also been observed. However, the effect was not as intense as the positive control (**Figure 96C and F**). This observation would suggest that *rac*-SK-3 can penetrate the cell. Hence lack of activity against 6-OHDA is more likely explained by *rac*-SK-3 been able to rich mitochondria and act on them (as the lesion of MPP<sup>+</sup> is strongly associated with mitochondria). Furthermore, co-treatment with *L*-SK-4 shown almost a dramatic cellular rescue even at 12.5  $\mu$ M (**Figure 96D**). The increase of the viability levels in combination with the reduced LDH been released at this concentration were significantly elevated compared with the respective levels of the positive control (**Figure 96D and F**). Interestingly, at high concentration an almost complete recovery has been notice (**Figure 96D**). These results also revealed that *rac*-SK-5 could demonstrated some minor potency at concentration as high as 500  $\mu$ M (**Figure 96E**)

The ability of the SK-n compounds to act as neuroprotective agents was also evaluated under fluorescent microscope. LUHMES cells were treated with MPP<sup>+</sup> in the presence of absence of SK-n compounds and DFP and imaging was occurred as mentioned in the previous section (8.2) (Figure 97).

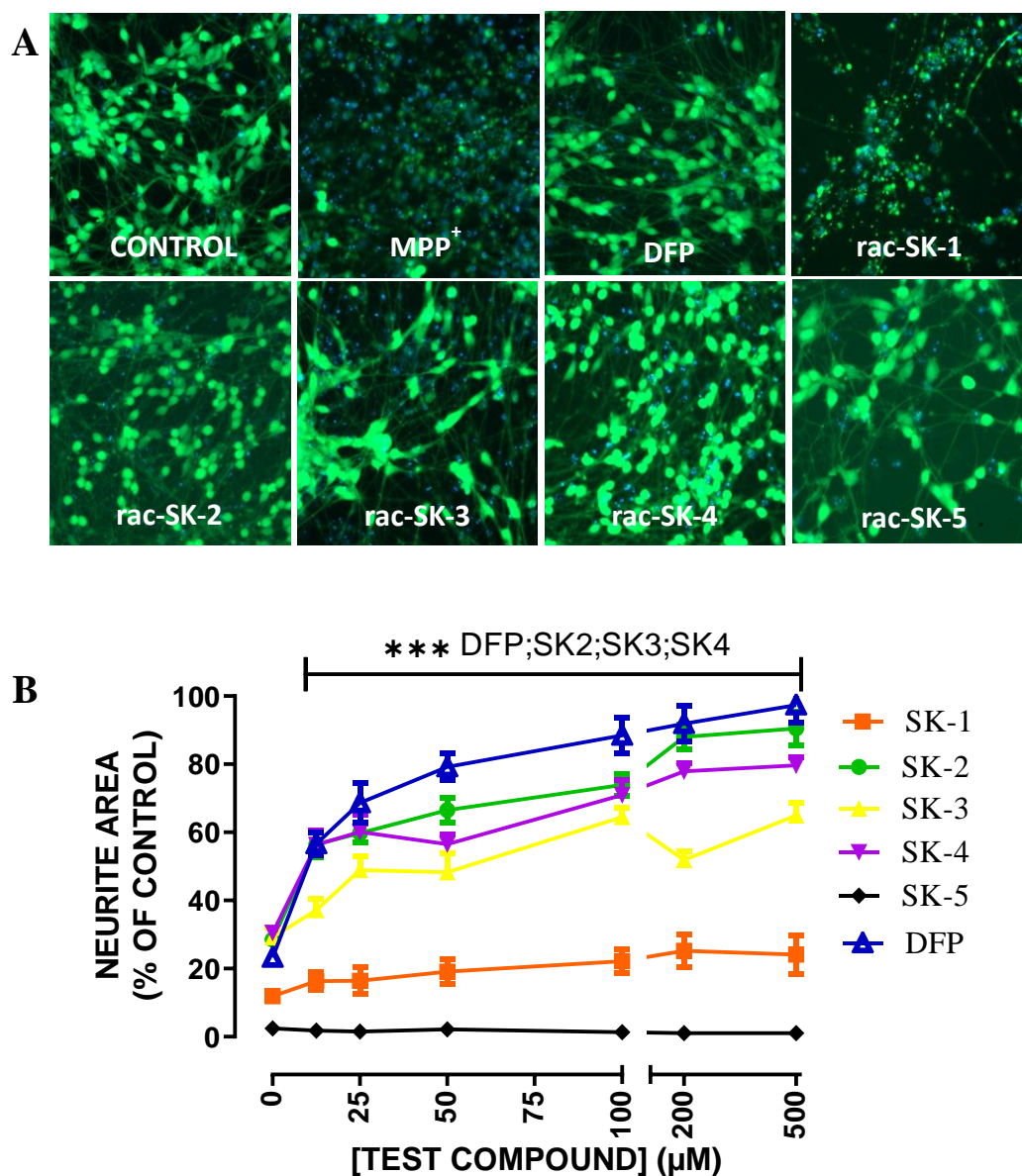


**Figure 97:** The ability of the SK-n compounds to protect from neuronal degradation phenotype been induced by MPP<sup>+</sup>. LUHMES cells were exposed to a range of 12.5-500 µM concentrations of each compound prior to the addition of MPP<sup>+</sup> (5 µM). (A) LUHMES cells were labelled with Calcein-AM (1 µM) and H-33342 (1 µg/mL). Images were collected using

automated microscope. **(B)** An algorithm quantified all calcein positive cells as viable and only H-33342 positive nuclei as “not viable” cells. All calcein positive pixels outside of these masks (somatic area) were counted as neurite area.

The results indicated that *rac*-SK-1 and 5 were the least active compounds (**Figure 97**). This is because the H33342 positively stained nucleus were dominating over Calcein stained features. In addition to this, the densitometric analysis does not show any significant elevation on the neurite area. In the case where cells were treated with both MPP<sup>+</sup> and *rac*-SK-2 or *L*-SK-4, a reverse phenotype was noticed (**Figure 97A**). Namely, the treatment with the compounds had the ability to protect the dopaminergic neuronal precursor cells from the cell death induced by toxin. In addition to this, a statistically significant increase ( $p < 0.001$ ) in the neurite area, has been noticed in a concentration as low as 25  $\mu$ M (**Figure 97B**). These observations seem to follow the same trend as the positive control (DFP) (**Figure 97B**). In addition to this, treatment with *rac*-SK-3 seems to induce statistically significant neuronal rescue at 25  $\mu$ M, however the cellular recovery was not as intense as it was in the case of *rac*-SK-2, *L*-SK-4 and DFP (**Figure 97B**).

The ability of DFP (as a 3, 4-HOPO) to rescue from the lesion induced by the treatment with MPP<sup>+</sup> has been documented before.<sup>309,668,669</sup> Interestingly, in this case it can be observed that HOPOs do not follow the same trend of activity as shown before for 6-OHDA. Namely, it is shown here that 3, 4-HOPOs > 1, 2-HOPO >> 3, 2-HOPO ~ hydroxypyranone. This suggests that the activity is guided by a more complex combination of molecular properties. To the very best of our knowledge, there is not any documented statements that proves that activity of 1, 2- and 3, 2-HOPO against MPP<sup>+</sup> induced toxicity, only using 6-OHDA.

#### **8.4 In vitro model of ferroptosis.**

In this section an *in vitro* model of ferroptosis as an alternative parkinsonian induced phenotype, was generated by the exposure of LUHMES cells to erastin, which is an eradicator of RAS and small t antigen (ST) expressing cells.<sup>670–672</sup> Similar to other conditions, the SK-n

compounds were pre-applied to the cells in a range of concentrations (12.5-500  $\mu\text{M}$ ) 1 hr prior to the addition erastin (1.25  $\mu\text{M}$ ) and cells were incubated for 24 hr before taking any measurements. As described above, the cytotoxic ability of the SK-n compounds has been assessed via resazurin reduction and LDH release assay (**Figure 98**).

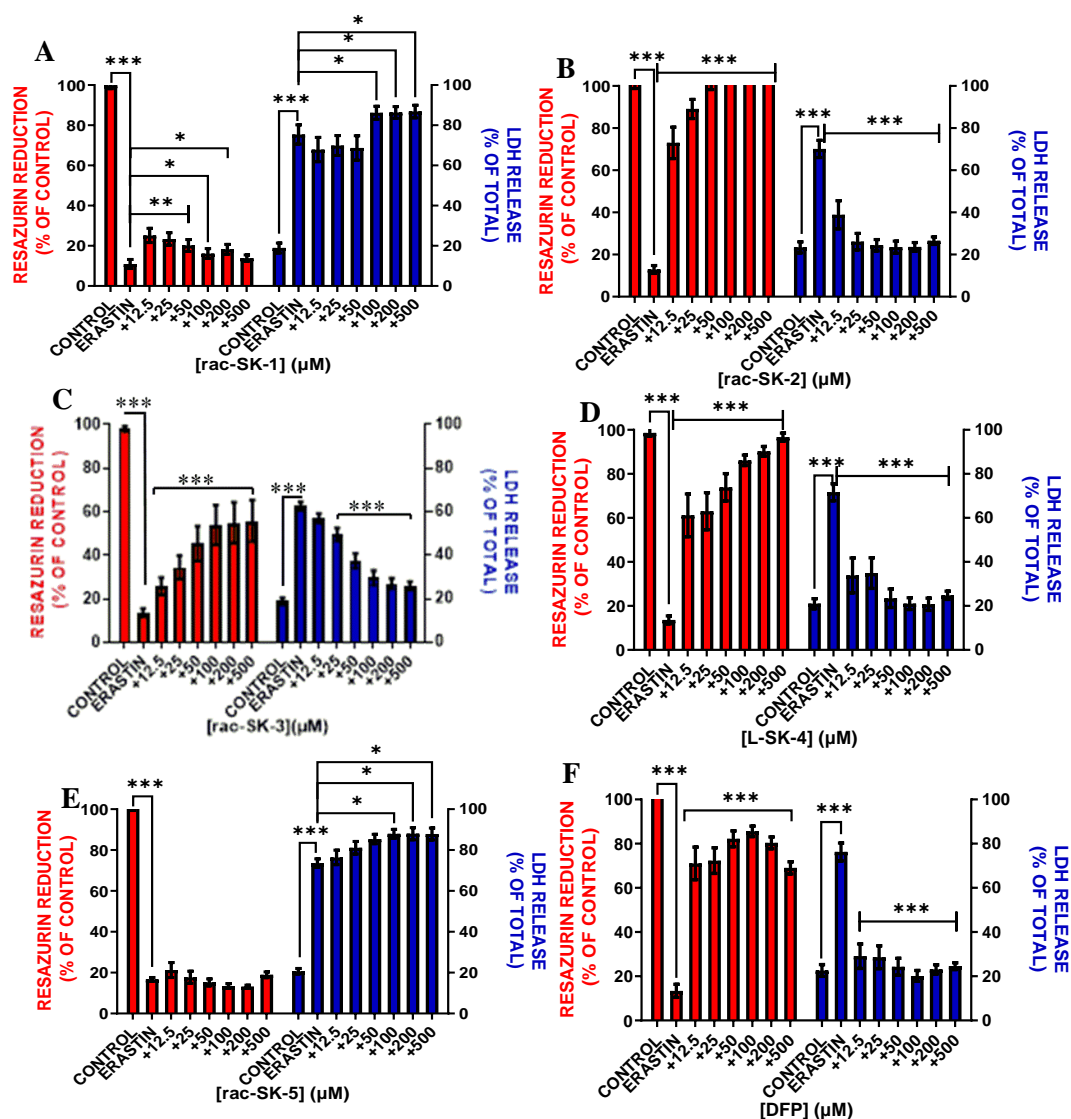


**Figure 98:** The neuroprotective capacity of the SK-n compounds against erastin induced ferroptosis. LUHMES cells were exposed to a range of 12.5-500  $\mu\text{M}$  concentrations of the SK-n compounds prior to the addition of erastin (1.25  $\mu\text{M}$ ). Red bars represent viability assays performed by means of resazurin reduction whereas the blue bars show the outcome of LDH

release assay. Data shown are means  $\pm$  SD of at least 3 replicates from 3 independent experiments.

The results revealed the treatment of LUHMES cells with erastin caused a statistical significant reduction of the % of viable cells. The induction of erastin's toxicity was also demonstrated by the statistically significant elevation of LDH levels extracellularly (**Figure 98**). Interestingly, when cells were exposed to *rac*-SK-1 (12.5-50 $\mu$ M) a statistically significant ( $p < 0.001$ ) elevation of the viable cells (indicating cellular protection) has been noticed, whereas at higher concentration  $\leq 50 \leq 500 \mu$ M the effect seems to be abolished (**Figure 98A**). The similar pattern seems to be reflected into the LDH release profile. The treatment with the *rac*-SK-1 compound could not manage to induce any statistically significant decrease of the previously elevated levels of extracellular LDH (**Figure 98A**). In contrast, the treatment in the range of 100-500  $\mu$ M cause a statistical elevation ( $p < 0.05$ ) of LDH implying in that way that the compound acquires a cytotoxic rather than neuroprotective profile (**Figure 98A**). The ability of *rac*-SK-2 to act an excellent neuroprotective potency against erastin induced parkinsonian phenotype is demonstrated in (**Figure 98B**). The results show a sharp elevation with statistical significance ( $p < 0.001$ ) of viability levels in the cell groups exposed to the *rac*-SK-2 even at the lowest concentration (12.5  $\mu$ M) (**Figure 98B**). The same pattern is also reflected into the LDH release profile. Treatment with *rac*-SK-2 managed to decrease dramatically the elevated by erastin levels of LDH; bringing the LDH levels to the same magnitude as to the untreated control (**Figure 98B**). Interestingly, it seems that *rac*-SK-2 was even more potent when compared to the positive control (DFP) (**Figure 98B** and **F**). Additionally, a neuroprotective potency seems to be illustrated by the treatment with *rac*-SK-3 (**Figure 98C**). Despite, the statistically significant elevation of the viable levels and the drop of the extracellularly LDH, the magnitude of protection was not as effective as it was in the case of the *rac*-SK-2. In the case of *L*-SK-4, the same pattern as *rac*-SK-2 seems to be repeated in almost the same magnitude (**Figure 98D**). Eventually, the neuroprotective inability of *rac*-

SK-5 has been assessed with the results showing the disability of the compound to protect cells. Interestingly, at the concentration range (100-500  $\mu$ M) the compound excretes a cytotoxic character as a statistically significant elevation ( $p < 0.05$ ) of the LDH levels has been noticed (**Figure 98F**).

The neuroprotective properties of the SK-n against erastin's toxicity has been visualised under fluorescent microscope and the neurite area has been measured as described before (**Figure 99**). The results suggested that neither *rac*-SK-1 nor *rac*-SK-5 have any neuroprotective capacity since the H33346 stained nucleus (non-viable cells) are the main observable features. This observation is also confirmed by neurite area determination, as the densitometry results did not show any increased in the neurite area. Additionally, the potency of *rac*-SK-2, 3 and *L*-SK-4 is also validated by the Calcein-AM stained cells, which seems to be the most prevalent features. Furthermore, densitometry, validated those findings as there was a statistically significant elevation of the neurite are of the cell groups been exposed to *rac*-SK-2, 3 and *L*-SK-4 respectively. The increase in the neurite is been noticed mainly at 25  $\mu$ M and becomes plateau even at the higher concentrations (**Figure 99**).

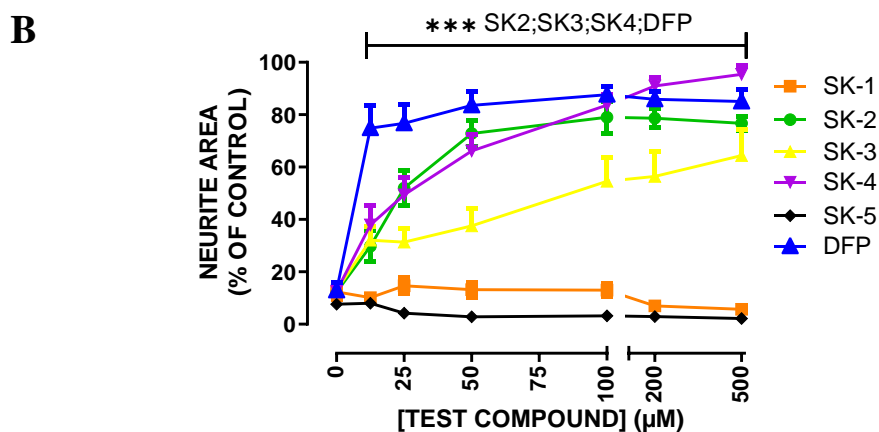
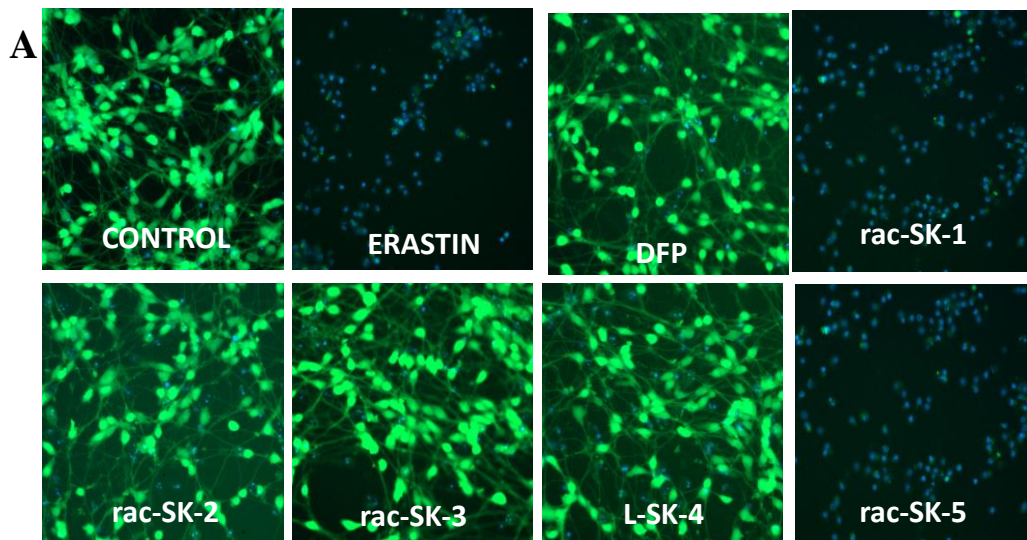


**Figure 99:** The ability of the SK-n compounds to protect from ferroptosis been induced by erastin. LUHMES cells have been exposed to a range of 12.5-500 µM concentrations of each compound prior to the addition of erastin (1.25 µM). (A) LUHMES cells were labelled with Calcein-AM (1 µM) and H-33342 (1 µg/ mL). Images were collected using automated microscope. (B) An algorithm quantified all calcein positive cells as viable and only H-33342 positive nuclei as “not viable” cells. All calcein positive pixels outside of these masks (somatic area) were counted as neurite area.

The ability of *rac*-SK-2 and *L*-SK-4 to protect cells from the erastin induced ferroptosis was correlated (by means of cytotoxicological evaluation as well as neurite area determination) with the neuroprotective capacity of two ferroptosis inhibitors; Ferrostatin-1 (**Figure 100A**) and Liproxstatin-1 (**Figure 100B**) which have been introduced as alternative positive controls.

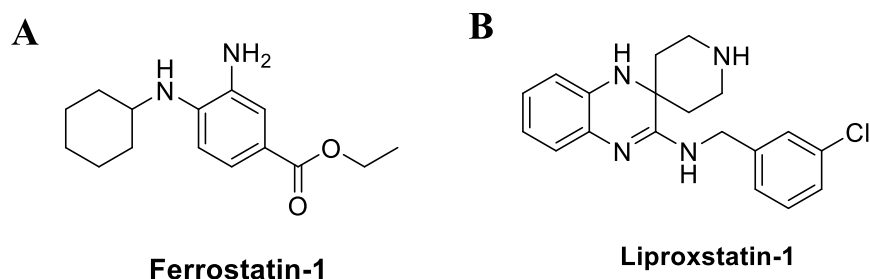


**Figure 100:** Structure of (A) Ferrostatin-1 and (B) Liproxstatin-1

Ferrostatin-1 has the ability to inhibit ferroptosis been induced by erastin by trapping peroxy radicals preventing in that way the autooxidation of lipids.<sup>257,673–675</sup> In addition to this, it has been proven that Ferrostatin-1 prevents the cell death been induced by *L*-glutamate in a rat organotypic hippocampal slice culture model.<sup>676</sup> On the other hand, Liproxstatin-1 can inhibits ferroptosis by preventing the suppression of glutathione peroxidase (Gpx4) by ferroptotic agents.<sup>674,677–679</sup> LUHMES cells have been treated with the ferroptosis inhibitors 1 hr prior to exposure to erastin in a range of concentrations (0.3-10  $\mu$ M) and were incubated for 24 hrs before taking any measurements. The results suggested that both compounds manage to protect from the neurotoxicity of erastin as there is a statistically significant elevation of the viable cells even at the lowest concentration (0.3-10  $\mu$ M) of the inhibitor (**Figure 101**).

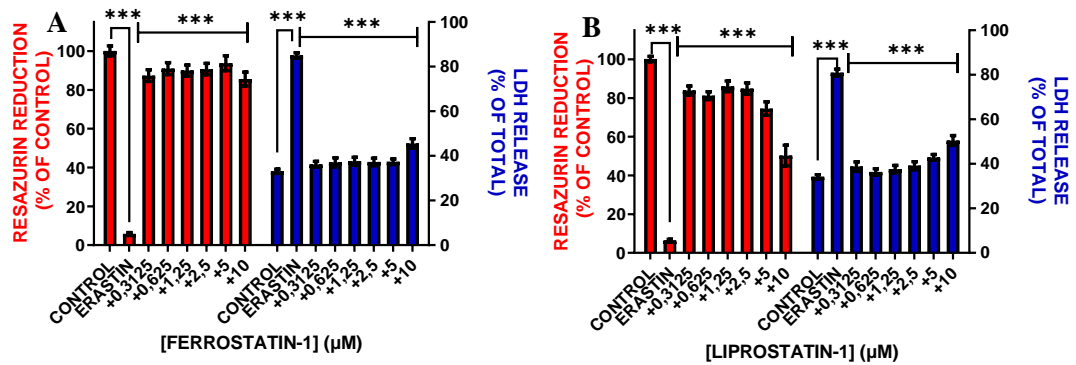


**Figure 101:** The ability of Ferrostatin-1 and Liproxstatin-1 to inhibit the erastin induced ferroptosis. LUHMES cells were exposed to a range of 0.3125-10  $\mu\text{M}$  concentrations of each inhibitor prior to the addition of erastin (1.25  $\mu\text{M}$ ). Red bars represent the viability assays performed by means of resazurin reduction whereas the blue bars show the outcome of LDH release assay. Data shown are means  $\pm$  SD of at least 3 replicates from 3 independent experiments.

More specifically, Ferrostatin-1 elevated the viable levels by approximately 70% and the effect seems to be retained in a non-dose dependent manner as the effect reached plateau for all the concentrations. In the addition to this, the treatment lowers, in a statistically significant manner, the elevated (by erastin) LDH levels, demonstrating in that way its neuroprotective capacity. Similar observations have been exported for Liproxstatin-1. However, in this case high concentrations of the inhibitor seems to lower the neuroprotective capacity as the levels of viable cells were considerably lower compared to the lowest concentrations. Moreover, this observation seems to be reflected to the percentage of the LDH been release extracellularly, as at high concentrations the respective percentage tends to be elevated.

In addition to this the neurite area of the cell groups been exposed to erastin has been measured in the presence or the absence of either Ferrostatin-1 or Liproxstatin-1 (**Figure 102**).

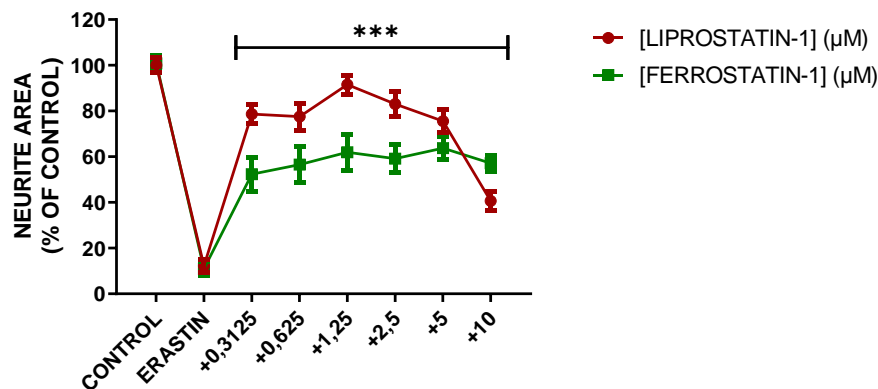


**Figure 102:** The ability of Ferrostatin-1 and Liproxstatin-1 to inhibit the erastin induced ferroptosis. LUHMES cells were exposed to a range of 0.3125-10  $\mu\text{M}$  concentrations of each inhibitor prior to the addition of erastin (1.25  $\mu\text{M}$ ). LUHMES cells were labelled with Calcein-AM (1  $\mu\text{M}$ ) and H-33342 (1  $\mu\text{g}/\text{mL}$ ). Images were collected using automated microscope. All calcein positive pixels outside of these masks (somatic area) were counted as neurite area.

According to the results, a statistically significant elevation of the neurite area was noticed in both cells groups that were with Ferrostatin-1 and Liproxstatin-1 confirming the above findings. In the case of Ferrostatin-1, increasing concentrations of the inhibitor doesn't seem to influence the neurite area whereas in the case of Liproxstatin-1 at concentrations higher than 1.25  $\mu\text{M}$  a decrease in the neurite area is noticed. These results suggest, that the active compounds; *rac*-SK-2 and *L*-SK-4 can act as inhibitors of ferroptosis as both compounds shown the same phenotype as the Ferrostatin-1 and Liproxstatin-1. However, the mode of inhibition seems to be different.

### 8.5 *In vitro* validation of Structure Activity Relationship (SAR)

In order to examine the SAR of *L*-SK-4, two control compounds have been designed and synthesised; SK-4C1, which has the site for metal coordination blocked and SK-4C2, which is a primary amine without the carboxylated group. The justification of the design and synthesis of the control compounds can be found in 7.2 and 7.2.2. Briefly, LUHMEN cells,

were treated with the control compounds (12.5-500  $\mu\text{M}$ ) 1 hr prior to the addition of erastin (1.25  $\mu\text{M}$ ) and they incubated for 24 hr before taking any measurements (**Figure 103**).

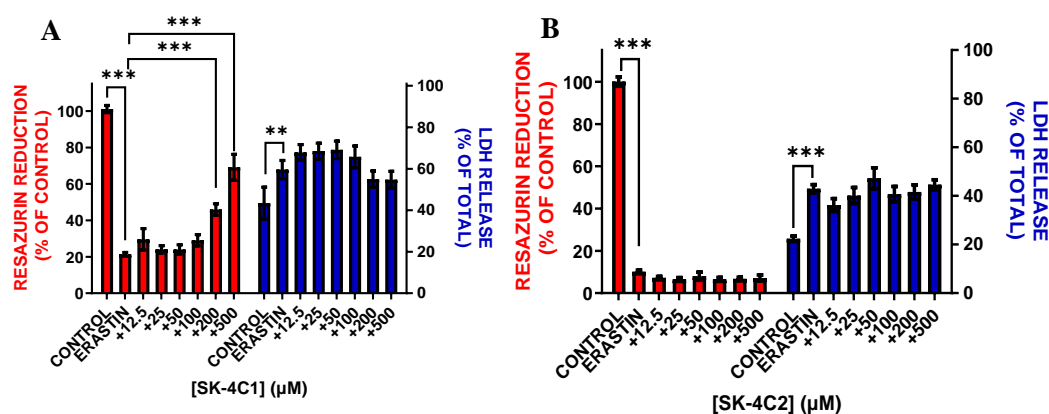


**Figure 103:** The ability of the control compounds; SK-4C1 and SK-4C2 to inhibit Erastin induced ferroptosis. LUHMES cells were exposed to a range of 12.5-500  $\mu\text{M}$  concentrations of each inhibitor prior to the addition of erastin (1.25  $\mu\text{M}$ ). Red bars represent the viability assays performed by means of resazurin reduction whereas the blue bars show the outcome of LDH release assay. Data shown are means  $\pm$  SD of at least 3 replicates from 3 independent experiments.

The results suggested that SK4C1 compound did not manage to rescue neuronal cells at concentrations of 12.5-100  $\mu\text{M}$ . Interestingly, at concentrations of 200 and 500  $\mu\text{M}$  a statistically significant elevation of the viability levels was observed. The reasons are not clear. This might be attributed to the fact that the compound might be de-methylated by cells upon compounds insertion. It is known that cells expressing P450 enzymes have the capacity to metabolically de-methylate allyl ether substrates. However, to the best of our knowledge there is no literature report that claims the expression of any class of P450 enzymes in LUHMES cells. Some level of metal chelation (hence cell protection) might be occurred through the amino acid vector as it is known that amino acids can act as metal chelators. In contrast there was not any significant dropped of the levels of LDH. On the other hand, SK4C2 did not show any cell rescue, (as it was expected) due to the fact that this control compound lacks the amino

acid moiety, preventing it in that way to exploit LAT-1 (if LUHMES cells express this particular transporter). This particular control compound it is expected to be in its protonated state at physiological pH, and possibly it cannot diffuse through the neuronal cells (and consequently BBB) due to its hydrophilic character (**Figure 104**).

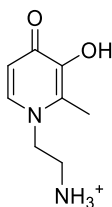


**Figure 104:** Structure of SK-4C2 at physiological pH.

The neurite area determination also confirmed the above findings as none of the control compounds could exert any neuroprotective property. The neurite area of the treated with the control compounds cell groups remain steady in the same levels as to those of erastin (**Figure 105**).

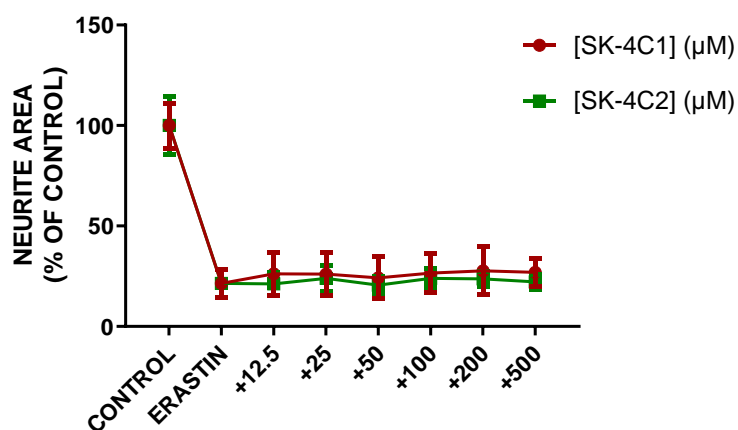


**Figure 105:** The ability of the control compounds; SK-4C1 and SK-4C2 c to protect from ferroptosis been induced by erastin. LUHMES cells have been exposed to a range of 12.5-500 µM concentrations of each compound prior to the addition of erastin (1.25 µM). LUHMES cells were labelled with Calcein-AM (1 µM) and H-33342 (1 µg/ mL). Images were collected using automated microscope. All calcein positive pixels outside of these masks (somatic area) were counted as neurite area.

## 8.6 Antioxidant properties of SK-n.

### 8.6.1 Interaction of the SK-n compounds with superoxide

The neuroprotective capacity of the synthesised SK-n compounds is shown and validated in the previous sections. In this section, an attempt to document any antioxidant potency (by means of ROS or RNS scavenging) towards the deamination of the mode of action of compounds is presented. Primarily the ability of the SK-n compounds to interact with trap superoxide radicals has been examined in LUHMES cells, using xanthine oxidase alone with its substrate as a source of superoxide anions (**Figure 106A**).

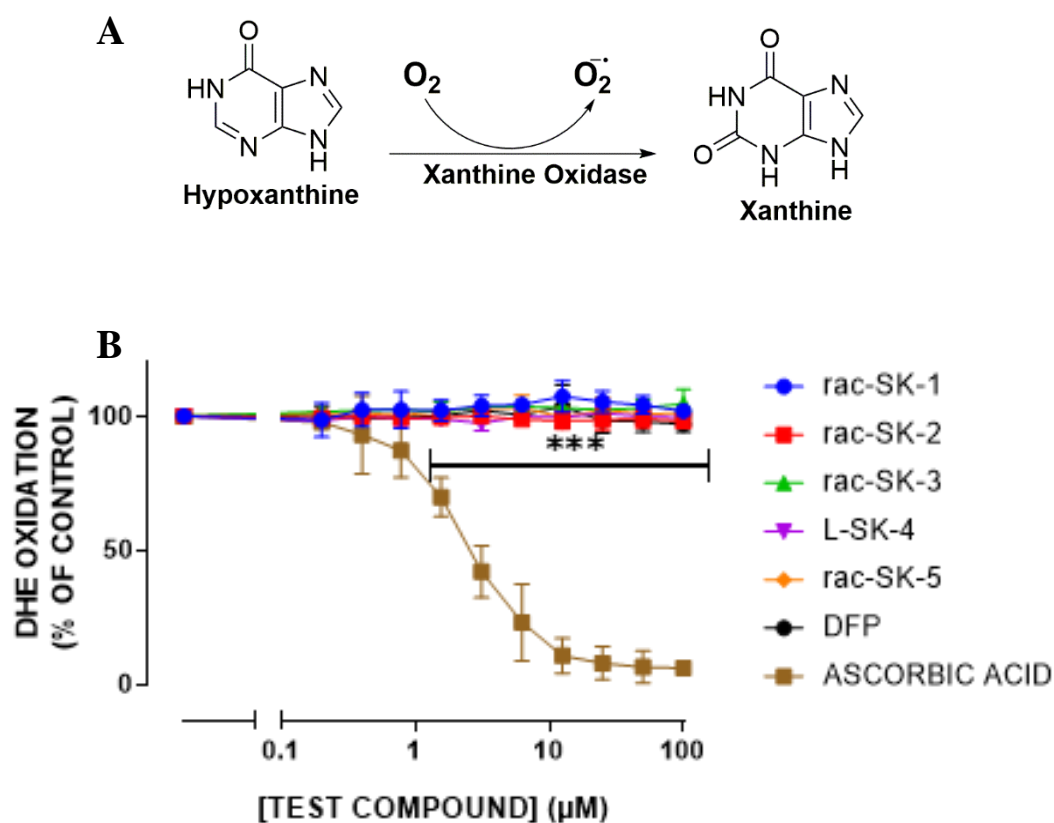


**Figure 106:** (A) Generation of superoxide radicals by the reduction of molecular oxygen and oxidation of hypoxanthine into xanthine in a reaction catalysed by xanthine oxidase. (B) Briefly, LUHMES cells were treated with the SK-n compounds (0.1-100  $\mu\text{M}$ ) in the presence of xanthine oxidase (1 mU/mL), hypoxanthine (500  $\mu\text{M}$ ) and DHE (5  $\mu\text{M}$ ). The levels of DHE

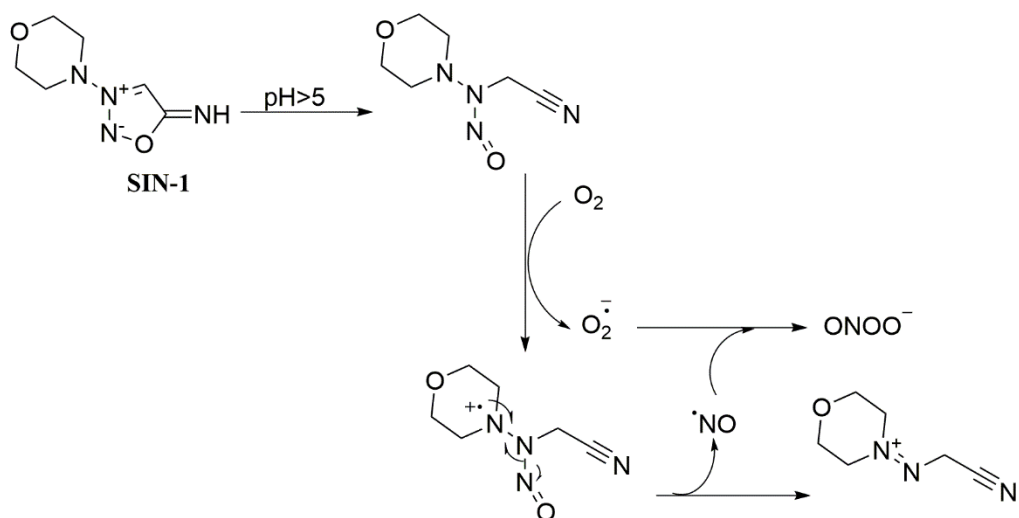
oxidation were representative for the Antioxidant capacity of SK-n compounds against superoxide anions.

According to the results obtained, none of the examined compounds had the ability to trap superoxide anions, whereas the positive control (ascorbic acid) shown a massive superoxide scavenging at a concentration of 1  $\mu$ M (**Figure 106B**) as it was demonstrated before.<sup>680-682</sup> In the case of *L*-SK-4 and *rac*-SK-2, those findings are in agreement with the literature as it has been previously documented that 3, 4-HOPOs derivatives are extremely poor radical scavengers.<sup>441</sup> In addition to this, Ramsaywack S and co-workers support this statement by proving with kinetics of radicals autoxidation that indeed HOPO are not antioxidant by trapping ROS as it has previously suggested.<sup>394,396,438</sup> However, they can exert antioxidant capacity by preventing the radical oxidation catalysed by toxic metals.<sup>438</sup> The application of these findings can be applied in this case, as the ability of the SK-n compounds to protect neuronal cells against the oxidative damage is not linked to ROS trapping. On the contrary, they protect neuronal cells by preventing the oxidation catalysed by both;  $\text{Fe}^{3+}$  and  $\text{Cu}^{2+}$  during the Haber-Weiss reaction (in a stoichiometric ratio 3:1 for complete redox silencing).<sup>417,434,438,440,441,443,444</sup> Moreover, according to the literature, 3-hydroxy-2(1H)-pyridinones (3, 2 HOPOs) are significantly better ROS traps compared to 3, 4-HOPOs and least active when compared to other classes of chelators including hydroxamic acids and phenols. In our case *rac*-SK-5, a 3, 2-HOPO was expected to demonstrate some scavenging activity, such observation has not been noticed.<sup>441</sup> On the other hand, *rac*-SK-1, which shares the same pyranone core with maltol, was also expected to present some activity as it has been previously proven that maltol can exhibit some minor trapping activity (however more active compared to DFP).<sup>441</sup> Finally, to the very best of our knowledge, there is exciting work that shows the ability of 1-hydroxy-2(1H)-pyridinones (1, 2-HOPO) to trap ROS.<sup>683</sup> Although our data suggested that 1,2 HOPOs (by means of *rac*-SK-3) are not capable for trapping ROS.

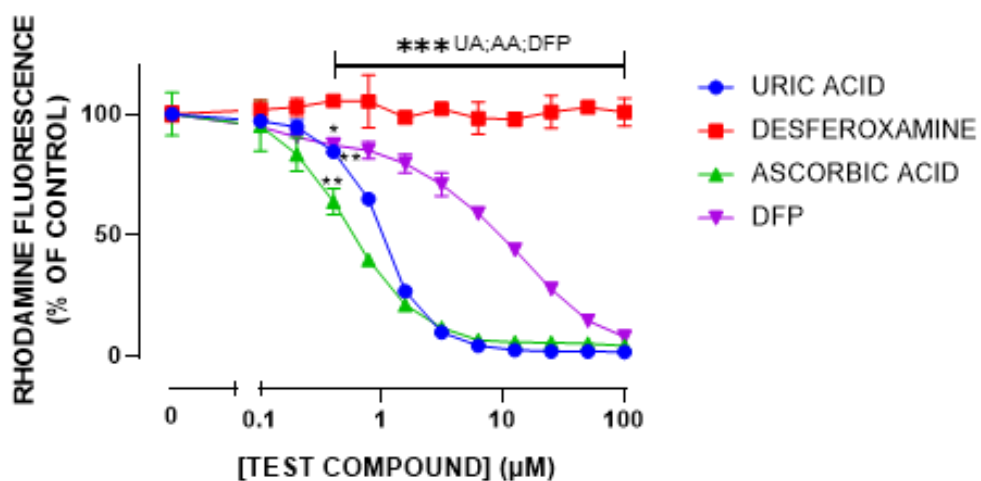
### 8.6.2 Interactions of SK-n compounds with peroxyxynitrite

The antioxidant capacity of the SK-n compounds to scavenge peroxyntirite species was assessed on LUHMES cells, using 3-Morpholinosydnnonimine hydrochloride (SIN-1) as a generator of peroxyntirite (Figure 107A).

**A**



**B**



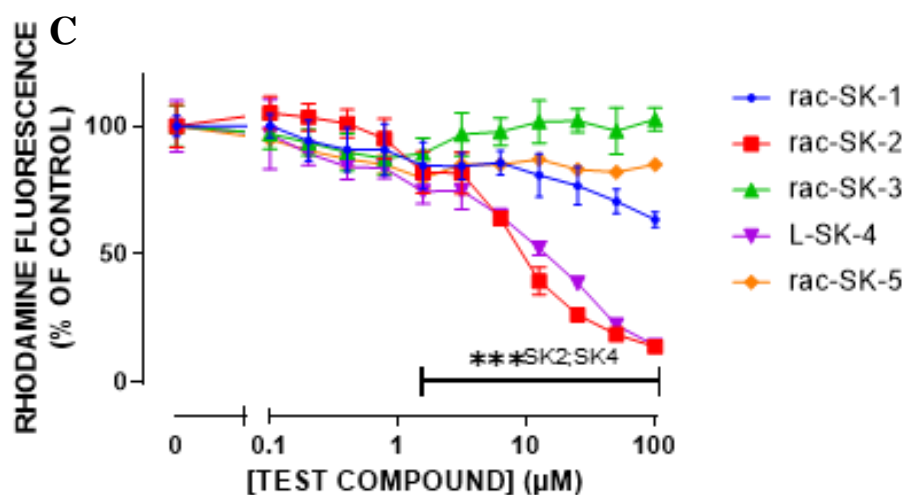


**Figure 107:** (A) Proposed mechanism for the formation of peroxynitrite species. Briefly, LUHMES cells were treated with the SK-n compounds (0.1-100  $\mu\text{M}$ ) in the presence of SIN-1 (5  $\mu\text{M}$ ). As readout, DHR 123 (1  $\mu\text{M}$ ) was added and its oxidation was followed by the detection of Rhodamine fluorescence. (B) Antioxidant capacity against peroxynitrite of known scavengers and chelators and (C) Antioxidant capacity of the SK- compounds against peroxynitrite species.

The results suggested that all the examined compounds, except *rac*-SK-3 shown some antioxidant capacity against peroxynitrite species but not in the same magnitude (**Figure 107C**). Namely, exposure of the LUHMES cells with *rac*-SK-1, 3 and 5 shown some decrease in the fluorescence intensity of rhodamine in a dose-dependent manner (**Figure 107C**). However, the observed decreased is not of statistically significant even after treatment with 100  $\mu\text{M}$  of each compound. In contrast, exposure of the cells to *rac*-SK-2 and *L*-SK-4 (respectively) shown a dramatic decrease in the rhodamine fluorescence intensity, in a dose-dependent manner, meaning that both compounds were able to counteract with peroxynitrite species or react with SIN-1 (**Figure 107C**). In addition to this, it seems that both compounds are significantly better peroxynitrite scavengers compared to desferoxamine and less active compared to uric and ascorbic acid (**Figure 107B**).<sup>684-687</sup> Furthermore, more *L*-SK-4 and *rac*-SK-2 shown a similar potency as DFP. This could be attributed to the fact that either the SK-

n compounds (as nucleophiles) reacted themselves with SIN-1, thus preventing the elimination of NO $\cdot$  and consequently, the formation of ONOO $\cdot$ . Additionally it has been previously shown that peroxyntirite can nitrate tyrosine at the ortho position. Initially, reaction of peroxyntirite with carbon dioxide lead to the formation nitrocarbonate (**Figure 108**). Homolysis of nitrocarbonate, generates carbonate and nitrite radical (**Figure 108**). Afterwards, the carbonate radical abstracts homolytically the phenolic proton of tyrosine, generating tyrosyl radicals. Then, it was suggested that the nitrite radical can react with the tyrosyl radical at the *ortho* position forming 3-nitrotyrosine. Beside this reaction, it has been previously demonstrated, that tyrosyl radicals can react with themselves and dimerised forming the oxidation product; 3,3'-dityrosine. (**Figure 108**).<sup>688-691</sup>

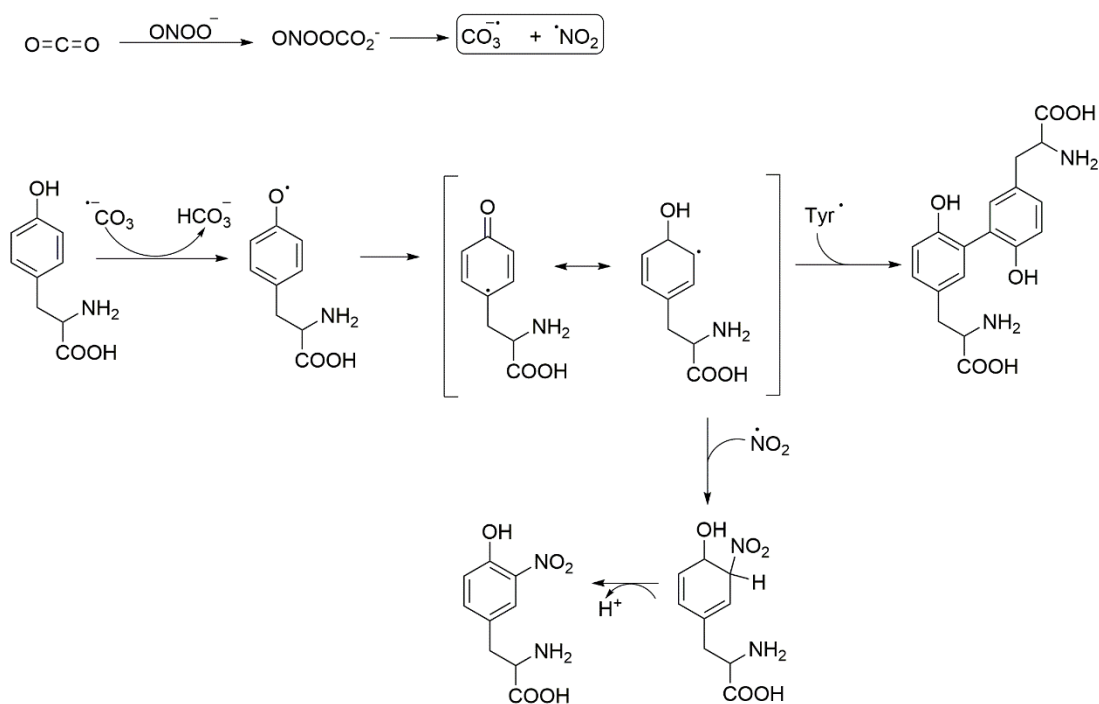


**Figure 108:** Proposed tyrosine oxidation pathways. Tyrosine is oxidised, by several oxidants, (eg CO $_3^{\cdot-}$ ) forming the tyrosyl radical which can react further with nitrite radical yielding nitrotyrosine or dimerised into the respective 3,3'-dityrosine.

Bases on the above, it can be hypothesised that the SK-n compounds reacted with nitrite radicals and nitrated (**Figure 109**).

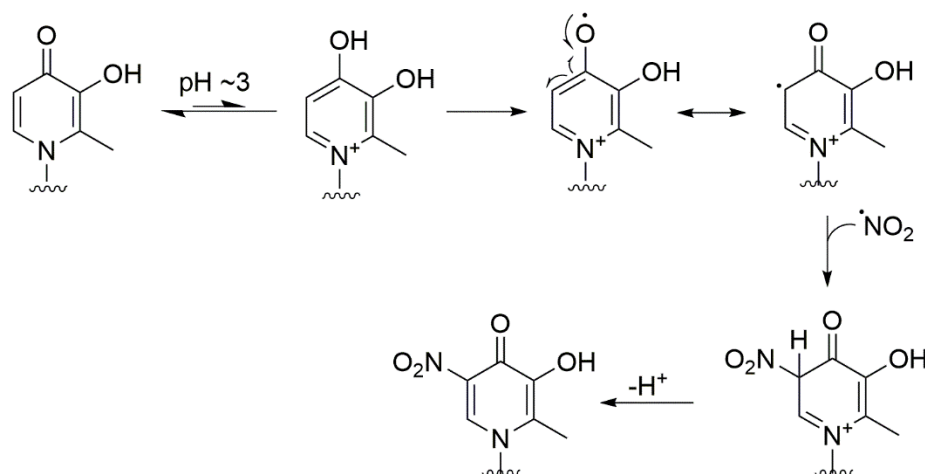


**Figure 109:** Proposed nitration mechanism of a 3, 4-HOPO.

This could explain the reduction of peroxyxynitrite concentration. Since the *pKa* of the *ipso* hydroxyl group differs across the series of HOPOs that could explain the potency of 3,4-HOPOs over the 3, 2- and 1, 2-HOPOs.

## 9 Final discussion

### 9.1 Summary and Conclusions

Due to high therapeutic potential of metal chelators against various types of cancer and neurodegenerative diseases, there is a need to develop novel ones or improved the already existing therapies in order to generate more robust compounds that would be able to reach the central nervous system (CNS) (in the case of PD) or the site of action while retaining their metal chelation properties [chelation of the redox active metals eg. Fe(III), Cu(II)]. Various mechanisms can be exploited to cross the BBB in order to reach the brain for the treatment of PD or brain metastatic cancers, a passive and several active routes eg. GLUT-1 and LAT-1 transporters. Herein, a series of novel hydroxypyridinone (HOPO) based metal chelators including a 1,2-HOPO (*rac*-SK-3 and *rac*-SK-6), 3,2-HOPO (*rac*-SK-5 and *rac*-SK-7), 3,4-HOPO (*rac*-SK-2, *L* and *D*-SK-4, *rac*-SK-8) and a hydroxypyranone (*rac*-SK-1) were designed, synthesised and characterised in terms of experimental calculation of their protonation constants ( $pK_a$ ) as well as their stability constant upon complexation with Fe(III), Cu(II) and Zn(III) and the exported data were in agreement with those of the literature which refers to closed analogues or parts of the molecule. The rational design behind the synthesis of this molecules was the introduction of an amino acid moiety in order to facilitate the transportation across the BBB (in case of PD) or the cell membrane (in case of melanoma cancer) using an active transport mechanism; the LAT-1 transporter, which has been shown that is overexpressed in BBB and in various cancer cells.

The scientific impact of the current work is reflected in various sectors of medicinal chemistry and drug design. Initially, novel compounds (*rac*-SK-1, *rac*-SK-3, *L/D*-SK-4, *rac*-SK-7, *L*-SK-8) have been synthesised and fully characterised. In addition to this, the biological evaluation of those compounds (*rac*-SK-1, *rac*-SK-2, *rac*-SK-3, *L/D*-SK-4, *rac*-SK-5) against an in vitro model of both melanoma cancer and PD, demonstrated a unique capacity to exhibit opposed dual mode action which includes in both cases the metal coordination and the

transportation through LAT-1. Additionally, it has been proven that these compounds can induce cytotoxicity against melanoma cancer and neuroprotection against PD. In addition to this, the extensive characterisation of the mode of cell death (in the case of cancer) shown significant insights into their mode of action. The outcome of this study, can lead us to the development of second generation of these compounds taking into consideration the structural optimization of the active compounds, aiming to reduce to EC<sub>50</sub> value that is associate with their activity and place them on the radar of pharmaceutical companies as potential candidates for development.

The biological evaluation of these (*rac*-SK-1, *rac*-SK-2, *rac*-SK-3, *L/D*-SK-4, *rac*-SK-5) molecules involved their screening against an *in vitro* model of malignant melanoma composed of human (A375, VVM1, Hs-294T) and rodent (B16F-10) melanoma cells as well as non-melanoma epidermoid carcinoma (A431) and immortalized, non-malignant keratinocyte (HaCaT) cells. The results obtained from the cytotoxicological assays revealed that the order of anticancer activity is as follow; *L*-SK-4 >>> *rac*-SK-2 ~ *rac*-SK-3 with the most active compound (*L*-SK-4) to have an EC<sub>50</sub> of 100 μM at 48 hr of exposure. Our data are in agreement with the already existing data that are reported in the literature concerning the anticancer activity of *L*-mimosine and DFP (as both compounds exhibit structural similarity with *L*-SK-4).<sup>138,139</sup> In example, the EC<sub>50</sub> value of those compounds is ~100 μM when their cytotoxicity was examined in various cell lines of prostate, breast and lung cancer.<sup>692-696</sup> However, due to the general high EC<sub>50</sub> value of *L*-SK-4 (100 μM) it can be concluded that overall the compound is not considered as cytotoxic. In example, cisplatin, which its anticancer capacity has been listed several times in the current literature, has an EC<sub>50</sub> value of ~6 μM on A375 whereas other chemotherapeutic drugs (that are used against melanoma) such as etoposide, topotecan and doxorubisine have EC<sub>50</sub> value of 10 μM, 1 μM and 35 μM respectively on the same working cell line (A375).<sup>697-699</sup>

In addition to this, the effect of structural changes was reflected into the biological activity and capacity of the SK series. Namely, the fact the *rac*-SK-1, 2, 3 and 5 did not shown any activity

(at low concentrations) can be attributed to several factors. In example, it might be that the compounds exploited LAT-1, however they could not develop interactions with the active site of the transporter and therefore their transportation was prevented. Furthermore, the solvation effect might be another reason that influence the capacity of these compounds as the water molecules displacement from the active site of the LAT-1 transporter by the compounds is not energetically favoured.<sup>700</sup> It has also been proven that the protonation state of these compounds at pH 7.4 can affect both the pFe value of the compounds (hence the metal binding) and also their transportation ability as LAT-1 transporter can accommodate neutral species, whereas *rac*-SK-1, 2, 3 and 5 are expected to be charged at physiological pH. Another possible factor that prevent the activity of these molecules can be attributed to possible formation of interactions with the proteins that are located in the cell surface and are responsible for the recognition of xenobiotics (eg p-glycoproteins).<sup>701,702</sup> Interactions with such proteins can prevent their cellular uptake and hence its activity. Also, the lack of activity of these compounds might be due to a result of their rapid metabolism once they enter the cell. Also, the lack of activity of these compounds might be due to a result of the rapid metabolism once they enter the cell.

Afterwards, the selectivity of this compound to target specifically melanoma cells and not the cancerous (control) cells, has also been evaluated and interestingly, the results shown a significant preference of cytotoxicity induction in melanoma cell line (A375) as the control cell lines (A431 and HaCaT) appeared to be more resistant to the treatment. The next part of the biological evaluation involved a descriptive characterisation of the mode of action of the active molecule using flow cytometry and western immunoblotting approach. The results suggested that at the given concentration of 100  $\mu$ M the compound has the ability to elevate the levels of ROS almost three times higher compared to the untreated control with the effect being sustained over the course of 72 hr. The elevation of ROS levels was accompanied with cell cycle growth arrest at the G1 phase in a similar way as *L*-mimosine does and also the activation of both intrinsic and extrinsic apoptosis. Moreover, a detailed characterisation of

the induced oxidative stress has been constructed by measuring the levels of ROS induction in a various concentrations of drug at several time points proving that the maximum ROS of induction was denoted at 100  $\mu$ M whereas at higher concentrations the ROS levels were dropped. Additionally, the ROS elevation was found to selectively been induced on melanoma cell lines (A375, VVM1, Hs-294T and B16F-10) rather than the control cell lines (A431 and HaCaT). Furthermore, the levels of lipid peroxidation (by means of MDA), protein carbonylation as well as the levels of DNA oxidative damage (by means of 8-OHdG) have been determined experimentally. The results shown that during the first 48 hr all the examined metabolites reached the maximum level and afterwards the effect either dropped or sustained whereas during the first 24 hr there was not any significant alteration regardless the elevation of ROS. Furthermore, the addition of ROS scavenger (GSH) confirmed that the apoptosis is ROS driven as ROS abolishment prevented the activation of apoptosis. A detailed metabolomic approach has confirmed significant changes in the lipidomic profile of A375 cells, upon exposure to 100  $\mu$ M L-SK-4 for 24 hr. The results shown that there was a significant elevation in the production of sphingolipids. To this end, we correlate that ROS induction with the activation of apoptosis and the sphingolipids elevation by the use of an inhibitor of the *de novo* synthesis of sphingolipids (myriocin). The overall relation suggests that upon exposure to L-SK-4, there is a massive increase in the production of ROS, which stimulated that biosynthesis of sphingolipids as an adaptation of the response mechanism of the cell. Afterwards, the elevation of sphingolipids and more specifically the elevation of ceramide triggers the direct activation of the extrinsic apoptosis via FASL activation and indirectly the activation of intrinsic apoptosis by means of mitochondrial depolarisation and formation of apoptosome. In addition to this, it appears that after 48 and 72 hr of exposure the cell is unable to counteract the amount of ROS that been produced as the oxidative stress is in a progressive stage, hence the apoptosis reached it maximum levels.

The formation of ROS via redox cycle of hydrogen peroxide catalysed by Fe(III) or Cu(II) has been shown to contribute in the development of PD. Herein, it has been demonstrated that the

use iron chelators based on the HOPO core can act as neuroprotective agents against a variety of PD-induced neurotoxins including; 6-hydroxydopamine (6-OHDA), which generates superoxide radicals, 1-methyl-4-phenylpyridinium (MPP<sup>+</sup>), a mitochondrial complex I inhibitor, and the ferroptosis activator, erastin in an *in vitro* model of immortalised human dopaminergic neuronal precursor cells (LUHMES). The results suggested that the neuroprotective capacity of the compound varies across the different toxins. Namely, the neuroprotective effectiveness trend of the HOPO compounds against 6-OHDA was; *rac*-SK-2 > *L*-SK-4 >>> *rac*-SK-5 whereas *rac*-SK-1 and *rac*-SK-3 were totally inactive. Additionally, the respective trend on MPP<sup>+</sup> and erastin was *rac*-SK2 ~ *L*-SK-4 ~ *rac*-SK-3 >>> *rac*-SK-5 and *rac*-SK-2 ~ 4 >> *rac*-SK-3 respectively. Once again *rac*-SK-1 and *rac*-SK-5 were not shown any neuroprotective ability. The possible reason that prevent there activity might be their protonation state at physiological pH, the solvation effect (that is related to the transporter) and also the development of interactions between the cell surface and the compounds. Furthermore, an attempt to characterise the antioxidant capacity of the chelators has been conducted by examining whether the compounds can act as superoxide and/or peroxynitrite scavengers. The results obtained suggested that none of the chelators could act as superoxide scavengers. Although it appeared that *rac*-SK-2 and *L*-SK-4 can act as peroxynitrite scavengers.

In order to validate which structural features were essential for the transportation and the action of the compound, a series of control compounds of the potent *L*-SK-4 have also been designed and screened against both melanoma cancer as well as PD cell lines. The exported data documented that that the HOPO core is essential for the metal binding and the amino acid side vector for the transportation using the LAT-1 as the various control compounds didn't show any anticancer activity against melanoma and or any neuroprotection against PD. Additionally, in order to confirm that the active compounds are using the LAT-1 transporter, A375 cells have been treated with both *L*-SK-4 and three competitive (non-specific) LAT-1 substrates (BCH and *L* and *D*- 2-amino-3-(2-naphthyl) propanoic acid) and a LAT-1 inhibitor (*L*-

thyroxin) (separately). The outcome of this analysis shown a significant cell rescue rather than cell death demonstrating in that way that the inhibition of the LAT-1, prevent the entrance of the molecule to the cell and hence its action. Therefore, the control compounds of the associated molecule supported the rational design behind it. These compounds, therefore, constitute a new develop on the therapeutic ability of HOPOs, that deserves further studies.

## 9.2 Further studies

This research has identified many avenues of interest that would lead in a better understanding of how metal chelators can have multiple mode of actions (eg, cytotoxicity against cancer, neuroprotection against PD) and how to design new improved compounds of this class.

### 9.2.1 Novel Molecules

One of the most promising research direction that maybe highly beneficial to pharmaceutical sector is the synthesis of more lipophilic analogues of the above series capable to penetrate BBB that would lower the  $EC_{50}$  value and increase the therapeutic index using computational modelling tools based on the newly discovered structure of human LAT-1. This structural optimisation of the active compounds would facilitate the transportation to the brain, hence it could be used for the treatment of both neurodegenerative diseases and brain metastatic cancers (**Figure 110A, B, C**). Additionally, the synthesis of a glycosylated masked analogue of L-SK-4 would be noteworthy compound as it would combined essential features for both activity and transportation including; the HOPO core, the pro-chelator masked with glucose hydroxyl group, and the amino acid vector that would allow the transportation through LAT-1. These chemical modifications would lead to the formation of a prodrug that would hydrolysed *in situ* and release the active L-SK-4 (**Figure110D**). Alternatively, the addition of sugar maybe facilitates the transportation through the GLUT-1 transporter.

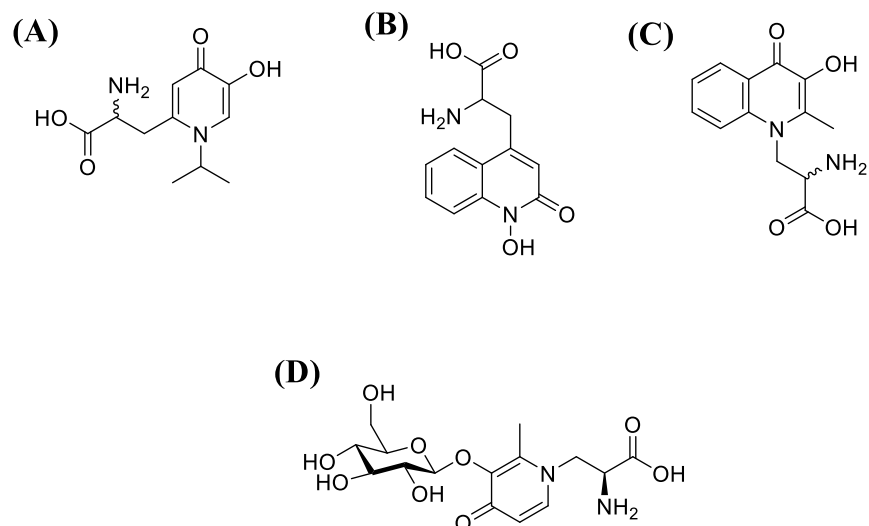


**Figure 110:** Proposed compounds with increased lipophilicity and a suggested pro-drug form of L-SK-4 in an attempt to optimise its structure for the improvement of BBB penetration.

### 9.2.2 Mode of action

In the case of cancer evaluation, we could potentially measure the liable iron pool in the different organelles and also calculate how much of the active compound enters the cell in order to have a better understating of the mode of action of the chelator; *L*-SK-4. This can give insights into the stoichiometry of the total iron and the chelator and consequently an understanding whether the chelator acts as pro-oxidant or anti-oxidant. Additionally, a metabolic analysis of the active compound could be of high interest as the mode action could be relied on its metabolites rather than the actual molecule itself. Another potential orientation and improvement of the current study would be the combinational therapy, where the synthesised HOPOs would be administered in combination with already existing chemotherapeutic agents and try to identify synergies. Furthermore, the use of *in vivo* models could be a powerful tool that would allow the determination of both the pharmacokinetic and the pharmacodynamics properties of the synthesised molecules.

From the point of view of application of metal chelators against PD, a potent development of the research would be the use of animal models (*in vivo*) that we could use the *loco motor*

phenotype as an end point of the activity of the compounds. Furthermore, the ability of the synthesized molecules to act as COMT inhibitors (due to the structural similarities with the currently existing COMT inhibitors) could give a better understanding on the mode of action of these molecules. Finally, racemic resolution of *rac*-SK-2 and *rac*-SK-3 followed by biological evaluation of the pure enantiomers could potentially increase the therapeutic index and lower the EC<sub>50</sub>.

## 10 Experimental procedures – organic synthesis

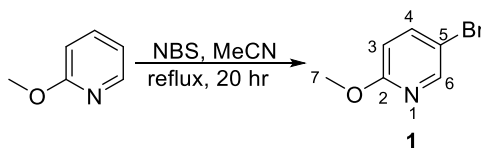
### 10.1 Equipment and chemical reagents.

All chemical reagents were purchased from Sigma-Aldrich (St. Louis, MO, USA), Alfa Aesar (Lancashire, UK), Fluorochem (Derbyshire, UK), TCI (Oxford, UK) and were used without any further purification unless otherwise specified. All chemical solvents were purchased from Fisher Scientific (Hampton, NH, USA) and Sigma Aldrich (St. Louis, MO, USA), at either HPLC or reagent grade. When required, solvents were dried over activated 3 or 4 Å molecular sieves. **NMR Spectroscopy** was performed on JEOL ELS400 Delta Spectrometer at frequencies of 400 MHz for  $^1\text{H}$  NMR, 101 MHz for  $^{13}\text{C}$  NMR. Chemical shifts were recorded as parts per million (ppm) with tetramethylsilane (TMS) as the internal standard. Solvents used included deuterated dimethyl sulfoxide ( $\text{DMSO-}d_6$ ), deuterated chloroform ( $\text{CDCl}_3$ ), deuterated methanol ( $\text{CD}_3\text{OD}$ ), deuterated water ( $\text{D}_2\text{O}$ ) and deuterated TFA ( $\text{CF}_3\text{CO}_2\text{D}$ ). Chemical shifts were observed with integrals, splitting and J values, multiplicity of the signals were recorded as singlet (s), doublet (d), triplet (t), quartet (q). In addition, the multiplicities (which have further coupling) were recorded e.g. double doublet (dd). For broad signal (br) is indicated. **High Resolution Mass Spectrometry (HRMS)** was carried out at Northumbria University using Thermo Q-Exactive spectrometer with electrospray ionisation (ESI) (Thermo Fisher Scientific, Cramlington, UK). **High Performance Liquid Chromatography (HPLC)** (Agilent Technologies, 1260 Infinity) analysis was carried out at Northumbria University using Phenomenex Column (HYPERASIL 5u C18, 150x4.60 mm). **Automated Flash Chromatography** was performed on Biotage® Isolera One using Biotage® SNAP-Ultra flash chromatography cartridges 10-100g size (Biotage, Uppsala, Sweden). **Melting points** were recorded in open capillary tubes using a Stanford Research System MPa160 Melting Point Apparatus and are reported uncorrected.

## 10.2 Synthesis of 1.2 HOPOs

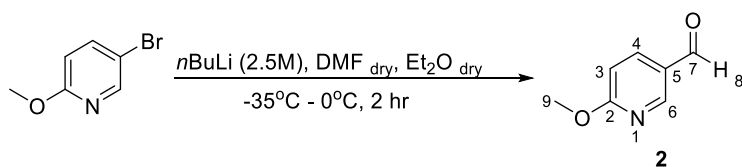
### 10.2.1 Synthesis of *rac*-SK-3

#### 10.2.1.1 Synthesis of 5-bromo-2-methoxypyridine (**1**)



The product was prepared based upon a literature procedure.<sup>500</sup> In a solution of 2-methoxypyridine (15 g, 138 mmol, 1 eq) in acetonitrile (415 mL), *N*-bromosuccinimide (30 g, 169 mmol, 1.22 eq) was added and the resulting mixture was refluxed for 20 hr. Upon completion of the reaction, as indicated by TLC (SiO<sub>2</sub>, eluent: Petroleum Ether 60-80: Ethyl acetate, 8:2; UV-light), the mixture was filtered over a pad of silica. The solvent was evaporated, under reduced pressure, affording the crude product as orange oil which was then purified by an automated flash chromatography column (Isolera); R<sub>f</sub> = 0.83 (Petrol Ether 60-80: Ethyl acetate, 95:5; UV light) affording intermediate (**1**) as a pale-yellow oil (4.7 g, 25 mmol, 18%). <sup>1</sup>H-NMR (400 MHz, CDCl<sub>3</sub>) δ<sub>H</sub>: 3.90 (s, 3H, H-7), 6.64 (d, *J* = 8.8 Hz, 1H, H-3), 7.61 (dd, *J* = 2.8 Hz, *J* = 8.8 Hz, 1H, H-4), 8.18 (d, *J* = 2.8 Hz, 1H, H-6) ppm; <sup>13</sup>C-NMR (100 MHz, CDCl<sub>3</sub>) δ<sub>C</sub>: 53.6 (C-7), 111.6 (C-5), 112.5 (C-3), 140.9 (C-4), 147.5 (C-6), 162.8 (C-2) ppm.

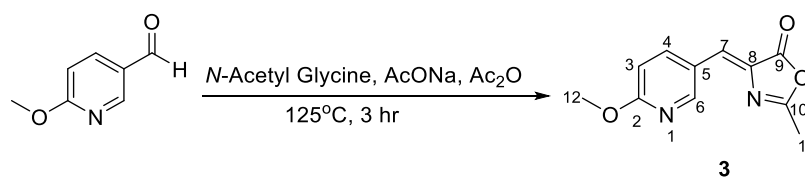
#### 10.2.1.2 Synthesis of 6-methoxypyridine-3-carbaldehyde (**2**)



The product was prepared based upon a literature procedure.<sup>500</sup> In a solution of 5-bromo-2-methoxypyridine (**1**) (4.7 g, 25 mmol, 1 eq) in dry diethyl ether (50 mL) and under inert atmosphere, *n*-Butyl Lithium (2.5 M in hexanes, 12 mL, 30 mmol, 1.2 eq) was added at -35°C, and stirred until the formation of a brown precipitate. Then, dry *N,N*-dimethyl formamide (5.4

mL, 70 mmol, 2.8 eq) was added dropwise for 5 min. The resulting mixture was stirred at 0°C (~2 hr), under inert atmosphere. Upon completion of the reaction, as it was indicated by TLC (SiO<sub>2</sub>, eluent Petroleum Ether 60:80: ethyl acetate, 80:20; UV light), the reaction was quenched by aqueous solution of ammonium chloride (5%, 25 mL). The aqueous layer was extracted with dichloromethane (3 x 50 mL). The combined organic extracts were dried over magnesium sulphate and concentrated under reduced pressure, forming the crude product as orange oil. The crude product was purified by automated flash chromatography column (Isolera); R<sub>f</sub> = 0.43 (Petrol Ether 60-80: diethyl ether, 60:40; UV light) affording intermediate **2** as yellow crystals (2.53 g, 16.7 mmol, 67%). Mp: 42-44°C, [lit: 42-46°C].<sup>500</sup> <sup>1</sup>H-NMR (400 MHz, CDCl<sub>3</sub>) δ<sub>H</sub>: 4.03 (s, 3H, H-9), 6.84 (d, J = 8.4 Hz, 1H, H-3), 8.05 (dd, J = 2.4 Hz, J = 8.4 Hz, 1H, H-4), 8.63 (d, J = 2.4 Hz, 1H, H-6), 9.96 (s, 1H, H-8) ppm; <sup>13</sup>C-NMR (100 MHz, CDCl<sub>3</sub>) δ<sub>C</sub>: 54.4 (C-9), 112.2 (C-4), 126.7 (C-6), 137.5 (C-5), 153.5 (C-3), 167.8 (C-2), 189.6 (C-7) ppm.

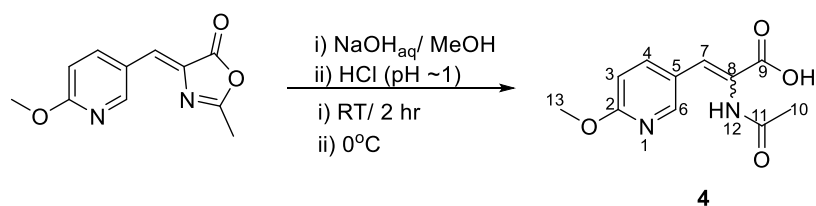
### 10.2.1.3 Synthesis of 4-[(6-methoxypyridin-3-yl)methylidene]-2-methyl-4,5-dihydro-1,3-oxazol-5-one (**3**)



The synthesis was performed according to a modified method that was previously published.<sup>503</sup> Briefly, in a solution of 6-methoxypyridine-3-carbaldehyde (**2**) (1.84 g, 12.17 mmol, 1 eq) in acetic anhydride (8 mL), a sample of *N*-acetyl glycine (2.04 g, 17.44 mmol, 1.5 eq.) and a sample of sodium acetate (1.5 g, 18.29 mmol, 1.5 eq) were added sequentially. The resulting mixture was stirred at 125°C for 4 hr. Upon completion of the reaction, the mixture was poured into ice-water and stirred for a further 1 hr leading to the formation of a yellow solid of the crude product which was collected by vacuum filtration, washed with water and dried in air.

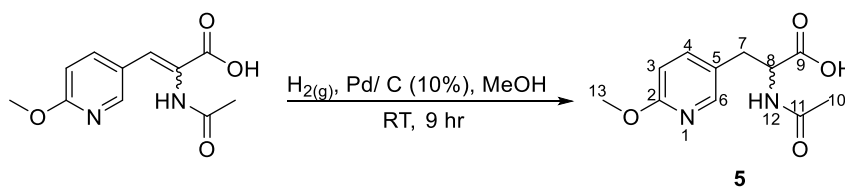
The crude product was purified by recrystallization from methanol affording the pure product (**3**) as pale-yellow solid (1.66 g, 7.6 mmol, 63%). Mp: 152-154°C. <sup>1</sup>H-NMR (400 MHz, CDCl<sub>3</sub>) δ<sub>H</sub>: 2.40 (s, 3H, H-11), 4.00 (s, 3H, H-12), 6.83 (d, *J* = 8.8 Hz, 1H, H-3), 7.12 (s, 1H, H-7), 8.6 (d, *J* = 2.4 Hz, H-6), 8.67 (dd, *J* = 2.4 Hz, *J* = 8.8 Hz, H-4) ppm; <sup>13</sup>C-NMR (100 MHz, CDCl<sub>3</sub>,) δ<sub>C</sub>: 15.8 (C-11), 54.1 (C-12), 111.8 (C-3), 123.3 (C-7), 128.1 (C-5), 132.0 (C-8), 140.9 (C-4), 152.1 (C-6), 165.4 (C-10), 165.7 (C-9), 167.7 (C-2) ppm. HRMS (ESI) for C<sub>11</sub>H<sub>10</sub>N<sub>2</sub>O<sub>3</sub>; Theoretical [M+H]: 219.0769. Measured [M+H]: 219.0766.

#### 10.2.1.4 Synthesis of 2-acetamido-3-(6-methoxypyridin-3-yl)prop-2-enoic acid (**4**)



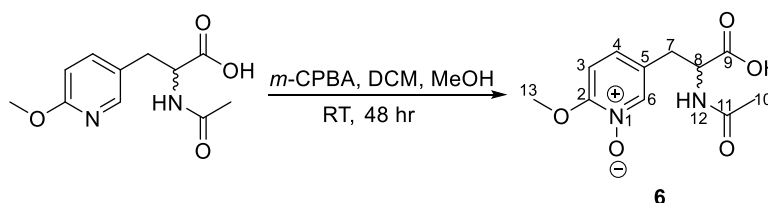
The synthesis was performed according to a modified method previously published.<sup>505</sup> Briefly, a sample of 4-[(6-methoxypyridin-3-yl)methylidene]-2-methyl-4,5-dihydro-1,3-oxazol-5-one (**3**) (2 g, 9.16 mmol) was dissolved in a mixture of water (30 mL)/acetone (50 mL) and the resulting mixture was refluxed for 9 hr. The solution was allowed to cool down to RT and then was concentrated, under reduced pressure, forming the crude product as yellow solid. The crude product was purified by recrystallization from methanol affording (**4**) as pale brown crystals (1.76 g, 7.45 mmol, 81%). Mp: 162-164°C. <sup>1</sup>H-NMR (400 MHz, DMSO-*d*<sub>6</sub>) δ<sub>H</sub>: 2.00 (s, 3H, H-10), 3.89 (s, 3H, H-13), 6.88 (d, *J* = 8.8 Hz, 1H, H-3), 7.25 (s, 1H, H-7), 7.98 (dd, *J* = 2.4 Hz, *J* = 8.8 Hz, 1H, H-4), 8.40 (d, *J* = 2.4 Hz, 1H, H-6), 9.48 (s, 1H, H-12) ppm; <sup>13</sup>C-NMR (100 MHz, DMSO-*d*<sub>6</sub>) δ<sub>C</sub>: 23.2 (C-10), 54.0 (C-13), 111.1 (C-3), 124.1 (C-7), 127.1 (C-5), 128.7 (C-8), 139.8 (C-4), 149.7 (C-6), 164.1 (C-10), 166.8 (C-9), 169.7 (C-2) ppm. HRMS (ESI) for C<sub>11</sub>H<sub>12</sub>N<sub>2</sub>O<sub>4</sub>; Theoretical [M+H]: 237.0875. Measured [M+H]: 237.0871.

### 10.2.1.5 Synthesis of *rac*-2-acetamido-3-(6-methoxypyridin-3-yl)propanoic acid (**5**)



In a suspension of 2-acetamido-3-(6-methoxypyridin-3-yl)prop-2-enoic acid (**4**) (1.76 g, 7.45 mmol) in methanol (50 mL), Pd/C (10%) was added. The reaction mixture was stirred under hydrogen gas at RT for 9 hr. Upon completion of the reaction, the solution mixture was filtrated over a pad of Celite and concentrated under reduced pressure forming a yellow slurry. The resulting slurry was purified by automated flash chromatography column (Isolera™ Biotech) ( $\text{SiO}_2$ );  $R_f = 0.89$  (dichloromethane: methanol 9:1; UV light) affording (**5**) as a pale-yellow oil which was solidified on standing (940 mg, 3.94 mmol, 53%). Mp: 181-183°C.  $^1\text{H-NMR}$  (400 MHz,  $\text{CD}_3\text{OD}$ )  $\delta_{\text{H}}$ : 2.01 (3H, s, H-10), 2.95-2.30 (1H, m, H-7), 3.20-3.25 (m, 1H, H-7), 3.95 (s, 3H, H-13), 4.70-4.73 (m, 1H, H-8), 6.83 (d,  $J = 8.4$  Hz, 1H, H-3), 7.67 (dd,  $J = 2.4$  Hz,  $J = 8.4$  Hz, 1H, H-4), 8.15 (d,  $J = 2.4$  Hz, 1H, H-6) ppm;  $^{13}\text{C-NMR}$  (100 MHz,  $\text{CD}_3\text{OD}$ )  $\delta_{\text{C}}$ : 21.6 (C-10), 34.1 (C-7), 53.4 (C-13), 54.1 (C-8), 110.7 (C-3), 126.4 (C-4), 140.7 (C-5), 147.2 (C-6), 164.0 (C-2), 172.5 (C-11), 173.7 (C-9) ppm. HRMS (ESI) for  $\text{C}_{11}\text{H}_{14}\text{N}_2\text{O}_4$ ; Theoretical  $[\text{M}+\text{H}]$ : 238.0953. Measured  $[\text{M}+\text{H}]$ : 238.0961.

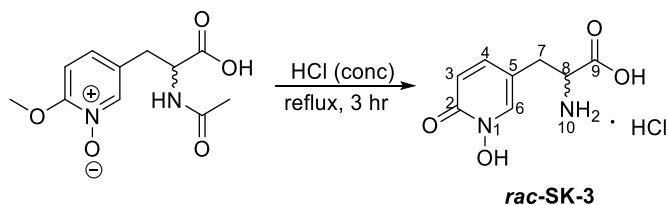
### 10.2.1.6 Synthesis of *rac*-5-(2-carboxy-2-acetamidoethyl)-2-methoxypyridin-1-ium-1-olate (**6**)



In a suspension of 2-acetamido-3-(6-methoxypyridin-3-yl)propanoic acid (**5**) (560 mg, 2.35 mmol, 1 eq) in a solution mixture of dichloromethane/methanol (9:1, 30mL) a sample of *m*-chloroperoxy benzoic acid (1 g, 5.8 mmol, 2.5 eq) was added. The resulting mixture was stirred

at RT for 48 hr under nitrogen atmosphere. Upon completion of the reaction, the solvents were removed under reduced pressure and the resulting yellowish slurry residue was washed several times with diethyl ether. Filtration of the product led to isolation of the title compound (**6**) as a white powder (460 mg, 1.80 mmol, 77%). Mp: 189-192°C. <sup>1</sup>H-NMR (400 MHz, DMSO-*d*<sub>6</sub>)  $\delta_H$ : 1.79 (s, 3H, H-10), 2.71-2.77 (m 1H, H-7), 2.95-2.99 (m, 1H, H-7), 3.93 (s, 3H, H-13), 4.38-4.43 (m, 1H, H-8), 7.13 (d, *J* = 8.7 Hz, 1H, H-12), 7.23 (dd, *J* = 2.0 Hz, *J* = 8.7 Hz, 1H, H-3), 8.11 (d, *J* = 2.0 Hz, 1H, H-6), 8.23 (d, 1H, *J* = 8.7 Hz, H-4) ppm; <sup>13</sup>C-NMR (100 MHz, DMSO-*d*<sub>6</sub>)  $\delta_C$ : 22.8 (C-10), 33.2 (C-7), 53.2 (C-8), 57.5 (C-13), 109.0 (C-3), 128.1 (C-6), 128.3 (C-5), 139.9 (C-4), 157.5 (C-2), 169.8 (C-11), 173.2 (C-9) ppm. HRMS (ESI) for C<sub>11</sub>H<sub>15</sub>N<sub>2</sub>O<sub>5</sub>; Theoretical [M+H]: 255.0908. Measured [M+H]: 255.0912.

#### 10.2.1.7 *rac*-2-amino-3-(1-hydroxy-6-oxo-1,6-dihydropyridin-3-yl)propanoic acid (*rac*-SK-3)

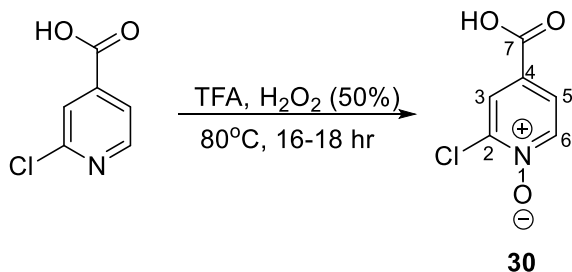


A sample of *rac*-5-(2-carboxy-2-acetamidoethyl)-2-methoxypyridin-1-ium-1-olate (**6**) (460 mg, 1.80 mmol) was dissolved in concentrated solution of HCl (20 mL). The resulting mixture was refluxed for 3 hr. Upon completion of the reaction, the mixture was concentrated to dryness leading to the formation of brownish crystals the target molecule (300 mg, 1.51 mmol, 84%). Mp: 120-122°C. <sup>1</sup>H-NMR (400 MHz, D<sub>2</sub>O/CF<sub>3</sub>COOD 8:2)  $\delta_H$ : 2.96-3.10 (2H, m, H-7), 4.13 (d, *J* = 4.8 Hz, 1H, H-8), 6.63 (t, *J* = 9.2 Hz, 1H, H-4), 7.43 (d, *J* = 9.2 Hz, 1H, H-3), 7.94 (s, 1H, H-6), 8.49 (s, 3H, H-10) ppm; <sup>13</sup>C-NMR (100 MHz, D<sub>2</sub>O/CF<sub>3</sub>COOD 8:2)  $\delta_C$ : 31.4 (C-7), 52.9 (C-8), 118.9 (C-3), 136.6 (C-5), 140.7 (C-6), 140.8 (C-4), 157.8 (C-2), 170.4 (C-9) ppm. For analytical purposes, a small portion of the titled molecule was dissolved in water and basified (pH 5.0) with ammonium hydroxide solution and kept at 5°C for several weeks until

precipitation. HRMS (ESI) for C<sub>8</sub>H<sub>10</sub>N<sub>2</sub>O<sub>4</sub>; Theoretical [M+H]: 199.0718. Measured [M+H]: 199.0711.

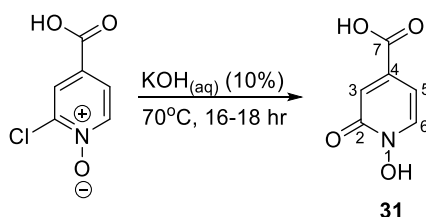
## 10.2.2 Synthesis of *rac*-SK-6

### 10.2.2.1 Synthesis of 4-carboxy-2-chloropyridin-1-ium-1-olate (**30**)



A sample of 2-chloroisonicotinic acid (5.1 g, 32.37 mmol) was dissolved in trifluoroacetic acid (90 mL) and mixed with hydrogen peroxide (50% in water, 12 mL). The resulting solution was heated at 80 °C overnight. Upon completion of the reaction, half of the volume was evaporated under reduced pressure and then diethyl ether (200 mL) was added leading to the precipitation of a beige powder of the title compound (**30**) that was isolated by vacuum filtration (4.92 g, 28.35 mmol, 88%). Mp: 178-183 °C [lit. 175-185 °C].<sup>703</sup> <sup>1</sup>H-NMR (400 MHz, DMSO-*d*<sub>6</sub>) δ<sub>H</sub>: 7.76 (s, 1H, H-3), 7.78 (d, *J*=2.4 Hz, 1H, H-5), 8.55 (d, *J*= 2.4 Hz, 1H, H-6) ppm; <sup>13</sup>C-NMR (100 MHz, DMSO-*d*<sub>6</sub>) δ<sub>C</sub>:125.0 (C-5), 127.6 (C-2), 127.8 (C-3), 141.2 (C-6), 141.3 (C-4), 164.6 (C-7) ppm.

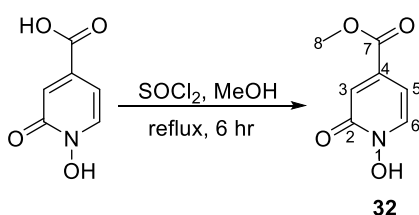
### 10.2.2.2 Synthesis of 1-hydroxy-2-oxo-1,2-dihydropyridine-4-carboxylic acid (**31**)



The product was prepared based upon a literature procedure.<sup>704</sup> A sample of 4-carboxy-2-chloropyridin-1-ium-1-olate (**30**) (3.94 g, 51.51 mmol) was dissolved in aqueous solution of potassium hydroxide (10%, 150 mL). The resulting solution mixture was heated at 70°C

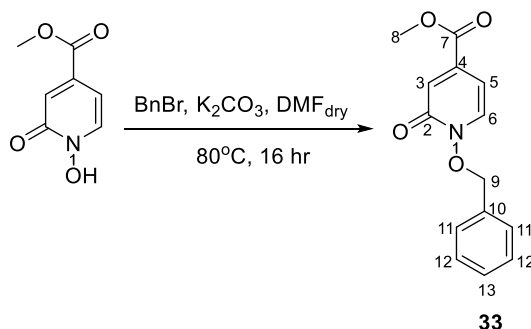
overnight. Then it was allowed to cool at RT and concentrated hydrochloric acid was added until pH 1. White crystals of the title compound (**31**) were precipitated and collected by filtration and allowed to dry in air (7.34, 47.38 mmol, 92%). Mp: 179-182°C. <sup>1</sup>H-NMR (400 MHz, DMSO-*d*<sub>6</sub>) δ<sub>H</sub>: 6.58 (dd, *J* = 2.0 Hz, 7.0 Hz, 1H, H-5), 6.99 (d, *J* = 2.0 Hz, 1H, H-3), 8.04 (d, *J* = 7.0 Hz, 1H, H-6) ppm; <sup>13</sup>C-NMR (100 MHz, DMSO-*d*<sub>6</sub>) δ<sub>C</sub>: 103.5 (C-5), 150.5 (C-3), 136.9 (C-6), 140.2 (C-4), 157.9 (C-2), 166.0 (C-7) ppm. HRMS (ESI) for C<sub>6</sub>H<sub>5</sub>NO<sub>4</sub>; Theoretical [M+H]: 156.0296. Measured [M+H]: 156.0292.

### 10.2.2.3 Synthesis of methyl 1-hydroxy-2-oxo-1,2-dihydropyridine-4-carboxylate (**32**)



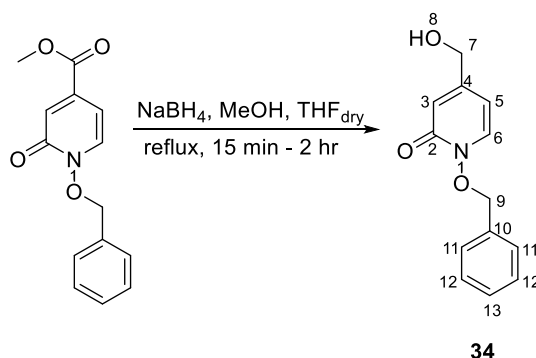
The product was prepared based upon a similar literature procedure.<sup>704,525</sup> In a suspension of 1-hydroxy-2-oxo-1,2-dihydropyridine-4-carboxylic acid (**31**) (7 g, 45.13 mmol, 1 eq) in dry methanol (180 mL), cooled to 0 °C, thionyl chloride (15 mL, 190 mmol, 14.6 eq) was added dropwise over a period of 1 hr. Then resulting mixture was refluxed for 6 hr. Upon completion of the reaction, solvents were evaporated to dryness and the resulting residue was co-evaporated several times with toluene affording the title compound (**32**) as off-white crystals (7.25, 42.56 mmol, 95%). Mp: 190-191°C. <sup>1</sup>H-NMR (400 MHz, DMSO-*d*<sub>6</sub>) δ<sub>H</sub>: 2.46 (s, 3H, H-8), 6.66 (d, *J* = 6.8 Hz, 1H, H-5), 6.99 (br, 1H, H-3), 8.06 (d, *J* = 6.8 Hz, 1H, H-6) ppm; <sup>13</sup>C-NMR (100 MHz, DMSO-*d*<sub>6</sub>) δ<sub>C</sub>: 53.4 (C-8), 103.3 (C-5), 120.5 (C-3), 137.4 (C-6), 138.8 (C-4), 157.8 (C-2), 164.9 (C-7) ppm. HRMS (ESI) for C<sub>7</sub>H<sub>7</sub>NO<sub>4</sub>; Theoretical [M+H]: 170.0453. Measured [M+H]: 170.0443.

#### 10.2.2.4 Synthesis of methyl 1-(benzyloxy)-2-oxo-1,2-dihydropyridine-4-carboxylate (33)



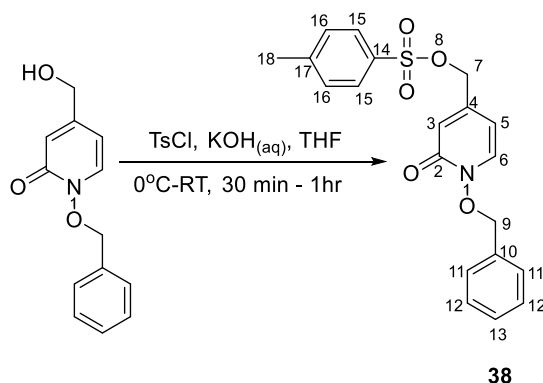
The product was prepared based upon a similar literature procedure with some modifications.<sup>705</sup> In a suspension of potassium carbonate (18 g, 129 mmol, 3 eq.) in dry *N,N*-dimethylformamide (160 mL), methyl 1-hydroxy-2-oxo-1,2-dihydropyridine-4-carboxylate (**32**) (7.25, 42.86 mmol, 1 eq) and benzyl bromide (6.1 mL, 51.43 mmol, 1.2 eq) was added. The resulting solution mixture was stirred at 80°C for 16 hr and then it was allowed to cool at RT. The excess of solvents were removed under reduced pressure and the resulting slurry was taken up in dichloromethane (30 mL) and washed with water (2x25 mL). The organic layer was dried over magnesium sulphate and concentrated under reduced pressure affording the crude product as black oil. Purification by automated flash chromatography column (Isolera);  $R_f = 0.52$  (Petrol Ether 60-80: ethyl acetate, 1:1; UV light) title compound (**33**) as a dark orange oil (6 g, 23.14 mmol, 54%). <sup>1</sup>H-NMR (400 MHz, CDCl<sub>3</sub>)  $\delta_H$ : 3.88 (s, 3H, H-8), 5.28 (s, 2H, H-9), 6.40 (dd,  $J = 2.4$  Hz,  $J = 5.2$  Hz, 1H, H-5), 7.13 (d,  $J = 2.4$  Hz, 1H, H-3), 7.32 (d,  $J = 5.2$  Hz, 1H, H-6), 7.33-7.4 (m, 5H, H-11, H-12, H-13) ppm; <sup>13</sup>C-NMR (100 MHz, CDCl<sub>3</sub>)  $\delta_C$ : 53.0 (C-8), 78.5 (C-9), 103.2 (C-5), 124.6 (C-2), 128.4 (*Ar*), 128.9 (*Ar*), 128.9 (*Ar*), 129.6 (*Ar*), 130.2 (*Ar*), 133.4 (*Ar*), 158.4 (C-2), 164.7 (C-7) ppm. HRMS (ESI) for C<sub>14</sub>H<sub>13</sub>NO<sub>4</sub>; Theoretical [M+H]: 260.0922. Measured [M+H]: 260.0936.

### 10.2.2.5 Synthesis of 1-(benzyloxy)-4-(hydroxymethyl)-1,2-dihydropyridin-2-one (34)



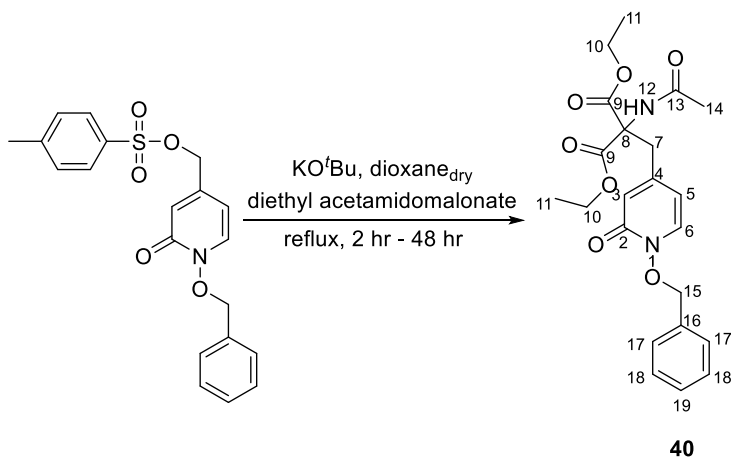
In a suspension of methyl 1-(benzyloxy)-2-oxo-1,2-dihydropyridine-4-carboxylate (**33**) (5 g, 19.28 mmol, 1 eq), in dry tetrahydrofuran (100 mL), sodium borohydride (6 g, 139 mmol, 7.2 eq) was added. The resulting mixture was refluxed for 15 min. Then methanol (12 mL) was added dropwise at refluxing temperature for a period of 2 hr. The reflux was continued for further 20 min and upon completion of the reaction as it was indicated by TLC (SiO<sub>2</sub>, eluent; hexanes: ethyl acetate, 5:2; UV light) the reaction mixture was cooled to 0°C and it was quenched carefully by the addition of a saturated aqueous solution of ammonium chloride (25 mL). The resulting solution was stirred for further 15 min before it was concentrated under reduced pressure. The resulting slurry residue was extracted from dichloromethane (3x50 mL). The combined organic extracts were dried over magnesium sulphate and concentrated under reduced pressure affording compound **34** as a pale yellow oil (4.22 g, 18.25 mmol, 95 %), *R*<sub>f</sub> = 0.35 that solidified on standing. Mp: 49-52°C. <sup>1</sup>H-NMR (400 MHz, CDCl<sub>3</sub>) δ<sub>H</sub>: 4.43 (s, 2H, H-7), 4.64 (s, 1H, H-8), 5.17 (s, 2H, H-9), 5.92 (d, *J* = 5.2 Hz, 1H, H-5), 6.65 (s, 1H, H-3), 7.03 (d, *J* = 5.2 Hz, 1H, H-6), 7.25-7.35 (m, 5H, H-11, H-12, H-13) ppm; <sup>13</sup>C-NMR (100 MHz, CDCl<sub>3</sub>) δ<sub>C</sub>: 62.4 (C-7), 78.7 (C-9), 104.2 (C-5), 117.3 (C-3), 127.0 (*Ar*), 128.5 (*Ar*), 128.8 (*Ar*), 129.5 (*Ar*), 134.7 (C-6) 152.1 (C-4), 158.9 (C-2) ppm. HRMS (ESI) for C<sub>13</sub>H<sub>13</sub>NO<sub>3</sub>; Theoretical [M+H]: 232.0973. Measured [M+H]: 232.0976.

### 10.2.2.6 Synthesis of [1-(benzyloxy)-2-oxo-1,2-dihydropyridin-4-yl]methyl 4-methylbenzene-1-sulfonate (**38**)



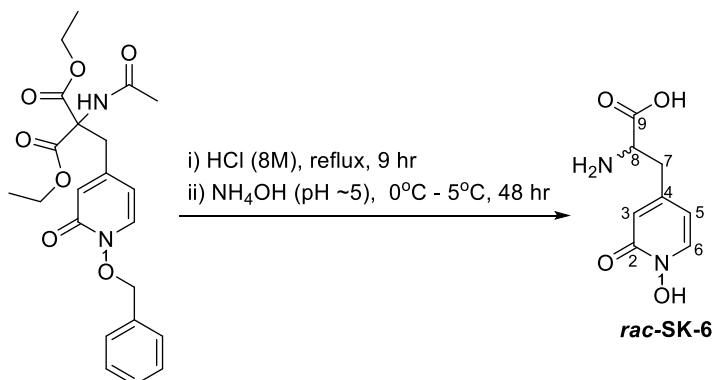
The product was prepared based upon a literature procedure with some modifications.<sup>705</sup> In a suspension of 1-(benzyloxy)-4-(hydroxymethyl)-1,2-dihydropyridin-2-one (**34**) (830 mg, 3.72 mmol, 1 eq) in tetrahydrofuran (10 mL) potassium hydroxide (320 mg, 5.56 mmol, 1.5 eq.) in water (3 mL) was added. The resulting solution was cooled to 0°C and then tosyl chloride (786 mg, 4.12 mmol, 1.2 eq) in tetrahydrofuran (10 mL) was added dropwise over a period of 30 min. The resulting solution was stirred until it reached RT. Upon completion of the reaction as it was indicated by TLC (SiO<sub>2</sub>, eluent; petroleum ether 60:80: ethyl acetate, 1:1; UV light) the reaction was quenched by the addition of saturated aqueous solution of sodium hydrogen carbonate (20 mL) and extracted from ethyl acetate (3x50 mL). The combined organic extracts were dried over magnesium sulphate and concentrated under reduced pressure, affording the title compound (**38**) as a white solid (1.0 g, 2.59 mmol, 70%). Mp: 159-163°C. <sup>1</sup>H-NMR (400 MHz, CDCl<sub>3</sub>) δ<sub>H</sub>: 2.44 (s, 3H, H-18), 4.8 (s, 2H, H-7), 5.24 (s, 2H, H-9), 5.86 (d, *J*= 7.2 Hz, 1H, H-5), 6.52 (s, 1H, H-3), 7.06 (d, *J*= 7.2 Hz, 1H, H-6), 7.25-7.36 (m, 7H, H-11, H-12, H-13, H-16), 7.80 (d, *J*= 8.4 Hz, 2H, H-15) ppm; <sup>13</sup>C-NMR (100 MHz, CDCl<sub>3</sub>) δ<sub>C</sub>: 21.8 (C-18), 68.5 (C-7), 78.6 (C-9), 102.8 (C-5), 120.1 (C-3), 120.2 (*Ar*), 127.1 (*Ar*), 128.1 (*Ar*), 128.7 (*Ar*), 128.9 (*Ar*), 130.2 (C-6), 133.2 (*Ar*), 137.0 (C-4), 140.3 (*Ar*), 146.2 (C-4), 158.2 (C-2) ppm. HRMS (ESI) for C<sub>20</sub>H<sub>19</sub>NO<sub>5</sub>S; Theoretical [M+H]: 386.1062. Measured [M+H]: 386.1039.

**10.2.2.7 Synthesis of 1,3-diethyl 2-[[1-(benzyloxy)-2-oxo-1,2-dihydropyridin-4-yl]methyl]-2-acetamidopropanedioate (40)**



The product was prepared based upon a similar literature procedure with some modifications.<sup>527</sup> In a solution of diethyl acetamidomalonate (820 mg, 3.77 mmol, 1.1 eq) in dry dioxane (30 mL), potassium *tert*-butoxide (460 mg, 4.1 mmol, 1.2 eq) were added and the resulting solution was heated at 60°C for 2 hr. Afterwards, a solution of [1-(benzyloxy)-2-oxo-1,2-dihydropyridin-4-yl]methyl 4-methylbenzene-1-sulfonate (**38**) (1.43 g, 3.5 mmol, 1 eq) in dry dioxane (10 mL) was added dropwise at the same temperature over a period of 2 hr. The resulting solution mixture was allowed to reflux for 48 hr. Upon completion of the reaction, solvents were evaporated to dryness and the resulting slurry was taken up in water and extracted with dichloromethane (3x50 mL). The combined organic extracts were dry with magnesium sulphate and concentrated under reduced pressure affording the title compound (**40**) as a yellow oil (1.01 g, 2.55 mmol, 73%). <sup>1</sup>H-NMR (400 MHz, CDCl<sub>3</sub>) δ<sub>H</sub>: 1.29 (t, *J*= 7.2 Hz, 6H, H-11), 2.02 (s, 3H, H-14), 4.26 (q, *J*= 7.2 Hz, 4H, H-10), 4.53 (s, 2H, H-7), 5.17 (s, 2H, H-15), 5.58 (d, *J*= 6.8 Hz 1H, H-5), 6.63 (s, 1H, H-3), 6.65 (d, *J*= 6.8 Hz, 1H, H-6), 7.24-7.38 (m, 5H, H-17, H-18, H-19) 7.27 (s, 1H, H-12) ppm; <sup>13</sup>C-NMR (100 MHz, CDCl<sub>3</sub>) δ<sub>C</sub>: 14.1 (C-11), 22.4 (C-14), 40.1 (C-7), 60.7 (C-10), 62.5 (C-8), 77.1 (C-9), 114.1 (C-5), 120.0 (C-3), 128.3 (*Ar*), 128.9 (*Ar*), 129.7 (*Ar*), 134.82 (*Ar*), 142.3 (C-6), 150.1 (C-4), 159.3 (C-2), 168.4 (C-9), 170.0 (C-13) ppm. HRMS (ESI) for C<sub>22</sub>H<sub>26</sub>N<sub>2</sub>O<sub>7</sub>; Theoretical [M+H]: 431.1818. Measured [M+H]: 431.1823.

### 10.2.2.8 Synthesis of 2-amino-3-(1-hydroxy-2-oxo-1,2-dihydropyridin-4-yl)propanoic acid (*rac*-SK-6)

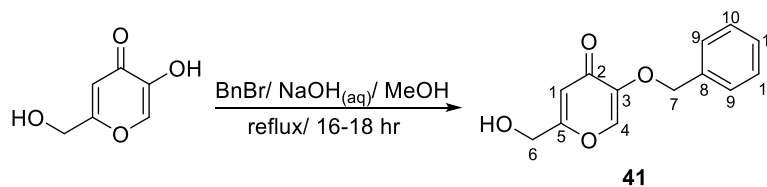


A suspension of 1,3-diethyl 2-[[1-(benzyloxy)-2-oxo-1,2-dihydropyridin-4-yl]methyl]-2-acetamidopropanedioate (**40**) (500 mg, 1.16 mmol) in HCl (8M, 20 mL) was allowed to reflux for 9 hr. Upon completion of the reaction, the solvents were removed under reduced pressure, forming a brown solid which was dissolved in water (20 mL). The solution was treated with charcoal, filtered and the pH of the filtrate was adjusted to 5 by the dropwise addition of conc. ammonium hydroxide. The resulting solution was kept at 5°C for 48 hr until complete precipitation. The titled compound (*rac*-SK-6) was afforded as yellow/brown crystals (53 mg, 0.26 mmol, 23%). Mp: 189-193°C. <sup>1</sup>H-NMR (400 MHz, D<sub>2</sub>O/CF<sub>3</sub>COOD) δ<sub>H</sub>: ppm; 2.93-3.11 (m, 2H, H-7), 4.19 (t, *J* = 4.8 Hz, 1H, H-8), 6.29-6.31 (dd, *J* = 7.2 Hz, *J* = 2.0 Hz, 1H, H-5), 6.48 (d, *J* = 2.0 Hz, 1H, H-3), 7.69 (d, *J* = 7.2 Hz, 1H, H-6) ppm; <sup>13</sup>C-NMR (100 MHz, D<sub>2</sub>O/CF<sub>3</sub>COOD) δ<sub>C</sub>: 35.9 (C-7), 53, 1 (C8), 108.9 (C-5), 115.92 (C-3), 136.3 (C-6), 152.2 (C-4), 158.4 (C-2), 173.3 (C-9) ppm. HRMS (ESI) for C<sub>8</sub>H<sub>10</sub>N<sub>2</sub>O<sub>4</sub>; Theoretical [M+H]: 199.0718. Measured [M+H]: 199.0709.

### 10.3 Synthesis of 3,2-HOPOs

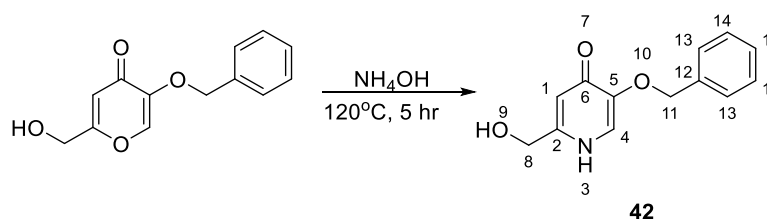
#### 10.3.1 Synthesis of *rac*-SK-5

##### 10.3.1.1 Synthesis of 5-(benzyloxy)-2-(hydroxymethyl)-4H-pyran-4-one (**41**)



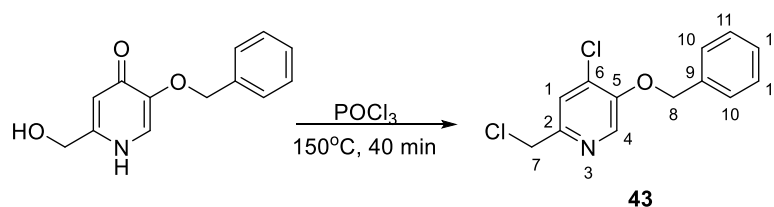
The synthesis was performed according to a modified method previously published.<sup>706</sup> A sample of kojic acid (20 g, 141 mmol, 1 eq) was dissolved in methanol (30 mL) and mixed with a solution of sodium hydroxide (6.2 g, 155 mmol) in water (30 mL). The mixture was heated to reflux for 40 min followed by the dropwise addition of benzyl bromide (19 mL, 155 mmol, 1.1 eq). The mixture was allowed to reflux overnight. Upon completion of the reaction, the solvents were evaporated under reduced pressure to give the crude product as yellowish crystals which were washed with diethyl ether and then with water. The crude product was recrystallized from isopropanol and dried in the air affording the pure product (**41**) as white crystals (29 g, 125 mmol, 87%). Mp: 126-129°C [lit: 128-130°C].<sup>706</sup> <sup>1</sup>H-NMR (400 MHz, DMSO-*d*<sub>6</sub>) δ<sub>H</sub>: 4.30 (s, 2H, H-7), 4.95 (s, 2H, H-6), 6.20 (s, 1H, H-4), 7.25-7.37 (m, 6H, H-1, H-9, H-10, H-11) ppm; <sup>13</sup>C-NMR (100 MHz, DMSO-*d*<sub>6</sub>) δ<sub>C</sub>: 60.3 (C-6), 71.0 (C-7), 111.6 (C-1), 128.6 (*Ar*), 128.7 (*Ar*), 128.9 (*Ar*), 136.6 (C-8), 141.6 (C-4), 147.1 (C-3), 168.6 (C-3), 173.8 (C-2) ppm.

##### 10.3.1.2 Synthesis of 5-(benzyloxy)-2-(hydroxymethyl)-1,4-dihydropyridin-4-one (**42**)



Prepared according to the literature.<sup>498</sup> In a stainless-steel bomb, concentrated ammonium hydroxide (40 mL) was mixed with a sample of 5-(benzyloxy)-2-(hydroxymethyl)-4*H*-pyran-4-one (**41**) (25 g, 107.64 mmol). The resulting mixture was heated at 120°C for 5 hr. Upon completion of the reaction, volatiles were removed under reduced pressure. The resulting slurry was extracted with hot acetone, filtrated and washed with excess of hot acetone affording the titled compound (**42**) as brown crystal (20 g, 86.48 mmol, 80%). M.p: 228-232°C [lit. 230-235°C]<sup>498</sup>. <sup>1</sup>H-NMR (400 MHz, DMSO-*d*<sub>6</sub>) δ<sub>H</sub>: 4.34 (s, 2H, H-8), 5.00 (s, 2H, H-11), 6.23 (s, 1H, H-1), 7.25-7.35 (m, 6H, H-4, H-13, H-14, H-15) ppm; <sup>13</sup>C-NMR (100 MHz, DMSO-*d*<sub>6</sub>) δ<sub>C</sub>: 60.3 (C-8), 70.9 (C-11), 112.0 (C-1), 124.0 (C-4), 128.2 (*Ar*), 128.4 (*Ar*), 128.8 (*Ar*), 137.8 (*Ar*), 147.0 (C-2), 149.7 (C-5), 171.6 (C-6) ppm.

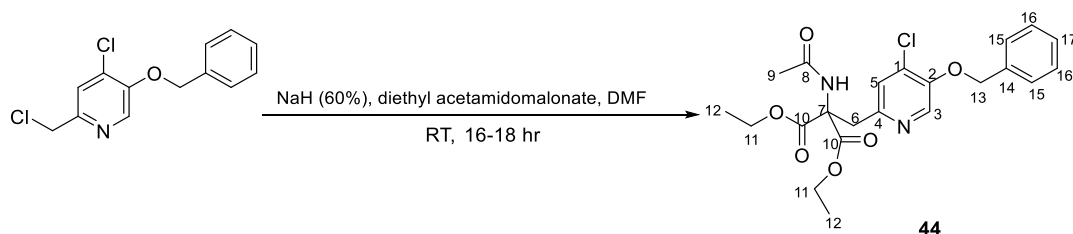
### 10.3.1.3 Synthesis of 5-(benzyloxy)-4-chloro-2-(chloromethyl)pyridine (**43**)



Prepared according to the literature.<sup>498</sup> A sample of 5-(benzyloxy)-2-(hydroxymethyl)-1,4-dihydropyridin-4-one (**42**) (13.84 g, 60 mmol) was added to a suspension of phosphorus oxychloride (42 mL), in portions, thus increasing the temperature of the reaction. After the solution mixture was returned back to RT, it was heated at 150°C for 40 min. Upon completion of the reaction, the mixture was poured into ice-water and stirred vigorously. Addition of more ice into the stirred mixture enhanced the hydrolysis of phosphorous oxychloride and led to the precipitation of the pure product (**43**) (14.5 g, 60 mmol, 87%) as a black solid which was isolated by filtration and left to dry overnight. Mp: 77-79°C [lit: 80-81°C]<sup>498</sup>. <sup>1</sup>H-NMR (400 MHz, DMSO-*d*<sub>6</sub>) δ<sub>H</sub>: 4.34 (s, 2H, H-7), 5.00 (s, 2H, H-8), 7.28-7.44 (m, 5H, H-10, H-11, H-12), 7.75 (s, 1H, H-1), 8.51 (s, 1H, H-4) ppm; <sup>13</sup>C-NMR (100 MHz, DMSO-*d*<sub>6</sub>) δ<sub>C</sub>: 45.4 (C-

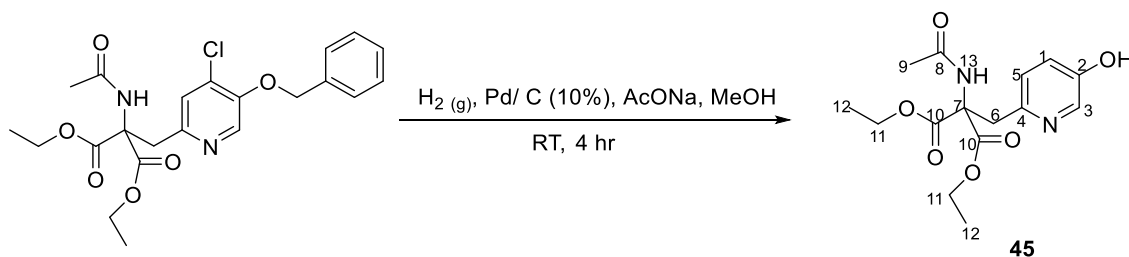
7), 71.5 (C-8), 125.7 (C-1), 128.2 (*Ar*), 128.4 (*Ar*), 128.8 (*Ar*), 129.1 (C-6), 133.1 (C-2), 135.5 (*Ar*), 136.2 (C-4), 149.4 (C-5) ppm.

#### 10.3.1.4 Synthesis of 1,3-diethyl-2-[[5-(benzyloxy)-4-chloropyridin-2-yl]methyl]-2-acetamidopropane dioate (**44**)



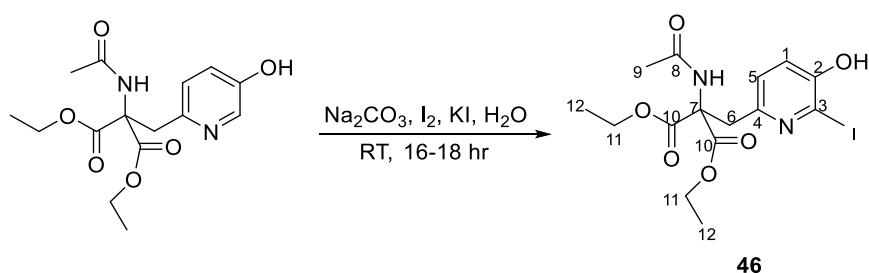
Prepared according to the literature.<sup>498</sup> In dry *N,N*-dimethylformamide (62 mL) sodium hydride (60% in mineral oil, 2.16 g, 54 mmol, 1.7 eq) was added. The solution was stirred at RT and then diethyl acetamidomalonate (11.25 g, 51.8 mmol, 1.7 eq) was added in portion evolving hydrogen gas. Upon ceasing of hydrogen gas evolution, 5-(benzyloxy)-4-chloro-2-(chloromethyl)pyridine (**43**) (13.84 g, 51.6 mmol, 1 eq) was added. The resulting solution mixture was stirred overnight at RT. Upon completion of the reaction, acetic acid (25 mL) was added to neutralise the reaction mixture which was then concentrated, under reduced pressure, and the resulting syrup was dissolved in water (200 mL) and extracted with diethyl ether (2 x 80 mL). The combined organic extracts were washed with brine, dried over magnesium sulphate and concentrated under reduced pressure, affording the titled compound (**44**) as white crystals which was recrystallized from ethanol (22.7 g, 50.6 mmol, 98%). Mp: 119-122°C [Lit=118-120°C]<sup>498</sup>. <sup>1</sup>H-NMR (400 MHz, DMSO-*d*<sub>6</sub>)  $\delta_H$ : 1.18 (t, *J*= 7.2 Hz, 6H, H-12), 1.82 (s, 3H, H-9), 3.50 (s, 2H, H-6), 4.08 (q, *J*= 7.2 Hz, 4H, H-11), 5.25 (s, 2H, H-13), 7.13 (1H, s, NH), 7.30-7.44 (m, 5H, H-15, H-16, H-17), 8.02 (s, 1H, H-5), 8.34 (s, 1H, H-3) ppm; <sup>13</sup>C-NMR (100 MHz, DMSO-*d*<sub>6</sub>)  $\delta_C$ : 14.3 (C-12), 22.5 (C-9), 40.1 (C-6), 62.3 (C-11), 66.6 (C-13), 71.1 (C-7), 125.8 (C-5), 128.2 (C-1), 128.7 (*Ar*), 129.1 (*Ar*), 131.3 (*Ar*), 136.0 (*Ar*), 136.6 (C-3), 149.6 (C-2), 149.9 (C-4), 167.5 (C-10), 169.9 (C-8) ppm.

### 10.3.1.5 Synthesis of 1,3-diethyl 2-acetamido-2-[(5-hydroxypyridin-2-yl) methyl] propanedioate (45)



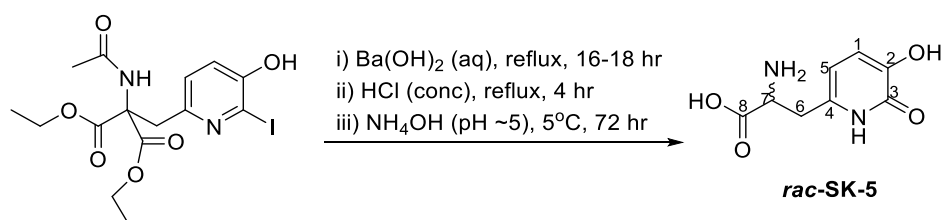
Prepared according to the literature.<sup>498</sup> A suspension of diethyl 2-[(5-(benzyloxy)-4-chloropyridin-2-yl)methyl]-2-acetamidopropanedioate (**44**) (6 g, 13.36 mmol, 1 eq) in methanol (75 mL), sodium acetate (6 g, 73.14 mmol, 5.5eq) and a catalytic amount of 10% Pd/C was stirred vigorously under hydrogen atmosphere. Upon completion of the reaction (4 hr), as indicated by TLC (SiO<sub>2</sub>, ethyl acetate 100%), the solution mixture was filtered over a pad of Celite, washed with methanol and diluted with water (150 mL) forming the titled compound (**45**) as white crystals which were isolated by filtration (2.94 g, 9.06 mmol, 68%). Mp: 152-154°C [Lit: 150-153°C].<sup>498</sup> <sup>1</sup>H-NMR (400 MHz, DMSO-*d*<sub>6</sub>)  $\delta$ <sub>H</sub>: 1.1 (t, *J* = 7.2 Hz, 6H, H-12), 1.81 (s, 3H, H-9), 3.43 (s, 2H, H-6), 4.07 (q, *J* = 7.2 Hz, 4H, H-11), 6.78 (d, *J* = 8.8 Hz, 1H, H-5), 6.99 (dd, *J* = 3.2 Hz, *J* = 8.8 Hz, 1H, H-1), 7.87 (s, 1H, H-13), 7.91 (d, *J* = 3.2 Hz, 1H, H-3) ppm; <sup>13</sup>C-NMR (100 MHz, DMSO-*d*<sub>6</sub>)  $\delta$ <sub>C</sub>: 13.8 (C-12), 23.2 (C-9), 42.3 (C-6), 63.5 (C-11), 65.2 (C-7), 124.1 (C-1), 128.0 (C-5), 137.9 (C-3), 147.5 (C-4), 153.0 (C-2), 166.2 (C-10), 170.4 (C-8) ppm.

### 10.3.1.6 Synthesis of 1,3-diethyl-2-acetamido-2-[(5-hydroxy-6-iodopyridin-2-yl)methyl] propanedioate (46)



Prepared according to the literature.<sup>498</sup> A sample of diethyl 2-acetamido-2-[(5-hydroxypyridin-2-yl)methyl] propanedioate (2.5 g, 7.7 mmol, 1 eq) (**45**) was dissolved in water (70 mL) containing sodium carbonate (1.54 g, 13.97 mmol, 1.8 eq). A solution of iodine (1.92 g, 15.13 mmol, 2 eq) and potassium iodide (2.32 g, 13.97 mmol) in water (50 mL) was added dropwise to the previous solution. The resulting mixture was stirred overnight at RT. Upon completion of the reaction, the solution mixture was neutralized with glacial acetic acid (5 mL), leading to the precipitation of the title compound, which was collected by filtration, washed with water and dried at 90°C. The title compound (**46**) was obtained as a white powder (3.39 g, 7.54 mmol, 98%). M.p: 200-203°C. [Lit: 196-197°C]<sup>498</sup>. <sup>1</sup>H-NMR (400 MHz, DMSO-*d*<sub>6</sub>)  $\delta$ <sub>H</sub>: 1.1 (t, *J* = 7.2 Hz, 6H, H-12), 1.81 (s, 3H, H-9), 3.43 (s, 2H, H-6), 4.07 (q, *J* = 7.2 Hz, 4H, H-11), 6.78 (d, *J* = 8.8 Hz, 1H, H-5), 6.99 (dd, *J* = 3.2 Hz, *J* = 8.8 Hz, 1H, H-1), 7.87 (s, 1H, -NH), 7.91 (d, *J* = 3.2 Hz, 1H, -OH) ppm; <sup>13</sup>C-NMR (100 MHz, DMSO-*d*<sub>6</sub>)  $\delta$ <sub>C</sub>: 14.3 (C-12), 22.6 (C-9), 39.9 (C-6), 66.8 (C-11), 69.0 (C-7) 122.8 (*Ar*), 125.1 (*Ar*), 137.6 (*Ar*), 146.5 (*Ar*), 152.8 (*Ar*), 167.7 (C-10), 169.7 (C-8) ppm.

### 10.3.1.7 Synthesis of *rac*-2-amino-3-(5-hydroxy-6-oxo-1,6-dihydropyridin-2-yl)propanoic acid (*rac*-SK-5)

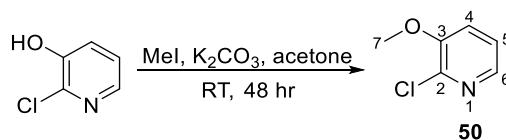


Prepared according to the literature.<sup>498</sup> A mixture of barium hydroxide (7.1 g, 41.43 mmol, 4.7 eq) and diethyl 2-acetamido-2-[(5-hydroxy-6-iodopyridin-2-yl)methyl] propanedioate (**46**) (4 g, 8.88 mmol, 1 eq) in water (70 mL) was refluxed for 24 hr. Upon completion of the reaction, the resulting barium salt was collected by filtration and refluxed with concentrated HCl (50

mL) for 1 hr. Once again, upon completion of the reaction, the solution mixture was evaporated to dryness yielding a yellowish salt of the crude product which was dissolved in water (20 mL), treated with charcoal and filtered. The pH of the filtrates was adjusted to 5.0 by addition of concentrated ammonia and cooled at 5°C for 72 hr leading to precipitation of the titled compound appearing as white crystals (1.67 g, 8.44 mmol, 95%). M.p: 193-195°C. [Lit: 196-197°C]<sup>498</sup>. <sup>1</sup>H-NMR (400 MHz, DMSO-*d*<sub>6</sub>) δ<sub>H</sub>: 2.86-2.99 (m, 2H, H-6), 4.07 (t, J= 7.6 Hz, 1H, H-7), 6.06 (d, J= 7.2 Hz, 1H, H-5), 6.75 (d, J= 7.2 Hz, 1H, H-1) ppm; <sup>13</sup>C-NMR (100 MHz, DMSO-*d*<sub>6</sub>) δ<sub>C</sub>: 32.4 (C-6), 52.0 (C-7), 110.8 (C-5), 121.2 (C-1), 131.3 (C-2), 144.7 (C-4), 159.0 (C-3), 170.3 (C-8) ppm. HRMS (ESI) for C<sub>8</sub>H<sub>10</sub>N<sub>2</sub>O<sub>4</sub>; Theoretical [M+H]: 199.0718. Measured [M+H]: 199.0711.

### 10.3.2 Synthesis of *rac*-SK-7

#### 10.3.2.1 Synthesis of 2-chloro-3-methoxy pyridine (**50**)

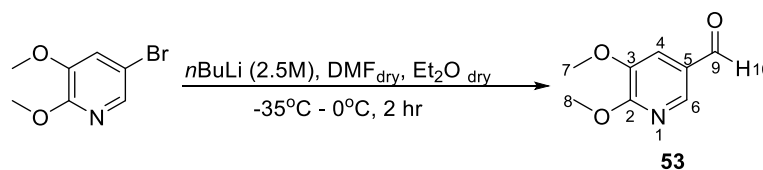


The synthesis was performed according to a modified method previously published.<sup>538</sup> In a solution of 2-chloro-3-hydroxy pyridine (20 g, 125.36 mmol, 1 eq) in acetone (1 L), iodomethane (11 mL, 169.23 mmol, 1.35 eq) and potassium carbonate (35 g, 253.24 mmol, 2 eq) were added. The reaction was stirred for 48 hr at RT and upon completion of the reaction as it was indicated by TLC (SiO<sub>2</sub>, eluent; ethyl acetate: petrol ether 60:80, 1:1; UV light) (R<sub>f</sub> = 0.73) water (100 mL) and ethyl acetate (200 mL) was added and the aqueous phase was extracted with ethyl acetate (3x100 mL). The combined organic extracts were, washed with brine, dried over anhydrous magnesium sulphate and concentrated under reduced pressure affording the titled compound (**50**) as brown oil (17.63 g, 122.8 mmol, 98%). <sup>1</sup>H-NMR (400 MHz, CDCl<sub>3</sub>) δ<sub>H</sub>: 3.91 (s, 3H, H-7), 7.18 (s (br), 2H, H-4, H-5), 7.98 (s (br), 1H, H-6) ppm; <sup>13</sup>C-NMR (100 MHz, CDCl<sub>3</sub>) δ<sub>C</sub>: 56.0 (C-7), 122.0 (C-5), 122.39 (C-4), 140.2 (C-2), 141.5



The synthesis was performed according to a modified method previously published.<sup>540</sup> In a solution mixture of dichloromethane-saturated sodium bicarbonate (1:2, 250 mL: 133 mL), 2,3- dimethoxypyridine (**51**) (8.34 g, 59.93 mmol, 1 eq) was added and cooled to 0°C. Then bromine (3.1 mL, 59.93 mmol, 1eq) was added and the solution mixture was stirred for 2 hr at RT. The process of the reaction was monitor by TLC (SiO<sub>2</sub>, eluent; petrol ether 60:80: ethyl acetate, 6:4; UV light) and after two hours another 0.5 eq of bromine was added. After 4 hr the starting material had been consumed and the reaction was quenched by the addition of sodium thiosulphate (20 g) and extracted with dichloromethane (3x100 mL). The combined organic extracts were dried over anhydrous magnesium sulphate and concentrated under reduced pressure affording a brown oil a non-separable mixture (11.25 g, 51.59 mmol). <sup>1</sup>H-NMR (of the major product) (**52**) (400 MHz, CDCl<sub>3</sub>) δ<sub>H</sub>: 3.82 (s, 3H, H-7), 3.97 (s, 3H, H-8), 7.09 (d, *J*= 1.6 Hz, 1H, H-4), 7.73 (d, *J*= 1.6 Hz, 1H, H-6) ppm; <sup>13</sup>C-NMR (100 MHz, CDCl<sub>3</sub>) δ<sub>C</sub>: 52.7 (C-7), 55.8 (C-8), 113.1 (C-5), 123.2 (C-4), 140.5 (C-6), 145.91 (C-3), 154.34 (C-2) ppm.

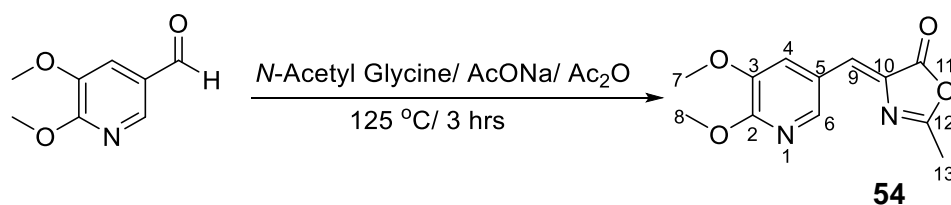
#### 10.3.2.4 Synthesis of 5,6-dimethoxypyridine-3-carbaldehyde (**53**)



The synthesis was performed according to a modified method previously published.<sup>708</sup> In a solution of 5-bromo-2,3-dimethoxypyridine (**52**) (10 g, 45.86 mmol, 1 eq) in anhydrous diethyl ether (50 mL), under nitrogen atmosphere and cooled down to -35°C, *n*BuLi (2.5 M in hexanes) (22 mL, 55.03 mmol, 1.2 eq) was added. The resulting solution was stirred until a brown precipitate formed. Then anhydrous *N,N*- dimethylformamide (9.9 mL, 128.4 mmol, 2.8 eq) was added slowly and the mixture was allowed to stir until the temperature reached 0°C. Upon completion of the reaction as it was indicated by TLC (SiO<sub>2</sub>, eluent; petrol ether 60:80: diethyl ether, 6:4; UV light) *R<sub>f</sub>* (0.85) the reaction was quenched carefully by the

addition of aqueous solution of ammonium chloride (5%, 50 mL). Then the aqueous layer was extracted with dichloromethane (3x100 mL). The combined organic extracts were washed with water, brine, dried over anhydrous magnesium sulphate and concentrated under reduced pressure affording the crude compound as orange oil which was solidified on standing. The solid was purified by recrystallization from methanol forming the title compound (**53**) as pale yellow crystals (4.06 g, 24.3 mmol, 53%). Mp: 125-127°C [lit: 123°C].<sup>708</sup> <sup>1</sup>H-NMR (400 MHz, CDCl<sub>3</sub>) δ<sub>H</sub>: 3.94 (s, 3H, H-7), 4.12 (s, 3H, H-8), 7.48 (s, 1H, H-4), 8.21 (s, 1H, H-6), 9.94 (s, 1H, H-4) ppm; <sup>13</sup>C-NMR (100 MHz, CDCl<sub>3</sub>) δ<sub>C</sub>: 52.7 (C-7), 56.4 (C-7), 120.7 (C-4), 125.4 (C-5), 141.6 (C6), 146.0 (C-3), 157.1 (C-2), 190.3 (C-9) ppm.

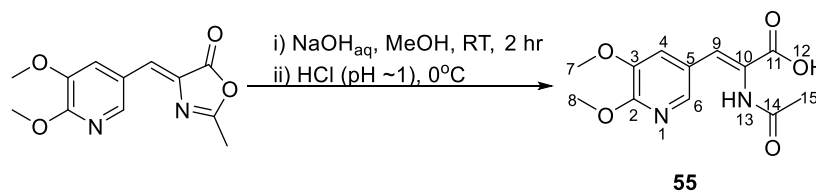
#### 10.3.2.5 Synthesis of 4-[(5,6-dimethoxypyridin-3-yl)methylidene]-2-methyl-4,5-dihydro-1,3-oxazol-5-one (**54**)



The synthesis was performed according to a modified method previously published.<sup>505</sup> A mixture of 5,6-dimethoxypyridine-3-carbaldehyde (**53**) (2 g, 11.96 mmol, 1eq), *N*-acetyl glycine (1.82 g, 15.6 mmol, 1.3 eq) and sodium acetate (1.3 g, 15.6 mmol, 1.3 eq) in acetic anhydride (10 mL) was heated at 125°C for three hours. Upon completion of the reaction, ice (~50 g) was added into the solution mixture and stirred vigorously until a yellow precipitate formed. The crude product was collected by filtration and washed with excess of diethyl ether. Then it was recrystallized from methanol affording the title compound (**54**) as pale yellow crystals (2.55 g, 9.57 mmol, 80%). Mp: 158-160°C. <sup>1</sup>H-NMR (400 MHz, CDCl<sub>3</sub>) δ<sub>H</sub>: 2.38 (s, 3H, H-13), 3.92 (s, 3H, H-7), 4.06 (s, 3H, H-8), 7.07 (s, 1H, H-9), 8.04 (d, *J* = 1.6 Hz, 1H, H-4), 8.26 (d, *J* = 1.6 Hz, 1H, H-6) ppm; <sup>13</sup>C-NMR (100 MHz, CDCl<sub>3</sub>) δ<sub>C</sub>: 23.3 (C-13), 52.5 (C-7), 55.8 (C-8), 121.4 (C-4), 121.7 (C-5), 131.8 (C-9), 131.3 (C-10), 144.0 (C-6), 147.2 (C-3),

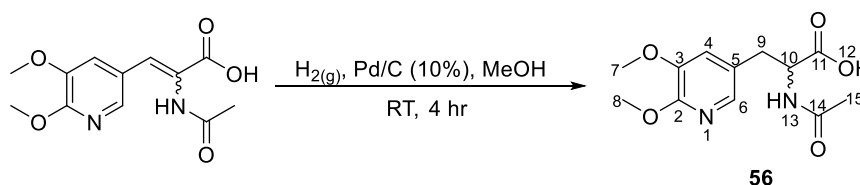
154.5 (C-2), 162.5 (C-12), 166.23 (C-11) ppm. HRMS (ESI) for C<sub>12</sub>H<sub>12</sub>N<sub>2</sub>O<sub>4</sub>; Theoretical [M+H]: 249.0797. Measured [M+H]: 249.0785.

### 10.3.2.6 Synthesis of *rac*-3-(5,6-dimethoxypyridin-3-yl)-2-acetamidoprop-2-enoic acid (**55**)



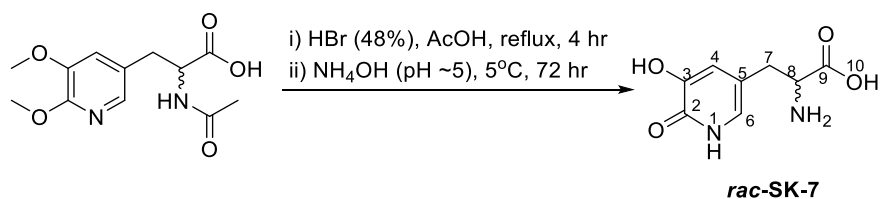
The synthesis was performed according to a modified method previously published.<sup>505</sup> In a suspension of 4-[(5,6-dimethoxypyridin-3-yl)methylidene]-2-methyl-4,5-dihydro-1,3-oxazol-5-one (**54**) (1.5 g, 6.04 mmol, 1 eq) in methanol (30 mL) sodium hydroxide (290 mg, 7.25 mmol, 1.2 eq) in water (final pH~8-9) was added. The resulting solution was stirred at RT for 2 hours before methanol was removed under reduced pressure. The resulting aqueous solution was acidified to pH 1 and cooled at 0°C for maximal precipitation. The resulting crystals were collected by filtration and washed with cold ether affording the title compound (**55**) as beige crystals (1.53g, 5.74 mmol, 95%). Mp: 192°C. <sup>1</sup>H-NMR (400 MHz, DMSO-*d*<sub>6</sub>) δ<sub>H</sub>: 1.95 (s, 3H, H-15), 3.74 (s, 3H, H-7), 3.84 (s, 3H, H-8), 7.19 (s, 1H, H-9), 7.50 (s, 1H, H-4), 7.90 (s, 1H, H-6), 9.48 (s, 1H, H-13) ppm; <sup>13</sup>C-NMR (100 MHz, DMSO-*d*<sub>6</sub>) δ<sub>C</sub>: 23.2 (C-15), 52.5 (C-7), 22.8 (C-8), 119.2 (C-4), 122.9 (C-5), 125.8 (C-9), 126.8 (C-10), 141.5 (C-6), 145.2 (C-3), 154.4 (C-2), 166.5 (C-11), 168.5 (C-14) ppm. HRMS (ESI) for C<sub>12</sub>H<sub>14</sub>N<sub>2</sub>O<sub>5</sub>; Theoretical [M+H]: 267.0980. Measured [M+H]: 267.0969.

### 10.3.2.7 Synthesis of *rac*-3-(5,6-dimethoxypyridin-3-yl)-2-acetamidopropanoic acid (**56**)



In a suspension of *rac*-(2*Z*)-3-(5,6-dimethoxypyridin-3-yl)-2-acetamidoprop-2-enoic acid (**55**) (1 g, 3.75 mmol, 1 eq) in methanol (30 mL) a catalytic amount of Pd/C (10%) was added. The resulting solution was stirred under hydrogen atmosphere for 4 hours. Upon completion of the reaction, as it was indicated by <sup>1</sup>H-NMR, Celite was added into the solution mixture and filtrated through a pad of Celite which was then washed sequentially with ethyl acetate and methanol. The filtrates were concentrated under reduced pressure affording the title compound (**56**) as beige crystals (633 mg, 2.36 mmol, 63%). Mp: 201-203°C. <sup>1</sup>H-NMR (400 MHz, DMSO-*d*<sub>6</sub>) δ<sub>H</sub>: 1.79 (s, 3H, H-15), 2.71-2.80 (m, 1H, H-9), 2.95-2.99 (m, 1H, H-9), 3.75 (s, 3H, H-7), 3.83 (s, 3H, H-8), 4.35-4.40 (m, 1H, H-10), 7.17 (s, 1H, H-4), 7.50 (s, 1H, H-6), 8.13 (d, *J*= 8.0 Hz, 1H, H-13) ppm; <sup>13</sup>C-NMR (100 MHz, DMSO-*d*<sub>6</sub>) δ<sub>C</sub>: 22.9 (C-15), 34.1 (C-9), 52.8 (C-7), 55.8 (C-7), 56.07 (C-10), 120.6 (C-4), 124.9 (C-5), 138.8 (C-6), 144.6 (C-3), 151.7 (C-2), 170.8 (C-14), 172.9 (C-11) ppm. HRMS (ESI) for C<sub>12</sub>H<sub>16</sub>N<sub>2</sub>O<sub>5</sub>; Theoretical [M+H]: 269.1137. Measured [M+H]: 269.1168.

### 10.3.2.8 Synthesis of *rac*-2-amino-3-(5-hydroxy-6-oxo-1,6-dihydropyridin-3-yl)propanoic acid (*rac*-SK-7)



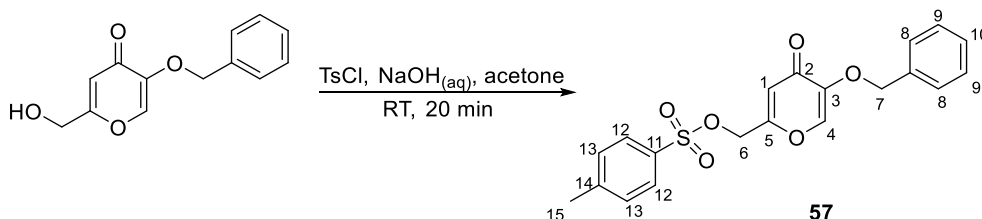
In a solution mixture of HBr (48%, 15 mL) and glacial acetic acid (15 mL), *rac*-3-(5,6-dimethoxypyridin-3-yl)-2-acetamidopropanoic acid (**56**) (500 mg, 1.86 mmol). The resulting solution was stirred under reflux for 4 hr. Upon completion of the reaction the reaction mixture concentrated under reduced pressure, and the resulting crystals were taken up in water and the pH was adjusted to 5 by the dropwise addition of ammonium hydroxide. The final solution was kept at 5°C for 72 hr and the pure off white crystals formed of the titled compound (*rac*-SK-7) were collect by filtration (178 mg, 0.74 mmol, 40%). Mp: 199°C. <sup>1</sup>H-

NMR (400 MHz, D<sub>2</sub>O/CF<sub>3</sub>COOD 8:2):  $\delta_{\text{H}}$ : 2.91-3.11 (m, 1H, H-7), 2.95-2.99 (m, 1H, H-7), 4.31 (s, 1H, H8), 6.72 (s, 1H, H-4), 6.85 (s, 1H, H-6) ppm; <sup>13</sup>C-NMR (100 MHz, D<sub>2</sub>O/CF<sub>3</sub>COOD 8:2):  $\delta_{\text{C}}$ : 32.3 (C-7), 53.1 (C-8), 112.4 (C-5), 129.3 (C-4), 132.8 (C-6), 147.6 (C-3), 158.5 (C-2), 172.6 (C-9) ppm. HRMS (ESI) for C<sub>8</sub>H<sub>10</sub>N<sub>2</sub>O<sub>4</sub>; Theoretical [M+H]: 199.0718. Measured [M+H]: 199.0713.

## 10.4 Synthesis of 3, 4-HOPOS

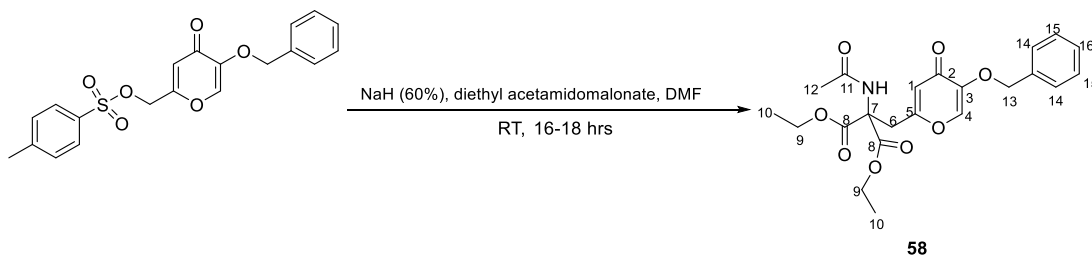
### 10.4.1 Synthesis of *rac*-SK-1 and *rac*-SK-2

#### 10.4.1.1 Synthesis of [5-(benzyloxy)-4-oxo-4H-pyran-2-yl]methyl 4-methylbenzene-1-sulfonate (**57**)



The synthesis was performed according to a modified method previously published.<sup>543</sup> A sample of 5-(benzyloxy)-2-(hydroxymethyl)-4H-pyran-4-one (**41**) (25 g, 108 mmol, 1 eq) was dissolved in acetone (350 mL) and mixed by vigorous stirring with tosyl chloride (21 g, 110 mmol, 1.1 eq) at RT, followed by the addition of a solution of sodium hydroxide (4.3g, 72 mmol) in water (18 mL). The mixture was stirred at RT for 20 min. The crude product was precipitated upon addition of water (50 mL). The crude product was purified by recrystallization from methanol/water affording the pure compound (**57**) as pale yellow crystals (38 g, 98 mmol, 94%). Mp: 111-114°C [lit: 112°C]<sup>543</sup>. <sup>1</sup>H-NMR (400 MHz, DMSO-*d*<sub>6</sub>)  $\delta_{\text{H}}$  2.47 (s, 3H, H-15), 4.77 (s, 2H, H-6), 5.02 (s, 2H, H-7), 6.33 (s, 1H, H-1), 7.25-7.36 (m, 7H, H-8, H-9, H-10, H-13), 7.75 (s, 1H, H-1), 7.76 (d, *J* = 8 Hz, 2H, H-12) ppm; <sup>13</sup>C-NMR (100 MHz, DMSO-*d*<sub>6</sub>)  $\delta_{\text{C}}$  = 21.8 (C-15), 66.0 (C-6), 71.9 (C-7), 115.5 (C-1), 127.8 (*Ar*), 128.1 (*Ar*), 128.6 (*Ar*), 128.9 (*Ar*), 130.2 (*Ar*), 132.3 (*Ar*), 135.5 (*Ar*), 141.5 (C-4), 145.8 (*Ar*), 147.4 (C-3), 158.7 (C-5), 174.0 (C-2) ppm. HRMS (ESI) for C<sub>20</sub>H<sub>18</sub>O<sub>6</sub>S; Theoretical [M+H]: 387.0902. Measured [M+H]: 387.0890.

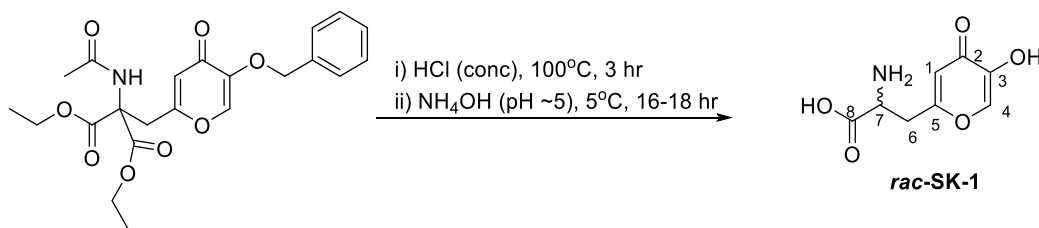
#### 10.4.1.2 Synthesis of 1,3-diethyl 2-[[5-(benzyloxy)-4-oxo-4H-pyran-2-yl]methyl]-2-acetamidopropanedioate (**58**)



The synthesis was performed according to a modified method previously published.<sup>497</sup> In a solution of diethyl acetamidomalonate (10 g, 46 mmols) in dry *N,N*-dimethyl formamide (70 mL), sodium hydride (60% in mineral oil, 2 g, 50 mmol) was added in portions. Upon the evolution of hydrogen gas, a sample of [5-(benzyloxy)-4-oxo-4H-pyran-2-yl]methyl 4-methylbenzene-1-sulfonate (**57**) (8.5 g, 22 mmol) was added to the solution mixture and the final mixture was stirred overnight protected from moisture at RT. Upon completion of the reaction, the solvents were removed under reduced pressure forming a brown residue which was mixed with water (100 mL) and stirred vigorously forming the crude product as a brown solid which was filtered and left to dry overnight. The crude product was purified by recrystallization (acetone/petroleum ether 60:80) affording the pure compound (**58**) as light orange crystals (9.21 g, 21mmol, 95 %). Mp: 117-120°C [lit: 117-118°C].<sup>17</sup> <sup>1</sup>H-NMR (400 MHz, DMSO-*d*<sub>6</sub>) δ<sub>H</sub> 1.18 (t, *J*= 7.2 Hz, 6H, H-10), 1.92 (s, 3H, H-12), 3.35 (s, 2H, H-6), 4.85 (s, 2H, H-13), 4.14 (q, *J*<sub>1</sub>= 7.2 Hz, 4H, H-9), 6.05 (s, 1H, H-1), 7.35-7.37 (m, 5H, H-14, H-15, H-16), 8.08 (s, 1H, H-4), 8.45 (s, 1H, -NH) ppm; <sup>13</sup>C-NMR (100 MHz, DMSO-*d*<sub>6</sub>) δ<sub>C</sub>= 14.3 (C-10), 22.4 (C-12), 31.2 (C-6), 62.8 (C-9), 65.6 (C-7), 71.0 (C-13), 116.1 (C-4), 128.7 (*Ar*), 128.8 (*Ar*), 129.0 (*Ar*), 136.5 (*Ar*), 142.0 (C-1), 147.2 (C-3), 163.2 (C-8), 167.0 (C-11), 170.4 (C-5), 173.4 (C-2) ppm. HRMS (ESI) for C<sub>22</sub>H<sub>25</sub>NO<sub>8</sub>; Theoretical [M+H]: 432.1658. Measured [M+H]: 432.1656.

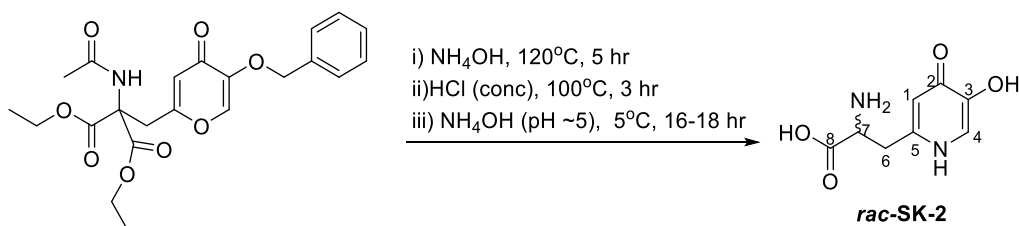
### 10.4.1.3 Synthesis of 2-amino-3-(5-hydroxy-4-oxo-4H-pyran-2-yl)propanoic acid

#### (*rac*-SK-1)



A solution of conc. hydrochloric acid (40 mL) and 1, 3-diethyl 2-[[5-(benzyloxy)-4-oxo-4H-pyran-2-yl] methyl]-2-acetamidopropanedioate (**58**) (5.1 g, 11.84 mmol) was refluxed at 100°C for 3 hr. Upon completion of the reaction, the solvents were removed under reduced pressure, forming a brown solid which was dissolved in water (20 mL). The solution was treated with charcoal, filtered and the pH of the filtrate was adjusted to 5 by the dropwise addition of conc. ammonium hydroxide. The resulting solution was kept overnight at 5°C and white crystals precipitated. The crystals were collected, washed with water, acetone, light petroleum and dried in the air affording the pure compound (***rac*-SK-1**) as white crystals (2.10 g, 10.54 mmol, 89%), Mp: 116-117°C. <sup>1</sup>H-NMR (400 MHz, D<sub>2</sub>O/CF<sub>3</sub>COOD 8:2) δ<sub>H</sub>: 2.63-2.75 (m, 2H, H-6), 3.84 (t, J= 6.8 Hz, 1H, H-7), 5.97 (s, 1H, H-1), 7.45 (1H, s, H-4) ppm; <sup>13</sup>C-NMR (100 MHz, D<sub>2</sub>O/CF<sub>3</sub>COOD 8:2): δ<sub>C</sub>= 32.9 (C-6), 50.0 (C-7), 116.4 (C-1), 119.3 (C-4), 142.5 (C-3), 144.2 (C-5), 169.4 (C-8), 175.5 (C-2) ppm. HRMS (ESI) for C<sub>8</sub>H<sub>9</sub>NO<sub>5</sub>; Theoretical [M+H]: 200.0558. Measured [M+H]:200.0550.

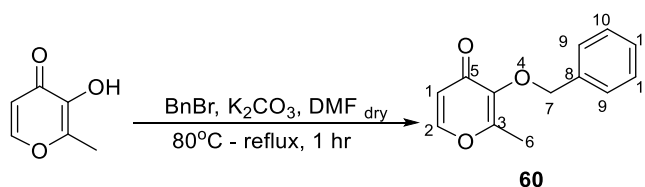
#### 10.4.1.3.1 Synthesis of 2-amino-3-(5-hydroxy-4-oxo-1,4-dihydropyridin-2-yl)propanoic acid (*rac*-SK-2)



Prepared according to the literature.<sup>497</sup> A portion of 1,3-diethyl 2-([5-(benzyloxy)-4-oxo-4H-pyran-2-yl]methyl)-2-acetamidopropanedioate (**58**) (4.2 g, 9.73 mmol) was mixed with a solution of conc. ammonium hydroxide (25 mL) and the mixture was heated for 5 hr in a stainless steel bomb at 120°C. Upon completion of the reaction the mixture was evaporated to dryness and the resulting solid was dissolved in a solution of conc. HCl (30 mL). The resulting mixture was refluxed at 100 °C for 3 hr. The solvents were evaporated and the resulting crystals were dissolved in water (20 mL). The solution was treated with charcoal, filtered and the pH was adjusted to 5 using ammonia solution. The resulting solution was kept overnight at 5 °C forming white crystals. The crystals were collected, washed with water, acetone, and light petroleum and dried affording the pure compound (*rac*-**SK-2**) as white crystals (1.76 g, 8.9 mmol, 91%) Mp: >250 °C [lit: >250°C].<sup>497</sup> <sup>1</sup>H-NMR (400 MHz, D<sub>2</sub>O/CF<sub>3</sub>COOD 8:2): δ<sub>H</sub> 2.73-2.75 (m, 2H, H-6), 3.71 (t, *J* = 6.8 Hz, 1H, H-7), 6.52 (s, 1H, H-1), 7.3 (s, 1H, H-4) ppm; <sup>13</sup>C-NMR (100 MHz, D<sub>2</sub>O/CF<sub>3</sub>COOD): δ<sub>C</sub> 30.1 (C-6), 51.2 (C-7), 113.6 (C-1), 116.4 (C-4), 142.5 (C-3), 143.4 (C-5), 168.7 (C-8), 169.0 (C-2) ppm. HRMS (ESI) for C<sub>8</sub>H<sub>10</sub>N<sub>2</sub>O<sub>4</sub>; Theoretical [M+H]: 197.0718. Measured [M+H]: 197.0699.

## 10.4.2 Synthesis of *D*-SK-4

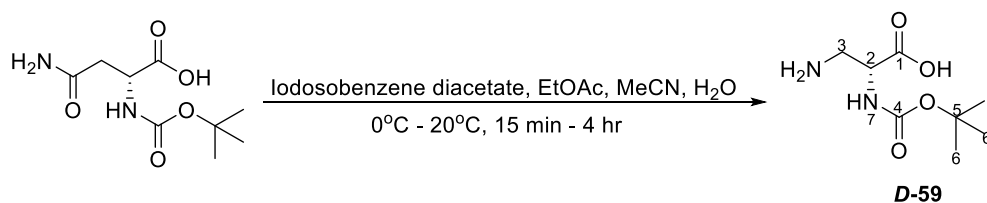
### 10.4.2.1 Synthesis of 3-(benzyloxy)-2-methyl-1,4-dihydropyridin-4-one (**60**)



Prepared according to the literature.<sup>544</sup> In a solution of maltol (10 g, 79.26 mmol, 1 eq) in *N,N*-dimethyl formamide (100 mL) a solution of benzyl bromide (9.42 mL, 79.26 mmol, 1 eq) was added. The solution mixture was stirred at 80°C for 15 min. Then a sample of potassium carbonate (12.05 g, 87.18 mmol, 1.1 eq) was added to the reaction mixture and the final mixture was refluxed for further 1 hr. Upon completion of the reaction the excess of inorganic

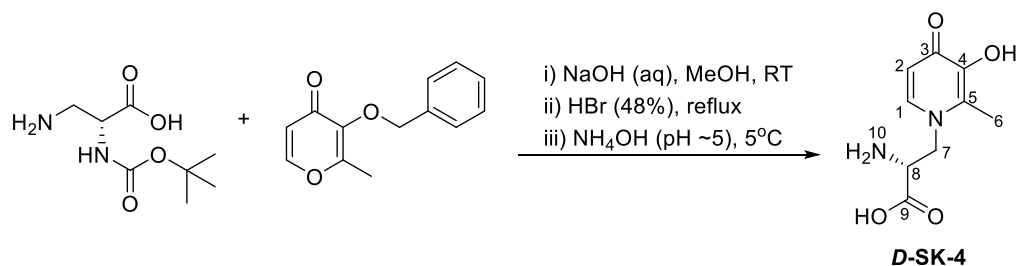
salt was removed by filtration and the filtrates were concentrated under reduced pressure. The resulting residue was dissolved in tetrahydrofuran (50 mL) and any remaining of the inorganic salt was removed by filtration. Finally, the filtrate was concentrated under reduced pressure affording the title compound (**60**) as a viscous orange oil (16.28 g, 75.29 mmol, 95%). <sup>1</sup>H-NMR (400 MHz, CDCl<sub>3</sub>) δ<sub>H</sub>: 2.00 (s, 3H, H-6), 5.07 (s, 2H, H-7), 6.28 (d, *J* = 5.6 Hz, 1H, H-1), 7.25-7.33 (m, 5H, H-9, H-10, H-11), 7.53 (d, *J* = 5.6 Hz, 1H, H-2) ppm; <sup>13</sup>C-NMR (100 MHz, CDCl<sub>3</sub>) δ<sub>C</sub>: 14.6 (C-6), 73.3 (C-7), 116.8 (C-1), 128.2 (Ar), 128.3 (Ar), 128.8 (Ar), 136.7 (Ar), 143.6 (C-4), 153.9 (C-2), 159.8 (C-3), 175.02 (C-5) ppm.

#### 10.4.2.2 Synthesis of (2R)-3-amino-2-[[*tert*-butoxy]carbonyl]amino]propanoic acid (**D-59**)



Prepared according to the literature.<sup>545</sup> In a solution mixture composed of ethyl acetate (24 mL), acetonitrile (24 mL) and water (12 mL), *N*-Boc-*D*-asparagine (5.0 g, 21.5 mmol, 1 eq) and iodosobenzene diacetate (8.32 g, 25.8 mmol, 1.2 eq) were added. The resulting slurry, was stirred at 16°C for 30 min and then at RT for 4 hr. Upon completion of the reaction, the mixture was cooled at 0°C for 15 min forming a white salt which was collected by filtration. The filtercake was then washed with cold ethyl acetate (30 mL) affording compound (**D-59**) as a white solid (3.34 g, 16.35 mmol, 76%). Mp: 203-207°C [lit: 207-212°C]<sup>545</sup>. <sup>1</sup>H-NMR (400 MHz, DMSO-*d*<sub>6</sub>) δ<sub>H</sub>: 1.33 (s, 9H, H-6), 2.67-2.73 (m, 1H, H-3), 2.93-2.98 (m, 1H, H-3), 3.57 (m, 2H, H-2), 6.14 (s, br, 1H, H-7) ppm; <sup>13</sup>C-NMR (100 MHz, DMSO-*d*<sub>6</sub>) δ<sub>C</sub>: 28.6 (C-6), 41.2 (C-3), 51.3 (C-2), 78.7 (C-5), 155.6 (C-4), 171.6 (C-1) ppm.

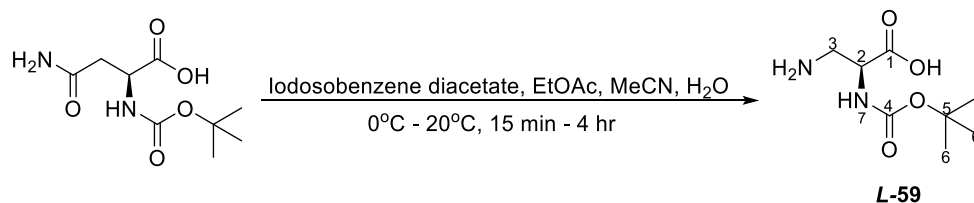
### 10.4.2.3 Synthesis of 2-amino-3-(3-hydroxy-2-methyl-4-oxo-1,4-dihydropyridin-1-yl)propanoic acid (*D-SK-4*)



A sample of 3-(benzyloxy)-2-methyl-1,4-dihydropyridin-4-one (**60**) (4.9 g, 22.66 mmol, 1 eq) was mixed with a sample of (2R)-2-amino-2-[[tert-butoxy]carbonyl]acetic acid (**D-59**) (2.9 g, 14.2 mmol, 0.6 eq.) and dissolved in water (100 mL), ethanol (100 mL) containing sodium hydroxide (2 g, 50 mmol). The resulting solution was allowed to stir at RT for 8 days. Then, the solution was acidified to pH 2 by the addition of conc. hydrochloric acid. The excess of solvents were removed under reduced pressure. The resulting residue was mixed with hydrobromic acid (48% w/v, 20 mL) and refluxed for 20 min. The solution mixture was concentrated under reduced pressure, and then the resulting solid was dissolved in water (20 mL), treated with charcoal and basified (pH 5) by the addition of ammonium hydroxide solution. The resulting solution was cooled to 5°C for 72 hr, where brown crystals were precipitated. The crystals were collected washed with a small portion of water and dried on air affording the title compound (**D-SK-4**) as pale brown crystals (3.23 g, 14.27 mmol, 63%). Mp: 165-168°C [lit: 167-168°C].<sup>7</sup> <sup>1</sup>H-NMR (400 MHz, D<sub>2</sub>O/CF<sub>3</sub>COOD)  $\delta_{\text{H}}$ : 1.90 (s, 3H, H-6), 3.86 (t,  $J=7.2$  Hz, 1H, H-8), 4.07-4.31 (m, 2H, H-7), 6.43 (d,  $J=8$  Hz, 1H, H-2), 7.35 (d,  $J=8$  Hz, 1H, H-1) ppm; <sup>13</sup>C-NMR (100 MHz, D<sub>2</sub>O/CF<sub>3</sub>COOD)  $\delta_{\text{C}}$ : 13.4 (C-6), 49.17 (C-7), 52.24 (C-8), 119.54 (C-2), 141.59 (C-1), 143.28 (C-5), 147.33 (C-4), 170.96 (C-8), 176.7 (C-3) ppm. HRMS (ESI) for C<sub>9</sub>H<sub>12</sub>N<sub>2</sub>O<sub>4</sub>; Theoretical [M+H]: 213.0869. Measured [M+H]: 213.0899.

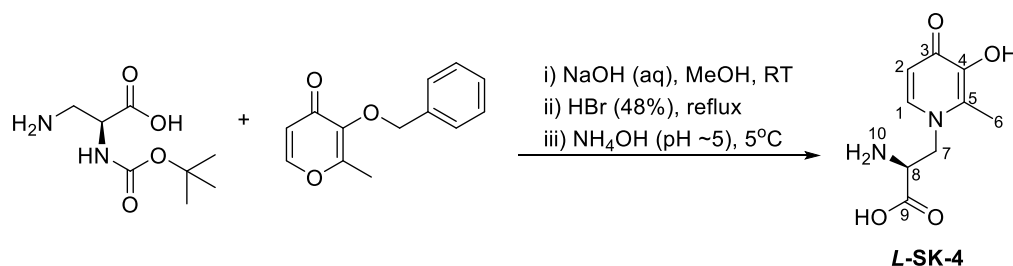
### 10.4.3 Synthesis of *L*-SK-4

#### 10.4.3.1 Synthesis of (2*S*)-3-amino-2-[[*tert*-butoxy]carbonyl]amino}propanoic acid (*L*-59)



Prepared according to the literature.<sup>545</sup> In a solution mixture composed of ethyl acetate (24 mL), acetonitrile (24 mL) and water (12 mL), *N*-Boc-*L*-asparagine (5.0 g, 21.5 mmol, 1 eq) and iodosobenzene diacetate (8.32 g, 25.8 mmol, 1.2 eq) were added. The resulting slurry, was stirred overnight at RT. Upon completion of the reaction, the mixture was concentrated and the resulting slurry was sonicated with ethyl acetate (30 mL). The precipitate was filtrate and filtercake was washed with cooled ethyl acetate (30 mL) affording compound (*L*-59) as a white solid (3.94 g, 19.3 mmol, 90%). Mp. 200-204°C [lit: 207-212°C].<sup>545</sup> <sup>1</sup>H-NMR (400 MHz, DMSO-*d*<sub>6</sub>) δ<sub>H</sub>: 1.35 (s, 9H, H-6), 2.67-2.74 (m, 1H, H-3), 2.95-2.97 (m, 1H, H-3), 3.57 (m, 2H, H-2), 6.13 (s, br, 1H, H-7) ppm; <sup>13</sup>C-NMR (100 MHz, DMSO-*d*<sub>6</sub>) δ<sub>C</sub>: 28.5 (C-6), 41.4 (C-3), 51.6 (C-2), 78.6 (C-5), 155.6 (C-4), 171.6 (C-1) ppm.

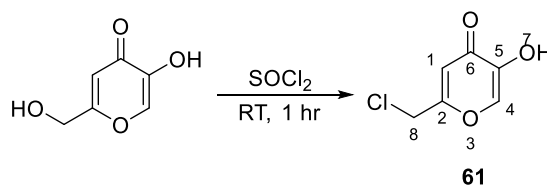
#### 10.4.3.2 Synthesis of 2-amino-3-(3-hydroxy-2-methyl-4-oxo-1,4-dihydropyridin-1-yl)propanoic acid (*L*-SK-4)



A sample of 3-(benzyloxy)-2-methyl-1,4-dihydropyridin-4-one (**60**) (3.88 g, 17.93 mmol, 1 eq) was mixed with a sample of (2S)-2-amino-2-[[tert-butoxy)carbonyl]amino}acetic acid (3.94 g, 19.3 mmol, 1.1 eq.) and dissolved in water (200 mL), ethanol (100 mL) containing sodium hydroxide (2 g, 50 mmol). The resulting solution was allowed to stir at RT for 8 days. Then, the solution was acidified to pH 2 by the addition of conc. hydrochloric acid. The excess of solvents were removed under reduced pressure. The resulting residue was mixed with hydrobromic acid (48% w/v, 20 mL) and refluxed for 20 min. The solution mixture was concentrated under reduced pressure, and then the resulting solid was dissolved in water (20 mL), treated with charcoal and basified (pH 5) by the addition of ammonium hydroxide solution. The resulting solution was cooled to 5°C for 72 hr, where brown solid were precipitated. The solid was collected washed and purified by recrystallization from water/methanol, affording the title compound (**L-SK-4**) as pale brown crystals (1.78 g, 8.43 mmol, 47%). Mp: 163-168°C. <sup>1</sup>H-NMR (400 MHz, D<sub>2</sub>O/CF<sub>3</sub>COOD, 8:2) δ<sub>H</sub>: 1.92 (s, 3H, H-6), 3.85 (t, *J* = 7.2 Hz, 1H, H-8), 4.07-4.31 (m, 2H, H-7), 6.44 (d, *J* = 8 Hz, 1H, H-2), 7.36 (d, *J* = 8 Hz, 1H, H-1) ppm; <sup>13</sup>C-NMR (100 MHz, D<sub>2</sub>O/CF<sub>3</sub>COOD) δ<sub>C</sub>: 13.4 (C-6), 49.2 (C-7), 52.2 (C-8), 119.54 (C-2), 141.7 (C-1), 143.3 (C-5), 147. (C-4), 170.9 (C-8), 176.7 (C-3) ppm. HRMS (ESI) for C<sub>9</sub>H<sub>12</sub>N<sub>2</sub>O<sub>4</sub>; Theoretical [M+H]: 213.0869. Measured [M+H]: 213.0865.

#### 10.4.4 Synthesis of **L-SK-8**

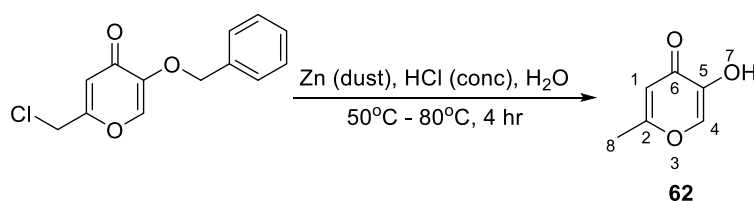
##### 10.4.4.1 Synthesis of 2-(chloromethyl)-5-hydroxy-4H-pyran-4-one (**61**)



The synthesis was performed according to a modified method previously published.<sup>550</sup> A sample of kojic acid (10 g, 70.37 mmol, 1 eq) was dissolved in thionyl chloride (15 mL, 201.7 mmol, 2.9 eq). The resulting solution was stirred at RT until yellow crystals of the title

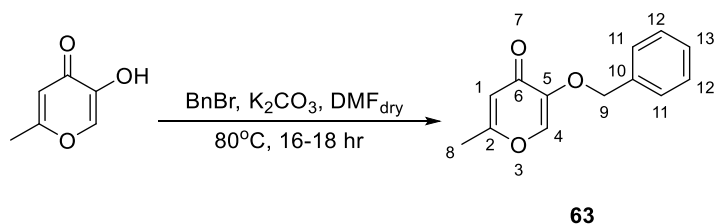
compound were precipitated. The crystals were collect by filtration and washed with excess of hexanes, affording compound **61** as off-white crystals (11.15 g, 69.45 mmol, 97%). Mp: 166-167°C [lit: 166-167°C]<sup>550</sup>. <sup>1</sup>H-NMR (400 MHz, DMSO-*d*<sub>6</sub>) δ<sub>H</sub>: 4.62 (s, 2H, H-8), 5.65 (s, br, 1H, H-7), 6.53 (s, 1H, H-1), 8.1 (s, 1H, H-4) ppm; <sup>13</sup>C-NMR (100 MHz, DMSO-*d*<sub>6</sub>) δ<sub>C</sub>: 41.8 (C-8), 113.8 (C-1), 140.7 (C-4), 146.6 (C-5), 162.2 (C-2), 174.3 (C-6) ppm.

#### 10.4.4.2 Synthesis of 5-hydroxy-2-methyl-4H-pyran-4-one (**62**)



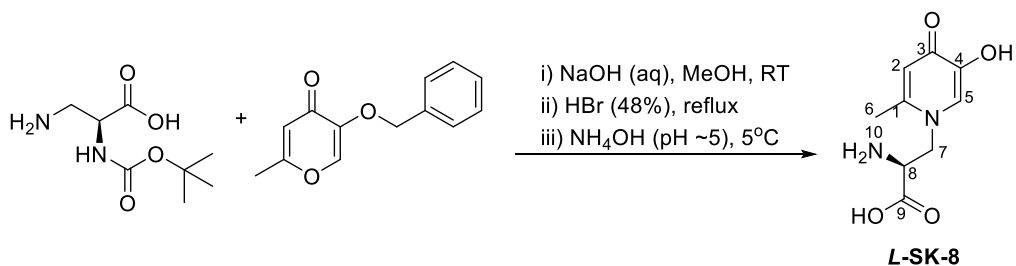
The synthesis was performed according to a modified method previously published.<sup>549</sup> A suspension of 2-(chloromethyl)-5-hydroxy-4H-pyran-4-one (**61**) (5 g, 31.14 mmol, 1 eq) in distilled water (60 mL) was heated at 50°C and stirred until complete dissolution. Then, zinc dust (4.1 g, 62.45 mmol, 2 eq) was added followed by the dropwise addition of concentrated hydrochloric acid (13 mL), for 1 hr maintaining the reaction temperature between 70-80°C. The reaction mixture was stirred for further 4 hr at the same temperature. Upon completion of the reaction, the solution mixture was filtered whilst hot in order to remove the zinc residues. Then, the filtrates were extracted (5x) with a mixture of ethyl acetate (10 mL) and dichloromethane (50 mL). The combined organic extracts were dried over magnesium sulphate and concentrated under reduced pressure affording the title compound (**62**) as white solid (3.23 g, 25.61 mmol, 82%). Mp: 148-150°C [lit: 145-150°C]<sup>549</sup>. <sup>1</sup>H-NMR (400 MHz, DMSO-*d*<sub>6</sub>): δ<sub>H</sub>: 3.32 (s, 3H, H-8), 6.19 (s, br, 1H, H-7), 7.93 (s, 1H, H-1), 8.9 (s, 1H, H-4) ppm; <sup>13</sup>C-NMR (100 MHz, DMSO-*d*<sub>6</sub>) δ<sub>C</sub>: 19.6 (C-8), 112.4 (C-1), 140.2 (C-4), 145.4 (C-5), 166.5 (C-2), 174.7 (C-6) ppm.

#### 10.4.4.3 Synthesis of 5-(benzyloxy)-2-methyl-4H-pyran-4-one (63)



The synthesis was performed according to a modified method previously published.<sup>564</sup> In a stirred solution of 5-hydroxy-2-methyl-4H-pyran-4-one (**62**) (2 g, 15.86 mmol, 1 eq) in dry *N,N*-dimethylformamide (100 mL), potassium carbonate (4.82 g, 34.9 mmol, 2.2 eq.) and benzyl bromide (2.26 mL, 19 mmol, 1.2 eq) were added. The resulting solution mixture was stirred overnight at 80°C. Upon completion of the reaction, the solvents were evaporated to dryness and the resulting slurry was taken up with water (30 mL). Then, it was extracted with dichloromethane (3x50 mL). The combined organic extracts were washed with sodium hydroxide (1M, 50 mL) dried over magnesium sulphate and concentrated under reduced pressure affording compound **63** as a dark red oil that solidified on standing (2.33 g, 10.78 mmol, 68%). Mp: 50-52°C [lit: 48-53°C].<sup>564</sup> <sup>1</sup>H-NMR (400 MHz, DMSO-*d*<sub>6</sub>) δ<sub>H</sub>: 3.32 (s, 3H, H-8), 4.88 (s, 2H, H-9), 6.2 (s, 1H, H-1), 7.26-7.37 (m, 5H, H-11, H-12, H-13), 8.08 (s, 1H, H-4) ppm; <sup>13</sup>C-NMR (100 MHz, DMSO-*d*<sub>6</sub>) δ<sub>C</sub>: 19.5 (C-8), 70.9 (C-9), 113.9 (C-1), 128.6 (*Ar*), 128.7 (*Ar*), 128.9 (*Ar*), 136.8 (C-10), 141.8 (C-4), 146.8 (C-5), 165.8 (C-2), 173.7 (C-6) ppm.

#### 10.4.4.4 Synthesis of (2S)-2-amino-3-(5-hydroxy-2-methyl-4-oxo-1,4-dihydropyridin-1-yl)propanoic acid (L-SK-8)

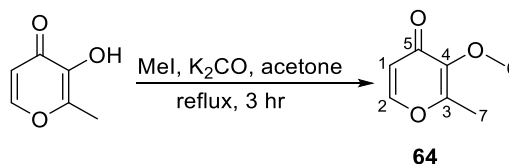


In a solution mixture of ethanol: water (42 mL: 85 mL) sodium hydroxide pellets (370 mg, 9.25 mmol, 1 eq) were added adjusting the pH to 12. To this solution mixture, 5-(benzyloxy)-2-methyl-4H-pyran-4-one (**63**) (2.0 g, 9.25 mmol, 1eq) and (2S)-3-amino-2-[(tert-butoxy)carbonyl]amino}propanoic acid (**L-59**) (1.89 g, 9.25 mmol, 1 eq) were added. The resulting solution mixture was stirred at RT for 8 days. Upon completion of the reaction, the pH was adjusted to 2 by the careful addition of conc. Hydrochloric acid. Then the solvents were evaporated to dryness under reduced pressure. To the resulting residue, hydrobromic acid (30%, 20 mL) was added and the suspension was refluxed for 20 min and then it was evaporated to dryness forming the crude product as brown solid. The crude product was dissolved in water (20 mL) and the pH was adjusted to 5 by the dropwise addition of ammonium hydroxide solution. The resulting solution was kept in at 5°C for two weeks where white crystals of compound (**L-SK-8**) were formed. The crystalline product was collected by vacuum filtration and washed with cold water affording compound (**L-SK-8**) as pure white needles (350 mg, 1.65 mg, 18%). Mp: 172-173°C. <sup>1</sup>H-NMR (400 MHz, D<sub>2</sub>O/CF<sub>3</sub>COOD, 8:2): δ<sub>H</sub>: 1.8 (s, 3H, H-7), 3.79 (t, *J* = 7.6 Hz, 1H, H-9), 3.9-3.95 (m, 1H, H-8), 4.1-4.16 (m, 1H, H-9), 6.32 (s, 1H, H-1), 7.3 (s, 1H, H-4) ppm; <sup>13</sup>C-NMR (100 MHz, D<sub>2</sub>O/CF<sub>3</sub>COOD, 8:2): δ<sub>C</sub>: 17.9 (C-7), 50.9 (C-6), 52.7 (C-9), 114.2 (C-1), 130.6 (C-4), 143.2 (C-5), 160.0 (C-2), 161.2 (C-10), 167.2 (C-6) ppm. HRMS (ESI) for C<sub>9</sub>H<sub>12</sub>N<sub>2</sub>O<sub>4</sub>; Theoretical [M+H]: 213.0869. Measured [M+H]: 213.0823.

## 10.5 Synthesis of the control compounds

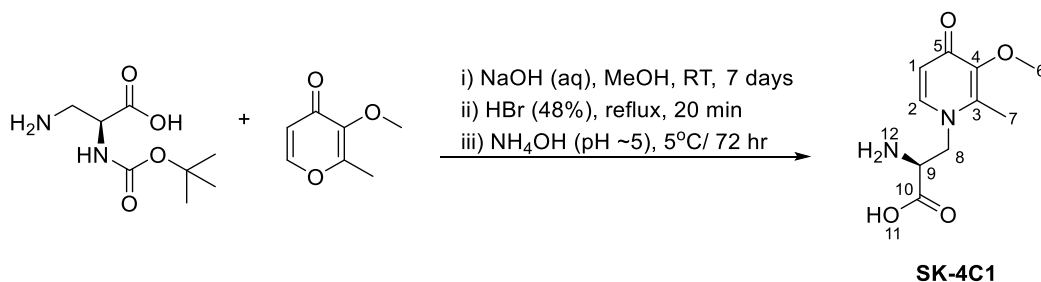
### 10.5.1 Synthesis of *L*-SK-4 control compounds

#### 10.5.1.1 Synthesis of 3-methoxy-2-methyl-4H-pyran-4-one (**64**)



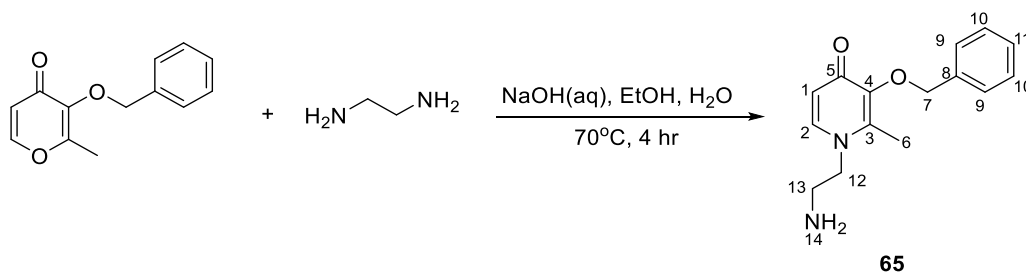
The synthesis was performed according to a modified method previously published.<sup>551</sup> In a suspension of maltol (5 g, 41.28 mmol, 1 eq.) in acetone (50 mL) potassium carbonate (16.4 g, 118.66 mmol, 3 eq) and iodomethane (7.4 g, 49.31 mmol, 1.2 eq) were added sequentially. The resulting solution mixture was refluxed for 3 hr. Upon completion of the reaction, the solvents were removed under reduced pressure and the resulting residue was partitioned in a mixture of dichloromethane/water (1:1) (100 mL). Then the aqueous phase was extracted with dichloromethane (3x50 mL). The combined organic extracts were washed with brine, dried over magnesium sulphate and concentrated under reduced pressure to afford compound (**64**) as a brown-orange oil (5.44 g, 38.85 mmol, 94%). <sup>1</sup>H-NMR (400 MHz, CDCl<sub>3</sub>) δ<sub>H</sub>: 2.13 (s, 3H, H-7), 3.65 (s, 3H, H-6), 6.14 (d, J= 10.8 Hz, 1H, H-1), 7.49 (s, J= 10.8 Hz, 1H, H-2) ppm; <sup>13</sup>C-NMR (100 MHz, CDCl<sub>3</sub>) δ<sub>C</sub>: 14.5 (C-7), 59.8 (C-6), 117.8 (C-1), 145.5 (C-2), 163.7 (C-3), 159.1 (C-4), 174.8 (C-5) ppm.

**10.5.1.2 Synthesis of (2S)-amino-3-(3-methoxy-2-methyl-4-oxo-1,4-dihydropyridin-1-yl)propanoic acid (SK-4C1)**



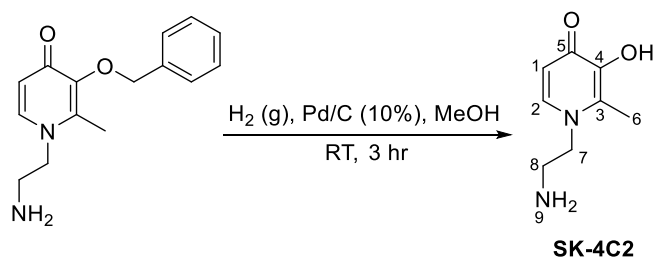
In a suspension of 3-methoxy-2-methyl-4H-pyran-4-one (**64**) (5.44 g, 38.85 mmol 1 eq) in water (145 mL) and ethanol (73 mL) containing sodium hydroxide (1.5 g, 37.5 mmol), a sample of 3-amino-2S-[[tert-butoxy]carbonyl]amino}propanoic acid (**L-59**) (2.11 g, 10.28 mmol, 0.3 eq) was added. The resulting solution mixture was stirred at RT for 7 days. Upon completion of the reaction, the pH was adjusted to 2 by the addition of conc. HCl and the solvents were evaporated to dryness under reduced pressure. The resulting residue was refluxed with hydrobromic acid (30% w/v, 20 mL) for 20 min. Then the solvents were evaporated and the residue was dissolved in water (30 mL), treated with charcoal and filtered. Addition of conc. ammonium hydroxide solution to the filtrates until pH 5 cause the crystallisation of the product which was collected and by filtration as a brown solid (2.37 g, 10.5 mmol, 42%). Mp: 170-173°C. <sup>1</sup>H-NMR (400 MHz, D<sub>2</sub>O/CF<sub>3</sub>COOD, 8:2) δ<sub>H</sub>: 2.13 (s, 3H, H-7), 3.27 (s, 3H, H-6), 4.09 (t, *J*= 7.2 Hz, 1H, H-9), 4.28-4.51 (m, 2H, H-8), 6.7 (d, *J*= 7.2 Hz, 1H, H-1), 7.76 (d, *J*= 7.2 Hz, 1H, H-2) ppm; <sup>13</sup>C-NMR (100 MHz, 400 MHz, D<sub>2</sub>O/CF<sub>3</sub>COOD, 8:2) δ<sub>C</sub>: 12.8 (C-7), 49.3 (C-6), 51.1 (C-8), 60.9 (C-9), 119.5 (C-1), 142.9 (C-2), 144.7 (C-3), 150.7 (C-4), 167.5 (C-10), 176.3 (C-5) ppm. HRMS (ESI) for C<sub>10</sub>H<sub>14</sub>N<sub>2</sub>O<sub>4</sub>; Theoretical [M+H]: 227.1031. Measured [M+H]: 227.1069.

### 10.5.1.3 Synthesis of 1-(2-aminoethyl)-3-(benzyloxy)-2-methyl-1,4-dihydropyridin-4-one (65)



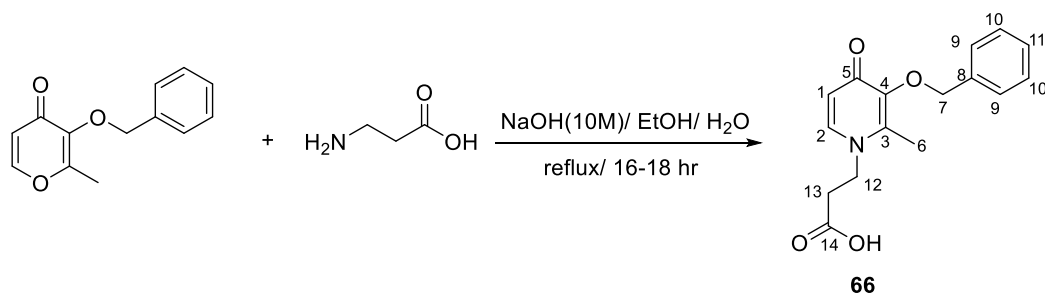
The synthesis was performed according to a modified method previously published.<sup>552</sup> In a suspension of 3-(benzyloxy)-2-methyl-1,4-dihydropyridin-4-one (**60**) (3 g, 13.9 mmol, 1 eq) in EtOH/water mixture (20/15 mL) sodium hydroxide (0.5 g, 12.5 mmol) was added. Ethylenediamine (3.3 mL, 49.3 mmol, 3.5 eq.) was added to the stirred solution was heated at 70°C for 4 hr and then it was allowed to cool to RT overnight. The solution mixture was acidified to pH 1 by the addition of concentrated hydrochloric acid. The resulting mixture was concentrated under reduced pressure affording an orange salt which was washed with excess of acetone. The salt was collected by filtration, dissolved in water (20 mL), basified to pH 12 by aqueous solution of sodium hydroxide (10 M) and extracted in dichloromethane (4x50 mL). The organic extracted were concentrated under reduced pressure affording the title compound (**65**) as brown oil (2.79 g, 10.8 mmol, 77%). <sup>1</sup>H-NMR (400 MHz, D<sub>2</sub>O)  $\delta_{\text{H}}$ : 2.30 (s, 3H, H-6), 3.30 (t,  $J=7.6$  Hz, 2H, H-13), 4.47 (t,  $J=7.6$  Hz, 2H, H-12), 5.01 (s, 2H, H-7), 7.03 (d,  $J=6.8$  Hz, 1H, H-1), 7.29-7.36 (m, 5H, H-9, H-10, H-11), 8.06 (d,  $J=6.8$  Hz, 1H, H-2) ppm; <sup>13</sup>C-NMR (100 MHz, D<sub>2</sub>O)  $\delta_{\text{C}}$ = 13.2 (C-6), 38.1 (C-13), 52.5 (C-12), 75.6 (C-7), 114.1 (C-1), 128.9 (*Ar*), 129.3 (*Ar*), 129.7 (*Ar*), 135.2 (*Ar*), 142.5 (C-2), 143.2 (C-3), 147.01 (C-4), 166.0 (C-5) ppm.

#### 10.5.1.4 Synthesis of 1-(2-aminoethyl)-3-(benzyloxy)-2-methyl-1,4-dihydropyridin-4-one (SK-4C2)



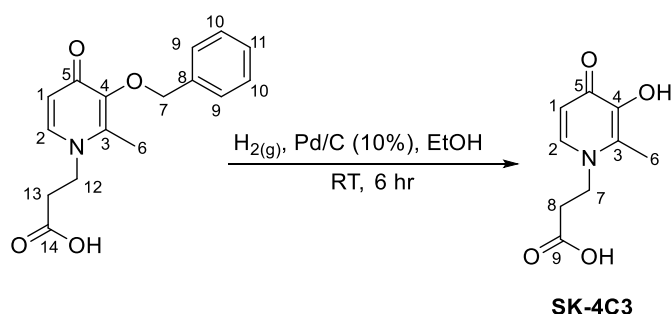
The synthesis was performed according to a modified method previously published.<sup>552</sup> In a suspension of 1-(2-aminoethyl)-3-(benzyloxy)-2-methyl-1,4-dihydropyridin-4-one (**65**) (2 g, 7.74 mmol, 1 eq) in methanol (30 mL) a catalytic amount of Pd/C (10%, 580 mg, 5.45 mmol, 0.7 eq.) was added. The reaction mixture was stirred under hydrogen gas at RT for 3 hr. Upon completion of the reaction, the solution mixture was filtrated over a pad of Celite, and concentrated under reduced pressure affording the title compound (**SK-4C2**) as pale yellow crystals (1.17 g, 6.97 mmol, 90%). Mp: 143-148°C. [lit: 142-146°C].<sup>552</sup> <sup>1</sup>H-NMR (400 MHz, D<sub>2</sub>O)  $\delta_{\text{H}}$ : 2.56 (s, 3H, H-6), 2.86 (t,  $J=6.8$  Hz, 2H, H-8), 4.52 (t,  $J=6.8$  Hz, 2H, H-7), 7.37 (d,  $J=6.8$  Hz, 1H, H-1), 8.28 (d,  $J=6.8$  Hz, 1H, H-2) ppm; <sup>13</sup>C-NMR (100 MHz, D<sub>2</sub>O)  $\delta_{\text{C}}$ : 12.9 (C-6), 34.1 (C-7), 52.1 (C-8), 111.0 (C-1), 138.9 (C-2), 142.4 (C-3), 143.2 (C-4), 159.0 (C-5) ppm. HRMS (ESI) for C<sub>8</sub>H<sub>12</sub>N<sub>2</sub>O<sub>2</sub>; Theoretical [M+H]: 169.0977. Measured [M+H]: 169.0859.

#### 10.5.1.5 Synthesis of 3-[3-(benzyloxy)-2-methyl-4-oxo-1,4-dihydropyridin-1-yl]propanoic acid (**66**)



The synthesis was performed according to a modified method previously published.<sup>553</sup> In a suspension of 3-(benzyloxy)-2-methyl-1,4-dihydropyridin-4-one (**60**) (14.0 g, 65.4 mmol, 1 eq) in a mixture of ethanol/H<sub>2</sub>O (1:1, 100 mL), β-alanine (7.0 g, 78.47 mmol, 1.2 eq) was added and the pH was adjusted to 13 by the addition of aqueous sodium hydroxide solution (10M, ~50 mL). The reaction mixture was refluxed overnight and then it was allowed to cool at RT. Then the reaction mixture volume was reduced by ~1/3 followed by the addition of water and the re-adjustment of pH to 4 by the dropwise addition of aqueous solution of hydrochloric acid (6M). The resulting solution was extracted with dichloromethane (4x75 mL). The combined organic extracts were washed with brine, dried over anhydrous magnesium sulphate and concentrated under reduced pressure to afford a pale brown solid of compound **66** (12.21 g, 42.5 mmol, 65%). Mp: 169-172°C [lit: 172-173°C].<sup>553</sup> <sup>1</sup>H-NMR (400 MHz, D<sub>2</sub>O/CF<sub>3</sub>COOD, 8:2) δ<sub>H</sub>: 2.10 (s, 3H, H-6), 2.70 (t, *J*= 7.0 Hz, 2H, H-13), 4.11 (t, *J*= 7.0 Hz, 2H, H-12), 5.21 (s, 2H, H-7) 6.42 (d, *J*= 7.5 Hz, 2H, H-1), 7.28-7.42 (m, 6H, H-2, H-9, H-10, H-11) ppm; <sup>13</sup>C-NMR (100 MHz, D<sub>2</sub>O/CF<sub>3</sub>COOD, 8:2) δ<sub>C</sub>: 12.8 (C-6), 34.73 (C-13), 46.5 (C-12), 71.3 (C-7), 118.4 (C-1), 127.1 (*Ar*), 127.6 (*Ar*), 128.3 (*Ar*), 135.3 (*Ar*), 141.8 (C-3), 143.6 (C-4), 142.8 (C-2), 174.5 (C-14), 176.4 (C-5) ppm.

#### 10.5.1.6 Synthesis of 3-(3-hydroxy-2-methyl-4-oxo-1,4-dihydropyridin-1-yl)propanoic acid (SK-4C3)

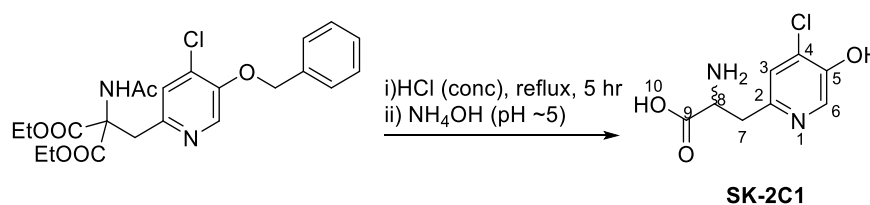


The synthesis was performed according to a modified method previously published.<sup>709</sup> In a suspension of 3-[3-(benzyloxy)-2-methyl-4-oxo-1,4-dihydropyridin-1-yl]propanoic acid (**66**) (1 g, 3.48 mmol, 1 eq) in ethanol (20 mL) a catalytic amount of Pd/C (10%) was added. The reaction mixture was stirred under hydrogen gas at RT for 6 hr. Upon completion of the

reaction, the solution mixture was filtrated over a pad of Celite, and concentrated under reduced pressure affording the crude compound as brown crystals which was then purified by recrystallization from acetone/ diethyl ether, forming the titled compound (**SK-4C3**) as white crystals (600 mg, 2.99 mmol, 86%). Mp: 207-208°C. [lit: 200-205°C]<sup>709</sup>. <sup>1</sup>H-NMR (400 MHz, D<sub>2</sub>O/CF<sub>3</sub>COOD, 8:2)  $\delta_{\text{H}}$ : 2.13 (s, 3H, H-6), 2.65 (t,  $J = 7.0$  Hz, 2H, H-8) 4.16 (t,  $J = 7.0$  Hz, 2H, H-7), 6.42 (d,  $J = 7.5$  Hz, 2H, H-2), 7.63 (d,  $J = 7.5$  Hz, 2H, H-1) ppm; <sup>13</sup>C-NMR (100 MHz, D<sub>2</sub>O/CF<sub>3</sub>COOD, 8:2)  $\delta_{\text{C}}$ : 11.2 (C-6), 35.0 (C-8), 46.9 (C-7), 119.0 (C-1), 132.4 (C-3), 140.1 (C-4), 142.2 (C-2), 176.5 (C-9), 178.1 (C-5) ppm. HRMS (ESI) for C<sub>9</sub>H<sub>11</sub>NO<sub>4</sub>; Theoretical [M+H]: 198.0766. Measured [M+H]: 198.0966.

## 10.5.2 Synthesis of *rac*-SK-2 control

### 10.5.2.1 Synthesis of *rac*-3-amino-3-(4-chloro-5-hydroxypyridin-2-yl)propanoic acid (**SK-2C1**)

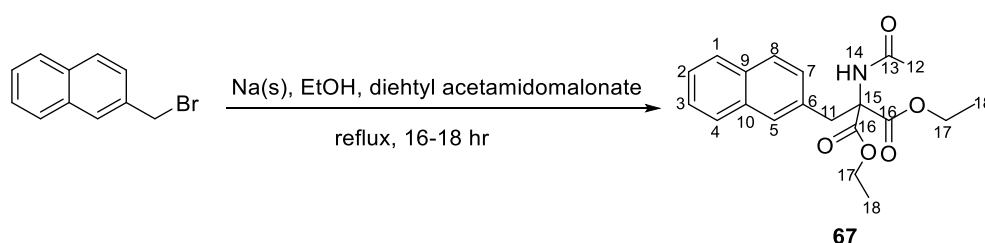


In a solution of conc. hydrochloric acid (25 mL), a sample of 1,3-diethyl 2-([5-(benzyloxy)-4-chloropyridin-2-yl]methyl)-2-acetamidopropanedioate (**44**) (3 g, 6.68 mmol) were added. The resulting solution mixture was refluxed for 5 hr and then the solution was evaporated to dryness, forming a yellow powder which was dissolved in water (10 mL), treated with charcoal and filtered. The pH of the filtrates was adjusted to 5 by the dropwise addition of conc. ammonium hydroxide solution, which was led to precipitation of the title compound (**SK2C-1**). The product was collected by filtration and washed with water, acetone and light petroleum affording compound (**SK-2C1**) as pale yellow crystals. (1.35 g, 6.34 mmol, 95%). Mp: 178-179°C. <sup>1</sup>H-NMR (400 MHz, D<sub>2</sub>O/CF<sub>3</sub>COOD; 8:2)  $\delta_{\text{H}}$ : 2.96-3.07 (m, 2H, H-7), 3.9 (t,  $J = 6.4$  Hz, 1-H, H-8). 7.49 (s, 1H, H-3), 7.75 (s, 1H, H-6) ppm; <sup>13</sup>C-NMR (100 MHz,

D<sub>2</sub>O/CF<sub>3</sub>COOD; 8:2)  $\delta_C$ : 31.6 (C-7), 51.0 (C-8), 116.3 (C-3), 119.2 (C-4), 140.6 (C-6), 151.6 (C-2), 160.6 (C-5), 168.7 (C-9) ppm.

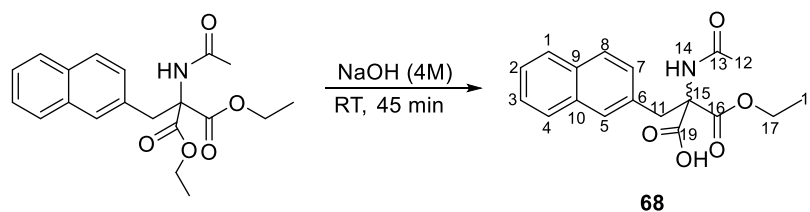
## 10.6 Synthesis of LAT-1 competitive substrate

### 10.6.1 Synthesis of 1,3-diethyl 2-acetamido-2-[(naphthalen-2-yl)methyl]propanedioate (**67**)



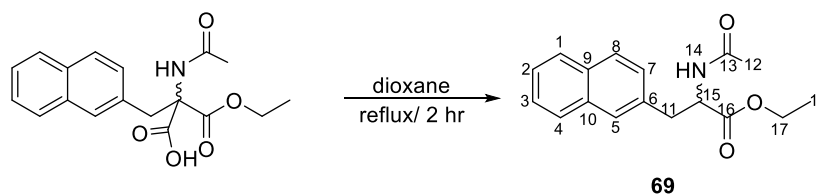
The synthesis was performed according to a modified method previously published.<sup>710</sup> In a stirred solution of ethanol (50 mL) cooled to 0°C and under nitrogen, metallic sodium (260 mg, 11.3 mmol, 1 eq) was added and allowed to stir until complete dissolution. Then diethyl acetamidomalonate (2.45 g, 11.3 mmol, 1 eq) was added and the resulting solution mixture was stirred for further 10 min before the addition of 2-(bromomethyl) naphthalene (2.5 g, 11.3 mmol, 1 eq). The resulting mixture was allowed to reflux overnight. Upon completion of the reaction, the solution was allowed to cool at RT before it was cooled at 0°C, where white crystals of the title compound (**67**) were precipitated. The crystals were collected by filtration and washed with excess of ethanol affording intermediate **67** as white crystals (3.1 g, 8.67 mmol, 77%). Mp: 117-122°C. [lit: 120-122°C]<sup>710</sup>. <sup>1</sup>H-NMR (400 MHz, DMSO-*d*<sub>6</sub>)  $\delta_H$ : 1.19 (t, *J* = 7.2 Hz, 6H, H-18), 1.97 (s, 3H, H-12), 3.60 (s, 2H, H-11), 4.18 (q, *J* = 7.2 Hz, 4H, H-17), 7.08 (d, *J* = 8.8 Hz, 1H, H-8), 7.42-7.46 (2H, H-2, H-3), 7.77 (s, 1H, H-5), 7.76-8.06 (m, 3H, H-1, H-4, H-13) ppm; <sup>13</sup>C-NMR (100 MHz, DMSO-*d*<sub>6</sub>)  $\delta_C$ : 14.4 (C-18), 22.7 (C-12), 38.2 (C-11), 62.4 (C-17), 67.7 (C-15), 126.29 (*Ar*), 126.58 (*Ar*), 126.59 (*Ar*), 127.88 (*Ar*), 128.01 (*Ar*), 128.7 (*Ar*), 129.2 (*Ar*), 132.6 (*Ar*), 133.35 (*Ar*), 133.4 (*Ar*), 165.7 (C-16), 170.2 (C-13) ppm.

### 10.6.2 Synthesis of *rac*-2-acetamido-3-ethoxy-2-[(naphthalen-2-yl)methyl]-3-oxopropanoic acid (**68**)



The synthesis was performed according to a modified method previously published.<sup>555</sup> In a suspension of 1,3-diethyl 2-acetamido-2-[(naphthalen-2-yl)methyl]propanedioate (**67**) (2.0 g, 5.59 mmol) in ethanol (15 mL), aqueous solution of sodium hydroxide (4M, 5 mL) was added and the resulting solution was stirred at RT for 45 min. The solution was then acidified to pH 2 by the addition of conc. HCl, and it was evaporated to dryness. The resulting white solid was washed with water and dried on air overnight affording the titled compound (**68**) as white solid (1.0 g, 3.21 mmol, 57%). Mp: 133-134°C [lit: 137-139°C].<sup>555</sup> <sup>1</sup>H-NMR (400 MHz, DMSO-*d*<sub>6</sub>)  $\delta_{\text{H}}$  = 1.19 (t, *J* = 6.8 Hz, 3H, H-18), 1.97 (s, 3H, H-12), 3.56-3.7 (m, 2H, H-11), 4.16 (q, *J* = 6.8 Hz, 2H, H-17), 7.17 (d, *J* = 8.4 Hz, 1H, H-7), 7.48-7.9 (m, 7H, H-1, H-2, H-3, H-4, H-8, H-5, H-14) ppm; <sup>13</sup>C-NMR (100 MHz, DMSO-*d*<sub>6</sub>)  $\delta_{\text{C}}$  = 14.3 (C-18), 22.7 (C-12), 38.4 (C-11), 61.9 (C-17), 67.5 (C-15), 116.9 (*Ar*), 119.8 (*Ar*), 126.1 (*Ar*), 126.5 (*Ar*), 127.8 (*Ar*), 127.9 (*Ar*), 128.0 (*Ar*), 128.7 (*Ar*), 129.0 (*Ar*), 133.8 (*Ar*), 167.9 (C-16), 169.5 (C-19), 169.9 (C-13) ppm.

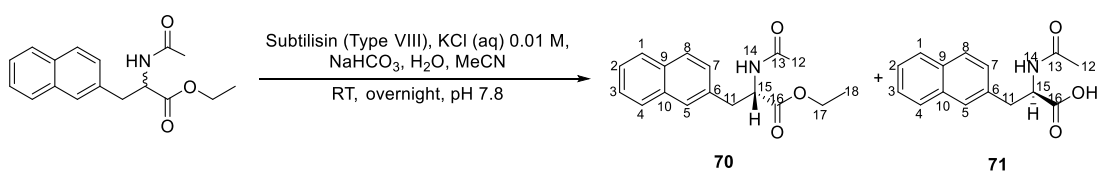
### 10.6.3 Synthesis of *rac*- ethyl 2-acetamido-3-(naphthalen-2-yl)propanoate (**69**)



The synthesis was performed according to a modified method previously published.<sup>555</sup> A solution of 2-acetamido-3-ethoxy-2-[(naphthalen-2-yl)methyl]-3-oxopropanoic acid (**68**) (900 mg, 2.86 mmol) in 1, 4-dioxane (20 mL) was refluxed for 2 hr . The solution was allowed to

cool at RT and then it was concentrated under reduced pressure affording a yellow slurry that it was taken up in ethyl acetate (20 mL) and washed with aqueous solution of sodium hydrogen carbonate (5%, 15 mL). The organic phase washed with brine, dried over anhydrous magnesium sulphate and concentrated under reduced pressure affording the titled intermediate (**69**) as a yellow oil which crystallized on standing (670 mg, 2.48 mmol, 87%). Mp: 133-134°C [lit: 137-139°C].<sup>555</sup> <sup>1</sup>H-NMR (400 MHz, DMSO-*d*<sub>6</sub>)  $\delta$ <sub>H</sub>: 1.06 (t, *J* = 8.4 Hz, 3H, H-18), 1.8 (s, 3H, H-12), 3.03-3.2 (m, 2H, H-11), 4.05 (q, *J* = 8.4 Hz, 2H, H-17), 4.53-4.58 (m, 1H, H-15), 7.4-7.55 (m, 3H, H-2, H-3, H-7), 7.72 (s, 1H, H-5), 8.41 (d, 1H, *J* = 4 Hz, H-7), 7.83-7.88 (m, 3H, H-1, H-4, H-8) ppm; <sup>13</sup>C-NMR (100 MHz, DMSO-*d*<sub>6</sub>)  $\delta$ <sub>C</sub>: 14.6 (C-18), 22.7 (C-12), 37.5 (C-11), 54.2 (C-15), 60.9 (C-17), 117.0 (*Ar*), 126.0 (*Ar*), 126.5 (*Ar*), 127.9 (*Ar*), 128.0 (*Ar*), 128.1 (*Ar*), 128.2 (*Ar*), 132.4 (*Ar*), 133.4 (*Ar*), 135.4 (*Ar*) 169.8 (C-16), 172.2 (C-13) ppm.

#### 10.6.4 Synthesis of ethyl (2*S*)-2-acetamido-3-(naphthalen-2-yl)propanoate (**70**) and (2*R*)-2-acetamido-3-(naphthalen-2-yl)propanoic acid (**71**)

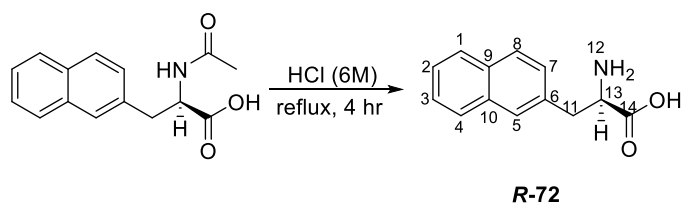


The synthesis was performed according to a modified method previously published.<sup>555</sup> In a suspension of *rac*- ethyl 2-acetamido-3-(naphthalen-2-yl)propanoate (**69**) (660 mg, 2.31 mmol, 1 eq) in a mixture of acetonitrile/water (1:1, 24 mL), an aqueous solution of potassium chloride (0.01 M, 20 mL) was added. The resulting mixture was stirred vigorously and sodium hydrogen carbonate (11.37 mg, 135.3  $\mu$ mol, 0.05 eq) was added followed by Subtilisin (Type VIII, 1.1 mg). The pH was maintained at 7.8 by the manual addition of fractions (5-10  $\mu$ L) of aqueous solution of sodium hydroxide (1M, 10 mL). The solution mixture was stirred at RT

until no more sodium hydroxide was used up (pH stabilization). Then the volatiles were removed under reduced pressure and the resulting off white solid of the (S)-ester (**70**) was removed by vacuum filtration and dried on air overnight (320 mg, 1.18 mmol, 51%). Mp: 133-134°C [lit: 137-139°C]<sup>555</sup>. <sup>1</sup>H-NMR (400 MHz, DMSO-*d*<sub>6</sub>)  $\delta_{\text{H}}$ : 1.06 (t, *J*= 8.4 Hz, 3H, H-18), 1.8 (s, 3H, H-12), 3.03-3.2 (m, 2H, H-11), 4.05 (q, *J*= 8.4 Hz, 2H, H-17), 4.53-4.58 (m, 1H, H-15), 7.4-7.55 (m, 3H, H-2, H-3, H-7), 7.72 (s, 1H, H-5), 8.41 (d, 1H, *J*= 4 Hz, H-7), 7.83-7.88 (m, 3H, H-1, H-4, H-8) ppm; <sup>13</sup>C-NMR (100 MHz, DMSO-*d*<sub>6</sub>)  $\delta_{\text{C}}$ : 14.6 (C-18), 22.7 (C-12), 37.5 (C-11), 54.2 (C-15), 60.9 (C-17), 117.0 (*Ar*), 126.0 (*Ar*), 126.5 (*Ar*), 127.9 (*Ar*), 128.0 (*Ar*), 128.1 (*Ar*), 128.2 (*Ar*), 132.4 (*Ar*), 133.4 (*Ar*), 135.4 (*Ar*), 169.8 (C-16), 172.2 (C-13) ppm

The filtrates were then extracted with ethyl acetate (3x30 mL) and then acidified to pH 1 with aqueous solution of hydrochloric acid (6 M, ~15 mL), and cooled to 0 °C for 5 hr. The white precipitate of the (R)-amino acid (**71**) was collected by filtration and dried on air overnight (250 mg, 0.96 mmol, 42%). Mp: 187-189°C [lit: 188-189°C].<sup>555</sup> <sup>1</sup>H-NMR (400 MHz, DMSO-*d*<sub>6</sub>)  $\delta_{\text{H}}$ : 1.73 (s, 3H, H-12), 2.94-3.33 (m, 2H, H-11), 4.46-4.85 (m, 1H, H-15), 7.37 (d, *J*= 8.4 Hz, 1H, H-7), 7.42-7.44 (m, 3H, H-1, H-4, H-8), 7.68 (s, 1H, H-5), 7.78-7.83 (m, 2H, H-2, H-3), 8.22 (d, 1H, *J*= 5.6 Hz, H-14) ppm; <sup>13</sup>C-NMR (100 MHz, DMSO-*d*<sub>6</sub>)  $\delta_{\text{C}}$ : 22.8 (C-12), 37.5 (C-11), 54.0 (C-15), 126.0 (*Ar*), 126.5 (*Ar*), 127.9 (*Ar*), 127.95 (*Ar*), 127.99 (*Ar*), 128.1 (*Ar*), 128.3 (*Ar*), 132.3 (*Ar*), 133.4 (*Ar*), 135.9 (*Ar*), 169.7 (C-16), 173.6 (C-13) ppm.

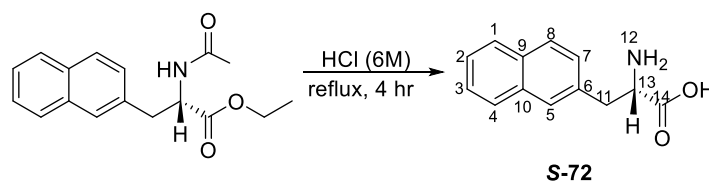
#### 10.6.5 Synthesis of (2R)-2-amino-3-(naphthalen-2-yl)propanoic acid (R-72)



The synthesis was performed according to a modified method previously published.<sup>555</sup> A suspension of (2S)-2-acetamido-3-(naphthalen-2-yl)propanoate (**71**) (200 mg, 0.74 mmol) in

aqueous hydrochloric acid (6M, 20 mL) was refluxed for 4 hr. Upon completion of the reaction the excess of solvents were removed under reduced pressure affording the titled compound as a white solid (154 mg, 0.67 mmol, 90%). Mp: 250-252°C [lit: 251-252°C].<sup>555</sup> <sup>1</sup>H-NMR (400 MHz, DMSO-*d*<sub>6</sub>)  $\delta_{\text{H}}$ : 3.18-3.26 (m, 2H, H-11), 4.20-4.23 (m, 1H, H-13), 7.35 (d, *J*= 8 Hz, 1H, H-7), 7.40-7.46 (m, 3H, H-1, H-4, H-8), 7.7 (s, 1H, H-5), 7.75-7.81 (m, 2H, H-2, H-3), 8.2 (s, 2H, H-12) ppm; <sup>13</sup>C-NMR (100 MHz, DMSO-*d*<sub>6</sub>)  $\delta_{\text{C}}$ : 36.3 (C-11), 53.6 (C-13), 111.1 (*Ar*), 114.0 (*Ar*), 114.1 (*Ar*), 116.8 (*Ar*), 128.2 (*Ar*), 158.3 (*Ar*), 158.7 (*Ar*), 158.7 (*Ar*), 159.1 (*Ar*), 159.5 (*Ar*), 173.2 (C-14) ppm.

#### 10.6.6 Synthesis of (2*S*)-2-amino-3-(naphthalen-2-yl)propanoic acid (**S-72**)



As described for (2*R*)-2-amino-3-(naphthalen-2-yl)propanoic acid (**R-72**). (155 mg, 0.72 mmol, 92%). Mp: 253-256°C [lit: 251-252°C].<sup>555</sup> <sup>1</sup>H-NMR (400 MHz, DMSO-*d*<sub>6</sub>)  $\delta_{\text{H}}$ : 3.18-3.26 (m, 2H, H-11), 4.2-4.23 (m, 1H, H-1), 7.35 (d, *J*= 8 Hz, 1H, H-7), 7.40-7.46 (m, 3H, H-1, H-4, H-8), 7.7 (s, 1H, H-5), 7.75-7.81 (m, 2H, H-2, H-3), 8.2 (s, 2H, H-12) ppm; <sup>13</sup>C-NMR (100 MHz, DMSO-*d*<sub>6</sub>)  $\delta_{\text{C}}$ : 36.3 (C-11), 53.6 (C-13), 111.1 (*Ar*), 114.0 (*Ar*), 114.1 (*Ar*), 116.8 (*Ar*), 128.2 (*Ar*), 158.3 (*Ar*), 158.7 (*Ar*), 158.7 (*Ar*), 159.1 (*Ar*), 159.5 (*Ar*), 173.2 (C-14) ppm.

## 11 Experimental procedures – Biological screening and evaluation of the SK-n compounds

### 11.1 Cell Culture and Methodologies

#### 11.1.1 Cell lines

The experimental model that has been used consisted of three different skin cell lines: (A) a normal immortalized keratinocyte (HaCaT) cell line, (B) an epidermoid carcinoma (A431) cell line and (C) a primary malignant melanoma (A375) cell line. In addition to these, the experimental model include a variation of malignant melanoma cell lines from different tissues including: (D) human brain metastatic malignant melanoma (VMM-1) cell line, (E) human lymph node metastatic malignant melanoma (Hs 294T) cell line as well as (F) murine malignant melanoma (B16 F10) cell line (**Table 24** and **25**).

**Table 24:** List of cell lines used for the in vitro human malignant melanoma model.

Cell line	Company
HaCaT	A kind gift from Dr Sharon Brody (Dermal Toxicology and Effects Group; Centre for Radiation, Chemical and Environmental Hazards; Public Health England, UK)
A431	Purchased from Sigma-Aldrich (St. Louis, MO, USA)
A375	Purchased from Sigma-Aldrich (St. Louis, MO, USA)
VMM-1	Purchased from ATCC (Manassas, VA, USA)
Hs 294T	Purchased from ATCC (Manassas, VA, USA)
B16 F10	Purchased from ATCC (Manassas, VA, USA)

**Table 25:** Characterization of the different cell lines used for the in vitro model of malignant melanoma.

Cell Line	HaCaT	A431	A375	VMM-1	Hs 294T	B16 F10
<b>Organism</b>	<i>Homo sapiens</i> (Human)					<i>Mus</i> <i>Musculus</i> (Mouse)
<b>Ethnicity</b>	Caucasian					-
<b>Gender</b>	Male	Female	Female	Male	Male	-
<b>Tissue</b>	Skin	Epidermis	Skin	Brain	Lymph node	Skin
<b>Morphology</b>	Monolayer, adherent	Epithelial, adherent	Epithelial, adherent	Epithelial, adherent	Mixed stellate and polygonal, adherent	Adherent Mixture of Spindle-shaped and epithelial-like cells
<b>Description</b>	In vitro spontaneously transformed keratinocytes from histologically normal skin	Established from solid tumors in the skin/epidermis	Derived from the skin	Established from brain metastatic malignant melanoma (Stage IV)	Established from lymph node malignant melanoma (Stage IV)	Derived from the parental B16 cell lines as they display significantly greater tissue-invasive abilities
<b>Disease</b>	N/A	Epidermoid Carcinoma		Malignant Melanoma		
<b>Tumorigenic</b>	No	Yes	Yes	Yes	Yes	Yes

### 11.1.2 Materials for cell culture

**Table 26:** List of materials used for cell cultures [unless stated, chemicals were from Sigma Aldrich (St. Louis, MO, USA), Invitrogen (Carlsbad, CA, USA) and were of analytical grade.

Reagents	Components
<b>Complete Growth Media for A375, A431 and HaCaT cells</b>	DMEM (Dulbecco's Modified Eagle Medium) (Labtech International Ltd, East Sussex, UK) high glucose was supplemented with 10 fetal bovine resume heat-inactivated (Labtech), 2 mM <i>L</i> -Glutamine (Labtech), and 1% (v/v) penicillin/streptomycin mix.
<b>Complete Growth Media for Hs 294T and B16 F10</b>	DMEM (Dulbecco's Modified Eagle Medium) (Labtech International Ltd, East Sussex, UK) high glucose was supplemented with 10 fetal bovine resume heat-inactivated (Labtech), 4 mM <i>L</i> -Glutamine (Labtech), and 1% (v/v) penicillin/streptomycin mix.
<b>Complete Growth Media for VMM-1</b>	RPMI-1640 (Labtech International Ltd, East Sussex, UK) high glucose was supplemented with 10 fetal bovine resume heat-inactivated (Labtech), 2 mM <i>L</i> -Glutamine (Labtech), and 1% (v/v) penicillin/streptomycin mix.
<b>Phosphate Buffer Saline (PBS) [1X]</b>	[NaCl]= 140 mM, [KCl]= 2.7 mM, [Na <sub>2</sub> HPO <sub>4</sub> ]= 10 mM, [KH <sub>2</sub> PO <sub>4</sub> ]= 1.7 mM, pH 7.4
<b>Trypsin-EDTA Solution [1X]</b>	Trypsin-EDTA 0.25% in PBS w/o Mg <sup>2+</sup> , w/o Ca <sup>2+</sup> (Labtech)
<b>Cell Culture plates &amp; flasks</b>	Corning Inc., NY, USA

### **11.1.3 Cells recovery**

All cell lines were stored under vapor phase of liquid nitrogen for long term storage in fetal bovin serum (FBS) containing 10% (v/v) DMSO. Prior to use, cells were rapidly thawed and resuspended in ~5 mL of complete growth media (depending of type of cell line) and centrifuged at 2000 *rpm* for 2 min at RT. The freezing media was aspirated and the cells were resuspended in complete growth media. Then the cells suspensions were transferred into a 25 cm<sup>3</sup> cell culture flask. All cell lines were authenticated with the STR method and were also tested for mycoplasma contamination. All cell lines were cultured for 15-20 passages before new stocks were utilized.

### **11.1.4 Cells propagation**

All cell lines were cultured in flasks containing complete growth media and maintained in 5% atmospheric CO<sub>2</sub>, at 37°C, in a humidified incubator. Cells were subcultured via trypsinization 2-3 times per week prior to reaching 100% confluence. More specifically, cells were washed with ~5 mL PBS after aspirating growth media and were then washed with 1 mL of trypsin-EDTA (1X). Fresh trypsin-EDTA was added in the flask (1 mL for A375, B16 F10 cells or 2 mL for HaCaT, A431, VMM-1 and Hs 294T cells) and then cells were placed in the incubator until they detached from the flask's surface (5-10 min depending on the cell line). The cells were then observed under the microscope to ensure that they had detached and 4-5 mL of complete growth media was added into the flask in order to deactivate trypsin-EDTA. Finally, cells were resuspended and the wanted number of them was returned in the flask while more media was added (10-15 mL).

### **11.1.5 Cells plating**

After trypsinization and suspension, the cells in complete growth media were transferred into a falcon tube and then centrifuged at 2,000 *rpm* for 2 min at room temperature. Media was then aspirated, and cells were thoroughly suspended in fresh media (5-12 mL according to the

size of cell pellet) while a 30  $\mu\text{L}$  sample was transferred into a microcentrifuge tube. An equal amount of trypan blue solution 0.4% (v/v) (HyClone Inc, South Logan, USA) was added, into the tube, and mixed with the sample of cell suspension. For the determination of cell number, 10  $\mu\text{L}$  of the previously mentioned mix was loaded into a Neubauer counting chamber (hemocytometer) and the number of viable cells were counted, under the microscope. The concentration of cells (number of cells/ mL) was calculated by using the following formula:

$$[\text{CELLS}] = \frac{N}{4} \times \text{DF} \times 10^4$$

Where  $N$ = the number of cells counted in the 4 squares of the counting chamber,  $\text{DF} = 2$  (1:1 dilution with trypan blue solution) and  $10^4$  = conversion factor to convert  $10^{-4}$  mL to 1 mL (calculated according to the dimensions of the small square). After estimating the concentration of cells in the suspension, the desired number of cells were seeded into 100  $\text{mm}^3$ , cell culture dishes, 96-well plates, etc. (according to the requirements of the various experimental protocols).

## 11.2 Morphological observation of cells

A375, A431 and HaCaT cells were seeded in 100 mm dishes and exposed to either complete medium only (control) or 100  $\mu\text{M}$  of L-SK-4 for 24, 48 and 72 hr. The density of A375 cells was  $1.4 \times 10^6$ ,  $0.7 \times 10^6$  and  $0.4 \times 10^6$  per dish and the density of A431 and HaCaT cells was  $1.8 \times 10^6$ ,  $1.0 \times 10^6$  and  $0.7 \times 10^6$  for 24, 48 and 72 hr, respectively. At the indicated time points, the morphology of cells was observed by an inverted phase contrast microscope (ZOE fluorescent cell imager, Bio-rad, CA, USA) and images were captured at 20x magnification.

## 11.3 Determination of cell viability – Alamar Blue Assay

### 11.3.1 Principle of the assay:

The assay is based on the ability of the indicator resazurin (blue dye) (non-fluorescent) to be uptaken and reduced by live cells into rezorufin (pink color, fluorescent) by the oxidation of the coenzyme  $\text{NADH}/\text{H}^+$ . (**Figure 111**).<sup>711</sup>

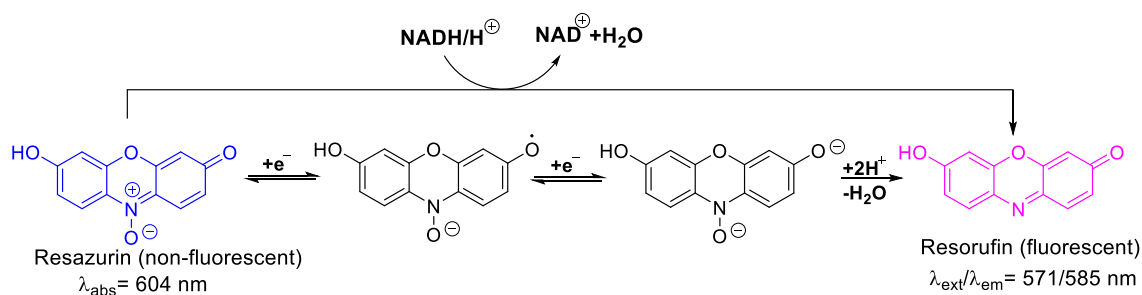


**Figure 111:** Reduction of the non-fluorescent reassuring into highly fluorescence resorufin by metabolically active (live) cells. The electrons required for the reduction reaction arise from the oxidation of the  $\text{NADH/H}^+$ .<sup>712</sup>

The detection of the levels of oxidation/reduction by means of absorbance or fluorescence intensity, indicates the quantitatively measure of cell viability.<sup>711</sup>

### 11.3.1.1 Experimental procedure:

The Alamar-blue assay was utilized in this set of experiments. A375, A431, and HaCaT cells were seeded in 100  $\mu\text{L}$ /well into 96-well plates and incubated overnight prior to exposure to each of the hydroxypyridone compounds (e.g. SK-n compounds). Density of A375 cells was 8,000, 4,000, 2,000 cells/well and for A431 and HaCaT cells 10,000, 5,000, 2,500 cells/well for 24, 48 and 72 hr, respectively. On the following day, cells were exposed to a range of concentrations of the SK-n compounds (10-1000  $\mu\text{M}$ ). In the case of co-treatments, A375 cells have been pretreated for 2 hr with either *L*-thyroxin (0.1-1 mM), BCH (0.5-10 mM), reduced-GSH (1.5-3 mM) or Myriocin (0-50  $\mu\text{M}$ ) prior to the addition of *L*-SK-4 (100  $\mu\text{M}$ ) over different incubation periods. For control conditions, cells were incubated with complete medium only. At the indicated time points, resazurin [dissolved in PBS (1mg/ mL final concentration)] was added in an amount equal to 1/10 of the volume in each well and incubated for 2-4 hr (depending on the type of cancer cell line), at 37°C. The plates were then centrifuged, and absorbance was recorded at 570 nm and 600 nm (reference wavelength) using a Spark multimode plate reader (Tecan, Switzerland). The levels of cell viability were estimated and expressed as percentage of control cells.

## 11.4 Flow Cytometry Methodologies

The following experiments have been done using FACS Canto II flow cytometer (BD Biosciences, San Jose, CA, USA). Details about the reagents that were used can be found on **Table 27**

**Table 27:** Reagents used in flow cytometry experiments

Reagent	Supplier	Item No
DHR 123	Sigma Aldrich Ltd	D1054
CellEvent Caspase 3/7	ThermoFisher Scientific Ltd	C10423
JC-1	Invitrogen	65-0851-38
FxCycle PI/RNase	ThermoFisher Scientific Ltd	F10797
DAPI	Sigma Aldrich Ltd	10236276001

### 11.4.1 Determination of ROS kinetics

#### 11.4.1.1 Principle of the assay:

Dihydrorhodamine 123 (DHR 123) is a non-fluorescent compound that reacts rapidly with either ROS or RNS and it is converted into rhodamine 123 which exhibits fluorescent intensity (**Figure 112A**).<sup>713</sup> In addition to this, 4',6 – diamidino-2-phenylindole (DAPI) is a fluorescent stain that can diffuse through the membranes of the dead cells only. Once it reaches the nucleus of the cell, it binds (by intercalation) to adenine-thymine rich regions of the major groove of the DNA (**Figure 112B**).<sup>714</sup> The utilization of DAPI aims to exclude the dead cells from the analysis, as ROS are generated by live cells.<sup>715,716</sup>

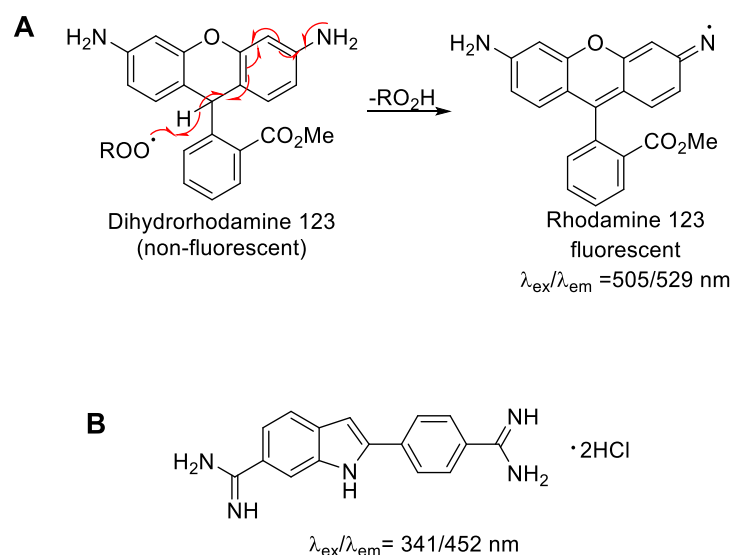


**Figure 112:** (A) DHR 123 is oxidized as illustrated by alkylperoxyl radicals into the fluorescence Rhodamine 123. (B) Structure of DAPI.<sup>713,716</sup>

The detection of the levels of rhodamine 123 by means of fluorescent intensity through flow cytometry, indicates the quantitatively the presence of ROS, whereas the fluorescent intensity of DAPI corresponds to the quantification of the dead cells.

#### 11.4.1.1.1 Experimental procedure:

Cells were seeded in 60 mm dishes ( $0.35 \times 10^6$ ,  $0.25 \times 10^6$  and  $0.15 \times 10^6$  per dish for A375), ( $0.45 \times 10^6$ ,  $0.35 \times 10^6$  and  $0.25 \times 10^6$  per dish for Hs 294T), ( $0.3 \times 10^6$ ,  $0.2 \times 10^6$  and  $0.1 \times 10^6$  per dish for B16-F10), ( $0.8 \times 10^6$ ,  $0.6 \times 10^6$  and  $0.4 \times 10^6$  per dish for VMM-1, HaCaT and A431) for 24, 48 and 72 hr, respectively and exposed to *L*-SK-4 (100  $\mu\text{M}$ ) with or without pretreatment with either reduced GSH (1.5 mM) or myriocin (50 nM). Then, they were harvested and washed twice with PBS and a single cell suspension of  $10^6$  cells/mL was prepared. DHR 123 (10  $\mu\text{M}$ ) was added in the suspension and incubated for 5 min at 37 °C. Then, DAPI (1  $\mu\text{M}$ ) was added to each sample and incubated for 5 min in order to determine the percent of dead cells in the suspension. Data acquisition and analysis of 10,000 events, for each sample. DAPI-positive cells were excluded from further analysis of the results.

## 11.4.2 Determination of apoptosis

### 11.4.2.1 Principle of the assay:

CellEvent Caspase 3/7 is a tetrapeptide (DVED) conjugated to a nucleic acid binding dye which is non-fluorescence. Upon activation of either caspase 3 or 7, in apoptotic cells, the bond between the DVED and the dye is cleaved (by caspase 3 or 7) liberating the dye which binds to the DNA and producing a fluorogenic response at 530 nm (**Figure 113**).<sup>717</sup>

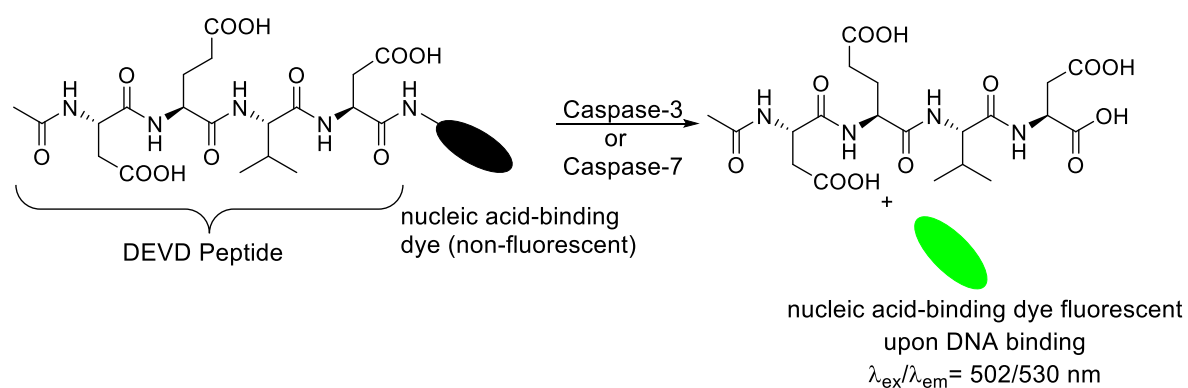


**Figure 113:** Activation of caspase 3/7 leads to the dissociation of the non-fluorescent dye from the DEVD peptide. Once it dissociated, it can reach the nucleus and upon DNA binding it emits fluorescent signal.

Once again DAPI is used in order to exclude dead (necrotic) cells from the analysis. The measured fluorescent intensity (through flow cytometry), indicates the quantitatively activation of caspase 3/7, whereas the fluorescent intensity of DAPI corresponds to the quantification of the dead (necrotic) cells.<sup>716,718</sup>

#### 11.4.2.1.1 Experimental procedure:

The CellEvent Caspase 3/7 Green flow cytometry assay kit was utilized for the detection of apoptosis according to the manufacturer's instructions. Cells were seeded and allowed to adhere overnight in 60 mm dishes ( $0.35 \times 10^6$ ,  $0.25 \times 10^6$  and  $0.15 \times 10^6$  per dish for A375), ( $0.45 \times 10^6$ ,  $0.35 \times 10^6$  and  $0.25 \times 10^6$  per dish for Hs 294T), ( $0.3 \times 10^6$ ,  $0.2 \times 10^6$  and  $0.1 \times$

$10^6$  per dish for B16-F10) ( $0.8 \times 10^6$ ,  $0.6 \times 10^6$  and  $0.4 \times 10^6$  for VMM1) per dish for 24, 48 and 72 hr, respectively and exposed to *L*-SK-4 (100  $\mu$ M) with or without pretreatment with either reduced GSH (1.5 mM) or myriocin (50 nM). Next, cells were harvested, washed twice with PBS and a single cell suspension of  $10^6$  cells/mL was prepared. Then, 0.5  $\mu$ L of CellEvent Caspase 3/7 Green detection reagent was added into 0.5 mL of each cell suspension and samples were incubated at 37°C for 30 min. Then, DAPI (1  $\mu$ M) was added to each sample and incubated for 5 min in order to determine the percent of dead cells in the suspension. Data acquisition and analysis of 20,000 events, for each sample. Caspase-3/7-positive cells were identified as apoptotic whereas DAPI-positive cells as necrotic.

### 11.4.3 Determination of mitochondria membrane depolarization

#### 11.4.3.1 Principle of the assay:

This principle of this assay is based into the ability of molecules to move across the membranes of mitochondria using the potential difference ( $\Delta\Psi$ ) between the exterior and the interior of the mitochondria.<sup>719</sup> Under pathological conditions mitochondrial membranes become permeable and the potential inside the membrane is decreased whereas the potential of the exterior space is increased.<sup>719</sup> Therefore, the high potential outside the membrane has the ability to pull 1,1',3,3'-tetraethyl-5-5',6,6' tetrachloroimidacarbocyanine iodide (JC-1) (Figure 114) stain inside mitochondrial forming aggregates with characteristic absorption/ emission properties.<sup>720</sup> In contrast, healthy mitochondria have higher interior potential preventing in that way the entrance of JC-1 into mitochondria. JC-1 that is accumulated in the exterior space forms monomers with characteristic absorption/ emission properties.<sup>720</sup>

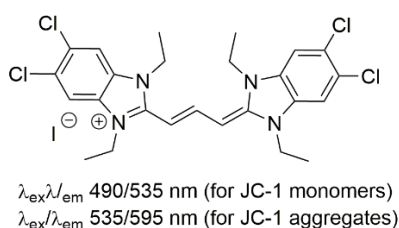


**Figure 114:** Structure of JC-1 stain.

#### 11.4.3.1.1 Experimental Procedure:

The JC-1 staining solution was used according to the manufacturer's instructions. The density of A375 cells was  $0.35 \times 10^6$ ,  $0.25 \times 10^6$  and  $0.15 \times 10^6$  cells per dish (60 mm) for 24, 48 and 72 hr, respectively. Following exposure to *L*-SK-4 (100  $\mu$ M) with or without pretreatment with myriocin (50 nM), cells were harvested and washed twice with PBS. Then, 0.3  $\mu$ L of the stain (JC-1: 0.1 mg/mL) was added into 0.3 mL of each cell suspension in PBS and samples were incubated at 37°C for 30 min. Afterwards cell suspensions were centrifuged at 1000 rpm for 5 min and the pellets were re-suspended in fresh PBS. Data acquisition and analysis of 10,000 events, for each sample.

#### 11.4.4 Determination of cell cycle kinetics

##### 11.4.4.1 Principle of the assay:

Propidium Iodide (PI) (**Figure 115**) is dye that has the ability to intercalate with the major groove of double stranded DNA upon cell death.<sup>721</sup> It can only penetrate the membranes of dead cells and therefore it can be used as an indicator for dead cells. Due to the fact that different quantities of DNA exist in the various stages of the cell cycle, PI can be used for the identification and quantification of the DNA that is presented in each phase based on the fluorescent intensity that PI arise upon DNA binding.<sup>721</sup>

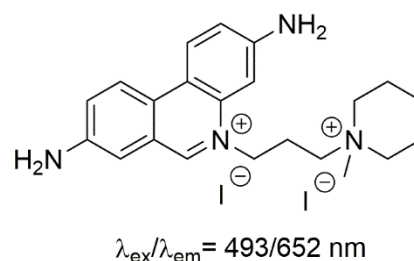


**Figure 115:** Structure of PI.

#### **11.4.4.1.1 Experimental procedure:**

The FxCycle PI/RNase staining solution was used according to the manufacturer's instructions. Following exposure to 100  $\mu$ M of L-SK-4, cells were harvested and washed twice with PBS. The density of; A375 cells was  $1.4 \times 10^6$ ,  $0.7 \times 10^6$  and  $0.4 \times 10^6$  cells per dish, A431 and HaCaT cells was  $1.8 \times 10^6$ ,  $1.0 \times 10^6$ ,  $0.7 \times 10^6$  for 24, 48 and 72 hr, respectively. Approximately  $0.5 \times 10^6$  cells were fixed in cold 70% ethanol, for 1 hr or longer, and kept at 4 °C until further processing. Cells were then washed twice with PBS to remove ethanol and finally suspended in FxCycle PI/RNase staining solution for 30 min at RT in the dark. Data acquisition and analysis of 10,000 events, for each sample.

#### **11.4.5 Protein Methodologies**

##### **11.4.5.1 Preparation of cell lysates and protein determination**

A375 cells were plated in 100 mm dishes and cultured overnight at 37°C at a density of  $1.4 \times 10^6$ ,  $0.7 \times 10^6$  and  $0.4 \times 10^6$  cells per dish for 24, 48 and 72 hr respectively. Next day, cells were treated with L-SK-4 (100  $\mu$ M) with or without pretreatment with either reduced GSH (1.5 mM) or Myriocin (50 nM) for 24, 48 and 72 hr and then trypsinized, washed twice with ice-cold PBS and pellets were collected after centrifugation at 2,000 rpm for 3 min at 4°C. Cell pellets were then lysed in lysis buffer (10 mM HEPES at pH 7.9, 10 mM KCl, 0.1 mM EDTA, 1.5 mM MgCl<sub>2</sub>, 0.2% NP40) and supplemented with Protease Inhibitor Tablets (Thermo Scientific, Waltham, MA, USA). Then, they were left on ice while periodically vortexed over a 30 min period and sonicated (three cycles at 10 amplitudes for 20 sec on ice) to disrupt cellular membranes. Cell lysates were centrifuged at full speed (15,000 rpm) for 10 min at 4°C and supernatants were transferred in new tubes. Protein content was determined by utilizing the BCA protein assay kit (Thermo Scientific, Waltham, MA, USA), according to the manufacturer's protocols. To carry out the protein concentration quantification, a standard curve using Bovine Serum Albumin (BSA) was used. Briefly, a series of various BSA

concentrations (0, 0.2, 0.5, 1, 2  $\mu\text{g}/\mu\text{L}$ ) were added into the wells of a 96-well plate by mixing the appropriate volumes of  $\text{dH}_2\text{O}$  and BSA stock to a final volume of 20  $\mu\text{L}$ . Samples were also added at a 1:10 dilution in duplicates. The appropriate volume of working reagent was prepared by mixing 50 parts of BCA reagent A with 1 part of BCA reagent B (50:1), and then 200  $\mu\text{L}$  was loaded in each well. The plate was covered and incubated at 37°C for 30 min. Finally, the plate was centrifuged at 2,000 *rpm* for 2 min before the absorbance was measured at 562nm by using a Spark multimode plate reader (Tecan, Switzerland). The unknown protein concentrations of the samples were calculated by generating a standard BSA curve. The required volume of samples was transferred to new microcentrifuge tubes and loading buffer (5X) was added as 4 parts of sample in 1 part of loading buffer. Then, the samples were either immediately used or they were stored at -20°C until future usage.

#### **11.4.5.2 Western immunoblotting**

Forty micrograms (40  $\mu\text{g}$ ) of cytoplasmic protein extracts were separated by SDS-polyacrylamide gels in SDS Running Buffer (1X) (**Table 28**) and transferred electrophoretically (120 V, 0.35 mA, 2 hr) onto PVDF membranes (either 0.45 or 0.2 $\mu\text{m}$ ) using mini gel tank and mini blot modules (Invitrogen, Carlsbad, CA, USA) using Transfer Buffer (1X). Then the blots were then blocked in 5% non-fat milk powder in TBST buffer (**Table 28**) for 2 hr at RT. After blocking, membranes were washed three times with TBST and incubated overnight at 4°C, under agitation, with the appropriate primary antibody and according to the manufacturer's protocol (**Table 29**). Next day, membranes were incubated with the appropriate horseradish peroxidase-conjugated secondary antibody (**Table 29**) for 1 hr at RT, under agitation, after being washed three times with TBST. Membranes were washed three times with TBST and labelled protein bands were detected by utilizing the SuperSignal West Pico PLUS Chemiluminescent Substrate kit from Thermo Scientific (Waltham, MA, USA) according to the manufacturer's protocol. Protein bands were visualized with the use of the G:BOX Chemi XX6/XX9 gel imaging system (Syngene, Cambridge, UK).

**Table 28:** List of Buffers used for Western Immunoblottings.

Buffer	Components
<b>SDS running buffer 10X</b>	[Tris Base] 250 mM, [Glycine]= 1% SDS, pH 8.3-8.5
<b>SDS running buffer 1X</b>	1:100 dilution of the SDS running buffer 10X
<b>Transfer Buffer 10X</b>	[Tris Base] 250 mM, [Glycine]= 1% SDS, pH 8.3-8.5
<b>Transfer Buffer 1X</b>	1:100 dilution of the Transfer Buffer 10X, 0.5% (v/v) [SDS]= (10% w/v), 20% MeOH, dH <sub>2</sub> O to bring buffer to desire volume
<b>Tris Buffered Saline-Tween 20 (TBST) 1X</b>	[Tris]= 20 mM, [NaCl]= 150 mM, 0.1% Tween 20 in dH <sub>2</sub> O, pH 7.6

**Table 29:** List of Antibodies used for Western Immunoblottings.

Antibody	Dilution	Blocking Buffer	Isotype	Company
<b>Anti-Caspase-8</b>	1:1000	5% BSA in TBST	Mouse	Cell Signaling
<b>Anti-Caspase-9</b>	1:1000	5% dry milk in TBST	Rabbit	Cell Signaling
<b>Anti-BID</b>	1:1000	5% dry milk in TBST	Rabbit	Cell Signaling
<b>Anti-Apaf-1</b>	1:1000	5% BSA in TBST	Rabbit	Cell Signaling
<b>Anti-BAX</b>	1:1000	5% BSA in TBST	Rabbit	Cell Signaling
<b>Anti-BAK</b>	1:1000	5% BSA in TBST	Rabbit	Cell Signaling
<b>Anti-FADD</b>	1:1000	5% BSA in TBST	Rabbit	Cell Signaling
<b>Anti-FAS</b>	1:1000	5% dry milk in TBST	Rabbit	Cell Signaling
<b>Anti-Tubulin</b>	1:20000	5% dry milk in TBST	Mouse	Sigma Aldrich
<b>Horse Anti-mouse conjugate Antibody</b>	1:2000	5% dry milk in TBST	Mouse	Cell Signaling
<b>Anti-HRP 2°</b>				

<b>Goat Anti-rabbit HRP conjugate</b>	1:2000	5% dry milk in TBST	Rabbit	Cell Signaling
<b>2° Antibody</b>				

#### 11.4.6 Biochemical Assays

**Table 30:** Details about the assays that have been used for the biochemical characterization.

Supplier	Assay	Item No
<b>Thiobarbituric acid (TBARS )</b>	Cambridge Bioscience Ltd Cambridge, UK	10009055
<b>Protein Carbonyl Colorimetric Assay</b>	Cambridge Bioscience Ltd, Cambridge, UK	10005020
<b>DNA oxidative Damage Elisa Assay</b>	Cambridge Bioscience Ltd, Cambridge, UK	589320

##### 11.4.6.1 TBARS assay

###### 11.4.6.1.1 Principle of the assay:

Malondialdehyde (MDA) is one of the major byproducts of lipid peroxidation, therefore its quantification can give insights into the magnitude of this effect.<sup>722</sup> MDA can react stoichiometrically under acidic conditions and heat with thiobarbituric acid forming a fluorescent adduct with characteristic excitation/ emission properties (**Figure 116**).<sup>723</sup>

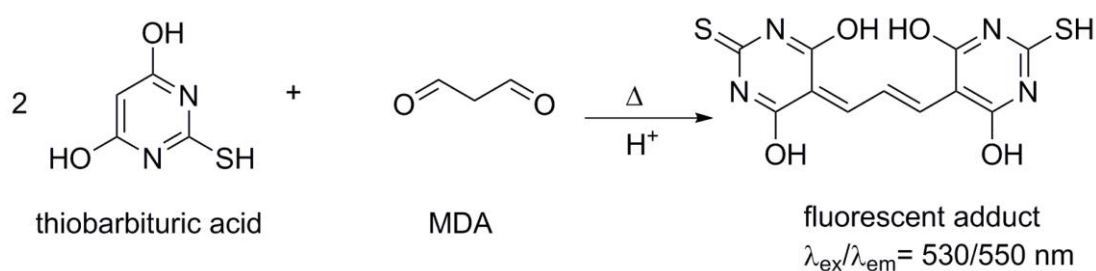


**Figure 116:** Stoichiometric reaction of MDA that produced as byproduct of lipid peroxidation with thiobarbituric acid.<sup>723</sup>

#### **11.4.6.1.1.1 Experimental procedure:**

For the determination of the concentration of malondialdehyde, A375 cells were plated in 100 mm dishes and cultured overnight at 37°C at a density of  $1.4 \times 10^6$ ,  $0.7 \times 10^6$  and  $0.4 \times 10^6$  cells per dish for 24, 48 and 72 hr respectively. Next day, cells were treated with *L*-SK-4 (100  $\mu$ M) and then trypsinised and washed twice with ice-cold PBS and pellets were collected after centrifugation at 2,000 *rpm* for 3 min at 4°C. The pellets were re-suspended in ice-cold PBS, and sonicated (three cycles at 10 amplitudes for 20 sec on ice). Afterwards 100  $\mu$ L of each sample has been mixed with 100  $\mu$ L of SDS solution and the final solution was mixed by swirling. Then, 4 mL of the color reagent was added and the solutions were heated at 95 °C for 1 hr. The reaction has been quenched by their immediate addition to ice for 10 min. After the incubation time, the vials were centrifuged at 1600 *g* at 4°C and allowed to equilibrate at room temperature for 30 min. Eventually, 150  $\mu$ L was loaded in triplicates into a 96 well plate and the absorbance was measured at 530 nm. A standard curve was generated using MDA in a range of concentrations (0-50  $\mu$ M). The results have been expressed as nmols of MDA/mg of protein.

#### **11.4.6.2 Protein Carbonyl Colorimetric Assay**

##### **11.4.6.2.1 Principle of the assay:**

The side chains of proteins tends to oxidised into the respective carbonyl compounds under oxidative stress conditions.<sup>724</sup> The identification and quantification of the protein carbonyl content, can give information about the magnitude of oxidative stress that it has been induced. In this assay the protein carbonyl content was determined using 2,4-dinitrophenylhydrazine (2,4-DNPH). Upon condensation of the carbonyl moiety of the protein with 2,4- DNPH a yellow/ orange adduct is formed with characteristic absorption properties (**Figure 117**).<sup>725</sup>

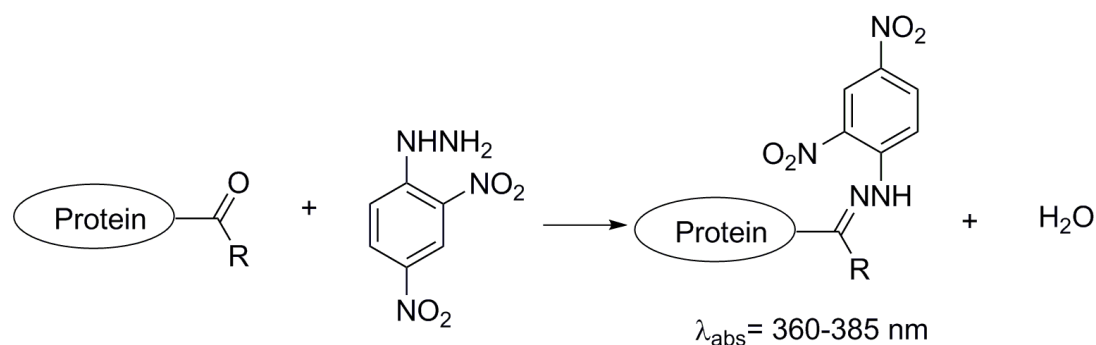


**Figure 117:** Reaction of protein carbonyl with 2,4-DNPH.<sup>725</sup>

#### 11.4.6.2.1.1 Experimental procedure:

For the determination of protein carbonyl content, A375 cells were plated in 100 mm dishes and cultured overnight at 37°C at a density of  $1.4 \times 10^6$ ,  $0.7 \times 10^6$  and  $0.4 \times 10^6$  cells per dish for 24, 48 and 72 hr respectively. Next day, cells were treated with L-SK-4 (100  $\mu\text{M}$ ) and then trypsinised and collected by centrifugation at 2000 g for 10 min at 4°C. The pellet was then re-suspended in PBS (containing 1 mM EDTA) and sonicated (three cycles at 10 amplitudes for 20 sec on ice). Then the cell suspensions were centrifuged at 10000 g for 15 min at 4°C and the supernatant was kept for assaying. A volume of 200  $\mu\text{L}$  of each sample was transferred into a 2 mL Eppendorf tubes (one tube was sample tube and the other was the control tube – for each of the assaying sample). Then 800  $\mu\text{L}$  of 2,4-DNPH was placed in the sample tube and 800  $\mu\text{L}$  of 2.5 M HCl was placed into the control tube. All the tubes were vortexed every 15 min at room temperature in the dark. Afterwards 1 mL of 20% TCA was added into each tube and then the samples were vortexed, incubated on ice for further 5 min and centrifuged at 10000 g for 10 min at 4°C. The supernatant was discarded, the pellets were re-suspended in 1 mL of ice-cold 10% TCA solution and then solutions were incubated on ice for 5 min. The tubes were then centrifuged at 10000 g for 10 min at 4°C. The supernatant was discarded and the pellet was taken up in ethanol/ ethyl acetate (1:1). The sample tubes were centrifuged at 10000 g for 10 min at 4°C. After repeating this procedure twice, the protein pellet was re-suspended in 500  $\mu\text{L}$  of guanidine hydrochloride and the final solutions were centrifuged at

10000 g for 10 min at 4°C to remove and left over debris. Afterwards, 220 µL of the supernatant (from the sample tube and control respectively) was loaded in triplicates in a 96 well plate and the absorbance was measured at 370 nm. The results were expressed as nmol/mL/mg protein/mL.

### 11.4.6.3 DNA oxidative Damage Elisa Assay

#### 11.4.6.3.1 Principle of the assay:

This principle of this assay is based on the competition between oxidised (damage) guanine and 8-OHG-acetylcholinesterase conjugate tracer for a limited amount of DNA oxidative damage monoclonal antibody. The amount of the tracer is held constant in the assay and the concentration of the oxidised guanine varies, the amount of the tracer that is capable to bind to the monoclonal antibody is inversly proportional to the concentration of the oxidised guanine (in the well). The DNA oxidative damage monoclonal antibody binds to the goat anti mouse polyclonal IgG which already coats the well (**Figure 118**).<sup>726</sup>

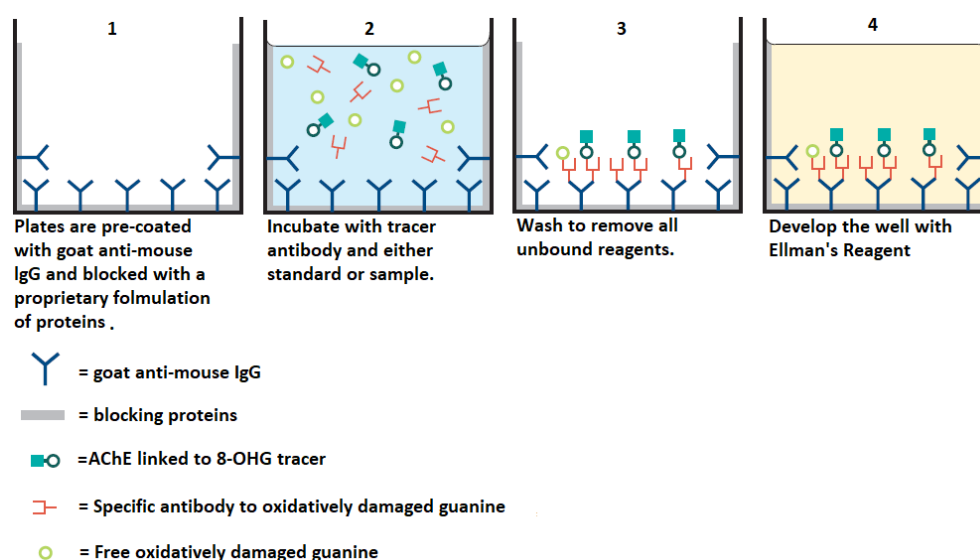


**Figure 118:** The principle of the DNA oxidative Damage Elisa assay for the determination and quantification of 8-OHdG.<sup>727</sup>

Then, the addition of Ellman's reagent (substrate of AChE) promote the enzymatic reaction where a product with distinct yellow colour is liberated and the spectrophotometric determination is proportional to the amount of DNA oxidative damage AChE tracer bound to the well and inverserly proportional to the amount of free 8-OHdG (**Figure 119**).<sup>727</sup>

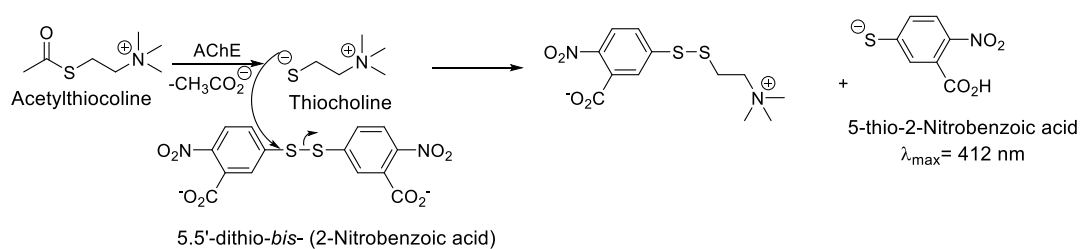


**Figure 119:** Enzymatic reaction where the tracer (Acetylthiocholine) is hydrolysed into the thiocholine which reacts further with 5,5'-dithio-bis-(2-nitrobenzoic acid) in order to produce 5-thio-2-nitrobenzoic acid which has a strong absorbance at 412 nm.<sup>727</sup>

#### 11.4.6.3.1.1 Experimental procedure:

For the determination of the concentration of 8-oxo2-deoxy guanosine (8-OHdG), A375 cells were plated in 100 mm dishes and cultured overnight at 37°C at a density of  $1.4 \times 10^6$ ,  $0.7 \times 10^6$  and  $0.4 \times 10^6$  cells per dish for 24, 48 and 72 hr respectively. Next day, cells were treated with L-SK-4 (100  $\mu\text{M}$ ) and then trypsinised and washed twice with ice-cold PBS and pellets were collected after centrifugation at 2,000 rpm for 3 min at 4°C. Then the dsDNA was extracted using the PureLinK™ Genomic DNA Mini Kit (Invitrogen- *K1820-01*) (Carlsbad, CA, USA) according to the manufacture's protocol, and it was converted into ssDNA by heat denaturation (98°C for 10 min, 0 °C for 30 sec). Afterwards, the ssDNA was digested to single nucleotides using Nuclease P1 (New England Biolabs) (0.5  $\mu\text{L}$  of Nuclease P1, 5  $\mu\text{L}$  of Nuclease P1 Buffer, 37°C for 30 min, and 75°C for 10 min for inactivation) followed by de-

phosphorylation of the nucleotide by incubating the samples with shrimp alkaline phosphatase (New England Biolabs) (1  $\mu$ L of shrimp alkaline phosphatase, 100  $\mu$ L shrimp alkaline phosphatase, 50  $\mu$ L dH<sub>2</sub>O, 37°C for 30 min, and 65°C for 5 min for inactivation). Then the plate was constructed according to the manufacture's recommendation. Then the reconstituted antibody was mixed with 60  $\mu$ L of antiserum dye and added to the wells (in a dilution 1:100) except the total activity, non-specific binding as well as the blank wells. The plate was then incubated at 4°C for 18 hr under continuous agitation. Next day, the wells were emptied, and washed 5 times with 100  $\mu$ L of Elisa Washing Buffer and then Ellman's reagent was added to each well. The plate was then incubated at room temperature and agitated in an orbital shaker for 3 hr. The absorbance was measured at 412 nm. The results were expressed as pg/mL/ng/ $\mu$ L.

## 11.5 Lipidomics

### 11.5.1 Lipidomic extraction protocol:

A375 cells were plated in 100 mm dishes and cultured overnight at 37 °C at a density of  $1.4 \times 10^6$  for 24 respectively Next day, cells were treated with *L*-SK-4 (100  $\mu$ M) and then trypsinised and collected by centrifugation at 2000 *rpm* for 3 min at 4°C. Approximately  $3 \times 10^6$  cells were washed with ice-cold PBS three times prior to extraction. Then the cell pellet was resuspended in 300  $\mu$ L of the extraction buffer (dichloromethane/methanol (3:1 v/v) chilled to 4°C) and cell lysis was induced by snap freezing the samples in liquid nitrogen for 1 min and thawed over ice. This was repeated 5 times to ensure full cell lysis. Afterwards, cell suspensions were then sonicated for 15 min and ultracentrifuged at 15000 *rpm* for 15 min. The entire supernatant was then transferred to 1.5 mL Eppendorf and allowed to evaporate at RT overnight under a fume hood. The dried down extracts were then reconstituted in 300  $\mu$ L of isopropyl alcohol/ acetonitrile/ water (2: 1: 1), sonicated for 15 min and ultracentrifuged at 15000 *rpm* for additional 15 min before transferring 100  $\mu$ L to 1.5ml autosampler vial with

200  $\mu$ L microinsert, capped and subjected to lipidomic characterization.

### **11.5.2 Sample analysis**

LC parameters: The chemical analysis was performed on a ThermoScientific Orbitap classic mass spectrometer system hyphenated to Dionex 3000 UHPLC system with the autosampler tray been set to 4°C. The separation was performed on a Waters C18 CSH analytical column, 2 x 100mm with a 1.7  $\mu$ m particle size. The column was maintained at 55°C with a flow rate of 400  $\mu$ L/min. A binary buffer system was used for the chromatographic separation. Buffer A was 60/40 (v/v ACN/MillQ water) and Buffer B (90/10 v/v isopropyl alcohol and ACN) with 10 mM ammonium formate in both and 0.1% formic acid.

### **11.5.3 LC profile**

Starting condition: 00.00 min 45% (B) → 11.00 min 65% (B) → 20.00 min 99% (B) → 24.00 min 99% (B) → 24.25 min 45% (B) → 28.50 min 45% (B).

### **11.5.4 Mass spectrometer**

The HESI source condition were as follows: Sheath gas flow: 50, Aux Gas flow: 13, Sweep gas flow: 3. Spray voltage was set 3.5 kV, Capillary temperature was set to 275°C S-lens RF level was set to 50 and the temperature of the HESI was set to 425 °C.

### **11.5.5 Mass spectral acquisition parameter**

Scan range was set from 300 to 2000 m/z at mass resolution of 140K with a scan rate of 1.6 scans/s with an automatic gain control of  $1 \times 10^6$  with a maximum injection time of 100 ms. MS1 profiling in positive polarity mode.

### **11.5.6 Peak table generations**

Compound discoverer V2, the alignment window was set to 0.25 min with mass tolerance of 5 ppm with (M-H)<sup>+</sup> adducts only. Quality control and extraction blanks was imbedded into the analysis for stability assessment and background subtractions.

### **11.5.7 Statistical analysis**

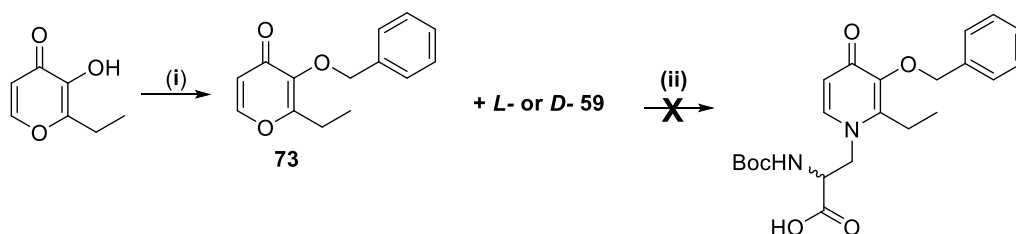
Data were expressed as mean values  $\pm$  standard deviation (SD) and comparisons were made between control and treated groups. Statistical analyses were performed by one-way ANOVA with Tukey's test for multiple comparisons after using the SPSS v.22 software. Finally, statistical significance was set at  $p < 0.05$ ,  $p < 0.01$  and  $p < 0.001$  and indicated as \* or # or  $\diamond$ , \*\* or ## or  $\diamond\diamond$  and \*\*\* or ### or  $\diamond\diamond\diamond$  respectively when compared to the respective control and/or positive control.

## 12 Appendices

### 12.1 Appendix I: derivatization of *L*-SK-4

Due to the exceptional results that *L*-SK-4 has been shown in biological evaluation against melanoma cancer and PD an attempt to optimize its structure has been contacted in order to increase the therapeutic index. The optimization aimed to increase the lipophilicity of the compound in order to improve the BBB penetration.

Therefore, the synthesis was initiated by using the ethyl maltol (2-ethyl-3-hydroxy-4-pyranone) rather than maltol. The first synthetic attempt was the same as it was described for *L* and *D*-SK-4. Namely, the synthesis was initiated with the benzyl protection of ethyl maltol follow by condensation with *N*-Boc-*L* or *D*-Asn respectively (**Scheme 41**).

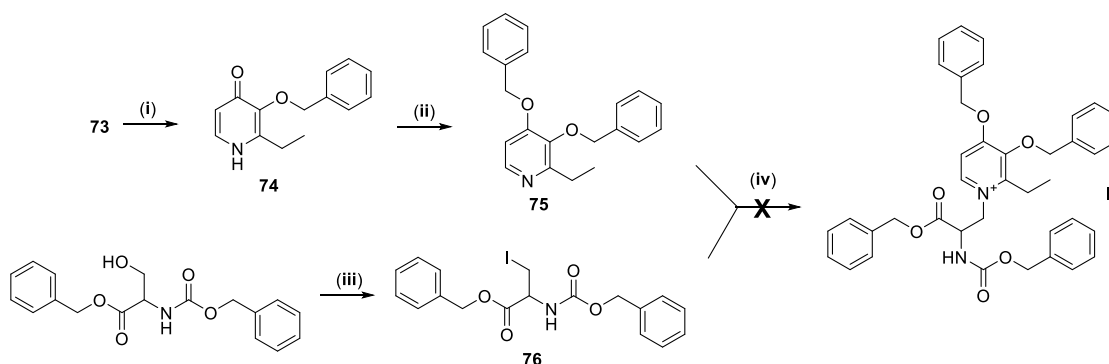


**Scheme 41:** Reagents and conditions: (i) BnBr, K<sub>2</sub>CO<sub>3</sub>, DMF, 80°C, 16 hr (73%); (ii) *L* or *D*-59, EtOH: H<sub>2</sub>O, various temperatures and times.

However, the reaction failed to proceed even after changing the temperature and the duration of the reaction.

An alternative approach has been followed according to which, the benzyl protected ethyl maltol was converted to the respective pyridone (**74**) by treatment with ammonium hydroxide in methanol in the presence of sodium hydroxide as it was previously reported in the literature

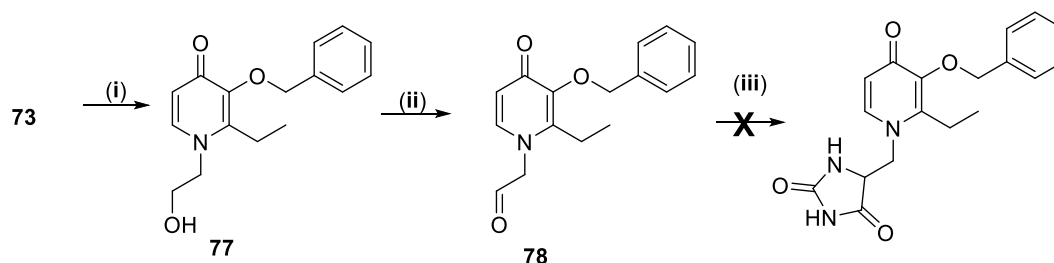
(Scheme 42).<sup>728</sup> Afterwards, by using the Mitsunobu reaction, using TPP, benzyl alcohol and DEAD, in dry THF -78°C underwent dibenylation (75) in a moderated yield (49%).<sup>728</sup>



**Scheme 42:** Reagents and conditions: (i)  $\text{NH}_4\text{OH}$ ,  $\text{NaOH}$ ,  $\text{EtOH}$ , reflux, 18 hr, 83%; (ii)  $\text{BnOH}$ ,  $\text{DEAD}$ ,  $\text{TPP}$ ,  $\text{THF}_{\text{dry}}$ ,  $-78^\circ\text{C}$ , 3 hr, 49%; (iii)  $\text{Imidazole}$ ,  $\text{TPP}$ ,  $\text{I}_2$ ,  $\text{DCM}_{\text{dry}}$ ,  $0^\circ\text{C}$  -  $20^\circ\text{C}$ , 4 hr 63%; (iv)  $\text{ACN}$ , various temperatures and times.

The formed intermediate (75) was then reacted with the iodoserine benzoyl protected intermediate (76) which was prepared according to the literature.<sup>729</sup> However, the reaction failed to proceed.

Eventually, in the last attempt, the benzyl protected intermediate (73) reacted with ethanolamine to give intermediate (77) which was then oxidized into the respective aldehyde in the presence of manganese dioxide in chloroform in excellent yield and purity (97%) (Scheme 43).<sup>730</sup>



**Scheme 43:** Reagents and conditions: (i)  $\text{Ethanolamine}$ ,  $\text{NaOH}$ ,  $\text{EtOH}$ , reflux, 16 hr, 67%; (ii)  $\text{MnO}_2$ ,  $\text{CHCl}_3$ , reflux, 2 hr, 97%, (iii)  $\text{KCN}$ ,  $(\text{NH}_4)_2\text{CO}_3$ ,  $\text{MeOH}$ ,  $\text{H}_2\text{O}$ , RT, 1 week.

Afterwards the hydantoin formation has been attempted as an amino acid precursor as it was described in (**Figure 46**) however the reaction failed once again.<sup>494</sup>

## 12.2 Appendix II: List of publications

- (I) Sotiris Kyriakou\*, Melina Mitsiogianni, Theodora Mantso, William Cheung, Stephen Todryk, Stephany Veuger, Aglaia Pappa, David Tetard and Mihalis I. Panayiotidis. Anticancer activity of a novel methylated analogue of L-mimosine against an *in vitro* model of human malignant melanoma. *Investigational New Drugs*. **2019**. *In Press*.
- (II) Sotiris Kyriakou\*, Theodora Mantso, William Cheung, Joao Victor de De Souza Cunha, Aglaia Pappa, Agnieszka Bronowska, David Tetard, Mihalis, I. Panayiotidis. A novel methylated analogue of L-mimosine exerts its therapeutic potency by promoting ROS and ceramide induced apoptosis *in vitro* model of melanoma cancer. *Molecular Cancer*. **2019**. *Submitted*.
- (III) Simon Gutbier\*, Sotiris Kyriakou\*, Stefan Schildknecht, Jeremy Brandel, Anna-Katharina Ückert, Markus Brüll, Frank Lewis, David Dickens, Liam Pearson, Joanna L. Elson, Sylvia Michel, Véronique Hubscher-Bruder, David Tetard, Marcel Leist and Ilse S. Pienaar Neuroprotection by novel hydroxypyridinone-based metal chelators in various models of parkinsonian neurodegeneration. *In preparation*.

### 13 List of References

- (1) ASC. Key Statistics for Basal and Squamous Cell Skin Cancers. 2019.
- (2) American Cancer Society. About Basal and Squamous Cell Skin Cancer.
- (3) Erb, P.; Ji, J.; Kump, E.; Mielgo, A.; Wernli, M. Apoptosis and Pathogenesis of Melanoma and Nonmelanoma Skin Cancer BT - Sunlight, Vitamin D and Skin Cancer; Reichrath, J., Ed.; Springer New York: New York, NY, 2008; pp 283–295.
- (4) Connolly, S. M.; Baker, D. R.; Coldiron, B. M.; Fazio, M. J.; Storrs, P. A.; Vidimos, A. T.; Zalla, M. J.; Brewer, J. D.; Smith Begolka, W.; Berger, T. G.; et al. AAD/ACMS/ASDSA/ASMS 2012 Appropriate Use Criteria for Mohs Micrographic Surgery: A Report of the American Academy of Dermatology, American College of Mohs Surgery, American Society for Dermatologic Surgery Association, and the American Society for Mohs Su. *J. Am. Acad. Dermatol.* **2012**, *67* (4), 531–550.
- (5) (NCRAS), N. C. R. and A. S. Non-melanoma skin cancer in England, Scotland, Northern Ireland and Ireland.
- (6) Brenn, T. Pleomorphic Dermal Neoplasms: A Review. *Adv. Anat. Pathol.* **2014**, *21*, 108–130.
- (7) Barton, V.; Armeson, K.; Hampras, S.; Ferris, L. K.; Visvanathan, K.; Rollison, D.; Alberg, A. J. Nonmelanoma Skin Cancer and Risk of All-Cause and Cancer-Related Mortality: A Systematic Review. *Arch. Dermatol. Res.* **2017**, *309* (4), 243–251.
- (8) de Vries, E.; Coebergh, J.-W. W. Melanoma Incidence Has Risen in Europe. *BMJ* **2005**, *331* (7518), 698.
- (9) Arnold, M.; Holterhues, C.; Hollestein, L. M.; Coebergh, J. W. W.; Nijsten, T.; Pukkala, E.; Holleczek, B.; Tryggvadóttir, L.; Comber, H.; Bento, M. J.; et al. Trends in Incidence and Predictions of Cutaneous Melanoma across Europe up to 2015. *J. Eur. Acad. Dermatology Venereol.* **2014**, *28* (9), 1170–1178.
- (10) CRUK. Melanoma skin cancer statistics.
- (11) Dennis, L. K. Melanoma Incidence by Body Site: Effects of Birth-Cohort Adjustment. *Arch. Dermatol.* **1999**, *135* (12), 1553–1554.
- (12) Stang, A.; Stabenow, R.; Eisinger, B.; Jöckel, K.-H. Site- and Gender-Specific Time Trend Analyses of the Incidence of Skin Melanomas in the Former German Democratic Republic (GDR) Including 19 351 Cases. *Eur. J. Cancer* **2003**, *39* (11), 1610–1618.
- (13) Pérez-Gómez, B.; Aragonés, N.; Gustavsson, P.; Lope, V.; López-Abente, G.; Pollán, M. Socio-Economic Class, Rurality and Risk of Cutaneous Melanoma by Site and Gender in Sweden. *BMC Public Health* **2008**, *8*, 33.
- (14) Bataille, V.; Winnett, A.; Sasieni, P.; Newton Bishop, J. A.; Cuzick, J. Exposure to the Sun and Sunbeds and the Risk of Cutaneous Melanoma in the UK: A Case–Control Study. *Eur. J. Cancer* **2004**, *40* (3), 429–435.
- (15) Parkin, D. M.; Mesher, D.; Sasieni, P. 13. Cancers Attributable to Solar (Ultraviolet) Radiation Exposure in the UK in 2010. *Br. J. Cancer* **2011**, *105* Suppl (Suppl 2), S66–S69.
- (16) Rushton, L.; J Hutchings, S. The Burden of Occupationally-Related Cutaneous

- Malignant Melanoma in Britain Due to Solar Radiation. *Br. J. Cancer* **2017**, *116* (4), 536–539.
- (17) Fu, S.; Wu, H.; Zhang, H.; Lian, C. G.; Lu, Q. DNA Methylation / Hydroxymethylation in Melanoma. *Oncotarget* **2017**, *8* (44), 78163–78173.
- (18) Russak, J. E.; Rigel, D. S. Risk Factors for the Development of Primary Cutaneous Melanoma. *Dermatol. Clin.* **2012**, *30* (3), 363–368.
- (19) Visvader, J. E. Cells of Origin in Cancer. *Nature* **2011**, *469* (7330), 314–322.
- (20) E Visvader, J.; J Lindeman, G. Cancer Stem Cells in Solid Tumours: Accumulating Evidence and Unresolved Questions. *Nat. Rev. Cancer* **2008**, *8*, 755–768.
- (21) Shiozawa, Y.; Nie, B.; Pienta, K. J.; Morgan, T. M.; Taichman, R. S. Cancer Stem Cells and Their Role in Metastasis. *Pharmacol. Ther.* **2013**, *138* (2), 285–293.
- (22) Klein-Szanto, A. J. P.; Ruggeri, B.; Bianchi, A.; Conti, C. J. Cellular and Molecular Changes During Mouse Skin Tumor Progression BT - Skin Carcinogenesis in Man and in Experimental Models. In *Skin Carcinogenesis in Man and in Experimental Models*; Hecker, E., Jung, E. G., Marks, F., Tilgen, W., Eds.; Springer Berlin Heidelberg: Berlin, Heidelberg, **1993**; pp 193–204.
- (23) Frame, S.; Balmain, A. Integration of Positive and Negative Growth Signals during Ras Pathway Activation in Vivo. *Curr. Opin. Genet. Dev.* **2000**, *10* (1), 106–113.
- (24) Bailleul, B.; Surani, M. A.; White, S.; Barton, S. C.; Brown, K.; Blessing, M.; Jorcano, J.; Balmain, A. Skin Hyperkeratosis and Papilloma Formation in Transgenic Mice Expressing a Ras Oncogene from a Suprabasal Keratin Promoter. *Cell* **1990**, *62* (4), 697–708.
- (25) Brown, K.; Strathdee, D.; Bryson, S.; Lambie, W.; Balmain, A. The Malignant Capacity of Skin Tumours Induced by Expression of a Mutant H-Ras Transgene Depends on the Cell Type Targeted. *Curr. Biol.* **1998**, *8* (9), 516–524.
- (26) Van Duuren, B. L. Chemical Structure, Reactivity, and Carcinogenicity of Halohydrocarbons. *Environ. Health Perspect.* **1977**, *21*, 17–23.
- (27) Monzani, E.; Facchetti, F.; Galmozzi, E.; Corsini, E.; Benetti, A.; Cavazzin, C.; Gritti, A.; Piccinini, A.; Porro, D.; Santinami, M.; et al. Melanoma Contains CD133 and ABCG2 Positive Cells with Enhanced Tumorigenic Potential. *Eur. J. Cancer* **2007**, *43* (5), 935–946.
- (28) Fang, D.; Nguyen, T. K.; Leishear, K.; Finko, R.; Kulp, A. N.; Hotz, S.; Van Belle, P. A.; Xu, X.; Elder, D. E.; Herlyn, M. A Tumorigenic Subpopulation with Stem Cell Properties in Melanomas. *Cancer Res.* **2005**, *65* (20), 9328 LP – 9337.
- (29) Kaplan, R. N.; Riba, R. D.; Zacharoulis, S.; Bramley, A. H.; Vincent, L.; Costa, C.; MacDonald, D. D.; Jin, D. K.; Shido, K.; Kerns, S. A.; et al. VEGFR1-Positive Haematopoietic Bone Marrow Progenitors Initiate the Pre-Metastatic Niche. *Nature* **2005**, *438* (7069), 820–827.
- (30) Topczewska, J.; Postovit, L.-M.; Margaryan, N.; Sam, A.; Hess, A.; W Wheaton, W.; J Nickoloff, B.; Topczewski, J.; J C Hendrix, M. Melanoma Pathogenesis and Nodal: A Partial Picture? Reply. *Nat. Med.* **2006**, *12*, 1231.
- (31) Massi, D.; Borgognoni, L.; Franchi, A.; Martini, L.; M Reali, U.; Santucci, M. Thick Cutaneous Malignant Melanoma: A Reappraisal of Prognostic Factors. *Melanoma Res.* **2000**, *10*, 153–164.

- (32) Croteau, W.; Jenkins, M. H.; Ye, S.; Mullins, D. W.; Brinckerhoff, C. E. Differential Mechanisms of Tumor Progression in Clones from a Single Heterogeneous Human Melanoma. *J. Cell. Physiol.* **2013**, 228 (4), 773–780.
- (33) Brinckerhoff, C. E. Cancer Stem Cells (CSCs) in Melanoma: There's Smoke, but Is There Fire? *J. Cell. Physiol.* **2017**, 232 (10), 2674–2678.
- (34) Ferrara, G.; Misciali, C.; Brenn, T.; Cerroni, L.; W Kazakov, D.; Perasole, A.; Russo, R.; Ricci, R.; Crisman, G.; Alessandro Fanti, P.; et al. The Impact of Molecular Morphology Techniques on the Expert Diagnosis in Melanocytic Skin Neoplasms. *Int. J. Surg. Pathol.* **2013**, 21.
- (35) Garbe, C.; Eigentler, T. K.; Keilholz, U.; Hauschild, A.; Kirkwood, J. M. Systematic Review of Medical Treatment in Melanoma: Current Status and Future Prospects. *Oncologist* **2011**, 16 (1), 5–24.
- (36) Bandarchi, B.; Ma, L.; Navab, R.; Seth, A.; Rasty, G. From Melanocyte to Metastatic Malignant Melanoma. *Dermatol. Res. Pract.* **2010**, 2010, 583748.
- (37) Marchesini, R.; Bono, A.; Bartoli, C.; Lualdi, M.; Tomatis, S.; Cascinelli, N. Optical Imaging and Automated Melanoma Detection: Questions and Answers. *Melanoma Res.* **2002**, 12, 279–286.
- (38) Balch, C. M.; Gershenwald, J. E.; Soong, S.-J.; Thompson, J. F.; Atkins, M. B.; Byrd, D. R.; Buzaid, A. C.; Cochran, A. J.; Coit, D. G.; Ding, S.; et al. Final Version of 2009 AJCC Melanoma Staging and Classification. *J. Clin. Oncol.* **2009**, 27 (36), 6199–6206.
- (39) Amin, M. B.; Greene, F. L.; Edge, S. B.; Compton, C. C.; Gershenwald, J. E.; Brookland, R. K.; Meyer, L.; Gress, D. M.; Byrd, D. R.; Winchester, D. P. The Eighth Edition AJCC Cancer Staging Manual: Continuing to Build a Bridge from a Population-Based to a More “Personalized” Approach to Cancer Staging. *CA. Cancer J. Clin.* **2017**, 67 (2), 93–99.
- (40) Cadet, J.; Grand, A.; Douki, T. Solar UV Radiation-Induced DNA Bipyrimidine Photoproducts: Formation and Mechanistic Insights BT - Photoinduced Phenomena in Nucleic Acids II: DNA Fragments and Phenomenological Aspects. In *Photoinduced Phenomena in Nucleic Acids II*; Barbatti, M., Borin, A. C., Ullrich, S., Eds.; Springer International Publishing: Cham, 2015; pp 249–275.
- (41) Joosse, A.; De Vries, E.; Van Eijck, C. H.; Eggermont, A. M. M.; Nijsten, T.; Coebergh, J. W. W. Reactive Oxygen Species and Melanoma: An Explanation for Gender Differences in Survival? *Pigment Cell Melanoma Res.* **2010**, 23 (3), 352–364.
- (42) De Gannes, G. C.; Ip, J. L.; Martinka, M.; Crawford, R. I.; Rivers, J. K. Early Detection of Skin Cancer by Family Physicians: A Pilot Project. *J. Cutan. Med. Surg. Inc. Med. Surg. Dermatology* **2004**, 8 (2), 103–109.
- (43) Kozar, I.; Cesi, G.; Margue, C.; Philippidou, D.; Kreis, S. Impact of BRAF Kinase Inhibitors on the MiRNomes and Transcriptomes of Melanoma Cells. *Biochim. Biophys. Acta - Gen. Subj.* **2017**, 1861 (11, Part B), 2980–2992.
- (44) Hartmann, S.; Brands, R. C.; Kuchler, N.; Fuchs, A.; Linz, C.; Kübler, A. C.; Müller-Richter, U. D. A. Melanoma-Associated Antigen Expression and the Efficacy of Tyrosine Kinase Inhibitors in Head and Neck Cancer. *Oncol. Lett.* **2015**, 10 (2), 1211–1217.
- (45) Weinstein, D.; Leininger, J.; Hamby, C.; Safai, B. Diagnostic and Prognostic Biomarkers in Melanoma. *J. Clin. Aesthet. Dermatol.* **2014**, 7 (6), 13–24.

- (46) Posch, C.; Vujic, I.; Monshi, B.; Sanlorenzo, M.; Weihsengruber, F.; Rappersberger, K.; Ortiz-Urda, S. Searching for the Chokehold of NRAS Mutant Melanoma. *J. Invest. Dermatol.* **2016**, *136* (7), 1330–1336.
- (47) Kawakami, A.; Fisher, D. E. The Master Role of Microphthalmia-Associated Transcription Factor in Melanocyte and Melanoma Biology. *Lab. Investig.* **2017**, *97* (6), 649–656.
- (48) Grimaldi, A. M.; Simeone, E.; Festino, L.; Vanella, V.; Strudel, M.; Ascierto, P. A. MEK Inhibitors in the Treatment of Metastatic Melanoma and Solid Tumors. *Am. J. Clin. Dermatol.* **2017**, *18* (6), 745–754.
- (49) Ribas, A.; T Flaherty, K. BRAF Targeted Therapy Changes the Treatment Paradigm in Melanoma. *Nat. Rev. Clin. Oncol.* **2011**, *8*, 426–433.
- (50) Latimer, N. R.; Bell, H.; Abrams, K. R.; Amonkar, M. M.; Casey, M. Adjusting for Treatment Switching in the METRIC Study Shows Further Improved Overall Survival with Trametinib Compared with Chemotherapy. *Cancer Med.* **2016**, *5* (5), 806–815.
- (51) Daponte, A.; Signoriello, S.; Maiorino, L.; Massidda, B.; Simeone, E.; Grimaldi, A. M.; Caracò, C.; Palmieri, G.; Cossu, A.; Botti, G.; et al. Phase III Randomized Study of Fotemustine and Dacarbazine versus Dacarbazine with or without Interferon- $\alpha$  in Advanced Malignant Melanoma. *J. Transl. Med.* **2013**, *11*, 38.
- (52) Simeone, E.; Grimaldi, A. M.; Festino, L.; Vanella, V.; Palla, M.; Ascierto, P. A. Combination Treatment of Patients with BRAF-Mutant Melanoma: A New Standard of Care. *BioDrugs* **2017**, *31* (1), 51–61.
- (53) Margolin, K. The Promise of Molecularly Targeted and Immunotherapy for Advanced Melanoma. *Curr. Treat. Options Oncol.* **2016**, *17* (9), 48.
- (54) Sim, G. C.; Chacon, J.; Haymaker, C.; Ritthipichai, K.; Singh, M.; Hwu, P.; Radvanyi, L. Tumor-Infiltrating Lymphocyte Therapy for Melanoma: Rationale and Issues for Further Clinical Development. *BioDrugs* **2014**, *28* (5), 421–437.
- (55) Rosenberg, S. A.; Dudley, M. E. Adoptive Cell Therapy for the Treatment of Patients with Metastatic Melanoma. *Curr. Opin. Immunol.* **2009**, *21* (2), 233–240.
- (56) Bright, R.; Coventry, B.; Eardley-Harris, N.; Briggs, N. Clinical Response Rates From Interleukin-2 Therapy for Metastatic Melanoma Over 30 Years' Experience: A Meta-Analysis of 3312 Patients. *J. Immunother.* **2016**, *40*, 1.
- (57) Anh Trinh, V.; Zobniw, C.; Hwu, W.-J. The Efficacy and Safety of Adjuvant Interferon-Alfa Therapy in the Evolving Treatment Landscape for Resected High-Risk Melanoma. *Expert Opin. Drug Saf.* **2017**, *16*.
- (58) Laks, S.; Brueske, K. A.; Hsueh, E. C. Neoadjuvant Treatment of Melanoma: Case Reports and Review. *Exp. Hematol. Oncol.* **2013**, *2* (1), 30.
- (59) González, N.; Ratner, D. Novel Melanoma Therapies and Their Side Effects. *Cutis* **2016**, *97*, 426–428.
- (60) Lee, D.; Porter, J.; Hertel, N.; Hatswell, A. J.; Briggs, A. Modelling Comparative Efficacy of Drugs with Different Survival Profiles: Ipilimumab, Vemurafenib and Dacarbazine in Advanced Melanoma. *BioDrugs* **2016**, *30* (4), 307–319.
- (61) Yun, S.; Vincelette, N. D.; Green, M. R.; Wahner Hendrickson, A. E.; Abraham, I. Targeting Immune Checkpoints in Unresectable Metastatic Cutaneous Melanoma: A Systematic Review and Meta-Analysis of Anti-CTLA-4 and Anti-PD-1 Agents

- Trials. *Cancer Med.* **2016**, *5* (7), 1481–1491.
- (62) Hassel, J. C.; Heinzerling, L.; Aberle, J.; Bähr, O.; Eigentler, T. K.; Grimm, M.-O.; Grünwald, V.; Leipe, J.; Reinmuth, N.; Tietze, J. K.; et al. Combined Immune Checkpoint Blockade (Anti-PD-1/Anti-CTLA-4): Evaluation and Management of Adverse Drug Reactions. *Cancer Treat. Rev.* **2017**, *57*, 36–49.
- (63) Quéreux, G.; Dréno, B. Fotemustine for the Treatment of Melanoma. *Expert Opin. Pharmacother.* **2011**, *12* (18), 2891–2904.
- (64) Diamantopoulos, P.; Gogas, H. Melanoma Immunotherapy Dominates the Field. *Ann. Transl. Med.* **2016**, *4* (14), 269.
- (65) Gampa, G.; Vaidhyanathan, S.; Sarkaria, J. N.; Elmquist, W. F. Drug Delivery to Melanoma Brain Metastases: Can Current Challenges Lead to New Opportunities? *Pharmacol. Res.* **2017**, *123*, 10–25.
- (66) Maret, W. The Metals in the Biological Periodic System of the Elements: Concepts and Conjectures. *International Journal of Molecular Sciences.* **2016**.
- (67) Fouani, L.; Menezes, S. V.; Paulson, M.; Richardson, D. R.; Kovacevic, Z. Metals and Metastasis: Exploiting the Role of Metals in Cancer Metastasis to Develop Novel Anti-Metastatic Agents. *Pharmacol. Res.* **2017**, *115*, 275–287.
- (68) Osredkar, J. Copper and Zinc, Biological Role and Significance of Copper/Zinc Imbalance. *J. Clin. Toxicol.* **2014**, *3* (1), 1–18.
- (69) PARISI, A. F.; VALLEE, B. L. Zinc Metalloenzymes: Characteristics and Significance in Biology and Medicine. *Am. J. Clin. Nutr.* **1969**, *22* (9), 1222–1239.
- (70) Elledge, S. J.; Zhou, Z.; Allen, J. B. Ribonucleotide Reductase: Regulation, Regulation, Regulation. *Trends Biochem. Sci.* **1992**, *17* (3), 119–123.
- (71) Gupta, S. K.; Shukla, V. K.; Vaidya, M. P.; Roy, S. K.; Gupta, S. Serum and Tissue Trace Elements in Colorectal Cancer. *J. Surg. Oncol.* **1993**, *52* (3), 172–175.
- (72) Gupte, A.; Mumper, R. J. Elevated Copper and Oxidative Stress in Cancer Cells as a Target for Cancer Treatment. *Cancer Treat. Rev.* **2009**, *35* (1), 32–46.
- (73) Nilsson, M.; Adamo, H.; Bergh, A.; Halin Bergström, S. Inhibition of Lysyl Oxidase and Lysyl Oxidase-Like Enzymes Has Tumour-Promoting and Tumour-Suppressing Roles in Experimental Prostate Cancer. *Sci. Rep.* **2016**, *6*, 19608.
- (74) Bhuvanasundar, R.; John, A.; Sulochana, K. N.; Coral, K.; Deepa, P. R.; Umashankar, V. A Molecular Model of Human Lysyl Oxidase (LOX) with Optimal Copper Orientation in the Catalytic Cavity for Induced Fit Docking Studies with Potential Modulators. *Bioinformation* **2014**, *10* (7), 406–412.
- (75) Serrano-Gomez, S. J.; Maziveyi, M.; Alahari, S. K. Regulation of Epithelial-Mesenchymal Transition through Epigenetic and Post-Translational Modifications. *Mol. Cancer* **2016**, *15* (1), 18.
- (76) MacDonald, G.; Nalvarte, I.; Smirnova, T.; Vecchi, M.; Aceto, N.; Doelemeyer, A.; Frei, A.; Lienhard, S.; Wyckoff, J.; Hess, D.; et al. Memo Is a Copper-Dependent Redox Protein with an Essential Role in Migration and Metastasis. *Sci. Signal.* **2014**, *7* (329), ra56 LP-ra56.
- (77) Coleman, J. E. ZINC PROTEINS: Enzymes, Storage Proteins, Transcription Factors, and Replication Proteins. *Annu. Rev. Biochem.* **1992**, *61* (1), 897–946.

- (78) Jacobsen, J. A.; Major Jourden, J. L.; Miller, M. T.; Cohen, S. M. To Bind Zinc or Not to Bind Zinc: An Examination of Innovative Approaches to Improved Metalloproteinase Inhibition. *Biochim. Biophys. Acta - Mol. Cell Res.* **2010**, *1803* (1), 72–94.
- (79) Uzzo, R. G.; Crispen, P. L.; Golovine, K.; Makhov, P.; Horwitz, E. M.; Kolenko, V. M. Diverse Effects of Zinc on NF-KB and AP-1 Transcription Factors: Implications for Prostate Cancer Progression. *Carcinogenesis* **2006**, *27* (10), 1980–1990.
- (80) Cai, M.-Y.; Luo, R.-Z.; Li, Y.-H.; Dong, P.; Zhang, Z.-L.; Zhou, F.-J.; Chen, J.-W.; Yun, J.-P.; Zhang, C. Z.-Y.; Cao, Y. High-Expression of ZBP-89 Correlates with Distal Metastasis and Poor Prognosis of Patients in Clear Cell Renal Cell Carcinoma. *Biochem. Biophys. Res. Commun.* **2012**, *426* (4), 636–642.
- (81) Borghaei, R. C.; Gorski, G.; Seutter, S.; Chun, J.; Khaselov, N.; Scianni, S. Zinc-Binding Protein-89 (ZBP-89) Cooperates with NF-KB to Regulate Expression of Matrix Metalloproteinases (MMPs) in Response to Inflammatory Cytokines. *Biochem. Biophys. Res. Commun.* **2016**, *471* (4), 503–509.
- (82) Zhang, C. Z. Y.; Chen, G. G.; Lai, P. B. S. Transcription Factor ZBP-89 in Cancer Growth and Apoptosis. *Biochim. Biophys. Acta - Rev. Cancer* **2010**, *1806* (1), 36–41.
- (83) Jung, M.; Mertens, C.; Tomat, E.; Brüne, B. Iron as a Central Player and Promising Target in Cancer Progression. *International Journal of Molecular Sciences*. 2019.
- (84) Kwok, J. C.; Richardson, D. R. The Iron Metabolism of Neoplastic Cells: Alterations That Facilitate Proliferation? *Crit. Rev. Oncol. Hematol.* **2002**, *42* (1), 65–78.
- (85) Bauckman, K.; Haller, E.; Taran, N.; Rockfield, S.; Ruiz-Rivera, A.; Nanjundan, M. Iron Alters Cell Survival in a Mitochondria-Dependent Pathway in Ovarian Cancer Cells. *Biochem. J.* **2015**, *466* (2), 401–413.
- (86) Steegmann-Olmedillas, J. L. The Role of Iron in Tumour Cell Proliferation. *Clin. Transl. Oncol.* **2011**, *13* (2), 71–76.
- (87) Fischer-Fodor, E.; Miklasova, N.; Berindan-Neagoe, I.; Saha, B. Iron, Inflammation and Invasion of Cancer Cells. *Med. Pharm. Reports* **2015**, *88* (3), 272–277.
- (88) Freitas, I.; Boncompagni, E.; Vaccarone, R.; Fenoglio, C.; Barni, S.; Baronzio, G. F. Iron Accumulation in Mammary Tumor Suggests a Tug of War between Tumor and Host for the Microelement. *Anticancer Res.* **2007**, *27* (5 A), 3059–3065.
- (89) Jian, J.; Yang, Q.; Shao, Y.; Axelrod, D.; Smith, J.; Singh, B.; Krauter, S.; Chiriboga, L.; Yang, Z.; Li, J.; et al. A Link between Premenopausal Iron Deficiency and Breast Cancer Malignancy. *BMC Cancer* **2013**, *13* (1), 307.
- (90) Rossiello, R.; Carriero, M. V.; Giordano, G. G. Distribution of Ferritin, Transferrin and Lactoferrin in Breast Carcinoma Tissue. *J. Clin. Pathol.* **1984**, *37* (1), 51 LP – 55.
- (91) Jézéquel, P.; Campion, L.; Spyrtos, F.; Loussouarn, D.; Campone, M.; Guérin-Charbonnel, C.; Joalland, M.-P.; André, J.; Descotes, F.; Grenot, C.; et al. Validation of Tumor-Associated Macrophage Ferritin Light Chain as a Prognostic Biomarker in Node-Negative Breast Cancer Tumors: A Multicentric 2004 National PHRC Study. *Int. J. Cancer* **2012**, *131* (2), 426–437.
- (92) Wang, W.; Deng, Z.; Hatcher, H.; Miller, L. D.; Di, X.; Tesfay, L.; Sui, G.; D&#039;Agostino, R. B.; Torti, F. M.; Torti, S. V. IRP2 Regulates Breast Tumor Growth. *Cancer Res.* **2014**, *74* (2), 497 LP – 507.
- (93) Greene, C. J.; Attwood, K.; Sharma, N. J.; Gross, K. W.; Smith, G. J.; Xu, B.;

- Kauffman, E. C. Transferrin Receptor 1 Upregulation in Primary Tumor and Downregulation in Benign Kidney Is Associated with Progression and Mortality in Renal Cell Carcinoma Patients. *Oncotarget* **2017**, 8 (63), 107052–107075.
- (94) Chanvorachote, P.; Luanpitpong, S. Iron Induces Cancer Stem Cells and Aggressive Phenotypes in Human Lung Cancer Cells. *Am. J. Physiol. Physiol.* **2016**, 310 (9), C728–C739.
- (95) Nicco, C.; Laurent, A.; Chereau, C.; Weill, B.; Batteux, F. Differential Modulation of Normal and Tumor Cell Proliferation by Reactive Oxygen Species. *Biomed. Pharmacother.* **2005**, 59 (4), 169–174.
- (96) Fruehauf, J. P.; Meyskens, F. L. Reactive Oxygen Species: A Breath of Life or Death? *Clin. Cancer Res.* **2007**, 13 (3), 789 LP – 794.
- (97) SINGH, K. K. Mitochondria Damage Checkpoint, Aging, and Cancer. *Ann. N. Y. Acad. Sci.* **2006**, 1067 (1), 182–190.
- (98) Burdon, R. H.; Gill, V.; Rice-Evans, C. Oxidative Stress and Tumour Cell Proliferation. *Free Radic. Res. Commun.* **1990**, 11 (1–3), 65–76.
- (99) Wang, Z.; Li, Y.; Sarkar, F. Signaling Mechanism(S) of Reactive Oxygen Species in Epithelial-Mesenchymal Transition Reminiscent of Cancer Stem Cells in Tumor Progression. *Curr. Stem Cell Res. Ther.* **2010**, 5 (1), 74–80.
- (100) Lau, S. T.; Lin, Z. X.; Leung, P. S. Role of Reactive Oxygen Species in Brucein D-Mediated P38-Mitogen-Activated Protein Kinase and Nuclear Factor-KB Signalling Pathways in Human Pancreatic Adenocarcinoma Cells. *Br. J. Cancer* **2010**, 102, 583.
- (101) McCarthy, N. Oncogene Detox Programme. *Nat. Rev. Cancer* **2011**, 11, 622.
- (102) Liu-Smith, F.; Dellinger, R.; Meyskens Jr, F. L. Updates of Reactive Oxygen Species in Melanoma Etiology and Progression. *Arch. Biochem. Biophys.* **2014**, 563, 51–55.
- (103) Heo, J.-R.; Lee, G.-A.; Kim, G.-S.; Hwang, K.-A.; Choi, K.-C. Phytochemical-Induced Reactive Oxygen Species and Endoplasmic Reticulum Stress-Mediated Apoptosis and Differentiation in Malignant Melanoma Cells. *Phytomedicine* **2018**, 39, 100–110.
- (104) Lin, S.; Zheng, W.; Liu, J.; Zhang, Y.; Qin, H.; Wu, H.; Xue, B.; Lu, Y.; Shen, P. Oxidative Stress in Malignant Melanoma Enhances TNF- $\alpha$  Secretion of Tumor-Associated Macrophages That Promote Cancer Cell Invasion. *Antioxid. Redox Signal.* **2013**, 19.
- (105) Russo, M. T.; De Luca, G.; Casorelli, I.; Degan, P.; Molatore, S.; Barone, F.; Mazzei, F.; Pannellini, T.; Musiani, P.; Bignami, M. Role of MUTYH and MSH2 in the Control of Oxidative DNA Damage, Genetic Instability, and Tumorigenesis. *Cancer Res.* **2009**, 69 (10), 4372 LP – 4379.
- (106) Kyriakou, S.; Mitsiogianni, M.; Mantso, T.; Cheung, W.; Todryk, S.; Veuger, S.; Pappa, A.; Tetard, D.; Panayiotidis, M. I. Anticancer Activity of a Novel Methylated Analogue of L-Mimosine against an in Vitro Model of Human Malignant Melanoma. *Invest. New Drugs* **2019**.
- (107) Carocho, M.; Ferreira, I. C. F. R. A Review on Antioxidants, Prooxidants and Related Controversy: Natural and Synthetic Compounds, Screening and Analysis Methodologies and Future Perspectives. *Food Chem. Toxicol.* **2013**, 51, 15–25.
- (108) Khan, N. M.; Sandur, S. K.; Checker, R.; Sharma, D.; Poduval, T. B.; Sainis, K. B. Pro-Oxidants Ameliorate Radiation-Induced Apoptosis through Activation of the

Calcium–ERK1/2–Nrf2 Pathway. *Free Radic. Biol. Med.* **2011**, *51* (1), 115–128.

- (109) León-González, A. J.; Auger, C.; Schini-Kerth, V. B. Pro-Oxidant Activity of Polyphenols and Its Implication on Cancer Chemoprevention and Chemotherapy. *Biochem. Pharmacol.* **2015**, *98* (3), 371–380.
- (110) Predebon, J. M.; Bond, R. D.; Brzozowski, J.; Jankowski, H.; Deane, F.; Tarleton, M.; Shaw, A. A.; McCluskey, A.; Bowyer, C. M.; Weidenhofer, J.; et al. The Bispidinone Derivative 3,7-Bis-[2-(S)-Amino-3-(1H-Indol-3-Yl)-Propionyl]-1,5-Diphenyl-3,7-Diazabicyclo[3.3.1]Nonan-9-One Dihydrochloride Induces an Apoptosis-Mediated Cytotoxic Effect on Pancreatic Cancer Cells In Vitro. *Molecules.* **2019**.
- (111) Juran, S.; Walther, M.; Stephan, H.; Bergmann, R.; Steinbach, J.; Kraus, W.; Emmerling, F.; Comba, P. Hexadentate Bispidine Derivatives as Versatile Bifunctional Chelate Agents for Copper(II) Radioisotopes. *Bioconjug. Chem.* **2009**, *20* (2), 347–359.
- (112) Heimburg, T.; Chakrabarti, A.; Lancelot, J.; Marek, M.; Melesina, J.; Hauser, A. T.; Shaik, T. B.; Duclaud, S.; Robaa, D.; Erdmann, F.; et al. Structure-Based Design and Synthesis of Novel Inhibitors Targeting HDAC8 from *Schistosoma Mansoni* for the Treatment of Schistosomiasis. *J. Med. Chem.* **2016**, *59* (6), 2423–2435.
- (113) Heimburg, T.; Kolbinger, F. R.; Zeyen, P.; Ghazy, E.; Herp, D.; Schmidt-kunz, K.; Melesina, J.; Shaik, T. B.; Erdmann, F.; Schmidt, M.; et al. Structure-Based Design and Biological Characterization of Selective Histone Deacetylase 8 (HDAC8) Inhibitors with Anti-Neuroblastoma Activity. *J. Med. Chem.* **2017**, *60* (24), 10188–10204.
- (114) Brard, L.; Granai, C. O.; Swamy, N. Iron Chelators Deferoxamine and Diethylenetriamine Pentaacetic Acid Induce Apoptosis in Ovarian Carcinoma. *Gynecol. Oncol.* **2006**, *100* (1), 116–127.
- (115) Salis, O.; Bedir, A.; Kilinc, V.; Alacam, H.; Gulten, S.; Okuyucu, A. The Anticancer Effects of Desferrioxamine on Human Breast Adenocarcinoma and Hepatocellular Carcinoma Cells. *Cancer Biomark* **2014**, *14*.
- (116) Potuckova, E.; Jansova, H.; Machacek, M.; Vavrova, A.; Haskova, P.; Tichotova, L.; Richardson, V.; Kalinowski, D. S.; Richardson, D. R.; Simunek, T. Quantitative Analysis of the Anti-Proliferative Activity of Combinations of Selected Iron-Chelating Agents and Clinically Used Anti-Neoplastic Drugs. *PLoS One* **2014**, *9* (2), e88754.
- (117) Dayani, P. N.; Bishop, M. C.; Black, K.; Zeltzer, P. M. Desferoxamine (DFO) – Mediated Iron Chelation: Rationale for a Novel Approach to Therapy for Brain Cancer. *J. Neurooncol.* **2004**, *67* (3), 367–377.
- (118) Ford, S. J.; Obeidy, P.; Lovejoy, D. B.; Bedford, M.; Nichols, L.; Chadwick, C.; Tucker, O.; Lui, G. Y. L.; Kalinowski, D. S.; Jansson, P. J.; et al. Deferasirox (ICL670A) Effectively Inhibits Oesophageal Cancer Growth in Vitro and in Vivo. *Br. J. Pharmacol.* **2013**, *168* (6), 1316–1328.
- (119) Kohno, J.; Hirano, N.; Sugawara, K.; Nishio, M.; Hashiyama, T.; Nakanishi, N.; Komatsubara, S. Structure of TMC-69, a New Antitumor Antibiotic from *Chrysosporium* Sp. TC 1068. *Tetrahedron* **2001**, *57* (9), 1731–1735.
- (120) Major Jourden, J. L.; Cohen, S. M. Hydrogen Peroxide Activated Matrix Metalloproteinase Inhibitors: A Prodrug Approach. *Angew. Chemie Int. Ed.* **2010**, *49* (38), 6795–6797.

- (121) Agrawal, A.; Romero-Perez, D.; Jacobsen, J. A.; Villarreal, F. J.; Cohen, S. M. Zinc-Binding Groups Modulate Selective Inhibition of MMPs. *ChemMedChem* **2008**, *3* (5), 812–820.
- (122) Zheng, B.; Yao, Y.; Liu, Z.; Deng, L.; Anglin, J. L.; Jiang, H.; Prasad, B. V. V.; Song, Y. Crystallographic Investigation and Selective Inhibition of Mutant Isocitrate Dehydrogenase. *ACS Med. Chem. Lett.* **2013**, *4* (6), 542–546.
- (123) Liu, Z.; Yao, Y.; Kogiso, M.; Zheng, B.; Deng, L.; Qiu, J. J.; Dong, S.; Lv, H.; Gallo, J. M.; Li, X.-N.; et al. Inhibition of Cancer-Associated Mutant Isocitrate Dehydrogenases: Synthesis, Structure–Activity Relationship, and Selective Antitumor Activity. *J. Med. Chem.* **2014**, *57* (20), 8307–8318.
- (124) Hanif, M.; Henke, H.; Meier, S. M.; Martic, S.; Labib, M.; Kandioller, W.; Jakupec, M. A.; Arion, V. B.; Kraatz, H. B.; Keppler, B. K.; et al. Is the Reactivity of M(II)-Arene Complexes of 3-Hydroxy-2(1 H)-Pyridones to Biomolecules the Anticancer Activity Determining Parameter? *Inorg. Chem.* **2010**, *49* (17), 7953–7963.
- (125) Puerta, D. T.; Lewis, J. A.; Cohen, S. M. New Beginnings for Matrix Metalloproteinase Inhibitors: Identification of High-Affinity Zinc-Binding Groups. *J. Am. Chem. Soc.* **2004**, *126* (27), 8388–8389.
- (126) Chapman, T. M.; Gillen, K. J.; Wallace, C.; Lee, M. T.; Bakrania, P.; Khurana, P.; Coombs, P. J.; Stennett, L.; Fox, S.; Bureau, E. A.; et al. Catechols and 3-Hydroxypyridones as Inhibitors of the DNA Repair Complex ERCC1-XPF. *Bioorganic Med. Chem. Lett.* **2015**, *25* (19), 4097–4103.
- (127) Saghaie, L.; Ashaehshoar, M. Synthesis, Analysis and Cytotoxic Evaluation of Some Hydroxypyridinone Derivatives on HeLa and K562 Cell Lines. *Res. Pharm. Sci.* **2013**, *8* (3), 185–195.
- (128) Saghaie, L.; Kafiri, M. Synthesis and Biological Evaluation of Bidentate 3-Hydroxypyridin-4-Ones Iron Chelating Agents. *Res. Pharm. Sci.* **2011**, *6* (2), 117–122.
- (129) Simonart, T.; Boelaert, J. R.; Mosselmans, R.; Andrei, G.; Noel, J. C.; De Clercq, E.; Snoeck, R. Antiproliferative and Apoptotic Effects of Iron Chelators on Human Cervical Carcinoma Cells. *Gynecol. Oncol.* **2002**, *85* (1), 95–102.
- (130) Jourden, J. L. M.; Daniel, K. B.; Cohen, S. M. Investigation of Self-Immolative Linkers in the Design of Hydrogen Peroxide Activated Metalloprotein Inhibitors. *Chem. Commun.* **2011**, *47* (28), 7968–7970.
- (131) Selig, R. A.; White, L.; Gramacho, C.; Sterling-Levis, K.; Fraser, I. W.; Naidoo, D. Failure of Iron Chelators to Reduce Tumor Growth in Human Neuroblastoma Xenografts. *Cancer Res.* **1998**, *58* (3), 473–478.
- (132) Jacobsen, J. A.; Major Jourden, J. L.; Miller, M. T.; Cohen, S. M. To Bind Zinc or Not to Bind Zinc: An Examination of Innovative Approaches to Improved Metalloproteinase Inhibition. *Biochim. Biophys. Acta - Mol. Cell Res.* **2010**, *1803* (1), 72–94.
- (133) Chenoufi, N.; Drénou, B.; Loréal, O.; Pigeon, C.; Brissot, P.; Lescoat, G. Antiproliferative Effect of Deferiprone on the Hep G2 Cell Line. *Biochem. Pharmacol.* **1998**, *56* (4), 431–437.
- (134) Yasumoto, E.; Nakano, K.; Nakayachi, T.; Morshed, S. R. M.; Hashimoto, K.; Kikuchi, H.; Nishikawa, H.; Kawase, M.; Sakagami, H. Cytotoxic Activity of Deferiprone, Maltol and Related Hydroxyketones against Human Tumor Cell Lines.

*Anticancer Res.* **2004**, *24* (2 B), 755–762.

- (135) Simões, R. V.; Veeraperumal, S.; Serganova, I. S.; Kruchevsky, N.; Varshavsky, J.; Blasberg, R. G.; Ackerstaff, E.; Koutcher, J. A. Inhibition of Prostate Cancer Proliferation by Deferiprone. *NMR Biomed.* **2017**, *30* (6), 1–11.
- (136) Nguyen, B. C. Q.; Tawata, S. The Chemistry and Biological Activities of Mimosine: A Review. *Phyther. Res.* **2016**, *1242* (April), 1230–1242.
- (137) Li, X. W.; Hu, C. P.; Li, Y. J.; Gao, Y. X.; Wang, X. M.; Yang, J. R. Inhibitory Effect of L-Mimosine on Bleomycin-Induced Pulmonary Fibrosis in Rats: Role of EIF3a and P27. *Int. Immunopharmacol.* **2015**, *27* (1), 53–64.
- (138) Prabhakaran, K., Harris, E. B., Kirchheimer, W. F. Suppression of Melanoma Development and Inhibition of Phenoloxidase by Mimosine. *Cytobios* **1973**, *1A*, 3–5.
- (139) Prabhakaran, K., Harris, E. B., Kirchheimer, W. F. A Specific Effect of Mimosine on Melanoma Cells. *Cytobios* **1973**, *7*, 254–252.
- (140) Gilberts, D., Neilson, A., Miyazawa H., DePamphilis, M., Burhans, W. Mimosine Arrests DNA Synthesis at Replication Fork by Inhibiting Deoxyribonucleotide Metabolism. *J. Biol. Chem.* **1995**, *270* (16), 9597–9606.
- (141) Tumey, L. N.; Bom, D.; Huck, B.; Gleason, E.; Wang, J.; Silver, D.; Brunden, K.; Boozer, S.; Rundlett, S.; Sherf, B.; et al. The Identification and Optimization of a N-Hydroxy Urea Series of Flap Endonuclease 1 Inhibitors. *Bioorg. Med. Chem. Lett.* **2005**, *15* (2), 277–281.
- (142) Chapman, T. M.; Wallace, C.; Gillen, K. J.; Bakrania, P.; Khurana, P.; Coombs, P. J.; Fox, S.; Bureau, E. A.; Brownlees, J.; Melton, D. W.; et al. N-Hydroxyimides and Hydroxypyrimidinones as Inhibitors of the DNA Repair Complex ERCC1–XPF. *Bioorg. Med. Chem. Lett.* **2015**, *25* (19), 4104–4108.
- (143) Finch, R. A.; Liu, M. C.; Grill, S. P.; Rose, W. C.; Loomis, R.; Vasquez, K. M.; Cheng, Y. C.; Sartorelli, A. C. Triapine (3-Aminopyridine-2-Carboxaldehyde-Thiosemicarbazone): A Potent Inhibitor of Ribonucleotide Reductase Activity with Broad Spectrum Antitumor Activity. *Biochem. Pharmacol.* **2000**, *59* (8), 983–991.
- (144) Popović-Bijelić, A.; Kowol, C. R.; Lind, M. E. S.; Luo, J.; Himo, F.; Enyedy, É. A.; Arion, V. B.; Gräslund, A. Ribonucleotide Reductase Inhibition by Metal Complexes of Triapine (3-Aminopyridine-2-Carboxaldehyde Thiosemicarbazone): A Combined Experimental and Theoretical Study. *J. Inorg. Biochem.* **2011**, *105* (11), 1422–1431.
- (145) Samuni, A. M.; Krishna, M. C.; DeGraff, W.; Russo, A.; Planalp, R. P.; Brechbiel, M. W.; Mitchell, J. B. Mechanisms Underlying the Cytotoxic Effects of Tachpyr - A Novel Metal Chelator. *Biochim. Biophys. Acta - Gen. Subj.* **2002**, *1571* (3), 211–218.
- (146) Bowen, T.; Planalp, R. P.; Brechbiel, M. W. Synthesis of Novel Hexadentate Ligand Derivatives for the Preparation of Gallium Radiopharmaceuticals. *Bioorganic Med. Chem. Lett.* **1996**, *6* (7), 807–810.
- (147) Camphausen, K.; Sproull, M.; Tantama, S.; Sankineni, S.; Scott, T.; Ménard, C.; Coleman, C. N.; Brechbiel, M. W. Evaluation of Copper Chelation Agents as Anti-Angiogenic Therapy. *Bioorganic Med. Chem.* **2003**, *11* (19), 4287–4293.
- (148) By S.V. Torti, F.M. Torti, S.P. Whitman, M.W. Brechbiel, G. Park, and R. P. P. Tumor Cell Cytotoxicity of a Novel Metal Chelator. *Blood* **1998**, *92* (4), 1384–1389.
- (149) Abeyasinghe, R. D.; Greene, B. T.; Haynes, R.; Willingham, M. C.; Turner, J.; Planalp, R. P.; Brechbiel, M. W.; Torti, F. M.; Torti, S. V. P53-Independent

Apoptosis Mediated by Tachpyridine. an Anti-Cancer Iron Chelator. *Carcinogenesis* **2001**, 22 (10), 1–8.

- (150) Childers, M. L.; Su, F.; Przyborowska, A. M.; Bishwokarma, B.; Park, G.; Brechbiel, M. W.; Torti, S. V.; Torti, F. M.; Broker, G.; Alexander, J. S.; et al. Pyridine-Ring Alkylation of Cytotoxic r-1,c-3,c-5-Tris[(2-Pyridylmethyl)- Amino]Cyclohexane Chelators: Structural and Electronic Properties of the Mn II, FeII, NiII, CuII and Zn II Complexes. *Eur. J. Inorg. Chem.* **2005**, No. 19, 3971–3982.
- (151) Lu, G. P. F. H.; Brechbiel, N. Y. M. W.; Planalp, S. V. T. F. M. T. R. P. Novel Iron Complexes and Chelators Based On. *J. Biol. Inorg. Chem.* **1998**, 3, 449–457.
- (152) Childers, M. L.; Cho, J.; Regino, C. A. S.; Brechbiel, M. W.; DiPasquale, A. G.; Rheingold, A. L.; Torti, S. V.; Torti, F. M.; Planalp, R. P. Influence of Ligand Structure on Fe(II) Spin-State and Redox Rate in Cytotoxic Tripodal Chelators. *J. Inorg. Biochem.* **2008**, 102 (1), 150–156.
- (153) Chong, H. S.; Torti, S. V.; Ma, R.; Torti, F. M.; Brechbiel, M. W. Synthesis and Potent Antitumor Activities of Novel 1,3,5-Cis,Cis- Triaminocyclohexane N-Pyridyl Derivatives. *J. Med. Chem.* **2004**, 47 (21), 5230–5234.
- (154) Zhai, S.; Yang, L.; Cui, Q. C.; Sun, Y.; Dou, Q. P.; Yan, B. Tumor Cellular Proteasome Inhibition and Growth Suppression by 8-Hydroxyquinoline and Clioquinol Requires Their Capabilities to Bind Copper and Transport Copper into Cells. *J. Biol. Inorg. Chem.* **2010**, 15 (2), 259–269.
- (155) Oliveri, V.; Vecchio, G. 8-Hydroxyquinolines in Medicinal Chemistry: A Structural Perspective. *Eur. J. Med. Chem.* **2016**, 120, 252–274.
- (156) Yan, X.; Yu, Y.; Ji, P.; He, H.; Qiao, C. Antitumor Activity of Endoperoxide-Iron Chelator Conjugates - Design, Synthesis and Biological Evaluation. *Eur. J. Med. Chem.* **2015**, 102, 180–187.
- (157) Shaw, A. Y.; Chang, C. Y.; Hsu, M. Y.; Lu, P. J.; Yang, C. N.; Chen, H. L.; Lo, C. W.; Shiau, C. W.; Chern, M. K. Synthesis and Structure-Activity Relationship Study of 8-Hydroxyquinoline- Derived Mannich Bases as Anticancer Agents. *Eur. J. Med. Chem.* **2010**, 45 (7), 2860–2867.
- (158) Madonna, S.; Béclin, C.; Laras, Y.; Moret, V.; Marcowycz, A.; Lamoral-Theys, D.; Dubois, J.; Barthelemy-Requin, M.; Lenglet, G.; Depauw, S.; et al. Structure-Activity Relationships and Mechanism of Action of Antitumor Bis 8-Hydroxyquinoline Substituted Benzylamines. *Eur. J. Med. Chem.* **2010**, 45 (2), 623–638.
- (159) Moret, V.; Laras, Y.; Cresteil, T.; Aubert, G.; Ping, D. Q.; Di, C.; Barthélémy-Requin, M.; Béclin, C.; Peyrot, V.; Allegro, D.; et al. Discovery of a New Family of Bis-8-Hydroxyquinoline Substituted Benzylamines with pro-Apoptotic Activity in Cancer Cells: Synthesis, Structure-Activity Relationship, and Action Mechanism Studies. *Eur. J. Med. Chem.* **2009**, 44 (2), 558–567.
- (160) Renaud, S.; Corcé, V.; Cannie, I.; Ropert, M.; Lepage, S.; Loréal, O.; Deniaud, D.; Gaboriau, F. Quilamine HQ1-44, an Iron Chelator Vectorized toward Tumor Cells by the Polyamine Transport System, Inhibits HCT116 Tumor Growth without Adverse Effect. *Biochem. Pharmacol.* **2015**, 96 (3), 179–189.
- (161) Chan, S. H.; Chui, C. H.; Chan, S. W.; Kok, S. H. L.; Chan, D.; Tsoi, M. Y. T.; Leung, P. H. M.; Lam, A. K. Y.; Chan, A. S. C.; Lam, K. H.; et al. Synthesis of 8-Hydroxyquinoline Derivatives as Novel Antitumor Agents. *ACS Med. Chem. Lett.* **2013**, 4 (2), 170–174.

- (162) Liu, Z. D.; Lockwood, M.; Rose, S.; Theobald, A. E.; Hider, R. C. Structure-Activity Investigation of the Inhibition of 3-Hydroxypyridin-4-Ones on Mammalian Tyrosine Hydroxylase. *Biochem. Pharmacol.* **2001**, *61* (3), 285–290.
- (163) Abeysinghe, R. D.; Roberts, P. J.; Cooper, C. E.; MacLean, K. H.; Hider, R. C.; Porter, J. B. The Environment of the Lipoxygenase Iron Binding Site Explored with Novel Hydroxypyridinone Iron Chelators. *J. Biol. Chem.* **1996**, *271* (14), 7965–7972.
- (164) Tricta, F.; Uetrecht, J.; Galanello, R.; Connelly, J.; Rozova, A.; Spino, M.; Palmblad, J. Deferiprone-Induced Agranulocytosis: 20 Years of Clinical Observations. *Am. J. Hematol.* **2016**, *91* (10), 1026–1031.
- (165) Kontoghiorghes, G. J. Ethical Issues and Risk/Benefit Assessment of Iron Chelation Therapy: Advances with Deferiprone/Deferoxamine Combinations and Concerns about the Safety, Efficacy and Costs of Deferasirox. *Hemoglobin* **2008**, *32* (1–2), 1–15.
- (166) Kratz, F.; Müller, I. A.; Ryppa, C.; Warnecke, A. Prodrug Strategies in Anticancer Chemotherapy. *ChemMedChem* **2008**, *3* (1), 20–53.
- (167) Akam, E. A.; Chang, T. M.; Astashkin, A. V.; Tomat, E. Intracellular Reduction/Activation of a Disulfide Switch in Thiosemicarbazone Iron Chelators. *Metallomics* **2014**, *6* (10), 1905–1912.
- (168) Chang, T. M.; Tomat, E. Disulfide/Thiol Switches in Thiosemicarbazone Ligands for Redox-Directed Iron Chelation. *Dalt. Trans.* **2013**, *42* (22), 7846–7849.
- (169) Akam, E. A.; Tomat, E. Targeting Iron in Colon Cancer via Glycoconjugation of Thiosemicarbazone Prochelators. *Bioconjug. Chem.* **2016**, *27* (8), 1807–1812.
- (170) Younes, M.; Lechago, L. V.; Somoano, J. R.; Mosharaf, M.; Lechago, J. Wide Expression of the Human Erythrocyte Glucose Transporter Glut1 in Human Cancers. *Cancer Res.* **1996**, *56* (5), 1164 LP – 1167.
- (171) Cao, J.; Cui, S.; Li, S.; Du, C.; Tian, J.; Wan, S.; Qian, Z.; Gu, Y.; Chen, W. R.; Wang, G. Targeted Cancer Therapy with a 2-Deoxyglucose-Based Adriamycin Complex. *Cancer Res.* **2013**, *73* (4), 1362 LP – 1373.
- (172) Liu, D.-Z.; Sinchaikul, S.; Reddy, P. V. G.; Chang, M.-Y.; Chen, S.-T. Synthesis of 2'-Paclitaxel Methyl 2-Glucopyranosyl Succinate for Specific Targeted Delivery to Cancer Cells. *Bioorg. Med. Chem. Lett.* **2007**, *17* (3), 617–620.
- (173) Lin, Y.-S.; Tungpradit, R.; Sinchaikul, S.; An, F.-M.; Liu, D.-Z.; Phutrakul, S.; Chen, S.-T. Targeting the Delivery of Glycan-Based Paclitaxel Prodrugs to Cancer Cells via Glucose Transporters. *J. Med. Chem.* **2008**, *51* (23), 7428–7441.
- (174) Murthy, R. S. *The World Health Report: 2001. Mental Health: New Understanding, New Hope.*; 2001.
- (175) Olesen, J.; Leonardi, M. The Burden of Brain Diseases in Europe. *Eur. J. Neurol.* **2003**, *10* (5), 471–477.
- (176) Ironside, A. H. P. and J. W. Molecular Pathology in Neurodegenerative Diseases. *Current Drug Targets.* 2012, pp 1548–1559.
- (177) Brown, R. C.; Lockwood, A. H.; Sonawane, B. R. Neurodegenerative Diseases: An Overview of Environmental Risk Factors. *Environ. Health Perspect.* **2005**, *113* (9), 1250–1256.
- (178) Johnson, I. P. Age-Related Neurodegenerative Disease Research Needs Aging

Models. *Front. Aging Neurosci.* **2015**, *7*, 168.

- (179) Dorsey, E. R.; Constantinescu, R.; Thompson, J. P.; Biglan, K. M.; Holloway, R. G.; Kieburtz, K.; Marshall, F. J.; Ravina, B. M.; Schifitto, G.; Siderowf, A.; et al. Projected Number of People with Parkinson Disease in the Most Populous Nations, 2005 through 2030. *Neurology* **2007**, *68* (5), 384–386.
- (180) DiNunzio, J.; Williams, R. CNS Disorders—Current Treatment Options and the Prospects for Advanced Therapies. *Drug Dev. Ind. Pharm.* **2008**, *34*, 1141–1167.
- (181) Bolognin, S.; Drago, D.; Messori, L.; Zatta, P. Chelation Therapy for Neurodegenerative Diseases. *Med. Res. Rev.* **2009**, *29* (4), 547–570. <https://doi.org/10.1002/med.20148>.
- (182) Dauer, W.; Przedborski, S. Parkinson's Disease: Mechanisms and Models. *Neuron* **2003**, *39* (6), 889–909.
- (183) Molina-Holgado, F.; Hider, R. C.; Gaeta, A.; Williams, R.; Francis, P. Metals Ions and Neurodegeneration. *BioMetals* **2007**, *20* (3), 639–654.
- (184) Nussbaum, R. L.; Ellis, C. E. Alzheimer's Disease and Parkinson's Disease. *N. Engl. J. Med.* **2003**, *348* (14), 1356–1364.
- (185) Parkinson, J. An Essay on the Shaking Palsy. *J. Neuropsychiatry Clin. Neurosci.* **2002**, *14* (2), 223–236.
- (186) Tysnes, O.-B.; Storstein, A. Epidemiology of Parkinson's Disease. *J. Neural Transm.* **2017**, *124* (8), 901–905.
- (187) Parkinson's-UK. The incidence and prevalence of Parkinson's in the UK report [nals/resources/incidence-and-prevalence-parkinsons-uk-report](https://www.parkinsons-uk.org/research-and-statistics/incidence-and-prevalence-parkinsons-uk-report).
- (188) Lai, B. C. L.; Marion, S. A.; Teschke, K.; Tsui, J. K. C. Occupational and Environmental Risk Factors for Parkinson's Disease. *Parkinsonism Relat. Disord.* **2002**, *8* (5), 297–309.
- (189) Aron, L. Genetic Analysis of Dopaminergic Neuron Survival. GDNF/Ret Signaling and the Parkinson's Disease-Associated Gene DJ-1, 2019.
- (190) Duffy, P. E.; Tennyson, V. M. Phase and Electron Microscopic Observations of Lewy Bodies and Melanin Granules in the Substantia Nigra and Locus Caeruleus in Parkinson's Disease\*†. *J. Neuropathol. Exp. Neurol.* **1965**, *24* (3), 398–414.
- (191) Davie, C. A. A Review of Parkinson's Disease. *Br. Med. Bull.* **2008**, *86* (1), 109–127.
- (192) Raffa, R. B.; Danah, J.; Tallarida, C. S.; Zimmerman, C.; Gill, G.; Baron, S. J.; Rawls, S. M. Potential of a Planarian Model to Study Certain Aspects of Anti-Parkinsonism Drugs. *Adv. Park. Dis.* **2013**, *02* (03), 70–74.
- (193) Mazzoni, P.; Shabbott, B.; Cortés, J. C. Motor Control Abnormalities in Parkinson's Disease. *Cold Spring Harb. Perspect. Med.* **2012**, *2* (6), a009282–a009282.
- (194) Nolden, L. F.; Tartavouille, T.; Porche, D. J. Parkinson's Disease: Assessment, Diagnosis, and Management. *J. Nurse Pract.* **2014**, *10* (7), 500–506.
- (195) Juárez Olguín, H.; Calderón Guzmán, D.; Hernández García, E.; Barragán Mejía, G. The Role of Dopamine and Its Dysfunction as a Consequence of Oxidative Stress. *Oxid. Med. Cell. Longev.* **2016**, 2016.
- (196) Neil, L. Parkinson's Disease Signs and Symptoms of Parkinson's Disease <https://www.webmd.com/parkinsons-disease/guide/parkinsons-common-symptoms>.

- (197) DeMaagd, G.; Philip, A. Parkinson's Disease and Its Management: Part 1: Disease Entity, Risk Factors, Pathophysiology, Clinical Presentation, and Diagnosis. *P T* **2015**, *40* (8), 504–532.
- (198) Crichton, R. R.; Dexter, D. T.; Ward, R. J. Metal Based Neurodegenerative Diseases—From Molecular Mechanisms to Therapeutic Strategies. *Coord. Chem. Rev.* **2008**, *252* (10), 1189–1199.
- (199) Obeso, J. A.; Rodriguez-Oroz, M. C.; Goetz, C. G.; Marin, C.; Kordower, J. H.; Rodriguez, M.; Hirsch, E. C.; Farrer, M.; Schapira, A. H. V.; Halliday, G. Missing Pieces in the Parkinson's Disease Puzzle. *Nat. Med.* **2010**, *16*, 653.
- (200) Shults, C. W. Lewy Bodies. *Proc. Natl. Acad. Sci. U. S. A.* **2006**, *103* (6), 1661–1668.
- (201) Xu, J.; Kao, S.-Y.; Lee, F. J. S.; Song, W.; Jin, L.-W.; Yankner, B. A. Dopamine-Dependent Neurotoxicity of  $\alpha$ -Synuclein: A Mechanism for Selective Neurodegeneration in Parkinson Disease. *Nat. Med.* **2002**, *8* (6), 600–606.
- (202) Lesage, S.; Brice, A. Parkinson's Disease: From Monogenic Forms to Genetic Susceptibility Factors. *Hum. Mol. Genet.* **2009**, *18* (R1), R48–R59.
- (203) Klein, C.; Westenberger, A. Genetics of Parkinson's Disease. *Cold Spring Harb. Perspect. Med.* **2012**, *2* (1), a008888–a008888.
- (204) Yoritaka, A.; Shimo, Y.; Shimo, Y.; Inoue, Y.; Yoshino, H.; Hattori, N. Nonmotor Symptoms in Patients with PARK2 Mutations. *Parkinsons. Dis.* **2011**, *2011*, 0–5.
- (205) Paisán-Ruiz, C.; Jain, S.; Evans, E. W.; Gilks, W. P.; Simón, J.; van der Brug, M.; de Munain, A. L.; Aparicio, S.; Gil, A. M.; Khan, N.; et al. Cloning of the Gene Containing Mutations That Cause PARK8-Linked Parkinson's Disease. *Neuron* **2004**, *44* (4), 595–600.
- (206) Sundal, C.; Fujioka, S.; Uitti, R. J.; Wszolek, Z. K. Autosomal Dominant Parkinson's Disease. *Parkinsonism Relat. Disord.* **2012**, *18*, S7–S10.
- (207) Polymeropoulos, M.; Lavedan, C.; Leroy, E.; Ide, S. E.; Dehejia, A.; Dutra, A. Mutation in the Alpha-Synuclein Gene Identified in Families with Parkinson's Disease. *Science* (80-. ). **1997**, *276*, 2045–2047.
- (208) Paridah, M. .; Moradbak, A.; Mohamed, A. .; Owolabi, F. abdulwahab taiwo; Asniza, M.; Abdul Khalid, S. H. . Mutations of PARK Genes and Alpha-Synuclein and Parkin Concentrations in Parkinson's Disease, A Synopsis of Parkinson's Disease,. *Intech* **2016**, 1–13.
- (209) Spinelli, K. J.; Taylor, J. K.; Osterberg, V. R.; Churchill, M. J.; Pollock, E.; Moore, C.; Meshul, C. K.; Unni, V. K. Presynaptic Alpha-Synuclein Aggregation in a Mouse Model of Parkinson's Disease. *J. Neurosci.* **2014**, *34* (6), 2037 LP – 2050.
- (210) Xu, L.; Pu, J. Alpha-Synuclein in Parkinson's Disease: From Pathogenetic Dysfunction to Potential Clinical Application. *Parkinsons. Dis.* **2016**, *2016*, 1720621.
- (211) Mizuno, Y.; Hattori, N.; Yoshino, H.; Asakawa, S.; Minoshima, S.; Shimizu, N.; Suzuki, T.; Chiba, T.; Tanaka, K. Chapter 28 - Parkin Mutations (Park 2). In *Genetics of Movement Disorders*; Pulst, S.-M. B. T.-G. of M. D., Ed.; Academic Press: San Diego, 2003; pp 305–314.
- (212) Solano, S. M.; Miller, D. W.; Augood, S. J.; Young, A. B.; Penney Jr, J. B. Expression of  $\alpha$ -Synuclein, Parkin, and Ubiquitin Carboxy-Terminal Hydrolase L1 mRNA in Human Brain: Genes Associated with Familial Parkinson's Disease. *Ann. Neurol.* **2000**, *47* (2), 201–210.

- (213) Zhu, M.; Cortese, G. P.; Waites, C. L. Parkinson's Disease-Linked Parkin Mutations Impair Glutamatergic Signaling in Hippocampal Neurons. *BMC Biol.* **2018**, *16* (1), 100.
- (214) Estrada, A. A.; Sweeney, Z. K. Chemical Biology of Leucine-Rich Repeat Kinase 2 (LRRK2) Inhibitors. *J. Med. Chem.* **2015**, *58* (17), 6733–6746.
- (215) Westerlund, M.; Ran, C.; Borgkvist, A.; Sterky, F. H.; Lindqvist, E.; Lundströmer, K.; Pernold, K.; Brené, S.; Kallunki, P.; Fisone, G.; et al. Lrrk2 and  $\alpha$ -Synuclein Are Co-Regulated in Rodent Striatum. *Mol. Cell. Neurosci.* **2008**, *39* (4), 586–591.
- (216) Parisiadou, L.; Yu, J.; Sgobio, C.; Xie, C.; Liu, G.; Sun, L.; Gu, X.-L.; Lin, X.; Crowley, N. A.; Lovinger, D. M.; et al. LRRK2 Regulates Synaptogenesis and Dopamine Receptor Activation through Modulation of PKA Activity. *Nat. Neurosci.* **2014**, *17* (3), 367–376.
- (217) Galter, D.; Westerlund, M.; Carmine, A.; Lindqvist, E.; Sydow, O.; Olson, L. LRRK2 Expression Linked to Dopamine-Innervated Areas. *Ann. Neurol.* **2006**, *59* (4), 714–719.
- (218) Henderson, M. X.; Sengupta, M.; McGeary, I.; Zhang, B.; Olufemi, M. F.; Brown, H.; Trojanowski, J. Q.; Lee, V. M. Y. LRRK2 Inhibition Does Not Impart Protection from  $\alpha$ -Synuclein Pathology and Neuron Death in Non-Transgenic Mice. *Acta Neuropathol. Commun.* **2019**, *7* (1), 28.
- (219) Atashrazm, F.; Dzamko, N. LRRK2 Inhibitors and Their Potential in the Treatment of Parkinson's Disease: Current Perspectives. *Clin. Pharmacol.* **2016**, *8*, 177–189.
- (220) Pickrell, A. M.; Youle, R. J. The Roles of PINK1, Parkin, and Mitochondrial Fidelity in Parkinson's Disease. *Neuron* **2015**, *85* (2), 257–273.
- (221) Barodia, S. K.; Creed, R. B.; Goldberg, M. S. Parkin and PINK1 Functions in Oxidative Stress and Neurodegeneration. *Brain Res. Bull.* **2017**, *133*, 51–59.
- (222) Pridgeon, J. W.; Olzmann, J. A.; Chin, L.-S.; Li, L. PINK1 Protects against Oxidative Stress by Phosphorylating Mitochondrial Chaperone TRAP1. *PLoS Biol.* **2007**, *5* (7), e172.
- (223) Priyadarshini, M.; Orosco, L. A.; Panula, P. J. Oxidative Stress and Regulation of Pink1 in Zebrafish (*Danio Rerio*). *PLoS One* **2013**, *8* (11), e81851–e81851.
- (224) Ishihara-Paul, L.; Hulihan, M. M.; Kachergus, J.; Upmanyu, R.; Warren, L.; Amouri, R.; Elango, R.; Prinjha, R. K.; Soto, A.; Kefi, M.; et al. PINK1 Mutations and Parkinsonism. *Neurology* **2008**, *71* (12), 896–902.
- (225) Kawajiri, S.; Saiki, S.; Sato, S.; Hattori, N. Genetic Mutations and Functions of PINK1. *Trends Pharmacol. Sci.* **2011**, *32* (10), 573–580.
- (226) Ramsden, D. B.; Parsons, R. B.; Ho, S. L.; Waring, R. H. The Aetiology of Idiopathic Parkinson's Disease. *Mol. Pathol.* **2001**, *54* (6), 369–380.
- (227) Sassi, C. Genetics of Parkinson Disease. *Genet. Med.* **2011**, *9* (12), 21–23.
- (228) Sofic, E.; Paulus, W.; Jellinger, K.; Riederer, P.; Youdim, M. B. H. Selective Increase of Iron in Substantia Nigra Zona Compacta of Parkinsonian Brains. *J. Neurochem.* **1991**, *56* (3), 978–982.
- (229) Dexter, D. T.; Wells, F. R.; Agid, F.; Agid, Y.; Lees, A. J.; Jenner, P.; Marsden, C. D. Increased nigral iron content in postmortem parkinsonian brain. *Lancet* **1987**, *330* (8569), 1219–1220.

- (230) Höck, A.; Demmel, U.; Schicha, H.; Kasperek, K.; Feinendegen, L. E. Trace Element Concentration In Human Brain: Activation Analysis Of Cobalt, Iron, Rubidium, Selenium, Zinc, Chromium, Silver, Cesium, Antimony And Scandium. *Brain* **1975**, 98 (1), 49–64.
- (231) Alam, Z. I.; Daniel, S. E.; Lees, A. J.; Marsden, D. C.; Jenner, P.; Halliwell, B. A Generalised Increase in Protein Carbonyls in the Brain in Parkinson's but Not Incidental Lewy Body Disease. *J. Neurochem.* **1997**, 69 (3), 1326–1329.
- (232) Dexter, D. T.; Wells, F. R.; Lee, A. J.; Agid, F.; Agid, Y.; Jenner, P.; Marsden, C. D. Increased Nigral Iron Content and Alterations in Other Metal Ions Occurring in Brain in Parkinson's Disease. *J. Neurochem.* **1989**, 52 (6), 1830–1836.
- (233) Gaeta, A.; Hider, R. C. The Crucial Role of Metal Ions in Neurodegeneration: The Basis for a Promising Therapeutic Strategy. *Br. J. Pharmacol.* **2005**, 146 (8), 1041–1059.
- (234) Fenton, H. J. H. Oxidation of Tartaric Acid in Presence of Iron. *J. Chem. Soc. Trans.* **1894**, 65, 899–910.
- (235) Eaton, J. W.; Qian, M. Molecular Bases of Cellular Iron Toxicity. *Free Radic. Biol. Med.* **2002**, 32 (9), 833–840.
- (236) Uversky, V.; Li, J.; Fink, A. L. Metal-Triggered Structural Transformations, Aggregation and Fibrillation of Human  $\alpha$ -Synuclein. A Possible Molecular Link between Parkinson's Disease and Heavy Metal Exposure. *J. Biol. Chem.* **2001**, 276, 44284–44296.
- (237) Giasson, B. I.; Duda, J. E.; Murray, I. V. J.; Chen, Q.; Souza, J. M.; Hurtig, H. I.; Ischiropoulos, H.; Trojanowski, J. Q.; -Y. Lee, V. M. Oxidative Damage Linked to Neurodegeneration by Selective  $\alpha$ -Synuclein Nitration in Synucleinopathy Lesions. *Science* (80-. ). **2000**, 290 (5493), 985 LP – 989.
- (238) Nagatsu, T.; Sawada, M. Cellular and Molecular Mechanisms of Parkinson's Disease: Neurotoxins, Causative Genes, and Inflammatory Cytokines. *Cell. Mol. Neurobiol.* **2006**, 26 (4), 779–800.
- (239) Bové, J.; Prou, D.; Perier, C.; Przedborski, S. Toxin-Induced Models of Parkinson's Disease. *NeuroRx* **2005**, 2 (3), 484–494.
- (240) Breese, G. R.; Traylor, T. D. Effect of 6-Hydroxydopamine on Brain Norepinephrine and Dopamine Evidence for Selective Degeneration of Catecholamine Neurons. *J. Pharmacol. Exp. Ther.* **1970**, 174 (3), 413–420.
- (241) Sossi, V.; Dinelle, K.; Jivan, S.; Fischer, K.; Holden, J. E.; Doudet, D. In Vivo Dopamine Transporter Imaging in a Unilateral 6-Hydroxydopamine Rat Model of Parkinson Disease Using <sup>11</sup>C-Methylphenidate PET. *J. Nucl. Med.* **2012**, 53 (5), 813–822.
- (242) Chotibut, T.; Apple, D. M.; Jefferis, R.; Salvatore, M. F. Dopamine Transporter Loss in 6-OHDA Parkinson's Model Is Unmet by Parallel Reduction in Dopamine Uptake. *PLoS One* **2012**, 7 (12), e52322–e52322.
- (243) Schapira, A. H. V. Complex I: Inhibitors, Inhibition and Neurodegeneration. *Exp. Neurol.* **2010**, 224 (2), 331–335.
- (244) Fato, R.; Bergamini, C.; Bortolus, M.; Maniero, A. L.; Leoni, S.; Ohnishi, T.; Lenaz, G. Differential Effects of Mitochondrial Complex I Inhibitors on Production of Reactive Oxygen Species. *Biochim. Biophys. Acta* **2009**, 1787 (5), 384–392.

- (245) Meredith, G. E.; Rademacher, D. J. MPTP Mouse Models of Parkinson's Disease: An Update. *J. Parkinsons. Dis.* **2011**, *1* (1), 19–33.
- (246) Przedborski, S.; Vila, M. MPTP: A Review of Its Mechanisms of Neurotoxicity. *Clin. Neurosci. Res.* **2001**, *1* (6), 407–418.
- (247) KOPIN, I. J. Features of the Dopaminergic Neurotoxin MPTP. *Ann. N. Y. Acad. Sci.* **1992**, *648* (1), 96–104.
- (248) Chiba, K.; Trevor, A.; Castagnoli, N. Metabolism of the Neurotoxic Tertiary Amine, MPTP, by Brain Monoamine Oxidase. *Biochem. Biophys. Res. Commun.* **1984**, *120* (2), 574–578.
- (249) Haga, H.; Matsuo, K.; Yabuki, Y.; Zhang, C.; Han, F.; Fukunaga, K. Enhancement of ATP Production Ameliorates Motor and Cognitive Impairments in a Mouse Model of MPTP-induced Parkinson's Disease. *Neurochem. Int.* **2019**, *129*, 104492.
- (250) Murphy, M. P.; Krueger, M. J.; Sablin, S. O.; Ramsay, R. R.; Singer, T. P. Inhibition of Complex I by Hydrophobic Analogues of N-Methyl-4-Phenylpyridinium (MPP+) and the Use of an Ion-Selective Electrode to Measure Their Accumulation by Mitochondria and Electron-Transport Particles. *Biochem. J.* **1995**, *306* ( Pt 2 (Pt 2)), 359–365.
- (251) Samantaray, S.; Banik, S. K. R. and N. L. Calpain as a Potential Therapeutic Target in Parkinsons Disease. *CNS & Neurological Disorders - Drug Targets.* 2008, pp 305–312.
- (252) Duchen, M. R. Mitochondria, Calcium-Dependent Neuronal Death and Neurodegenerative Disease. *Pflugers Arch.* **2012**, *464* (1), 111–121.
- (253) Chen, T. S.; Koutsilieri, E.; Rausch, W. D. MPP+ Selectively Affects Calcium Homeostasis in Mesencephalic Cell Cultures from Embryonal C57/B16 Mice. *J. Neural Transm. / Gen. Sect. JNT* **1995**, *100* (2), 153–163.
- (254) Ali, S. F.; David, S. N.; Newport, G. D.; Cadet, J. L.; Slikker Jr., W. MPTP-Induced Oxidative Stress and Neurotoxicity Are Age-Dependent: Evidence from Measures of Reactive Oxygen Species and Striatal Dopamine Levels. *Synapse* **1994**, *18* (1), 27–34.
- (255) Li, D. W.; Li, G. R.; Lu, Y.; Liu, Z. Q.; Chang, M.; Yao, M.; Cheng, W.; Hu, L. Sen.  $\alpha$ -Lipoic Acid Protects Dopaminergic Neurons against MPP + -Induced Apoptosis by Attenuating Reactive Oxygen Species Formation. *Int. J. Mol. Med.* **2013**, *32* (1), 108–114.
- (256) Zawada, W. M.; Banninger, G. P.; Thornton, J.; Marriott, B.; Cantu, D.; Rachubinski, A. L.; Das, M.; Griffin, W. S. T.; Jones, S. M. Generation of Reactive Oxygen Species in 1-Methyl-4-Phenylpyridinium (MPP+) Treated Dopaminergic Neurons Occurs as an NADPH Oxidase-Dependent Two-Wave Cascade. *J. Neuroinflammation* **2011**, *8*, 129.
- (257) Guiney, S. J.; Adlard, P. A.; Bush, A. I.; Finkelstein, D. I.; Ayton, S. Ferroptosis and Cell Death Mechanisms in Parkinson's Disease. *Neurochem. Int.* **2017**, *104*, 34–48.
- (258) Yu, H.; Guo, P.; Xie, X.; Wang, Y.; Chen, G. Ferroptosis, a New Form of Cell Death, and Its Relationships with Tumourous Diseases. *J. Cell. Mol. Med.* **2017**, *21* (4), 648–657.
- (259) Hider, R. C.; Kong, X. L. Glutathione: A Key Component of the Cytoplasmic Labile Iron Pool. *BioMetals* **2011**, *24* (6), 1179–1187.

- (260) Dexter, D.; Carter, C.; Agid, F.; Agid, Y.; Lees, A. J.; Jenner, P.; Marsden, C. D. Lipid peroxidation as cause of nigral cell death in parkinson's disease. *Lancet* **1986**, 328 (8507), 639–640.
- (261) Agmon, E.; Solon, J.; Bassereau, P.; Stockwell, B. Modeling the Effects of Lipid Peroxidation during Ferroptosis on Membrane Properties. *Sci. Rep.* **2018**, 8, 5155.
- (262) Freund, H.-J. Long-Term Effects of Deep Brain Stimulation in Parkinson's Disease. *Brain* **2005**, 128 (10), 2222–2223.
- (263) Follett, K. A.; Weaver, F. M.; Stern, M.; Hur, K.; Harris, C. L.; Luo, P.; Marks, W. J.; Rothlind, J.; Sagher, O.; Moy, C.; et al. Pallidal versus Subthalamic Deep-Brain Stimulation for Parkinson's Disease. *N. Engl. J. Med.* **2010**, 362 (22), 2077–2091.
- (264) Munhoz, R. P.; Picillo, M.; Fox, S. H.; Bruno, V.; Panisset, M.; Honey, C. R.; Fasano, A. Eligibility Criteria for Deep Brain Stimulation in Parkinson's Disease, Tremor, and Dystonia. *Can. J. Neurol. Sci. / J. Can. des Sci. Neurol.* **2016**, 43 (4), 462–471.
- (265) Spencer, D. D.; Robbins, R. J.; Naftolin, F.; Marek, K. L.; Vollmer, T.; Leranth, C.; Roth, R. H.; Price, L. H.; Gjedde, A.; Bunney, B. S.; et al. Unilateral Transplantation of Human Fetal Mesencephalic Tissue into the Caudate Nucleus of Patients with Parkinson's Disease. *N. Engl. J. Med.* **1992**, 327 (22), 1541–1548.
- (266) Mollers, S.; Dobrossy, M.; Nikkhah, G. Transplantation of Foetal Ventral Mesencephalic Grafts in Parkinson's Disease: A Still Evolving Concept with New Regulatory Challenges. In *Towards New Therapies for Parkinson's Disease*; 2011; pp 380–396.
- (267) Li, J.-Y.; Englund, E.; Widner, H.; Rehncróna, S.; Björklund, A.; Lindvall, O.; Brundin, P. Characterization of Lewy Body Pathology in 12- and 16-Year-Old Intrastratial Mesencephalic Grafts Surviving in a Patient with Parkinson's Disease. *Mov. Disord.* **2010**, 25 (8), 1091–1096.
- (268) Sanders, L.; Giudice, L.; Raffin, T. Ethics of Fetal Tissue Transplantation. *West. J. Med.* **1993**, 159, 400–407.
- (269) Coune, P. G.; Schneider, B. L.; Aebischer, P. Parkinson's Disease: Gene Therapies. *Cold Spring Harb. Perspect. Med.* **2012**, 2 (4), 1–15.
- (270) Kageyama, T.; Nakamura, M.; Matsuo, A.; Yamasaki, Y.; Takakura, Y.; Hashida, M.; Kanai, Y.; Naito, M.; Tsuruo, T.; Minato, N.; et al. The 4F2hc/LAT1 Complex Transports l-DOPA across the Blood–Brain Barrier. *Brain Res.* **2000**, 879 (1), 115–121.
- (271) Lin, J.; Raouf, D. A.; Thomas, D. G.; Greenson, J. K.; Giordano, T. J.; Robinson, G. S.; Bourner, M. J.; Bauer, C. T.; Orringer, M. B.; Beer, D. G. L-Type Amino Acid Transporter-1 Overexpression and Melphalan Sensitivity in Barrett's Adenocarcinoma. *Neoplasia* **2004**, 6 (1), 74–84.
- (272) Geier, E. G.; Schlessinger, A.; Fan, H.; Gable, J. E.; Irwin, J. J.; Sali, A.; Giacomini, K. M. Structure-Based Ligand Discovery for the Large-Neutral Amino Acid Transporter 1, LAT-1. *Proc. Natl. Acad. Sci.* **2013**, 110 (14), 5480–5485.
- (273) Palma, J.-A.; Norcliffe-Kaufmann, L.; Fuente-Mora, C.; Percival, L.; Spalink, C. L.; Kaufmann, H. 154 - Disorders of the Autonomic Nervous System: Autonomic Dysfunction in Pediatric Practice. In *Swaiman's Pediatric Neurology (Sixth Edition)*; Swaiman, K. F., Ashwal, S., Ferriero, D. M., Schor, N. F., Finkel, R. S., Gropman, A. L., Pearl, P. L., Shevell, M. I. B. T.-S. P. N. (Sixth E., Eds.; Elsevier, 2017; pp 1173–

1183.

- (274) Thorner, M. O. Dopamine is an important neurotransmitter in the autonomic nervous system. *Lancet* **1975**, 305 (7908), 662–665.
- (275) Rinne, U. K.; Mölsä, P. Levodopa with Benserazide or Carbidopa in Parkinson Disease. *Neurology* **1979**, 29 (12), 1584 LP – 1589.
- (276) Hinz, M.; Stein, A.; Cole, T. Parkinson's Disease: Carbidopa, Nausea, and Dyskinesia. *Clin. Pharmacol.* **2014**, 6, 189–194.
- (277) Scott, L. J. Opicapone: A Review in Parkinson's Disease. *Drugs* **2016**, 76 (13), 1293–1300.
- (278) Barbeau, A.; Mars, H.; Botez, M. I.; Joubert, M. Levodopa Combined with Peripheral Decarboxylase Inhibition in Parkinson's Disease. *Can. Med. Assoc. J.* **1972**, 106 (11), 1169–1174.
- (279) Tarazi, F. I. Neuropharmacology of Dopamine Receptors: Implications in Neuropsychiatric Diseases. *J. Sci. Res. Med. Sci.* **2001**, 3 (2), 93–104.
- (280) Xie, T.; Ho, S.-L.; Ramsden, D. Catechol-O-Methyltransferase Inhibitors in Parkinson's Disease. *Lancet* **1998**, 351 (9120), 1966.
- (281) Tsao, D.; Diatchenko, L.; Dokholyan, N. V. Structural Mechanism of S-Adenosyl Methionine Binding to Catechol O-Methyltransferase. *PLoS One* **2011**, 6 (8), e24287.
- (282) Learmonth, D. A.; Kiss, L. E.; Soares-da-Silva, P. The Chemistry of Catechol-O-Methyltransferase Inhibitors. In *Basic Aspects of Catechol-O-Methyltransferase and the Clinical Applications of its Inhibitors*; Nissinen, E. B. T.-I. R. of N., Ed.; Academic Press, 2010; Vol. 95, pp 119–162.
- (283) Antonini, A.; Abbruzzese, G.; Barone, P.; Bonuccelli, U.; Lopiano, L.; Onofri, M.; Zappia, M.; Quattrone, A. COMT Inhibition with Tolcapone in the Treatment Algorithm of Patients with Parkinson's Disease (PD): Relevance for Motor and Non-Motor Features. *Neuropsychiatr. Dis. Treat.* **2008**, 4 (1), 1–9.
- (284) Truong, D. D. Tolcapone: Review of Its Pharmacology and Use as Adjunctive Therapy in Patients with Parkinson's Disease. *Clin. Interv. Aging* **2009**, 4, 109–113.
- (285) Harrison, S. T.; Poslusney, M. S.; Mulhearn, J. J.; Zhao, Z.; Kett, N. R.; Schubert, J. W.; Melamed, J. Y.; Allison, T. J.; Patel, S. B.; Sanders, J. M.; et al. Synthesis and Evaluation of Heterocyclic Catechol Mimics as Inhibitors of Catechol-o-Methyltransferase (COMT). *ACS Med. Chem. Lett.* **2015**, 6 (3), 318–323.
- (286) Wallach, J.; Colestock, T.; Adejare, A. Receptor Targets in Alzheimer's Disease Drug Discovery. In *Alzheimer's Disease*; Adejare, A. B. T.-D. D. A. for the T. of N. D., Ed.; Academic Press, 2017; pp 83–107.
- (287) Di Monte, D. A.; DeLanney, L. E.; Irwin, I.; Royland, J. E.; Chan, P.; Jakowec, M. W.; Langston, J. W. Monoamine Oxidase-Dependent Metabolism of Dopamine in the Striatum and Substantia Nigra of l-DOPA-Treated Monkeys. *Brain Res.* **1996**, 738 (1), 53–59.
- (288) Finberg, J. P. M.; Rabey, J. M. Inhibitors of MAO-A and MAO-B in Psychiatry and Neurology. *Front. Pharmacol.* **2016**, 7, 340.
- (289) Giladi, N.; Asgharnejad, M.; Bauer, L.; Grieger, F.; Boroojerdi, B. Rotigotine in Combination with the MAO-B Inhibitor Selegiline in Early Parkinson's Disease: A Post Hoc Analysis. *J. Parkinsons. Dis.* **2016**, 6 (2), 401–411.

- (290) Waters, C. H. Side Effects of Selegiline (Eldepryl). *Top. Geriatr.* **1992**, *5* (1), 31–34.
- (291) Stocchi, F. Dopamine Agonists in Parkinson's Disease. *CNS Drugs* **1998**, *10* (3), 159–170.
- (292) Olanow, C. W. The Role of Dopamine Agonists in the Treatment of Early Parkinson's Disease. *Neurology* **2002**, *58* (suppl 1), S33 LP-S41.
- (293) Shill, H. A.; Stacy, M. Update on Ropinirole in the Treatment of Parkinson's Disease. *Neuropsychiatr. Dis. Treat.* **2009**, *5*, 33–36.
- (294) Parkes, J. D.; Marsden, C. D.; Donaldson, I.; Galea-Debono, A.; Walters, J.; Kennedy, G.; Asselman, P. Bromocriptine Treatment in Parkinson's Disease. *J. Neurol. Neurosurg. Psychiatry* **1976**, *39* (2), 184–193.
- (295) Constantinescu, R. Update on the Use of Pramipexole in the Treatment of Parkinson's Disease. *Neuropsychiatr. Dis. Treat.* **2008**, *4* (2), 337–352.
- (296) Chung, S. J.; Asgharnejad, M.; Bauer, L.; Benitez, A.; Boroojerdi, B.; Heidbrede, T.; Little, A.; Kim, H. J. Switching from an Oral Dopamine Receptor Agonist to Rotigotine Transdermal Patch: A Review of Clinical Data with a Focus on Patient Perspective. *Expert Rev. Neurother.* **2017**, *17* (7), 737–749.
- (297) Ford, C. P. The Role of D2-Autoreceptors in Regulating Dopamine Neuron Activity and Transmission. *Neuroscience* **2014**, *282*, 13–22.
- (298) De Mei, C.; Ramos, M.; Iitaka, C.; Borrelli, E. Getting Specialized: Presynaptic and Postsynaptic Dopamine D2 Receptors. *Curr. Opin. Pharmacol.* **2009**, *9* (1), 53–58.
- (299) Brown, F.; Campbell, W.; Mitchell, P. J.; Randall, K. Dopamine Autoreceptors and the Effects of Drugs on Locomotion and Dopamine Synthesis. *Br. J. Pharmacol.* **1985**, *84* (4), 853–860.
- (300) Borovac, J. A. Side Effects of a Dopamine Agonist Therapy for Parkinson's Disease: A Mini-Review of Clinical Pharmacology. *Yale J. Biol. Med.* **2016**, *89* (1), 37–47.
- (301) Deleu, D.; Hanssens, Y.; Northway, M. G. Subcutaneous Apomorphine. *Drugs Aging* **2004**, *21* (11), 687–709.
- (302) Chaudhuri, K. R.; Clough, C. Subcutaneous Apomorphine in Parkinson's Disease. *BMJ* **1998**, *316* (7132), 641.
- (303) Maramai, S.; Gemma, S.; Brogi, S.; Campiani, G.; Butini, S.; Stark, H.; Brindisi, M. Dopamine D3 Receptor Antagonists as Potential Therapeutics for the Treatment of Neurological Diseases. *Front. Neurosci.* **2016**, *10*, 451.
- (304) Bownik, A.; Sokołowska, N.; Slaska, B. Effects of Apomorphine, a Dopamine Agonist, on *Daphnia Magna*: Imaging of Swimming Track Density as a Novel Tool in the Assessment of Swimming Activity. *Sci. Total Environ.* **2018**, *635*, 249–258.
- (305) Barbeau, A. L-Dopa Therapy in Parkinson's Disease: A Critical Review of Nine Years' Experience. *Can. Med. Assoc. J.* **1969**, *101* (13), 59–68.
- (306) Gal, S.; Zheng, H.; Fridkin, M.; Youdim, M. B. H. Novel Multifunctional Neuroprotective Iron Chelator-Monoamine Oxidase Inhibitor Drugs for Neurodegenerative Diseases. In Vivo Selective Brain Monoamine Oxidase Inhibition and Prevention of MPTP-Induced Striatal Dopamine Depletion. *J. Neurochem.* **2005**, *95* (1), 79–88.
- (307) Geldenhuys, W. J.; Youdim, M. B. H.; Carroll, R. T.; Van der Schyf, C. J. The

Emergence of Designed Multiple Ligands for Neurodegenerative Disorders. *Prog. Neurobiol.* **2011**, *94* (4), 347–359.

- (308) Dexter, D. T.; Statton, S. A.; Whitmore, C.; Freinbichler, W.; Weinberger, P.; Tipton, K. F.; Della Corte, L.; Ward, R. J.; Crichton, R. R. Clinically Available Iron Chelators Induce Neuroprotection in the 6-OHDA Model of Parkinson's Disease after Peripheral Administration. *J. Neural Transm.* **2011**, *118* (2), 223–231.
- (309) Molina-Holgado, F.; Gaeta, A.; Francis, P. T.; Williams, R. J.; Hider, R. C. Neuroprotective Actions of Deferiprone in Cultured Cortical Neurones and SHSY-5Y Cells. *J. Neurochem.* **2008**, *105* (6), 2466–2476.
- (310) Bebbington, D.; Dawson, C.; Gaur, S.; Spencer, J. Prodrug and Covalent Linker Strategies for the Solubilization of Dual-Action Antioxidants/Iron Chelators. *Bioorg. Med. Chem. Lett.* **2002**, *12*, 3297–3300.
- (311) Workman, D. G.; Tsatsanis, A.; Lewis, F. W.; Boyle, J. P.; Mousadoust, M.; Hettiarachchi, N. T.; Hunter, M.; Peers, C. S.; Tétard, D.; Duce, J. A. Protection from Neurodegeneration in the 6-Hydroxydopamine (6-OHDA) Model of Parkinson's with Novel 1-Hydroxypyridin-2-One Metal Chelators. *Metallomics* **2015**, *7* (5), 867–876.
- (312) Perez, C. A.; Tong, Y.; Guo, M. Iron Chelators as Potential Therapeutic Agents for Parkinson's Disease. *Curr. Bioact. Compd.* **2008**, *4* (3), 150–158.
- (313) Liddell, J. R.; Obando, D.; Liu, J.; Ganio, G.; Volitakis, I.; Mok, S. S.; Crouch, P. J.; White, A. R.; Codd, R. Lipophilic Adamantyl- or Deferasirox-Based Conjugates of Desferrioxamine B Have Enhanced Neuroprotective Capacity: Implications for Parkinson Disease. *Free Radic. Biol. Med.* **2013**, *60*, 147–156.
- (314) Rodríguez-Rodríguez, C.; Telpoukhovskaia, M.; Orvig, C. The Art of Building Multifunctional Metal-Binding Agents from Basic Molecular Scaffolds for the Potential Application in Neurodegenerative Diseases. *Coord. Chem. Rev.* **2012**, *256* (19), 2308–2332.
- (315) Gomes, L. M. F.; Vieira, R. P.; Jones, M. R.; Wang, M. C. P.; Dyrager, C.; Souza-Fagundes, E. M.; Da Silva, J. G.; Storr, T.; Beraldo, H. 8-Hydroxyquinoline Schiff-Base Compounds as Antioxidants and Modulators of Copper-Mediated A $\beta$  Peptide Aggregation. *J. Inorg. Biochem.* **2014**, *139*, 106–116.
- (316) Oliveri, V.; Bellia, F.; Grasso, G. I.; Pietropaolo, A.; Vecchio, G. Trehalose-8-Hydroxyquinoline Conjugates as Antioxidant Modulators of A $\beta$  Aggregation. *RSC Adv.* **2016**, *6* (53), 47229–47236.
- (317) Wang, L.; Esteban, G.; Ojima, M.; Bautista-Aguilera, O. M.; Inokuchi, T.; Moraleda, I.; Iriepa, I.; Samadi, A.; Youdim, M. B. H.; Romero, A.; et al. Donepezil + Propargylamine + 8-Hydroxyquinoline Hybrids as New Multifunctional Metal-Chelators, ChE and MAO Inhibitors for the Potential Treatment of Alzheimer's Disease. *Eur. J. Med. Chem.* **2014**, *80*, 543–561.
- (318) Porter, J. B.; Abeysinghe, R. D.; Hoyes, K. P.; Barra, C.; Huehns, E. R.; Brooks, P. N.; Blackwell, M. P.; Araneta, M.; Brittenham, G.; Singh, S.; et al. Contrasting Interspecies Efficacy and Toxicology of 1, 2 -Diethyl 1–3 -Hydroxypyridin-4-One, CP9 4, Relates to Differing Metabolism of the Iron Chelating Site. *Br. J. Haematol.* **1993**, *85* (1), 159–168.
- (319) Singh, S.; Epemolu, R. O.; Dobbin, P. S.; Tilbrook, G. S.; Ellis, B. L.; Damani, L. A.; Hider, R. C. Urinary Metabolic Profiles in Human and Rat of 1,2-Dimethyl- and 1,2-Diethyl-Substituted 3-Hydroxypyridin-4-Ones. *Drug Metab. Dispos.* **1992**, *20* (2), 256 LP – 261.

- (320) Roy, S.; Preston, J. E.; Hider, R. C.; Ma, Y. M. Glucosylated Deferiprone and Its Brain Uptake: Implications for Developing Glucosylated Hydroxypyridinone Analogues Intended to Cross the Blood–Brain Barrier. *J. Med. Chem.* **2010**, *53* (15), 5886–5889.
- (321) Pontikoglou, C.; Papadaki, H. A. Idiosyncratic Drug-Induced Agranulocytosis: The Paradigm of Deferiprone. *Hemoglobin* **2010**, *34* (3), 291–304.
- (322) Mao, X.; Schimmer, A. D. The Toxicology of Clioquinol. *Toxicol. Lett.* **2008**, *182* (1), 1–6.
- (323) Faux, N. G.; Ritchie, C. W.; Gunn, A.; Rembach, A.; Tsatsanis, A.; Bedo, J.; Harrison, J.; Lannfelt, L.; Blennow, K.; Zetterberg, H.; et al. PBT2 Rapidly Improves Cognition in Alzheimer’s Disease: Additional Phase II Analyses. *J. Alzheimer’s Dis.* **2010**, *20* (2), 509–516.
- (324) Murthy, L. I. Inhibition of Phenylalanine Hydroxylase Activity by  $\alpha$ -Methyl Tyrosine, a Potent Inhibitor of Tyrosine Hydroxylase. *Life Sci.* **1975**, *17* (12), 1777–1783.
- (325) Daubner, S. C.; Le, T.; Wang, S. Tyrosine Hydroxylase and Regulation of Dopamine Synthesis. *Arch. Biochem. Biophys.* **2011**, *508* (1), 1–12.
- (326) Pardridge, W. M. Blood-Brain Barrier Drug Targeting: The Future of Brain Drug Development. *Mol. Interv.* **2003**, *3* (2), 90–105.
- (327) Bentivoglio, M.; Kristensson, K. Tryps and Trips: Cell Trafficking across the 100-Year-Old Blood-Brain Barrier. *Trends Neurosci.* **2014**, *37* (6), 325–333.
- (328) Ghose, A. K.; Viswanadhan, V. N.; Wendoloski, J. J. A Knowledge-Based Approach in Designing Combinatorial or Medicinal Chemistry Libraries for Drug Discovery. 1. A Qualitative and Quantitative Characterization of Known Drug Databases. *J. Comb. Chem.* **1999**, *1* (1), 55–68.
- (329) Pardridge, W. M.; Oldendorf, W. H.; Cancilla, P.; Frank, H. J. L. Blood-Brain Barrier: Interface Between Internal Medicine and the Brain. *Ann. Intern. Med.* **1986**, *105* (1), 82–95.
- (330) Norinder, U.; Haeberlein, M. Computational Approaches to the Prediction of the Blood–Brain Distribution. *Adv. Drug Deliv. Rev.* **2002**, *54* (3), 291–313.
- (331) Lipinski, C. A. Lead- and Drug-like Compounds: The Rule-of-Five Revolution. *Drug Discov. Today Technol.* **2004**, *1* (4), 337–341.
- (332) Obermeier, B.; Daneman, R.; Ransohoff, R. M. Development, Maintenance and Disruption of the Blood-Brain Barrier. *Nat. Med.* **2013**, *19* (12), 1584–1596.
- (333) Abbott, N. J. Dynamics of CNS Barriers: Evolution, Differentiation, and Modulation. *Cell. Mol. Neurobiol.* **2005**, *25* (1), 5–23.
- (334) Abbott, N. J.; Patabendige, A. A. K.; Dolman, D. E. M.; Yusof, S. R.; Begley, D. J. Structure and Function of the Blood–Brain Barrier. *Neurobiol. Dis.* **2010**, *37* (1), 13–25.
- (335) Wolburg, H.; Noell, S.; Mack, A.; Wolburg-Buchholz, K.; Fallier-Becker, P. Brain Endothelial Cells and the Glio-Vascular Complex. *Cell Tissue Res.* **2009**, *335* (1), 75–96.
- (336) Agúndez, J. A. G.; Jiménez-Jiménez, F. J.; Alonso-Navarro, H.; García-Martín, E. Drug and Xenobiotic Biotransformation in the Blood-Brain Barrier: A Neglected

Issue. *Front. Cell. Neurosci.* **2014**, *8*, 335.

- (337) Daneman, R.; Prat, A. The Blood-Brain Barrier. *Cold Spring Harb. Perspect. Biol.* **2015**, *7* (1), a020412–a020412.
- (338) Minn, A.; Ghersi-Egea, J.-F.; Perrin, R.; Leininger, B.; Siest, G. Drug Metabolizing Enzymes in the Brain and Cerebral Microvessels. *Brain Res. Rev.* **1991**, *16* (1), 65–82.
- (339) Calias, P.; Banks, W. A.; Begley, D.; Scarpa, M.; Dickson, P. Intrathecal Delivery of Protein Therapeutics to the Brain: A Critical Reassessment. *Pharmacol. Ther.* **2014**, *144* (2), 114–122.
- (340) Shilo, M.; Sharon, A.; Baranes, K.; Motiei, M.; Lellouche, J. P. M.; Popovtzer, R. The Effect of Nanoparticle Size on the Probability to Cross the Blood-Brain Barrier: An in-Vitro Endothelial Cell Model. *J. Nanobiotechnology* **2015**, *13* (1), 1–7.
- (341) Kreuter, J. Mechanism of Polymeric Nanoparticle-Based Drug Transport across the Blood-Brain Barrier (BBB). *J. Microencapsul.* **2013**, *30* (1), 49–54.
- (342) Olivier, J.-C. Drug Transport to Brain with Targeted Nanoparticles. *NeuroRx* **2005**, *2* (1), 108–119.
- (343) Pardridge, W. M. Drug Transport across the Blood-Brain Barrier. *J. Cereb. Blood Flow Metab.* **2012**, *32* (11), 1959–1972.
- (344) Lipinski, C. A.; Lombardo, F.; Dominy, B. W.; Feeney, P. J. Experimental and Computational Approaches to Estimate Solubility and Permeability in Drug Discovery and Development Settings IPII of Original Article: S0169-409X(96)00423-1. The Article Was Originally Published in Advanced Drug Delivery Reviews 23 (1997) 3. *Adv. Drug Deliv. Rev.* **2001**, *46* (1), 3–26.
- (345) Lieb, W. R.; Stein, W. D. Non-Stokesian Nature of Transverse Diffusion within Human Red Cell Membranes. *J. Membr. Biol.* **1986**, *92* (2), 111–119.
- (346) Fischer, H.; Gottschlich, R.; Seelig, A. Blood-Brain Barrier Permeation: Molecular Parameters Governing Passive Diffusion. *J. Membr. Biol.* **1998**, *165* (3), 201–211.
- (347) Oldendorf, W. H. Lipid Solubility and Drug Penetration of the Blood Brain Barrier. *Proc. Soc. Exp. Biol. Med.* **1974**, *147* (3), 813–816.
- (348) Hitchcock, S. A.; Pennington, L. D. Structure–Brain Exposure Relationships. *J. Med. Chem.* **2006**, *49* (26), 7559–7583.
- (349) Daina, A.; Michielin, O.; Zoete, V. SwissADME: A Free Web Tool to Evaluate Pharmacokinetics, Drug-Likeness and Medicinal Chemistry Friendliness of Small Molecules. *Sci. Rep.* **2017**, *7* (October 2016), 1–13.
- (350) Daina, A.; Zoete, V. A BOILED-Egg To Predict Gastrointestinal Absorption and Brain Penetration of Small Molecules. *ChemMedChem* **2016**, *11* (11), 1117–1121.
- (351) Daina, A.; Michielin, O.; Zoete, V. ILOGP: A Simple, Robust, and Efficient Description of n-Octanol/Water Partition Coefficient for Drug Design Using the GB/SA Approach. *J. Chem. Inf. Model.* **2014**, *54* (12), 3284–3301.
- (352) Habgood, M. D.; Liu, Z. D.; Dehkordi, L. S.; Khodr, H. H.; Abbott, J.; Hider, R. C. Investigation into the Correlation between the Structure of Hydroxypyridinones and Blood–Brain Barrier Permeability. *Biochem. Pharmacol.* **1999**, *57* (11), 1305–1310.
- (353) Rautio, J.; Laine, K.; Gynther, M.; Savolainen, J. Prodrug Approaches for CNS

Delivery. *AAPS J.* **2008**, *10* (1), 92–102.

- (354) Anderson, B. D. Prodrugs for Improved CNS Delivery. *Adv. Drug Deliv. Rev.* **1996**, *19* (2), 171–202.
- (355) Pavan, B.; Dalpiaz, A.; Ciliberti, N.; Biondi, C.; Manfredini, S.; Vertuani, S. Progress in Drug Delivery to the Central Nervous System by the Prodrug Approach. *Molecules* **2008**, *13*, 1035–1065.
- (356) Habgood, M. D.; Begley, D. J.; Abbott, N. J. Determinants of Passive Drug Entry into the Central Nervous System. *Cell. Mol. Neurobiol.* **2000**, *20* (2), 231–253.
- (357) Oliveri, V.; Vecchio, G. Prochelator Strategies for Site-Selective Activation of Metal Chelators. *J. Inorg. Biochem.* **2016**, *162*, 31–43.
- (358) Zlokovic, B. V. The Blood-Brain Barrier in Health and Chronic Neurodegenerative Disorders. *Neuron* **2008**, *57* (2), 178–201.
- (359) Lee, G.; Dallas, S.; Hong, M.; Bendayan, R. Drug Transporters in the Central Nervous System: Brain Barriers and Brain Parenchyma Considerations. *Pharmacol. Rev.* **2001**, *53* (4), 569 LP – 596.
- (360) Begley, D. J. Delivery of Therapeutic Agents to the Central Nervous System: The Problems and the Possibilities. *Pharmacol. Ther.* **2004**, *104* (1), 29–45.
- (361) Pardridge, W. M. The Blood-Brain Barrier: Bottleneck in Brain Drug Development. *NeuroRx* **2005**, *2* (1), 3–14.
- (362) Löscher, W.; Potschka, H. Blood-Brain Barrier Active Efflux Transporters: ATP-Binding Cassette Gene Family. *NeuroRx* **2005**, *2* (1), 86–98.
- (363) Toda, R.; Kawazu, K.; Oyabu, M.; Miyazaki, T.; Kiuchi, Y. Comparison of Drug Permeabilities across the Blood–Retinal Barrier, Blood–Aqueous Humor Barrier, and Blood–Brain Barrier. *J. Pharm. Sci.* **2011**, *100* (9), 3904–3911.
- (364) Jong, A. Blood-Brain Barrier Drug Discovery for Central Nervous System Infections. *Curr. Drug Targets. Infect. Disord.* **2005**, *5*, 65–72.
- (365) Mäger, I.; Meyer, A. H.; Li, J.; Lenter, M.; Hildebrandt, T.; Leparç, G.; Wood, M. J. A. Targeting Blood-Brain-Barrier Transcytosis – Perspectives for Drug Delivery. *Neuropharmacology* **2017**, *120*, 4–7.
- (366) Jones, A. R.; Shusta, E. V. Blood-Brain Barrier Transport of Therapeutics via Receptor-Mediation. *Pharm. Res.* **2007**, *24* (9), 1759–1771.
- (367) Hervé, F.; Ghinea, N.; Scherrmann, J.-M. CNS Delivery via Adsorptive Transcytosis. *AAPS J.* **2008**, *10* (3), 455–472.
- (368) Song, X.; Li, R.; Deng, H.; Li, Y.; Cui, Y.; Zhang, H.; Dai, W.; He, B.; Zheng, Y.; Wang, X.; et al. Receptor Mediated Transcytosis in Biological Barrier: The Influence of Receptor Character and Their Ligand Density on the Transmembrane Pathway of Active-Targeting Nanocarriers. *Biomaterials* **2018**, *180*, 78–90.
- (369) Lu, W.; Xiong, C.; Zhang, R.; Shi, L.; Huang, M.; Zhang, G.; Song, S.; Huang, Q.; Liu, G.-Y.; Li, C. Receptor-Mediated Transcytosis: A Mechanism for Active Extravascular Transport of Nanoparticles in Solid Tumors. *J. Control. Release* **2012**, *161* (3), 959–966.
- (370) Xiao, G.; Gan, L. S. Receptor-Mediated Endocytosis and Brain Delivery of Therapeutic Biologics. *Int. J. Cell Biol.* **2013**, *2013*.

- (371) Lajoie, J. M.; Shusta, E. V. Targeting Receptor-Mediated Transport for Delivery of Biologics across the Blood-Brain Barrier. *Annu. Rev. Pharmacol. Toxicol.* **2015**, *55*, 613–631.
- (372) Fishman, J. B.; Rubin, J. B.; Handrahan, J. V.; Connor, J. R.; Fine, R. E. Receptor-Mediated Transcytosis of Transferrin across the Blood-Brain Barrier. *J. Neurosci. Res.* **1987**, *18* (2), 299–304.
- (373) Dehouck, B.; Fenart, L.; Dehouck, M. P.; Pierce, A.; Torpier, G.; Cecchelli, R. A New Function for the LDL Receptor: Transcytosis of LDL across the Blood-Brain Barrier. *J. Cell Biol.* **1997**, *138* (4), 877–889.
- (374) Chen, Y.-W.; Boyartchuk, V.; Lewis, B. C. Differential Roles of Insulin-like Growth Factor Receptor- and Insulin Receptor-Mediated Signaling in the Phenotypes of Hepatocellular Carcinoma Cells. *Neoplasia* **2009**, *11* (9), 835–845.
- (375) Pardridge, W. Blood-Brain Barrier Endogenous Transporters as Therapeutic Targets: A New Model for Small Molecule CNS Drug Discovery. *Expert Opin. Ther. Targets* **2015**, *19*.
- (376) Khan, N. U.; Miao, T.; Ju, X.; Guo, Q.; Han, L. 6 - Carrier-Mediated Transportation through BBB. In *A Focus on Nanotechnology and Nanoparticulates*; Gao, H., Gao, X. B. T.-B. T. D. D. S., Eds.; Academic Press, 2019; pp 129–158.
- (377) Ennis, S. R.; Ren, X.; Betz, A. L. Mechanisms of Sodium Transport at the Blood-Brain Barrier Studied with In Situ Perfusion of Rat Brain. *J. Neurochem.* **1996**, *66* (2), 756–763.
- (378) Cornford, E. M.; Diep, C. P.; Pardridge, W. M. Blood-Brain Barrier Transport of Valproic Acid. *J. Neurochem.* **1985**, *44* (5), 1541–1550.
- (379) Li, J. Y.; Boado, R. J.; Pardridge, W. M. Cloned Blood-Brain Barrier Adenosine Transporter Is Identical to the Rat Concentrative Na<sup>+</sup> Nucleoside Cotransporter CNT2. *J. Cereb. Blood Flow Metab.* **2001**, *21* (8), 929–936.
- (380) Müller, J.; Lips, K. S.; Metzner, L.; Neubert, R. H. H.; Koepsell, H.; Brandsch, M. Drug Specificity and Intestinal Membrane Localization of Human Organic Cation Transporters (OCT). *Biochem. Pharmacol.* **2005**, *70* (12), 1851–1860.
- (381) Pardridge, W. M.; Sakiyama, R.; Fierer, G. Transport of Propranolol and Lidocaine through the Rat Blood-Brain Barrier. Primary Role of Globulin-Bound Drug. *J. Clin. Invest.* **1983**, *71* (4), 900–908.
- (382) Bouw, M. R.; Xie, R.; Tunblad, K.; Hammarlund-Udenaes, M. Blood-Brain Barrier Transport and Brain Distribution of Morphine-6-Glucuronide in Relation to the Antinociceptive Effect in Rats--Pharmacokinetic/Pharmacodynamic Modelling. *Br. J. Pharmacol.* **2001**, *134* (8), 1796–1804. <https://doi.org/10.1053/bjph.2001.1348>
- (383) McAllister, M. S.; Krizanac-Bengez, L.; Macchia, F.; Naftalin, R. J.; Pedley, K. C.; Mayberg, M. R.; Marroni, M.; Leaman, S.; Stanness, K. A.; Janigro, D. Mechanisms of Glucose Transport at the Blood-Brain Barrier: An in Vitro Study. *Brain Res.* **2001**, *904* (1), 20–30.
- (384) Cheeseman, C. I. Hexose Transport Across Mammalian Epithelia BT - Epithelial Transport Physiology. In *Epithelial Transport Physiology*; Gerencser, G. A., Ed.; Humana Press: Totowa, NJ, 2010; pp 323–352.
- (385) Barrett, M. P.; Walmsley, A. R.; Gould, G. W. Structure and Function of Facultative Sugar Transporters. *Curr. Opin. Cell Biol.* **1999**, *11* (4), 496–502.

- (386) Wood, I.; Trayhurn, P. Glucose Transporters (GLUT and SGLT): Expanded Families of Sugar Transport Proteins. *Br. J. Nutr.* **2003**, *89*, 3–9.
- (387) Baldwin, S. A. Mammalian Passive Glucose Transporters: Members of an Ubiquitous Family of Active and Passive Transport Proteins. *Biochim. Biophys. Acta - Rev. Biomembr.* **1993**, *1154* (1), 17–49.
- (388) Manolescu, A. R.; Witkowska, K.; Kinnaird, A.; Cessford, T.; Cheeseman, C. Facilitated Hexose Transporters: New Perspectives on Form and Function. *Physiology* **2007**, *22* (4), 234–240.
- (389) Sun, L.; Zeng, X.; Chuangye, Y.; Sun, X.; Gong, X.; Rao, Y.; Yan, N. Crystal Structure of a Bacterial Homologue of Glucose Transporters GLUT1-4. *Nature* **2012**, *490*, 361–366.
- (390) Kumagai, A. K. Glucose Transport in Brain and Retina: Implications in the Management and Complications of Diabetes. *Diabetes. Metab. Res. Rev.* **1999**, *15* (4), 261–273.
- (391) Kalaria, R. N.; Gravina, S. A.; Schmidley, J. W.; Perry, G.; Harik, S. I. The Glucose Transporter of the Human Brain and Blood-Brain Barrier. *Ann. Neurol.* **1988**, *24* (6), 757–764.
- (392) Pardridge, W.; Boado, R.; Farrell, C. Brain-Type Glucose Transporter (GLUT-1) Is Selectively Localized to the Blood-Brain Barrier: Studies with Quantitative Western Blotting and in Situ Hybridization. *J. Biol. Chem.* **1990**, *265*, 18035–18040.
- (393) Carruthers, A.; DeZutter, J.; Ganguly, A.; Devaskar, S. U. Will the Original Glucose Transporter Isoform Please Stand Up! *Am. J. Physiol. Endocrinol. Metab.* **2009**, *297* (4), E836–E848.
- (394) Scott, L. E.; Telpoukhovskaia, M.; Rodríguez-Rodríguez, C.; Merkel, M.; Bowen, M. L.; Page, B. D. G.; Green, D. E.; Storr, T.; Thomas, F.; Allen, D. D.; et al. N-Aryl-Substituted 3-( $\beta$ -D-Glucopyranosyloxy)-2-Methyl-4(1H)-Pyridinones as Agents for Alzheimer's Therapy. *Chem. Sci.* **2011**, *2* (4), 642–648.
- (395) Schugar, H.; Green, D. E.; Bowen, M. L.; Scott, L. E.; Storr, T.; Böhmerle, K.; Thomas, F.; Allen, D. D.; Lockman, P. R.; Merkel, M.; et al. Combating Alzheimer's Disease With Multifunctional Molecules Designed for Metal Passivation. *Angew. Chemie Int. Ed.* **2007**, *46* (10), 1716–1718.
- (396) Green, D. E.; Bowen, M. L.; Scott, L. E.; Storr, T.; Merkel, M.; Böhmerle, K.; Thompson, K. H.; Patrick, B. O.; Schugar, H. J.; Orvig, C. In Vitro Studies of 3-Hydroxy-4-Pyridinones and Their Glycosylated Derivatives as Potential Agents for Alzheimer's Disease. *Dalt. Trans.* **2010**, *39* (6), 1604–1615.
- (397) Storr, T.; Merkel, M.; Song-Zhao, G. X.; Scott, L. E.; Green, D. E.; Bowen, M. L.; Thompson, K. H.; Patrick, B. O.; Schugar, H. J.; Orvig, C. Synthesis, Characterization, and Metal Coordinating Ability of Multifunctional Carbohydrate-Containing Compounds for Alzheimer's Therapy. *J. Am. Chem. Soc.* **2007**, *129* (23), 7453–7463.
- (398) Verrey, F.; Closs, E. I.; Wagner, C. A.; Palacin, M.; Endou, H.; Kanai, Y. CATs and HATs: The SLC7 Family of Amino Acid Transporters. *Pflügers Arch.* **2004**, *447* (5), 532–542.
- (399) Fotiadis, D.; Kanai, Y.; Palacín, M. The SLC3 and SLC7 Families of Amino Acid Transporters. *Mol. Aspects Med.* **2013**, *34* (2), 139–158.

- (400) Napolitano, L.; Scalise, M.; Galluccio, M.; Pochini, L.; Albanese, L. M.; Indiveri, C. LAT1 Is the Transport Competent Unit of the LAT1/CD98 Heterodimeric Amino Acid Transporter. *Int. J. Biochem. Cell Biol.* **2015**, *67*, 25–33.
- (401) Braun, D.; Kinne, A.; Bräuer, A. U.; Sapin, R.; Klein, M. O.; Köhrle, J.; Wirth, E. K.; Schweizer, U. Developmental and Cell Type-Specific Expression of Thyroid Hormone Transporters in the Mouse Brain and in Primary Brain Cells. *Glia* **2011**, *59* (3), 463–471.
- (402) Kanai, Y.; Segawa, H.; Miyamoto, K. I.; Uchino, H.; Takeda, E.; Endou, H. Expression Cloning and Characterization of a Transporter for Large Neutral Amino Acids Activated by the Heavy Chain of 4F2 Antigen (CD98). *J. Biol. Chem.* **1998**, *273* (37), 23629–23632.
- (403) Pardridge, W. M. Brain Metabolism: A Perspective from the Blood-Brain Barrier. *Physiol. Rev.* **1983**, *63* (4), 1481–1535.
- (404) Meier, C.; Ristic, Z.; Klauser, S.; Verrey, F. Activation of System L Heterodimeric Amino Acid Exchangers by Intracellular Substrates. *EMBO J.* **2002**, *21* (4), 580–589.
- (405) Singh, N.; Ecker, F. G. Insights into the Structure, Function, and Ligand Discovery of the Large Neutral Amino Acid Transporter 1, LAT1. *International Journal of Molecular Sciences*. 2018.
- (406) Fort, J.; De La Ballina, L. R.; Burghardt, H. E.; Ferrer-Costa, C.; Turnay, J.; Ferrer-Orta, C.; Usón, I.; Zorzano, A.; Fernández-Recio, J.; Orozco, M.; et al. The Structure of Human 4F2hc Ectodomain Provides a Model for Homodimerization and Electrostatic Interaction with Plasma Membrane. *J. Biol. Chem.* **2007**, *282* (43), 31444–31452.
- (407) Costa, M.; Rosell, A.; Álvarez-Marimon, E.; Zorzano, A.; Fotiadis, D.; Palacín, M. Expression of Human Heteromeric Amino Acid Transporters in the Yeast *Pichia Pastoris*. *Protein Expr. Purif.* **2013**, *87* (1), 35–40.
- (408) Rosell, A.; Meury, M.; Álvarez-Marimon, E.; Costa, M.; Pérez-Cano, L.; Zorzano, A.; Fernández-Recio, J.; Palacín, M.; Fotiadis, D. Structural Bases for the Interaction and Stabilization of the Human Amino Acid Transporter LAT2 with Its Ancillary Protein 4F2hc. *Proc. Natl. Acad. Sci.* **2014**, *111* (8), 2966 LP – 2971.
- (409) Yan, R.; Zhao, X.; Lei, J.; Zhou, Q. Structure of the Human LAT1–4F2hc Heteromeric Amino Acid Transporter Complex. *Nature* **2019**, *568* (7750), 127–130.
- (410) Gao, X.; Zhou, L.; Jiao, X.; Lu, F.; Yan, C.; Zeng, X.; Wang, J.; Shi, Y. Mechanism of Substrate Recognition and Transport by an Amino Acid Antiporter. *Nature* **2010**, *463* (7282), 828–832.
- (411) Ma, D.; Lu, P.; Yan, C.; Fan, C.; Yin, P.; Wang, J.; Shi, Y. Structure and Mechanism of a Glutamate–GABA Antiporter. *Nature* **2012**, *483* (7391), 632–636.
- (412) Shaffer, P. L.; Goehring, A.; Shankaranarayanan, A.; Gouaux, E. Structure and Mechanism of a Na<sup>+</sup>-Independent Amino Acid Transporter. *Science* (80-. ). **2009**, *325* (5943), 1010 LP – 1014.
- (413) O., O.; O.A., F.; J.I., O.; M.M., A.; A.O., K.; E.M., O. Estimation of the Kinetic Parameters of the Inhibition of Tyrosinase by an Extract of *S. Mombin* (Root Bark) and the Investigation of Likely Interactions of Composite Phytochemicals Using Molecular Docking Calculations. *Am. J. Pharmacol. Sci.* **2018**, *6* (1), 13–18.
- (414) Olivares, D.; Huang, X.; Branden, L.; Greig, H. N.; Rogers, T. J. Physiological and

Pathological Role of Alpha-Synuclein in Parkinson's Disease Through Iron Mediated Oxidative Stress; The Role of a Putative Iron-Responsive Element. *International Journal of Molecular Sciences*. 2009.

- (415) Segura-Aguilar, J.; Paris, I.; Muñoz, P.; Ferrari, E.; Zecca, L.; Zucca, F. A. Protective and Toxic Roles of Dopamine in Parkinson's Disease. *J. Neurochem.* **2014**, *129* (6), 898–915.
- (416) Bisaglia, M.; Filograna, R.; Beltramini, M.; Bubacco, L. Are Dopamine Derivatives Implicated in the Pathogenesis of Parkinson's Disease? *Ageing Res. Rev.* **2014**, *13*, 107–114.
- (417) Merkofer, M.; Kissner, R.; Hider, R. C.; Brunk, U. T.; Koppenol, W. H. Fenton Chemistry and Iron Chelation under Physiologically Relevant Conditions: Electrochemistry and Kinetics. *Chem. Res. Toxicol.* **2006**, *19* (10), 1263–1269.
- (418) Zhou, T.; Ma, Y.; Kong, X.; Hider, R. C. Design of Iron Chelators with Therapeutic Application. *Dalt. Trans.* **2012**, *41* (21), 6371–6389.
- (419) Crisponi, G.; Remelli, M. Iron Chelating Agents for the Treatment of Iron Overload. *Coord. Chem. Rev.* **2008**, *252* (10), 1225–1240.
- (420) Liu, Z. D.; Khodr, H. H.; Liu, D. Y.; Lu, S. L.; Hider, R. C. Synthesis, Physicochemical Characterization, and Biological Evaluation of 2-(1'-Hydroxyalkyl)-3-Hydroxypyridin-4-Ones: Novel Iron Chelators with Enhanced  $\text{PFe}^{3+}$  Values. *J. Med. Chem.* **1999**, *42* (23), 4814–4823.
- (421) Hider, R. C.; Kong, X. Chemistry and Biology of Siderophores. *Nat. Prod. Rep.* **2010**, *27* (5), 637–657.
- (422) Loper, J. E.; Henkels, M. D. Utilization of Heterologous Siderophores Enhances Levels of Iron Available to *Pseudomonas Putida* in the Rhizosphere. *Appl. Environ. Microbiol.* **1999**, *65* (12), 5357–5363.
- (423) Pearson, R. G. Hard and Soft Acids and Bases. *J. Am. Chem. Soc.* **1963**, *85* (22), 3533–3539. <https://doi.org/10.1021/ja00905a001>.
- (424) Martell, A. E., Smith, R. M. *Critical Stability Constant*, vol. 1-6.; Springer, Ed.; Plenum Press: London, 1989.
- (425) Harris, D. C.; Aisen, P. Facilitation of Fe(II) Antioxidation by Fe(III) Complexing Agents. *Biochim. Biophys. Acta - Gen. Subj.* **1973**, *329* (1), 156–158.
- (426) M, H. J. Physicochemical Characterisation of Chelation and Transport of Iron by Low Molecular Weight Chelators, Duke University, 2010.
- (427) Rodgers, S. J.; Raymond, K. N. Ferric Ion Sequestering Agents. 11. Synthesis and Kinetics of Iron Removal from Transferrin of Catechoyl Derivatives of Desferrioxamine B. *J. Med. Chem.* **1983**, *26* (3), 439–442.
- (428) Carrano, C. J.; Raymond, K. N. Ferric Ion Sequestering Agents. 2. Kinetics and Mechanism of Iron Removal from Transferrin by Enterobactin and Synthetic Tricatechols. *J. Am. Chem. Soc.* **1979**, *101* (18), 5401–5404. <https://doi.org/10.1021/ja00512a047>.
- (429) Albert-Gary, A.M, Crumbliss, A. L. Metal Ions in Biological Systems; CRC PRESS, 1998; pp 239–327.
- (430) Barbeau, K.; Rue, E. L.; Bruland, K. W.; Butler, A. Photochemical Cycling of Iron in the Surface Ocean Mediated by Microbial Iron(III)-Binding Ligands. *Nature* **201AD**,

- (431) Clarke, E. T.; Martell, A. E. 1-Methyl-3-Hydroxy-2-Pyridinone and 1,4-Dihydroxy-2-Pyridinone Complexes of the Trivalent Metal Ions of Fe(III), Ga(III), Al(III), In(III) and Gd(III): Potentiometric and Spectrophotometric Determination of Stabilities. *Inorganica Chim. Acta* **1992**, *196* (2), 185–194.
- (432) Xu, J.; Kullgren, B.; Durbin, P. W.; Raymond, K. N. Specific Sequestering Agents for the Actinides. 28. Synthesis and Initial Evaluation of Multidentate 4-Carbamoyl-3-Hydroxy-1-Methyl-2(1H)-Pyridinone Ligands for in Vivo Plutonium(IV) Chelation. *J. Med. Chem.* **1995**, *38* (14), 2606–2614.
- (433) May, S. W.; Oldham, C. D.; Mueller, P. W.; Padgett, S. R.; Sowell, A. L. Protocatechuate 3,4-Dioxygenase. *J. Biol. Chem.* **1982**, *257* (21), 12746–12751.
- (434) Devanur, L. D.; Neubert, H.; Hider, R. C. The Fenton Activity of Iron(III) in the Presence of Deferiprone. *J. Pharm. Sci.* **2008**, *97* (4), 1454–1467.
- (435) Graf, E.; Mahoneys, J. R.; Bryant, R. G.; Eaton, J. W. Iron-Catalyzed Hydroxyl Radical Formation. *J. Biol. Chem.* **1984**, *259* (6), 3620–3624.
- (436) Timoshnikov, V. A.; Kobzeva, T. V.; Polyakov, N.; Kontoghiorghes, G. Inhibition of Fe(2+) and Fe(3+) Induced Hydroxyl Radical Production by the Iron Chelating Drug Deferiprone. *Free Radic. Biol. Med.* **2014**, *78*.
- (437) A. Timoshnikov, V.; Kobzeva, T.; Selyutina, O.; Polyakov, N.; Kontoghiorghes, G. Effective Inhibition of Copper-Catalyzed Production of Hydroxyl Radicals by Deferiprone. *JBIC J. Biol. Inorg. Chem.* **2019**.
- (438) Ramsaywack, S.; M Vogels, C.; Ricker, L.; Westcott, S.; Barclay, L. *Pyridinones Are Not Antioxidants As Shown by Kinetics of Free Radical Autoxidation, but They Prevent Radical Oxidations Catalyzed by Toxic Heavy Metals*; 2013; Vol. 26.
- (439) Devos, D.; Moreau, C.; Devedjian, J. C.; Kluza, J.; Petrault, M.; Laloux, C.; Jonneaux, A.; Ryckewaert, G.; Garçon, G.; Rouaix, N.; et al. Targeting Chelatable Iron as a Therapeutic Modality in Parkinson's Disease. *Antioxid. Redox Signal.* **2014**, *21* (2), 195–210.
- (440) Timoshnikov, V. A.; Kobzeva, T. V.; Polyakov, N. E.; Kontoghiorghes, G. J. Inhibition of Fe<sup>2+</sup>- and Fe<sup>3+</sup>- Induced Hydroxyl Radical Production by the Iron-Chelating Drug Deferiprone. *Free Radic. Biol. Med.* **2015**, *78*, 118–122.
- (441) Kayyali, R.; Pannala, A. S.; Khodr, H.; Hider, R. C. Comparative Radical Scavenging Ability of Bidentate Iron(III) Chelators. *Biochem. Pharmacol.* **1998**, *55* (8), 1327–1332.
- (442) Dobbin, P. S.; Hider, R. C.; Hall, A. D.; Taylor, P. D.; Sarpong, P.; Porter, J. B.; Xiao, G.; van der Helm, D. Synthesis, Physicochemical Properties, and Biological Evaluation of N-Substituted 2-Alkyl-3-Hydroxy-4(1H)-Pyridinones: Orally Active Iron Chelators with Clinical Potential. *J. Med. Chem.* **1993**, *36* (17), 2448–2458.
- (443) Chaves, S.; Canário, S.; Carrasco, M. P.; Mira, L.; Santos, M. A. Hydroxy(Thio)Pyrone and Hydroxy(Thio)Pyridinone Iron Chelators: Physico-Chemical Properties and Anti-Oxidant Activity. *J. Inorg. Biochem.* **2012**, *114*, 38–46.
- (444) Merkofer, M.; Kissner, R.; Hider, R. C.; Koppenol, W. H. Redox Properties of the Iron Complexes of Orally Active Iron Chelators CP20, CP502, CP509, and ICL670. *Helv. Chim. Acta* **2004**, *87* (12), 3021–3034.
- (445) Streater, M.; Taylor, P. D.; Hider, R. C.; Porter, J. Novel 3-Hydroxy-2(1H)-

Pyridinones. Synthesis, Iron(III)-Chelating Properties, and Biological Activity. *J. Med. Chem.* **1990**, *33* (6), 1749–1755.

- (446) Workman, D. G.; Hunter, M.; Dover, L. G.; Tétard, D. Synthesis of Novel Iron(III) Chelators Based on Triaza Macrocyclic Backbone and 1-Hydroxy-2(H)-Pyridin-2-One Coordinating Groups and Their Evaluation as Antimicrobial Agents. *J. Inorg. Biochem.* **2016**, *160*, 49–58.
- (447) Boukhalifa, H.; Crumbliss, A. L. Chemical Aspects of Siderophore Mediated Iron Transport. *Biometals* **2002**, *15* (4), 325–339.
- (448) Moridani, M. Y.; Tilbrook, G. S.; Khodr, H. H.; Hider, R. C. Synthesis and Physicochemical Assessment of Novel 2-Substituted 3-Hydroxypyridin-4-Ones, Novel Iron Chelators. *J. Pharm. Pharmacol.* **2002**, *54* (3), 349–364.
- (449) Chiswell, B.; Litster, D. S. The Multidentate Chemistry of Manganese(II). Part VI. Tridentate Nitrogenous Ligands Complexes. *Inorganica Chim. Acta* **1978**, *29*, 25–36.
- (450) Sankaralingam, M.; Saravanan, N.; Anitha, N.; Suresh, E.; Palaniandavar, M. Biomimetic Iron(III) Complexes of Facially and Meridionally Coordinating Tridentate 3N Ligands: Tuning of Regioselective Extradial Dioxygenase Activity in Organized Assemblies. *Dalt. Trans.* **2014**, *43* (18), 6828–6841.
- (451) Drew, M. G. B.; Iveson, P. B.; Hudson, M. J.; Liljenzin, J. O.; Spjuth, L.; Cordier, P.-Y.; Enarsson, Å.; Hill, C.; Madic, C. Separation of Americium(III) from Europium(III) with Tridentate Heterocyclic Nitrogen Ligands and Crystallographic Studies of Complexes Formed by 2,2':6',2''-Terpyridine with the Lanthanides. *J. Chem. Soc. Dalt. Trans.* **2000**, No. 5, 821–830.
- (452) Hider, R. C.; Hall, A. D. 2 Clinically Useful Chelators of Tripositive Elements. *Prog. Med. Chem.* **1991**, *28*, 41–173.
- (453) Bernhardt, P. V.; Caldwell, L. M.; Chaston, T. B.; Chin, P.; Richardson, D. R. Cytotoxic Iron Chelators: Characterization of the Structure, Solution Chemistry and Redox Activity of Ligands and Iron Complexes of the Di-2-Pyridyl Ketone Isonicotinoyl Hydrazone (HPKIH) Analogues. *J. Biol. Inorg. Chem.* **2003**, *8* (8), 866–880.
- (454) Sigel, A.; Sigel, H. Metal Ions in Biological Systems, Volume 35: Iron Transport and Storage Microorganisms, Plants, and Animals. *Met. Based. Drugs* **1998**, *5* (5), 262.
- (455) D Habgood, M.; Dong Liu, Z.; S Dehkordi, L.; Khodr, H.; Abbott, J.; Hider, R. Investigation into the Correlation between the Structure of Hydroxypyridinones and Blood-Brain Barrier Permeability - Part 32: An Analysis of Water-Octanol and Water-Alkane Partitioning and the  $\Delta\log P$  Parameter of Seiler. *Biochem. Pharmacol.* **1999**, *57*, 1305–1310.
- (456) FAGERHOLM; NILSSON; KNUTSON; LENNERNÄS. Jejunal Permeability in Humans In vivo and Rats In situ: Investigation of Molecular Size Selectivity and Solvent Drag. *Acta Physiol. Scand.* **1999**, *165* (3), 315–324.
- (457) Maxton, D. G.; Bjarnason, I.; Reynolds, A. P.; Catt, S. D.; Peters, T. J.; Menzies, I. S. Lactulose 51Cr-Labelled Ethylenediaminetetra-Acetate, L- Rhamnose and Polyethyleneglycol 500 as Probe Markers for Assessment in Vivo of Human Intestinal Permeability in Vivo of Human Intestinal Permeability. *Clin. Sci.* **1986**, *71* (1), 71 LP – 80. <https://doi.org/10.1042/cs0710071>.
- (458) Kim, M. Absorption of Polyethylene Glycol Oligomers (330-1122 Da) Is Greater in the Jejunum than in the Ileum of Rats. *J. Nutr.* **1996**, *126* (9), 2172–2178.

- (459) Liu, D. Y.; Liu, Z. D.; Hider, R. C. Oral Iron Chelators – Development and Application. *Best Pract. Res. Clin. Haematol.* **2002**, *15* (2), 369–384.
- (460) Yokel, R. A.; Fredenburg, A. M.; Meurer, K. A.; Skinner, T. L. Influence of Lipophilicity on the Bioavailability and Disposition of Orally Active 3-Hydroxypyridin-4-One Metal Chelators. *Drug Metab. Dispos.* **1995**, *23* (10), 1178–1180.
- (461) Liu, J.; Yu, K.; Zhu, W. Amino Acid Sensing in the Gut and Its Mediation in Gut-Brain Signal Transduction. *Anim. Nutr.* **2016**, *2* (2), 69–73.
- (462) Hider, R. C.; Singh, S.; Porter, J. B. Iron Chelating Agents with Clinical Potential. *Proc. R. Soc. Edinburgh. Sect. B. Biol. Sci.* **1992**, *99* (1–2), 137–168.
- (463) Abeysinghe, R. D.; Roberts, P. J.; Cooper, C. E.; MacLean, K. H.; Hider, R. C.; Porter, J. B. The Environment of the Lipoxygenase Iron Binding Site Explored with Novel Hydroxypyridinone Iron Chelators. *J. Biol. Chem.* **1996**, *271* (14), 7965–7972.
- (464) Hider, R. C. Potential Protection from Toxicity by Oral Iron Chelators. *Toxicol. Lett.* **1995**, *82–83*, 961–967.
- (465) Uchino, H.; Kanai, Y.; Kim, D. K.; Wempe, M. F.; Chairoungdua, A.; Morimoto, E.; Anders, M. W.; Endou, H. Transport of Amino Acid-Related Compounds Mediated by L-Type Amino Acid Transporter 1 (LAT1): Insights Into the Mechanisms of Substrate Recognition. *Mol. Pharmacol.* **2002**, *61* (4), 729–737.
- (466) Smith, Q. R. Carrier-Mediated Transport to Enhance Drug Delivery to Brain. *Int. Congr. Ser.* **2005**, *1277*, 63–74.
- (467) Gao, X.; Zhou, L.; Jiao, X.; Lu, F.; Yan, C.; Zeng, X.; Wang, J.; Shi, Y. Mechanism of Substrate Recognition and Transport by an Amino Acid Antiporter. *Nature* **2010**, *463* (7282), 828–832.
- (468) Napolitano, L.; Galluccio, M.; Scalise, M.; Parravicini, C.; Palazzolo, L.; Eberini, I.; Indiveri, C. Novel Insights into the Transport Mechanism of the Human Amino Acid Transporter LAT1 (SLC7A5). Probing Critical Residues for Substrate Translocation. *Biochim. Biophys. Acta - Gen. Subj.* **2017**, *1861* (4), 727–736.
- (469) Ylikangas, H.; Peura, L.; Malmioja, K.; Leppänen, J.; Laine, K.; Poso, A.; Lahtela-Kakkonen, M.; Rautio, J. Structure–Activity Relationship Study of Compounds Binding to Large Amino Acid Transporter 1 (LAT1) Based on Pharmacophore Modeling and in Situ Rat Brain Perfusion. *Eur. J. Pharm. Sci.* **2013**, *48* (3), 523–531.
- (470) Cramer, R. D.; Patterson, D. E.; Bunce, J. D. Comparative Molecular Field Analysis (CoMFA). 1. Effect of Shape on Binding of Steroids to Carrier Proteins. *J. Am. Chem. Soc.* **1988**, *110* (18), 5959–5967.
- (471) Cramer, R. D. Topomer CoMFA: A Design Methodology for Rapid Lead Optimization. *J. Med. Chem.* **2003**, *46* (3), 374–388.
- (472) SCHMIDT, L. H.; FRADKIN, R.; SULLIVAN, R.; FLOWERS, A. COMPARATIVE PHARMACOLOGY OF ALKYLATING AGENTS. 3. TOXICITY DATA ON MONKEYS AND DOGS. *Cancer Chemother. reports* **1965**, *18*, SUPPL 2:1017+.
- (473) WHITE, F. R. Sarcosylsin and Related Compounds. *Cancer Chemother. reports* **1960**, *6*, 61–93.
- (474) Larionov, L. F.; Khokhlov, A. S.; Shkodinskaja, E. N.; Vasina, O. S.; Troosheikina, V. I.; Novikova, M. A. STUDIES ON THE ANTI-TUMOUR ACTIVITY OF p-DI-

- (2-CHLOROETHYL) AMINOPHENYLALANINE (SARCOLYSINE). *Lancet* **1955**, 266 (6882), 169–171.
- (475) Bergel, F.; Stock, J. A. Cyto-Active Amino-Acid and Peptide Derivatives. Part I. Substituted Phenylalanines. *J. Chem. Soc.* **1954**, No. 0, 2409–2417.
- (476) Augustyn, E.; Finke, K.; Zur, A. A.; Hansen, L.; Heeren, N.; Chien, H.-C.; Lin, L.; Giacomini, K. M.; Colas, C.; Schlessinger, A.; et al. LAT-1 Activity of Meta-Substituted Phenylalanine and Tyrosine Analogs. *Bioorg. Med. Chem. Lett.* **2016**, 26 (11), 2616–2621.
- (477) Huttunen, K. M.; Gynther, M.; Huttunen, J.; Puris, E.; Spicer, J. A.; Denny, W. A. A Selective and Slowly Reversible Inhibitor of L-Type Amino Acid Transporter 1 (LAT1) Potentiates Antiproliferative Drug Efficacy in Cancer Cells. *J. Med. Chem.* **2016**, 59 (12), 5740–5751.
- (478) Kongpracha, P.; Nagamori, S.; Wiriyasermkul, P.; Tanaka, Y.; Kaneda, K.; Okuda, S.; Ohgaki, R.; Kanai, Y. Structure-Activity Relationship of a Novel Series of Inhibitors for Cancer Type Transporter L-Type Amino Acid Transporter 1 (LAT1). *J. Pharmacol. Sci.* **2017**, 133 (2), 96–102.
- (479) Zhou, P.; Qiu, W.-Y.; Liu, S.; Jin, N.-Z. Halogen as Halogen-Bonding Donor and Hydrogen-Bonding Acceptor Simultaneously in Ring-Shaped H<sub>3</sub>N·X(Y)·HF (X = Cl, Br and Y = F, Cl, Br) Complexes. *Phys. Chem. Chem. Phys.* **2011**, 13, 7408–7418.
- (480) Brammer, L.; Bruton, E. A.; Sherwood, P. Understanding the Behavior of Halogens as Hydrogen Bond Acceptors. *Cryst. Growth Des.* **2001**, 1 (4), 277–290.
- (481) Scholfield, M. R.; Zanden, C. M. Vander; Carter, M.; Ho, P. S. Halogen Bonding (X-Bonding): A Biological Perspective. *Protein Sci.* **2013**, 22 (2), 139–152.
- (482) YUNGER, L. M.; CRAMER, R. D. Measurement and Correlation of Partition Coefficients of Polar Amino Acids. *Mol. Pharmacol.* **1981**, 20 (3), 602 LP – 608.
- (483) Chollet, J.-F.; Delétage, C.; Faucher, M.; Miginiac, L.; Bonnemain, J.-L. Synthesis and Structure-Activity Relationships of Some Pesticides with an  $\alpha$ -Amino Acid Function. *Biochim. Biophys. Acta - Gen. Subj.* **1997**, 1336 (2), 331–341.
- (484) Ylikangas, H.; Malmioja, K.; Peura, L.; Gynther, M.; Nwachukwu, E. O.; Leppänen, J.; Laine, K.; Rautio, J.; Lahtela-Kakkonen, M.; Huttunen, K. M.; et al. Quantitative Insight into the Design of Compounds Recognized by the L-Type Amino Acid Transporter 1 (LAT1). *ChemMedChem* **2014**, 9 (12), 2699–2707.
- (485) Thomas, A.; Giacomini, K.; Zur, A.; Colas, C.; Hansen, L.; Heeren, N.; Augustyn, E.; Chien, H.-C.; Springer, S. *Reevaluating the Substrate Specificity of the L-Type Amino Acid Transporter (LAT1)*; 2018; Vol. 61.
- (486) Uchino, H.; Takeda, E.; Kanai, Y.; Segawa, H.; Endou, H.; Miyamoto, K. Expression Cloning and Characterization of a Transporter for Large Neutral Amino Acids Activated by the Heavy Chain of 4F2 Antigen (CD98). *J. Biol. Chem.* **2002**, 273 (37), 23629–23632.
- (487) Li, S.; Whorton, A. R. Identification of Stereoselective Transporters for S -Nitroso-L-Cysteine. *J. Biol. Chem.* **2005**, 280 (20), 20102–20110.
- (488) Matharu, J.; Oki, J.; Worthen, D. R.; Smith, Q. R.; Crooks, P. A. Regiospecific and Conformationally Restrained Analogs of Melphalan and DL-2-NAM-7 and Their Affinities for the Large Neutral Amino Acid Transporter (System LAT1) of the

Blood-Brain Barrier. *Bioorg. Med. Chem. Lett.* **2010**, *20* (12), 3688–3691.

- (489) Ohshima, Y.; Hanaoka, H.; Tominaga, H.; Kanai, Y.; Kaira, K.; Yamaguchi, A.; Nagamori, S.; Oriuchi, N.; Tsushima, Y.; Endo, K.; et al. Biological Evaluation of 3-[<sup>18</sup>F]Fluoro- $\alpha$ -Methyl-d-Tyrosine (d-[<sup>18</sup>F]FAMT) as a Novel Amino Acid Tracer for Positron Emission Tomography. *Ann. Nucl. Med.* **2013**, *27* (4), 314–324.
- (490) Li, J. J. Strecker Amino Acid Synthesis BT - Name Reactions: A Collection of Detailed Mechanisms and Synthetic Applications Fifth Edition. In *Name Reactions*; Li, J. J., Ed.; Springer International Publishing: Cham, 2014; pp 591–592.
- (491) Harusawa, S.; Hamada, Y.; Shioiri, T. Diethyl Phosphorocyanidated (DEPC). A Novel Reagent for the Classical Strecker's  $\alpha$ -Amino Nitrile Synthesis. *Tetrahedron Lett.* **1979**, *20* (48), 4663–4666.
- (492) Rajic, Z.; Zorc, B.; Raic-Malic, S.; Ester, K.; Kralj, M.; Pavelic, K.; Balzarini, J.; De Clercq, E.; Mintas, M. Hydantoin Derivatives of L- and D-Amino Acids: Synthesis and Evaluation of Their Antiviral and Antitumoral Activity. *Molecules* **2006**, *11* (11), 837–848.
- (493) Las Heras-Vázquez, F.; Clemente-Jiménez, J.; Martínez-Rodríguez, S.; Rodríguez-Vico, F. Optically Pure  $\alpha$ -Amino Acids Production by the “Hydantoinase Process.” *Recent Pat. Biotechnol.* **2008**, *2*, 35–46.
- (494) Brien, B O; Johnson, T. Hydantoins: A New Method for of Phenylalanine. *J. Biol. Chem.* **1912**, *12* (2), 205–2013.
- (495) Gibson, M. S.; Bradshaw, R. W. The Gabriel Synthesis of Primary Amines. *Angew. Chemie Int. Ed. English* **1968**, *7* (12), 919–930.
- (496) Kunishima, M.; Friedman, J. E.; Rokita, S. E. Transition-State Stabilization by a Mammalian Reductive Dehalogenase. *J. Am. Chem. Soc.* **1999**, *121* (19), 4722–4723.
- (497) Harris, R. L. N. Potential Wool Growth Inhibitors. Synthesis of DL- $\alpha$ -Amino- $\beta$ -(5-Hydroxy-4-Oxo-3,4-Dihydropyrimidin-2-Yl)Propionic Acid, a Pyrimidine Analogue of Mimosine. *Aust. J. Chem.* **1976**, *29* (6), 1335–1339.
- (498) Harris, R. L. N.; Teitei, T. Potential Wool Growth Inhibitors. 2(1H)-Pyridone Analogues of Mimosine. *Aust. J. Chem.* **1977**, *30* (3), 649–655.
- (499) Hutchinson, J. H.; Halczenko, W.; Brashear, K. M.; Breslin, M. J.; Coleman, P. J.; Duong, L. T.; Fernandez-Metzler, C.; Gentile, M. A.; Fisher, J. E.; Hartman, G. D.; et al. Nonpeptide Av $\beta$ 3 Antagonists. 8. In Vitro and in Vivo Evaluation of a Potent Av $\beta$ 3 Antagonist for the Prevention and Treatment of Osteoporosis. *J. Med. Chem.* **2003**, *46* (22), 4790–4798.
- (500) Struk, Ł.; Sośnicki, J. G. Noncryogenic Synthesis of Functionalized 2-Methoxypyridines by Halogen-Magnesium Exchange Using Lithium Dibutyl(Isopropyl)Magnesate(1-) and Lithium Chloride. *Synthesis (Stuttg.)* **2012**, *44* (5), 735–746.
- (501) Lee, C.-Y.; Chen, Y.-C.; Lin, H.-C.; Jhong, Y.; Chang, C.-W.; Tsai, C.-H.; Kao, C.-L.; Chien, T.-C. Facile Synthesis of 4-Arylidene-5-Imidazolinones as Synthetic Analogs of Fluorescent Protein Chromophore. *Tetrahedron* **2012**, *68* (29), 5898–5907.
- (502) Issa, D. A. E.; Habib, N. S.; Abdel Wahab, A. E. Design{,} Synthesis and Biological Evaluation of Novel 1{,}2{,}4-Triazolo and 1{,}2{,}4-Triazino[4{,}3-a]Quinoxalines as Potential Anticancer and Antimicrobial Agents. *Med. Chem.*

*Commun.* **2015**, *6* (1), 202–211.

- (503) Liu, S.; Shang, R.; Shi, L.; Wan, D. C. C.; Lin, H. Synthesis and Biological Evaluation of 7H-Thiazolo[3,2-b]-1,2,4-Triazin-7- One Derivatives as Dual Binding Site Acetylcholinesterase Inhibitors. *Eur. J. Med. Chem.* **2014**, *81*, 237–244.
- (504) Döbler, C.; Kreuzfeld, H.-J.; Krause, H. W.; Michalik, M. Unusual Amino Acids IV. Asymmetric Synthesis of Thienylalanines. *Tetrahedron: Asymmetry* **1993**, *4* (8), 1833–1842.
- (505) Arava, V. R.; Amasa, S. R.; Goud Bhatthula, B. K.; Kompella, L. S.; Matta, V. P.; Subha, M. C. S. Asymmetric Synthesis of Unnatural Amino Acids and Tamsulosin Chiral Intermediate. *Synth. Commun.* **2013**, *43* (21), 2892–2897.
- (506) The, C. P.; Thi, T. A. D.; Hoang, T. P.; Ngo, Q. A.; Doan, D. T.; Thi, T. H. N.; Thi, T. P.; Thi, T. H. V.; Jean, M.; van de Weghe, P.; et al. Synthesis of New Simplified Hemiasterlin Derivatives with  $\alpha,\beta$ -Unsaturated Carbonyl Moiety. *Bioorg. Med. Chem. Lett.* **2014**, *24* (10), 2244–2246.
- (507) Jursic, B. S.; Sagiraju, S.; Ancalade, D. K.; Clark, T.; Stevens, E. D. Practical Preparation of Z- $\alpha$ -(N-Acetylamino)- and Z- $\alpha$ -(N-Benzoylamino)- $\alpha,\beta$ -unsaturated Acids. *Synth. Commun.* **2007**, *37* (10), 1709–1714.
- (508) Adger, B. M.; Ayrey, P.; Bannister, R.; Forth, M. A.; Hajikarimian, Y.; Lewis, N. J.; O'Farrell, C.; Owens, N.; Shamji, A. Synthesis of 2-Substituted 4-Pyridylpropionates. Part 2. Alkylation Approach. *J. Chem. Soc. Perkin Trans. 1* **1988**, No. 10, 2791–2796.
- (509) Mayhoub, A. S.; Marler, L.; Kondratyuk, T. P.; Park, E.-J.; Pezzuto, J. M.; Cushman, M. Optimization of the Aromatase Inhibitory Activities of Pyridylthiazole Analogues of Resveratrol. *Bioorg. Med. Chem.* **2012**, *20* (7), 2427–2434.
- (510) Batist, G.; Katki, A. G.; Klecker, R. W.; Myers, C. E. Selenium-Induced Cytotoxicity of Human Leukemia Cells: Interaction with Reduced Glutathione. *Cancer Res.* **1986**, *46* (11), 5482 LP – 5485.
- (511) Ramos, J. F.; Webster, T. J. Cytotoxicity of Selenium Nanoparticles in Rat Dermal Fibroblasts. *Int. J. Nanomedicine* **2012**, *7*, 3907–3914.
- (512) Olm, E.; Fernandes, A. P.; Hebert, C.; Rundlöf, A.-K.; Larsen, E. H.; Danielsson, O.; Björnstedt, M. Extracellular Thiol-Assisted Selenium Uptake Dependent on the Cystine Transporter Explains the Cancer-Specific Cytotoxicity of Selenite. *Proc. Natl. Acad. Sci.* **2009**, *106* (27), 11400 LP – 11405.
- (513) Negoro, K.; Yonetoku, Y.; Misawa-Mukai, H.; Hamaguchi, W.; Maruyama, T.; Yoshida, S.; Takeuchi, M.; Ohta, M. Discovery and Biological Evaluation of Novel 4-Amino-2-Phenylpyrimidine Derivatives as Potent and Orally Active GPR119 Agonists. *Bioorg. Med. Chem.* **2012**, *20* (17), 5235–5246.
- (514) Subramanyam, C.; Noguchi, M.; Weinreb, S. M. An Approach to Amphimedine and Related Marine Alkaloids Utilizing an Intramolecular Kondrat'eva Pyridine Synthesis. *J. Org. Chem.* **1989**, *54* (23), 5580–5585.
- (515) Omura, K.; Sharma, A. K.; Swern, D. Dimethyl Sulfoxide-Trifluoroacetic Anhydride. New Reagent for Oxidation of Alcohols to Carbonyls. *J. Org. Chem.* **1976**, *41* (6), 957–962.
- (516) Kippo, T.; Fukuyama, T.; Ryu, I. Regioselective Radical Bromoallylation of Allenes Leading to 2-Bromo-Substituted 1,5-Dienes. *Org. Lett.* **2011**, *13* (15), 3864–3867.

- (517) Cabezon, B.; Cao, J.; Raymo, F. M.; Stoddart, J. F.; White, A. J. P.; Williams, D. J. Self-Complementary [2]Catenanes and Their Related [3]Catenanes. *Chem. – A Eur. J.* **2000**, *6* (12), 2262–2273.
- (518) Storr, T.; Cameron, B. R.; Gossage, R. A.; Yee, H.; Skerlj, R. T.; Darkes, M. C.; Fricker, S. P.; Bridger, G. J.; Davies, N. A.; Wilson, M. T.; et al. RuIII Complexes of Edta and Dtpa Polyaminocarboxylate Analogues and Their Use as Nitric Oxide Scavengers. *Eur. J. Inorg. Chem.* **2005**, *2005* (13), 2685–2697.
- (519) Waghray, D.; Zhang, J.; Jacobs, J.; Nulens, W.; Basarić, N.; Meervelt, L. Van; Dehaen, W. Synthesis and Structural Elucidation of Diversely Functionalized 5,10-Diaza[5]Helicenes. *J. Org. Chem.* **2012**, *77* (22), 10176–10183.
- (520) O'Donnell, M. J. Benzophenone Schiff Bases of Glycine Derivatives: Versatile Starting Materials for the Synthesis of Amino Acids and Their Derivatives. *Tetrahedron* **2019**, *75* (27), 3667–3696.
- (521) Perez, M.; Echeverria, P.-G.; Martinez-Arripe, E.; Ez Zoubir, M.; Touati, R.; Zhang, Z.; Genet, J.-P.; Phansavath, P.; Ayad, T.; Ratovelomanana-Vidal, V. An Efficient Stereoselective Total Synthesis of All Stereoisomers of the Antibiotic Thiamphenicol through Ruthenium-Catalyzed Asymmetric Reduction by Dynamic Kinetic Resolution. *European J. Org. Chem.* **2015**, *2015* (27), 5949–5958.
- (522) Bremberg, U.; Rahm, F.; Moberg, C. Palladium-Catalyzed Allylic Alkylation Using Pyridino-Oxazolines and Quinolino-Oxazolines as Ligands—Influence of Steric Factors. *Tetrahedron: Asymmetry* **1998**, *9* (19), 3437–3443.
- (523) Caron, S.; Do, N. M.; Sieser, J. E. A Practical, Efficient, and Rapid Method for the Oxidation of Electron Deficient Pyridines Using Trifluoroacetic Anhydride and Hydrogen Peroxide–Urea Complex. *Tetrahedron Lett.* **2000**, *41* (14), 2299–2302.
- (524) Campeau, L.-C.; Schipper, D. J.; Fagnou, K. Site-Selective Sp<sup>2</sup> and Benzylic Sp<sup>3</sup> Palladium-Catalyzed Direct Arylation. *J. Am. Chem. Soc.* **2008**, *130* (11), 3266–3267.
- (525) Boechat, N.; da Costa, J. C. S.; de Souza Mendonça, J.; de Oliveira, P. S. M.; Vinícius Nora De Souza, M. A Simple Reduction of Methyl Aromatic Esters to Alcohols Using Sodium Borohydride–Methanol System. *Tetrahedron Lett.* **2004**, *45* (31), 6021–6022.
- (526) Wang, J.; Gondrand, C.; Touti, F.; Hasserodt, J. A Pair of Highly Biotolerated Diamagnetic and Paramagnetic Iron(II) Complexes Displaying Electroneutrality. *Dalt. Trans.* **2015**, *44* (35), 15391–15395.
- (527) Zhang, Q.; Ren, H.; Baker, G. L. An Economical and Safe Procedure to Synthesize 2-Hydroxy-4-Pentynoic Acid: A Precursor towards ‘Clickable’ Biodegradable Polylactide. *Beilstein J. Org. Chem.* **2014**, *10*, 1365–1371.
- (528) Gagnot, G.; Hervin, V.; Coutant-Flexer, E.; Desmons, S.; Baatallah, R.; Monnot, V.; L Janin, Y. Synthesis of Unnatural  $\alpha$ -Amino Esters Using Ethyl Nitroacetate and Condensation or Cycloaddition Reactions. *Beilstein J. Org. Chem.* **2018**, *14*, 2846–2852.
- (529) Fioravanti, S.; Pellacani, L.; Cecilia Vergari, M. ChemInform Abstract: Fluorinated  $\beta$ -Nitro Amines by a Selective ZrCl<sub>4</sub>-Catalyzed Aza-Henry Reaction of (E)-Trifluoromethyl Aldimines. *Org. Biomol. Chem.* **2012**, *10*, 8207–8210.
- (530) Ballesteros, P.; Claramunt, R. M.; Elguero, J. Study of the Catalytic Properties of Tris (3,6-Dioxaheptyl) Amine (Tda-1) in Heteroaromatic Nucleophilic Substitution of Chloropyridines and Their n-Oxides. *Tetrahedron* **1987**, *43* (11), 2557–2564.

- (531) Chang, M.-Y.; Chen, S.-T.; Chang, N.-C. A Synthesis of Racemic Thalidomide. *Synth. Commun.* **2003**, *33* (8), 1375–1382.
- (532) Yavari, I.; Norouzi-Arasi, H. Triphenylphosphine-Catalyzed Nucleophilic  $\alpha$ -Addition to Alkyl Propiolates Synthesis of  $\alpha$ -Substituted Alkyl Acrylates. *Phosphorus. Sulfur. Silicon Relat. Elem.* **2002**, *177* (1), 87–92.
- (533) Medvecký, M.; Linder, I.; Schefzig, L.; Reissig, H.-U.; Zimmer, R. Iodination of Carbohydrate-Derived 1,2-Oxazines to Enantiopure 5-Iodo-3,6-Dihydro-2H-1,2-Oxazines and Subsequent Palladium-Catalyzed Cross-Coupling Reactions. *Beilstein J. Org. Chem.* **2016**, *12*, 2898–2905.
- (534) Collier, P. N.; Patel, I.; Taylor, R. J. K. Heck Reactions of Amino Acid Building Blocks: Application to the Synthesis of Pyrrololine Analogues. *Tetrahedron Lett.* **2002**, *43* (18), 3401–3405.
- (535) Dygos, J. H.; Yonan, E. E.; Scaros, M. G.; Goodmonson, O. J.; Getman, D. P.; Periana, R. A.; Beck, G. R. A Convenient Asymmetric Synthesis of the Unnatural Amino Acid 2,6-Dimethyl-L-Tyrosine. *Synthesis (Stuttg.)* **1992**, *8*, 741–743.
- (536) Harrington, P. J.; Hegedus, L. S.; McDaniel, K. F. Palladium-Catalyzed Reactions in the Synthesis of 3- and 4-Substituted Indoles. 2. Total Synthesis of the N-Acetyl Methyl Ester of (.+.-)-Clavicipitic Acids. *J. Am. Chem. Soc.* **1987**, *109* (14), 4335–4338.
- (537) Cardellicchio, C.; Fiandanese, V.; Marchese, G.; Naso, F.; Ronzini, L. Synthesis of  $\alpha$ -Amino Acid Derivatives by Copper(I)-Catalyzed Conjugate Addition of Grignard Reagents to Methyl 2-Acetamidoacrylate. *Tetrahedron Lett.* **1985**, *26* (36), 4387–4390.
- (538) Yang, J.; Liu, S.; Zheng, J.-F.; Zhou, J. (Steve). Room-Temperature Suzuki–Miyaura Coupling of Heteroaryl Chlorides and Tosylates. *European J. Org. Chem.* **2012**, *2012* (31), 6248–6259.
- (539) Testaferri, L.; Tiecco, M.; Tingoli, M.; Bartoli, D.; Massoli, A. The Reactions of Some Halogenated Pyridines with Methoxide and Methanethiolate Ions in Dimethylformamide. *Tetrahedron* **1985**, *41* (7), 1373–1384.
- (540) Parhi, A. K.; Xiang, A.; Bauman, J. D.; Patel, D.; Vijayan, R. S. K.; Das, K.; Arnold, E.; LaVoie, E. J. Phenyl Substituted 3-Hydroxypyridin-2(1H)-Ones: Inhibitors of Influenza A Endonuclease. *Bioorg. Med. Chem.* **2013**, *21* (21), 6435–6446.
- (541) Stogryn, E. L. 5-Hetarylmethylene-2,4-Diaminopyrimidines. *J. Heterocycl. Chem.* **1974**, *11* (2), 251–253.
- (542) G J Kontoghiorghes, L Sheppard, A V Hoffbrand, J Charalambous, J Tikerpae, M. J. P. Iron Chelation Studies Using Desferrioxamine and the Potential Oral Chelator, 1,2-Dimethyl-3-Hydroxypyrid-4-One, in Normal and Iron Loaded Rats. *J. Clin. Pathol.* **1987**, *40* (4), 404–408.
- (543) Thomas, F. A. The Oxidation of the Side Chain in Kojic Acid Benzyl Ether. *J. Chem. Soc.* **1962**, *334*, 439–442.
- (544) Kawasuji, T.; Johns, B. A.; Yoshida, H.; Weatherhead, J. G.; Akiyama, T.; Taishi, T.; Taoda, Y.; Mikamiyama-Iwata, M.; Murai, H.; Kiyama, R.; et al. Carbamoyl Pyridone HIV-1 Integrase Inhibitors. 2. Bi- and Tricyclic Derivatives Result in Superior Antiviral and Pharmacokinetic Profiles. *J. Med. Chem.* **2013**, *56* (3), 1124–1135.

- (545) Mitra, R.; Ganesh, K. N. PNAs Grafted with ( $\alpha/\gamma$ , R/S)-Aminomethylene Pendants: Regio and Stereo Specific Effects on DNA Binding and Improved Cell Uptake. *Chem. Commun.* **2011**, 47 (4), 1198–1200.
- (546) Katuri, J. V. P.; Nagarajan, K. Hofmann Rearrangement of Primary Carboxamides and Cyclic Imides Using DCDMH and Application to the Synthesis of Gabapentin and Its Potential Peptide Prodrugs. *Tetrahedron Lett.* **2019**, 60 (7), 552–556.
- (547) Zagulyaeva, A. A.; Banek, C. T.; Yusubov, M. S.; Zhdankin, V. V. Hofmann Rearrangement of Carboxamides Mediated by Hypervalent Iodine Species Generated in Situ from Iodobenzene and Oxone: Reaction Scope and Limitations. *Org. Lett.* **2010**, 12 (20), 4644–4647.
- (548) Maloney, P. R.; Khan, P.; Hedrick, M.; Gosalia, P.; Milewski, M.; Li, L.; Roth, G. P.; Sergienko, E.; Suyama, E.; Sugarman, E.; et al. Discovery of 4-Oxo-6-((Pyrimidin-2-Ylthio)methyl)-4H-Pyran-3-Yl 4-Nitrobenzoate (ML221) as a Functional Antagonist of the Apelin (APJ) Receptor. *Bioorg. Med. Chem. Lett.* **2012**, 22 (21), 6656–6660.
- (549) Credille, C. V.; Dick, B. L.; Morrison, C. N.; Stokes, R. W.; Adamek, R. N.; Wu, N. C.; Wilson, I. A.; Cohen, S. M. Structure–Activity Relationships in Metal-Binding Pharmacophores for Influenza Endonuclease. *J. Med. Chem.* **2018**, 61 (22), 10206–10217.
- (550) Credille, C. V.; Chen, Y.; Cohen, S. M. Fragment-Based Identification of Influenza Endonuclease Inhibitors. *J. Med. Chem.* **2016**, 59 (13), 6444–6454.
- (551) Ehrlich, M.; Carell, T. Total Syntheses and Biological Evaluation of 3-O-Methylfunicone and Its Derivatives Prepared by TMPZnCl·LiCl-Mediated Halogenation and Carbonylative Stille Cross-Coupling. *European J. Org. Chem.* **2013**, 2013 (1), 77–83.
- (552) Jin, B.; Zheng, R.; Peng, R.; Chu, S. Synthesis of New Bis(3-Hydroxy-4-Pyridinone) Ligands as Chelating Agents for Uranyl Complexation. *Molecules*. 2016, pp 1–11.
- (553) Ciupa, A.; De Bank, P. A.; Caggiano, L. Multicellular Aggregation of Maltol-Modified Cells Triggered by Fe<sup>3+</sup> Ions. *Chem. Commun.* **2013**, 49 (86), 10148–10150.
- (554) Singh, N.; Scalise, M.; Galluccio, M.; Wieder, M.; Seidel, T.; Langer, T.; Indiveri, C.; Ecker, G. F. Discovery of Potent Inhibitors for the Large Neutral Amino Acid Transporter 1 (LAT1) by Structure-Based Methods. *Int. J. Mol. Sci.* **2019**, 20 (1).
- (555) Rodriguez, M.; Bernad, N.; Galas, M. C.; Lignon, M. F.; Laur, J.; Aumelas, A.; Martinez, J. Synthesis and Biological Activities of Cholecystokinin Analogues Substituted in Position 30 by 3-(1-Naphthyl)-l-Alanine [Nal(1)] or 3-(2-Naphthyl)-l-Alanine [Nal(2)]. *Eur. J. Med. Chem.* **1991**, 26 (3), 245–253.
- (556) Gans, P.; Sabatini, A.; Vacca, A. Investigation of Equilibria in Solution. Determination of Equilibrium Constants with the HYPERQUAD Suite of Programs. *Talanta* **1996**, 43 (10), 1739–1753.
- (557) Alderighi, L.; Gans, P.; Ienco, A.; Peters, D.; Sabatini, A.; Vacca, A. Hyperquad Simulation and Speciation (HySS): A Utility Program for the Investigation of Equilibria Involving Soluble and Partially Soluble Species. *Coord. Chem. Rev.* **1999**, 184 (1), 311–318.
- (558) Stunzi, H.; Harris, L. N.; Perrin, D. D.; Teitei, T. Stability Constants for Metal Complexation by Isomers of Mimosine and Related Compounds. *Aust. J. Chem.* **1980**, 33 (10), 2207–2220.

- (559) Yue, J. L.; Martell, A. E. Potentiometric and Spectrophotometric Determination of Stabilities of the 1-Hydroxy-2-Pyridinone Complexes of Trivalent and Divalent Metal Ions. *Inorganica Chim. Acta* **1993**, *214* (1), 103–111.
- (560) Scarrow, R. C.; Riley, P. E.; Abu-Dari, K.; White, D. L.; Raymond, K. N. Ferric Ion Sequestering Agents. Synthesis, Structures, and Thermodynamics of Complexation of Cobalt(III) and Iron(III) Tris Complexes of Several Chelating Hydroxypyridinones. *Inorg. Chem.* **1985**, *24* (6), 954–967.
- (561) Chruscinska, E.; Garribba, E.; Micera, G.; Panzanelli, A. L-Mimosine, an Amino Acid with Maltol-Type Binding Properties toward Copper(II), Oxovanadium(IV) and Other Metal Ions. *J. Inorg. Biochem.* **1999**, *75* (3), 225–232.
- (562) Lachowicz, J. I.; Nurchi, V. M.; Crisponi, G.; Jaraquemada-Pelaez, M. G.; Arca, M.; Pintus, A.; Santos, M. A.; Quintanova, C.; Gano, L.; Szwczuk, Z.; et al. Hydroxypyridinones with Enhanced Iron Chelating Properties. Synthesis, Characterization and in Vivo Tests of 5-Hydroxy-2-(Hydroxymethyl)Pyridine-4(1H)-One. *Dalt. Trans.* **2016**, *45* (15), 6517–6528.
- (563) Boroujeni, H. C.; Gharib, F. Thermodynamic Investigation on Acid-Base Equilibria of Deferiprone and Deferasirox at Different Ionic Strengths and Various Temperatures. *J. Chem. Thermodyn.* **2016**, *103*, 366–373.
- (564) Xie, Y.-Y.; Lu, Z.; Kong, X.-L.; Zhou, T.; Bansal, S.; Hider, R. Systematic Comparison of the Mono-, Dimethyl- and Trimethyl 3-Hydroxy-4(1H)-Pyridones – Attempted Optimization of the Orally Active Iron Chelator, Deferiprone. *Eur. J. Med. Chem.* **2016**, *115*, 132–140.
- (565) Naik, D. V. Interaction of Kojic Acid with Gold(III) Ions. *Anal. Chim. Acta* **1979**, *106* (1), 147–150.
- (566) Nurchi, V. M.; Crisponi, G.; Lachowicz, J. I.; Murgia, S.; Pivetta, T.; Remelli, M.; Rescigno, A.; Niclós-Gutiérrez, J.; González-Pérez, J. M.; Domínguez-Martín, A.; et al. Iron(III) and Aluminum(III) Complexes with Hydroxypyridone Ligands Aimed to Design Kojic Acid Derivatives with New Perspectives. *J. Inorg. Biochem.* **2010**, *104* (5), 560–569.
- (567) Saghaie, L.; Hider, R. C. Synthesis and Physico-Chemical Properties of a Series of Bidentate 3-Hydroxypyridin-4-Ones Iron Chelating Agents. *Res. Pharm. Sci.* **2008**, *3* (April), 21–30.
- (568) Liu, Y.; He, Q. The Route of Nanomaterials Entering Brain. In *Neurotoxicity of Nanomaterials and Nanomedicine*; Jiang, X., Gao, H. B. T.-N. of N. and N., Eds.; Academic Press, 2017; pp 33–57.
- (569) Nurchi, V. M.; Crisponi, G.; Pivetta, T.; Donatoni, M.; Remelli, M. Potentiometric, Spectrophotometric and Calorimetric Study on Iron(III) and Copper(II) Complexes with 1,2-Dimethyl-3-Hydroxy-4-Pyridinone. *J. Inorg. Biochem.* **2008**, *102* (4), 684–692.
- (570) Cusnir, R.; Imberti, C.; Hider, R.; J. Blower, P.; Ma, M. *Hydroxypyridinone Chelators: From Iron Scavenging to Radiopharmaceuticals for PET Imaging with Gallium-68*; 2017; Vol. 18.
- (571) Merkofer, M.; Kissner, R.; Hider, R. C.; Brunk, U. T.; Koppenol, W. H. Fenton Chemistry and Iron Chelation under Physiologically Relevant Conditions: Electrochemistry and Kinetics. *Chem. Res. Toxicol.* **2006**, *19* (10), 1263–1269.
- (572) Sun, Y.; Pham, A. N.; Waite, T. D. Mechanism Underlying the Effectiveness of

Deferiprone in Alleviating Parkinson's Disease Symptoms. *ACS Chem. Neurosci.* **2018**, *9* (5), 1118–1127.

- (573) Pham, A. N.; Xing, G.; Miller, C. J.; Waite, T. D. Fenton-like Copper Redox Chemistry Revisited: Hydrogen Peroxide and Superoxide Mediation of Copper-Catalyzed Oxidant Production. *J. Catal.* **2013**, *301*, 54–64.
- (574) Wang, F.; Jiao, P.; Qi, M.; Frezza, M.; Dou, Q. P.; Yan, B. Turning Tumor-Promoting Copper into an Anti-Cancer Weapon via High-Throughput Chemistry. *Curr. Med. Chem.* **2010**, *17* (25), 2685–2698.
- (575) Hennemann, G.; Docter, R.; Friesema, E. C. H.; De Jong, M.; Krenning, E. P.; Visser, T. J. Plasma Membrane Transport of Thyroid Hormones and Its Role in Thyroid Hormone Metabolism and Bioavailability. *Endocr. Rev.* **2001**, *22* (4), 451–476.
- (576) Vijay, N.; Morris, M. E. Role of Monocarboxylate Transporters in Drug Delivery to the Brain. *Curr. Pharm. Des.* **2014**, *20* (10), 1487–1498.
- (577) Kim, C. S.; Cho, S. H.; Chun, H. S.; Lee, S. y; Ndou, H. E. BCH, an Inhibitor of System L Amino Acid Transporters, Induces Apoptosis in Cancer Cells. *Biol. Pharm. Bull.* **2008**, *31* (6), 1096–1100.
- (578) Yans, Z.; Hinkleg, P. M.; York, N. Saturable, Stereospecific Transport of 3,5,3'-Triiodo-L-Thyronine and L-Thyroxine into GH4C1 Pituitary Cells. *J. Biol. Chem.* **1993**, *268* (27), 20179–20184.
- (579) Friesema, E. C. H.; Docter, R.; Moerings, E. P. C. M.; Verrey, F.; Krenning, E. P.; Hennemann, G.; Visser, T. J. Thyroid Hormone Transport by the Heterodimeric Human System L Amino Acid Transporter. *Endocrinology* **2001**, *142* (10), 4339–4348.
- (580) H. Ylikangas, K. Malmioja, L. Peura, M. Gynther, E. O. Nwachukwu, J. Leppänen, K. Laine, J. Rautio, M. Lahtela-Kakkonen, K. M. Huttunen, A. P. Quantitative Insight into the Design of Compounds Recognized by the L-Type Amino Acid Transporter 1 (LAT1). *ChemMedChem* **2014**, *9*, 2699-2707.
- (581) Haase, C.; Bergmann, R.; Fuechtner, F.; Hoepping, A.; Pietzsch, J. L-Type Amino Acid Transporters LAT1 and LAT4 in Cancer: Uptake of 3-O-Methyl-6-<sup>18</sup>F-Fluoro-L-Dopa in Human Adenocarcinoma and Squamous Cell Carcinoma In Vitro and In Vivo. *J. Nucl. Med.* **2007**, *48* (12), 2063–2071.
- (582) Gynther, M.; Laine, K.; Ropponen, J.; Leppänen, J.; Mannila, A.; Nevalainen, T.; Savolainen, J.; Järvinen, T.; Rautio, J. Large Neutral Amino Acid Transporter Enables Brain Drug Delivery via Prodrugs. *J. Med. Chem.* **2008**, *51* (4), 932–936.
- (583) Kramlinger, V. M.; Rojas, M. A.; Kanamori, T.; Guengerich, F. P. Cytochrome P450 3A Enzymes Catalyze the O6-Demethylation of Thebaine, a Key Step in Endogenous Mammalian Morphine Biosynthesis. *J. Biol. Chem.* **2015**, *290* (33), 20200–20210.
- (584) Kulp, K. S.; Vulliet, P. R. Mimosine Blocks Cell Cycle Progression by Chelating Iron in Asynchronous Human Breast Cancer Cells. *Toxicol. Appl. Pharmacol.* **1996**, *139* (2), 356–364.
- (585) Hughes, T. A.; Cook, P. R. Mimosine Arrests the Cell Cycle after Cells Enter S-Phase. *Exp. Cell Res.* **1996**, *222* (2), 275–280.
- (586) Alexiou, G.; Gerogianni, P.; Vartholomatos, E.; P. Kyritsis, A. *Deferiprone Enhances Temozolomide Cytotoxicity in Glioma Cells*; 2016; Vol. 34.
- (587) Khodaverdian, V.; Tapadar, S.; MacDonald, I. A.; Xu, Y.; Ho, P. Y.; Bridges, A.;

- Rajpurohit, P.; Sanghani, B. A.; Fan, Y.; Thangaraju, M.; et al. Deferiprone: Pan-Selective Histone Lysine Demethylase Inhibition Activity and Structure Activity Relationship Study. *Sci. Rep.* **2019**, *9* (1), 1–17.
- (588) Patil, V.; Sodji, Q. H.; Kornacki, J. R.; Mrksich, M.; Oyelere, A. K. 3-Hydroxypyridin-2-Thione as Novel Zinc Binding Group for Selective Histone Deacetylase Inhibition. *J. Med. Chem.* **2013**, *56* (9), 3492–3506.
- (589) Lee, J.-C.; Chiang, K.-C.; Feng, T.-H.; Chen, Y.-J.; Chuang, S.-T.; Tsui, K.-H.; Chung, L.-C.; Juang, H.-H. The Iron Chelator, Dp44mT, Effectively Inhibits Human Oral Squamous Cell Carcinoma Cell Growth in Vitro and in Vivo. *Int. J. Mol. Sci.* **2016**, *17* (9), 1435.
- (590) Cooper, C. E.; Lynagh, G. R.; Hoyes, K. P.; Hider, R. C.; Cammack, R.; Porter, J. B. The Relationship of Intracellular Iron Chelation to the Inhibition and Regeneration of Human Ribonucleotide Reductase. *J. Biol. Chem.* **1996**, *271* (34), 20291–20299.
- (591) Nagamani, M.; Prahaladu, P.; Vijayababu, P. V. S. S.; Ashalata, K.; Kusuma Kumari, P.; Kumari, K. L. Lipid Peroxidation Product As A Marker Of Oxidative Stress In Psoriasis-A Case Control Study In North Coastal Andhra Pradesh. *IOSR J. Dent. Med. Sci. e-ISSN* **2015**, *14* (5), 18–20.
- (592) Rappaport, Z. H. Robotics and Artificial Intelligence: Jewish Ethical Perspectives. *Acta Neurochir. Suppl.* **2006**, *98*, 9–12.
- (593) Berlett, B. S.; Stadtman, E. R. Protein Oxidation in Aging and Disease. *Free Radic. Biol. Med.* **2003**, *27* (1988), S4.
- (594) Dalle-Donne, I.; Rossi, R.; Giustarini, D.; Milzani, A.; Colombo, R. Protein Carbonyl Groups as Biomarkers of Oxidative Stress. *Clin. Chim. Acta* **2003**, *329* (1–2), 23–38.
- (595) Collins, A. R. Oxidative DNA Damage, Antioxidants, and Cancer. *BioEssays* **1999**, *21* (3), 238–246.
- (596) Serdar, M.; Sertoglu, E.; Uyanik, M.; Tapan, S.; Akin, K.; Bilgi, C.; Kurt, I. Comparison of 8-Hydroxy-2'-Deoxyguanosine (8-OHdG) Levels Using Mass Spectrometer and Urine Albumin Creatinine Ratio as a Predictor of Development of Diabetic Nephropathy. *Free Radic. Res.* **2012**, *46* (10), 1291–1295.
- (597) Mena, S.; Rodriguez, M. L.; Ortega, A.; Priego, S.; Obrador, E.; Asensi, M.; Petschen, I.; Cerdá, M.; Brown, B. D.; Estrela, J. M. Glutathione and Bcl-2 Targeting Facilitates Elimination by Chemoradiotherapy of Human A375 Melanoma Xenografts Overexpressing Bcl-Xl, Bcl-2, and Mcl-1. *J. Transl. Med.* **2012**, *10*, 8.
- (598) Wang, L.; Leite de Oliveira, R.; Huijberts, S.; Bosdriesz, E.; Pencheva, N.; Brunen, D.; Bosma, A.; Song, J.-Y.; Zevenhoven, J.; Los-de Vries, G. T.; et al. An Acquired Vulnerability of Drug-Resistant Melanoma with Therapeutic Potential. *Cell* **2018**, *173* (6), 1413–1425.e14.
- (599) KARG, E.; TUNEK, A.; BRÖTELL, H.; ROSENGREN, E.; RORSMAN, H. Alteration of Glutathione Level in Human Melanoma Cells: Effect of N-Acetyl-L-Cysteine and Its Analogues. *Pigment Cell Res.* **1990**, *3* (1), 11–15.
- (600) Zhou, M.; Li, Y.; Hu, Q.; Bai, X.-C.; Huang, W.; Yan, C.; Scheres, S. H. W.; Shi, Y. Atomic Structure of the Apoptosome: Mechanism of Cytochrome c- and DATP-Mediated Activation of Apaf-1. *Genes Dev.* **2015**, *29* (22), 2349–2361.
- (601) Shakeri, R.; Kheirollahi, A.; Davoodi, J. Apaf-1: Regulation and Function in Cell Death. *Biochimie* **2017**, *135*, 111–125.

- (602) Fulda, S. Targeting Extrinsic Apoptosis in Cancer: Challenges and Opportunities. *Semin. Cell Dev. Biol.* **2015**, *39*, 20–25.
- (603) Yuan, S.; Akey, C. W. Apoptosome Structure, Assembly, and Procaspase Activation. *Structure* **2013**, *21* (4), 501–515.
- (604) Liu, X.; Li, P.; Zhang, P.; Zhou, L.; Zheng, X.; Liu, Y.; Zhao, T.; Li, Q. Caspase-9: Structure, Mechanisms and Clinical Application. *Oncotarget* **2017**, *8* (14), 23996–24008.
- (605) Hu, Q.; Wu, D.; Chen, W.; Yan, Z.; Shi, Y. Proteolytic Processing of the Caspase-9 Zymogen Is Required for Apoptosome-Mediated Activation of Caspase-9. *J. Biol. Chem.* **2013**, *288* (21), 15142–15147.
- (606) Green, D. R. Cell Death and the Immune System: Getting to How and Why. *Immunol. Rev.* **2017**, *277* (1), 4–8.
- (607) Shen, S.; Li, C.; Dai, M.; Yan, X. Induction of Huh-7 Cell Apoptosis by HCV Core Proteins via CK1 $\alpha$ -P53-Bid Signaling Pathway. *Mol. Med. Rep.* **2018**, *17* (6), 7559–7566.
- (608) Scorrano, L.; Ashiya, M.; Buttle, K.; Weiler, S.; Oakes, S. A.; Mannella, C. A.; Korsmeyer, S. J. A Distinct Pathway Remodels Mitochondrial Cristae and Mobilizes Cytochrome c during Apoptosis. *Dev. Cell* **2002**, *2* (1), 55–67.
- (609) Kantari, C.; Walczak, H. Caspase-8 and Bid: Caught in the Act between Death Receptors and Mitochondria. *Biochim. Biophys. Acta - Mol. Cell Res.* **2011**, *1813* (4), 558–563.
- (610) Brentnall, M.; Rodriguez-Menocal, L.; De Guevara, R. L.; Cepero, E.; Boise, L. H. Caspase-9, Caspase-3 and Caspase-7 Have Distinct Roles during Intrinsic Apoptosis. *BMC Cell Biol.* **2013**, *14*, 32.
- (611) Gonzalez, F.; Pariselli, F.; Jalmar, O.; Dupaigne, P.; Sureau, F.; Dellinger, M.; Hendrickson, E. A.; Bernard, S.; Petit, P. X. Mechanistic Issues of the Interaction of the Hairpin-Forming Domain of TBid with Mitochondrial Cardiolipin. *PLoS One* **2010**, *5* (2), e9342.
- (612) Wright, K. M.; Vaughn, A. E.; Deshmukh, M. *Apoptosome Dependent Caspase-3 Activation Pathway Is Non-Redundant and Necessary for Apoptosis in Sympathetic Neurons*; 2007; Vol. 14.
- (613) Würstle, M. L.; Rehm, M. A Systems Biology Analysis of Apoptosome Formation and Apoptosis Execution Supports Allosteric Procaspase-9 Activation. *J. Biol. Chem.* **2014**, *289* (38), 26277–26289.
- (614) Yuan, S.; Yu, X.; Asara, J. M.; Heuser, J. E.; Ludtke, S. J.; Akey, C. W. The Holo-Apoptosome: Activation of Procaspase-9 and Interactions with Caspase-3. *Structure* **2011**, *19* (8), 1084–1096.
- (615) Zou, H.; Yang, R.; Hao, J.; Wang, J.; Sun, C.; Fesik, S. W.; Wu, J. C.; Tomaselli, K. J.; Armstrong, R. C. Regulation of the Apaf-1/Caspase-9 Apoptosome by Caspase-3 and XIAP. *J. Biol. Chem.* **2003**, *278* (10), 8091–8098.
- (616) Franco, R.; Cidlowski, J. A. Apoptosis and Glutathione: Beyond an Antioxidant. *Cell Death Differ.* **2009**, *16* (10), 1303–1314.
- (617) Pahl, P. M. B.; Horwitz, M. A.; Horwitz, K. B.; Horwitz, L. D. Desferri-Exochelin Induces Death by Apoptosis in Human Breast Cancer Cells but Does Not Kill Normal Breast Cells. *Breast Cancer Res. Treat.* **2001**, *69* (1), 69–79.

- (618) Moon, J.-H.; Jeong, J.-K.; Park, S. *Deferoxamine Inhibits TRAIL-Mediated Apoptosis via Regulation of Autophagy in Human Colon Cancer Cells*; 2014; Vol. 33.
- (619) Zou, X.; Feng, Z.; Li, Y.; Wang, Y.; Wertz, K.; Weber, P.; Fu, Y.; Liu, J. Stimulation of GSH Synthesis to Prevent Oxidative Stress-Induced Apoptosis by Hydroxytyrosol in Human Retinal Pigment Epithelial Cells: Activation of Nrf2 and JNK-P62/SQSTM1 Pathways. *J. Nutr. Biochem.* **2012**, *23* (8), 994–1006.
- (620) Franco, R.; Panayiotidis, M. I.; Cidlowski, J. A. Glutathione Depletion Is Necessary for Apoptosis in Lymphoid Cells Independent of Reactive Oxygen Species Formation. *J. Biol. Chem.* **2007**, *282* (42), 30452–30465.
- (621) Franco, R.; Panayiotidis, M. I.; Cidlowski, J. A. Glutathione Depletion Is Necessary for Apoptosis in Lymphoid Cells Independent of Reactive Oxygen Species Formation. *J. Biol. Chem.* **2007**, *282* (42), 30452–30465.
- (622) Armstrong, J. S.; Steinauer, K. K.; Hornung, B.; Irish, J. M.; Lecane, P.; Birrell, G. W.; Peehl, D. M.; Knox, S. J. Role of Glutathione Depletion and Reactive Oxygen Species Generation in Apoptotic Signaling in a Human B Lymphoma Cell Line. *Cell Death Differ.* **2002**, *9* (3), 252–263.
- (623) Dumitru, C. A.; Zhang, Y.; Li, X.; Gulbins, E. Ceramide: A Novel Player in Reactive Oxygen Species-Induced Signaling? *Antioxid. Redox Signal.* **2007**, *9* (9), 1535–1540.
- (624) Young, M. M.; Kester, M.; Wang, H.-G. Sphingolipids: Regulators of Crosstalk between Apoptosis and Autophagy. *J. Lipid Res.* **2013**, *54* (1), 5–19.
- (625) Venkataraman, K.; Futerman, A. H. Ceramide as a Second Messenger: Sticky Solutions to Sticky Problems. *Trends Cell Biol.* **2000**, *10* (10), 408–412.
- (626) Gault, C. R.; Obeid, L. M.; Hannun, Y. A. An Overview of Sphingolipid Metabolism: From Synthesis to Breakdown. *Adv. Exp. Med. Biol.* **2010**, *688*, 1–23.
- (627) Andrieu-Abadie, N.; Gouazé, V.; Salvayre, R.; Levade, T. Ceramide in Apoptosis Signaling: Relationship with Oxidative Stress. *Free Radic. Biol. Med.* **2001**, *31* (6), 717–728.
- (628) van Blitterswijk, W. J.; van der Luit, A. H.; Veldman, R. J.; Verheij, M.; Borst, J. Ceramide: Second Messenger or Modulator of Membrane Structure and Dynamics? *Biochem. J.* **2003**, *369* (Pt 2), 199–211.
- (629) Sanvicens, N.; Cotter, T. G. Ceramide Is the Key Mediator of Oxidative Stress-Induced Apoptosis in Retinal Photoreceptor Cells. *J. Neurochem.* **2006**, *98* (5), 1432–1444.
- (630) Posse de Chaves, E. I. Sphingolipids in Apoptosis, Survival and Regeneration in the Nervous System. *Biochim. Biophys. Acta - Biomembr.* **2006**, *1758* (12), 1995–2015.
- (631) Poloni, J.; Chapola, H.; Feltes, B. C.; Bonatto, D. *The Importance of Sphingolipids and Reactive Oxygen Species in Cardiovascular Development*; 2014; Vol. 106.
- (632) Nikolova-Karakashian, M. N.; Reid, M. B. Sphingolipid Metabolism, Oxidant Signaling, and Contractile Function of Skeletal Muscle. *Antioxid. Redox Signal.* **2011**, *15* (9), 2501–2517.
- (633) Kimura, K.; Markowski, M.; Edsall, L. C.; Spiegel, S.; Gelmann, E. P. Role of Ceramide in Mediating Apoptosis of Irradiated LNCaP Prostate Cancer Cells. *Cell Death Differ.* **2003**, *10* (2), 240–248.
- (634) Huang, C.; Freter, C. Lipid Metabolism, Apoptosis and Cancer Therapy. *Int. J. Mol.*

*Sci.* **2015**, *16* (1), 924–949.

- (635) Giussani, P.; Tringali, C.; Riboni, L.; Viani, P.; Venerando, B. Sphingolipids: Key Regulators of Apoptosis and Pivotal Players in Cancer Drug Resistance. *Int. J. Mol. Sci.* **2014**, *15* (3), 4356–4392.
- (636) Meyer, S. G. E.; Wendt, A. E.; Scherer, M.; Liebisch, G.; Kerkweg, U.; Schmitz, G.; de Groot, H. Myriocin, an Inhibitor of Serine Palmitoyl Transferase, Impairs the Uptake of Transferrin and Low-Density Lipoprotein in Mammalian Cells. *Arch. Biochem. Biophys.* **2012**, *526* (1), 60–68.
- (637) Li, H.; Yun, H.-Y.; Baek, K.; Kwon, N.; Park, K.-C.; Kim, D.-S. *Myriocin, a Serine Palmitoyltransferase Inhibitor, Increases Melanin Synthesis in Mel-Ab Cells and a Skin Equivalent Model*; 2014; Vol. 69.
- (638) Lee, Y.-S.; Choi, K.-M.; Choi, M.-H.; Ji, S.-Y.; Lee, S.; Sin, D.-M.; Oh, K.-W.; Lee, Y.-M.; Hong, J.-T.; Yun, Y.-P.; et al. Serine Palmitoyltransferase Inhibitor Myriocin Induces Growth Inhibition of B16F10 Melanoma Cells through G2/M Phase Arrest. *Cell Prolif.* **2011**, *44* (4), 320–329.
- (639) Glaros, E. N.; Kim, W. S.; Garner, B. Myriocin-Mediated up-Regulation of Hepatocyte ApoA-I Synthesis Is Associated with ERK Inhibition. *Clin. Sci. (Lond)*. **2010**, *118* (12), 727–736.
- (640) Caretti, A.; Torelli, R.; Perdoni, F.; Falleni, M.; Tosi, D.; Zulueta, A.; Casas, J.; Sanguinetti, M.; Ghidoni, R.; Borghi, E.; et al. Inhibition of Ceramide de Novo Synthesis by Myriocin Produces the Double Effect of Reducing Pathological Inflammation and Exerting Antifungal Activity against *A. Fumigatus* Airways Infection. *Biochim. Biophys. Acta - Gen. Subj.* **2016**, *1860* (6), 1089–1097.
- (641) Li, J.; Yu, W.; Tiwary, R.; Park, S.-K.; Xiong, A.; Sanders, B. G.; Kline, K.  $\alpha$ -TEA-Induced Death Receptor Dependent Apoptosis Involves Activation of Acid Sphingomyelinase and Elevated Ceramide-Enriched Cell Surface Membranes. *Cancer Cell Int.* **2010**, *10*, 40.
- (642) Grassmé, H.; Jekle, A.; Riehle, A.; Schwarz, H.; Berger, J.; Sandhoff, K.; Kolesnick, R.; Gulbins, E. CD95 Signaling via Ceramide-Rich Membrane Rafts. *J. Biol. Chem.* **2001**, *276* (23), 20589–20596.
- (643) Coe, G. L.; Redd, P. S.; Paschall, A. V.; Lu, C.; Gu, L.; Cai, H.; Albers, T.; Lebedyeva, I. O.; Liu, K. Ceramide Mediates FasL-Induced Caspase 8 Activation in Colon Carcinoma Cells to Enhance FasL-Induced Cytotoxicity by Tumor-Specific Cytotoxic T Lymphocytes. *Sci. Rep.* **2016**, *6*, 30816.
- (644) Grullich, C.; Sullards, M. C.; Fuks, Z.; Merrill, A. H.; Kolesnick, R. CD95(Fas/APO-1) Signals Ceramide Generation Independent of the Effector Stage of Apoptosis. *J. Biol. Chem.* **2000**, *275* (12), 8650–8656.
- (645) Grassmé, H.; Cremesti, A.; Kolesnick, R.; Gulbins, E. Ceramide-Mediated Clustering Is Required for CD95-DISC Formation. *Oncogene* **2003**, *22* (35), 5457–5470.
- (646) Siskind, L. J. Mitochondrial Ceramide and the Induction of Apoptosis. *J. Bioenerg. Biomembr.* **2005**, *37* (3), 143–153.
- (647) Parra, V.; Moraga, F.; Kuzmicic, J.; López-Crisosto, C.; Troncoso, R.; Torrealba, N.; Criollo, A.; Díaz-Elizondo, J.; Rothermel, B. A.; Quest, A. F. G.; et al. Calcium and Mitochondrial Metabolism in Ceramide-Induced Cardiomyocyte Death. *Biochim. Biophys. Acta* **2013**, *1832* (8), 1334–1344.

- (648) Kogot-Levin, A.; Saada, A. Ceramide and the Mitochondrial Respiratory Chain. *Biochimie* **2014**, *100*, 88–94.
- (649) Hearps, A. C.; Burrows, J.; Connor, C. E.; Woods, G. M.; Lowenthal, R. M.; Ragg, S. J. Mitochondrial Cytochrome c Release Precedes Transmembrane Depolarisation and Caspase-3 Activation during Ceramide-Induced Apoptosis of Jurkat T Cells. *Apoptosis* **2002**, *7* (5), 387–394.
- (650) German, O. L.; Miranda, G. E.; Abrahan, C. E.; Rotstein, N. P. Ceramide Is a Mediator of Apoptosis in Retina Photoreceptors. *Invest. Ophthalmol. Vis. Sci.* **2006**, *47* (4), 1658–1668.
- (651) Dadsena, S.; Bockelmann, S.; Mina, J. G. M.; Hassan, D. G.; Korneev, S.; Razzera, G.; Jahn, H.; Niekamp, P.; Müller, D.; Schneider, M.; et al. Ceramides Bind VDAC2 to Trigger Mitochondrial Apoptosis. *Nat. Commun.* **2019**, *10* (1), 1832.
- (652) Scharstuhl, A.; Mutsaers, H. A. M.; Pennings, S. W. C.; Russel, F. G. M.; Wagener, F. A. D. T. G. Involvement of VDAC, Bax and Ceramides in the Efflux of AIF from Mitochondria during Curcumin-Induced Apoptosis. *PLoS One* **2009**, *4* (8), e6688–e6688.
- (653) Peña-Blanco, A.; García-Sáez, A. J. Bax, Bak and beyond — Mitochondrial Performance in Apoptosis. *FEBS J.* **2018**, *285* (3), 416–431.
- (654) Martínez-Abundis, E.; Correa, F.; Pavón, N.; Zazueta, C. Bax Distribution into Mitochondrial Detergent-Resistant Microdomains Is Related to Ceramide and Cholesterol Content in Postischemic Hearts. *FEBS J.* **2009**, *276* (19), 5579–5588.
- (655) Jain, A.; Beutel, O.; Ebell, K.; Korneev, S.; Holthuis, J. C. M. Diverting CERT-Mediated Ceramide Transport to Mitochondria Triggers Bax-Dependent Apoptosis. *J. Cell Sci.* **2017**, *130* (2), 360 LP – 371.
- (656) I Giles, G. *The Redox Regulation of Thiol Dependent Signaling Pathways in Cancer*; 2006; Vol. 12.
- (657) Ganesan, V.; Perera, M. N.; Colombini, D.; Datskovskiy, D.; Chadha, K.; Colombini, M. Ceramide and Activated Bax Act Synergistically to Permeabilize the Mitochondrial Outer Membrane. *Apoptosis* **2010**, *15* (5), 553–562.
- (658) Chipuk, J. E.; McStay, G. P.; Bharti, A.; Kuwana, T.; Clarke, C. J.; Siskind, L. J.; Obeid, L. M.; Green, D. R. Sphingolipid Metabolism Cooperates with BAK and BAX to Promote the Mitochondrial Pathway of Apoptosis. *Cell* **2012**, *148* (5), 988–1000.
- (659) Yabu, T.; Shiba, H.; Shibasaki, Y.; Nakanishi, T.; Imamura, S.; Touhata, K.; Yamashita, M. Stress-Induced Ceramide Generation and Apoptosis via the Phosphorylation and Activation of NSMase1 by JNK Signaling. *Cell Death Differ.* **2015**, *22* (2), 258–273.
- (660) Kolesnick, R.; Fuks, Z. Radiation and Ceramide-Induced Apoptosis. *Oncogene* **2003**, *22* (37), 5897–5906.
- (661) Kannan, R.; Jin, M.; Gamulescu, M.-A.; Hinton, D. Ceramide-Induced Apoptosis: Role of Catalase and Hepatocyte Growth Factor. *Free Radic. Biol. Med.* **2004**, *37* (2), 166–175.
- (662) Hofmann, K.; Dixit, V. M. Ceramide in Apoptosis—Does It Really Matter? *Trends Biochem. Sci.* **1998**, *23* (10), 374–377.
- (663) Haimovitz-Friedman, A.; Kolesnick, R. N.; Fuks, Z. Ceramide Signaling in Apoptosis. *Br. Med. Bull.* **1997**, *53* (3), 539–553.

- (664) Burgess, J.; Rangel, M. *Hydroxypyranones, Hydroxypyridinones, and Their Complexes*; 2008; Vol. 60.
- (665) Scarrow, R. C.; Riley, P. E.; Abu-Dari, K.; White, D. L.; Raymond, K. N. Ferric Ion Sequestering Agents. 13. Synthesis, Structures, and Thermodynamics of Complexation of Cobalt(III) and Iron(III) Tris Complexes of Several Chelating Hydroxypyridinones. *Inorg. Chem.* **1985**, *24* (6), 954–967.
- (666) T Dexter, D.; A Statton, S.; Whitmore, C.; Freinbichler, W.; Weinberger, P.; F Tipton, K.; Della Corte, L.; Ward, R.; Crichton, R. *Clinically Available Iron Chelators Induce Neuroprotection in the 6-OHDA Model of Parkinson's Disease after Peripheral Administration*; 2010; Vol. 118.
- (667) Kim-Han, J. S.; Antenor-Dorsey, J. A.; O'Malley, K. L. The Parkinsonian Mimetic, MPP+, Specifically Impairs Mitochondrial Transport in Dopamine Axons. *J. Neurosci.* **2011**, *31* (19), 7212–7221.
- (668) Ito, K.; Eguchi, Y.; Imagawa, Y.; Akai, S.; Mochizuki, H.; Tsujimoto, Y. MPP+ Induces Necrostatin-1-and Ferrostatin-1-Sensitive Necrotic Death of Neuronal SH-SY5Y Cells. *Cell Death Discov.* **2017**, *3*, 1–10.
- (669) Aguirre, P.; Mena, N. P.; Carrasco, C. M.; Muñoz, Y.; Pérez-Henríquez, P.; Morales, R. A.; Cassels, B. K.; Méndez-Gálvez, C.; García-Beltrán, O.; González-Billault, C.; et al. Iron Chelators and Antioxidants Regenerate Neuritic Tree and Nigrostriatal Fibers of MPP+/MPTP-Lesioned Dopaminergic Neurons. *PLoS One* **2015**, *10* (12), 1–15.
- (670) Xie, Y.; Hou, W.; Song, X.; Yu, Y.; Huang, J.; Sun, X.; Kang, R.; Tang, D. Ferroptosis: Process and Function. *Cell Death Differ.* **2016**, *23* (3), 369–379.
- (671) Stockwell, B. R.; Friedmann Angeli, J. P.; Bayir, H.; Bush, A. I.; Conrad, M.; Dixon, S. J.; Fulda, S.; Gascón, S.; Hatzios, S. K.; Kagan, V. E.; et al. Ferroptosis: A Regulated Cell Death Nexus Linking Metabolism, Redox Biology, and Disease. *Cell* **2017**, *171* (2), 273–285.
- (672) Dixon, S. J.; Lemberg, K. M.; Lamprecht, M. R.; Skouta, R.; Zaitsev, E. M.; Gleason, C. E.; Patel, D. N.; Bauer, A. J.; Cantley, A. M.; Yang, W. S.; et al. Ferroptosis: An Iron-Dependent Form of Nonapoptotic Cell Death. *Cell* **2012**, *149* (5), 1060–1072.
- (673) Miotto, G.; Rossetto, M.; Roveri, A.; Venerando, R.; Vučković, A.-M.; Di Paolo, M. L.; Bosello-Travain, V.; Zaccarin, M.; Maiorino, M.; Toppo, S.; et al. P-250 - Insight the Mechanism of Ferroptosis Inhibition by Ferrostatin-1. *Free Radic. Biol. Med.* **2018**, *120*, S120–S121.
- (674) Zilka, O.; Shah, R.; Li, B.; Friedmann Angeli, J. P.; Griesser, M.; Conrad, M.; Pratt, D. A. On the Mechanism of Cytoprotection by Ferrostatin-1 and Liproxstatin-1 and the Role of Lipid Peroxidation in Ferroptotic Cell Death. *ACS Cent. Sci.* **2017**, *3* (3), 232–243.
- (675) Angeli, J. P. F.; Shah, R.; Pratt, D. A.; Conrad, M. Ferroptosis Inhibition: Mechanisms and Opportunities. *Trends Pharmacol. Sci.* **2017**, *38* (5), 489–498.
- (676) Cater, H. L.; Gitterman, D.; Davis, S. M.; Benham, C. D.; Morrison III, B.; Sundstrom, L. E. Stretch-Induced Injury in Organotypic Hippocampal Slice Cultures Reproduces in Vivo Post-Traumatic Neurodegeneration: Role of Glutamate Receptors and Voltage-Dependent Calcium Channels. *J. Neurochem.* **2007**, *101* (2), 434–447.
- (677) Yang, W. S.; Stockwell, B. R. Ferroptosis: Death by Lipid Peroxidation. *Trends Cell*

*Biol.* **2016**, *26* (3), 165–176.

- (678) Li, X.; Duan, L.; Yuan, S.; Zhuang, X.; Qiao, T.; He, J. Ferroptosis Inhibitor Alleviates Radiation-Induced Lung Fibrosis (RILF) via down-Regulation of TGF-B1. *J. Inflamm.* **2019**, *16* (1), 11.
- (679) Li, Y.; Feng, D.; Wang, Z.; Zhao, Y.; Sun, R.; Tian, D.; Liu, D.; Zhang, F.; Ning, S.; Yao, J.; et al. Ischemia-Induced ACSL4 Activation Contributes to Ferroptosis-Mediated Tissue Injury in Intestinal Ischemia/Reperfusion. *Cell Death Differ.* **2019**, 1–16.
- (680) Nimse, S. B.; Pal, D. Free Radicals, Natural Antioxidants, and Their Reaction Mechanisms. *RSC Adv.* **2015**, *5* (35), 27986–28006.
- (681) Dunford, A. N. D. H. B. The Oxidation of Ascorbic Acid and Hydroquinone by Perhydroxyl Radicals. A Flash Photolysis Study. *Can. J. Chem.* **1979**, *57* (12), 3017–3022.
- (682) Kaneko, M.; Fukuda, M.; Sano, T.; Ohnishi, T.; Hosokawa, Y.; Matsui, S.; Matumoto, Y. ESR Spin Trapping Study on Ability of Ascorbic Acid as Superoxide Radical Scavenger. *J. Japanese Stomatol. Soc.* **1997**, *46* (3), 216–222.
- (683) Sato, E.; Kohno, M.; Nakashima, T.; Niwano, Y. Ciclopirox Olamine Directly Scavenges Hydroxyl Radical. *Int. J. Dermatol.* **2008**, *47* (1), 15–18.
- (684) Hooper, D. C.; Spitsin, S.; Kean, R. B.; Champion, J. M.; Dickson, G. M.; Chaudhry, I.; Koprowski, H. Uric Acid, a Natural Scavenger of Peroxynitrite, in Experimental Allergic Encephalomyelitis and Multiple Sclerosis. *Proc. Natl. Acad. Sci. U. S. A.* **1998**, *95* (2), 675–680.
- (685) Hooper, D. C.; Scott, G. S.; Zborek, A.; Mikheeva, T.; Kean, R. B.; Koprowski, H.; Spitsin, S. V. Uric Acid, a Peroxynitrite Scavenger, Inhibits CNS Inflammation, Blood–CNS Barrier Permeability Changes, and Tissue Damage in a Mouse Model of Multiple Sclerosis. *FASEB J.* **2000**, *14* (5), 691–698.
- (686) Schildknecht, S.; Pape, R.; Müller, N.; Robotta, M.; Marquardt, A.; Bürkle, A.; Drescher, M.; Leist, M. Neuroprotection by Minocycline Caused by Direct and Specific Scavenging of Peroxynitrite. *J. Biol. Chem.* **2011**, *286* (7), 4991–5002.
- (687) Bartesaghi, S.; Trujillo, M.; Denicola, A.; Folkes, L.; Wardman, P.; Radi, R. Reactions of Desferrioxamine with Peroxynitrite-Derived Carbonate and Nitrogen Dioxide Radicals. *Free Radic. Biol. Med.* **2004**, *36*, 471–483.
- (688) Beasley, A. S.; Anderson, C.; McArthur, J.; Sacktor, N.; Nath, A.; Cotter, R. J. Characterization of Nitrotyrosine-Modified Proteins in Cerebrospinal Fluid. *Clin. Proteomics* **2010**, *6* (1), 29–41.
- (689) Bartesaghi, S.; Radi, R. Fundamentals on the Biochemistry of Peroxynitrite and Protein Tyrosine Nitration. *Redox Biol.* **2018**, *14*, 618–625.
- (690) Franco, M.; Estevez, A. Reactive Nitrogen Species in Motor Neuron Apoptosis. In *Amyotrophic Lateral Sclerosis*; 2012; pp 1–24.
- (691) Zou, M.; Shi, C.; Cohen, R. That Is Associated with Thromboxane/Prostaglandin H2 Receptor-Mediated Apoptosis and Adhesion Molecule Expression in Cultured Human Aortic Endothelial Cells. *Diabetes* **2002**, *51* (January), 198–203.
- (692) Suresh, V. Inhibition of Prostate Cancer Proliferation by Deferiprone. *NMR Biomed.* **2017**, *30*, 1–12.

- (693) Saghaie, L.; Sadeghi-Aliabadi, H.; Ashaehshoar, M. Synthesis, Analysis and Cytotoxic Evaluation of Some Hydroxypyridinone Derivatives on HeLa and K562 Cell Lines. *Res. Pharm. Sci.* **2013**, *8* (3), 185–195.
- (694) Chenoufi, N.; Drénou, B.; Loréal, O.; Pigeon, C.; Brissot, P.; Lescoat, G. Antiproliferative Effect of Deferiprone on the Hep G2 Cell Line. *Biochem. Pharmacol.* **1998**, *56* (4), 431–437.
- (695) Chang, H.-C.; Lee, T.-H.; Chuang, L.-Y.; Yen, M.-H.; Hung, W.-C. Inhibitory Effect of Mimosine on Proliferation of Human Lung Cancer Cells Is Mediated by Multiple Mechanisms. *Cancer Lett.* **1999**, *145* (1), 1–8.
- (696) Huq, A. M.; Wai, L. K.; Rullah, K.; Mohd Aluwi, M. F. F.; Stanslas, J.; Jamal, J. A. Oestrogenic Activity of Mimosine on MCF-7 Breast Cancer Cell Line through the ER $\alpha$ -Mediated Pathway. *Chem. Biol. Drug Des.* **2019**, *93* (3), 222–231.
- (697) van der Walt, N. B.; Zakeri, Z.; Cronjé, M. J. The Induction of Apoptosis in A375 Malignant Melanoma Cells by *Sutherlandia Frutescens*. *Evid. Based. Complement. Alternat. Med.* **2016**, *2016*, 4921067.
- (698) Pfister, T. D.; Reinhold, W. C.; Agama, K.; Gupta, S.; Khin, S. A.; Kinders, R. J.; Parchment, R. E.; Tomaszewski, J. E.; Doroshov, J. H.; Pommier, Y. Topoisomerase I Levels in the NCI-60 Cancer Cell Line Panel Determined by Validated ELISA and Microarray Analysis and Correlation with Indenoisoquinoline Sensitivity. *Mol. Cancer Ther.* **2009**, *8* (7), 1878–1884.
- (699) Liu, J.; Jiang, G.; Mao, P.; Zhang, J.; Zhang, L.; Liu, L.; Wang, J.; Owusu, L.; Ren, B.; Tang, Y.; et al. Down-Regulation of GADD45A Enhances Chemosensitivity in Melanoma. *Sci. Rep.* **2018**, *8* (1), 1–11.
- (700) Wong, S. E.; Lightstone, F. C. Accounting for Water Molecules in Drug Design. *Expert Opin. Drug Discov.* **2011**, *6* (1), 65–74.
- (701) Amin, M. L. P-Glycoprotein Inhibition for Optimal Drug Delivery. *Drug Target Insights* **2013**, *7*, 27–34.
- (702) Schinkel, A. H. P-Glycoprotein, a Gatekeeper in the Blood-Brain Barrier. *Adv. Drug Deliv. Rev.* **1999**, *36* (2–3), 179–194.
- (703) Jankowiak, A.; Kaszynski, P. 4-Substituted 1-Acyloxypyridine-2(1H)-Thiones: Experimental and Computational Studies of the Substituent Effect on Electronic Absorption Spectra. *J. Org. Chem.* **2009**, *74* (19), 7441–7448.
- (704) Workman, D. G.; Tsatsanis, A.; Lewis, F. W.; Boyle, J. P.; Mousadoust, M.; Hettiarachchi, N. T.; Hunter, M.; Peers, C. S.; Tétard, D.; Duce, J. A. Protection from Neurodegeneration in the 6-Hydroxydopamine (6-OHDA) Model of Parkinson's with Novel 1-Hydroxypyridin-2-One Metal Chelators. *Metallomics* **2015**, *7* (5), 867–876.
- (705) Burgada, R.; Bailly, T.; Noël, J. P.; Gomis, J. M.; Valleix, A.; Ansoborlo, E.; Hengé-Napoli, M. H.; Paquet, F.; Gourmelon, P. Synthesis of 3,4,3 LI 1,2 HOPO Labelled with <sup>14</sup>C. *J. Label. Compd. Radiopharm.* **2001**, *44* (1), 13–19.
- (706) Barfoot, C. W.; Brown, P.; Dabbs, S.; Davies, D. T.; Hennessy, A. J.; Miles, T. J.; Pearson, N. D. The Design of Efficient and Selective Routes to Pyridyl Analogues of 2,3-Dihydro-1,4-Benzodioxin-6-Carbaldehyde. *Tetrahedron Lett.* **2010**, *51* (38), 5038–5040.
- (707) Trecourt, F.; Mallet, M.; Mongin, O.; Queguiner, G. Total Synthesis of (+)-Atpenin B. An Original “Clockwise” Functionalization of 2-Chloropyridine. *J. Org. Chem.*

**1994**, 59 (21), 6173–6178.

- (708) Ohtsu, H.; Itokawa, H.; Xiao, Z.; Su, C.-Y.; Shih, C. C.-Y.; Chiang, T.; Chang, E.; Lee, Y.; Chiu, S.-Y.; Chang, C.; et al. Antitumor Agents 222. Synthesis and Anti-Androgen Activity of New Diarylheptanoids. *Bioorg. Med. Chem.* **2003**, 11 (23), 5083–5090.
- (709) Dobbin, P. S.; Hider, R. C.; Hall, A. D.; Taylor, P. D.; Sarpong, P.; Porter, J. B.; Xiao, G.; van der Helm, D. Synthesis, Physicochemical Properties, and Biological Evaluation of N-Substituted 2-Alkyl-3-Hydroxy-4(1H)-Pyridinones: Orally Active Iron Chelators with Clinical Potential. *J. Med. Chem.* **1993**, 36 (17), 2448–2458.
- (710) Combret, Y.; Duflos, J.; Dupas, G.; Bourguignon, J.; Quéguiner, G. Variations of the Nature of the Chiral Auxiliary with a Highly Enantioselective Chiral NADH Model. *Tetrahedron: Asymmetry* **1993**, 4 (7), 1635–1644.
- (711) Dos Santos, T.; Varela, J.; Lynch, I.; Salvati, A.; Dawson, K. A. Quantitative Assessment of the Comparative Nanoparticle-Uptake Efficiency of a Range of Cell Lines. *Small* **2011**, 7 (23), 3341–3349.
- (712) Khazalpour, S.; Nematollahi, D. Electrochemical Study of Alamar Blue (Resazurin) in Aqueous Solutions and Room-Temperature Ionic Liquid 1-Butyl-3-Methylimidazolium Tetrafluoroborate at a Glassy Carbon Electrode. *RSC Adv.* **2014**, 4 (17), 8431–8438.
- (713) Nemzer, B.; Chang, T.; Xie, Z.; Pietrkowski, Z.; Reyes, T.; Ou, B. Decrease of Free Radical Concentrations in Humans Following Consumption of a High Antioxidant Capacity Natural Product. *Food Sci. Nutr.* **2014**, 2 (6), 647–654.
- (714) Lamani, D. S.; Bhowmick, D.; Muges, G. Substituent Effects on the Stability and Antioxidant Activity of Spirodiazaselenuranes. *Molecules* **2015**, 20 (7), 12959–12978.
- (715) Johnson, M. B.; Criss, A. K. Fluorescence Microscopy Methods for Determining the Viability of Bacteria in Association with Mammalian Cells. *J. Vis. Exp.* **2013**, No. 79, 1–9.
- (716) Wen, J.; Krishan, A.; Thomas, R. a. Effect of PH and DAPI Concentration on Dual Parametric Analysis of DNA/DAPI Fluorescence and Electronic Nuclear Volume. *Cytometry* **2001**, 43 (1), 12–15.
- (717) Peterson, Q. P.; Goode, D. R.; West, D. C.; Botham, R. C.; Hergenrother, P. J. Preparation of the Caspase-3/7 Substrate Ac-DEVD-PNA by Solution-Phase Peptide Synthesis. *Nat. Protoc.* **2010**, 5, 294–302.
- (718) Putt, K. S.; Chen, G. W.; Pearson, J. M.; Sandhorst, J. S.; Hoagland, M. S.; Kwon, J.-T.; Hwang, S.-K.; Jin, H.; Churchwell, M. I.; Cho, M.-H.; et al. Small-Molecule Activation of Pro-caspase-3 to Caspase-3 as a Personalized Anticancer Strategy. *Nat. Chem. Biol.* **2006**, 2 (10), 543–550.
- (719) Sivandzade, F.; Bhalerao, A.; Cucullo, L. Analysis of the Mitochondrial Membrane Potential Using the Cationic JC-1 Dye as a Sensitive Fluorescent Probe. *Bio-protocol* **2019**, 9 (1), e3128.
- (720) Perelman, A.; Wachtel, C.; Cohen, M.; Haupt, S.; Shapiro, H.; Tzur, A. JC-1: Alternative Excitation Wavelengths Facilitate Mitochondrial Membrane Potential Cytometry. *Cell Death Dis.* **2012**, 3 (11), e430–e430.
- (721) Suzuki, T.; Fujikura, K.; Tetsuya, H.; Takata, K. Nuclear Staining for Laser Confocal

Microscopy. *Acta Histochem. Cytochem.* **1997**, *45* (1), 49–53.

- (722) Niedernhofer, L. J.; Daniels, J. S.; Rouzer, C. A.; Greene, R. E.; Marnett, L. J. Malondialdehyde, a Product of Lipid Peroxidation, Is Mutagenic in Human Cells. *J. Biol. Chem.* **2003**, *278* (33), 31426–31433.
- (723) Janero, D. R. Malondialdehyde and Thiobarbituric Acid-Reactivity as Diagnostic Indices of Lipid Peroxidation and Peroxidative Tissue Injury. *Free Radic. Biol. Med.* **1990**, *9* (6), 515–540.
- (724) Weber, D.; Davies, M. J.; Grune, T. Determination of Protein Carbonyls in Plasma, Cell Extracts, Tissue Homogenates, Isolated Proteins: Focus on Sample Preparation and Derivatization Conditions. *Redox Biol.* **2015**, *5*, 367–380.
- (725) Dalle-Donne, I.; Carini, M.; Orioli, M.; Vistoli, G.; Regazzoni, L.; Colombo, G.; Rossi, R.; Milzani, A.; Aldini, G. Protein Carbonylation: 2,4-Dinitrophenylhydrazine Reacts with Both Aldehydes/Ketones and Sulfenic Acids. *Free Radic. Biol. Med.* **2009**, *46* (10), 1411–1419.
- (726) Setyaningsih, Y.; Husodo, A. H.; Astuti, I. Detection of Urinary 8-Hydroxydeoxyguanosine (8-OHdG) Levels as a Biomarker of Oxidative DNA Damage among Home Industry Workers Exposed to Chromium. *Procedia Environ. Sci.* **2015**, *23*, 290–296.
- (727) Cayman, C. DNA/RNA Oxidative Damage (High Sensitivity) ELISA Kit.
- (728) Piyamongkol, S.; Liu, Z. D.; Hider, R. C. Novel Synthetic Approach to 2-(1'-Hydroxyalkyl)- and 2-Amido-3-Hydroxypyridin-4-Ones. *Tetrahedron* **2001**, *57* (16), 3479–3486.
- (729) Xu, M.-Y.; Jiang, W.-T.; Li, Y.; Xu, Q.-H.; Zhou, Q.-L.; Yang, S.; Xiao, B. Alkyl Carbagermatranes Enable Practical Palladium-Catalyzed Sp<sup>2</sup>–Sp<sup>3</sup> Cross-Coupling. *J. Am. Chem. Soc.* **2019**, *141* (18), 7582–7588.
- (730) Battah, S.; Hider, R. C.; MacRobert, A. J.; Dobbin, P. S.; Zhou, T. Hydroxypyridinone and 5-Aminolaevulinic Acid Conjugates for Photodynamic Therapy. *J. Med. Chem.* **2017**, *60* (8), 3498–3510.